

UNCLASSIFIED

AD NUMBER
AD073754
NEW LIMITATION CHANGE
TO Approved for public release, distribution unlimited
FROM Distribution authorized to DoD only; Administrative/Operational Use; APR 1955. Other requests shall be referred to Wright Air Development Center, Wright-Patterson AFB, OH 45433.
AUTHORITY
USAF HQS 88ABW, 88CG/SCCMF ltr, 17 Mar 2006

THIS PAGE IS UNCLASSIFIED

UNCLASSIFIED

AD NUMBER
AD073754
CLASSIFICATION CHANGES
TO
unclassified
FROM
confidential
AUTHORITY
30 Apr 1967, DoDD 5200.10

THIS PAGE IS UNCLASSIFIED

UNCLASSIFIED

AD NUMBER
AD073754
CLASSIFICATION CHANGES
TO
confidential
FROM
secret
AUTHORITY
30 Apr 1958, DoDD 5200.10

THIS PAGE IS UNCLASSIFIED

AD 73754

Armed Services Technical Information Agency

Reproduced by
DOCUMENT SERVICE CENTER
KNOTT BUILDING, DAYTON, 2, OHIO

This document is the property of the United States Government. It is furnished for the duration of the contract and shall be returned when no longer required, or upon recall by ASTIA to the following address:
Armed Services Technical Information Agency, Document Service Center,
Knott Building, Dayton 2, Ohio.

NOTICE: WHEN GOVERNMENT OR OTHER DRAWINGS, SPECIFICATIONS OR OTHER DATA ARE USED FOR ANY PURPOSE OTHER THAN IN CONNECTION WITH A DEFINITELY RELATED GOVERNMENT PROCUREMENT OPERATION, THE U. S. GOVERNMENT THEREBY INCURS NO RESPONSIBILITY, NOR ANY OBLIGATION WHATSOEVER; AND THE FACT THAT THE GOVERNMENT MAY HAVE FORMULATED, FURNISHED, OR IN ANY WAY SUPPLIED THE SAID DRAWINGS, SPECIFICATIONS, OR OTHER DATA IS NOT TO BE REGARDED BY IMPLICATION OR OTHERWISE AS IN ANY MANNER LICENSING THE HOLDER OR ANY OTHER PERSON OR CORPORATION, OR CONVEYING ANY RIGHTS OR PERMISSION TO MANUFACTURE, USE OR SELL ANY PATENTED INVENTION THAT MAY IN ANY WAY BE RELATED THERETO.

SECRET

SECRET

FC

Repro
BELL Aircraft CORPORATION
BUFFALO, N. Y. NEW YORK

TECHNICAL DATA

By: R. S. Postle L. C. Landphair
R. Decrevel P. B. McKowen
J. S. Isenberg A. J. Pallone
H. K. Cheng F. S. Roehrs
W. J. Gill C. M. Schmidt
A. J. Hanawalt

Approved: *P. C. Emmons* Date: April 23, 1955
P. C. Emmons

REPORT NO. ml43-945-012

MX-2276 ADVANCE STRATEGIC WEAPON SYSTEM

AERODYNAMICS

DATE

U.S.A.O.

NOTICE: This document contains information affecting the national defense of the United States within the meaning of the Espionage Laws, Title 18 U.S.C., Sect. 793 and 794. Its transmission or the revelation of its contents in any manner to an unauthorized person is prohibited by law.

Best Available Copy

REPRODUCTION-AUTHORIZED

55BN976

SECRET

OCT 29 1955

55RD7-6515

SECRET

13296
AD

NOTICE: Except as hereinafter listed or marked, Bell Aircraft Corporation has no positive knowledge of the existence of other copyright, proprietary, or patent information contained in this report.

NOTICE

BELL AIRCRAFT CORPORATION reserves all rights of whatsoever nature in and to the developments herein described which are claimed in issued and/or pending patents in BELL'S name, except as any of same are or may be licensed to the United States Government for its use.

SECRET

Best Available Copy

Report No. D143-945-012

55802-6515

SECRET

 By _____ Date _____
 Checked _____ Date _____

BELL Aircraft CORPORATION

 Model _____ Page 1
 Missile _____ Report D143-945-012
 Airplane _____

Foreword

During the period 1 April 1954 to 2 May 1955 the Bell Aircraft Corporation conducted a study program for the New Development Office, Bombardment Aircraft Branch, WADO, in accordance with USAF Contract No. AF33(616)-2419 RDO No. R441-47. The objective of this study was to investigate the possible design and development problems associated with flight in the speed and altitude regimes of the weapon system outlined in Bell Aircraft Report D143-945-010. The results of this study will provide the firm technical foundations necessary for planning future programs, funds, and facilities.

The work accomplished during this program is reported in the following reports:

D143-945-012	Aerodynamics
D143-945-013	Structures
D143-945-014	Preliminary Global System Study
D143-945-015	Radar
D143-945-016	Navigation and Control
D143-945-017	Propulsion
D143-945-018	Final Summary Report

In the present report the pages are numbered by sections. In the interest of reading convenience, the symbols, references, tables and figures generally are arranged at the ends of the major sub-sections to which they are pertinent.

SECRET

SECRET

By _____ Date _____

BELL *Aircraft* CORPORATION

Model _____ Page 11

Checked _____ Date _____

Missile _____
Airplane _____ Report W43-945-012

Index

<u>Section</u>	<u>Title</u>
1.	Introduction
2.	Summary
3.	Conclusions and Recommendations
4.	General Aerodynamics
	4.1 Introduction
	4.2 Configuration
	4.3 Atmosphere
	4.4 Glide Performance
	4.5 Flight Mechanics
	4.6 Aerodynamic Heating
	4.7 Stability and Control
	4.8 Stage Separation
	4.9 Missile Trajectories
5.	Applied Research
	5.1 Introduction
	5.2 Fundamental Equations: Flow Regimes
	5.3 Bow Shock - Boundary Layer Interaction
	5.4 Ultra - High Temperature Phenomena
	5.5 Transpiration Cooling
	5.6 Inviscid Hypersonic Flow
	5.7 Transition
6.	Test Facilities

Appendices

4 A	Compressible Skin Friction and Heat Transfer Methods
4 B	Equations of Motion
5 A	Shock - Boundary Layer Interaction (Upper)
5 B	Shock - Boundary Layer Interaction (Lower)
5 C	Radiative Heat Transfer
5 D	Piston Analogy

SECRET

Section I
Introduction

The data presented in this report are the results of a study of the aerodynamic problems involved in the design of the MX-2276 weapon system. This weapon system, which is substantially as described in original proposal presented in Bell Aircraft Report D143-945-010, encounters regimes of flight wherein little previous attention has been given to the design of a workable flight vehicle.

It is essential to the development of such a system, that reliable methods of estimating the necessary aerodynamic parameters be determined. In the original study referenced above, the basic intent was to demonstrate feasibility and to generally outline some of the more critical problem areas. To accomplish this, approximate means of estimating the aerodynamic parameters were utilized and some preliminary investigations into the accuracy of these parameters were conducted. In addition, preliminary conclusions were reached as to the desired flight path and range capability of the weapon, and a tentative configuration was established. The feasibility of the weapon system was demonstrated in a preliminary manner.

The purpose of present study was to investigate the major problem areas in greater detail. In particular, the investigations were directed into the areas of 1) hypersonic lift and drag, 2) heat transfer, 3) performance calculation, 4) stability and control, and 5) launch and stage separation, with major attention given to the first three items. It was not intended that this study should include any optimization of the vehicle, but rather that the results would define the future development programs required to arrive at a workable weapon system.

In order to initiate the present study it was necessary to define a method of approach. The configuration originally proposed is sufficiently representative of the ultimate weapon to justify its use as a basis of study of the aerodynamic problems and no attempt was made to alter the design in the light of new findings. The flight path recommended as most efficient in the original study, that is, initial ascent of the vehicle to its maximum velocity followed by a continuous unpowered glide to the end of flight, was chosen, since this flight path penetrates most deeply into the realms of flight at hypersonic velocities and extreme altitudes.

It was planned that the initial phase of the study would be involved in an overall investigation of present outside activities and a review of the available technological information. With the compiling of this data, the study would then be divided into two general fields involving 1) General Aerodynamics wherein the presently available methods of analysis would be applied to the study of the problem

SECRET

By _____	Date _____	BELL <i>Aircraft</i> CORPORATION	Model _____	Page 1-2
Checked _____	Date _____		Missile _____	Report D143-945-012

areas, and 2) Applied Research where fundamental theories and analytical methods would be investigated to determine regions of applicability and to define the regions and problems wherein basic information is presently lacking.

A general summary of results is presented and the conclusion and recommendations derived from the study are listed. The technical information supporting these results follows and is divided into the two major fields of General Aerodynamics and Applied Research.

SECRET

SECRET

By _____ Date _____
Checked _____ Date _____

BELL Aircraft CORPORATION

Model _____ Page 2-1
Missile _____
Airplane _____ Report M43-Section 2Summary2.1 Configuration

The configuration presented in the original work has been retained for this study since optimization of the shape was not required. It is considered that the original configuration is sufficiently representative for use in the present study.

2.2 Atmosphere

Recent data obtained from sounding rocket firings has shown the NACA standard atmospheric characteristics to be in considerable error at altitudes over 100,000 ft. An atmospheric variation based on the data obtained from these firings has been proposed. Since the variations are large enough to produce significant changes in the present analysis, the work performed in the latter part of this study and that generally presented herein has been based on the proposed atmosphere.

Since the MX-2276 glide range is on the order of half the circumference of the earth and the flight duration is short, subsequent analysis should consider the atmospheric variations which may be encountered. These may be large according to the available data.

2.3 General Aerodynamics

The aerodynamics of the MX-2276 system is treated in Section 4 (General Aerodynamics) in terms of the application of available methods and extensions of available methods, and the new methods which have been derived in the present study. The analyses are generally concerned with the study of the glide phase of the third stage since it is felt that it is in this phase that most of the important aerodynamic problems occur.

2.3.1 Performance

The MX-2276 Stage III maximum L/D glide characteristics have been completely reevaluated above $M = 4$, generally using extension of inviscid flow theories and flat plate boundary layer theories. Boundary layer transition was assumed to occur at 2.8 million local Reynolds number.

The maximum L/D's vary approximately from 4 to 5 during the glide period and are very close to those originally predicted. The equilibrium altitudes, however, are considerably lower at the higher speeds; the original prediction was 259,000 ft. for the 22,000 fps initial speed, the present is 214,000 ft. This is partially due to

Form 24-1 Rev. 3-53

SECRET

By _____ Date _____

BELL Aircraft CORPORATION

Model _____ Page 2-2

Checked _____ Date _____

Missile _____ Report D143-945-012
Airplane _____

to adopting the new pressure-altitude variation. The non-rotating earth glide range for the aircraft with bomb load was found to be 10,670 nautical miles from the initial speed of 22,000 feet per second to zero final speed, while the corresponding glide range without bomb load was 10,000 nautical miles.

A preliminary investigation into the effects of shock wave boundary layer interaction on wing L/D's has been made. It was found that at the present equilibrium glide altitude there are appreciable effects on surface pressures and skin frictions but that the summation of these effects in L/D's produces only small changes from the no interaction L/D_{max} values. The differences in pressure result in an increase in lift, however, which will in turn increase the equilibrium altitude somewhat. Since L/D_{max} varies with altitude, differences in L/D_{max} may result. This effect has not been studied at present.

No new studies on the ascent path have been attempted since these would lie more in the field of design optimization. Studies of this type should receive future consideration however, to determine the effects of the path on ascent performance and on stage separation problems.

2.3.2 Equations of Motion

The equations of linear and angular motion of a hypersonic vehicle have been derived for flight about a rotating earth. For the present study, only earth attraction, curvature and rotation need be considered, the effects of the earth's orbital path and the attractions of other heavenly bodies being small. These equations form the basis on which glide paths, maneuvering characteristics and stability and control may be accurately analyzed.

2.3.3 Flight Paths

The new linear equations of motion which include the effects of earth rotation have been applied to the determination of glide range to demonstrate the effects on the flight paths. Numerical integration of these equations has been accomplished with IBM computing machinery. The results indicate that for an initial velocity of 22,000 ft./sec., earth rotation causes a 25% increase in glide range for flight about the equator to the east, as compared to the glide range about a non-rotating earth, and a 15% reduction in glide range for flight about the equator to the west. These effects are appreciable and must be considered in the design of a vehicle to accomplish a given task.

A study of the feasibility of flying at altitudes higher than the equilibrium altitude for maximum L/D of the present third stage has been made in order to investigate possible heat transfer

Checked _____	Date _____	BELL Aircraft CORPORATION	Model _____	Page 2-3
			Missile _____	
			Airplane _____	Report D113-245-012

reductions. The study included the effects of 1) lowered wing loading, 2) increased lift coefficient and 3) partial lift paths. The present wing loading is already close to a practical minimum, and the partial lift trajectories result in flight path oscillations which will tend to increase peak heating loads. Flight at a lift coefficient greater than that for maximum lift-drag ratio results in only a small saving within the critical areas of heating and a large loss in glide range. These results, which are based on inviscid flow methods, indicate therefore, that the prospect of an appreciable heat reduction is not favorable. The effects of shock boundary layer interaction on these results have not been considered in detail at present.

A possible method of navigation would be to follow great circle paths about the earth, however flight on a great circle with zero aerodynamic side force, will require that the aircraft be rolled in order to utilize aerodynamic lift to counter the Coriolis forces caused by earth rotation. An investigation has shown that a maximum roll of 22° will be required for the present third stage and that the normal load factor will vary a maximum of $\pm 38\%$ from the load factor presently required at the maximum flight velocity about a non-rotating earth. Maneuvering from one great circle path to another will require additional roll and normal load factor and only moderate rates of turn can be achieved with relatively large increments of normal load and roll. Further studies of the details of flight programming, heating and load limitations are required.

2.3.4 Aerodynamic Heating

Assuming a thin outer skin insulated from the inner structure, a number of equilibrium wall temperatures have been estimated for the Stage III configuration for the glide conditions determined in performance estimation. The compressible boundary layer heat transfer coefficients were determined by the reference temperature method, local surface flow conditions were estimated from inviscid theory.

The reference temperature method has been shown to give good results in the supersonic region of flight. This method has been extended to hypersonic flight by extrapolation from the presently known variation of the properties of air with temperature. Obviously then, the accuracy of this method in predicting surface temperatures in hypersonic flight is uncertain.

The most severe temperatures are found on the bottom of the body and wings. The temperatures one foot from the nose are approximately 2000° at the initial glide speeds and indicate the probable need for cooling close to the nose. The temperatures drop rapidly with distance aft until transition (assumed at 2.8 million local Reynolds number) is reached where they rise appreciably and remain essentially constant for the remaining distance aft. The temperature

SECRET

By _____	Date _____	BELL Aircraft CORPORATION	Model _____	Page 2-4
Checked _____	Date _____		Missile _____	Report D143-945-12

for the turbulent flow regions which cover large areas on the bottom are on the order of 1700°F for much of the glide, and are approximately 600°F greater than if the boundary layer were laminar. The importance of transition and its determination is evident from this. In view of the present lack of knowledge as to where transition will occur it is obvious that this is a major uncertainty of the system.

The variations of equilibrium temperature of the bottom surface with angle of attack and with changes in surface emissivity at the $M = 20$ point on the glide path were estimated. The need for a high coefficient of emissivity is demonstrated; a decrease in emissivity coefficient from .9 to .6 increases the surface temperature by 200°F to 300°F. Angle of attack is shown to be extremely important, the temperature rising approximately 100°F per degree. It is apparent that maneuvers such as pull-ups and turns will be strongly temperature limited.

The above analyses did not include the effects of shock boundary layer interaction or slip flow. A check of the effects of shock boundary layer interaction on the wing surface temperatures was made. The effect is greatest at the leading edge and decreases downstream. Inclusion of interaction gave very slightly higher temperatures on the lower surface; a 40°F increase at the 6 inch station, the severest condition considered. Interaction caused considerable change in the wing upper surface temperatures; for the 6 inch station at $M = 20$ a 700°F increase, at $M = 16$ a 300°F increase, at $M = 10$ a 80°F increase. It is obvious that shock - boundary layer interaction is an important consideration but it is also of interest that its neglect on the lower surface was not critical for the present flight plan.

Other than a determination of the regions in which slip flow may occur, it was not possible to investigate this effect in the present study.

Temperatures and heat fluxes in the stagnation areas of leading edges and noses have been estimated for the $M = 21.5$ and $M = 16$ conditions on the flight path. These are based on the assumption that the incompressible theories for predicting heat fluxes in such areas can be applied to the subsonic flow behind the normal shock waves produced by the leading edges and nose. The temperatures and heat fluxes are very severe. It is evident from them that the leading edge heating will present one of the most difficult design problems. It appears that considerable cooling of these areas will be necessary.

It should be noted however, that the methods employed are only approximate and that further study of the effects on leading edge heating of hypersonic viscous flow are required and in addition should consider the effects of variation of the profile shape.

Form 14-1 Rev. 3-53

SECRET

By _____ Date _____

Checked _____ Date _____

BELL Aircraft CORPORATION

Model _____ Page 2-5
Missile _____
Airplane _____ Report D1113-915-012

To evaluate the merit of transpiration cooling the quantities of air injection necessary to cool the first foot and the first 10 ft. of the lower surface to 1600°R (though not the leading edge radius itself) have been estimated for the Stage III glide. Approximately 1200 lbs. of air are required to cool the first foot of the wing. This is felt to be a practical quantity and to indicate the feasibility of this method of cooling, particularly since there is promise of considerable reduction in the coolant rate from the above through use of better coolants than air, which was used because the theory in its present state of development applied only to injection of air into air.

The present study has left the temperatures in the base areas of the body and wing completely undefined. These areas of the vehicle lie in a highly complex mixture of boundary layer flow which available analytical methods are unable to describe. Determination of the temperatures and heat fluxes in various base areas will probably rest on future experimental investigations.

2.3.5 Stability and Control

A hypersonic vehicle of the type of the MX-2276 will be required to be controllable over a wide range of flight velocities. Stability and control characteristics of aircraft up to low supersonic speeds are presently understood to a reasonable degree. In the hypersonic flight regime, new conditions are encountered and new equations governing the motion of the vehicle at hypervelocities have been derived. The equations show that stability and control analysis at these speeds will be a task of appreciable magnitude. Considerable effort must be applied to the determination of static and dynamic aerodynamic parameters, for which little work has been done to date, using the available methods of approach.

Some preliminary estimates show that static longitudinal stability and control can be achieved at $M = 20$. These approximate estimates were based on inviscid flow theories. Tentative estimates show that the effects of fluid viscosity, i.e. boundary layer interaction, can be appreciable at high altitudes and high Mach numbers and should be given further consideration.

2.3.6 Separation

As originally described, the MX-2276 System requires three stages of boost. Three separable configurations, the first and second stage boosters and the glide vehicle, are assembled adjacent to one another in a parallel arrangement. As the final stage is accelerated to the initial glide conditions, the first and second stage boosters separate and drop away as their fuel loads are expended. The aerodynamics of these separations is considered in a qualitative manner hereinafter. No definite conclusions as to the

SECRET

By _____ Date _____

BELL Aircraft CORPORATION

Model _____ Page 2-6

Checked _____ Date _____

Missile _____
Airplane _____ Report DTIC-945-012

practicability of the original booster-vehicle configurations for separation are made. It is recommended that when preliminary design of the system is begun, booster-vehicle combinations be put into aerodynamic test as soon as possible as it is believed this is the only way of evaluating them in a sufficiently quantitative manner.

2.3.7 Missile Trajectories

Some approximate estimates of the zero lift trajectories of the MX-2276 missile have been made, assuming constant drag coefficients, to determine the line of sight angle from the carrier to the missile during the fall and the time and range increments between the time at which the carrier passes over the target and impact to the missile. These estimates were made to illustrate the mechanics of the missile drop and serve as preliminary design information for the missile tracking and guidance system.

2.4 Applied Research

The Applied Research Section, Section 5, is concerned with the existence and accuracy of methods for analyzing the force and heat loads to which the MX-2276 aircraft will be subjected and with the major flow problems which need be solved in order to provide an adequate set of methods. One of the primary aims was to point out the "new" or "unconventional" phenomena of the hypersonic flight which are not apparent or do not occur at ordinary supersonic speeds and to provide means for assessing their importance.

2.4.1 Flow Regions

One approach centered about a critical investigation of the foundations of basic concepts of hypersonic flow theory to indicate the nature and types of flow patterns which could be expected to obtain; it was desired to determine both the physical problems and the basic flow equations which could adequately and consistently describe these flow problems. To this end, an analysis of the flow about a flat plate flying in the range of speeds and altitudes corresponding to the flight plan of MX-2276 was made, delineating the nature and the extent of the various flow regions. In attempting to build up an overall picture of the various flow regions, however, details of the flow about a plate for various Mach number - Reynolds number combinations were required, but since there are very few experiments in the high M, low Re range of interest, these details for the present study were derived from theory. In particular, it was found that the boundary layer slip and bow shock-boundary layer interaction phenomena could be appreciable in parts of the Mach number Reynolds number range of interest here.

SECRET

By _____	Date _____	BELL <i>Aircraft</i> CORPORATION	Model _____	Page 2-7
Checked _____	Date _____		Missile _____	Report D113-945-012
			Airplane _____	

2.4.2 Shock Boundary Layer Interaction

A survey was then made of the various shock-boundary interaction theories to compile and correlate the information on this phenomena for use in building up a picture of the various flow regions and for predicting the pressure, shear, and heating parameters on a body in hypersonic flight. There were, however, several different theories predicting different results for some cases of shock-boundary layer interaction, while other cases of interest, e.g., the expansion side of a plate at angle of attack, had not been considered at all. It was necessary, therefore, to go into shock interaction theory in some detail in order to evaluate these theories. As a result, some improvements were made on existing theory, (flat plate, zero angle) and new theory and numerical results were obtained for the cases of interaction on a flat plate at positive and negative angles of attack. It is shown that the increases in pressure and skin friction coefficient due to shock interaction for all cases can be correlated in a general but simple and convenient form.

2.4.3 High Temperature Phenomena

Another line of approach followed in this study was to make probing investigations into the nature and magnitude of "new" effects arising from the high temperatures which would be realized in the boundary layer and behind strong shocks in hypersonic flight. To this end studies were made of the emissivity of air - which governs radiative heat transfer - of the effect of dissociation of the air on convective heat transfer and of real gas effects on shock flow relations. In these cases determination of even the order of magnitude of an effect involved detailed investigations.

In considering whether or not the intensely hot air in the boundary layer radiates an appreciable amount of heat to the adjacent structure, the first step is to estimate the emissivity of air at temperatures of the order of 10,000°R and low densities. The estimates obtained from air analysis based on the quantum mechanical aspects of kinetic theory show that the order of magnitude of the emissivity of air at the temperatures under consideration is sufficiently high so that radiative heat transfer appears to be an important factor. It remains, however, to solve the flow equations in the boundary layer including a radiative heat transfer term, in order to determine the exact way in which radiation will qualitatively and quantitatively affect the overall heat transfer picture. A prerequisite to such a detailed study is a precise knowledge of the emissivity as a function of wave length, pressure and temperature. A theory has been developed to compute this quantity; it was not, however, possible in this study to carry out the detailed numerical calculations.

Some brief thoughts and remarks on the calculation of the transport properties of dissociated gases are given and an investigation

SECRET

By _____ Date _____

BELL Aircraft CORPORATION

Model _____ Page 2-8

Checked _____ Date _____

Missile _____ Report D1143-945-012
Airplane _____

of the effects of assumed equilibrium dissociation of air on the boundary layer characteristics is reported. The results of the latter study show that skin friction and heat transfer are essentially unaffected by dissociation so long as both the stream and body temperatures are below dissociation values. It appears that a similar result holds in the stagnation region of a blunt-nosed body.

A recently completed program (at Bell Aircraft Corporation) to compute basic tables of flow parameters for both shock flow and isentropic flow, incorporating real gas effects up to dissociation temperatures, is discussed. Since the gas flow tables are basic to any numerical analysis of the flow, it was important to determine how the actual behavior of air at high temperatures differs from that described by the standard ideal gas tables, and thus the real gas flow tables were needed as a standard comparison. A numerical comparison at typical flow conditions of interest was made. It is of particular interest to the performance and viscous heating analyses that real gas effects on the flow adjacent to surfaces at reasonably low angles of attack (e.g. the Stage III lower surfaces) are small.

2.4.4 Transpiration Cooling

A survey and evaluation of the existing theoretical and experimental literature on the aerodynamic aspects of transpiration cooling was made seeking a basis for the calculation of coolant requirements. Practically all of the theoretical studies examined were restricted to supersonic flow at low Mach number, generally less than $M = 3$. Hence it was deemed necessary to develop new solutions to the equations of the compressible laminar boundary layer including the effects of transpiration cooling for Mach numbers up to 20. As the end result, an approximate theoretical method was developed for computing the rate of mass flow injection of coolant required to keep a surface at a given (arbitrary) temperature under given initial free stream conditions.

The theory applies to a laminar boundary layer, which is most pertinent to the present case, as transpiration cooling will most probably be confined to the severely heated areas near the leading edges where the flow is expected to be laminar. It is probable that the injection of the relatively small amounts of coolant into the boundary layer will not destabilize the laminar flow. In the strict sense air must be used as the coolant because the theory is based on homogenous boundary layer considerations for which the coolant and boundary layer flows must be of the same gas; but it is believed that a dissimilar coolant can be handled with sufficient accuracy through a simple extension of the present theory. A set of exemplary design charts were calculated using air as the coolant.

Form 14-1 Rev. 3-53

SECRET

By _____ Date _____
Checked _____ Date _____

BELL Aircraft CORPORATION

Model _____ Page 2-9
Missile _____
Airplane _____ Report D113-945-012

2.4.5 Hypersonic Inviscid Flow Theory

The detailed investigation of shock-interaction theory led to a thorough study of hypersonic inviscid flow theory, since results of the latter have an important influence on the results of interaction theory based on the two layer model. Furthermore, the so-called "Newtonian flow" approximation of inviscid hypersonic flow is an important practical method for determining pressure distributions on a body where viscous effects do not predominate, and hence the applicability and limits of this approximation were given consideration. Some contributions to an understanding of an improvement in accuracy of the approximate hypersonic inviscid theory have been made.

2.4.6 Boundary Layer Transition

In any practical computation of friction drag or aerodynamic heating, the state of the boundary layer must first be assumed, i.e., a knowledge of the transition point is required. Unfortunately, the present state of reliable knowledge on this subject leaves much to be desired. The effect and the importance of the many variables which could effect transition and the mechanism of transition itself is not yet understood; hence the assumptions of theory are incomplete and experiments are not fully controlled. The best that can be done at the present time is to assume a transition Reynolds number based on the trends exhibited by available wind tunnel and flight test data. In the original work and the present study a transition Reynolds number $Re = 2.8$ million at all Mach numbers was assumed. This appears to have been conservatively low judging from the trends exhibited by the test data available, and from discussions with several experimenters during visits to other research agencies.

2.5 Facilities

The test facilities which would be pertinent to an MX-2276 development program have been considered and the range of coverage has been reviewed, for those facilities which are presently available, or are presently under development and will be available in the near future. Simultaneous simulation of all the flight parameters encountered in the flight of MX-2276 is difficult in earth-bound test facilities. However, the various types of wind tunnels and ballistic ranges which are in or approaching operation will enable investigations of the problem areas over much of the flight regime to be encountered. This data can be augmented and extended by flight test vehicles. Several test vehicles (the HTV and NACA PARD) are presently being developed which will approach the ultimate MX-2276 flight conditions.

By _____ Date _____

BELL *Aircraft* CORPORATIONModel _____ Page 3-1

Checked _____ Date _____

Missile _____
Airplane _____ Report DL43-945-012Section 3Conclusions and Recommendations3.1 Conclusions

The conclusions derived from the problem study of the aerodynamics of the MX 2276 system are enumerated in brief here. These generally concern the Stage III hypersonic, high altitude glide which is considered the most critical operational phase with respect to aerodynamics.

3.1.1 General Aerodynamics3.1.1.1 Performance

- a. Maximum L/D's of 4 to 5 between $M = 4$ and 20 which will give the desired 10,000 mile range for an initial glide velocity of 22,000 fps, appear attainable for glide configurations of the type originally presented for the system. This is based on theoretical analyses which are direct extensions of those which have been experimentally confirmed at lower supersonic Mach numbers but which do not account for the additional hypersonic and low density flight phenomena that may occur.
- b. Inclusion of shock-boundary layer interaction effects for the glide conditions, considered to be the most important of the hypersonic phenomena, caused significant increases in the wing lift and drag but when these were summed produced only small changes in wing L/D. Similar analysis is required for the body.
- c. Upper surfaces (expansion sides) are of secondary importance in their effects on performance. It may be possible to modify the upper wing profile, e.g. increasing the thickness of the airfoil aft for better structure and stowage, with little loss in aerodynamic performance.

3.1.1.2 Flight Mechanics

- a. Equations of motion including the effects of the earth rotation which are necessary to the study of very high speed flight have been derived and utilized.
- b. Effects of earth rotation on range are considerable and must be included in the consideration of specific glide paths.
- c. Flight constrained to great circle courses on the earth will produce appreciable additional loads which must be included in considering the overall L/D and the aerodynamic heating.

By _____	Date _____	BELL Aircraft CORPORATION	Model _____	Page 3-2
Checked _____	Date _____		Missile _____	Report D143-945-012

- d. Programming the Stage III flight altitude higher than that for maximum L/D glide by using higher lift coefficients than those for maximum L/D by attempting partial lifting paths, in order to reduce viscous heating, does not appear profitable.

3.1.1.3 Aerodynamic Heating

- a. For the glide path calculated for Stage III, the surface temperatures appear tolerable after approximately the first two feet where they are less than 1800°F.
- b. If transition occurs at 2.8 million Reynolds number (the number assumed during this study for lack of better information) turbulent boundary layer flow would exist over much of the lower surface of Stage III and temperatures there would be on the order of 1700°F for the higher speed portion of flight.
- c. If the above areas were laminar instead of turbulent, they would be approximately 600° cooler which indicates the importance of obtaining better knowledge concerning transition.
- d. Surface emissivity also plays an important role in determining temperature. A value of 0.9 was generally used in this work and variations from this caused significant changes.
- e. Increases in angle of attack at the higher glide speeds, as needed for maneuvers, will produce large surface temperature changes, on the order of 100° per degree angle of attack increase. This is an important consideration as maneuvers will undoubtedly be limited by such heating.
- f. The leading edge temperatures estimated are beyond tolerable materials limits; cooling in considerable quantity appears definitely necessary. The leading edge heating problem is seen to be an extremely important one which may greatly effect design considerations, e.g. sweepback and leading edge radius as well as provision for cooling.
- g. Transpiration cooling merits attention; it is indicated to be an efficient means though it has not been possible to evaluate it to the extent desired during the present study.
- h. Inclusion of shock boundary layer interaction effects in the prediction of wall temperatures did not produce appreciably greater temperatures on the bottom surface.

By _____ Date _____

Checked _____ Date _____

BELL *Aircraft* CORPORATIONModel _____ Page 3-3Missile _____
Airplane _____ Report D143-945-012

For the upper surfaces; however, interaction increased the temperatures significantly over large areas and it is evident that interaction effects must be considered there if any accuracy of prediction is to be achieved.

3.1.1.4 Stability and Control

- a. It is evident that the additional forces induced by the rotating earth will complicate stability and control analyses.
- b. An analysis based on inviscid flow theory indicates aerodynamic stability can be attained at $M = 20$ with a reasonable configuration.
- c. A check of boundary layer interaction effects shows these to be important to stability at the higher glide Mach numbers and definitely to be included in future stability analyses.
- d. Control appears feasible using conventional types of aerodynamic surfaces according to inviscid flow analyses. Boundary layer interaction should also be included in control analyses as it may modify control effectiveness.

3.1.1.5 Separation

- a. No definite conclusions as to the practicability of the original parallel stage configurations were reached. A quantitative analysis of separation was not made during the present study.
- b. It is believed that test results are necessary to achieve quantitative evaluations of the separation configurations.

3.1.2 Applied Research

3.1.2.1 Flow Regions

- a. Boundaries delineating certain regions of fluid flow - or flight - in which "new" or "unconventional" flow phenomena become significant have been derived.
- b. In some areas appreciable interaction of the boundary layer with the bow shock will occur.

By _____	Date _____	BELL Aircraft CORPORATION	Model _____	Page 3-4
Checked _____	Date _____		Missile _____	Report DL43-945-012

- c. It is shown that slip in the boundary layer may be a significant consideration.
- d. Temperatures produced by strong shock waves or by viscous heating in the boundary layer will be large enough to produce large percentages of dissociation in the air.

3.1.2.2 Shock-Boundary Layer Interaction

- a. Existing theory for shock-boundary layer interaction has been improved for the case of zero angle of attack, flat plate flow. A new theory has been developed for interaction on a plate at positive and negative angle of attack.
- b. The increases in pressure and skin friction coefficient due to shock interaction, both weak and strong, can be correlated in a general but simple and convenient form.

3.1.2.3 High Temperature Phenomena

- a. Radiation of heat from the hot boundary layer air appears to be an important quantity which should be considered in the boundary layer and heat balance equations.
- b. A theory has been developed to compute the emissivity of air.
- c. While not done in the present study, emissivities of air should be calculated and included in the heating analyses.
- d. Equilibrium dissociation of the air in the boundary layer has no appreciable effect on skin friction and heat transfer if (as in the practical case) the wall and local stream temperature are below that which produces dissociation.
- e. Tables of basic flow relations for shock and isentropic expansion flow considering air as a real gas have been calculated at Bell Aircraft and have been used in the present study.
- f. There is little information available on the thermodynamic properties of air (including the transport properties) at temperatures elevated through the range where dissociation and ionization occur. This basic information deserves much research effort.

By _____ Date _____

BELL *Aircraft* CORPORATION

Model _____ Page 3-5

Checked _____ Date _____

Missile _____
Airplane _____ Report D1143-945-012

3.1.2.4 Transpiration Cooling

- a. A theoretical method has been developed for predicting transpiration coolant requirements under hypersonic flight conditions. It applies to laminar boundary layer flow when air is used as a coolant.
- b. This method of cooling appears favorable and should be studied further; particularly, the method should be extended to other coolants which have better cooling qualities than air.

3.1.3.5 Transition

- a. There is essentially no theoretical or hypersonic test information which will allow reliable quantitative prediction of transition Reynold's number.
- b. The best that can be done at present is to assume a transition Reynold's number based on available test trends.
- c. The transition Reynold's number of 2.8 million used in the present study is believed conservative in the light of recent hypersonic wind tunnel tests.
- d. The problem must receive much attention because of its demonstrated importance to the skin temperature and skin friction.
- e. It is believed that theoretical investigations are not sufficient for this problem and that test information, preferably from free flight or ballistic tests, are necessary.

3.1.3 Facilities

- a. There are a number of wind tunnel and ballistic facilities available now for investigating the hypersonic aerodynamic problems of the MX 2276; many more facilities, larger in size and/or covering greater flow ranges, are planned or in development.
- b. Flight test vehicles approaching the ultimate MX 2276 flight conditions are being developed and are in initial flight test now.
- c. These facilities, having many diverse abilities, will allow experimental investigation of about all aerodynamic problems: Configuration evaluations, boundary layer investigation, high temperature flow aero-thermodynamic effects.

SECRET

By _____ Date _____

Checked _____ Date _____

BELL Aircraft CORPORATION

Model _____ Page 3-6

Missile _____ Report D113-915-012
Airplane _____

3.2 Recommendations

As a result of the problem study of MX-2276 aerodynamics the investigations listed in Tables 3.2-1, 3.2-2, and 3.2-3 are recommended. Primarily these are recommended with respect to further evaluating the aerodynamic problems of the system, but would provide basic design information also. Many of the analytical and theoretical investigations would be direct extensions of work done in the present study.

SECRET

By _____ Date _____
 Checked _____ Date _____

BELL Aircraft CORPORATION

Model _____ Page 3-7
 Missile _____
 Airplane _____ Report DL43-945-012

TABLE 3.2-1
RECOMMENDED AERODYNAMIC ANALYTICAL INVESTIGATIONS
TO BE PERFORMED BY BELL AIRCRAFT

<u>Area of Investigation</u>	<u>Item</u>	<u>Description</u>
1. Atmosphere	a. General characteristics of the atmosphere at high altitudes	Study the atmospheric information in greater detail for composition, pressure, temperature and density variations with altitude; particularly gradients of these quantities with time, and distance and direction about the earth; winds prevailing and possible.
2. Performance (L/D)	a. Skin Friction	Continue to evaluate methods of predicting skin friction at hypersonic Mach numbers. Study effects of boundary layer air radiation, boundary layer transition, wall temperature, injection or transpiration cooling, three dimensional configurations.
	b. Pressure Forces	Improve presently approximate methods of determining lift and drag of wings and bodies. Include effects of leading edge shape, i.e. finite radius
	c. Effects of control surface deflection on L/D at trim	Account for effects of trim on L/D; however, stability and control characteristics of the configuration must be known to do this.

By _____ Date _____

BELL Aircraft CORPORATION

Model _____ Page 3-8

Checked _____ Date _____

Missile _____ Report mlh-915-m2
Airplane _____

TABLE 3.2-1 (Cont'd)
RECOMMENDED AERODYNAMIC ANALYTICAL INVESTIGATIONS
TO BE PERFORMED BY BELL AIRCRAFT

<u>Area of Investigation</u>	<u>Item</u>	<u>Description</u>
2. Performance	d. Shock boundary layer interaction	Consider effects of shock boundary layer interaction on items a, b, c above in greater detail than possible in present study.
	a. L/D maximum glide	Determine methods of programming the L/D maximum glide. Include the effects of atmospheric variation and of dropping the bomb.
3. Flight Mechanics	b. New glide path courses	Investigation of glide paths following other than great circle courses on the earth in order to minimize losses due to earth rotation.
	c. Turns and Maneuvers	Study maneuverability limitations and correlate with navigational requirements.
4. Aerodynamic Heating	d. Ascent	Determine ascent performance for new glide paths. Consider various ascent programs and effects on performance and stage separation.
	a. Viscous heat transfer method	Continue to evaluate methods of predicting heat transfer at hypersonic Mach numbers. Study effects of boundary layer air radiation, boundary layer transition, wall temperature, three dimensional configurations.

SECRET

By _____ Date _____
Checked _____ Date _____

BELL Aircraft CORPORATION

Model _____ Page 3-3
Missile _____
Airplane _____ Report M112-915-012

TABLE 3.2-1 (Cont'd)
RECOMMENDED AERODYNAMIC ANALYTICAL INVESTIGATIONS
TO BE PERFORMED BY BELL AIRCRAFT

<u>Area of Investigation</u>	<u>Item</u>	<u>DESCRIPTION</u>
4. Aerodynamic Heating	b. Leading edge Heating	Expand upon present leading edge heating investigations; correlate available methods and study effects of sweep and leading edge profile.
	c. Transpiration cooling	Estimate coolant requirements for larger ranges of angle of attack and temperature of the cooled surface; include study of coolants other than air.
		Study transpiration cooling of the leading edge. This will require extension of the present transpiration cooling method which is for flat plate flow.
	d. Local heating	Examine effects of large temperature gradients which may occur in local areas, e.g. due to profile discontinuities, heat sinks, or transition.
		Consider heating in such areas as at the base of the body and the wing trailing edges.
	e. Effects of flight path programming on heating	Investigate effects of additional loads caused by earth rotation and maneuvers on the heat transfer and equilibrium temperatures.

SECRET

SECRET

By _____ Date _____
Checked _____ Date _____

BELL Aircraft CORPORATION

Model _____ Page 3-10
Missile _____
Airplane _____ Report D143-945-012

TABLE 3.2-1 (Cont'd)
RECOMMENDED AERODYNAMIC ANALYTICAL INVESTIGATIONS
TO BE PERFORMED BY BELL AIRCRAFT

<u>Area of Investigation</u>	<u>Item</u>	<u>Description</u>
5. Stability and control	a. Equations of motion	Continue the development of the equations of motion and express the applied forces and moments in terms of the aerodynamic coefficients. Study methods of evaluating these equations, considering the applicability of present supersonic stability criteria; include study of combined aero-servo and navigational problems.
	b. Stability parameters	Initiate study into methods of determining dynamic stability parameters in hypersonic viscous flow.

SECRET

SECRET

By _____ Date _____
 Checked _____ Date _____

ELL Aircraft COMPANIES Model _____ Page 3-11
 Missile _____
 Airplane _____ Report 0113-915-012

TABLE 3.2-2
RECOMMENDED THEORETICAL AERODYNAMIC INVESTIGATIONS

<u>Area of Investigation</u>	<u>Item</u>	<u>Description</u>	<u>Organizations</u>
1. Hypersonic flow	a. Basic equations	Continue study of the basic equations underlying flow at high velocities and altitudes. Extend scope of investigations to encompass arbitrary body shapes.	B.A.C. and pertinent outside organizations
2. Pressure forces	a. Arbitrary bodies and combinations	Investigate methods of analysis of inviscid flow about arbitrary shapes at hypersonic speeds ($M \gg 1$)	B.A.C. and pertinent outside organizations
3. Boundary layer	a. Leading edges	Investigate the effects of slip in the boundary layer flow at high M and low Re .	B.A.C. and pertinent outside organizations
	b. Air radiation	Study methods of solution of the equations of boundary layer flow which include the effects of air radiation within the layer.	B.A.C.

SECRET

SECRET

By _____ Date _____
Checked _____ Date _____

BELL Aircraft CORPORATION

Model _____ Page 3-12
Missile _____ Report ML-3-915-012
Airplane _____

TABLE 3.2-2 (Cont'd)

RECOMMENDED THEORETICAL AERODYNAMIC INVESTIGATIONS

<u>Area of Investigation</u>	<u>Item</u>	<u>Description</u>	<u>Organization</u>
3. Boundary layer (Cont'd)	c. Transverse curvature	Examine the effects of transverse curvature (e.g. small body radius) when the boundary layer thickness is large.	B.A.C.
	d. Shock interaction	Extend methods for predicting shock - boundary layer interaction to include two-dimensional flow around corners and three-dimensional shapes (e.g. cones and bodies of revolution at angle of attack).	B.A.C.
4. Thermodynamic properties of air	a. Transport properties	Calculate the transport properties of air at high temperatures. Consider the range of temperature for dissociation and ionization of air.	Extend work presently being done by other organizations.

SECRET

By _____ Date _____
 Checked _____ Date _____

BELL Aircraft CORPORATION

 Model _____ Page 3-13
 Missile _____ Report D143-945-012
 Airplane _____

TABLE 3-2-3

RECOMMENDED AERODYNAMIC TEST INVESTIGATIONS

<u>Area of Investigation</u>	<u>Item</u>	<u>Description</u>	<u>Possible Facilities*</u>
1. Laminar boundary layer flow	a. Basic skin friction and heating information	Tests of flat plate, cylindrical, or cone surfaces to determine C_f and/or h at various wall temperatures. There is little laminar data at any supersonic Mach no., none is known at hypersonic Mach nos., with which to check the compressible theory.	CIT Hypersonic W.T. $M = 5.8 - 8$ NACA PARD or HTV flight test $M \rightarrow 12$
	b. Three-dimensional configuration effects	Tests to determine effects of low aspect ratio and highly swept wings and wing-body combinations on the boundary layer and the skin friction and viscous heating; should be at flight Reynolds numbers.	NACA Hypersonic W.T. Langley 11 inch, $M = 7-10$ Ames 10 x 14 inch, $M = 6.3$

Note: * See Section 6 for a description of available facilities.

By _____ Date _____
 Checked _____ Date _____

BELL Aircraft CORPORATION

Model _____ Page 3-71
 Missile _____ Report DL3-945-012
 Airplane _____

TABLE 3.2-3 (Cont'd)
RECOMMENDED AERODYNAMICS TEST INVESTIGATIONS

<u>Area of Investigation</u>	<u>Item</u>	<u>Description</u>	<u>Possible Facilities</u>
1. Laminar boundary layer flow (Cont'd)	c. Boundary layer flow around corners	Tests to investigate the boundary layer flow about corners such as at the body cone-cylinder shoulder; at a deflected flap hinge line. In the present work it was necessary to make crude assumptions of this flow, e.g. in order to estimate the skin friction and heating after the nose cone shoulder.	NACA Hypersonic W.Ts. CIT Hypersonic W.Ts. NACA PARC or HTV flight tests. Some data of this type might be obtained coincident with tests of item la by instrumenting after the vehicle nose cone.
	d. Transpiration cooling	Tests of flat plate or cone having laminar boundary layer to determine effectiveness of transpiration cooling and obtain data for correlation with theory. Various injection rates, porosities, coolants should be checked. Interest is in both hypersonic and high temperature flow effects.	CIT Hypersonic W.T. PIBAL Hypersonic W.Ts. PIBAL Hydrogen - Oxygen W.T. Convair Hydrogen Oxygen W.T.

SECRET

By _____ Date _____

Checked _____ Date _____

BELL Aircraft CORPORATION

Model _____ Page 3-15

Missile _____ Report D013-915-012
Airplane _____

TABLE 3.2-3 (Cont'd)

RECOMMENDED AERODYNAMIC TEST INVESTIGATIONS

<u>Area of Investigation</u>	<u>Item</u>	<u>Description</u>	<u>Possible Facilities</u>
1. Laminar boundary layer flow (Cont'd)	e. Local heating	The viscous heating in areas where high local heat transfer and temperature gradients may occur should be investigated - as at boundary layer transition, corners and shoulders, and where structural attachments produce heat sinks.	As 1c above
2. Turbulent boundary layer flow	a. Same as 1a above	There are turbulent skin friction data available from hypersonic wind tunnel and free flight tests at $M < 10$, but not all in agreement, particularly with respect to effect of wall temperature. (See Appendix 4A).	
	b. Same as 1b above		
	c. Same as 1c above		

SECRET

By _____ Date _____
 Checked _____ Date _____

BELL Aircraft CORPORATION

Model _____ Page 3-16
 Missile _____
 Airplane _____ Report DL43-945-012

TABLE 3.2-3 (Cont'd)

RECOMMENDED AERODYNAMIC TEST INVESTIGATIONS

<u>Area of Investigation</u>	<u>Item</u>	<u>Description</u>	<u>Possible Facilities</u>
3. Transition	a. Basic information, smooth surfaces	Tests of cone and plate surfaces to determine maximum extent of laminous flow possible, i.e. transition Reynolds no. Effects of wall temperature variation should be included. Tests of this type on cones are being made at NOL and NOTS ballistic facilities at M→5. Plate or wing surface tests most probably require the larger flight test vehicles.	NOL Ballistic Range M→5 NOTS Ballistic Range and Light Gas Gun M→10 NACA PARD or HTV flight test, M→14
	b. Effects of surface roughness, typical construction, injection - as of transpiration coolant, and of corners	Cone, cone-cylinder, and plate surfaces as indicated. Roughness and three-dimensional corner effects can be investigated in ballistic facilities; other effects will require flight test. Wind tunnel testing should give relative or qualitative data on all. CIT has done some hypersonic transition work at M = 5.9 that is pertinent here.	As 3a above, and CIT Hypersonic W.T. Princeton Hypersonic W.T. NACA Hypersonic W.Ts.

By _____ Date _____
 Checked _____ Date _____

ELL Aircraft CORPORATION

Model _____ Page **3-17**
 Missile _____
 Airplane _____ Report **0113-945-012**

TABLE 3.2-3 (Cont'd)
RECOMMENDED AERODYNAMIC TEST INVESTIGATIONS

<u>Area of Investigation</u>	<u>Item</u>	<u>Description</u>	<u>Possible Facilities</u>
3. Transition (Cont'd)	c. Shock induced transition	Investigate effects of nose bow shock crossing the wing of wing body combination or the two-dimensional case of a shock wave impinging on a plate having laminar boundary layer.	CIT Hypersonic W.T. Princeton Hypersonic W.T., M \rightarrow 15 NACA Hypersonic W.T.
4. Pressure forces	a. Wings, bodies, wing plus body	Tests of several wings, bodies and combinations that could be considered basic in the MX-2276 system to provide data on lift, moment, and drag, and interaction effects between wing and bodies. Reynolds numbers should approximate those of MX-2276 flight.	NACA Hypersonic W.Ts. NACA PARC Flight Test, M \rightarrow 10. Ballistic facilities (most useful for drag)
	b. Control effectiveness	Tests of low aspect ratio three-dimensional wings with various flap and tip control surface configurations, including full blunt and wedge flaps. Reynolds numbers should approximate those of flight.	NACA Hypersonic W.Ts. M \rightarrow 10

SECRET

 By _____ Date _____
 Checked _____ Date _____

BELL Aircraft CORPORATION

 Model _____ Page 3-18
 Missile _____
 Airplane _____ Report D113-945-012

TABLE 3.2-3 (Cont'd)

RECOMMENDED AERODYNAMIC TEST INVESTIGATIONS

<u>Area of Investigation</u>	<u>Item</u>	<u>Description</u>	<u>Possible Facilities</u>
5. Shock-Boundary layer interaction	a. Two-dimensional investigations	Investigations of shock-boundary layer interaction near the leading edge have been carried out at the Princeton, CIT and NACA-Langley hypersonic W.T.s.; interaction at deflected controls at Princeton. These should be extended to Reynolds numbers pertinent to MI-2276, to realistic wall temperatures (cooled walls) and to more nose leading edge shapes. The effects of angle of attack and corners should be studied further, particularly negative angles (expansion) to determine whether interaction or separation exists.	Princeton Hypersonic W.T. CIT Hypersonic W.T. NACA Hypersonic W.T.
	b. Three-dimensional investigations	Investigations of interaction on nose shapes, bodies and wing body combinations are needed; none are presently available.	As above — Future larger W.T.s. e.g. ARDC 60x40 inch Hypersonic will be valuable here.

SECRET

SECRET

By _____ Date _____

Checked _____ Date _____

BELL Aircraft CORPORATION

Model _____ Page 3-19

Missile
Aircraft

Report D1143-945-012

TABLE 3.2-3 (Cont'd)

RECOMMENDED AERODYNAMIC TEST INVESTIGATIONS

<u>Area of Investigation</u>	<u>Item</u>	<u>Description</u>	<u>Possible Facilities</u>
6. Leading edge investigations	a. Drag	Systematic investigations of the effects of leading edge shape, radius, etc. on wing drag; should include sweep as a variable.	NACA Hypersonic W.Ts. M → 10
	b. Heating	As 6a above, but with respect to leading edge heating. The NACA in the Langley and Ames Hypersonic W.Ts. have made investigations of this type on cylindrical leading edges at M 7.	NACA Hypersonic W.Ts. M → 10 PIBAL Hypersonic W.T. M → 15
	c. Transpiration cooling	As 1d above but with respect to transpiration cooling of leading edges.	As 1d
7. Stability and control	a. Static forces and moments	These could be obtained under Items 4 above.	NACA PAED Free Flight Tests NACA Free Flight W.T.
	b. Dynamic testing	Ballistic and free-flight tests of bodies and body-wing combinations to determine stability parameters, particularly damping parameters.	

SECRET

SECRET

By _____ Date _____

Checked _____ Date _____

BELL *Aircraft* CORPORATION

Model _____ Page 3-20

Missile _____ Report D113-945-012
Airplane _____

TABLE 3.2-3 (Cont'd)

RECOMMENDED AERODYNAMIC TEST INVESTIGATIONS

<u>Area of Investigation</u>	<u>Item</u>	<u>Description</u>	<u>Possible Facilities</u>
8. Separation	a. Parallel stages	Sufficient insight into the parallel separation of stages at hypersonic speeds should be gained by arranging the stages of some of the vehicles called for in the previously outlined tests in parallel. The stability flights would be most suitable because of their instrumentation. Additional instrumentation in the parallel booster would be necessary, however.	NACA PARD Free Flight Test
9. Hypersonic-high temperature	a. Emissivity	Investigate the emissivity of air at very high temperatures - temperatures of the order reached inside the M = 10-20 boundary layer.	Cornell University
	b. Dissociation ionization relaxation	It is recommended that the general experimental research being done on these phenomenon be continued and augmented.	Shock tubes Impulse W.I.s. Hyperballistic facilities, i.e. light-gas guns.

SECRET

SECRET

By _____ Date _____

Checked _____ Date _____

BELL Aircraft CORPORATION

Model _____ Page 3-27

Missile
Airplane

Report D7113-915-012

TABLE 3.2-3 (Cont'd)

RECOMMENDED AERODYNAMIC TEST INVESTIGATIONS

<u>Area of Investigation</u>	<u>Item</u>	<u>Description</u>	<u>Possible Facilities</u>
10. Facilities	a. Summary	A continued survey of facilities of particular importance to MX-2276 is recommended as these are rapidly increasing in number and range of capabilities.	
	b. Development	In view of the great need for hypersonic test information, the further development of hypersonic and related facilities is certainly recommended.	

SECRET

By _____	Date _____	BELL Aircraft CORPORATION	Model _____	Page <u>4-1</u>
Checked _____	Date _____		Missile _____	Report <u>D143-945-012</u>
			Airplane _____	

SECTION 4

GENERAL AERODYNAMICS

4.1 Introduction:

The material presented in this section of the report encompasses those fields of general aerodynamics wherein the presently available methods of analysis may be applied to the study of problem areas.

The basic intent of the early analysis was to demonstrate the feasibility of a hypersonic weapon system and to outline the major problem areas. Approximate means of estimating the necessary aerodynamic parameters were therefore utilized, which in some cases were outright extrapolations of available supersonic analysis methods. Some preliminary investigations were conducted in order to roughly evaluate the accuracy of these approximate methods. Since the intent of the present study was to investigate these problem areas in greater detail and in addition to determine the extent of other problems, the original methods of study have been reviewed and where possible, have been improved and extended to give more accurate results.

In this regard, the following subjects have been considered: 1) atmospheric characteristics, 2) glide performance parameters, 3) flight mechanics, 4) the general field of aerodynamic heating including viscous heating, the specialized problem of leading edge heating, and transpiration cooling, 5) stability and control, 6) stage separation, and 7) missile trajectories. The results which have been obtained in the investigations of these subjects are presented in the following parts of this section.

In order to plan a program for the investigation of the basic problems and to hold the present investigation to applicable cases, it was necessary to first define the flight conditions under which it is expected that the MX-2276 system will operate. The flight path recommended as most efficient in the original study, that is, initial ascent of the vehicle to its maximum velocity followed by a continuous unpowered glide, was chosen since this path penetrates most deeply into the realms of flight at hypersonic velocities and extreme altitudes. For the intended purpose, it was felt that this path would be sufficient even though it might be modified by optimization in the future.

To illustrate the nature of this path, several flight limits of interest have been plotted on Figure 4.1-1, with the flight path as determined in the present study. It is reasoned that the very low static wing loading of $(W/S)_0 = 10$ psf. at a hypersonic lift coefficient of $C_L = 0.20$ defines an upper altitude limit for level flight

By _____ Date _____
 Checked _____ Date _____

BELL Aircraft CORPORATION

Model _____ Page 4-2
 Missile _____
 Airplane _____ Report D143-945-012

(and for maximum L/D glide). The effects of centrifugal forces involved in flying a circular path about the earth's center and the decrease in gravity with altitude are included in this limit curve. The satellite limit is that where the effective gravity is zero and no lift is required. The curve of 1800°F wall temperature approximates the temperature problem with respect to flight path. If 1800°F were the upper limit allowed for the configuration noted, flight would have to be above the curve (as it is for the present flight path) or cooling would be necessary. For the glide phase this also implied restrictions on wing loading and lift coefficient.

The dynamic pressures of the glide flight for the weights of the Stage III glide vehicle with and without payload are shown in Figure 4.1-2. It is evident that these remain appreciable throughout and indicate the feasibility of aerodynamic stability and control. Even at the highest altitudes reached the dynamic pressures are of the same order as for present low-speed aircraft.

Figure 4.1-3 illustrates some of the flow phenomena which must be considered in the aerodynamic analyses concerned with the flight path. The flight path is shown superimposed on a plot of boundary layer interaction and slip flow boundaries of fluid flow as they apply to a point one foot from the leading edge of a flat plate. In addition hypersonic flight, by shock waves or viscous forces, produces air flow temperatures sufficiently high to cause appreciable deviations from normal air properties, i.e. real gas effects, and in certain areas also dissociation of the air. A curve showing where approximately 5% equilibrium dissociation could occur in the boundary layer is also shown on Figure 4.1-2. These boundaries indicate where extension of the classical methods for supersonic analysis, e.g. inviscid flow theory, begin to become inapplicable and must be modified or replaced to account for the various phenomena. The above are treated in detail in the Section 5 and are discussed briefly where pertinent in the present section. The effects of shock boundary layer interaction, which have been found to be particularly significant, have been brought forward and applied to examples in the present section.

Figure 4.1-1

AERODYNAMIC FLIGHT LIMITS

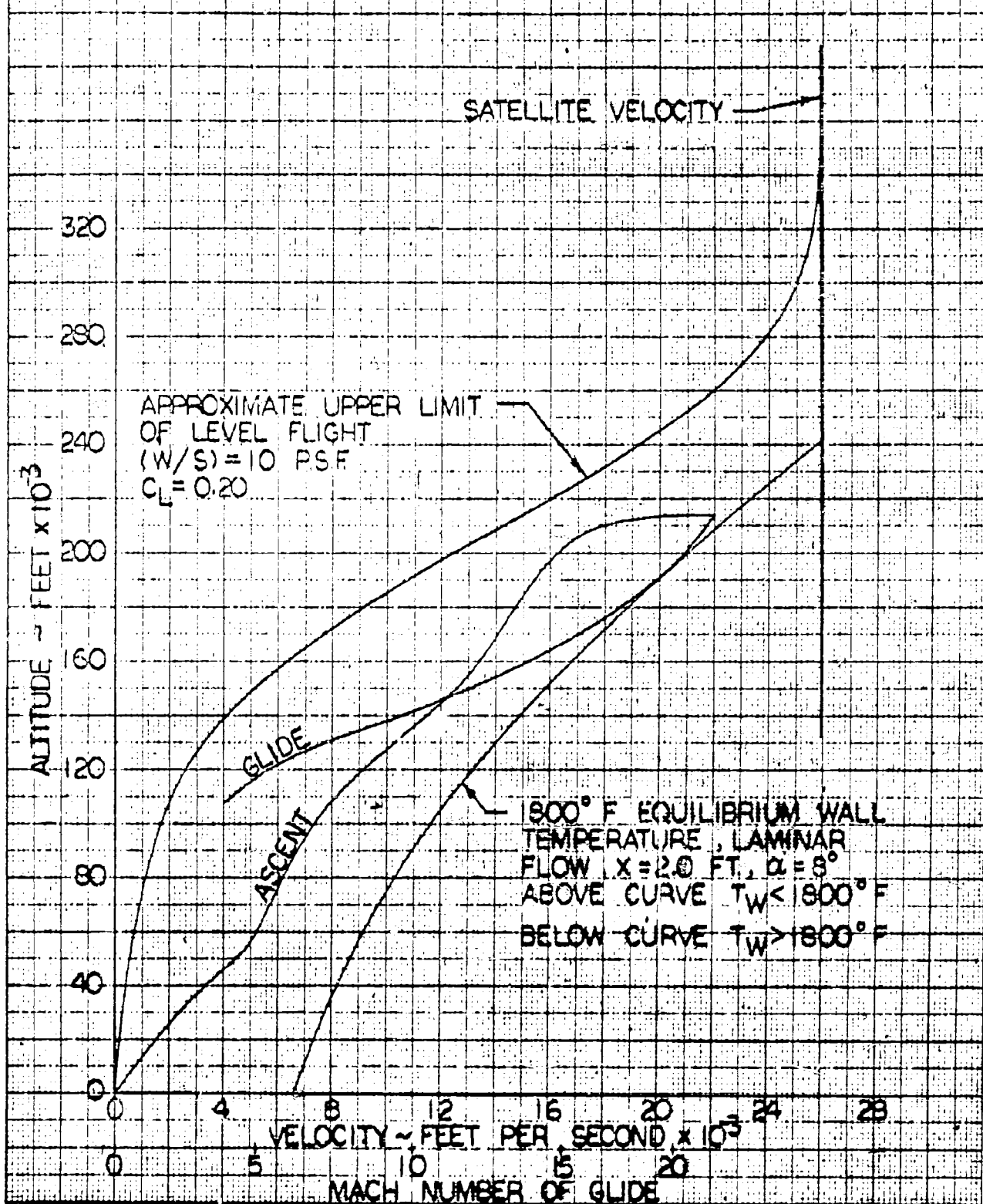
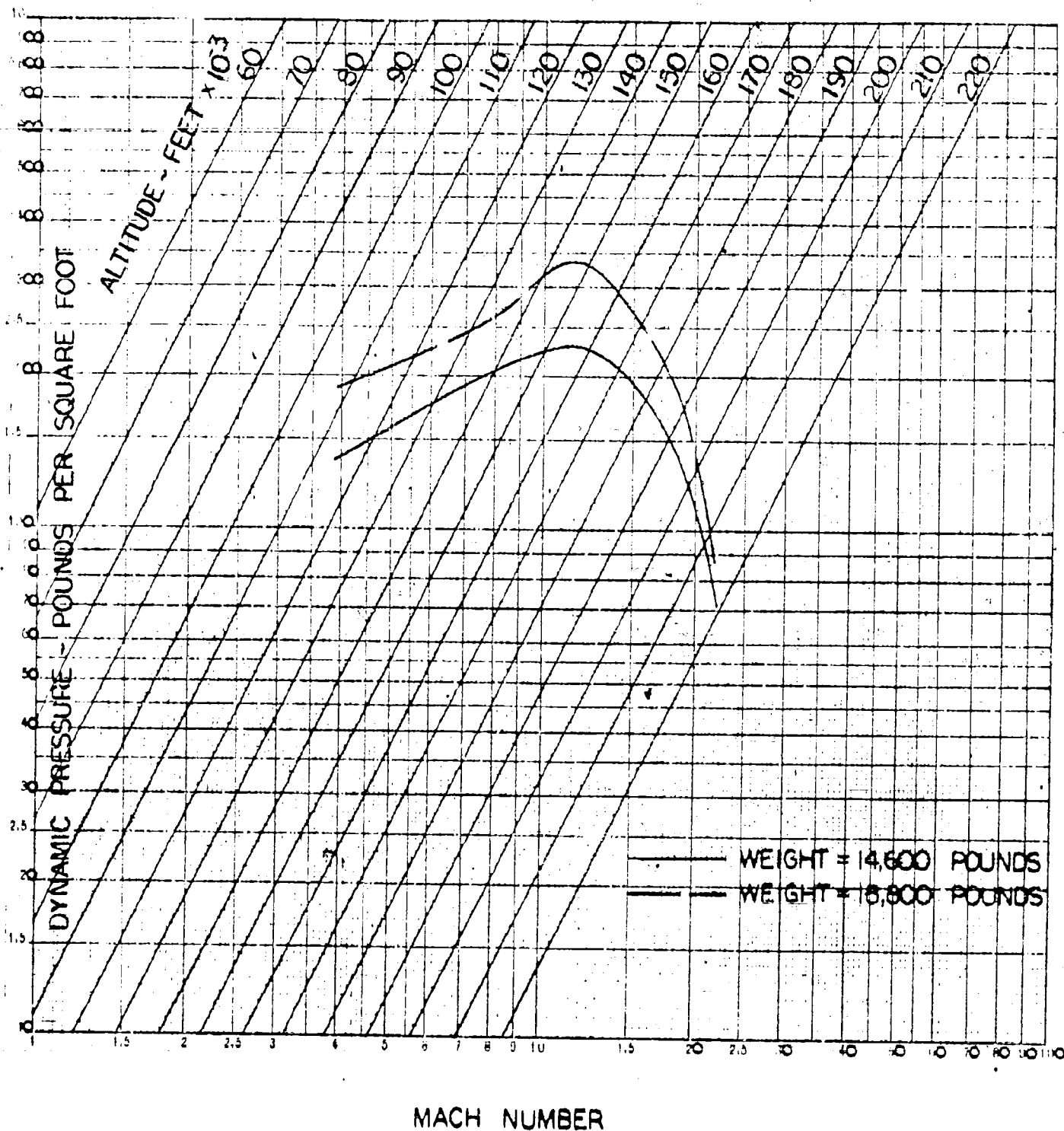


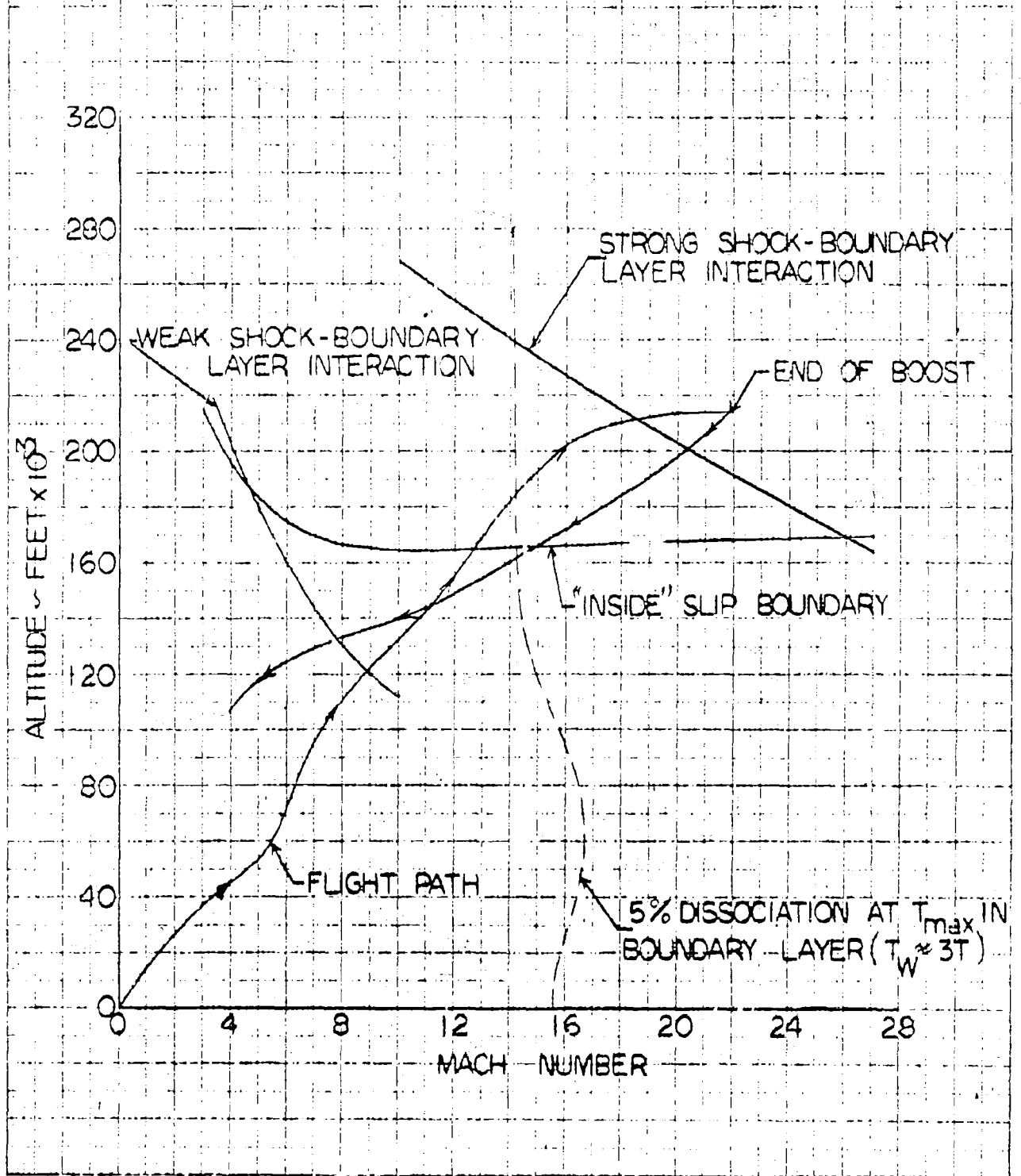
Figure 4.1-2

FREE STREAM DYNAMIC PRESSURE



FLIGHT REGIONS
ONE FOOT POINT ON FLAT PLATE

Figure 4.1-3



SECRET

By _____ Date _____

BELL Aircraft CORPORATION

Model _____ Page 4-6

Checked _____ Date _____

Missile _____
Airplane _____ Report D143-915-012

4.2 Configuration:

In certain of the aerodynamic investigations for the present study it was necessary to have a fairly specific configuration to evaluate. Since the study did not require development of better or optimized shapes, the configuration presented in the original work (Reference 4.2-1) was retained. The majority of the aerodynamic studies have been concerned with the hypersonic flight of the third stage, the glide vehicle; therefore, a fairly complete aerodynamic configuration description is presented here.

In the original layout of the third stage configuration the major consideration was given to obtaining good glide performance as the system performance potentialities were of greatest interest at that time; less attention was given to stability and control. The configuration certainly does not represent an aerodynamic optimum, but it was considered to be sufficiently realistic and typical of the class of vehicles in question for use in the present study. An additional advantage was that performance re-estimations could be directly compared with the original.

Figure 4.2-1 is a dimensional three view of Stage III as used herein. Table 4.2-1 presents the physical characteristics breakdown necessary for the aerodynamic estimations. Figure 4.2-2 shows the numerical identification of the various surface areas used throughout.

Some additional description may aid the reader. The body bottom is flat. The upper nose is a 5° cone whose axis is inclined 5° to the flat bottom; the nose sides are flat wedge surfaces, triangular in plan form from apex to body shoulder. The upper aft body is a cylindrical surface; the sides are flat surfaces vertical to the bottom and tangent to the upper cylinder. The wings are broken into two panels having different taper and sweep geometry but the same airfoil section. This section is 4% thick and of the modified wedge type. The bottom line is flat and in the same plane with the body bottom; the top is a wedge line from the leading edge to the mid-chord from whence it is a slab line parallel to the bottom. The trailing edge is a square base line (full blunt). The rocket motor fairings are essentially extensions of the wing upper wedge surface. The elevator-aileron controls are located in the outer wing panel only. The vertical tail section is a symmetrical, modified wedge of 5% thickness, made up of a forward wedge line, an aft slab line and a square base trailing edge. Nose and leading edge radii have not been defined and their effects have not been included (other than the assumption that they are small) in the majority of the analyses. The bomb is housed aft in the body between the rocket motors.

FORM 84-1 Rev. 3-53

SECRET

SECRET

By _____ Date _____

Checked _____ Date _____

BELL Aircraft CORPORATION

Model _____ Page 4-7

Missile _____
Airplane _____ Report D143-945-012

Section 4.2 References:

4.2-1 Strategic Weapon System: Bell Aircraft Corporation
Preliminary Design Report No. D143-945-010, dated
15 July 1953.

SECRET

SECRET

By _____ Date _____

BELL Aircraft CORPORATION

Model _____ Page 4-8

Checked _____ Date _____

Missile _____
Airplane _____ Report D113-945-012

TABLE 4.2-1

PHYSICAL CHARACTERISTICS OF STAGE III

<u>ITEM</u>	<u>UNITS</u>	<u>WING</u>	<u>ROCKET FIRINGS</u>	<u>VERTICAL TAIL</u>
S	sq. ft	905	289	104.5
S _{ex} = S _{ref.}	sq. ft.	615	289	104.5
S _B	sq. ft.	15.8	26.2	5.24
S _{in.} panel	sq. ft.	388	-	-
S _{out.} panel	sq. ft.	227	-	-
b	in.	472	85	123
b _{ex}	in.	412	85	123
b _{in.} panel	in.	170	-	-
b _{out.} panel	in.	242	-	-
c _R	in.	488	573	204
c _{Break}	in.	170	-	-
c _T	in.	100	414	40.8
λ in. panel	-	0.348	-	-
λ out. panel	-	0.588	-	-
λ	-	0.205	0.724	0.20
\bar{c} _{in.} panel	in.	337	-	-
\bar{c} _{out.} panel	in.	136	-	-
\bar{c}	in.	328	-	129.5
A	-	1.89	-	0.93
(t/c) _R	-	0.04	-	0.05
(t/c) _T	-	0.04	-	0.05
h/t	-	1.0	-	1.0

Form 14-1 Rev. 3-52

SECRET

SECRET

By _____ Date _____

BELL Aircraft CORPORATION

Model _____ Page 4-9

Checked _____ Date _____

Missile _____
Airplane _____ Report D113-945-012

ITEM	UNITS	WING	ROCKET FIRINGS	VERTICAL TAIL
$\Lambda_{\frac{0}{2}}$ in. panel	deg.	61.9	-	-
$\Lambda_{\frac{0}{2}}$ out. panel	deg.	16.1	-	-
$\Lambda_{\frac{0}{2}}$	deg.	-	-	33.6
Θ L.E.	deg.	4.58	-	2.87

ITEM	UNITS	BODY
F	sq. ft.	22.3
F cone or cyl. top	sq. ft.	9.8
F none wedge	sq. ft.	12.5
S _w cone	sq. ft.	110
S _w nose wedge	sq. ft.	71.6
S _w cyl. top	sq. ft.	360
S _w cyl. sides	sq. ft.	131
d hor.	in.	60
d vert.	in.	60
l	in.	896
l_N	in.	344
FR	-	14.93
FR _N	-	5.74
Θ_N	deg.	5.0
Θ_B	deg.	0

SECRET

SECRET

Figure 4.2-1

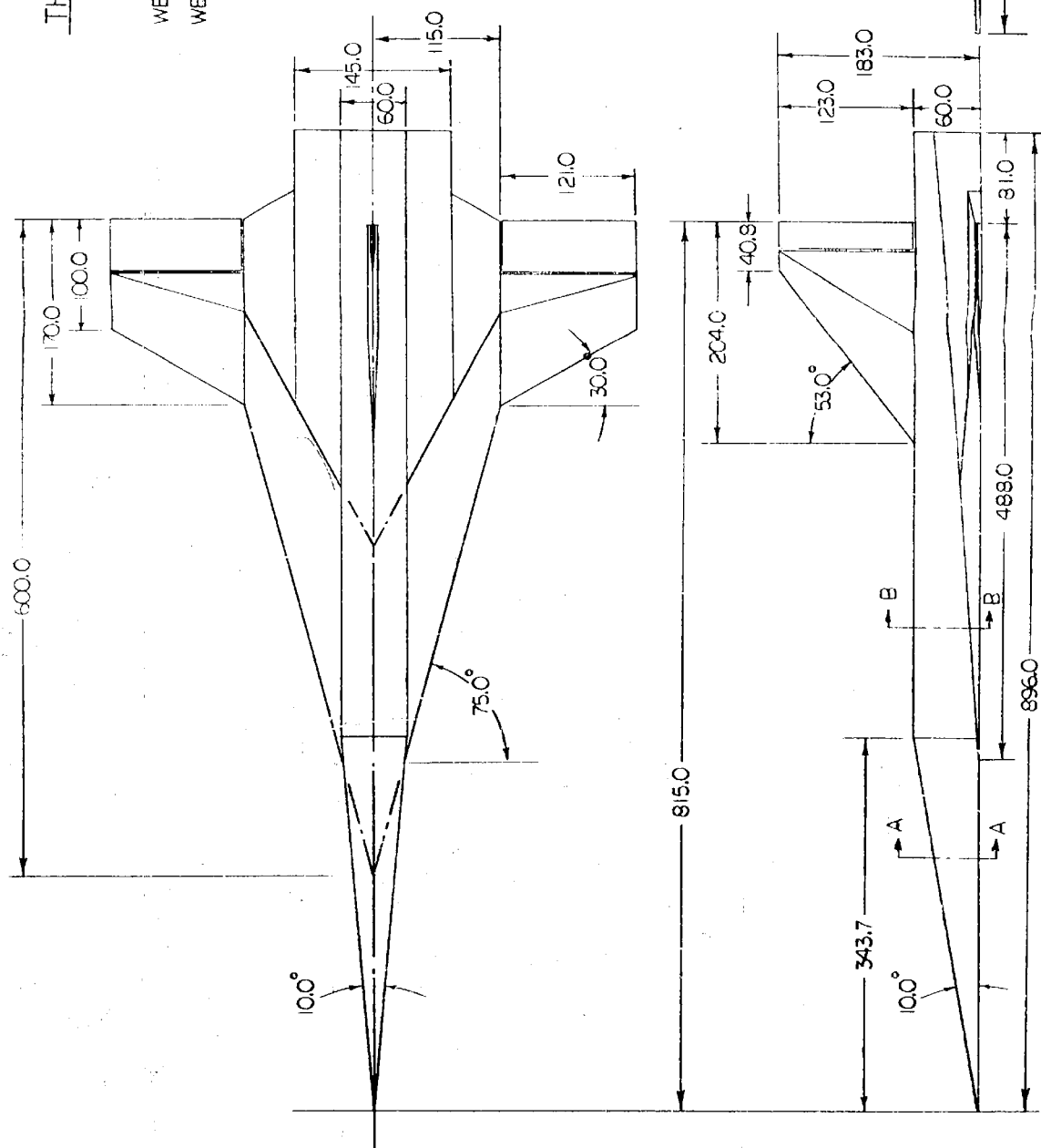
STAGE III

THREE VIEW ARRANGEMENT

SCALE = 1/100

WEIGHT EMPTY = 14,600 POUNDS

WEIGHT OF GLIDE BOMB = 4,200 POUNDS



SECRET

SECRET

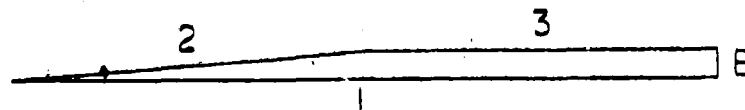
By _____ Date _____
Checked _____ Date _____

BELL Aircraft CORPORATION

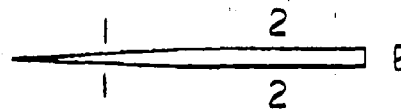
Model _____ Page 4-11
Missile _____
Airplane _____ Report D143-945-012

Figure 4.2-2

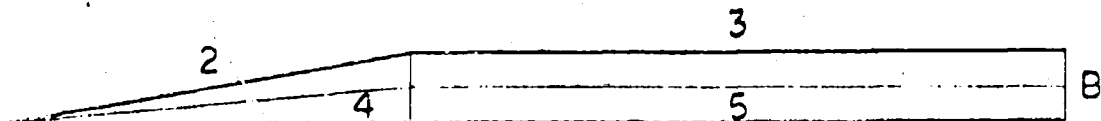
IDENTITY OF SURFACE AREAS



WING PROFILE



TAIL PROFILE



BODY PROFILE

By _____	Date _____	BELL Aircraft CORPORATION	Model _____	Page 4-12
Checked _____	Date _____		Missile _____	Report DL43-945-012

4.3 Atmospheric Data:

Until recently the variation of atmospheric characteristics with altitude presented by the NACA in Reference 4.3-1 has generally been used as a standard by the aviation industry. It was amended slightly up to 67,000 ft. altitude by Reference 4.3-2. In the past few years sounding rocket firings have shown this variation to be in considerable error, particularly at altitudes over 100,000 ft. and has led the Rocket Panel to recommend the atmospheric variation given in Reference 4.3-3, based on the sounding rocket findings. The original MX-2276 aerodynamic analyses were made using the Reference 4.3-1 atmosphere and this convention was carried through to the first portions of the present study. However, it was found that the Rocket Panel variations are large enough to produce significant changes in the present analyses; and since those are considered more realistic, it was considered necessary to adopt them as a new standard. The subsequent work in the present study was, therefore, based on the Rocket Panel altitude. Generally the data presented in this report is based on this altitude. When earlier work based on the Reference 4.3-1 altitude is presented the difference is stated. Within a particular study phase which utilized the older standard the comparative results are certainly still valid.

In the interest of convenience in usage, especially for the computation and use of the Bell Aircraft Corporation real gas tables, the Rocket Panel temperature variations have been approximated by linearizations. These are shown in Figure 4.3-1 which compares the several temperature altitude models. Figure 4.3-2 compares the various pressure models. The Air Force Geodetic Research Division has been compiling new atmospheric variations to be generally adopted in the U.S. in the near future. Recently preliminary information on this atmosphere was advanced to BAC. The temperature and pressure variations of this atmosphere are also shown on Figures 4.3-1 and 4.3-2. It will be noted that these vary somewhat with those of the Rocket Panel and of BAC, but not enough to cause appreciable differences in aerodynamic analyses.

The present analyses are based on the single temperature and pressure models discussed above. It should be remembered that the MX-2276 glide range is on the order of half the circumference of the earth and that this is traversed in little over an hour. In subsequent analyses, particularly with respect to flight programming, much more detail concerning the upper atmosphere must be known and considered: the prevailing winds, night-to-day variations, altitude and inter-continental variations, etc. The available information indicates such variations may be large.

SECRET

By _____ Date _____

Checked _____ Date _____

BELL *Aircraft* CORPORATION

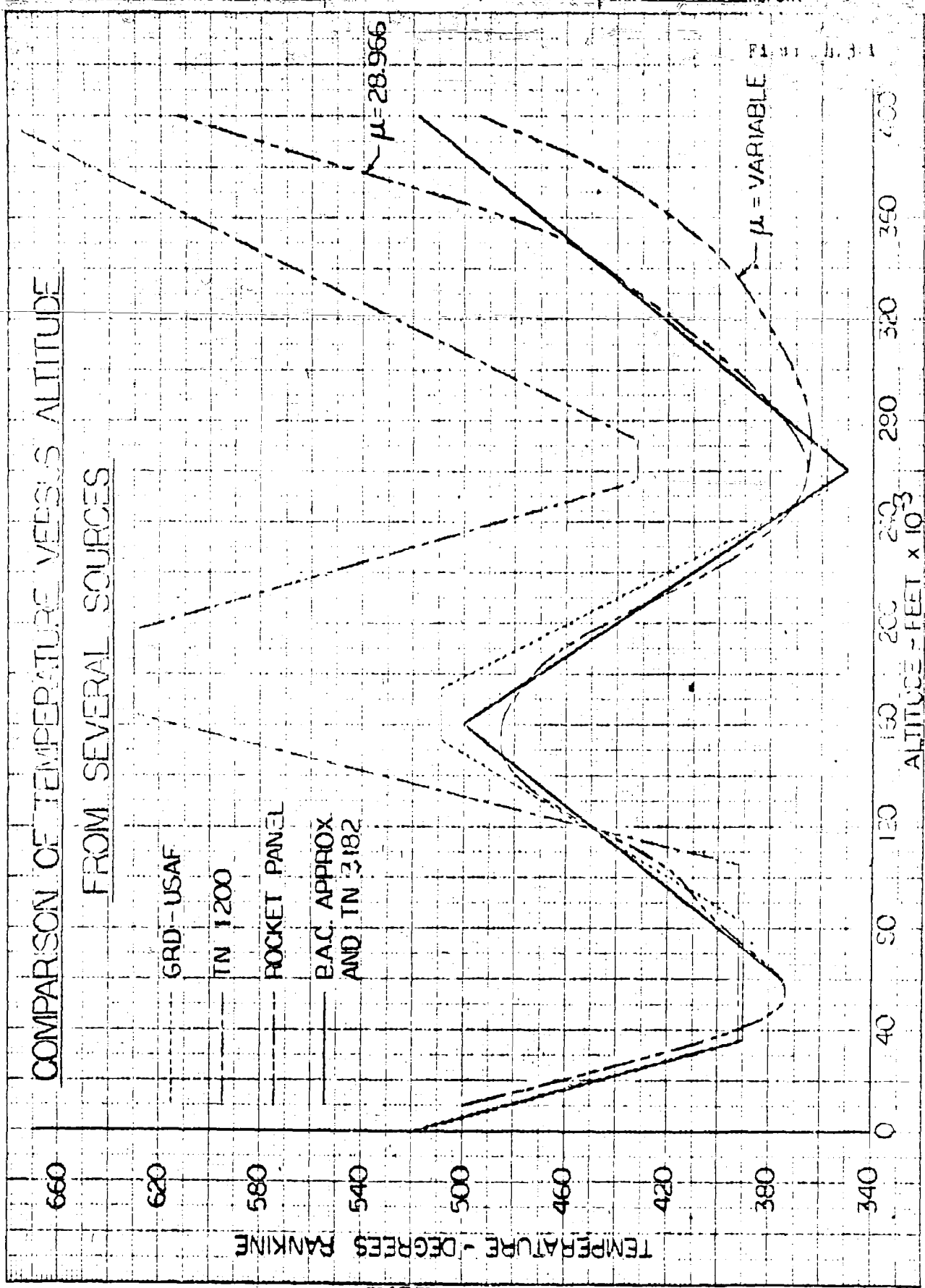
Model _____ Page 4-13

Missile _____
Airplane _____ Report D143-945-012

Section 4.3 References:

- 4.3-1 Warfield, C.N.: Tentative Tables for the Properties of the Upper Atmosphere; NACA Technical Note 1200, dated 1947.
- 4.3-2 Anon.; Manual of the ICAO Standard Atmosphere - Calculations by the NACA; NACA Technical Note 3182, dated May 1954.
- 4.3-3 The Rocket Panel: Pressures, Densities, and Temperatures in the Upper Atmosphere; Physical Review, Vol. 88, No. 5, pp 1027-1032, dated 12-1-52.
- 4.3-4 Minner, R.A.: Proposed United States Standard Atmosphere; ORD-USAFC Curve, dated 4-26-54.

SECRET



SECRET

ALTITUDE - FEET $\times 10^{-3}$

Report D143-945-012 Page 4-15

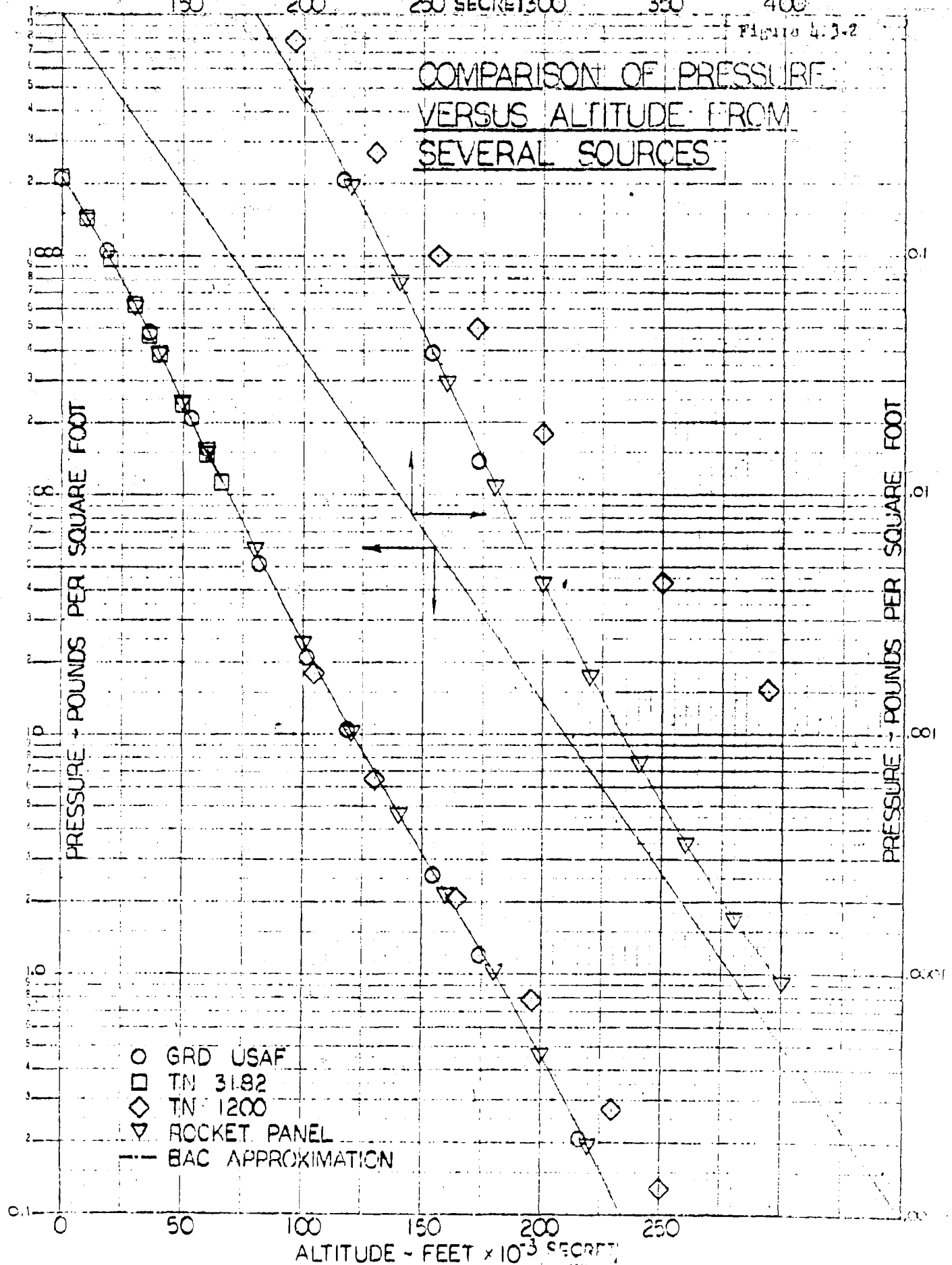
250 SECRET 300

350

400

Figure 4.3-2

COMPARISON OF PRESSURE VERSUS ALTITUDE FROM SEVERAL SOURCES



By _____ Date _____
 Checked _____ Date _____
BELL *Aircraft* CORPORATION
 Model _____ Page 4-16
 Missile _____
 Airplane _____ Report D143-945-012

4.4 Glide Performance of MX-2276 Stage III (Non-rotating earth)

A complete revaluation of the lift and drag coefficients and the maximum L/D characteristics of the aircraft has been made. These characteristics have been evaluated at $4 \leq M \leq 20$ since the major portion of the range (approximately 97%) is attained between these Mach numbers.

The aircraft has been broken down into a number of surfaces (similar to the breakdown in Reference 4.4-12) for convenience in determining these characteristics. Shock-expansion theories were employed herein to predict the local surface pressures and flow conditions, except in the case of the nose where the concept of Newtonian flow was used also. The lift and pressure drag for Stage III are to be found in Figures 4.4-19 and 4.4-20. The skin friction drag coefficients were determined from incompressible skin friction formulas modified for compressibility by reference temperature parameters. Boundary layer transition was assumed to occur at 2.8×10^6 local stream Reynolds number throughout. The Stage III skin friction drag coefficient may be viewed in Figure 4.4-26 where the effects of altitude and angle of attack are found to be of great importance in the higher Mach number region.

The time history of the Stage III glide is to be found in Figures 4.4-30 and 4.4-31 for the aircraft with and without a bomb load, respectively. Included in these figures are the equilibrium altitude, glide velocity, range, the aerodynamic characteristics (α , C_L and maximum L/D) and the wing equilibrium wall temperature at the one foot station.

The values of L/D_{\max} and altitude for the present estimation and those originally estimated (Reference 4.4-16) are compared in Figure 4.4-33. The L/D_{\max} curves are very similar. As a result the non-rotating earth glide range for the present calculation does not differ appreciably from the original. The equilibrium altitude is lower for the new calculation. The latter is partially due to the use of a new atmosphere as described earlier.

A preliminary investigation into the effects of shock wave boundary layer interaction on wing L/D 's has been made. It was found that at the present equilibrium glide altitude there are appreciable effects on surface pressures and skin frictions but that the summation of these effects in L/D 's produces only small changes from the no interaction L/D_{\max} values. The differences in pressure result in an increase in lift however, which will in turn increase the equilibrium altitude somewhat. Since L/D_{\max} is a function of altitude, differences in L/D_{\max} may result. This effect has not been studied at present. The results of this investigation are found in Figure 4.4-32.

By _____	Date _____	BELL Aircraft CORPORATION	Model _____	Page <u>4-17</u>
Checked _____	Date _____		Missile _____	Report <u>DL43-945-012</u>

Following are the methods of analysis used in determining the maximum L/D 's for the aircraft and the glide range

4.4.1 Lift and Pressure Drag

4.4.1.1 Lift and Pressure Drag Coefficients of Wing

Present linearized wing theories are not valid for determining wing aerodynamic characteristics over the Mach number range encountered in this analysis, so other means have to be considered. It has been shown in Reference 4.4-1, 4.4-2 and 4.4-3 that the exact two dimensional shock-expansion theories predicts lift and drag coefficients for three dimensional wings at Mach numbers 4 and up and for high Reynolds numbers, within a few percent of experimental values as shown in Figures 4.4-1, 4.4-2 and 4.4-3. These tests also indicate that at near hypersonic speeds the aerodynamic characteristics are little effected by planform and are dependent mostly upon section profile and thickness. This has already been pointed out in Reference 4.4-4 as has the fact that the two dimensional theory of Linnell (Reference 4.4-5) agrees very well with the exact shock-expansion theories and is easier to use in predicting the lift and drag coefficients. However, Linnell's theory does not yield the local stream to free stream temperature, density, and velocity ratios which are needed in the skin friction and skin temperature analyses. For this reason the more complete shock-expansion theories have been used. The local stream to free stream pressure, temperature, density, and velocity ratios, have been evaluated over adequate ranges of Mach number and angle of attack for the various wing surfaces from the shock flow tables in the case of compression and the isentropic expansion flow tables in the case of expansion as presented for air ($\gamma = 1.4$) in Reference 4.4-6. Typical values of these quantities are presented in Figures 4.4-4 thru 4.4-10 for the flat bottom surface.

The effect of rounding the leading edge on the subject wing has not been included in the analysis at this time. The meager amount of available supersonic tests showing the effect of leading edge radius on the aerodynamic characteristics of wings indicate that rounding the wing leading edge increased the drag coefficient a noticeable amount. This effect, however, is shown to diminish with increasing Mach number in the supersonic speed regime. It seems likely and reasonable that sweeping the leading edge would also decrease the magnitude of the drag increase.

The effect of leading edge radius on drag should be studied more critically in the future because relatively large radii may be dictated by aerodynamic heating considerations. In particular hypersonic tests to evaluate leading edge design are recommended.

The resulting wing lift and pressure drag coefficients shown in Figures 4.4-11 and 4.4-12 were obtained from the above by the following relation:

By _____ Date _____

BELL Aircraft CORPORATION

Model _____ Page 4-18

Checked _____ Date _____

Missile _____ Airplane _____ Report D143-945-012

$$C_L = C_N \cos \alpha - C_X \sin \alpha$$

$$C_D = C_X \cos \alpha + C_N \sin \alpha$$

where

$$C_N = C_{N_1} + C_{N_2} + C_{N_3}$$

$$= C_{p_1} \frac{c_1}{c} - C_{p_2} \frac{c_2}{c} - C_{p_3} \frac{c_3}{c}$$

$$= \frac{2}{\gamma M^2} \left[\left(\frac{P_1}{P_\infty} - 1 \right) - 0.5 \left(\frac{P_2}{P_\infty} - 1 \right) - 0.5 \left(\frac{P_3}{P_\infty} - 1 \right) \right]$$

$$C_X = C_{X_2} + C_{X_B}$$

$$= C_{p_2} \frac{t}{c} - C_{p_B} \frac{h}{c}$$

$$= \frac{P}{\gamma M^2} \left[0.04 \left(\frac{P_2}{P_\infty} - 1 \right) - 0.04 C_{p_B} \right]$$

C_{p_B} = base pressure coefficient from Figure 4.4-13 which is obtained by fairing data from Reference 4.4-7 into the vacuum pressure coefficient at approximately $M = 6.0$

C_N = normal force coefficient

C_X = axial force coefficient

C_p = pressure coefficient

c = surface chord

\bar{c} = mean chord of wing

M = free stream Mach number

$\frac{P}{P_\infty}$ = surface local stream pressure to free stream pressure

$\frac{t}{c}$ = surface maximum thickness ratio

$\frac{h}{c}$ = surface trailing edge height to chord ratio

α = angle of attack

γ = 1.4

Subscripts

1 = bottom surface of wing

2 = wedge surface of wing

3 = slab surface of wing

By _____ Date _____
 Checked _____ Date _____

BELL Aircraft CORPORATION

 Model _____ Page 4-19
 Missile _____
 Airplane _____ Report D143-945-012

4.4.1.2 Pressure Drag Coefficients of Vertical Tail

The pressure drag coefficients were obtained for this surface in the same manner as outlined in the wing section and are presented in Figure 4.4-14.

4.4.1.3 Lift and Pressure Drag Coefficients of Body

There are a few experiments available (References 4.4-1, 4.4-8 and 4.4-9) for bodies of the present type tested at supersonic Mach numbers up to approximately $M = 7$. The comparison of test and prediction is good when using the concept of Newtonian flow. The Newtonian (or impact) theory unfortunately does not predict the local stream to free stream temperature, density, and velocity ratios as do the shock-expansion theories. For this reason the shock-expansion theories were used where reasonable for the body also. Further, it is felt that the shock-expansion theories are actually more applicable to the prediction of the bottom parameters, most important of the body surfaces, since for the present configuration this surface is continuous with the wing bottom surfaces.

Newtonian theory was used in predicting the normal and axial force coefficients of the dropped nose cone. Several additional approximations were then necessary to obtain the cone surface local to free stream temperature, density, and velocity ratios needed for the skin friction calculations. When the body is at zero angle of attack, the cone axis angle of attack is 5° (in the sense of positive pressures on the surface) and the top cone element is at 10° . For this case the needed parameters were assumed conservatively as those of a 10° cone at zero angle of yaw - and were obtained for all Mach numbers from Reference 4.4-6. With the body at 5° angle of attack the nose cone axis is at zero angle of attack and the parameters for an unyawed 5° cone are pertinent and were used. At body angles of attack of 10° and greater, the top cone element is at zero angle of attack or less; for this case the cone surface local to free stream temperature, density, and velocity ratios were conservatively assumed to be one.

The local stream to free stream parameters on the top of the afterbody were approximated in the following manner. The parameters for the top cylinder element were found using the two dimensional shock-expansion theories - expanding from the conditions obtained for the nose cone. In determining the normal force coefficient on the complete cylinder the pressure coefficient was assumed to vary as follows from the cylinder top element to the vertical straight sides:

$$C_{p_3} = C'_{p_3} \sin \theta$$

Best Available Copy

By _____ Date _____
 Checked _____ Date _____

BELL Aircraft CORPORATION

Model _____ Page 4-20
 Missile _____
 Airplane _____ Report D143-945-012

where

C'_{p_3} = pressure coefficient of the top cylinder element

θ = radial angle of cylinder

and the normal force coefficient then becomes

$$\begin{aligned} C_{N_3} &= 2 \int_0^{\frac{\pi}{2}} C'_{p_3} \sin \theta r d\theta \\ &= 2C'_{p_3} r \int_0^{\frac{\pi}{2}} \sin^2 \theta d\theta \\ &= \frac{\pi r}{2} C'_{p_3} \end{aligned}$$

The local stream to free stream parameters of the nose wedge were obtained from the two dimensional shock flow tables for a 5° wedge. Free stream flight conditions were considered to be present on the straight vertical sides of the afterbody.

The body base drag coefficient was obtained from the data in References 4.4-10 and 4.4-11 which were faired into the vacuum pressure coefficient at approximately $M = 7.0$. Comparisons of the above method with experimental data are shown in Figures 4.4-15 and 4.4-16.

It is noted that the experimental body lift coefficients are lower than indicated by the present method; this is probably due to the three dimensional effects of the test data. However, the use of shock-expansion theories is believed to be in order since the bottom surface of the body is continuous with the wing bottom surface forming one surface which will experience essentially two dimensional flow.

The resulting body lift and pressure drag coefficients shown in Figures 4.4-17 and 4.4-18 were obtained from the above by the following relations:

$$C_L = C_N \cos \alpha - C_X \sin \alpha$$

$$C_D = C_X \cos \alpha + C_N \sin \alpha$$

where

$$C_N = C_{N_1} + C_{N_2} + C_{N_3}$$

$$= C_{p_1} \frac{S_1}{S_{ref}} + C_{N_2} \frac{S_2}{S_{ref}} + C_{N_3} \frac{S_3}{S_{ref}}$$

$$= \frac{2}{\gamma M^2} \left(\frac{p_1}{p_\infty} - 1 \right) \frac{S_1}{S_{ref}} + C_{N_2} \frac{S_2}{S_{ref}} + C_{N_3} \frac{S_3}{S_{ref}}$$

$$\begin{aligned}
 C_X &= C_{X_1} + C_{X_4} + C_{X_B} \\
 &= C_{X_1} \frac{S_1}{S_{ref}} + C_{p_4} \frac{S_4}{S_{ref}} - C_{p_B} \frac{S_B}{S_{ref}} \\
 &= C_{X_1} \frac{S_1}{S_{ref}} + \frac{2}{\gamma M^2} \left(\frac{p_4}{p_\infty} - 1 \right) \frac{S_4}{S_{ref}} - C_{p_B} \frac{S_B}{S_{ref}}
 \end{aligned}$$

- C_{N_2} = nose cone normal force coefficient from Equation 60 of Reference 12
- C_{X_2} = nose cone axial force coefficient from Equation 60 of Reference 12
- C_{p_B} = from Figure 4.4-13
- C_N = normal force coefficient
- C_X = axial force coefficient
- C_p = pressure coefficient
- S = surface area on which coefficients of a particular surface are based
- S_{ref} = reference area on which the coefficients of all surfaces are finally based
- M = free stream Mach number
- $\frac{p}{p_\infty}$ = surface local stream pressure to free stream pressure
- α = angle of attack
- γ = 1.4

and subscripts

- 1 = bottom surface of body
- 2 = conical surface of body nose
- 3 = circular cylinder surface of body
- 4 = wedge surfaces of body nose

4.4.1.4 Wing-Body Interference

Wing body interference effects, i.e. mutual upwash effects of the wing and body on each other, have not been included in the present analysis. There are indications from experiment that the effects are small to negligible in the lower hypersonic speed regime. Tests of a body with and without large fins at $M = 6.9$ in Reference 4.4-13 show that interference is not present. In discussions with NACA personnel during visits to their facilities it was expressed that the hypersonic interference effects were believed to be small or non-existent.

By _____ Date _____	BELL Aircraft CORPORATION	Model _____	Page 4-22
Checked _____ Date _____		Missile _____ Airplane _____	Report D1143-945-012

It should be noted, however, that the experimental data are for much higher Reynolds numbers ($Re \times 10^{-6} = 1$ to 6) than encountered on this aircraft in its glide path. The boundary layer thicknesses are probably small enough in these tests that they do not produce any noticeable interference effects.

In addition, the body and wing lower surfaces of the present configuration form a continuous surface which should tend to minimize interaction effects in that area. Since this bottom surface contributes almost the whole of the aerodynamic lift at high speeds, its effects predominate and a small overall interaction effect is indicated.

4.4.1.5 Stage III Total Lift and Pressure Drag Coefficients

The total lift coefficient of Stage III was found by the summation of the lift coefficients of the wing and body for several angles of attack and Mach numbers. The total lift coefficient of this aircraft is found in Figure 4.4-19 in carpet form.

The total pressure drag coefficient of Stage III was found by combining the pressure drag coefficients of the wing, tail, and body at several angles of attack and Mach numbers. The total pressure drag coefficient of the vehicle is shown in carpet form in Figure 4.4-20.

4.4.2 Skin Friction Drag Coefficients

4.4.2.1 Compressible Skin Friction Coefficients

The skin friction coefficients have been estimated through use of the well known incompressible skin friction relations extended to supersonic and hypersonic conditions by evaluating the air properties in these relations at a reference temperature - a weighted mean temperature which occurs within the boundary layer. This reference or effective temperature method has been widely adopted for engineering purposes. While originally derived as an approximation to the exact laminar compressible theory, it has proven equally useful for turbulent flow analysis as it has been found to correlate well with turbulent test data. The method is shown in more detail in Appendix 4A of this report where the skin friction coefficients are discussed in conjunction with the development of the compressible flow heat transfer coefficients.

The method of approach in the present estimations has been to express the local skin friction coefficient as the product of incompressible friction coefficient calculated from local stream conditions and a compressible correction factor which is dependent on the reference temperature.

$$C_{f_c} = C_{f_i} \left(\frac{C_{f_c}}{C_{f_i}} \right)$$

By _____	Date _____	BELL Aircraft Corporation	Model _____	Page 4-23
Checked _____	Date _____		Missile _____	Report D143-945-012

where

$$\left(\frac{C_{f_2}}{C_{f_1}}\right) = \frac{f(\rho_1, \mu_1)}{f(\rho_2, \mu_2)} = \frac{f(T_1)}{f(T_2)}$$

The compressible correction ratios for laminar and turbulent flows (see Appendix 4A) were calculated as a function of temperature to the extent possible using the actual viscosity variation with temperature from the NACA-NBS tables. However, a considerable extension of the correction curves is necessary to cover the range of reference temperatures encountered. A power law variation with temperature was selected as the best method of extending the data, that is

$$\left(\frac{C_{f_2}}{C_{f_1}}\right) = \left(\frac{T_1}{T_2}\right)^n$$

The values of $n = -0.17$ for laminar flow and -0.668 for turbulent flow were chosen as giving the best approximations and extensions to the actual property curves in the most critical range of temperatures, which was near the limits of the actual data (see Figure 4.4-21). The approximation also is seen to be reasonable at the lower temperature ratios; therefore, the power law variation was adopted throughout as it eliminates the necessity of calculating absolute temperatures in determining the compressibility correction, i.e. only the ratios $\frac{T_1}{T_2}$ is necessary and not T_1 and T_2 .

The compressible laminar skin friction coefficients were estimated from the widely accepted Blasius relation, which for average skin friction coefficient is

$$C_f = 1.328 / \sqrt{Re} \quad (\text{Reference 4.4-14, Section 14, p. 89})$$

For incompressible turbulent flow the Prandtl-Schlichting relation was used

$$C_f = 0.455 / (\log_{10} Re)^{2.58}$$

It may be noted there is some inconsistency here in that the simpler Blasius equation for turbulent skin friction was used in deriving the turbulent compressible correction (Appendix 4a). However, while the Prandtl-Schlichting relation is considered to have a wider range of applicability, the difference between the two in the Reynolds number range of present interest is not large, and it was felt that the less convenient form of compressibility correction derived from the more complicated Prandtl-Schlichting relation was not justified in view of the approximate nature of the overall method.

By _____ Date _____

Checked _____ Date _____

BELL Aircraft CORPORATION

Model _____ Page 4-24

Missile _____ Report D143-945-012
Airplane _____

The above relations give the skin friction coefficients for aerodynamically smooth surfaces. It is general practice in subsonic work to increase these to account for surface roughness, the amount of increase depending on the degree of roughness and class of construction. In the present case the relatively thicker hypersonic boundary layers are expected to be insensitive to the Stage III surface irregularities and the smooth surface relations are assumed applicable. This obviously must be checked by test when the outer surface construction has been developed and typical models can be made. There is little data available on the subject now. The trend of reduced roughness effects with increasing Mach number has been noted in recent boundary layer investigations in the CIT-JPL wind tunnels at $M = 2$ to $M = 4$ (discussed during a visit there). Recent data from free flight models fired to approximately $M = 2$ to investigate roughness effects at supersonic speeds (Reference 4.4-15) indicate open butt joints transverse to the local stream can be tolerated with very little or no friction drag increase over that of a completely smooth surface; exposed rivet heads and lap joint construction caused more significant increases but considerably less than would be predicted for the same construction under subsonic conditions.

The reference temperature is given by the following relations, which are graphically evaluated in Figure 4.4-22.

$$T' = 0.5 (T_W - T_\delta) + 0.22 (T_r - T_\delta)$$

or

$$\frac{T'}{T_\delta} = (0.5 - 0.22r) + 0.5 \frac{T_W}{T_\delta} + 0.22r \frac{T_t}{T_\delta}$$

where

 T_W = equilibrium wall temperature, °R T_δ = local free stream temperature, °R $T_r = r(T_t - T_\delta) + T_\delta$, °R T_t = stagnation temperature, °R r = recovery factor, 0.90 for turbulent flow and 0.85 for laminar flow

The local stream temperatures are determined from the shock flow or isentropic flow tables of Reference 4.4-6, depending upon the Mach number and attitude of the particular surface. The equilibrium wall temperatures are determined from the heat transfer analysis which in turn depends upon the flight path. Thus, it is an iterative process to obtain these temperatures. In this analysis the wall temperatures calculated for the original Stage III glide trajectory conditions at the 10 foot station on each surface were used as representative wall

By _____ Date _____

Checked _____ Date _____

BELL Aircraft CORPORATION

Model _____ Page 4-25

Missile _____ Report D143-945-012
Airplane _____

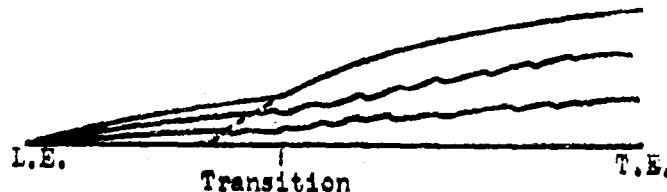
temperatures on the particular surface under analysis. This first approximation was sufficient as the T_w/T_g ratio was found to be relatively unimportant compared to T_t/T_g in determining T'/T_g at the higher Mach numbers.

The present theories on determining the point of transition from laminar to turbulent flow are incomplete and inadequate while the available experimental data show much scatter and inconsistencies, (see the discussion of transition in Section 5.7 for further detail). Thus, the assumption used in the proposal report, Reference 4.4-16, for this aircraft, that transition starts at a local stream Reynolds number of 2.8×10^6 , is used again at this time. This appears to be somewhat conservative when compared with recent hypersonic experiment, (Reference 4.4-17); however, until more adequate theories and/or systematized experiments are advanced it is felt that the present assumption is adequate. Even this low transition Reynolds number gives laminar flow on almost all of the aircraft throughout much of its flight path. The laminar distance is determined by

$$x_L = \frac{2.8 \times 10^6}{Re_g / x}$$

where Re_g / x is the local stream Reynolds number per foot. The laminar distance is shown in Figure 4.4-23 versus Re_g / x and the representative lengths used for the various aircraft components are also shown, indicating the Reynolds number per foot needed to obtain complete laminar flow.

A method has been presented in Reference 4.4-18 that allows one to determine the overall incompressible skin friction drag coefficient of a unit surface width when the boundary layer flow is mixed; that is when there is laminar flow on the forward part of the surface to the point of transition and then the remainder is in turbulent flow as typified by the model illustrated in the accompanying sketch.



By _____ Date _____
 Checked _____ Date _____

BELL Aircraft CORPORATION

Model _____ Page 4-26
 Missile _____
 Airplane _____ Report D1143-945-012

Essentially it is as follows. The skin friction drag of a surface results in an accumulating momentum loss in the boundary layer flow. The momentum loss at the transition point results from the preceding length of laminar flow. An effective turbulent length can be estimated which would produce the same momentum loss under the same local stream conditions. This effective length added to the turbulent flow length after the transition point gives a length of turbulent flow which would produce the same momentum loss at the trailing edge, and therefore, the same total friction drag, as does the total length of mixed flow. The overall average skin friction coefficient is the average turbulent coefficient for the effective plus real turbulent length times the ratio of this length to the actual surface length. The method has been compared in Reference 4.4-18 with experiment and found to be in good agreement.

The basic incompressible skin friction drag coefficient equations given previously are used to find the skin friction drag per unit width divided by the dynamic pressure as follows:

For laminar flow

$$\frac{D_{\text{unit}}}{q} = x C_{f_1} = 1.327 \sqrt{x} / \sqrt{Re_s / x}$$

For turbulent flow

$$\frac{D_{\text{unit}}}{q} = x C_{f_1} = 0.455 x / \left[\log_{10}(Re_s / x) + \log_{10} x \right]^{2.58}$$

where

x = length of surface, feet
 Re_s / x = local stream Reynolds number per foot

These equations have been plotted in Figures 4.4-24 and 4.4-25. They are most convenient for the skin friction coefficient calculation. As the above method states that across the transition point

$$(x C_{f_1})_L = (x C_{f_1})_T$$

and the effective turbulent length can be determined from $(x C_{f_1})_T$ and Re_s / x .

The method has been modified to account for compressible skin friction in the following manner:

$$(x C_{f_1})_L \left(\frac{C_{f_c}}{C_{f_1}} \right)_L = (x C_{f_1})_T \left(\frac{C_{f_c}}{C_{f_1}} \right)_T$$

By _____ Date _____

BELL *Aircraft* CORPORATIONModel _____ Page 4-27

Checked _____ Date _____

Missile _____ Report D143-945-012
Airplane _____

It is now possible to arrive at the compressible skin friction drag coefficient for any surface in a given flight condition once the local stream parameters, $\frac{T_s}{T_\infty}$, $\frac{Re_s}{Re_\infty}$, $\frac{q_s}{q_\infty}$ and T_w are known, using the

following steps:

1. Select various Mach numbers, altitude, and angles of attack.
2. The flight Reynolds number per foot may be obtained as well as the local stream to free stream Reynolds number ratio. Multiplying the two ratios together, $\frac{Re_s}{Re_\infty} \times \frac{Re_\infty}{Re_\infty}$, yields the surface local stream Reynolds number per foot.
3. Now the laminar flow length (x_L) may be determined for a surface by dividing the local stream Reynolds number for transition (2.8×10^6) by the local stream Reynolds number per foot for the particular surface.
4. The T'/T_s is next determined and the compressibility correction factors read for both types of flow from Figure 4.4-22.
5. Find $(x C_{f_1})_L$ from Figure 4.4-24, using $\frac{Re_s}{x}$ and x_L .
6. The turbulent incompressible $x C_f$ may be determined by equating the momentum loss in laminar flow at the point of transition to the turbulent momentum loss as stated before and solving for $(x C_{f_1})_T$.
7. The length necessary in turbulent flow to give the above calculated value of $(x C_{f_1})_T$ is found in the turbulent incompressible $x C_f$ graph, Figure 4.4-25.
8. Now the above determined length is added to the remaining length of the particular surface and a new $(x C_{f_1})_T$ is obtained from the same figure.
9. The compressible skin friction drag coefficient is now obtained by multiplying the $(x C_{f_1})_T$ by $\frac{(C_{f_c})}{(C_{f_1})_T}$ and dividing by the total length of the particular surface.
10. This coefficient is based upon the surface area and surface local stream dynamic pressure. To base the coefficient on the proper reference area and free stream dynamic pressure it is multiplied by the ratio of surface area to reference area and the ratio of surface local to free stream dynamic pressure.

If the laminar distance determined in Step 3 is longer than the surface length, Steps 6, 7, and 8 are not necessary and the laminar compressibility correction factor is used in Step 9 along with the laminar $x C_{f_1}$ corresponding to the length and Re_s/x for the particular surface.

By _____ Date _____

Checked _____ Date _____

BELL Aircraft CORPORATION

Model _____ Page 4-28

Missile _____ Report DML-3-945-012
Airplane _____

The method of calculating skin friction when there is transition present on the surface has also been adapted to the calculation of skin friction on a surface broken by a corner, e.g. the upper wing surface in going from areas (2) to (3). The type of flow prevailing before the corner is considered to be present after the corner, then the momentum loss at the corner is taken to be identical before and after the expansion around the corner and the laminar or turbulent incompressible $\times C_{f1}$ immediately after the corner can be determined. The equation for conditions across the transition point given above is modified for the corner calculation to:

$$(\times C_{f1})_2 \frac{(C_{fc})}{(C_{f1})_2} q_{\delta 2} = (\times C_{f1})_3 \frac{(C_{fc})}{(C_{f1})_3} q_{\delta 3}$$

where subscript 2 = condition ahead of corner
3 = condition behind corner

The length required to yield the $\times C_{f1}$ after the corner may be found from Figure 4.4-24 or 4.4-25 depending upon the type of flow involved. A new length for the surface is obtained by adding to the length just determined to the length of the surface after the corner and Steps 1 thru 10 in the previous discussion are repeated to obtain the skin friction drag coefficient of the entire surface.

It has been found in Reference 4.4-19 that the cone laminar boundary layer thickness at zero angle of attack with an attached shock wave is related to the flat plate boundary layer by:

$$\delta_C = \frac{1}{\sqrt{3}} \delta_{F.P.} = \frac{5.2 x_C}{\sqrt{3} \sqrt{Re}}$$

$$\text{and that } \tau_C = \sqrt{3} \tau_{F.P.} = \frac{0.664 \sqrt{3}}{\sqrt{Re}} q$$

so that the local skin friction coefficient is

$$c_{fC} = \sqrt{3} c_{fF.P.} = \frac{0.664 \sqrt{3}}{\sqrt{Re}}$$

and the average skin friction on a cone is

$$C_{fC} = \frac{2}{\sqrt{3}} C_{fF.P.}$$

where δ = boundary layer thickness
 τ = shear stress
 x = length

By _____ Date _____
 Checked _____ Date _____

BELL *Aircraft* CORPORATION

Model _____ Page 4-29
 Missile _____
 Airplane _____ Report D143-945-012

Re = local free stream Reynolds number from cone vertex
 or flat plate leading edge

c_f = local skin friction coefficient

C_f = average skin friction coefficient

q = local dynamic pressure

and the subscript C = cone
 F.P. = flat plate

The above correction has been used in determining the cone laminar skin friction drag coefficients, and also it has been applied in the same manner to the turbulent case.

A plot of the total aircraft skin friction drag coefficient is presented in Figure 4.4-26 and shows how the skin friction drag coefficient varies with an angle of attack and altitude.

The skin friction drag coefficients have been calculated for all surfaces independently and were broken down into the following surfaces and illustrated in Figure 4.2-2 of the Configuration Section:

- Wing - 1. Bottom surface (inner and outer panels)
 2. Upper surface wedge (inner and outer panels)
 3. Upper surface slab (inner and outer panels)

Tail - Wedge and slab

- Body - 1. Bottom surface
 2. Nose cone
 3. Afterbody circular cylinder top
 4. Nose wedge sides
 5. Afterbody straight vertical sides

4.4.3 Maximum Lift to Drag Ratios

The maximum L/D 's for the glide portion of this aircraft were obtained from the summation of the lifts of the various components divided by the summation of the various drags of each component for each Mach number, angle of attack, and altitude. It can be seen from the plots of these data in Figure 4.4-27 that altitude (200,000 feet and under) has little effect upon the maximum L/D 's at all Mach numbers, and the level of the maximum L/D 's does not noticeably change until after a Mach number of 10. The decrease in L/D 's above 200,000 feet are caused by increase in skin friction drag coefficients. Maximum L/D 's, angle of attack at maximum L/D , and lift coefficient at maximum L/D are plotted in Figure 4.4-28 versus altitude for constant Mach numbers.

By _____	Date _____	BELL Aircraft CORPORATION	Model _____	Page 4-30
Checked _____	Date _____		Missile _____	Report D143-945-012
			Airplane _____	

4.4.4 Glide Performance.

In equilibrium glide flight the maximum range is obtained at the attitude for maximum L/D. In other words in power off flight, the sum of the aircraft lift at maximum L/D and the centrifugal force due to the aircraft's circular motion about the earth is assumed to be balanced by the aircraft's weight, and the maximum range for this condition (as shown in another section of this report) occurs when the aircraft is flown at the attitude to obtain the maximum L/D at each combination of altitude and velocity.

The maximum range is obtained by integrating the maximum L/D with respect to the total energy available from the altitude and velocity, taking into account the effects of the centrifugal force and gravity variation with altitude on the weight. The range equation is repeated at this time and is for a non-rotating earth in the atmosphere described in Section 4.3.

$$R = \frac{1}{2g_0} \int_{U_2}^{U_1} \frac{(L/D)_{\max} dU}{g/g_0 - \frac{v^2}{g_0(r_0+h)}}$$

where

$$g/g_0 = \left(\frac{r_0}{h + r_0} \right)^2$$

$$U = v^2 + 2gh, \text{ feet}^2/\text{second}^2$$

$$g_0 = \text{acceleration of gravity at sea level, } 32.2 \text{ feet/second}^2$$

$$r_0 = \text{radius of the earth, } 20.9204 \times 10^6 \text{ feet}$$

$$h = \text{altitude of flight path above the earth, feet}$$

$$v = \text{velocity along the flight path, feet/second}$$

Integration of the above range equation yields maximum ranges of 10,670 nautical miles for a weight of 18,800 pounds (weight with bomb) and 10,000 nautical miles for a weight of 14,600 pounds (weight without bomb). The ranges for these two weights are shown in Figure 4.4-29 versus velocity. Thus, for any initial velocity and final velocity the maximum range can be obtained.

By _____	Date _____	BELL Aircraft CORPORATION	Model _____	Page <u>4-31</u>
Checked _____	Date _____		Missile _____	Report <u>DL13-945-012</u>
			Airplane _____	

Time histories from boost for these two weights are presented in Figure 4.4-30 and Figure 4.4-31.

4.4.5 Comparison of Original and Present Flight Paths

The maximum L/D ratios used in the original flight path for the 14,600 pounds condition (Reference 4.4-16) are compared in Figure 4.4-32 versus velocity with the maximum L/D's used in the present analysis. The L/D's from the present flight path are somewhat smaller than the previous values due to modifications in the methods used to predict the lift and drag coefficients.

The equilibrium altitudes for the two analyses are compared in the same figure and it is found that they are very similar except at the beginning of glide (velocities of 20,000 to 22,000 feet per second) where the present analysis indicates a lower altitude. This loss in altitude is due in part to the new atmosphere used in this study as explained in an earlier section.

As a result of the above losses the range is 9700 nautical miles for the present analysis compared to 10,160 nautical miles for the original analysis between the initial velocity of 22,000 feet per second and the final velocity of 4000 feet per second.

4.4.6 Additional Considerations

4.4.6.1 Shock Wave - Boundary Layer Interaction Effects on L/D

The effects of shock wave interaction with the boundary layer on the pressure coefficient and skin friction drag coefficient have been investigated for the present wing at Mach numbers of 20, 16 and 10 at the attitudes for maximum L/D without interaction. The method employed to determine these effects is described in Section 5.3 of this report.

The results of the investigation indicate that higher pressure coefficients are obtained when taking the interaction into account, giving approximately 24% increase in the normal force at the Mach numbers investigated and that the skin friction drag coefficient is increased approximately 42% for these speeds. The net results of these increases is that the lift-drag ratio is unaffected at Mach numbers 10 and 16 but is lowered somewhat at a Mach number of 20. The above results are shown in Figure 4.4-33.

This investigation has not been extensive enough to show how the attitude for maximum L/D or the equilibrium altitude change with the inclusion of these interactions as the interaction method was not available early enough in the present study for its incorporation in the complete L/D calculations.

Date _____

BELL Aircraft CORPORATION

Model _____

Page _____

4-32

Check _____

Date _____

Missile
Airplane

Report _____

D143-945-612

If the flight altitudes were increased through different flight programming or through a change in the Stage III configuration, the effects of shock boundary layer interaction would become more significant. This is shown by the simplified flat plate examples presented with the method discussion in Section 5.3.

4.4.6.2 Slip Flow Effects

The effects of boundary layer slip have not been accounted for in the present performance estimation though the development of flight regime boundaries presented in Section 5.2 indicates the slip regime is entered. An investigation of the quantitative effects of slip has not been made in the present study. However, the effects of slip (by definition) should be beneficial - reducing the skin friction - so that the exclusion of slip effects is considered to be conservative. Obviously the effect should be evaluated in future studies.

4.4.6.3 Ideal and Real Gas Effects

The present analysis has been made using the ideal gas tables of Reference 4.4-6. As shown in Section 5.4, the pressure ratio, local to free stream, is not effected by real gas effects, out to a Mach number of 22; thus the lift and pressure drag coefficients of this aircraft can not be effected appreciably. However, there is an effect on the local stream Mach number, tending to increase this function with increasing free stream Mach number; and the local to free stream temperature ratio is lowered with increasing Mach number. In as much as these variations are small in the Mach number and angle of attack ranges of immediate interest and the real gas calculations would entail considerable difficulty and labor, adding little to the accuracy of the study, the real gas effects have been set aside for this analysis.

By _____ Date _____
 Checked _____ Date _____

BELL Aircraft CORPORATION

Model _____ Page 4-33
 Missile _____
 Airplane _____ Report DL43-945-012

Section 4.4 Symbols

c	Surface chord, inches
\bar{c}	Mean chord, inches
C_D	Drag coefficient
C_f	Average skin friction coefficient
c_f	Local skin friction coefficient
C_L	Lift coefficient
C_N	Normal force coefficient
c_p	Pressure coefficient
C_X	Axial force coefficient
D	Drag, pounds
g	Acceleration of gravity, feet per square second
h	Altitude, feet
h	Height of wing trailing edge, inches
L	Lift, pounds
$L.E.$	Leading edge
L/D	Lift-drag ratio
M	Mach number
p	Pressure, pounds per square foot
q	Dynamic pressure, pounds per square foot
R	Range, nautical miles
Re	Reynolds number
$^{\circ}R$	Degrees Rankine
r	Radius of body, inches
r	Radius of earth, feet

SECRET

By _____

Date _____

BELL Aircraft CORPORATION

Model _____

Page _____

4-34

Checked _____

Date _____

Missile
Airplane

Report

D113-945-012

r Recovery factor
 S Area, square feet
 T Temperature, degrees
 T.E. Trailing Edge
 t/c Thickness ratio
 U Energy parameter, square feet per square second
 V Velocity, feet per second
 W Weight, pounds
 x Surface length used in skin friction calculations, feet
 α Angle of attack, degrees
 r Ratio of specific heats
 δ Boundary thickness, feet
 θ Body radial angle, degrees
 μ Coefficient of viscosity, slugs per foot second
 ρ Density, pounds per cubic foot
 τ Shear stress, pounds per square foot

Subscripts

1 Bottom surface
 2 Wing upper surface wedge or nose cone
 3 Wing upper surface slab or afterbody circular cylinder top
 4 Nose wedge sides
 5 Afterbody straight vertical sides
 ∞ Free stream conditions
 B Base
 B Body

Form 14-1 Rev. 1943

SECRET

By _____ Date _____

BELL Aircraft CORPORATIONModel _____ Page 4-35

Checked _____ Date _____

Missile _____
Airplane _____ Report D143-945-012

C Cone
c Compressible conditions
F.P. Flat plate
i Incompressible conditions
L Laminar flow
max. Maximum conditions
o Sea level conditions
p Pressure drag
r Recovery condition
ref. Reference
T Turbulent flow conditions
t Stagnation condition
V.T. Vertical tail
W Wall condition
W Wing
 $x C_f$ Skin friction parameter
 δ Local stream condition

Superscripts

()' Indicates reference or effective temperature condition
 unless otherwise noted
n Power law exponent

By _____	Date _____	BELL Aircraft CORPORATION	Model _____	Page 4-36
Checked _____	Date _____		Missile _____	Report D143-945-012

Section 4.4 References

- 4.4-1 McLellan, C. H.: Exploratory Wind Tunnel Investigation of Wings and Bodies at $M = 6.9$; Jour. of the Aero. Sciences, Vol. 18, No. 10, pp 641-648, dated October, 1951
- 4.4-2 McLellan, C. H., Bertram, M. H. and Moore, J. A.: An Investigation of Four Wings of Square Planform at a Mach Number of 6.86 in the Langley 11 Inch Hypersonic Tunnel; NACA Research Memorandum L51D17, dated June 19, 1951
- 4.4-3 Ulmann, E. F. and Lord, D. R.: An Investigation of Flow Characteristics at Mach Number 4.04 over 6 and 9% Thick Symmetrical Circular Arc Airfoil Having 30% Trailing Edge Flaps; NACA Research Memorandum L51D30, dated 1951
- 4.4-4 Anon: Interim Technical Report of MX-2276; Bell Aircraft Corporation Report No. D143-945-011, dated October 25, 1954.
- 4.4-5 Linnell, R. D.: Two Dimensional Airfoils in Hypersonic Flows; Jour. of the Aero. Sciences, Vol. 16, No. 1, dated January, 1949.
- 4.4-6 McKown, P. B.: Tables and Graphs for Compressible Flow; Bell Aircraft Corporation Aerodynamic Research Note No. 52, dated June 5, 1953.
- 4.4-7 Chapman, D. R., Winbrow, W. R. and Kester, R. H.: Experimental Investigation of Base Pressure on Blunt Trailing Edge Wings at Supersonic Velocities; NACA Technical Note No. 2611, dated 1952.
- 4.4-8 Dennis, D. H. and Cunningham, B. E.: Forces and Moments on Inclined Bodies at Mach Numbers from 3 to 6.3; NACA Research Memorandum A54E03, dated June 25, 1954.
- 4.4-9 Ridyard, H. W.: The Aerodynamic Characteristics of Two Series of Lifting Bodies at Mach Number 6.86; NACA Research Memorandum L54C15, dated May 1954.
- 4.4-10 Charters, A. C. and Turelsky, R. A.: Determination of Base Pressure from Free Flight Data; Ballistic Research Lab. Report No. 653, dated March 30, 1948.
- 4.4-11 Ritter, J. O., Jr. and Hamaker, F. M.: An Experimental Investigation of the Base Pressure Characteristics of Non Lifting Bodies of Revolution at Mach Numbers from 2.73 to 4.98; NACA Research Memorandum A52E20, dated September 17, 1952.

By _____	Date _____	BELL Aircraft CORPORATION	Model _____	Page 4-37
Checked _____	Date _____		Missile _____	Report DL43-945-012

- 4.4-12 William, E. P., et Al: Long Range Surface to Surface Rocket and Ramjet Missiles - Aerodynamics; Rand Corporation R-181, dated May 1, 1950.
- 4.4-13 McCaulley, W. D. and Feller, W. V.: An Investigation of the Characteristics of the NACA FN-10 (with and without fins) in the Langley 11 Inch Hypersonic Tunnel at a Mach Number of 6.9; NACA Research Memorandum L54I03, dated November 26, 1954.
- 4.4-14 Prandtl, L: The Mechanics of Viscous Fluids; Aerodynamic Theory; W. F. Durand, Vol. III, Division G, Durand Reprint Committee, 1943.
- 4.4-15 Hopko, R. N.: The Effect of Some Surface Roughness Elements on the Drag of a Body of Revolution at Supersonic Speeds; NACA Research Memorandum L54I21, dated November 24, 1954.
- 4.4-16 Anon: DL43 Bomi Strategic Weapon System; Bell Aircraft Corporation Report No. DL43-945-010, dated July 15, 1953.
- 4.4-17 Nagamatsu, H. T.: Summary of Recent GALTIT Hypersonic Experimental Investigations; Jour. of the Aero. Sciences, Vol. 22, No. 3, pp. 165-172, dated March, 1955.
- 4.4-18 Hall, C. F. and Fitzgerald, F. F.: An Approximate Method for Calculating the Effect of Surface Roughness on the Drag of an Airplane; NACA Research Memorandum A7B24, dated July 23, 1947.
- 4.4-19 Hantzsche, W. and Wendt, H.: The Laminar Boundary Layer on a Cone in a Supersonic Air Stream at Zero Angle of Attack; Project Rand, Douglas Aircraft Corporation, Inc., Translation RAT -6, dated November, 1947.

Figure 4.4-1

COMPARISON OF THEORETICAL AND EXPERIMENTAL
LIFT AND DRAG COEFFICIENTS AT $M=6.9$ FOR A WING
WITH 5 PERCENT SYMMETRICAL DOUBLE WEDGE
SECTIONS

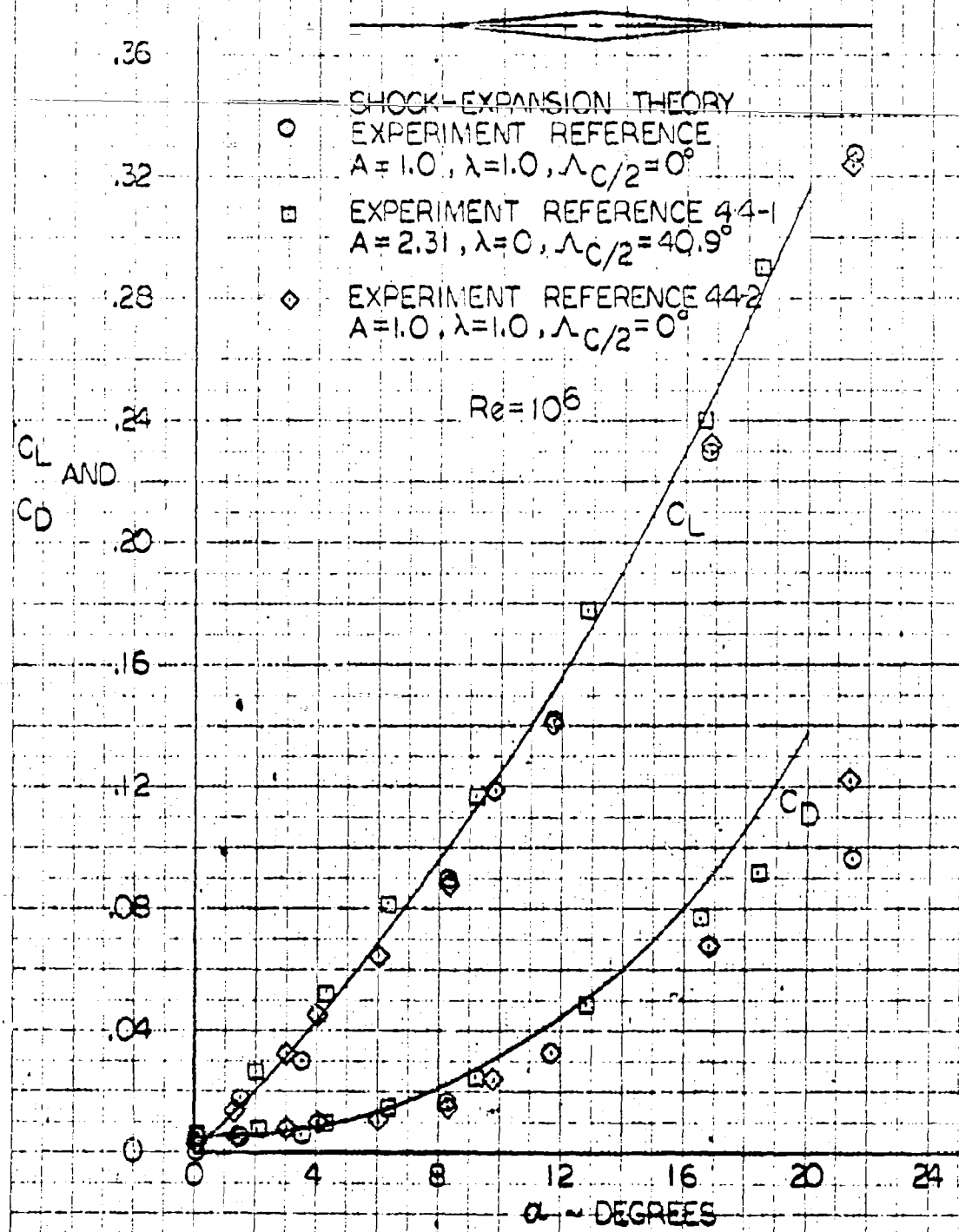


Figure L.4-2

COMPARISON OF THEORETICAL AND EXPERIMENTAL
LIFT AND DRAG COEFFICIENTS $M = 6.95$ FOR A WING
WITH 5 PERCENT HALF DOUBLE WEDGE SECTIONS

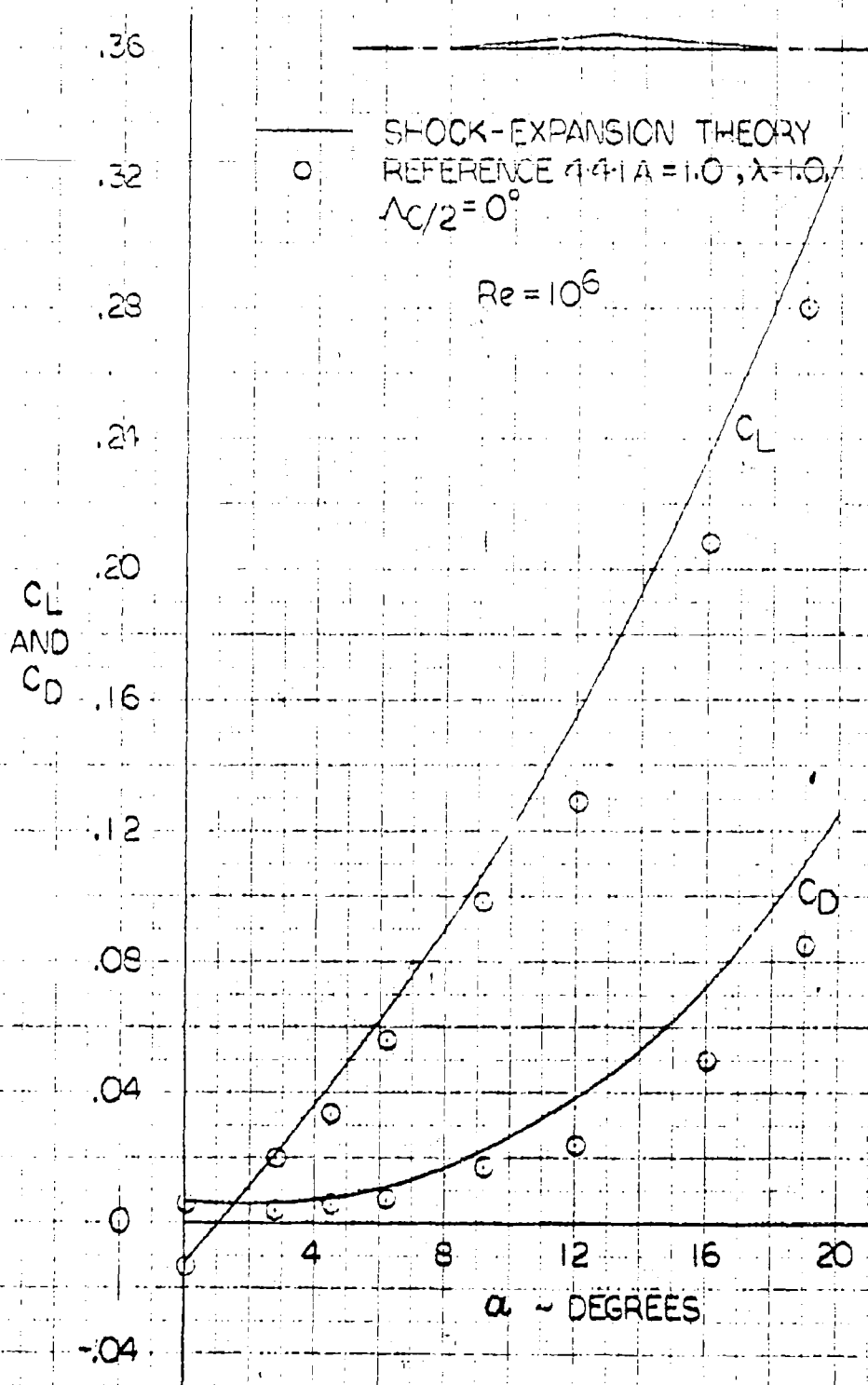
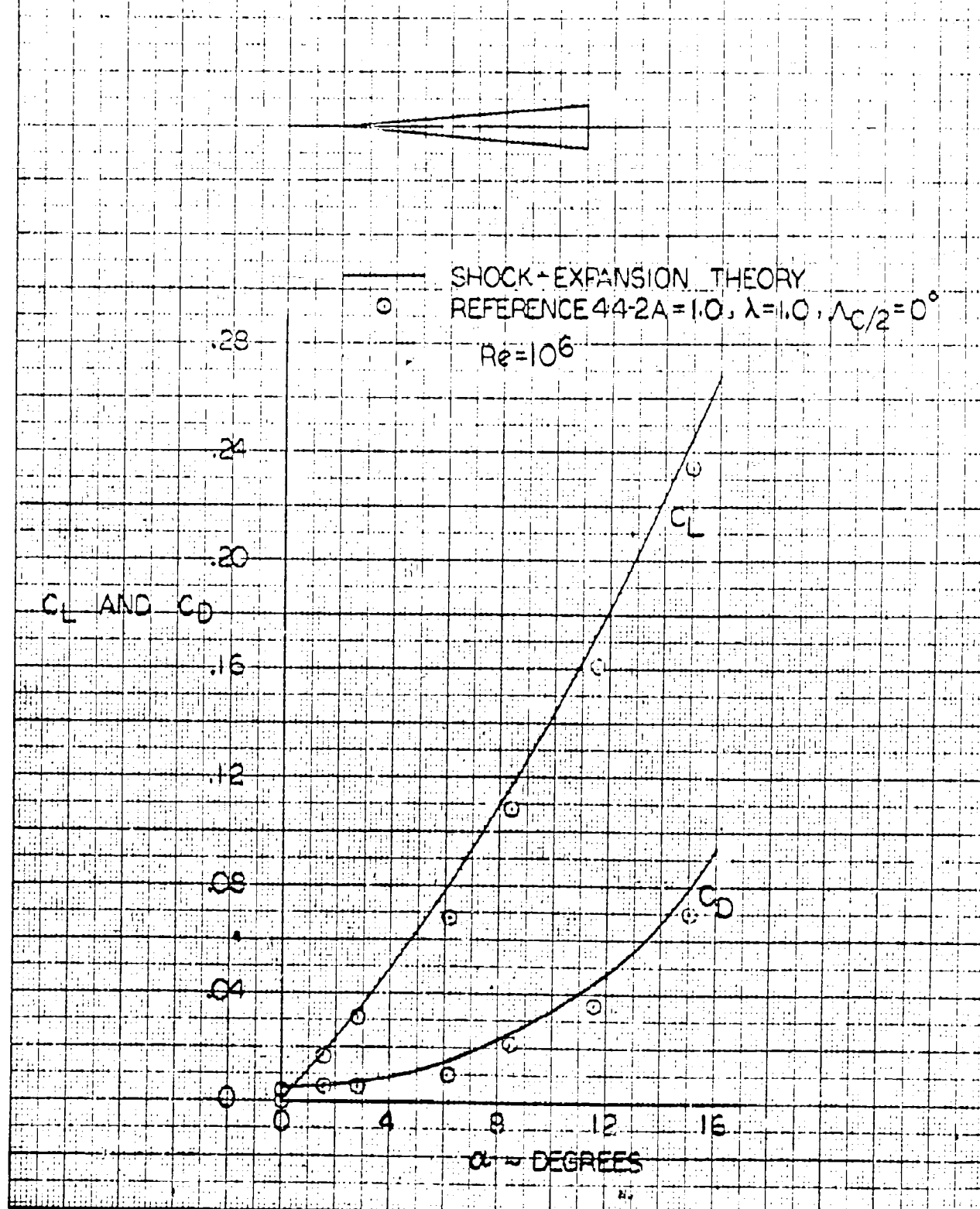


Figure 4.4-3
COMPARISON OF THEORETICAL AND EXPERIMENTAL
LIFT AND DRAG COEFFICIENTS $M=6.36$ FOR A WING
WITH 5 PERCENT SYMMETRICAL WEDGE SECTIONS

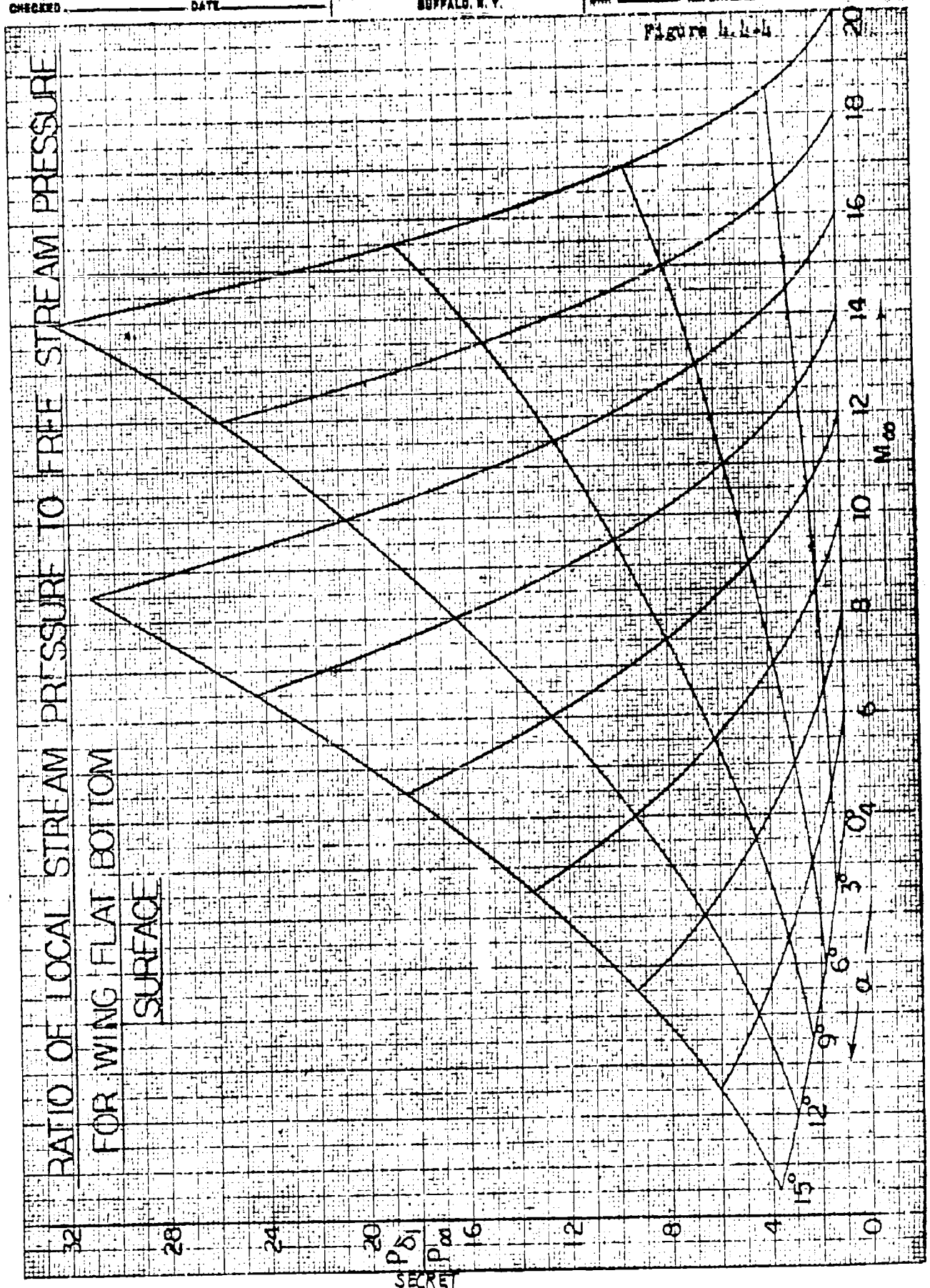


BY _____ DATE _____
 CHECKED _____ DATE _____

BELL **SECRET**
 AIRCRAFT CORPORATION
 BUFFALO, N. Y.

MODEL _____ PAGE 4-10
 SHEP _____ REPORT D143-945-012

Figure 4.4-4



SECRET

Figure 4.4-5

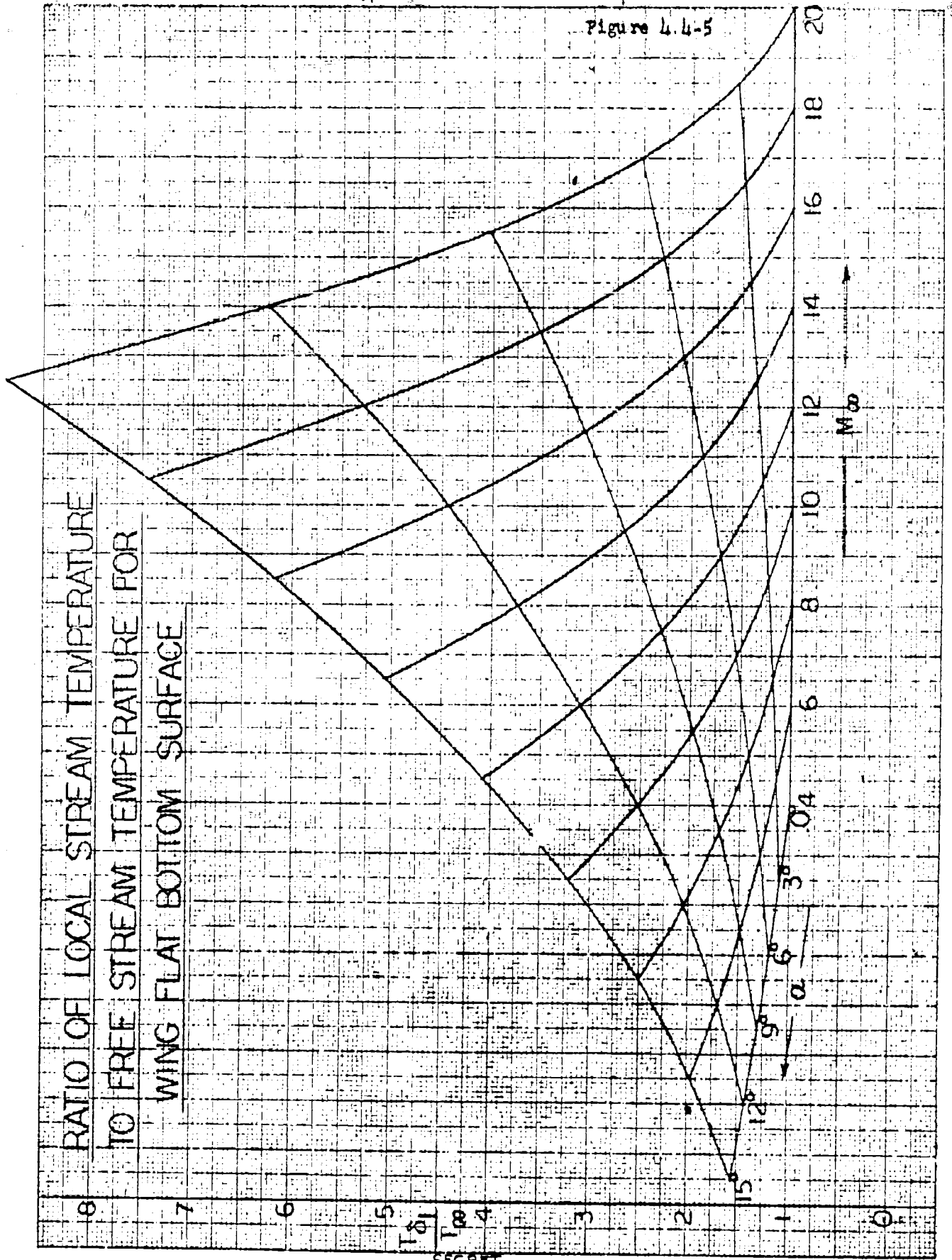
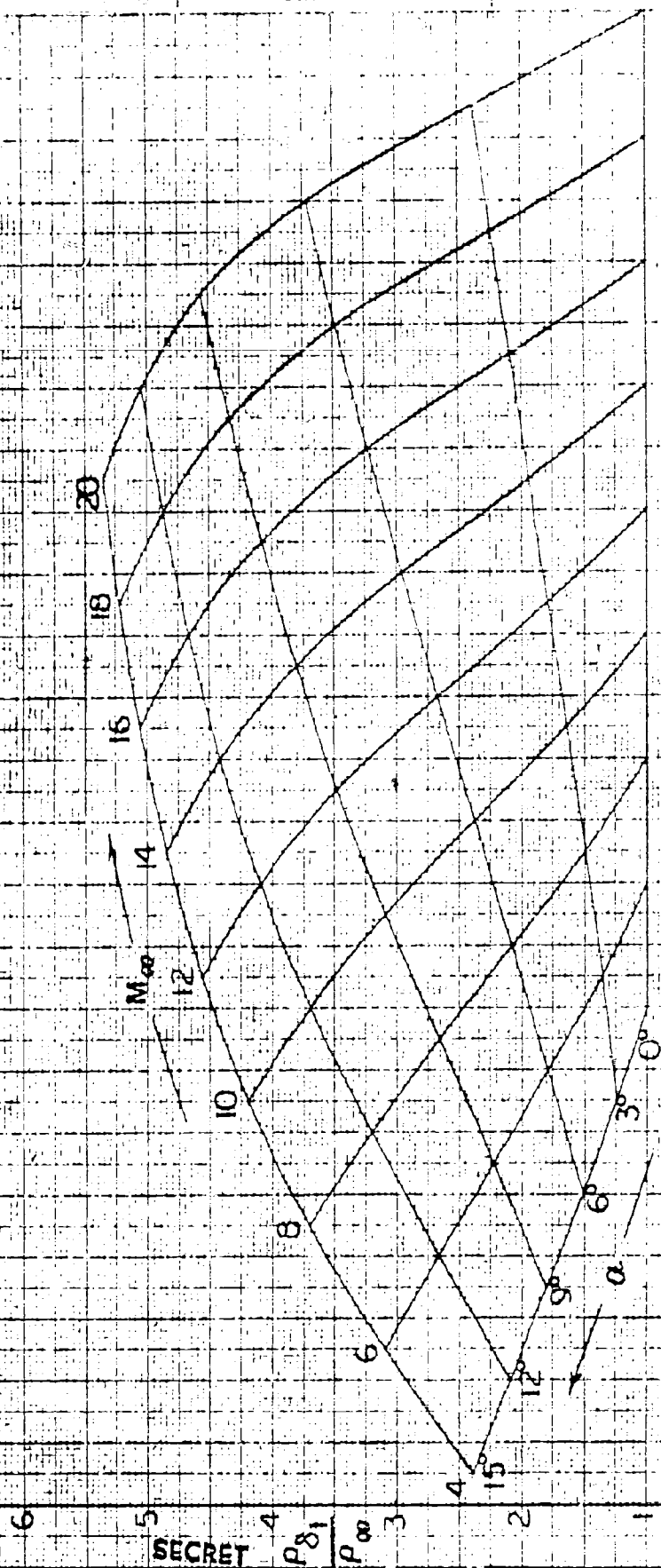


Figure 11-15

RATIO OF LOCAL STREAM DENSITY TO FREE STREAM
 DENSITY FOR WING FLAT BOTTOM SURFACE



BY _____ DATE _____
 CHECKED _____ DATE _____

SECRET
BELL Aircraft CORPORATION
 BUFFALO, N. Y.

MODEL _____ PAGE 4-44 OF _____
 SHIP _____ REPORT NL43-945-012

**RATIO OF LOCAL STREAM VELOCITY TO FREE STREAM
 VELOCITY FOR WING FLAT BOTTOM SURFACE**

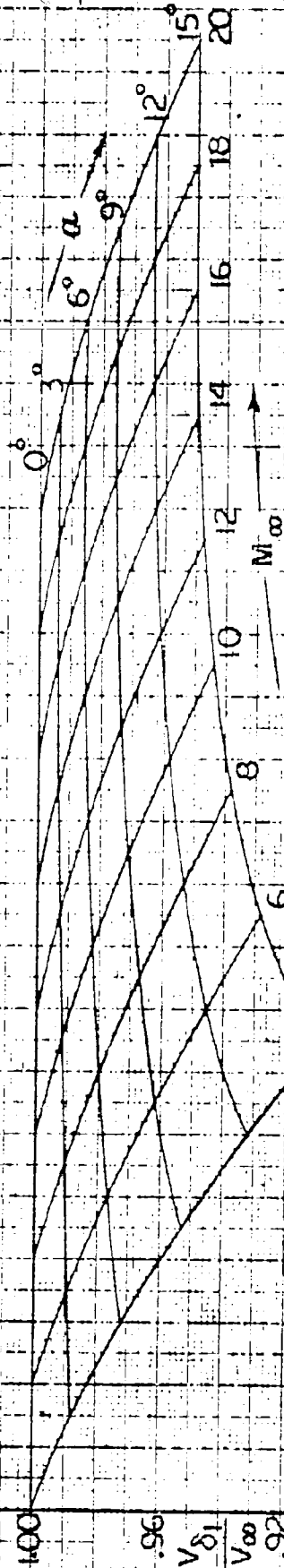


Figure 4.4-7

SECRET

Figure 1.1-8

RATIO OF LOCAL STREAM MACH NUMBER TO FREE
STREAM MACH NUMBER FOR WING FLAT BOTTOM
SURFACE

α 3° 0°
 6° 9° 12°

10
 8
 6
 4
 2
 0
 M_{∞}
 M_{∞}
 2
 0

10
 12
 14
 16
 18
 20

SECRET

BY _____ DATE _____
 CHECKED _____ DATE _____

SECRET
BELL Aircraft CORPORATION
 BUFFALO, N. Y.

MODEL _____ PAGE 1-16
 SHIP _____ REPORT D143-945-012

RATIO OF LOCAL STREAM REYNOLDS NUMBER TO FREE
STREAM REYNOLDS NUMBER FOR WING FLAT BOTTOM
SURFACE

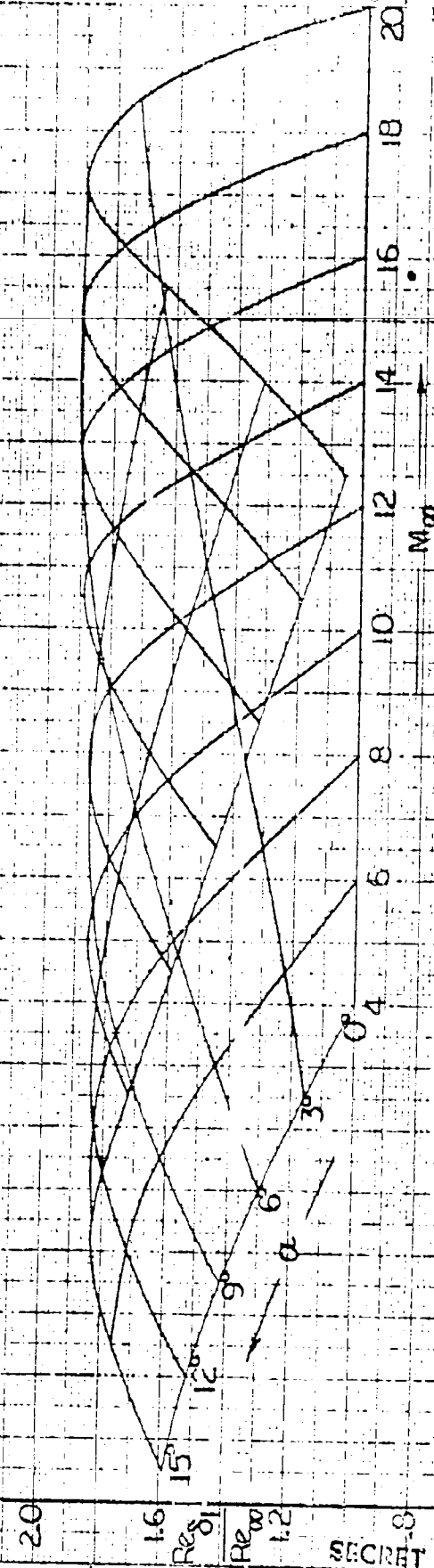


Figure 1.1.9

SECRET

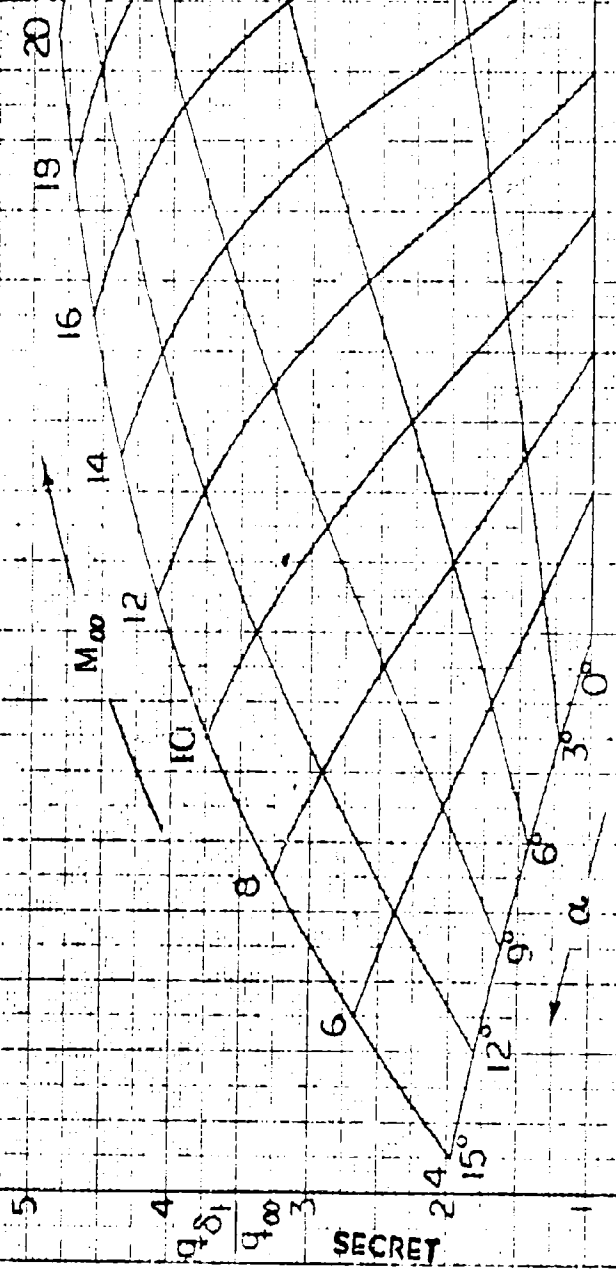
BY _____ DATE _____
 CHECKED _____ DATE _____

SECRET
BELL Aircraft CORPORATION
 BUFFALO, N. Y.

MODEL _____ REPORT _____
 SHIP _____

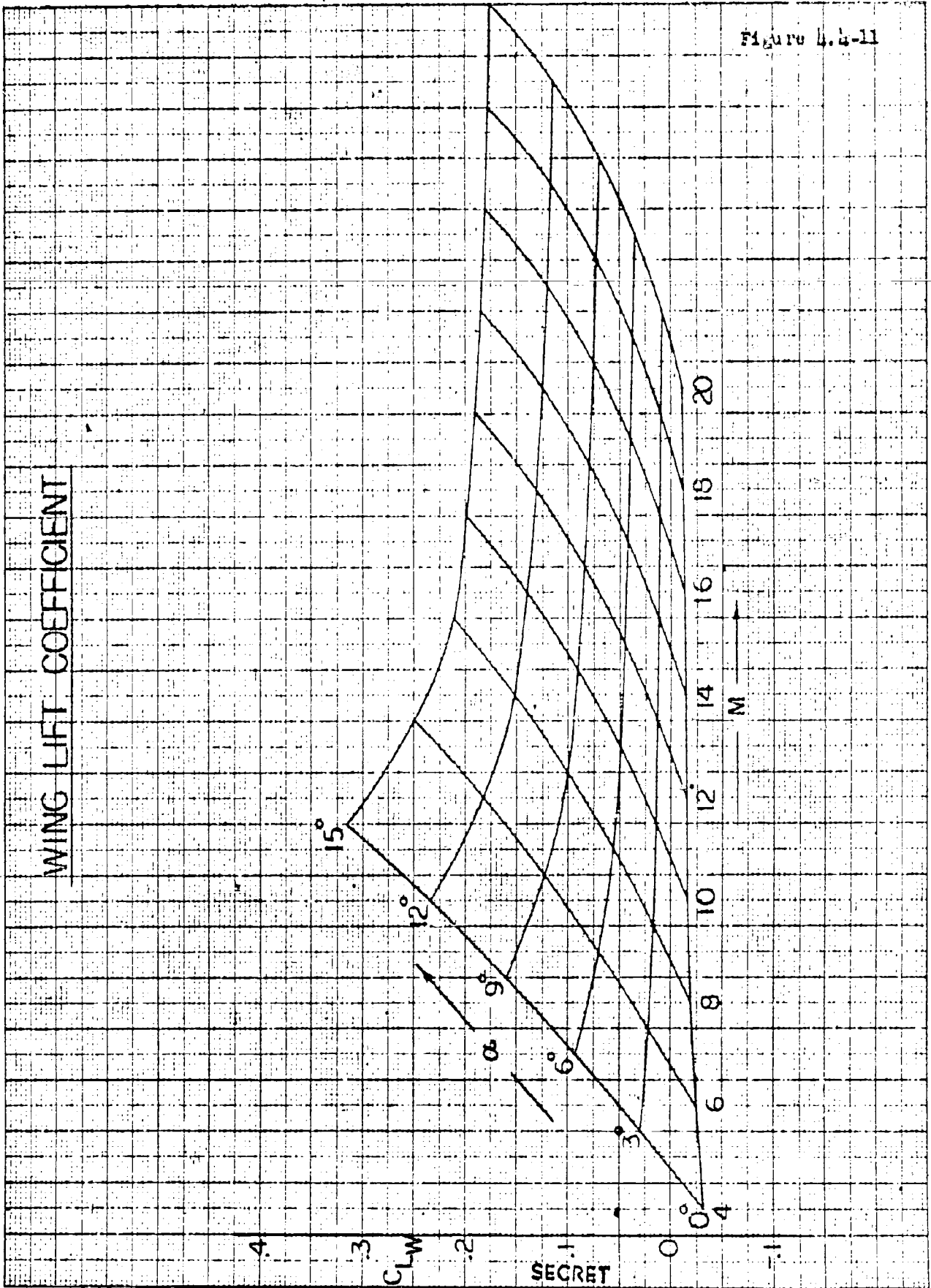
March 4, 1940

RATIO OF LOCAL STREAM DYNAMIC PRESSURE TO FREE
 STREAM DYNAMIC PRESSURE FOR WING FLAT BOTTOM
 SURFACE



SECRET

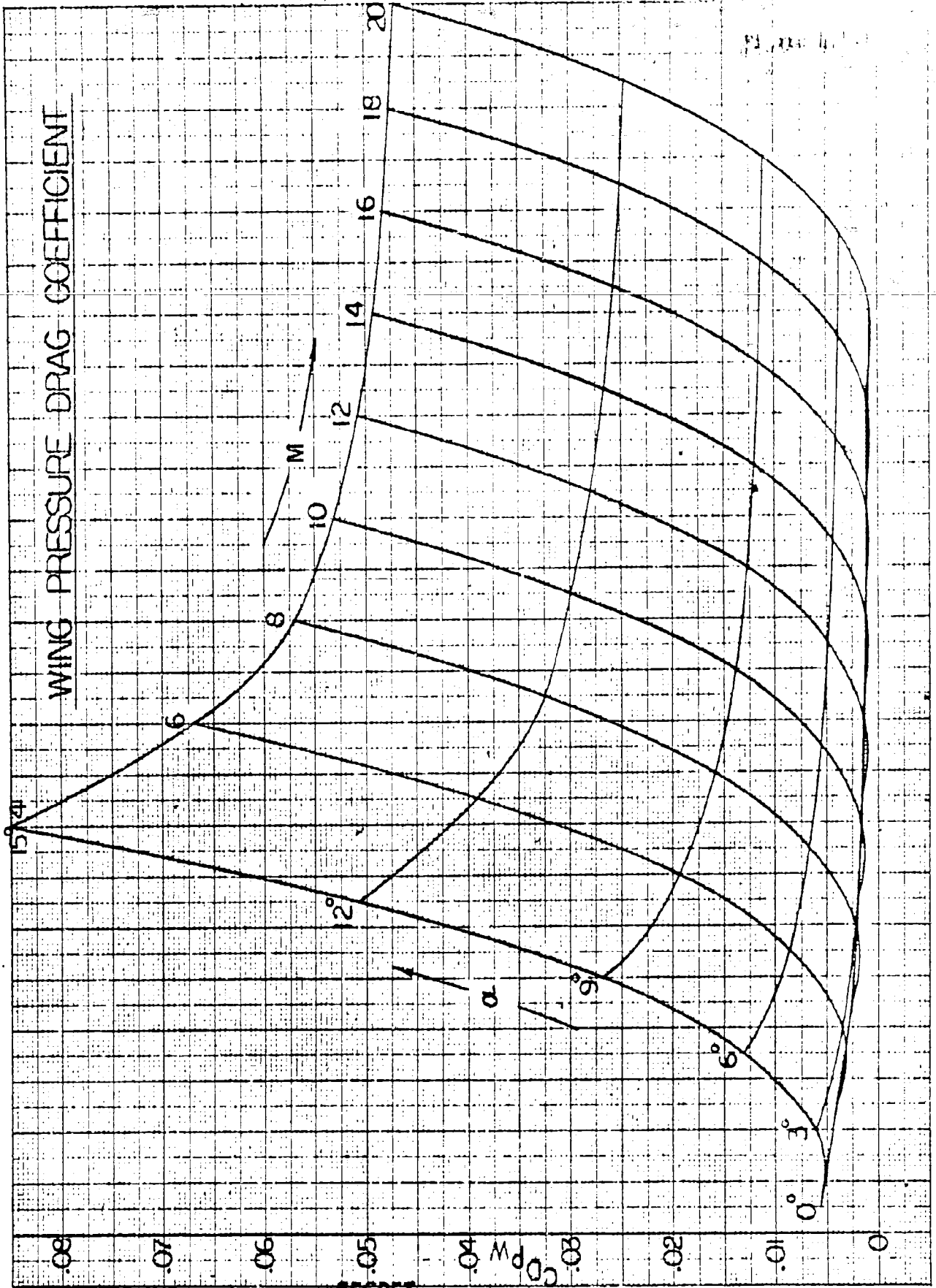
Figure 4.4-11



BY _____ DATE _____
 CHECKED _____ DATE _____

SECRET
 BELL Aircraft CORPORATION

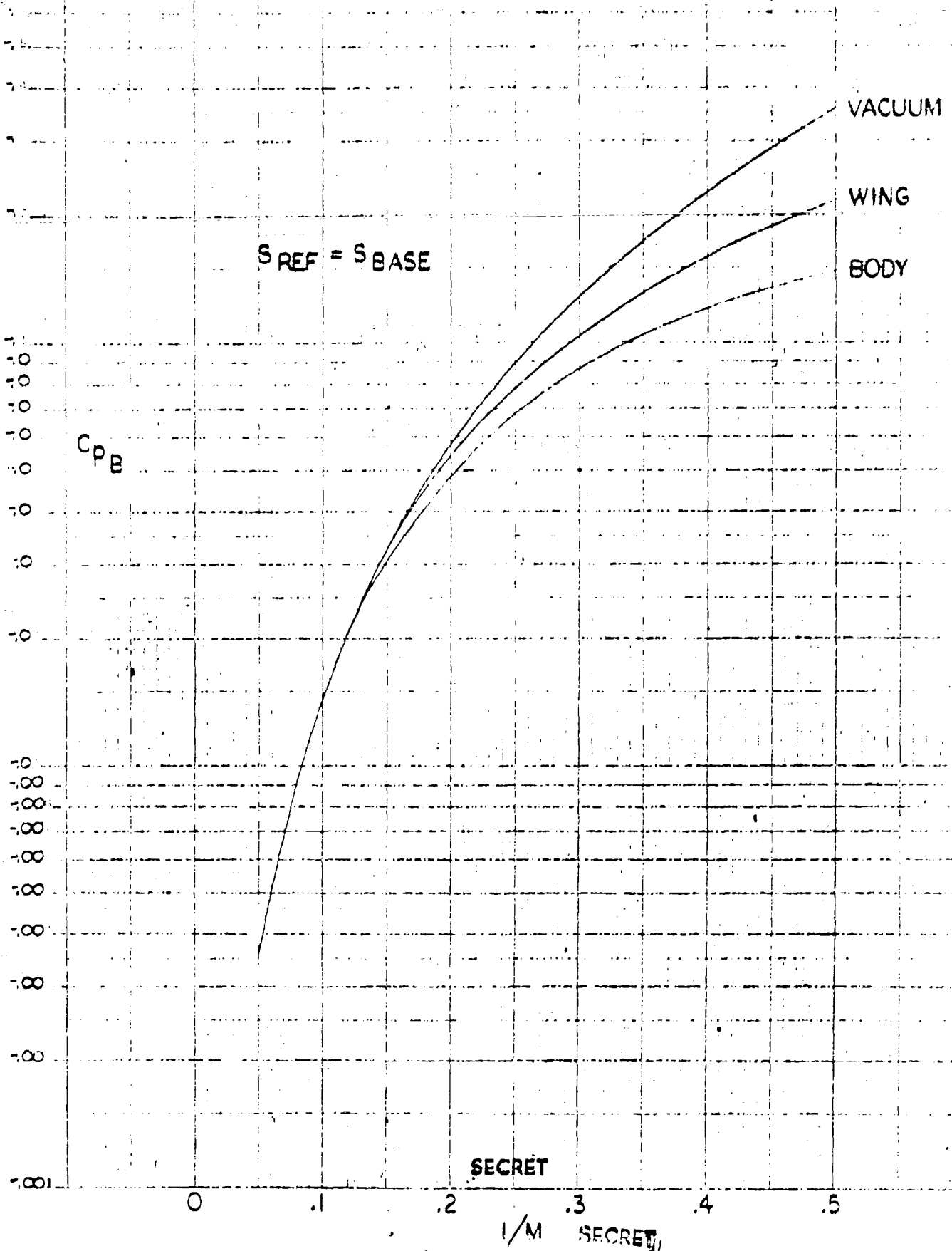
MODEL _____ PAGE 449
 SHIP _____ 143-945-01



SECRET

Figure 4.4-13

BASE PRESSURE COEFFICIENTS



SECRET

SECRET

BY _____ DATE _____
 CHECKED _____ DATE _____

SECRET
BELL Aircraft CORPORATION

MODEL _____ PAGE _____
 SHIP _____ REPORT _____

Figure 14b

VERTICAL TAIL PRESSURE DRAG COEFFICIENT

0.0010
 0.0008
 C_{DPT}
 0.0006
 0.0004
 0.0002
 0

2 4 6 8 10 12 14 16 18 20

1000 ft/sec

SECRET

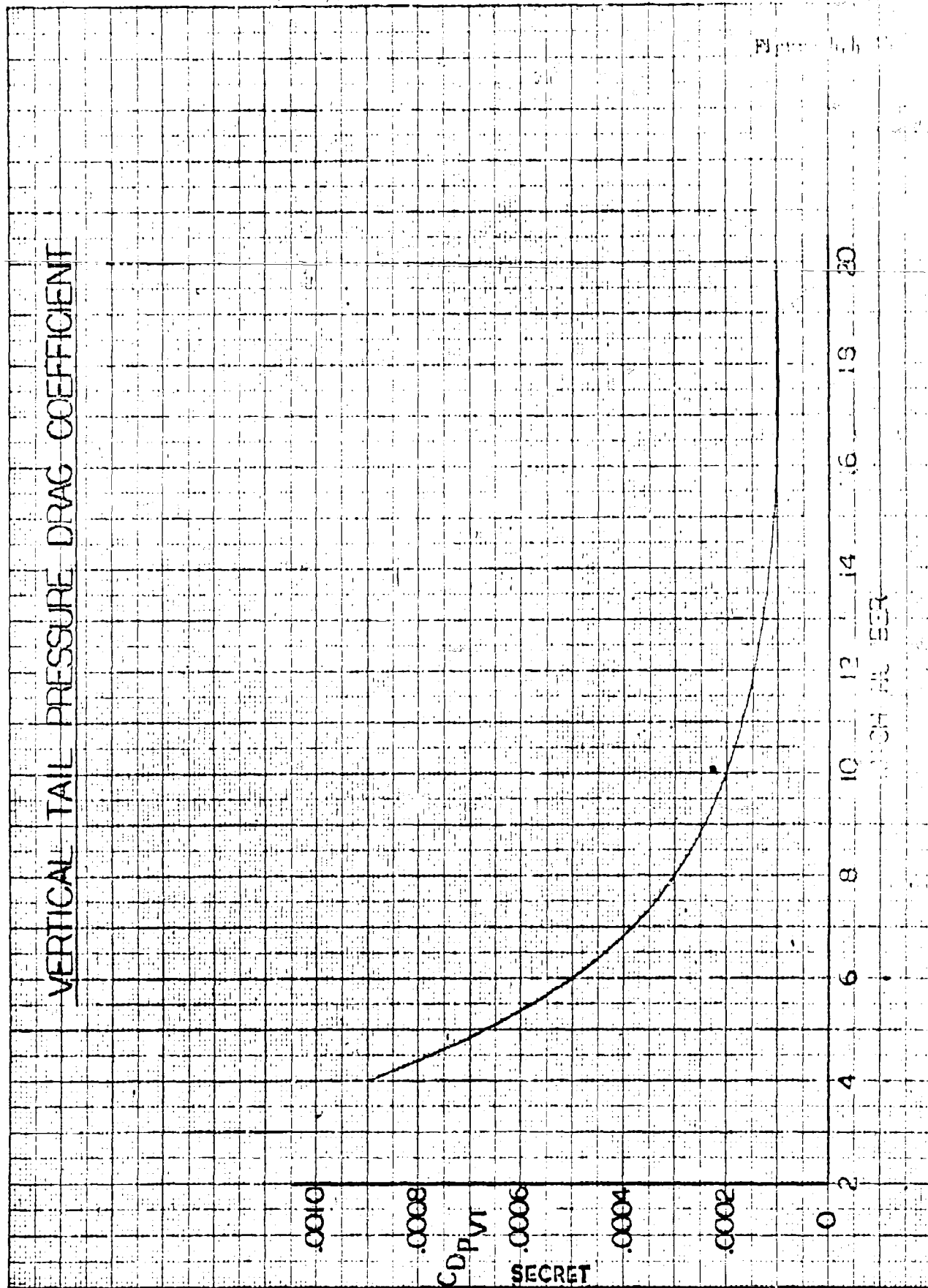
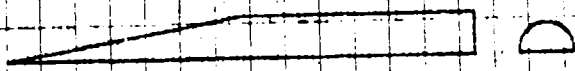


Figure 4.4-15

COMPARISON OF THEORETICAL AND EXPERIMENTAL
LIFT AND DRAG COEFFICIENTS AT $M=6.9$ FOR A
HALF CONE CYLINDER BODY (FLAT BOTTOM, $\theta_N=14^\circ$)



— COMBINED NEWTONIAN THEORY ON
 CONE AND SHOCK-EXPANSION THEORY
 ON REMAINDER OF BODY

○ EXPERIMENT REFERENCE 4-1

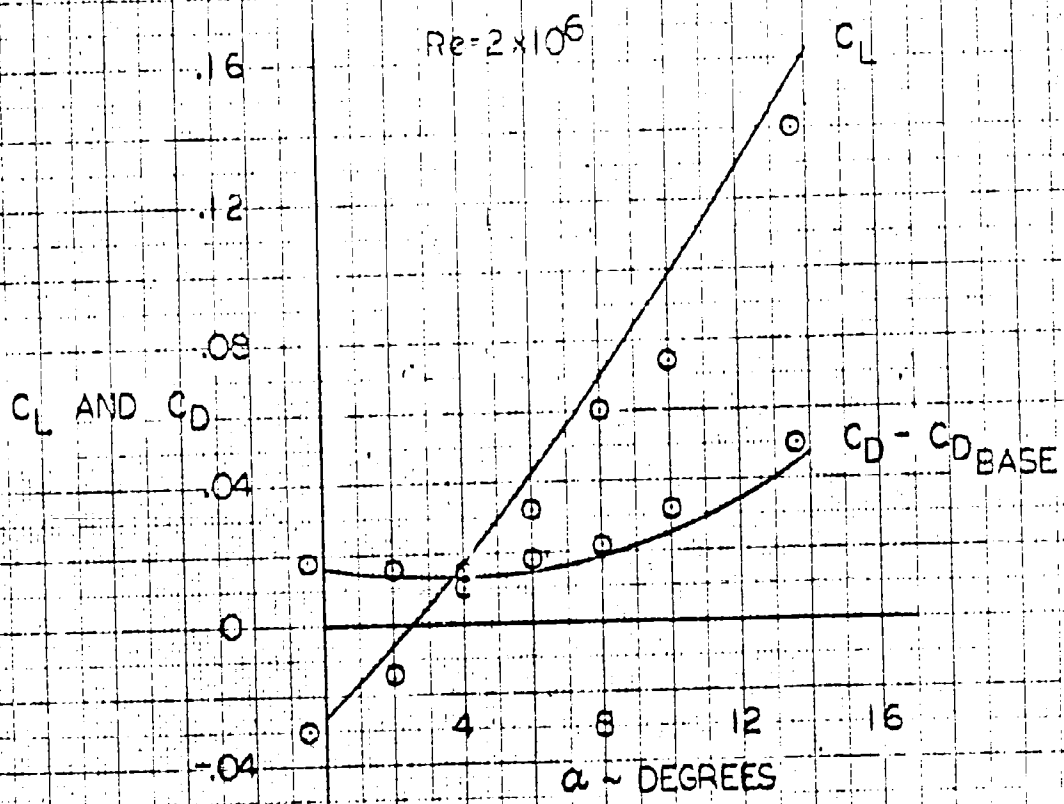
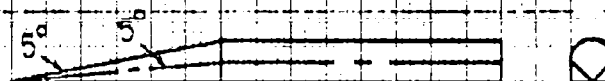


Figure 4.4-16

COMPARISON OF THEORETICAL AND EXPERIMENTAL
LIFT AND DRAG COEFFICIENTS AT $M=6.96$ FOR A
FLAT BOTTOM BODY WITH A 5° DROOPED CONICAL
NOSE



COMBINED NEWTONIAN THEORY ON CONE
 AND SHOCK-EXPANSION THEORIES ON
 REMAINDER OF BODY

○ EXPERIMENT REFERENCE 4-4-9

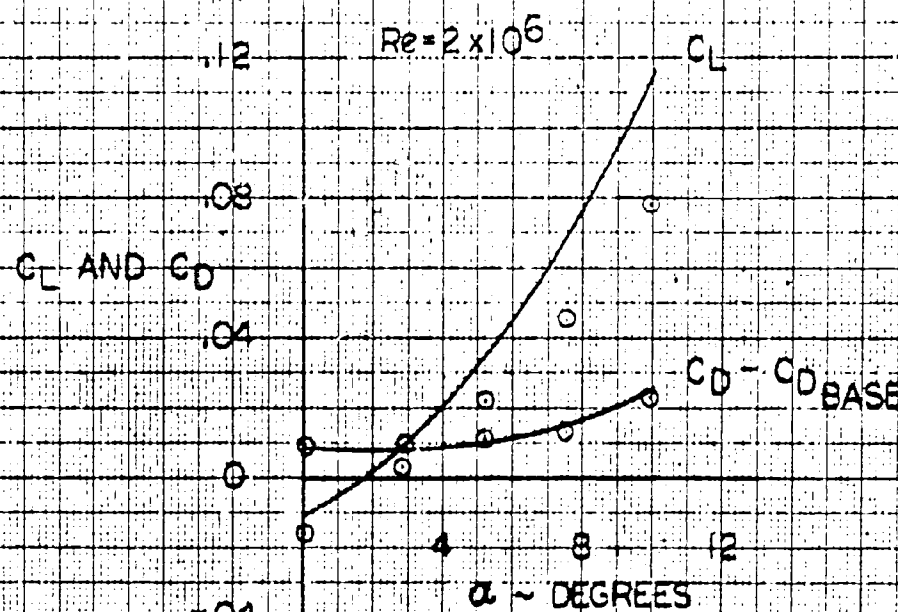
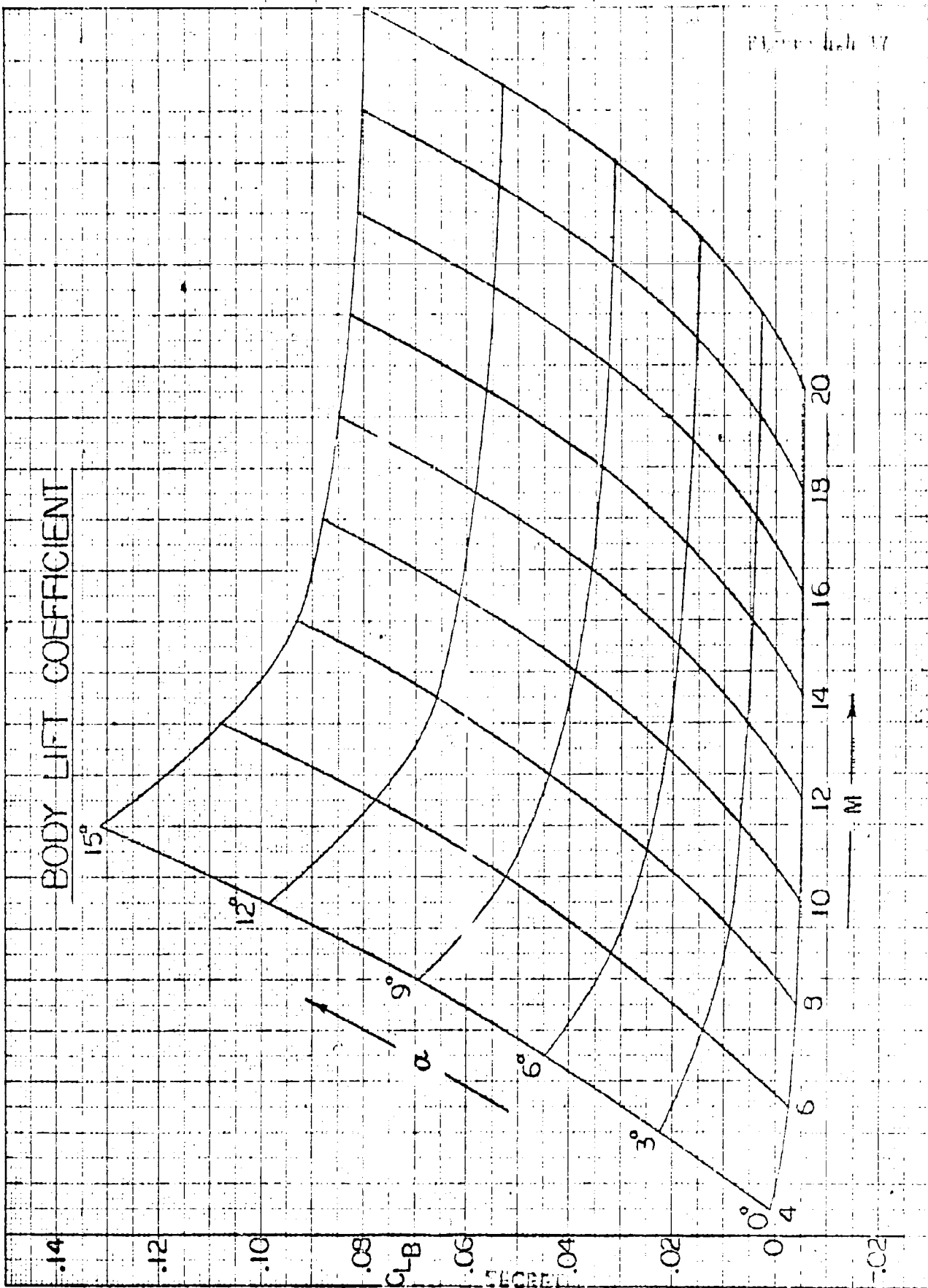


FIGURE 4-17

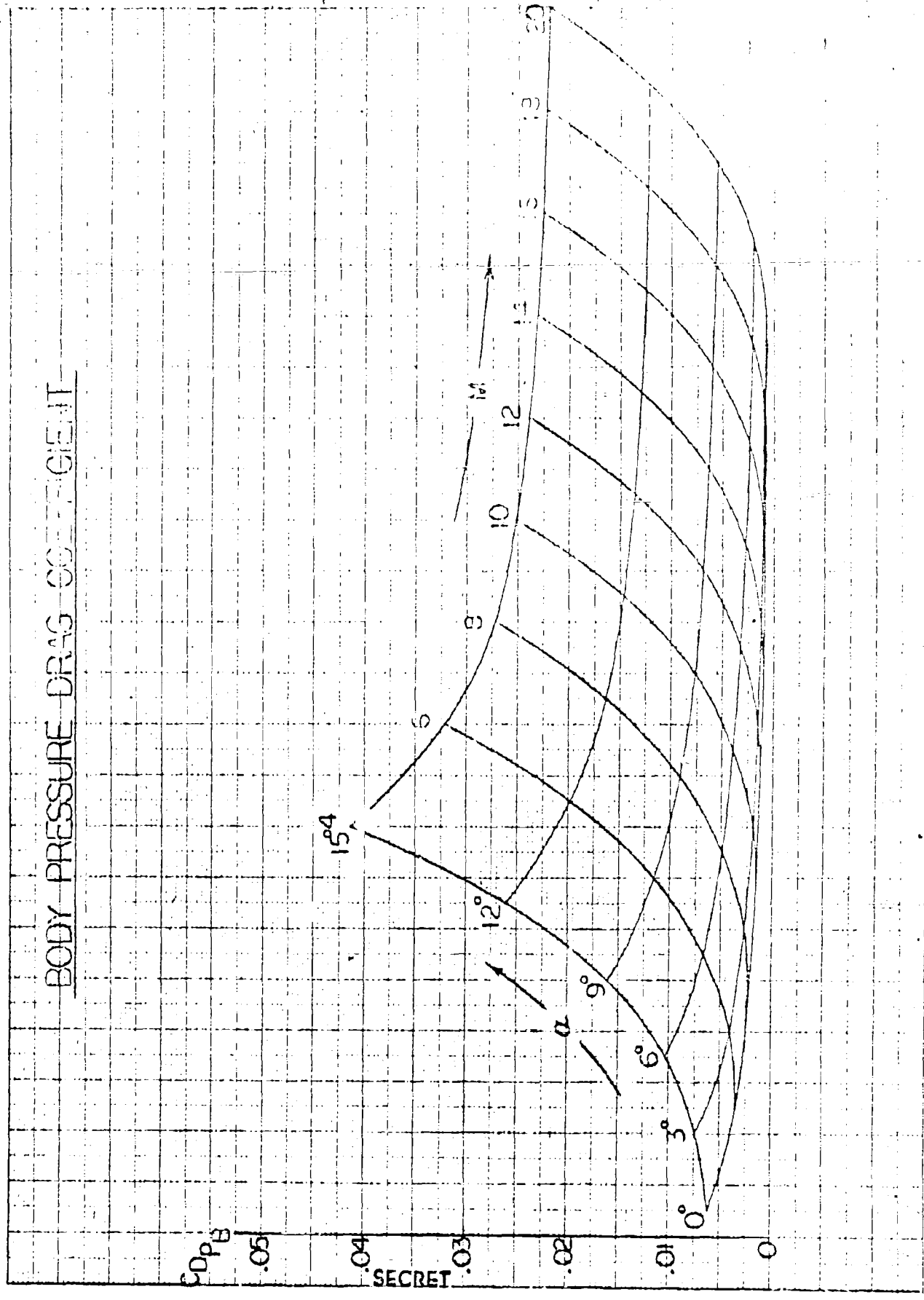


BY _____ DATE _____
 CHECKED _____ DATE _____

SECRET
BELL *Howell* CORPORATION

MODEL _____
 SIZE _____

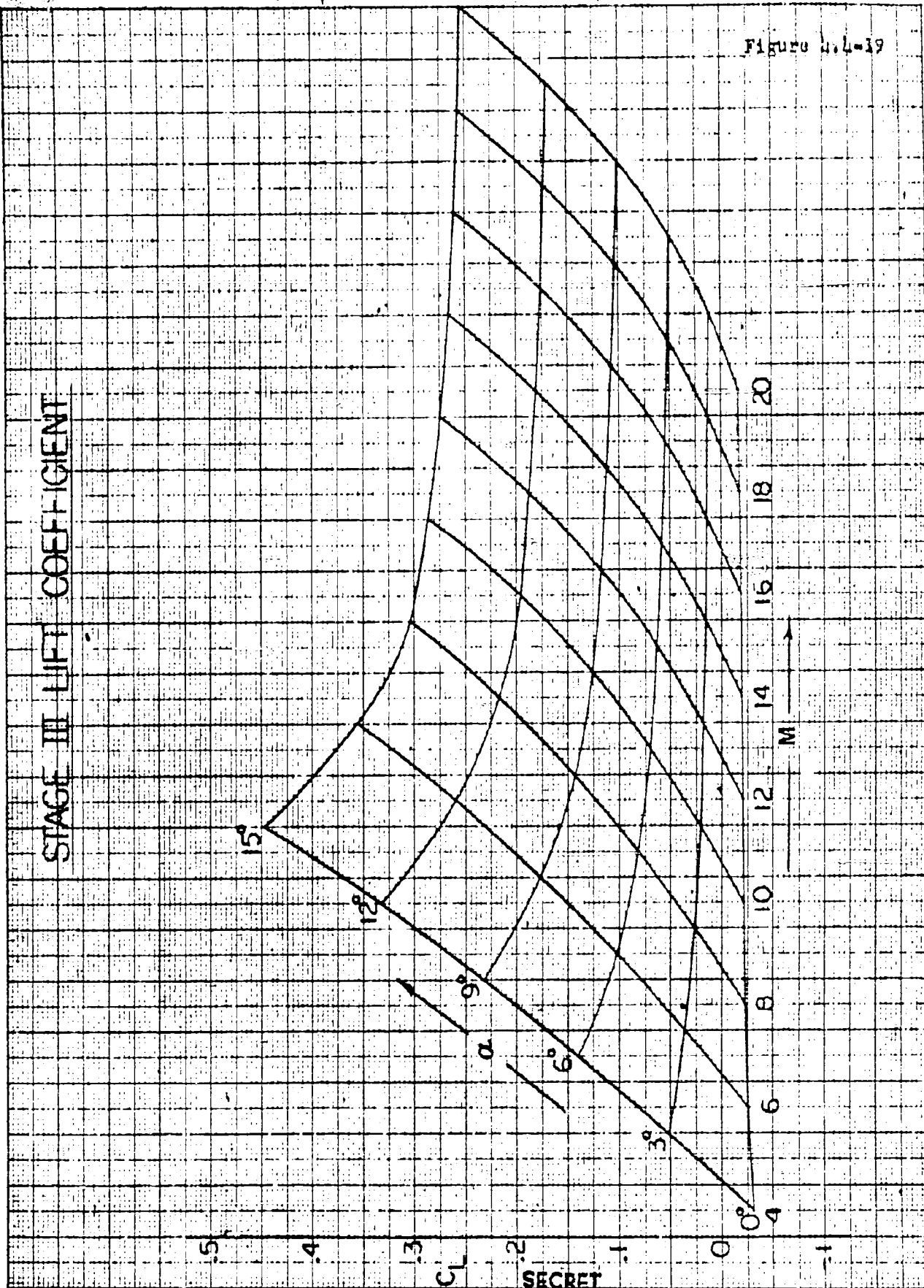
BODY PRESSURE DRAG COEFFICIENT



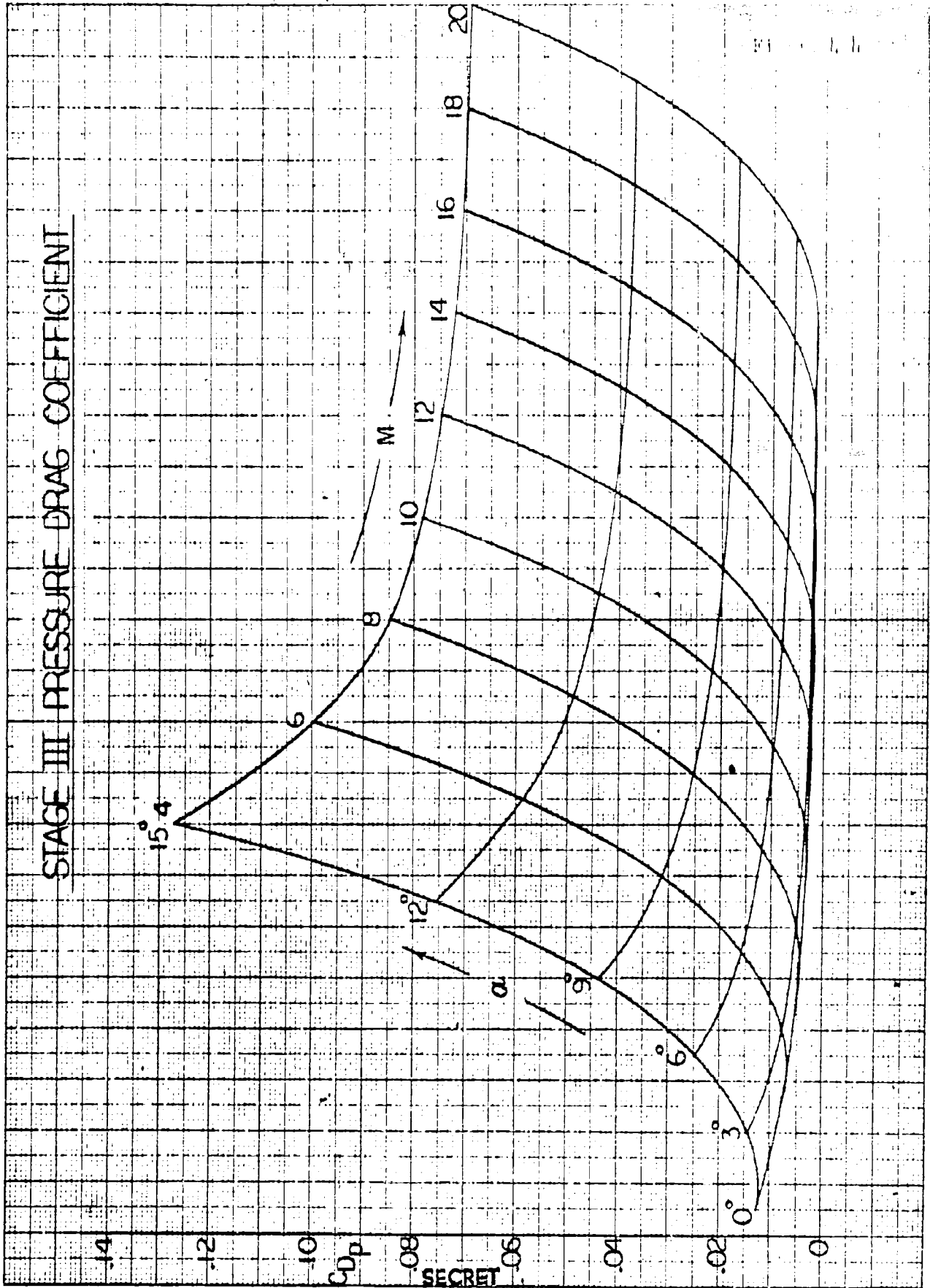
SECRET

STAGE III LIFT COEFFICIENT

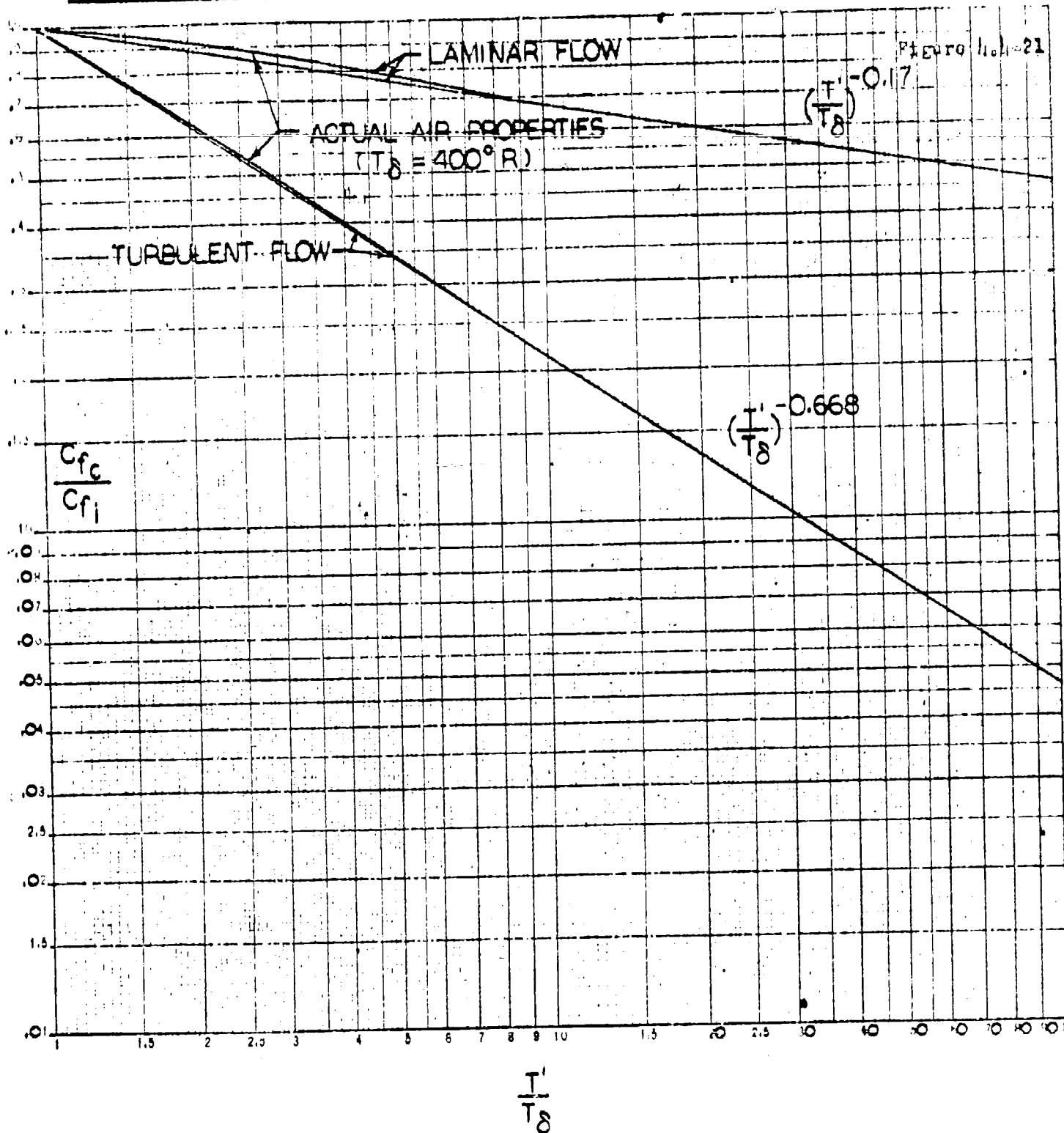
Figure 4.4-19



STAGE III PRESSURE DRAG COEFFICIENT



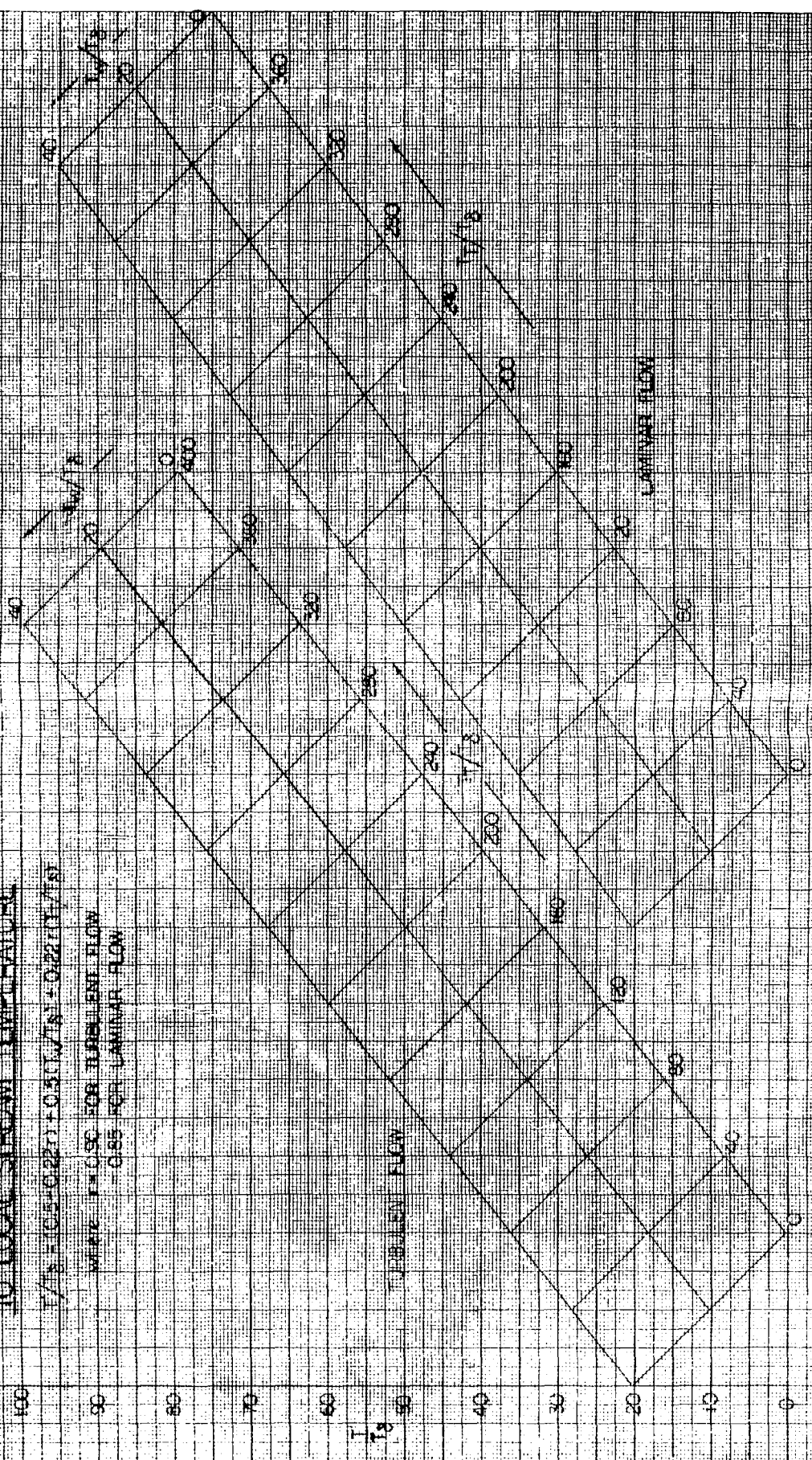
COMPARISON OF THE COMPRESSIBLE SKIN FRICTION TO INCOMPRESSIBLE SKIN FRICTION RATIO DETERMINED FROM ACTUAL AIR PROPERTIES AND POWER LAWS



**RATIO OF REFERENCE TEMPERATURE
 TO LOCAL STREAM TEMPERATURE**

$$T/T_s = (0.5 + 0.227) + 0.5(1/\sqrt{Re}) + 0.227(1/\sqrt{Re})^2$$

WHERE $T = 0.50$ FOR TURBULENT FLOW
 0.85 FOR LAMINAR FLOW



SECRET

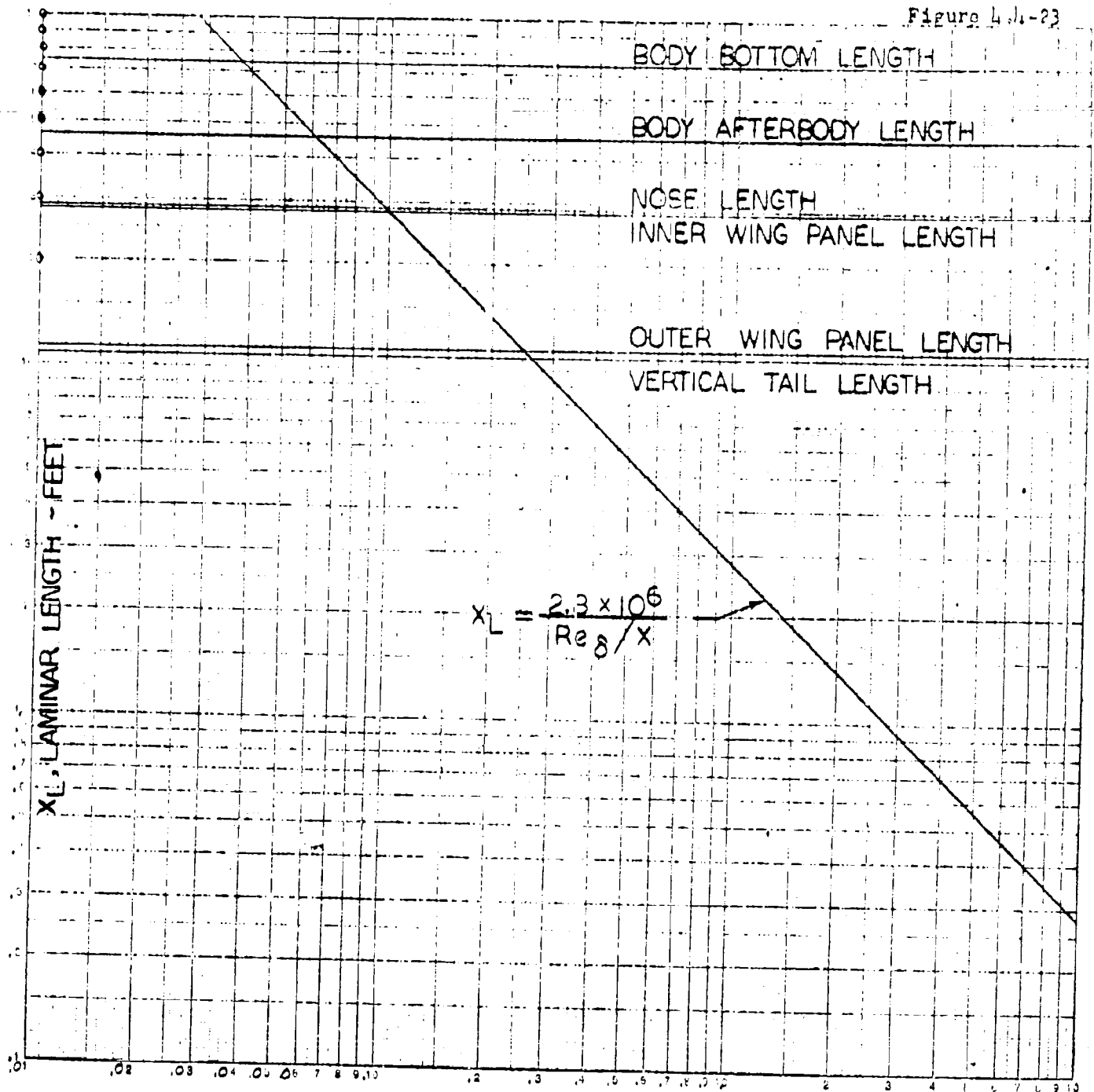
SECRET

SECRET

Page 4-60
Report D143-945-012

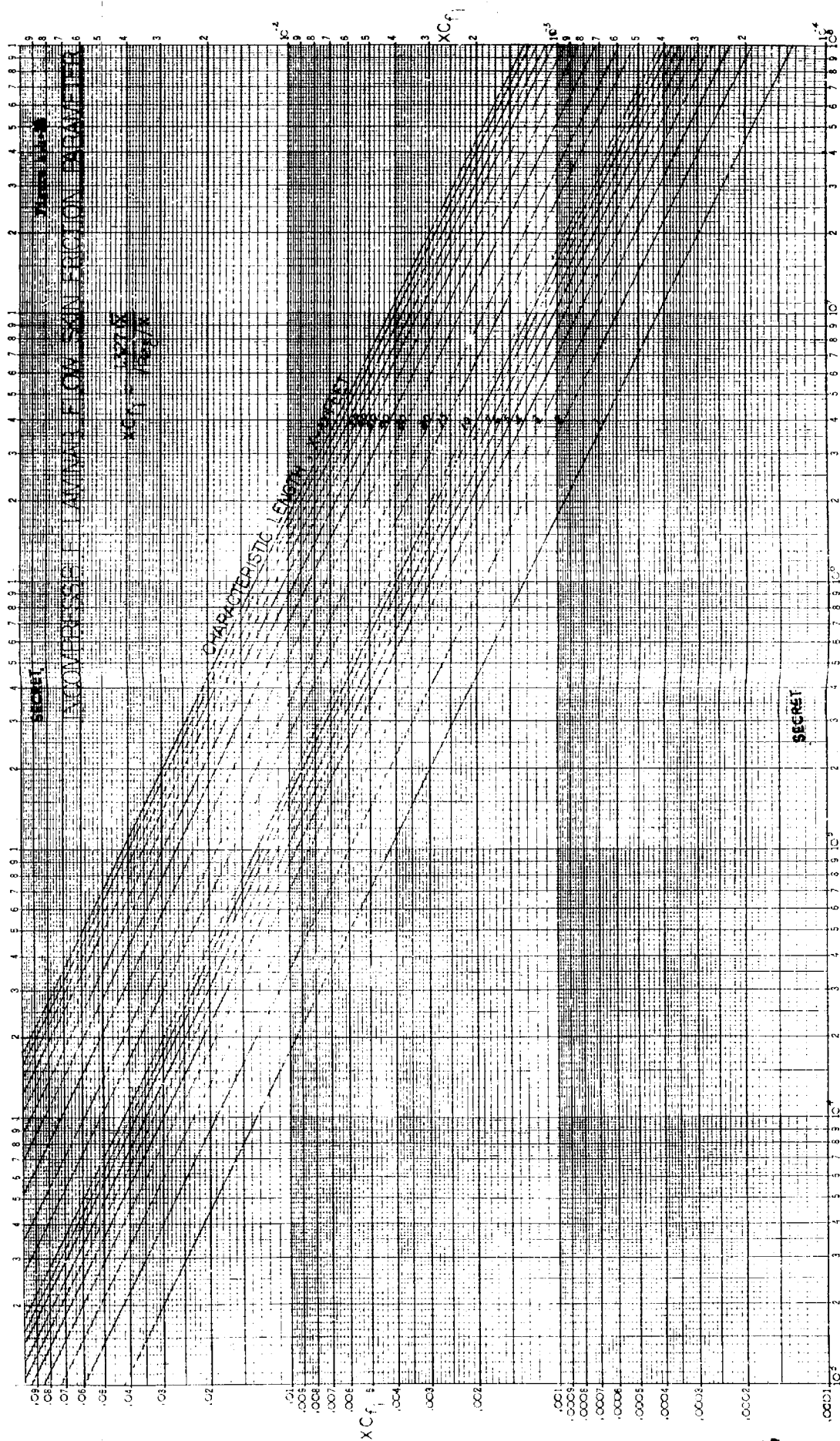
LAMINAR LENGTH VERSUS LOCAL FREE STREAM REYNOLDS NUMBER PER FOOT

Figure 4.4-23



Re_{δ}/x , LOCAL FREE STREAM REYNOLDS NUMBER
PER FOOT $\times 10^{-6}$

SECRET

LOCAL STREAM REYNOLDS NUMBER PER FOOT $\sim \text{Re}_x/x$

BY _____ DATE _____
CHECKED _____ DATE _____

BELL Aircraft CORPORATION

MODEL _____ PAGE **L-62**
SHIP _____ REPORT **DM3-915-012**

SECRET

INCOMPRESSIBLE TURBULENT SKIN FRICTION PARAMETER

$X C_{f_i}$ $0.055 X$
 10^{-4} 10^{-3} 10^{-2} 10^{-1}

CHARACTERISTIC LENGTH, X-FOOT

$X C_{f_i}$ 10^{-4} 10^{-3} 10^{-2} 10^{-1}

$X C_{f_i}$ 10^{-4} 10^{-3} 10^{-2} 10^{-1}

$X C_{f_i}$ 10^{-4} 10^{-3} 10^{-2} 10^{-1}

$X C_{f_i}$ 10^{-4} 10^{-3} 10^{-2} 10^{-1}

$X C_{f_i}$ 10^{-4} 10^{-3} 10^{-2} 10^{-1}

$X C_{f_i}$ 10^{-4} 10^{-3} 10^{-2} 10^{-1}

$X C_{f_i}$ 10^{-4} 10^{-3} 10^{-2} 10^{-1}

$X C_{f_i}$ 10^{-4} 10^{-3} 10^{-2} 10^{-1}

$X C_{f_i}$ 10^{-4} 10^{-3} 10^{-2} 10^{-1}

$X C_{f_i}$ 10^{-4} 10^{-3} 10^{-2} 10^{-1}

$X C_{f_i}$ 10^{-4} 10^{-3} 10^{-2} 10^{-1}

$X C_{f_i}$ 10^{-4} 10^{-3} 10^{-2} 10^{-1}

$X C_{f_i}$ 10^{-4} 10^{-3} 10^{-2} 10^{-1}

$X C_{f_i}$ 10^{-4} 10^{-3} 10^{-2} 10^{-1}

$X C_{f_i}$ 10^{-4} 10^{-3} 10^{-2} 10^{-1}

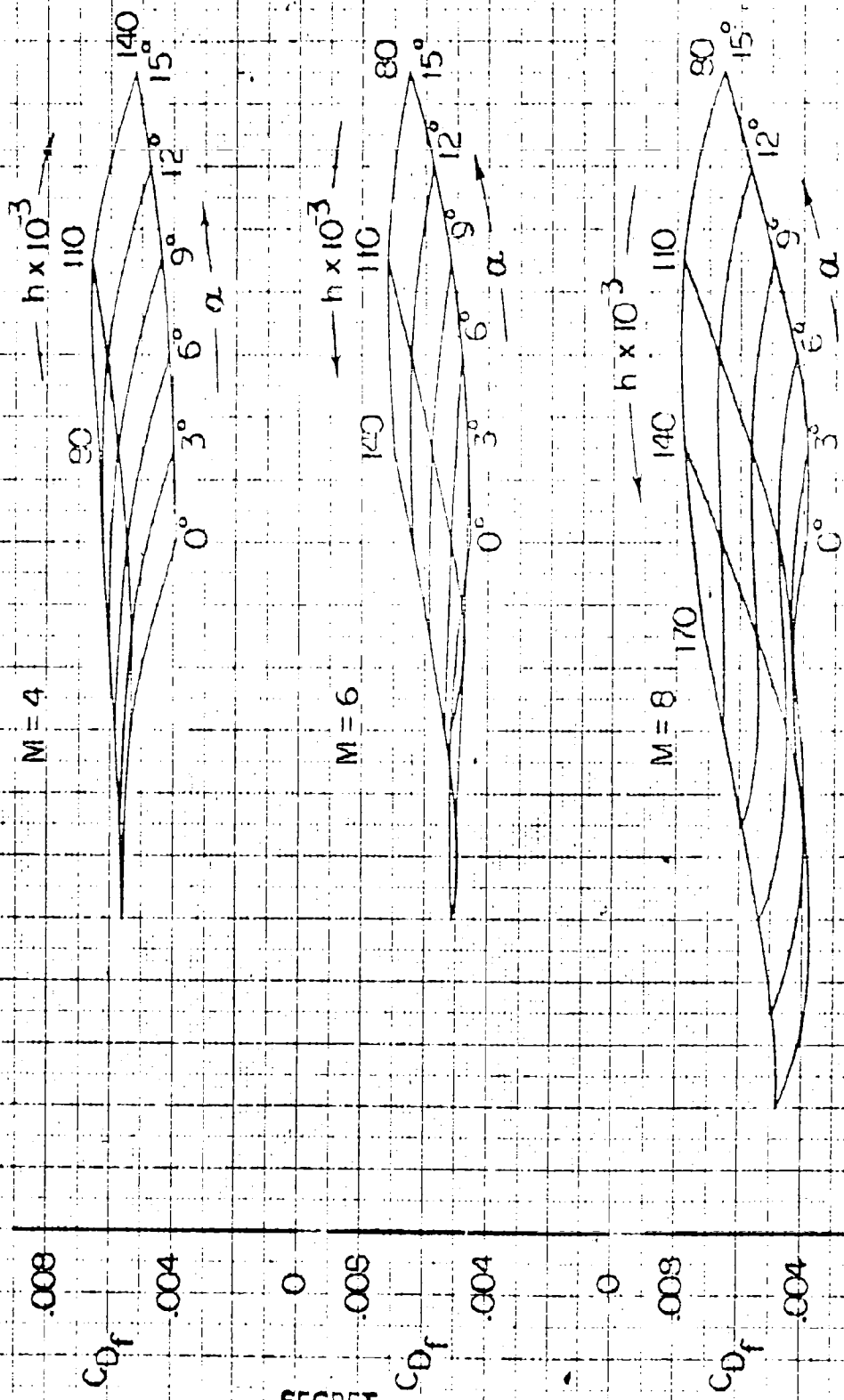
$X C_{f_i}$ 10^{-4} 10^{-3} 10^{-2} 10^{-1}

$X C_{f_i}$ 10^{-4} 10^{-3} 10^{-2} 10^{-1}

SECRET

LOCAL STREAM REYNOLDS NUMBER PER FOOT $\sim R_{S/X}$

STAGE III SKIN FRICTION DRAG COEFFICIENT



STAGE III SKIN FRICTION DRAG COEFFICIENT

$M = 10$

15° 250

12°

9°

6°

3°

0°

$h \times 10^3$

200

170

140

110

0.028

0.024

0.020

0.016

0.012

0.008

0.004

0

C_{Df}

SECRET

STAGE III SKIN FRICTION DRAG COEFFICIENT

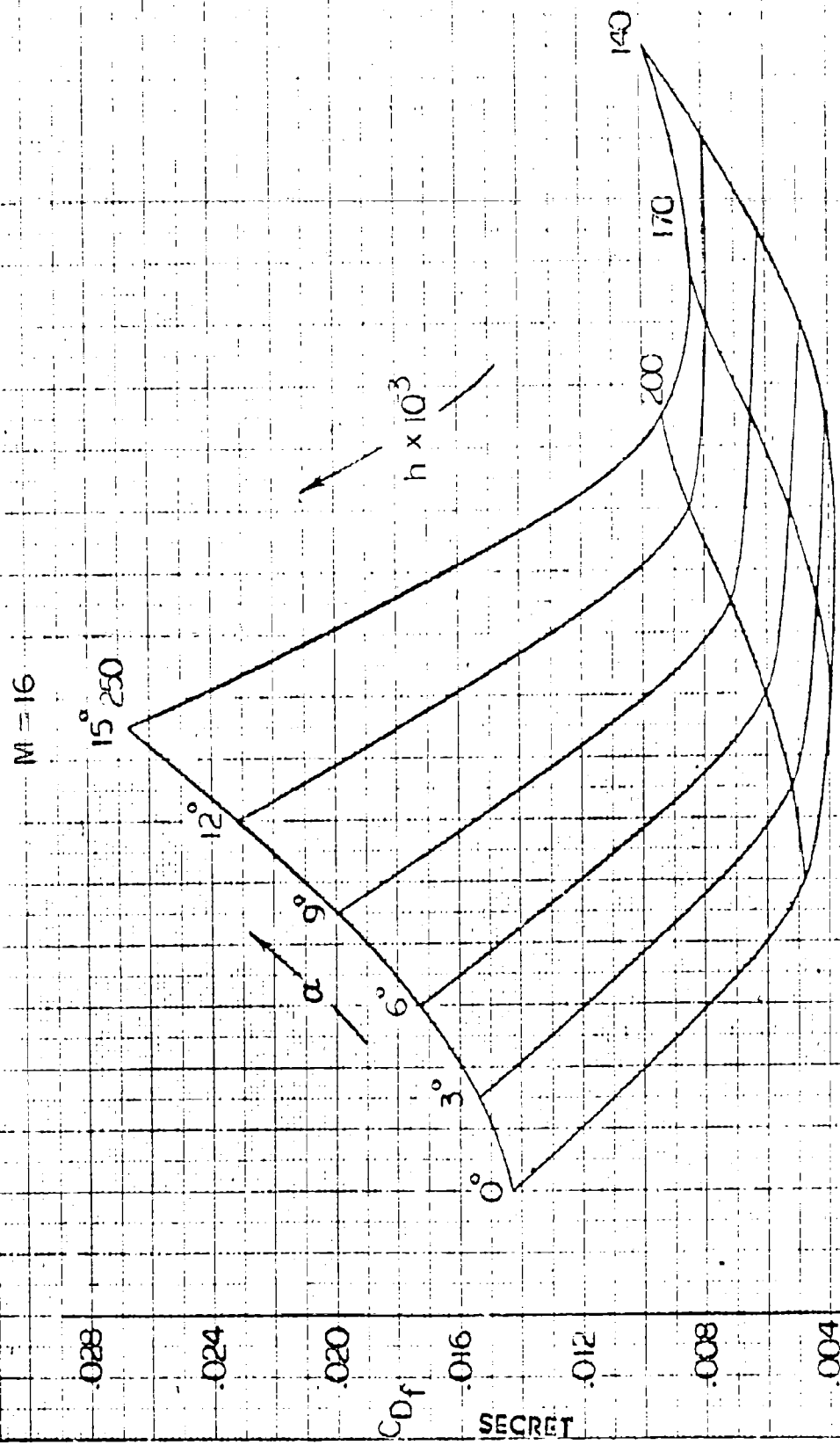
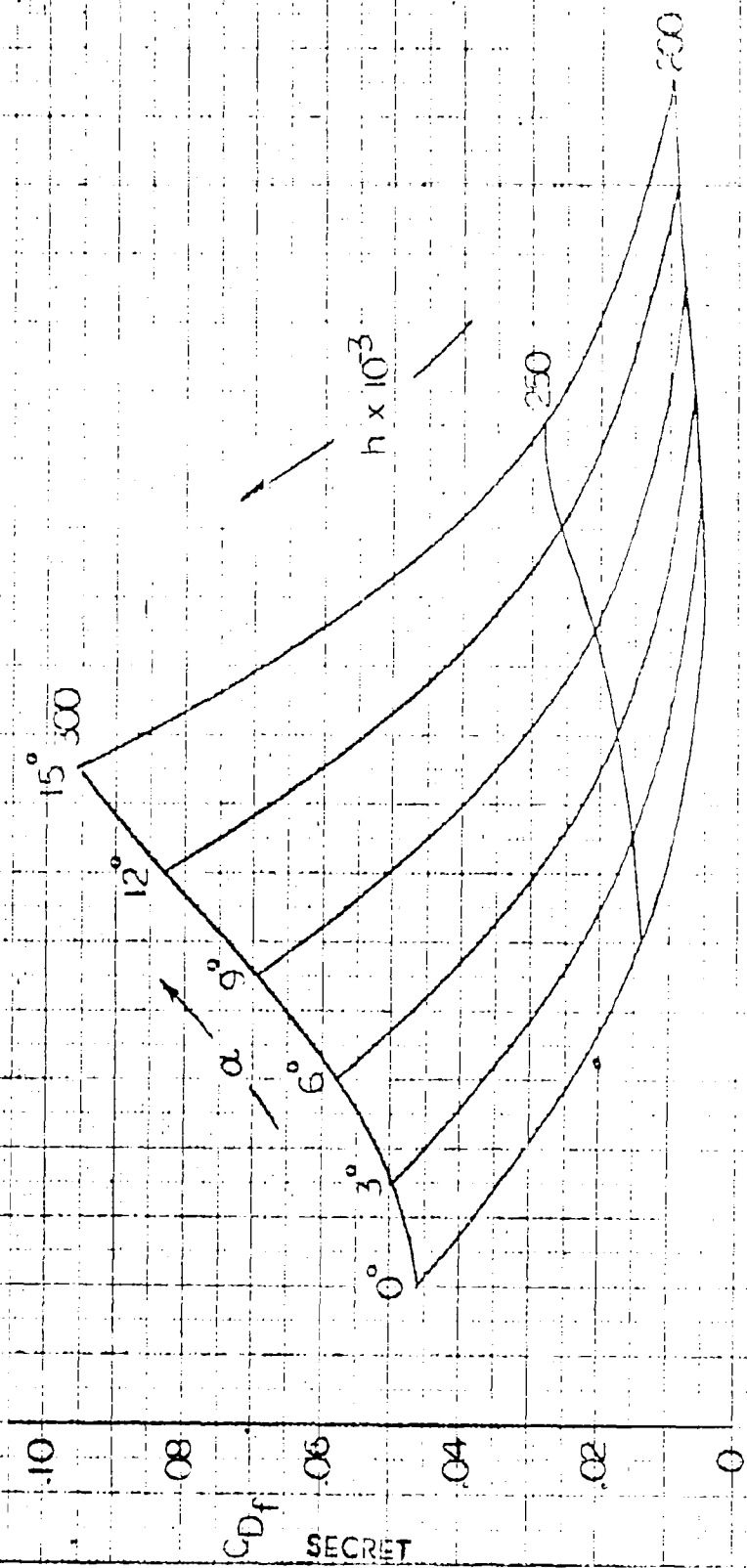


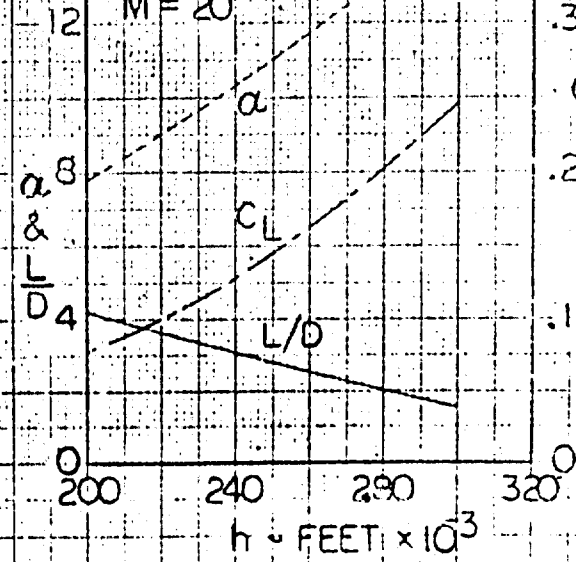
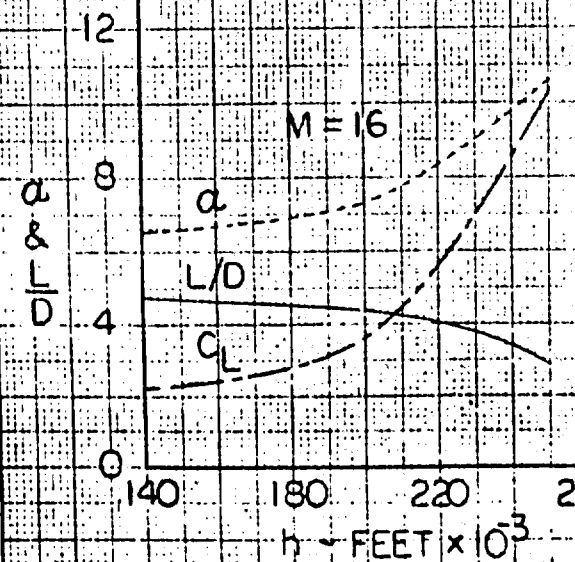
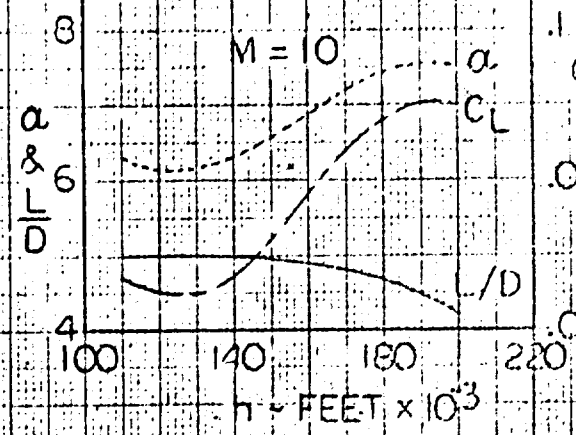
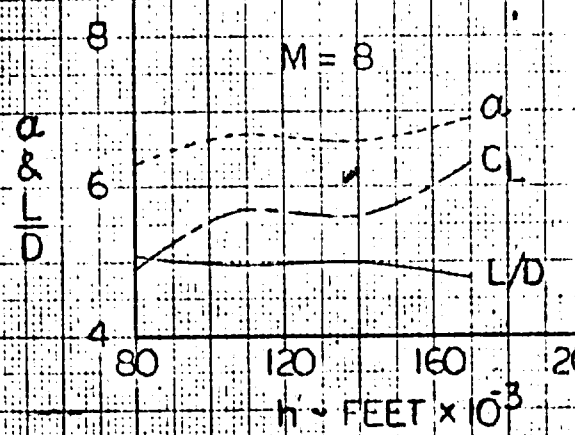
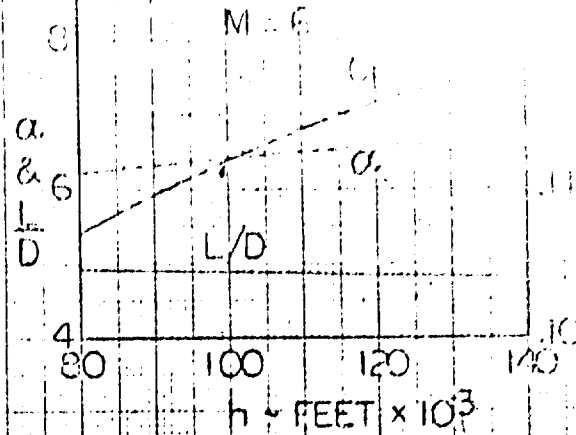
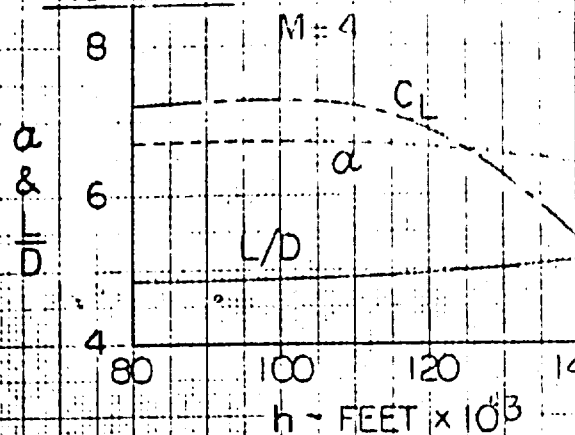
Figure 4-10-1

STAGE III SKIN FRICTION DRAG COEFFICIENT

$M = 20$

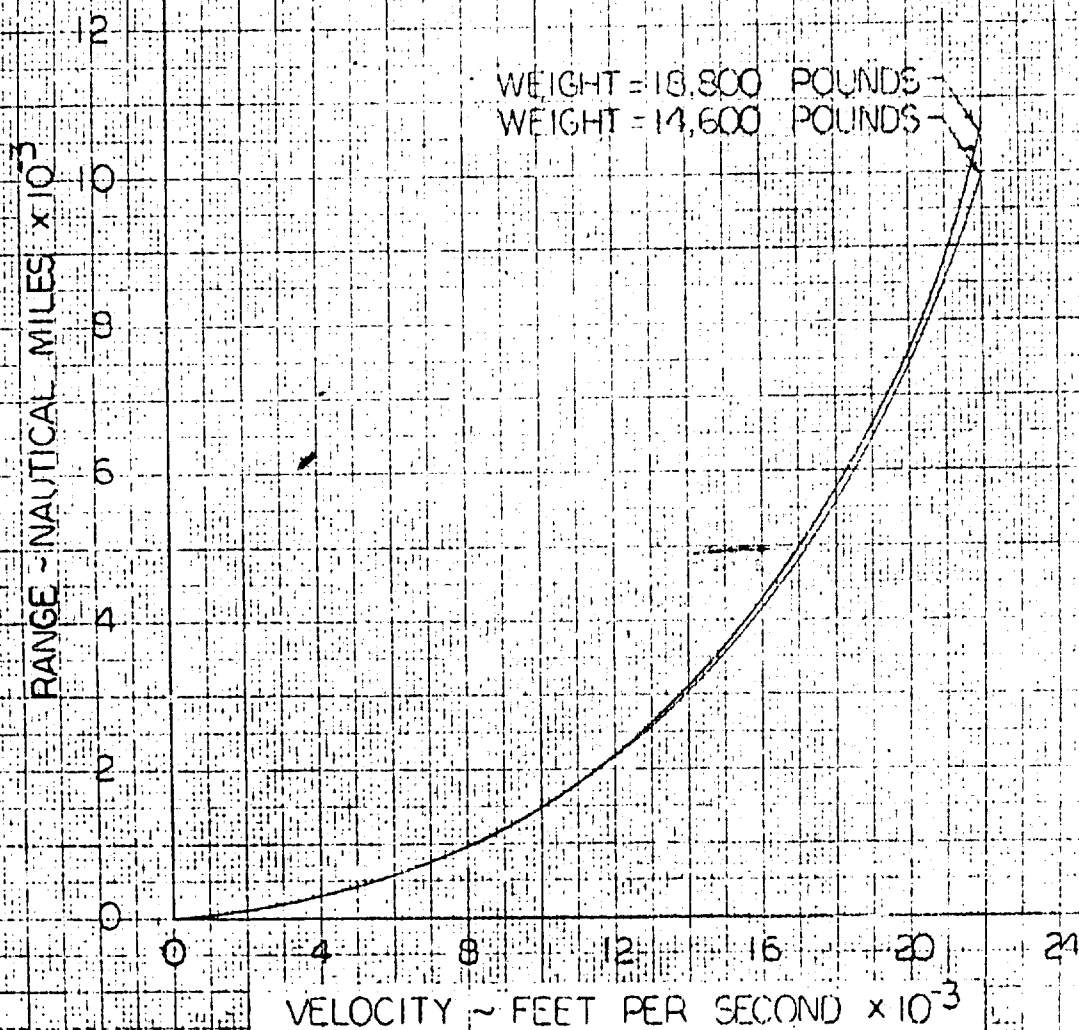


SUMMARY OF MAXIMUM LIFT DRAG RATIOS WITH CORRESPONDING
 LIFT COEFFICIENTS AND ANGLE OF ATTACK AT CONSTANT
 NUMBERS

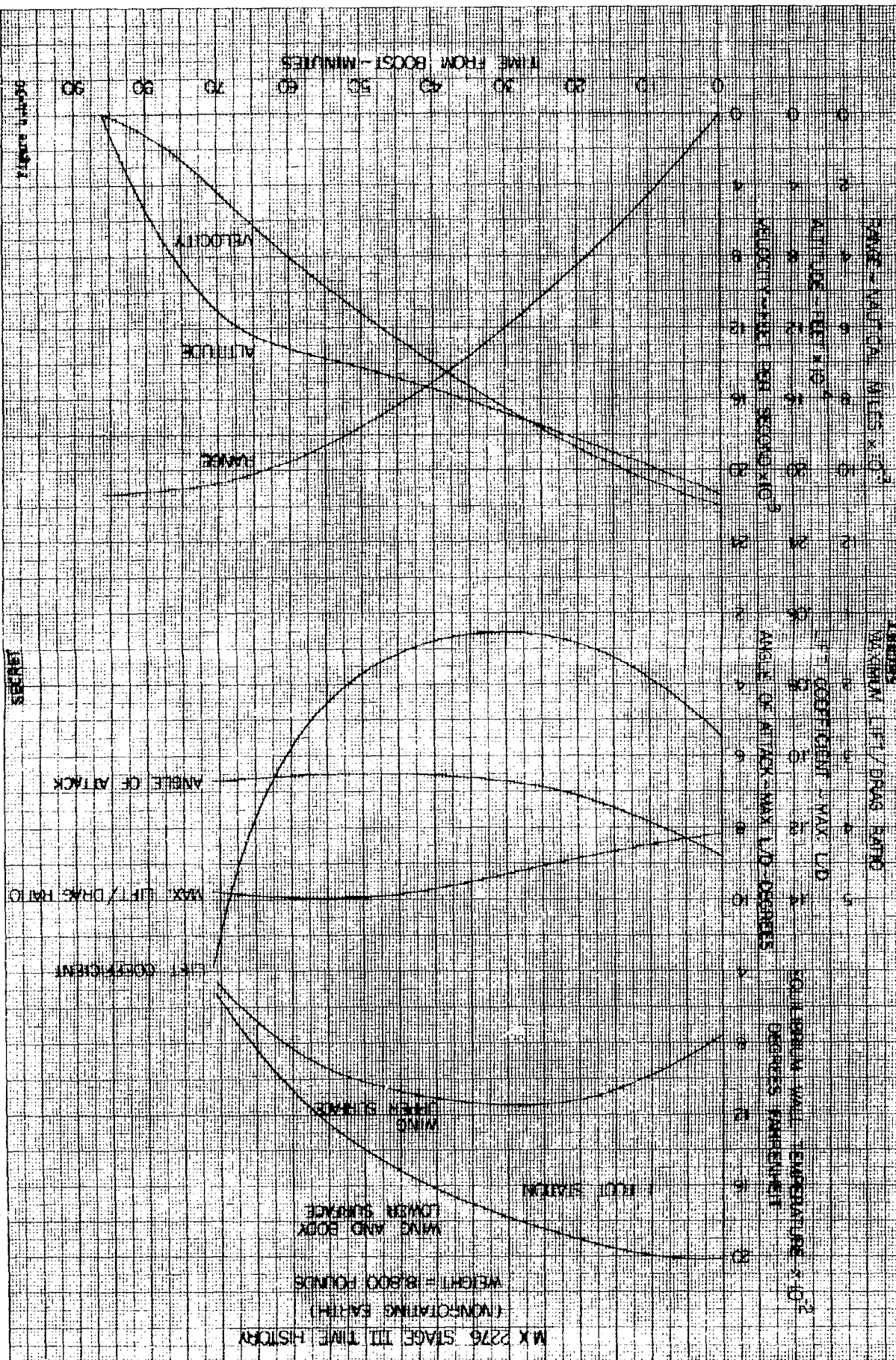


SECRET

MX 242 VERGIL FLIGHT (VERGIL) (NON-ROTATING EARTH)



SECRET



SECRET

Figure 111-31

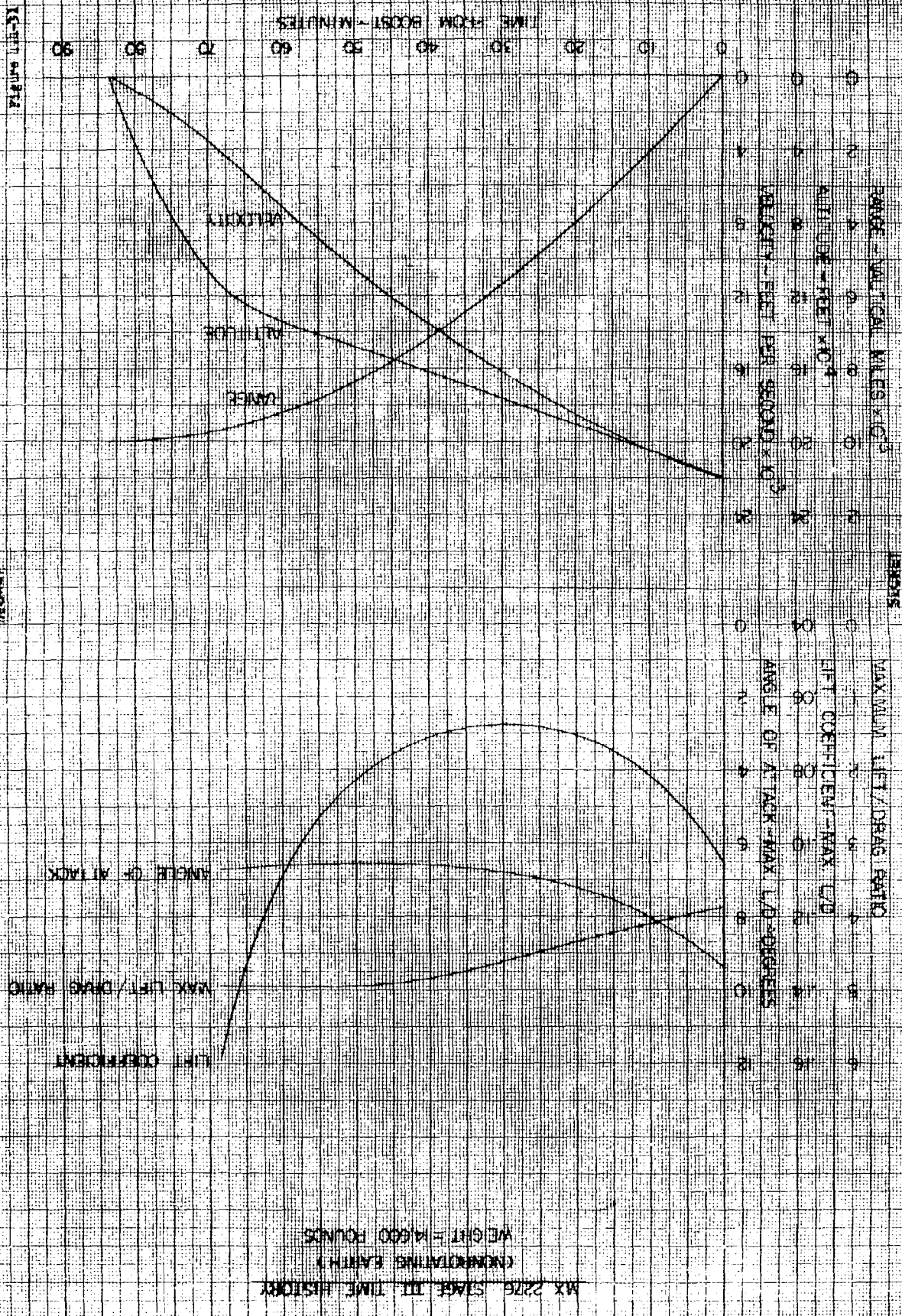


Figure 4.4-32

COMPARISON OF ORIGINAL AND PRESENT FLIGHT PATHS

WEIGHT = 14,600 POUNDS

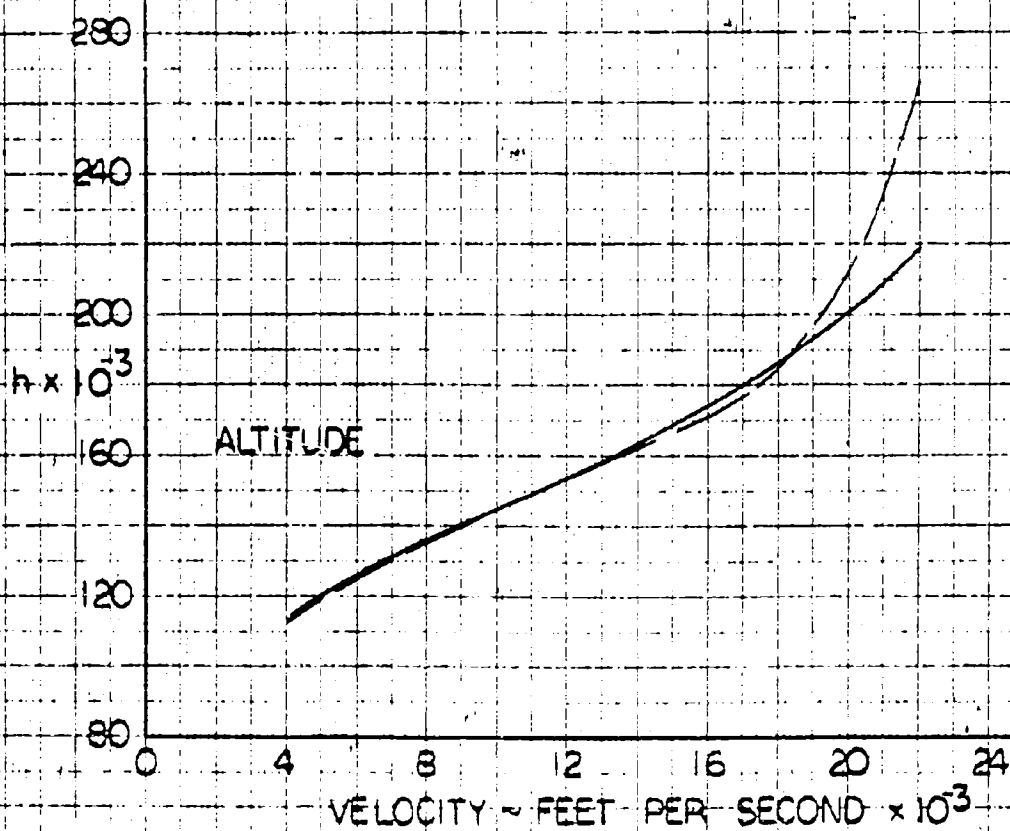
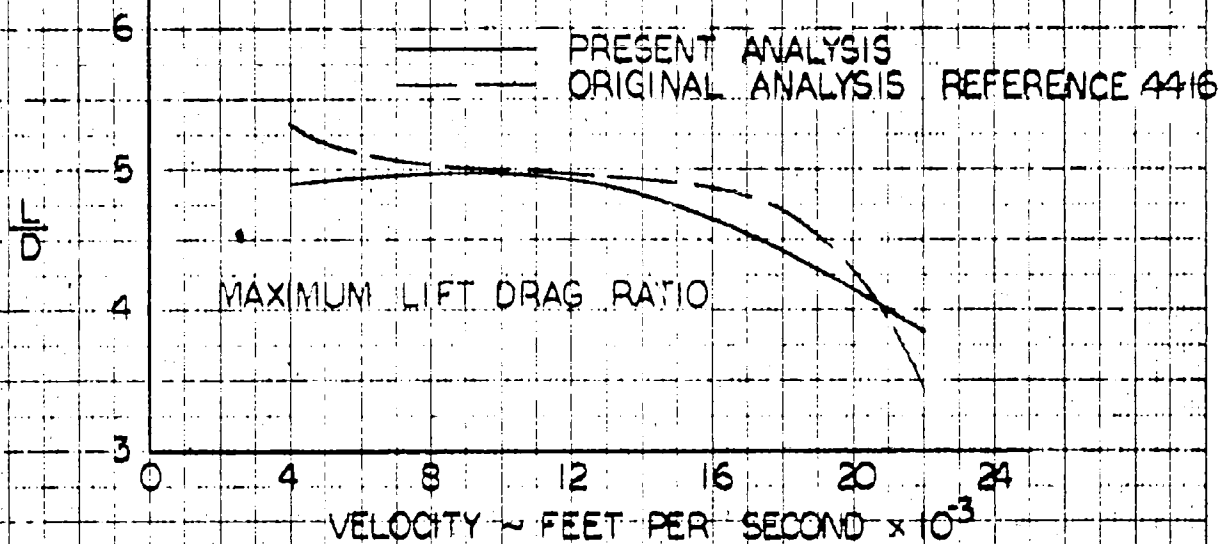
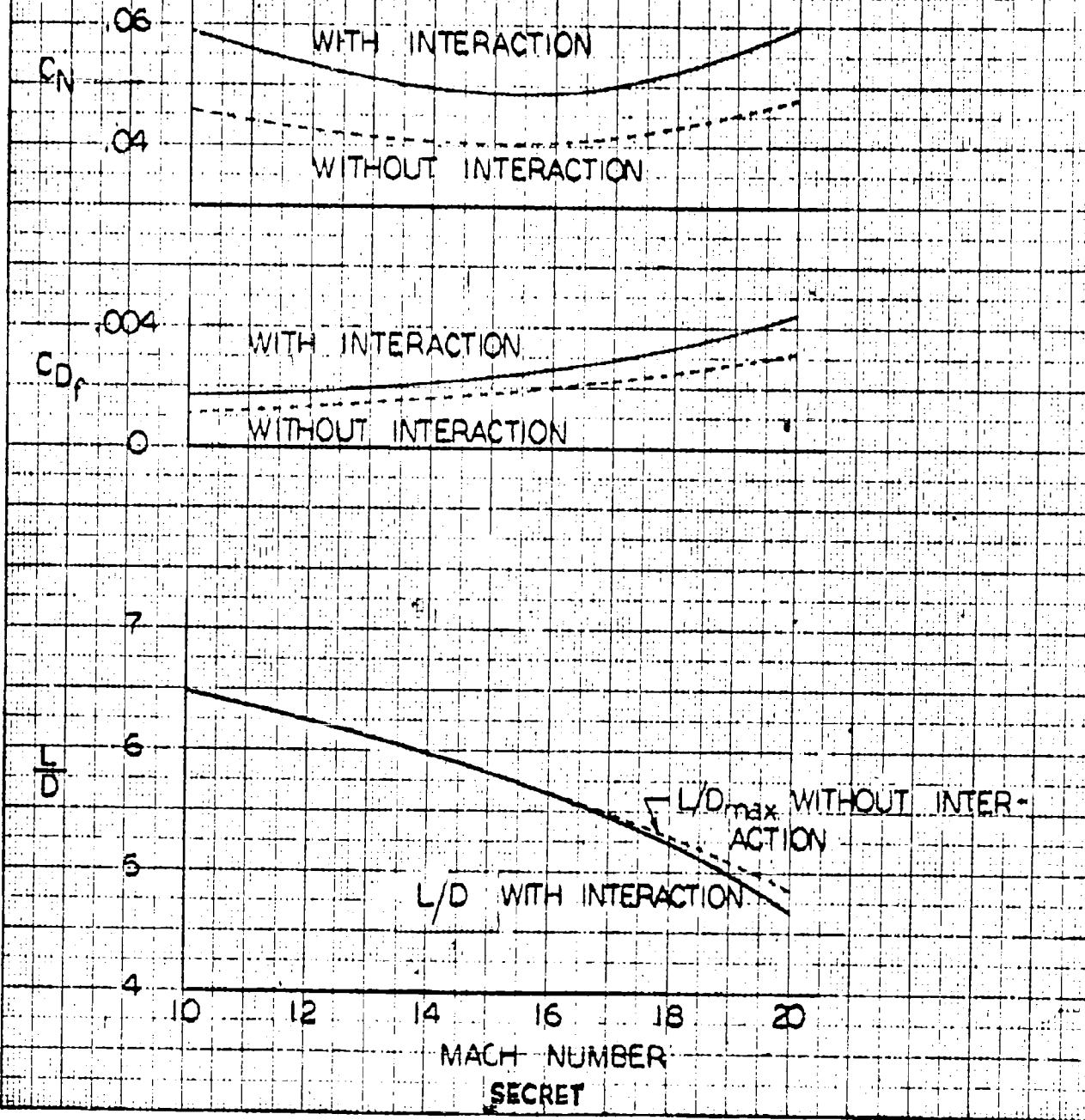


Figure 4.4-33

EFFECT OF SHOCK WAVE - BOUNDARY LAYER INTERACTION
ON WING AERODYNAMIC CHARACTERISTICS AT THE
CONDITIONS FOR MAXIMUM LIFT DRAG WITHOUT
INTERACTION



By _____ Date _____
 Checked _____ Date _____

BELL Aircraft CORPORATION

Model _____ Page 4-74
 Missile _____
 Airplane _____ Report D143-945-017

4.5 Flight Mechanics

The equations of motion of the vehicle have been analyzed in order to determine the effects of three-dimensional motion about a moving earth. While for preliminary evaluations of vehicle performance it is sufficient to consider only two-dimensional motion and to neglect earth motion, a more detailed study of the problems involved in hypersonic flight requires, as its foundation, equations which more accurately describe the motion of the vehicle. This is essential in both performance and stability analysis. It was the aim of this study not only to show the problems involved in obtaining satisfactory performance and stability, but also to indicate the difficulties which are encountered in attempting to analyze these factors. The detailed derivation of the equations of linear and angular motion is presented in Appendix 4B. As shown, these equations are highly complex and cumbersome to apply. The following sections present the results of some preliminary applications of these equations, in order to illustrate the significance of the new terms which appear. It is demonstrated that future studies should include considerable investigation of the equations in order to fully determine their significance in the design of a hypersonic vehicle.

4.5.1 Effects of Earth Rotation on Glide Range

In order to become more familiar with the new terms in the linear equations of motion and to demonstrate the differences in glide trajectories typical of the MX-2276 when great circle courses in various directions about the rotating earth are taken, several glide trajectories have been calculated with the aid of IBM computing machinery. A step-by-step integration of the equations using variable aerodynamic parameters results in a time-consuming process even with the aid of computing equipment. Since the same purpose of illustrating earth rotation effects is accomplished using constant aerodynamic parameters over the velocity range, typical constant values of wing loading, lift-drag ratio and lift coefficient for maximum lift-drag ratio were assumed for most of the calculations. These values were taken as $W/S = 22.0$, $L/D = 4$ and $C_L = 0.09$.

For flight about the equator the calculation of the glide trajectory reduces to a two-dimensional problem since for this case the Coriolis and centrifugal forces act in the vertical directions. For flight to the east the Coriolis force adds to centrifugal force, reducing the lift required for any given velocity and hence reduces the drag, thereby increasing the glide range. For flight to the west the opposite effect occurs and the glide range is reduced accordingly. The results of these calculations are presented in figure 4.5.1-1 together with the glide range which is obtained from the assumed parameters when the rotation of the earth is neglected ($\Omega = 0$). It is apparent from these results that the earth rotation has a strong

By _____ Date _____	BELL <i>Aircraft</i> CORPORATION	Model _____	Page 4-75
Checked _____ Date _____		Missile _____ Airplane _____	Report DL43-945-012

effect on the range of a hypersonic glide vehicle in east-west flight. For the given assumptions and for an initial velocity of 22,000 feet per second relative to the surface of the earth, a 25% increase in range results for flight about the equator to the east, and a 15% reduction in range results for flight to the west as compared to the range calculated for a nonrotating earth.

Flight about the poles of a rotating earth results in a three dimensional problem since in this case components of the centrifugal and Coriolis forces act along both the normal and lateral axis of the vehicle. For this condition then, glide range may be calculated in several ways. First, the flight of the vehicle may be conducted so that the angle of roll is maintained at zero value. For this case it is then necessary to yaw the vehicle in order to provide the lateral forces with which flight is maintained on a great circle polar path. The disadvantage of this approach is that the vehicle will most likely be less efficient in generating aerodynamic forces in yaw than in generating lift forces (i.e. $Y/D \ll L/D$), hence some penalty will be paid in order to maintain a zero roll angle great circle path. The other alternative for such a path is to utilize increased lift force to overcome the lateral components of centrifugal and Coriolis forces. This will require rolling the aircraft to some bank angle so that the vertical component of lift force will maintain the desired glide path while the horizontal component of lift force is employed to maintain the desired great circle path. Calculation of either of these paths requires a highly detailed computational program. An insight to the effects of earth rotation on great circle polar flight can be obtained however, with the assumption that total drag is given by the expression

$$D = \frac{(L + Y)}{\left(\frac{L}{D}\right)_{\text{Max.}}}$$

where

D = total drag

$\left(\frac{L}{D}\right)_{\text{Max.}}$ = maximum lift-drag ratio

L = lift for maximum L/D

Y = side force required to maintain the great circle polar path at zero roll angle

While this assumption is conservative to some extent, it serves to illustrate the effects on glide range. The results of IBM glide range computation using the above expression, and the previously assumed aerodynamic parameters are presented in figure 4.5.1-2 together with the glide range about a non-rotating earth. These results

By _____ Date _____

Checked _____ Date _____

BELL Aircraft CORPORATION

Model _____ Page 4-76

Missile _____ Report D143-945-012
Airplane _____

together with the previous results for east-west flight, demonstrate the large effect of earth rotation on the glide range of a hypersonic vehicle and indicate, particularly for flight at or near an east-west direction, that these effects must be considered in designing a hypersonic glide vehicle to meet specified performance requirements.

4.5.2 High Altitude Trajectories

In general the heat transfer from the boundary layer to the adjacent aircraft surface decreases as the local airflow density is decreased. From this it is indicated that the heat transfer will decrease with increases in flight altitude, which suggests that the MX-2276 temperature problems might be alleviated to some extent if higher flight paths than originally proposed are taken. There are several ways of achieving flight paths at altitudes higher than the original MX-2276 path (flight where the altitude is determined by the lift coefficient for maximum L/D); increasing the altitudes by (1) decreasing the wing loading, (2) increasing the lift coefficients, or (3) by flying a partial lifting path above the original equilibrium path.

An indication of the effects of wing loading on heat transfer can be obtained in the viscous heating section of this report wherein temperatures of the third stage of MX-2276 are presented with and without the bomb (see section 4.6). However, because the wing loading of the present configuration is already quite low (less than 25 psf), the second and third methods have been given the most consideration.

Figure 4.5.2-1 presents an example of the effect of increasing the angle of attack, and thus the lift coefficient, thereby increasing the glide altitude at a given velocity. The convective heating and equilibrium temperatures shown were estimated from the method outlined in Appendix 4A, and are for the one foot station of the wing. This point was chosen as more significant in the study of the overall heating problem, since the temperatures of the leading edge stagnation points will be considerably affected by changes in altitude (see Section 4.6), the leading edges present a localized problem, while the heat transfer of such surfaces as the wings and the body presents the generalized problem. The effects of shock-boundary layer interaction were not included and it was assumed that flow on the upper wing surface continues to expand with increasing altitude, although separation of the flow is actually quite probable. It will be noted that the more severe lower surface temperature is not significantly relieved by increasing the altitude through increasing the angle of attack. This is because the local lower surface pressure and velocity remain nearly the same through the angle of attack and altitude variations, since the lift force required to support the vehicle is essentially constant with altitude at a given velocity. While the upper surface temperature and heating are considerably reduced, these are

By _____	Date _____	BELL <i>Aircraft</i> CORPORATION	Model _____	Page <u>4-77</u>
Checked _____	Date _____		Missile _____	Report <u>DH3-945-012</u>
			Airplane _____	

relatively less critical than for the lower surface. Increasing the angle of attack from 8° , which is approximately the angle for maximum L/D (and thus represents the condition we wish to improve) to 15° yields a relatively small decrease in the total heating. The penalty in making such a change is shown by the range curves calculated for constant 8° and 15° angle of attack, the 8° curve approximating the maximum L/D glide range. These curves are presented in Figure 4.5.2-2. The loss of 3000 miles range for an initial glide speed of 22,000 fps appears to be a large penalty for the heating reduction obtained, particularly since the more critical lower surface temperatures and heating are not appreciably reduced. Some improvement in the range might be attained by programming the angle of attack from 15° to 8° as the heating falls off with decreasing velocity, but an inspection of the variation of temperature with altitude indicates that the critical heating range may extend down to 10,000 to 12,000 fps and programming back to the angle of attack for maximum L/D below these velocities would bring only a small gain in range. Apparently, then increasing angle of attack is generally disadvantageous. However, the results of the above work are preliminary since the effects of shock-boundary layer interaction have not been included. From the results of the studies of shock-boundary layer interaction discussed in Section 5.3, it is apparent that heat transfer, lift, drag and lift drag ratio will be affected, in particular the lift coefficient for maximum L/D. The methods have been derived from which an evaluation of this affect may be made - however, it was not possible to do so within the time period of the present study.

The third method of achieving higher altitude flight, the partial lifting path, requires that the initial flight path angle be greater than the initial angle for a maximum L/D glide, since by the very nature of the partial lift path, the flight path angle will be decreasing rapidly at the outset. Increases in the initial flight path angle can be easily attained by programming the ascent path to the desired final angle. Such a program will in itself result in a higher initial altitude. Thus at first glance the partial lift path appears advantageous. This advantage disappears however, when the results of the trajectory calculations presented in Figure 4.5.2-3 are studied. These results were obtained from an IBM integration of the equations of linear motion for a non-rotating earth. For these calculations, the lift coefficient and lift-drag ratio for an angle of attack of 8° were chosen. Shown in this figure are the first 700 seconds of an equilibrium glide and also the trajectory for a final ascent path angle (initial partial lift path angle) of 0.75° . As would be expected, the initially inclined partial lift flight path degenerates very quickly into an oscillation about the equilibrium glide path and approaches the well known skip trajectory. In this respect, the partial lift path possesses the disadvantages of the skip path wherein high loads, temperatures and heat fluxes are encountered at the bottom of the oscillation. For example, at $t = 250$ secs. on the partial lift path,

By _____ Date _____
 Checked _____ Date _____

BELL Aircraft CORPORATION

Model _____ Page 4-78
 Missile _____
 Airplane _____ Report D113-945-012

based on the NACA standard atmosphere, assuming laminar flow and an emissivity of 0.9, the equilibrium wall temperature at the one foot point of the bottom surface would be of the order of 2100°F while at the same time, and for the same conditions, the equilibrium wall temperature on the glide path would be about 1870°F.

The only method which might possibly reduce the temperatures and loads in the partial lift paths would be to make the first descent very long so that the first pull out would be accomplished near the end of flight. This, however, would require unreasonably high initial altitudes and final ascent path inclinations approaching the values of a ballistic path. While the effects of shock-boundary layer interaction have not been included in this study of partial lift paths - it is doubtful that any significant changes would result since the inherent nature of the path would be unchanged.

4.5.3 Flight Path Heading Control

In order to accomplish a given mission, that is, to deliver the hypersonic vehicle between two designated points on the surface of the earth, it is necessary to arrive at a means by which the vehicle may be guided between the specified positions. The problem is complicated by the rotation of the earth, which in effect means that a vehicle which is guided to a specific point on the surface of the earth is being directed at a target which is moving in space. It may be most convenient to accomplish this navigation by conventional means, that is, for flight between two designated points to follow the connecting path of a great circle on the surface of the earth.

In the trajectory study section it was indicated that flight about a great circle which is inclined with respect to the earth's equator results in components of the centrifugal and Coriolis forces that lie along the lateral axis of the vehicle. It was pointed out in that section that a possible method of countering these lateral forces lies in rolling the vehicle to a bank angle wherein the horizontal component of lift force balances the Coriolis force components. The feasibility of such a program depends upon the degree of roll angle and the amount of lift required, since it must be remembered that increasing lift results in increasing temperatures on the lifting surfaces, while excessive roll angles may have an adverse effect upon the guidance equipment. An expression for the roll angle, when the lateral aerodynamic force is zero, can be obtained from the linear equations of motion. From equation 4B-17b for $Y/M = 0$, $\gamma = 0$

$$\tan \phi = \frac{v \dot{\xi} - 2V \Omega \cos \lambda - r \Omega^2 \sin \lambda \cos \lambda - \frac{V^2}{r} \cos \xi \cot \lambda}{g - \frac{V^2}{r} - 2V \Omega \sin \lambda \cos \xi - r \Omega^2 \sin^2 \lambda} \quad (1)$$

By _____	Date _____	BELL Aircraft CORPORATION	Model _____	Page 4-79
Checked _____	Date _____		Missile _____	Report D113-945-012
			Airplane _____	

now for the great circle path it can be shown that

$$\cos \xi_{G.C.} = \frac{\cos \xi_0}{\sin \lambda} \quad (2)$$

where the notation is that shown in Figure 4.5.3-2. Differentiating this expression results in

$$\dot{\xi}_{G.C.} = \left(\frac{\cos \xi_{G.C.} \cos \lambda}{\sin \xi_{G.C.} \sin \lambda} \right) \dot{\lambda}$$

however

$$\dot{\lambda} = \frac{V}{r} \sin \xi$$

so that

$$\dot{\xi}_{G.C.} = \frac{V}{r} \cos \xi_{G.C.} \cot \lambda \quad (3)$$

Substituting these expressions into equation (1) gives the roll angle required to follow a great circle path with zero lateral aerodynamic force.

$$\tan \phi = \frac{-2V \Omega \cos \lambda - r \Omega^2 \cos \lambda \cos \xi_0}{g - \frac{V^2}{r} - 2V \Omega \cos \xi_0 - r \Omega^2 \sin^2 \lambda} \quad (4)$$

The maximum roll angle will occur at the highest velocity. Figure 4.5.3-3 presents the roll angle required to fly a great circle path at a velocity of 22,000 ft./sec. It is observed that at this velocity the maximum angle of roll which is required at any point on the surface of the earth is approximately 22 degrees. The determination of whether a roll angle of this magnitude is excessive or not will depend upon the characteristics of the guidance system.

The lift required to maintain the glide path when the vehicle is rolled to follow a great circle path may be determined as follows. If normal load factor is defined as

$$n = \frac{L + T \sin \psi}{g M}$$

By _____ Date _____
 Checked _____ Date _____

BELL Aircraft CORPORATION

 Model _____ Page 4-80
 Missile _____
 Airplane _____ Report D143-945-012

then for a glide path, where the thrust (T) is zero

$$n_N = \frac{L}{S M}$$

so that normal load factor is a direct expression of lift. Substituting this expression into equation (4B-17c) and together with equation (4B-17b) results (for $\gamma = 0$) in

$$g(n_N) \cos \phi = g - \frac{v^2}{r} - 2v\Omega \sin \lambda \cos \xi - r\Omega^2 \sin^2 \lambda \quad (5)$$

where the angle ϕ is defined by equation (1). For great circle flight then,

$$g(n_N)_{G.C.} \cos \phi_{G.C.} = g - \frac{v^2}{r} - 2v\Omega \cos \xi_0 - r\Omega^2 \sin^2 \lambda \quad (6)$$

where the angle $\phi_{G.C.}$ is defined by equation (4). The value of $n_{N,G.C.}$

which is determined from equation (6) is presented in Figure 4.5.3-4 for a velocity of 22,000 feet per second. As can be seen from these results, the value of $n_{N,G.C.}$ which is required for great circle flight

is greatly influenced by the inclination of the great circle. It is interesting to compare this with the load factor which is obtained when rotation of the earth is neglected, in which case any great circle path may be followed at zero roll angle and with a load factor given by

$$n_N = 1 - \frac{v^2}{gr}$$

which is identical with the load factor obtained for a rotating earth at the values $\lambda = 0^\circ$, $\xi_0 = \pm 90^\circ$. The extreme values of load factor in banked flight about a great circle on a rotating earth can be seen to differ by $\pm 38\%$ from the non-rotating earth load factor at $V = 22,000$ fps.

The above discussion has been concerned only with the load factors which are required for banked flight about a given great circle. Since it will be highly probable that deviations from a desired flight path along a great circle will occur due to cross winds, guidance errors, etc., or that a given flight plan will call for changes in the great circle path, an investigation of the ability of the vehicle to change heading is in order. In equation (1), ξ may be expressed as

$$\dot{\xi} = \dot{\xi}_{G.C.} + \Delta \dot{\xi} \quad (8)$$

By _____ Date _____

BELL Aircraft CORPORATION

Model _____ Page 4-81

Checked _____ Date _____

Missile _____
Airplane _____ Report D143-945-012

where $\dot{\xi}_{G.C.}$ = rate of change of ξ to follow a great circle path
 $\Delta \dot{\xi}$ = rate of turn from an instantaneous great circle

Substituting this expression into equation (1), rearranging and utilizing equation (4) results in

$$\tan \phi = \frac{V \Delta \dot{\xi}}{g - \frac{V^2}{r} - 2V\Omega \cos \xi_0 - r\Omega^2 \sin^2 \lambda} + \tan \phi_{G.C.} \quad (9)$$

The normal load factor required to hold $\delta = 0$ in the turn may be deduced from figure 4.5.3-1.

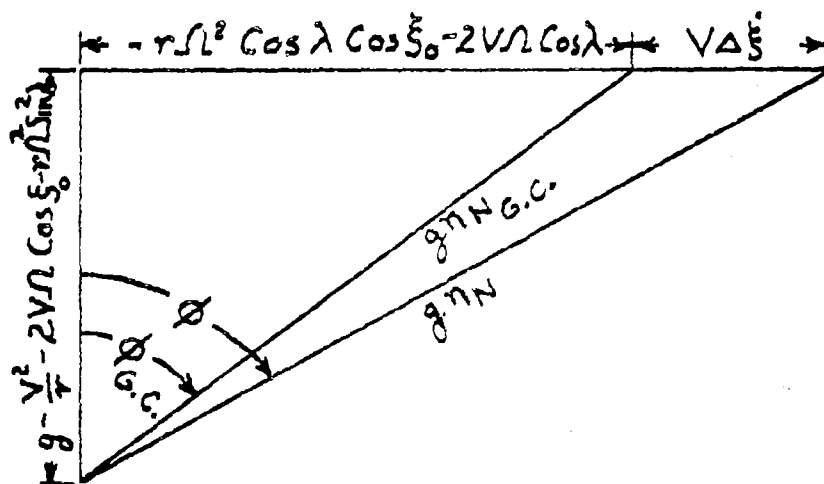


Figure 4.5.3-1

from this figure, it is seen that

$$(g_{NN})^2 = (g_{NN_{G.C.}})^2 + (V\Delta \dot{\xi})^2 - 2(g_{NN_{G.C.}})(V\Delta \dot{\xi}) \cos (90 + \phi_{G.C.})$$

or

$$(g_{NN})^2 = (g_{NN_{G.C.}})^2 + (V\Delta \dot{\xi})^2 + 2(g_{NN_{G.C.}})(V\Delta \dot{\xi}) \sin \phi_{G.C.} \quad (10)$$

SECRET

By _____ Date _____

Checked _____ Date _____

BELL Aircraft CORPORATION

Model _____ Page 4-82
Missile _____
Airplane _____ Report D143-945-012

but

$$\sin \theta_{G.C.} = - \left(\frac{1}{g n_{G.C.}} \right) (r \Omega^2 \cos \lambda \cos \xi_0 + 2V \Omega \cos \lambda) \quad (11)$$

combining equations (10) and (11) and solving for n_N gives

$$(n_N)^2 = (n_{G.C.})^2 + \left(\frac{V \Delta \xi}{g} \right)^2 - \left(\frac{V \Delta \xi}{g} \right) \left(\frac{r \Omega^2 \cos \lambda \cos \xi_0 + 2V \Omega \cos \lambda}{g} \right) \quad (12)$$

which is the normal load factor in a level flight, coordinated banked turn ($Y/M = 0, \delta = 0$) from an instantaneous great circle path. As an example of the maneuverability which can be expected for given normal load factors, figure 4.5.3-5 presents the rate of turn ($\Delta \xi$) as a function of the ratio of normal load factor in a turn to normal load factor for banked great circle flight, for flight at the equator, and where the initial heading is toward the poles (i.e. $\lambda = 90^\circ, \xi_0 = \pm 90^\circ$). From these results it is evident that a considerable increase in normal load factor (and hence lift) is required to obtain even moderate turning rates, as would be expected for hypersonic flight. While the magnitude of normal load factor is not large by conventional standards - it presents a serious problem for a hypersonic vehicle since it occurs in a flight regime wherein temperatures and loads are already critical. Further study is required into the details of flight path programming, flight path errors, and temperature and load limitations before a full evaluation of the maneuvering capabilities of a hypersonic glide vehicle can be made.

SECRET

EFFECT OF EARTH ROTATION ON GLIDE RANGE
 EQUATORIAL FLIGHT ($\lambda = 90^\circ$) Figure 4.5-1-1

(L/D) ASSUMED CONSTANT AT 4.0

C_L FOR (L/D) ASSUMED = .09

$W/S = 22$

INITIAL EQUILIBRIUM ALTITUDE (V = 22,000)

EAST	250,000
$\Omega = 0$	234,000
WEST	223,000

RANGE - 1000'S NAUT MILES

FLIGHT TO EAST
 NO EARTH ROTATION ($\Omega = 0$)
 FLIGHT TO WEST

VELOCITY - 1000'S FT/SEC

EFFECT OF EARTH ROTATION ON GLIDE RANGE
 FLIGHT ON A GREAT CIRCLE THROUGH POLES
 ZERO BANK ANGLE

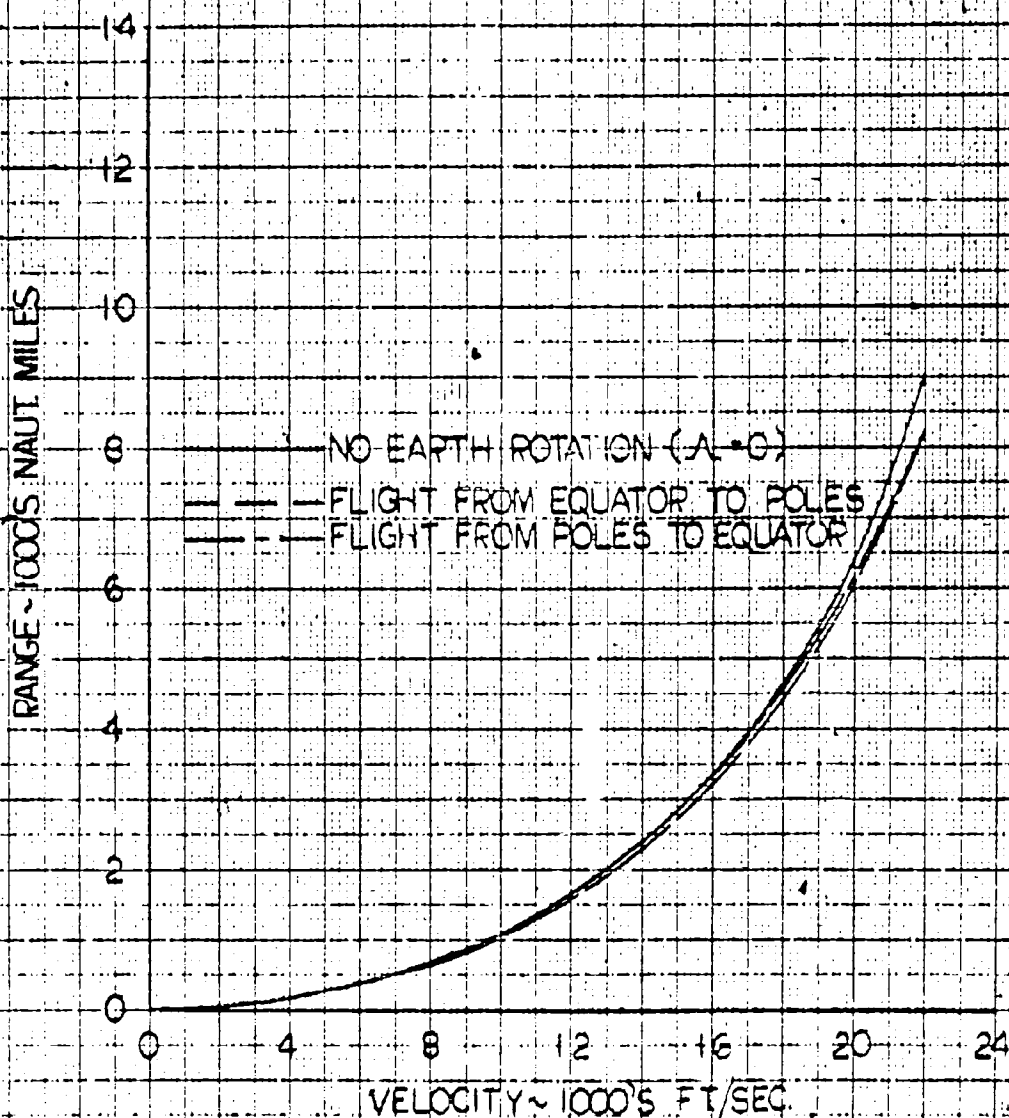
Figure 4.5.1-2

$(\frac{L}{D})$ ASSUMED CONSTANT AT 4.0

C_L FOR $(\frac{L}{D})$ ASSUMED = 0.9

$\frac{W}{S} = 22$

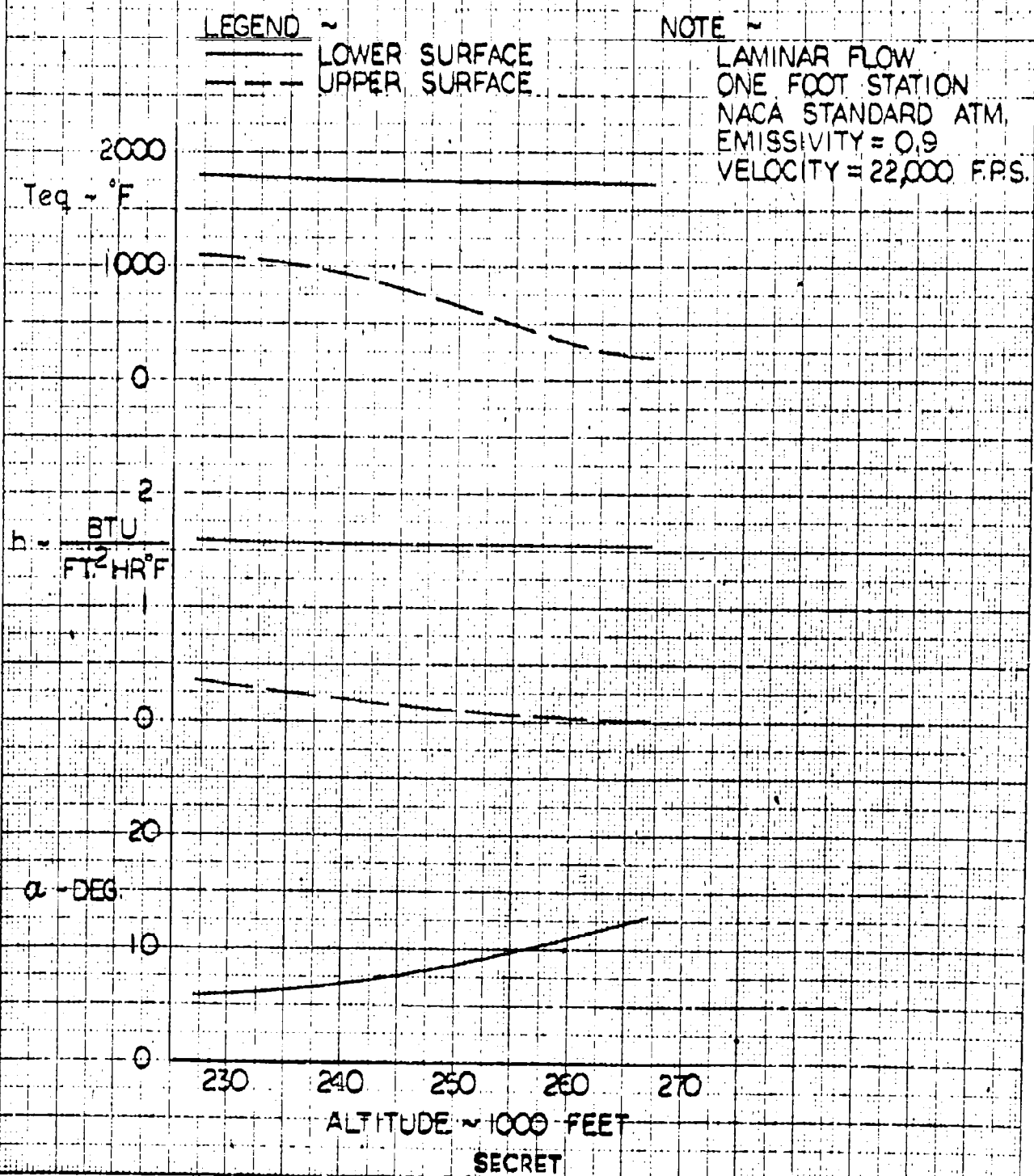
INITIAL ALTITUDE = 23,400 FT. AT $V = 22,000$



SECRET

MX 2276 STAGE III
EFFECT OF ALTITUDE ON EQUILIBRIUM TEMPERATURE
WITH CONSTANT LIFT AND AIRSPEED

Figure 4.5.2-1a



MX 2276 STAGE III

Figure 1.5.2-1b

EFFECT OF ALTITUDE ON BALANCED HEAT FLOW
WITH CONSTANT LIFT AND VELOCITY

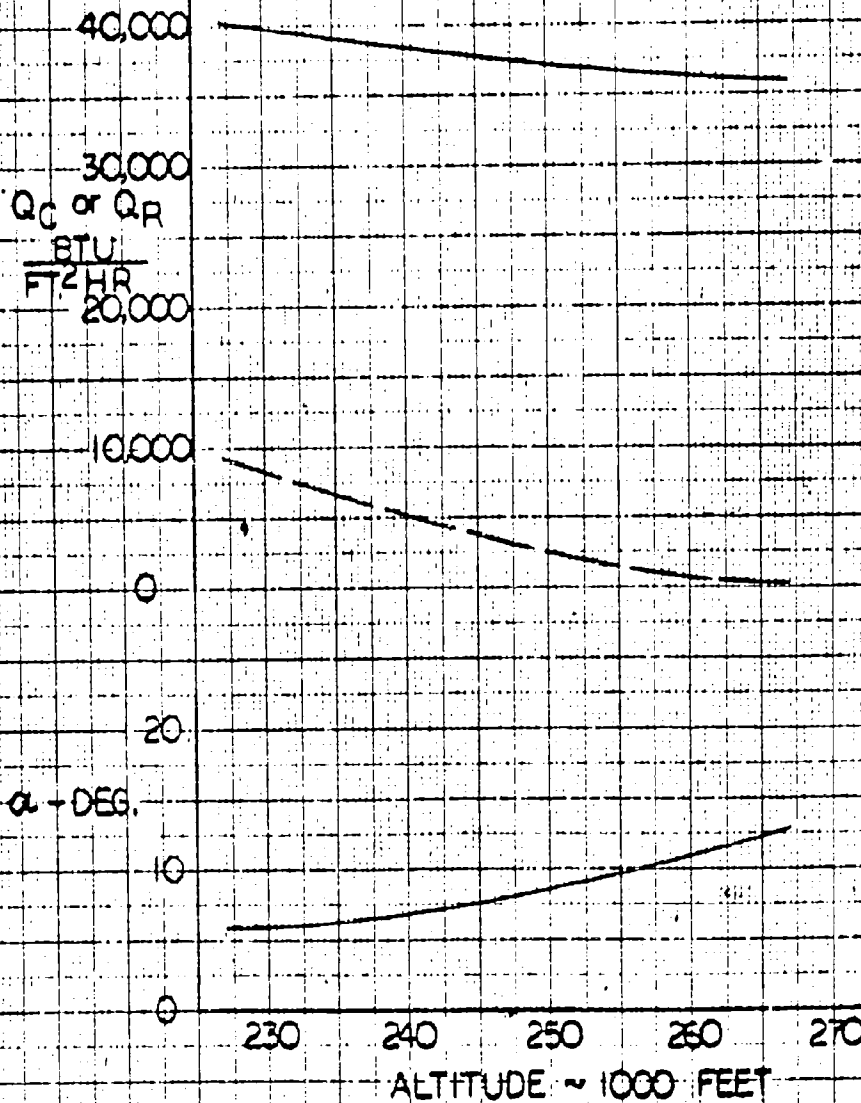
$(Q_C = Q_R)$

LEGEND ~

—— LOWER SURFACE
--- UPPER SURFACE

NOTE ~

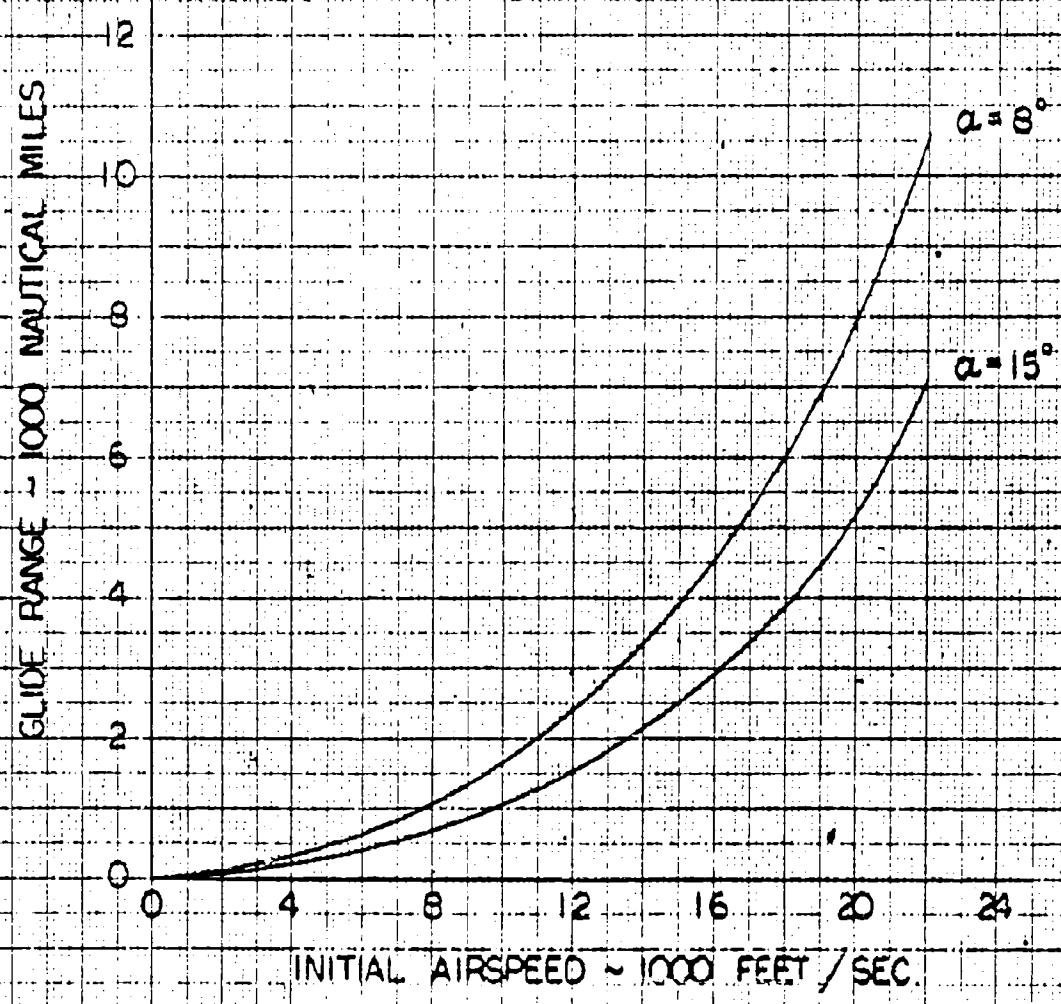
LAMINAR FLOW
ONE FOOT STATION
NACA STANDARD ATM.
EMISSIVITY = 0.9
VELOCITY = 22,000 FPS.



SECRET

MX 2276 STAGE III
EFFECT OF ANGLE OF ATTACK ON GLIDE RANGE
NACA STANDARD ATMOSPHERE

Figure 4.5.2-2



MX-2276 STAGE 3

Figure 4.5.2-3

COMPARISON OF PARTIAL LIFT AND GLIDE TRAJECTORIES

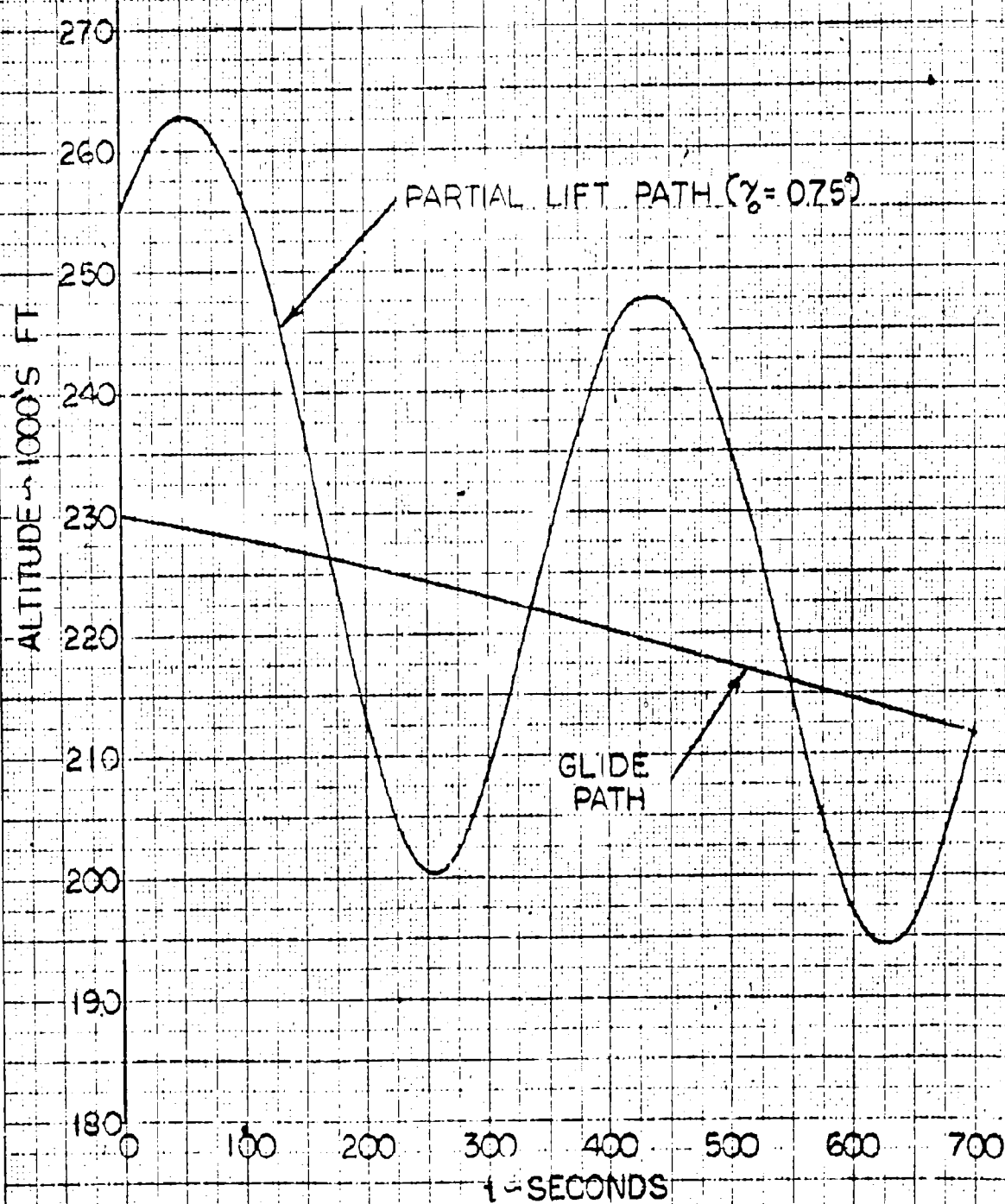
$$\alpha = 8^\circ$$

$$\Omega = 0$$

$$V_0 = 22000 \text{ FT SEC}$$

$$W/S = 22$$

NACA STANDARD ATMOSPHERE



SECRET

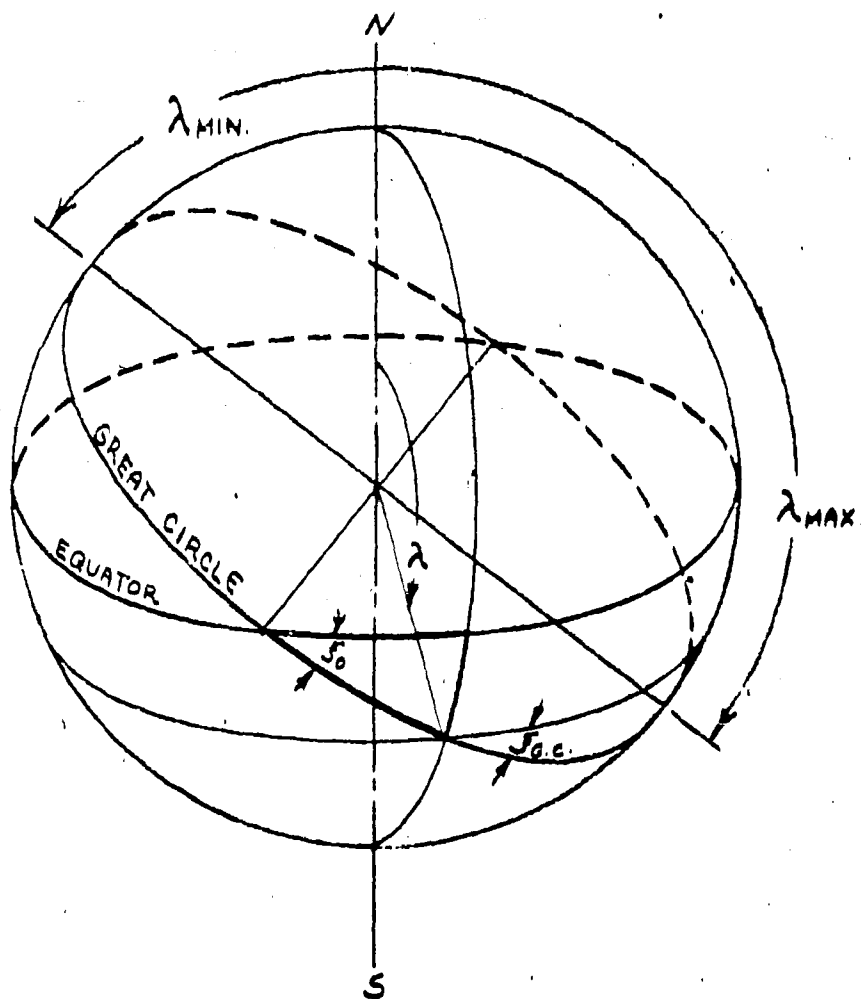
BY _____ DATE _____
CHECKED _____ DATE _____

SECRET
BELL *Telephone* CORPORATION

MODEL _____ PAGE **4-89**
AIRPLANE _____ REPORT **D143-945-012**

Figure 4.5.3-2

ORIENTATION OF GREAT CIRCLE



Form 4.5.3-2 Rev. 1049

SECRET

Figure 4.5.3-3

MX-2276 STAGE 3

BANK ANGLE FOR GREAT CIRCLE FLIGHT

$V = 22,000$ FT./SEC

$\gamma = 0$

$h = 200,000$ FT

$\gamma/M = 0$

λ_{MIN}
 $\lambda = 30^\circ$

$\lambda = 60^\circ$

$\lambda = 90^\circ$ (EQUATOR)

$\lambda = 120^\circ$

$\lambda = 150^\circ$

λ_{MAX}

$\xi \sim \text{DEGS}$

ϕ - BANK ANGLE - DEGS

SECRET

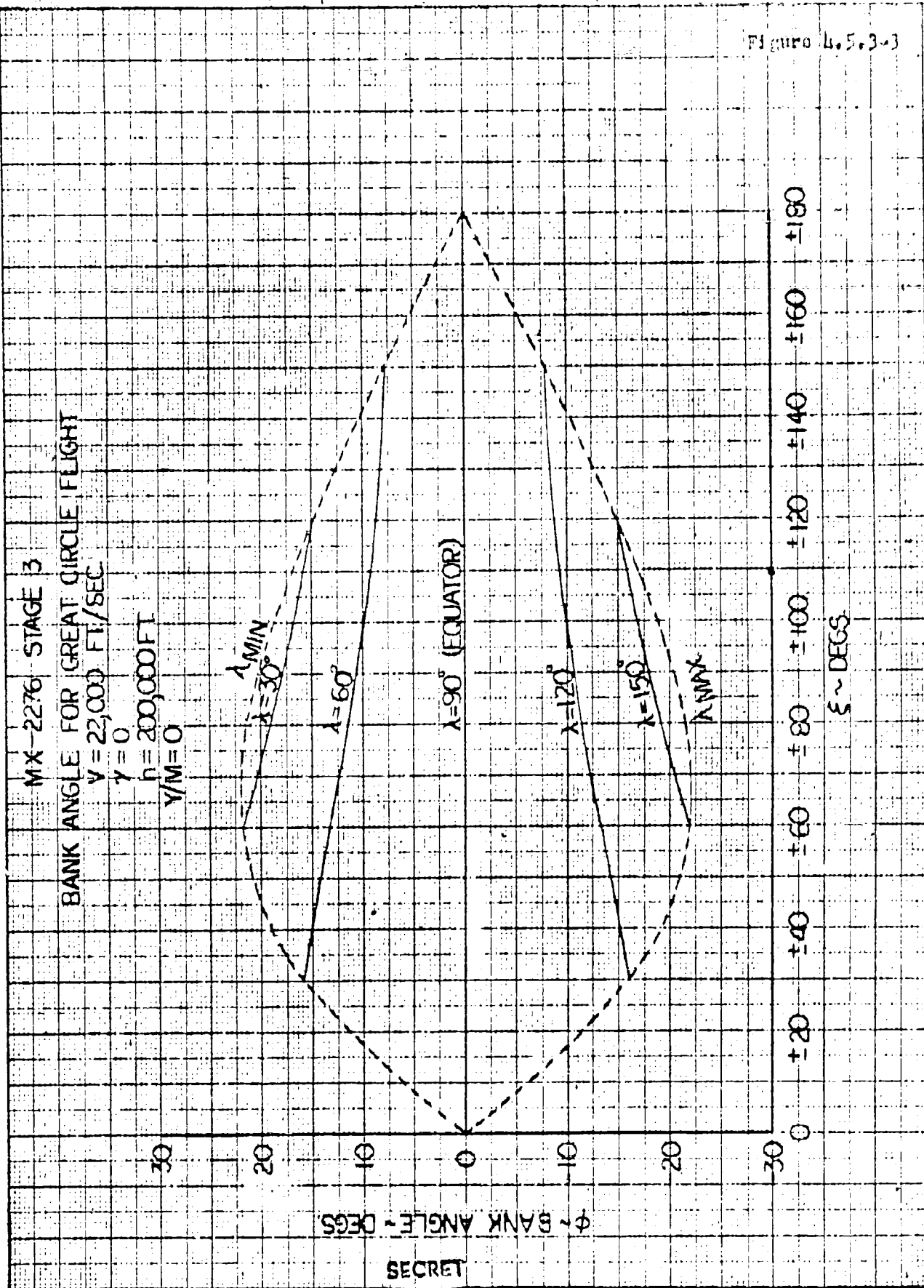


FIGURE 4.5.3.1

MX-2276 STAGE 3
 NORMAL LOAD FACTOR FOR BANKED
 GREAT CIRCLE FLIGHT
 $V = 22,000 \text{ FT/SEC.}$

$\gamma = 0$
 $h = 200,000 \text{ FT}$
 $\gamma/N = 0$

$\lambda = 30^\circ, 150^\circ$
 $\lambda = 60^\circ, 120^\circ$
 $\lambda = 90^\circ \text{ (EQUATOR)}$

4

3

n_{NGC}

2

1

0 $\pm 20^\circ$ $\pm 40^\circ$ $\pm 60^\circ$ $\pm 80^\circ$ $\pm 100^\circ$ $\pm 120^\circ$ $\pm 140^\circ$ $\pm 160^\circ$ $\pm 180^\circ$
 ϕ - DEGS

MX-2276 STAGE 3
RATE OF TURN FROM AN INSTANTANEOUS
GREAT CIRCLE
V = 22000 FT/SEC.

Figure L.5.3.3

$\gamma = 0$
 $\lambda = 90^\circ$
 $\xi_0 = \pm 90^\circ$
 $h = 200,000$ FT

$\Delta \dot{\xi}$ ~ RATE OF TURN FROM AN INSTANTANEOUS GREAT CIRCLE ~ DEG/SEC

± 14
 ± 12
 ± 10
 ± 08
 ± 06
 ± 04
 ± 02
 0

$\frac{\eta_N}{\eta_{NCG}}$ ~ RATIO OF NORMAL LOAD FACTORS

By _____ Date _____
Checked _____ Date _____BELL *Aircraft* CORPORATIONModel _____ Page 4-93
Missile _____
Airplane _____ Report D1143-945-01

4.6 Aerodynamic Heating

4.6.1 Problem Area

Aerodynamic heating of the structure at the hypersonic conditions necessary to achieve the desired performance poses a severe problem to the MX-2276 system. The heating rates will be high; wall temperatures near the upper working limits for even the best materials must be endured and in certain areas cooling will be needed. Thus accurate prediction of the aerodynamic heating is required. However, the speeds and flow conditions contemplated are generally beyond present experience. In order to estimate the aerodynamic heating parameters it is necessary to extend the present method of analyses beyond the speeds and conditions at which there is any data to substantiate their accuracy. In view of this, during the study considerable effort was expended on prediction of heat transfer parameters and on the effects of the various phenomena that may be encountered as a result of the hypersonic flight.

Herein are presented estimations of wall and leading edge temperatures and transpiration cooling requirements pertinent to the flight of Stage III. The methods adopted or derived for predicting these quantities are described or referenced and some of the qualifications as to their use and validity are discussed.

The major aerodynamic heating problem exists during the glide portion of the MX-2276 path. Because of the high speeds and relatively slow decelerations in the glide, i.e. long duration of flight, the Stage III vehicle was the most extensive object of the analysis during this study. Transient effects are important in Stage I because of the high rates of acceleration and deceleration giving a short flight time; however, the maximum speed conditions of this stage are relatively low, Mach number 5 at 70,000 feet, and a more conventional structure, less limited by temperature in choice of materials, could be used for this configuration. Stage II temperature problems did not appear serious enough to merit an investigation in this study because its time of flight is also very short and it is expendable at end of boost.

The walls of the Stage III vehicle are considered to be of a sandwich type construction, i.e. a cool primary structure separated from a thin outer skin. Transient effects for such an outside skin are not significant so that the results given in this section pertain to equilibrium temperatures associated with various sections of the vehicle over its glide path.

By _____ Date _____

BELL Aircraft CORPORATION

Model _____ Page 4-94

Checked _____ Date _____

Missile _____ Airplane _____ Report D113-945-012

4.6.2 Viscous Heating

4.6.2.1 The Heat Balance Equation

Wall temperatures and heat transfer to aircraft surfaces are determined from a summation of the heat flux both into and away from the surface. For the case of the wall isolated from the rest of the structure, where heat is neither conducted into or away from the surface, the heat fluxes which must be considered are those which result from convection or radiation. It is generally considered that the heat fluxes which are involved are those which result from convection from the boundary layer into the wall, radiation from the surrounding environment into the wall and radiation from the wall to surrounding environment. This may be expressed in a general equation of heat balance per unit area of surface as*

$$h_c(T_r - T_w) + \alpha G - \epsilon \sigma T_w^4 = 3600 \text{ wcy } \frac{dT_w}{dt}$$

which equates the total heat flux to the rate of change of wall temperature. The condition wherein heat flux into the surface is balanced by heat flux out (hence the wall temperature remains constant) is referred to as the condition of equilibrium wall temperature. For this case the heat balance equation reduces to

$$h_c(T_r - T_w) + \alpha G - \epsilon \sigma T_w^4 = 0$$

where the term $h_c(T_r - T_w)$ expresses the heat convected into the wall from the boundary layer, αG represents the heat radiated, both solar and nocturnal, into the wall from the surrounding environment and the term $\epsilon \sigma T_w^4$ expresses the heat radiated out from the wall.

4.6.2.2 Radiation

It should be noted that the equation as presented (and which was employed in the analysis reported in this section) does not allow for radiation of heat from the hot boundary layer to the wall. An investigation of this source of heat flux has been initiated during the present study and is discussed in detail in Section 5.4. A preliminary evaluation of this quantity has indicated that it may have important effects and should receive further consideration in future studies.

For the present study, the weighted mean average of solar and nocturnal radiation is small and was generally neglected. It may be

* The symbols employed here are defined in Appendix 4A

By _____ Date _____
 Checked _____ Date _____

BELL *Aircraft* CORPORATION

Model _____ Page 4-95
 Missile _____
 Airplane _____ Report DL43-945-012

observed that the remaining radiation term, $\epsilon \sigma T_w^4$, is highly influenced by the emissivity, ϵ , of the surface and should receive careful consideration. A value of $\epsilon = 0.9$ was generally used throughout this study. This is a high value but it appears to be attainable for certain surfaces as indicated in References 4.6-1 and 4.6-2; however, more research on the problem is definitely necessary as it may materially affect the vehicle design. The effects of varying emissivity are illustrated later in this section.

4.6.2.3 Convection from Viscous Heating

The convective heat flux into the surface is governed by the compressible heat transfer coefficient, h_0 . A review of the literature and discussion with research agencies has disclosed several methods for evaluating this coefficient. For laminar boundary layer flow, exact solutions for the compressible heat transfer coefficient have been obtained which are generally considered as reliable throughout the range of temperature conditions wherein the properties of air are adequately known at present. However, due to the current lack of understanding of the mechanism of turbulent flow, similar solutions for the compressible turbulent boundary layer do not exist.

Approximate methods are available which combine theoretical and empirical results to obtain solutions which have been shown to give good results for both laminar and turbulent flow. The method chosen for this study makes use of the well known constant property relations for incompressible laminar and turbulent flow and extends these to the supersonic and hypersonic regions by evaluating the air properties at a weighted mean reference temperature, T' , which occurs within the boundary layer. A brief exposition of this method, hereafter referred to as the T' method, is given in Appendix 4A. In the strictest sense, this method is only applicable to two dimensional flow over a flat plate with zero streamwise pressure and temperature gradients. The method applies directly to two-dimensional flow over a wedge with no temperature gradient however, if the local stream conditions are used. It has been found also, that similarity exists between cone flow and flat plate flow, and that when conditions on the surface of the cone are used a correction of $\sqrt{3}$ times the resulting plate coefficients for laminar flow and 1.15 times the plate coefficients for turbulent flow gives good results for flow over the cone. The flow along the surface of a cylinder can be approximated closely by direct application of the flat plate method at the local conditions, as long as the radius of the cylinder remains large with respect to the thickness of the boundary layer.

As was noted above, the method assumes zero streamwise pressure and temperature gradients. The surface shapes contemplated for the MX-2276 are generally very thin or slender and for such shapes, the available compressible flow results have shown the effects of pressure

By _____ Date _____
 Checked _____ Date _____

BELL Aircraft CORPORATION

Model _____ Page 4-96
 Missile _____
 Airplane _____ Report D143-945-012

gradient on skin friction and heat transfer to be small (see References 4.6-3 and 4.6-4) except in the immediate vicinity of the leading edges of the wing and the nose of the body where large changes in profile shape occur. Heat transfer to these surfaces are treated later in this section. For the remainder of the surfaces where changes in profile shape are small, it appears that the effects of pressure gradient may be neglected.

The effects of streamwise temperature gradient on heat transfer coefficient have also been examined. A typical example of the streamwise variation of the equilibrium wall temperature in the vicinity of a leading edge in laminar flow is given by

$$T_w = T_r (.333 - .646 x^* + .792 x^{*2} - .3125 x^{*3})$$

where

$$T_r = 6000^\circ\text{R}$$

$$x^* = \frac{x}{l}$$

Using this variation of wall temperature in the method of Reference 4.6-5, which is essentially reproduced in Reference 4.6-4, showed no significant change from the heat transfer coefficient obtained for a constant wall temperature. This result appears somewhat contrary to the results obtained by Chapman and Rubesin in Reference 4.6-5. However, the example presented therein is unrealistic for a vehicle of the type of MX-2276, since in order to point up the importance of temperature gradient along the wall, a wall temperature higher than the recovery temperature was assumed. On the basis of this investigation, it was concluded that temperature gradient does not significantly alter the overall heat flux within the laminar flow region; however, further investigations are required in the region of boundary layer transition, at body and wing shoulders, and regions of attachment of the outer skin to the primary structure where large local gradients may exist and may have an effect on the heat flux in these local areas.

At the hypersonic speeds under consideration the heat generated within the boundary layer will be sufficient to produce dissociation of the air components. The resultant dissociated gas mixture will have different physical properties from normal air and would alter the boundary layer heat transfer mechanism to the skin. A preliminary study has been carried out to investigate the effects of equilibrium dissociation of air on the characteristics of the compressible laminar boundary layer over a flat plate when the wall temperature is assumed uniform and below dissociation temperatures (Section 5.4). The results show that the skin friction and the heat transfer are essentially unaffected by dissociation although the thickness of the

By _____ Date _____

BELL

CORPORATION

Model _____ Page 4-97

Checked _____ Date _____

Missile

Airplane

Report D143-945-012

boundary layer is reduced and the maximum temperature in the layer is considerably decreased. Thus, extension of the present method into ranges where dissociation may occur appears to be a reasonable expedient, since for structural reasons the wall temperatures will necessarily be below air dissociation temperatures.

The previous discussion has outlined the method employed in this section to evaluate the compressible heat transfer coefficient and has considered the effects of pressure and temperature gradients and of dissociation of the air in the boundary layer. This method is based on a model of the flow which assumes that the flow can be described by the combination of an outer stream where the flow is essentially inviscid and an inner boundary layer where the viscous effects predominate. It is assumed that the pressures in the boundary layer are established by the outer stream and that no further interaction occurs. The flight of the third stage of the MX-2276, however, takes it into flow regimes where the boundary layers become very thick and where the interaction between the inviscid stream and the viscous boundary layer can no longer be neglected. In this regime the interaction between the boundary layer and the shock waves results in induced local pressure and shearing stress. This shock boundary layer interaction has been investigated in Section 5.3. In order to illustrate the effects of this interaction an example is presented later in this section. Since the presently available shock-boundary layer theory is not able to treat all the profile shapes involved in the MX-2276 vehicle, it has been necessary to neglect this effect in the general analysis.

In order to calculate the compressible heat transfer coefficient, it is necessary to establish the point at which the transition from laminar to turbulent boundary layer flow occurs. As discussed in Section 5.7, it is difficult to fix this transition point accurately. For this analysis transition of the boundary layer was assumed to occur at a local stream Reynolds number of 2.8 million as was done in the performance studies. This is perhaps a rather conservative estimate of the location of transition. If the transition Reynolds number were increased to say 10 million, which seems to be indicated by some test results, it would reduce the heating by an appreciable amount. This is demonstrated in the presentation of results. The local Reynolds number and the local stream conditions were determined from the inviscid shock and expansion theories relating local and free stream conditions, and the atmospheric conditions outlined in Section 4.3.

4.6.2.4 Results of Analysis Using T' Method

The equilibrium temperatures for the one foot station both top and bottom of the wing for the Stage III glide are given in Figure 4.6.2-1. These are based on the flight plan for the 18,800# vehicle

given in Figure 4.4-30. Since the local stream Reynolds number is below 2.8 million for these stations over the entire glide path, the results for laminar flow are shown. The temperature of the bottom surface is highest at burnout and decreases with time. On the other hand, the temperature of the upper wing reaches a peak during the glide about 30 minutes after power shut off. The reasons for this are two-fold: (1) the angle of attack decreases which means there is a smaller angle of expansion and (2) the effect of expansion on local conditions is relatively lower per degree at lower Mach numbers.

A calculation was made to compare the temperature on the bottom of the wing at $M = 16$ on the 18,800 lbs. vehicle to the same point on the 14,600 lbs. vehicle (after bomb release). The temperature was reduced from 1825° to 1755°F which is a relatively small reduction compared to the 22% change in wing loading that was effected. This is due in large part to the fourth power radiation term in the heat balance equation. It also indicates that a large change in wing loading will be necessary to strongly influence the surface temperatures. Since the present wing loading is already near a practical minimum ($W/S = 30.6$ or 23.8 with or without payload respectively), further appreciable reduction in surface temperature by decreasing wing loading does not seem possible. Conversely, if subsequent design shows a larger wing loading is necessary, the accompanying temperature rise would be small. This reasoning, of course, applies particularly to the case of radiation cooling.

In order to give a representative picture of the equilibrium temperatures on the vehicle as a whole over the flight path, profiles of equilibrium temperatures at three specific Mach numbers for the 18,800 lbs. configuration have been computed. The particular flight conditions that were chosen are the following:

<u>TIME</u> <u>(sec)</u>	<u>MACH</u> <u>NUMBER</u>	<u>VELOCITY</u> <u>(ft./sec.)</u>	<u>ALTITUDE</u> <u>(ft.)</u>	<u>ANGLE OF ATTACK</u> <u>(degrees)</u>
10	20	20,640	198,000	7.7
27	16	17,200	172,000	6.8
52	10	10,680	140,000	6.4

Figure 4.6.2-2 gives equilibrium temperature profiles on the bottom of the body and wing for the three flight conditions discussed. The point of transition is shown in this and subsequent figures as being at a local stream Reynolds number of 2.8 million. For the bottom the transition point is located at 40, 18, and 9 feet for Mach numbers 20, 16, and 10 respectively. If the transition were delayed to $Re = 10$ million, it would materially reduce the heating problem as shown by the extension of the laminar curves beyond transition. In particular it would move the transition point back so that the bottom of the body would be completely laminar at $M = 20$, laminar back to 64 feet at $M = 16$, and 32 feet at $M = 10$. The method for determining the effective

By _____ Date _____

BELL *Aircraft* CORPORATION

Model _____ Page 4-99

Checked _____ Date _____

Missile _____
Airplane _____ Report D143-945-012

length for turbulent flow is outlined in the skin friction discussion. The effect of the steep temperature gradient on the heat flux in the region of laminar flow has been examined and a discussion appears above. In general it was found that the effects of this gradient are small.

The abrupt temperature rise shown at transition will not actually occur. Transition requires a finite length so that the increase should occur over an extended region. However, there is insufficient information available to define this region and its actual profile.

It should be noted that the maximum temperature experienced over the bottom of the body and wing is below 1800°F except for the first two feet. Also over the region of turbulence it should be noted that 1700°F is a representative maximum temperature for the higher speeds.

The wing upper surface temperature profile is shown in Figure 4.6.2-3. These temperatures were computed for the mean wing panel chords shown in this figure. In turning the corner at the intersection of the wedge and slab surfaces, the effective lengths which were added to the slab chord in the skin friction calculation were employed here also. The flow was laminar for all three Mach numbers. The dashed lines indicate the shoulder between the wedge and the slab for both inner (long chord) and outer panel. There is a marked gradient in temperature as a function of distance on the wedge varying from a maximum of 1300°F at the 6 inch station to about 800°F at the shoulder of the outer panel. It will be noted that there is a drop in temperature after the shoulder to about 200°F at the high Mach number and increasing to about 400°F at the Mach 10 condition.

The temperatures on top of the cone-body combination are shown in Figure 4.6.2-4. At the Mach number 20 condition, the flow is laminar for the entire length of the body. The discontinuity at 26.7 feet is due to the cone-cylinder shoulder. Transition occurs on the cone at 20 feet and 12 feet for the Mach number 16 and 10 conditions respectively.

The discontinuity in the temperature profiles at the wing upper surface break and body shoulder, would not occur in practice. It should be the subject of boundary layer and temperature gradient studies as detailed design will certainly be affected by the profile in these regions. Because the temperatures in these regions did not appear critical in overall magnitude this discontinuity was not considered further in the present study.

Finally Figure 4.6.2-5 gives the temperature profiles for the side of the body. These are very similar to the profiles for the top of the body, particularly regarding location of transition. The temperatures in front of the shoulder are very similar to those on the top of the cone. Behind the shoulder the side temperatures are considerably higher because the wall is essentially at zero tangency angle with the free stream, whereas the top is assumed to be in a region of 6° to 8° expansion.

By _____ Date _____

BELL Aircraft CORPORATION

Model _____ Page 4-100

Checked _____ Date _____

Missile _____ Airplane _____ Report D143-945-012

In order to illustrate the combined effects of varying body length, emissivity, and angle of attack on the temperature on the bottom surface, Figures 4.6.2-6 and 4.6.2-7 are presented for laminar and turbulent flow respectively. One particular flight condition at Mach number 20 was chosen for this representation. The effect of body length has been noted previously. The importance of the coefficient of emissivity of the aircraft surfaces is demonstrated. The selection of surface finish for the glide vehicle merits careful appraisal with respect to emissivity.

Angle of attack is a particularly significant parameter showing a variation of approximately 100°F per degree angle of attack for laminar flow. For turbulent flow this variation is about 150°F. In the light of this it is evident that maneuvers requiring additional angles of attack and control deflection may produce critical heating loads on the surfaces. It is apparent that pull-up and turns would be temperature limited rather than "g" limited; e.g. at the beginning of glide flight the aerodynamic lift provides about one third of the lifting force; therefore in order to provide a one "g" maneuver it would be necessary to increase the angle of attack greatly. Such an increase in angle of attack would be intolerable from a temperature standpoint.

4.6.2.5 Effect of Shock-Boundary Layer Interaction on Equilibrium Temperature

At hypersonic speeds it is known that the shock wave interacts with the boundary layer. This interaction is greatest at the nose or leading edge and decreases downstream. The magnitude of this interaction and its effect on equilibrium temperatures has been estimated from two dimensional analyses for the top and bottom of the wing aft of the six inch station at the angle of attack and equilibrium altitude for (L/D) maximum with no interaction. On the bottom surface the equilibrium temperature is increased by not more than 1.5% (40°F). On the upper surface the effect is considerable, there being an increase in temperature from 1100°F to 1800°F at the six inch station and Mach number 20. At lower Mach numbers and greater distances aft the shock-boundary layer interaction effect is not as great (Figure 4.6.2-8). Thus, within the limitations of the present flight path it may be concluded that the T' method appears to be in considerable error on the upper wing but gives good results on the compression surfaces, which are more critical temperature-wise.

In making the above calculations the method used for predicting interaction effects was that shown in Section 5.3. This gave the effect of interaction on the skin friction coefficient which was put in the form of a percentage increase over the basic Crocco coefficient. For the present flight path this effect can be applied to the heat transfer coefficient directly. The heat balance equation was modified to

$$\frac{c_{f,inter}}{c_{f,c}} \cdot h_c (T_r - T_w) + \alpha G - \epsilon \sigma T_w^4 = 0$$

By _____ Date _____
Checked _____ Date _____

BELL Aircraft CORPORATION

Model _____ Page 4-101
Missile _____
Airplane _____ Report D143-945-012

Use of the above approximate relation between skin friction and heat transfer is felt to be somewhat conservative in predicting interaction effects on the bottom and top surfaces.

It should be noted that the interaction effects shown for the wing top apply to the forward, wedge surface only; interaction effects on the upper surface after the shoulder were not investigated in the present study. Obviously this region will be affected, if only from alteration of the boundary layer at the shoulder by interaction on the forward wedge. Three dimensional interaction on the body cone and cylinder also were not treated during the present study, but effects of the same order of magnitude as for the wing surfaces would be expected for the same local compression or expansion conditions.

It was pointed out above that the comparison was made at the equilibrium altitude and angle of attack for (L/D) maximum with no interaction. Since shock-boundary layer interaction affects pressure distribution and hence lift at a given angle of attack, the angle of attack and equilibrium altitude for (L/D) maximum will change when interaction is considered (see Section 4.4). This effect has not been considered in detail in the present study and requires further consideration.

4.6.3 Leading Edge Heating

Temperatures and heat fluxes in the stagnation areas of leading edges and noses have been estimated for two conditions on the flight path presented in the performance section. These are shown in Tables 4.6.3-1. The estimations are based on an extension of the theory of Squire (Reference 4.6-16) for a cylindrical leading edge normal to the flow and the theory of Silbulkin (Reference 4.6-17) for a hemispherical nose and are discussed in more detail in Appendix 5B. The theories are for incompressible flow, it is assumed that they apply to the subsonic flows behind the normal shock waves at the leading edge and nose stagnation areas. Dissociation effects have not been included though the air temperatures behind the shock are certainly sufficient to produce some dissociation. At the present the dissociation properties of air are not well enough known to predict quantitatively how this process will be affected. However, it is not believed dissociation will tend to increase the temperatures shown.

The equilibrium temperatures are severe and indicate the necessity for either a super-material or considerable cooling. It is of interest that the smaller radii shapes produce the higher temperatures. It should be remembered that the temperatures and heat fluxes shown are only for areas near the stagnation points.

An extension of Silbulkin's theory has been proposed by Koshkin in Reference 4.6-18 to predict the heat transfer distribution from the stagnation point to the shoulder or 90° point on spheres and cylinders.

By _____ Date _____

BELL Aircraft CORPORATION

Model _____ Page 4-102

Checked _____ Date _____

Missile _____ Airplane _____ Report D243-945-072

This theory indicates a reduction in heat transfer coefficient from the stagnation point to the shoulder, as would be expected. However, this theory has not been evaluated in the present study. References 4.6-19 and 4.6-20 present the results of tests of hemispheres at Mach numbers of 1.90 and 4.87. These results also exhibit appreciable reduction in heat transfer coefficients from the stagnation point to the shoulder of the models. A number of low subsonic results show the average flux on cylinders from 0° to 90° to be 80% to 90% of the stagnation area flux.

The temperatures and heat fluxes in Table I are given for an unswept leading edge. In tests at $M \sim 7$ (unpublished) the NACA has found that the heat transfer to the front half of a cylinder is reduced by sweepback at a rate on the order of the cosine of the sweep angle, i.e. unit $Q_\Delta \approx \cos \Delta$. Since the relation between leading edge

$$Q_\Delta = 0$$

length and sweep is wing-span/ $\cos \Delta$, the total heat input is not reduced by sweep as is the local heating. Thus, it appears that, if the leading edges is to be cooled entirely by an internal coolant, sweepback in terms of necessary coolant is not a prime consideration. However, if significant radiation cooling is present, for a given surface temperature the total radiation will increase directly as the leading edge area increases with sweep (i.e. $A_\Delta / A_\Delta = 0 = \frac{1}{\cos \Delta}$

for a constant leading edge radius) and a definite overall gain is realized from sweep.

A parallel to the above can be seen in the effect of leading edge radius; the unit stagnation point heat transfer decreases with increasing radius so that the total radiation for a constant surface temperature would grow faster than the total heating. However, in this case the local heating does not increase inversely as the area increases as it does with sweep case - but at a lesser rate, and one must be specific about the relative magnitude of the radiation before a definite overall advantage can be stated. If the leading edge were almost completely cooled by radiation there would be a gain. Obviously the effect of leading edge radius on drag would become an important consideration here also.

It is evident from the temperatures and heat fluxes shown that leading edge heating will present one of the most severe aero-structural design problems. Emphasis should be placed upon it in future studies. It appears that cooling will be necessary. The transpiration cooling work done for the wedge surface areas should be extended to the leading edge case in view of the effectiveness of this method of cooling. The actual gains available from sweep and increased leading edge radius should be carefully examined and the aircraft shape assessed in that light.

By _____ Date _____
 Checked _____ Date _____
BELL *Aircraft* CORPORATION
 Model _____ Page 4-103
 Missile _____
 Airplane _____ Report D143-945-012
TABLE 4.6-1STAGNATION POINT CONDITIONSASSUMPTIONS

1. No Dissociation
2. Emissivity = 0.8

A. EQUILIBRIUM WALL TEMPERATURESFlight Pt.

<u>Model</u>	<u>h = 214,000 ft., M = 21.9</u>	<u>h = 172,000 ft., M = 16</u>
1/2-inch Sphere	6126°R	5828°R
2-inch Sphere	5237°R	5008°R
1/2-inch Cylinder	5929°R	5643°R
2-inch Cylinder	5064°R	4845°R

B. HEAT FLUX THROUGH SURFACE: (BTU/sq. ft.-sec.)

<u>Model</u>	<u>h = 214,000 ft, M=21.9</u>		<u>h = 172,000 ft, M = 16</u>	
	<u>T_w = 1500°R</u>	<u>T_w = 3000°R</u>	<u>T_w = 1500°R</u>	<u>T_w = 3000°R</u>
1/2-inch Sphere	720.6	628.6	657.2	550.7
2-inch Sphere	359.3	298.8	327.6	259.8
1/2-inch Cylinder	621.4	538.0	566.7	470.8
2-inch Cylinder	309.7	253.4	282.3	219.8

By _____	Date _____	BELL Aircraft CORPORATION	Model _____	Page 4-104
Checked _____	Date _____		Missile _____	Report D113-915-012

4.6.4 Transpiration Cooling

For the higher glide velocity conditions the temperatures for the first several feet of surface appear critical enough to require cooling. Transpiration cooling has been studied as a means of accomplishing this. In this method of cooling a coolant gas is passed through a porous outer skin into the boundary layer where it modifies the boundary layer flow profiles such that the heat transfer to the surface is reduced. The effectiveness of this method of cooling has been proven in low speed tests though there is virtually no quantitative experimental information at hypersonic speeds upon which estimates may be based.

A transpiration cooling theory has been developed in the present study and is discussed in some detail in the Applied Research Section, along with more background on transpiration cooling. The theory applies to a laminar boundary layer. This is most pertinent to the present case as transpiration cooling will most probably be confined to the severely heated areas near the leading edges where the flow is expected to be laminar. It is probable that the injection of relatively small amounts of coolant into the boundary layer will not destabilize the laminar flow. In the strict sense air must be used as the coolant because the theory is based on homogeneous boundary layer consideration for which the coolant and boundary layer flows must be of the same gas; but it is believed that a dissimilar coolant can be handled with sufficient accuracy through a simple extension of the present theory.

To evaluate the merit of transpiration cooling the quantities of air injection necessary to cool the first foot and the first 10 feet of the lower surface (though not the leading edge radius itself) to 1600°R have been estimated for the Stage III (18,800 lbs. G.W.) glide conditions. The average coolant flow per square foot for these conditions is shown in Figure 4.6.4-1. The total quantities of coolant air necessary are found to be 6.68 and 30.82 lbs. per square foot of surface cooled for the ten and one foot surface length respectively. Thus, for example, to cool the first foot of the approximately 40 foot span of the third stage 1230 lbs. of coolant air would be required. This is felt to be a practical quantity, in view of the relatively low arbitrary temperature of 1600°R which was chosen, and indicates the feasibility and effectiveness of this method of cooling.

There is considerable promise of further reduction in the coolant rate from the above through use of better coolants than air. Water may be much better because it adds a high heat of vaporization to the process. It is believed its use would at least halve the above coolant requirement. It is concluded that transpiration cooling definitely merits future development. The effects of shock-boundary layer interaction and slip flow, which may both be strong near the leading edge, are not accounted for in the present theory and should be included in future studies.

By _____	Date _____	BELL Aircraft CORPORATION	Model _____	Page 4-105
Checked _____	Date _____		Missile _____	Report 0143-945-012

Section 4.6 - References

- 4.6-1 McAdams, W.H.: Heat Transmission; McGraw Hill Book Company, Inc., Third Edition, 1954.
- 4.6-2 Johnson, H.A., et al: A Design Manual for Determining the Thermal Characteristics of High Speed Heat Transfer; University of California, Department of Mechanical Engineering Research Projects USAAF TR No. 5632, 1947.
- 4.6-3 Chapman, D.R. and R.H. Kester: Turbulent Boundary Layer and Skin Friction Measurement in Axial Flow Along a Cylinder at Mach Numbers Between 0.5 and 3.6; NACA TN 3097, March 1954.
- 4.6-4 Eckert, E.R.G.: Survey of Heat Transfer at High Speeds; WADC Technical Report No. 54-70, April 1954.
- 4.6-5 Chapman, R. and M.W. Rubesin: Temperature and Velocity Profiles in the Compressible Laminar Boundary Layer with Arbitrary Distribution of Surface Temperature, Journal of the Aeronautical Sciences, Vol. 16, No. 9, pp 587-595, 1949.
- 4.6-6 William, E.P., L.W. Drones, J.H. Humbziokar, R.J. Lew, H.A. Lieski, L.L. Moore, and G.B.M. Young: Long Range Surface-to-Surface Rocket and Rocket Missiles - Aerodynamics; The Rand Corporation, Report 181, 1 May 1950.
- 4.6-7 Kumm, E.L.: Engineering Considerations in Supersonic Heat Transfer; (Talk), Redstone Arsenal, Aerophysics Development Corporation, 7 April 1954.
- 4.6-8 Rubesin, M.W. and H.A. Johnson: A Critical Review of Skin Friction and Heat Transfer Solutions of the Laminar Boundary Layer of a Flat Plate; Transactions of the American Society of Mechanical Engineers, Vol. 71, No. 4, pp 385-388, 1949.
- 4.6-9 Sommer, Simon C. and B.J. Short: Free Flight Measurements of Skin Friction of Turbulent Boundary Layers with High Rates of Heat Transfer at High Supersonic Speeds; Institute of Aeronautical Sciences, Preprint No. 518, January 1955.
- 4.6-10 Van Driest, E.R.: Investigation of Laminar Boundary Layer in Compressible Fluids Using the Crocco Method; NACA TN 2597, January 1952.
- 4.6-11 --: NBS - NACA Tables of Thermal Properties of Gases; U.S. Department of Commerce, National Bureau of Standards.

By _____	Date _____	BELL Aircraft CORPORATION	Model _____	Page <u>4-106</u>
Checked _____	Date _____		Missile _____	Report <u>D143-945-012</u>
			Airplane _____	

- 4.6-12 Van Driest, E.R.: Turbulent Boundary Layer in Compressible Fluids; Journal of the Aeronautical Sciences, Vol. 18, No. 3, pp 145 - 160, 216, March 1951.
- 4.6-13 Sieff, A., S.C. Sommer, and B.J. Short: Some Free Flight Measurements of Turbulent Skin Friction and Heat Transfer at High Supersonic Speeds; NACA Conference on Aerodynamics of High Speed Aircraft, July 1953.
- 4.6-14 Lobb, R.K., E.M. Winkler, and J. Persh: Experimental Investigation of Turbulent Boundary Layers in Hypersonic Flow; Institute of the Aeronautical Society, Preprint No. 452, January 1954.
- 4.6-15 Eggers, A.J., Jr.: One Dimensional Flow of an Imperfect Diatomic Gas; NACA TN 1861, 1949.
- 4.6-16 Goldstein, L.: Modern Developments in Fluid Dynamics, first edition, Vol. 2, p 631, Oxford University Press, London (1938).
- 4.6-17 Sibulkin: Heat Transfer Near the Forward Stagnation Point of a Body of Revolution, Journal of the Aeronautical Sciences, Vol. 19, No. 8, August 1952, pp. 570-571.
- 4.6-18 Korobkin, I.: Discussions of Laminar Heat Transfer Coefficients for Spheres and Cylinders in Incompressible Flow, Paper present at A.S.M.E. Fall Meeting in Milwaukee, Wisc., 9 September 1954.
- 4.6-19 Gruenewald, K.H. and Lobb, R.K.: New Laminar and Turbulent Heat Transfer Data applicable to Practical Body Shapes for High Mach Number Flight, Preprint of the Third Naval Symposium on Aerobalistics, Technical Session IV, 20 October 1954.
- 4.6-20 Stine, H.A. and Waulass, K.: Theoretical and Experimental Investigation of Aerodynamic Heating and Isothermal Heat Transfer Parameter on a Hemispherical Nose with Laminar Boundary Layer at Supersonic Mach Numbers, NACA TN 3344, December 1954.

Best Available Copy

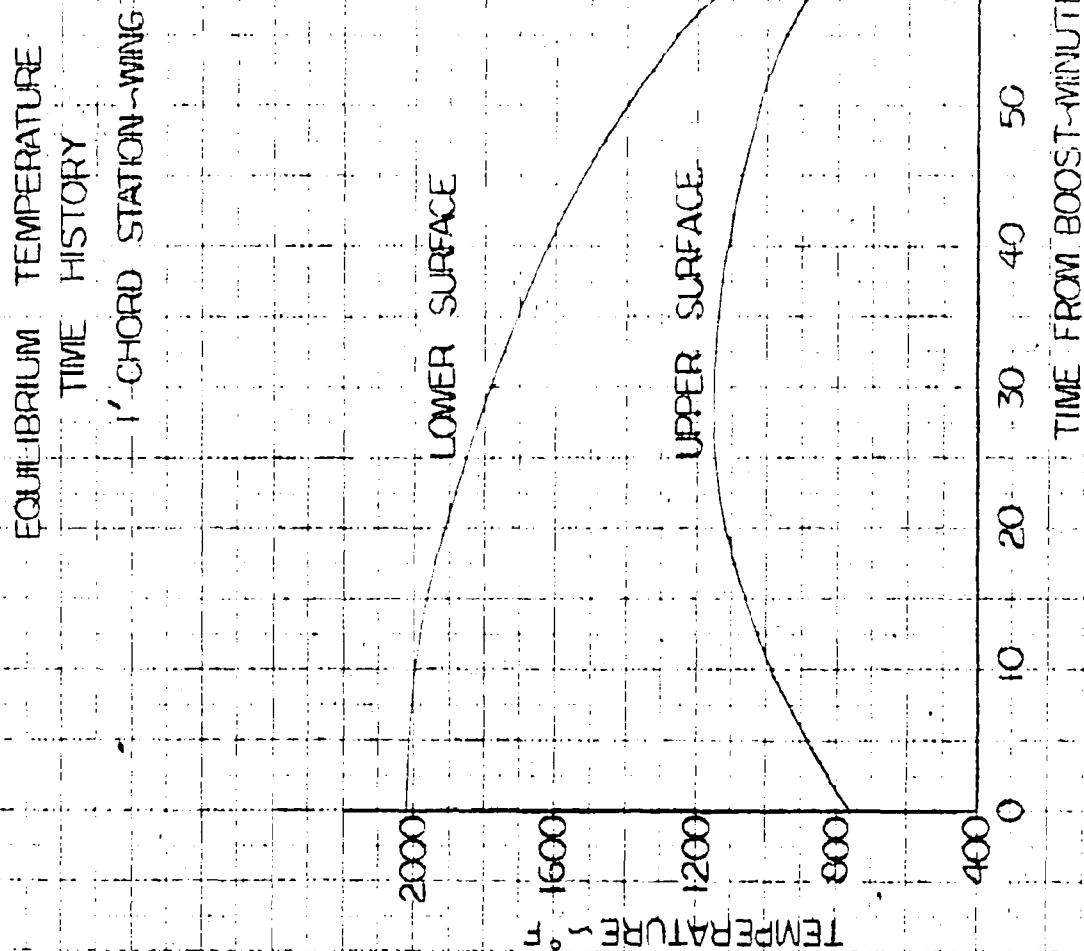
SECRET

BY _____ DATE _____
CHECKED _____ DATE _____

BELL Aircraft ENGINEERING

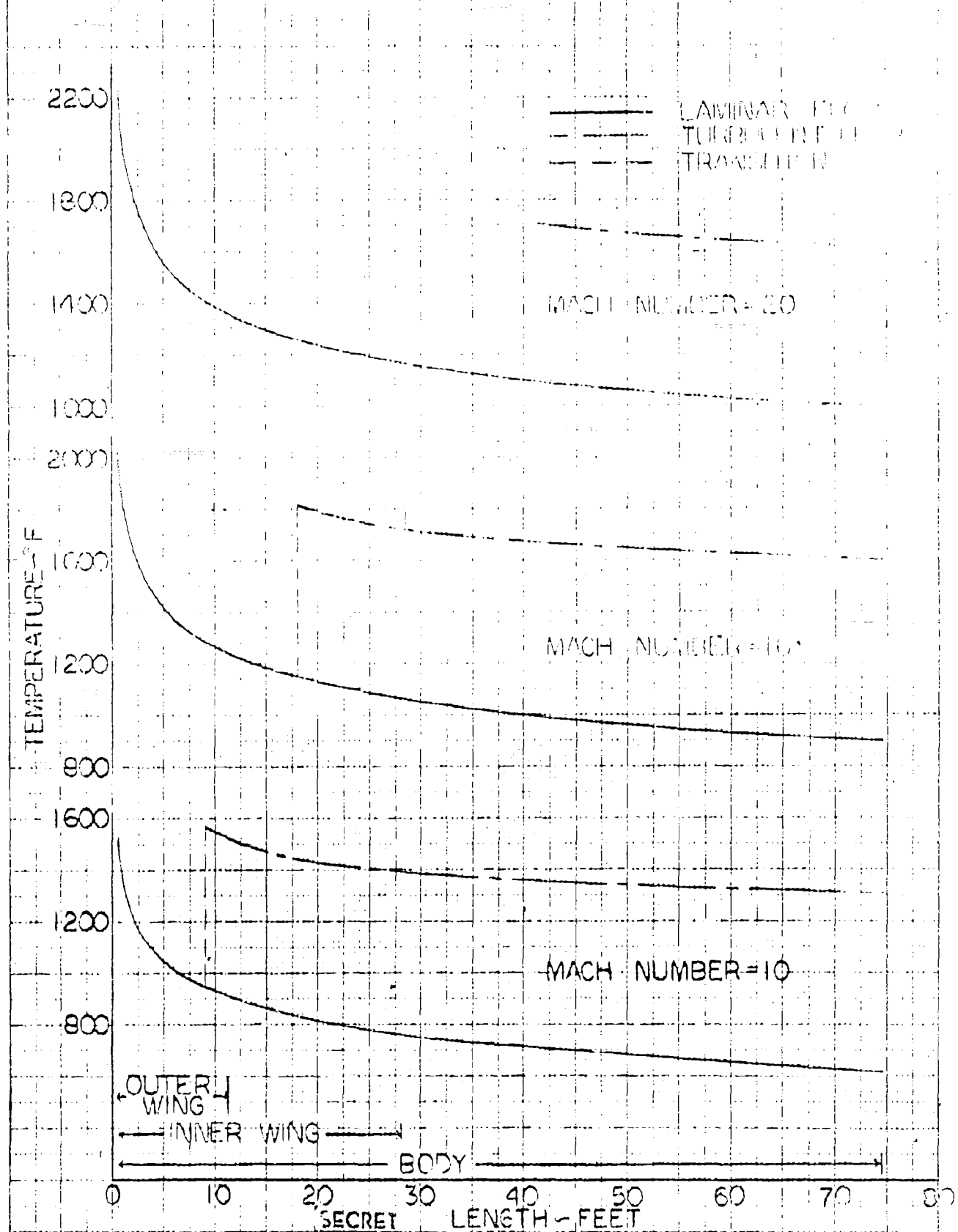
MODEL _____ PAGE 1-107
SHIP _____ REPORT 1113-915-100

Figure 4.6.2-1



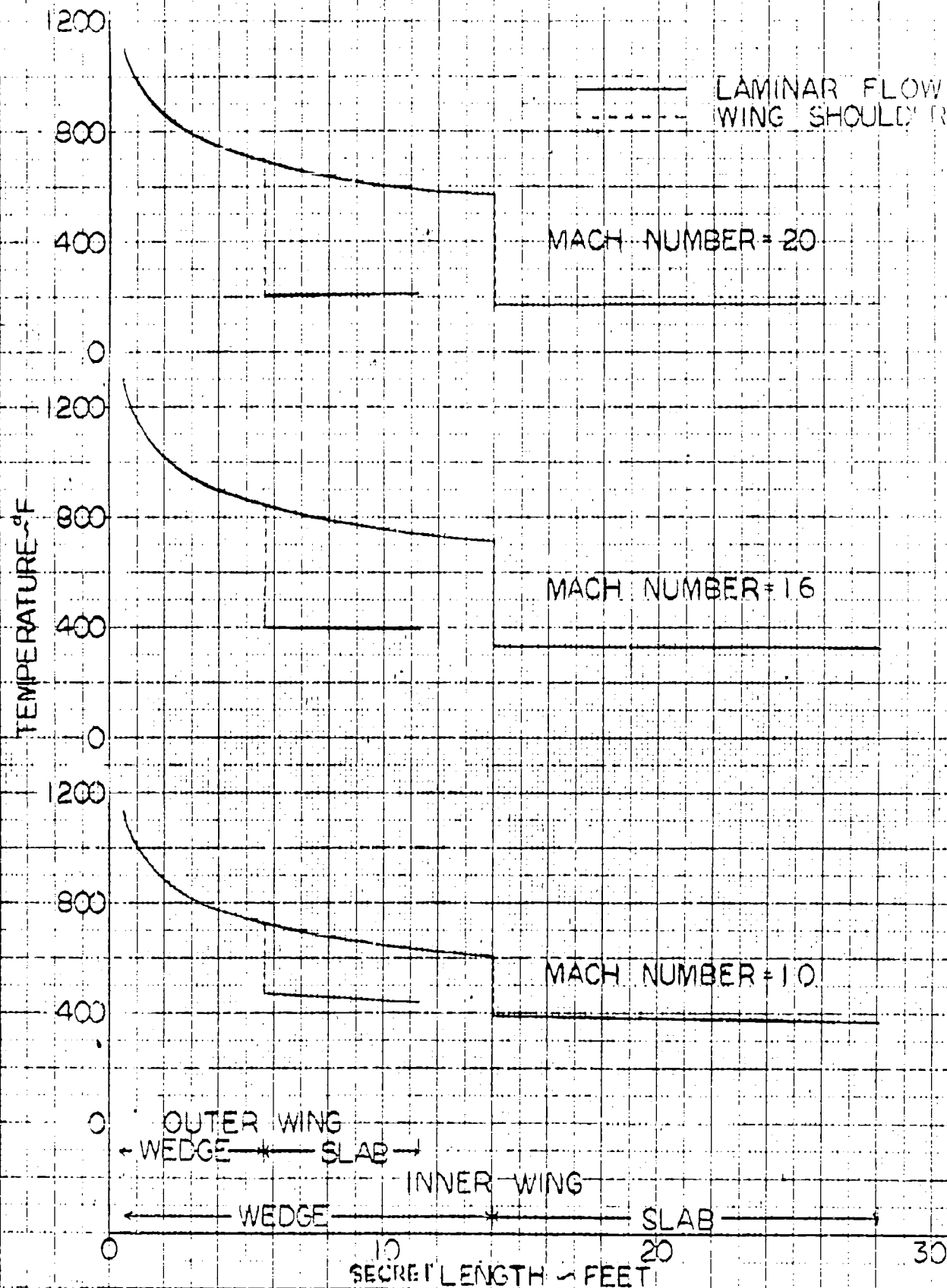
SECRET

EQUILIBRIUM TEMPERATURE BOTTOM OF BODY AND WING



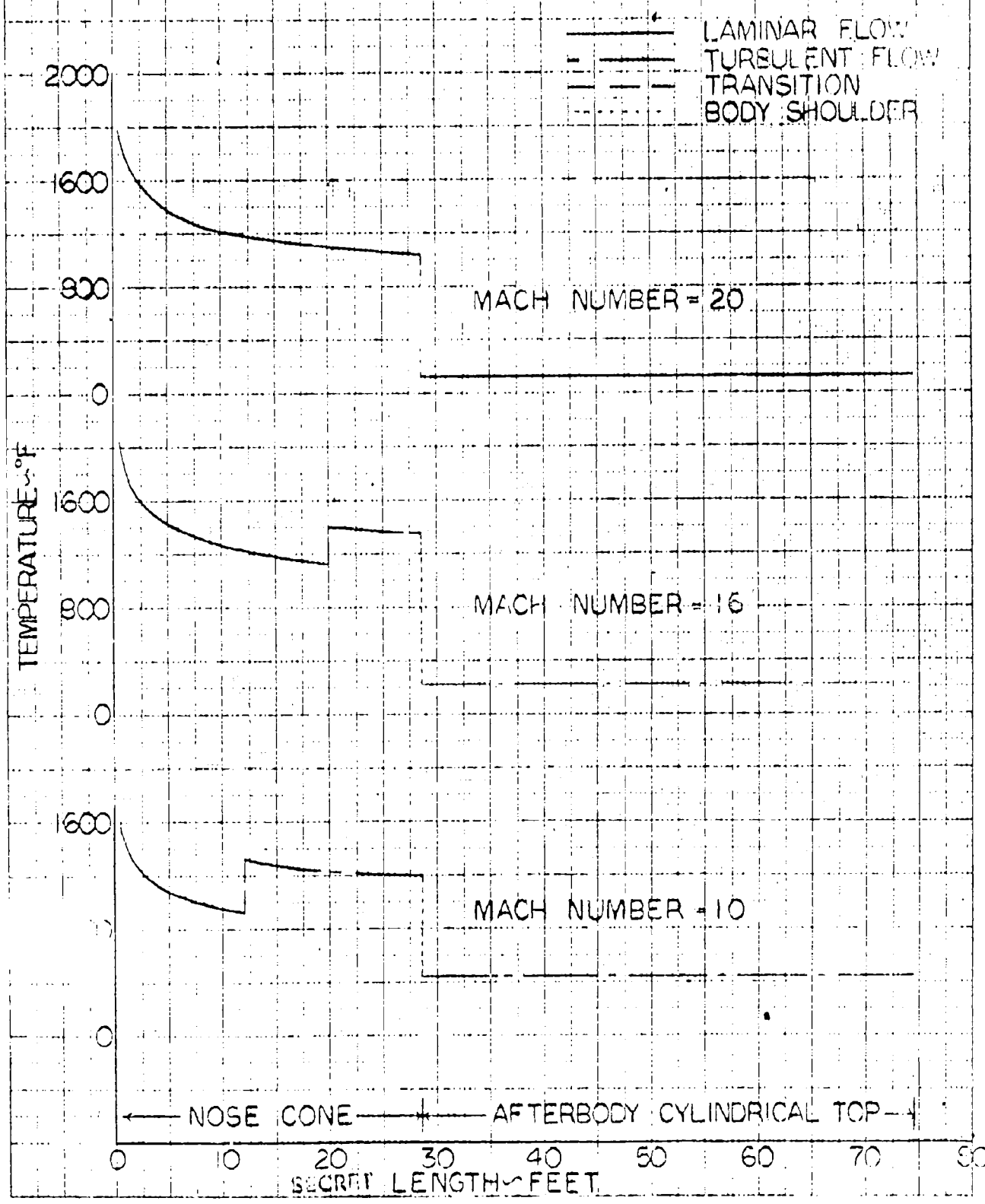
EQUILIBRIUM TEMPERATURE TOP OF WING

Figure 4-109



EQUILIBRIUM TEMPERATURE
TOP OF BODY

Figure 4.6.1-4

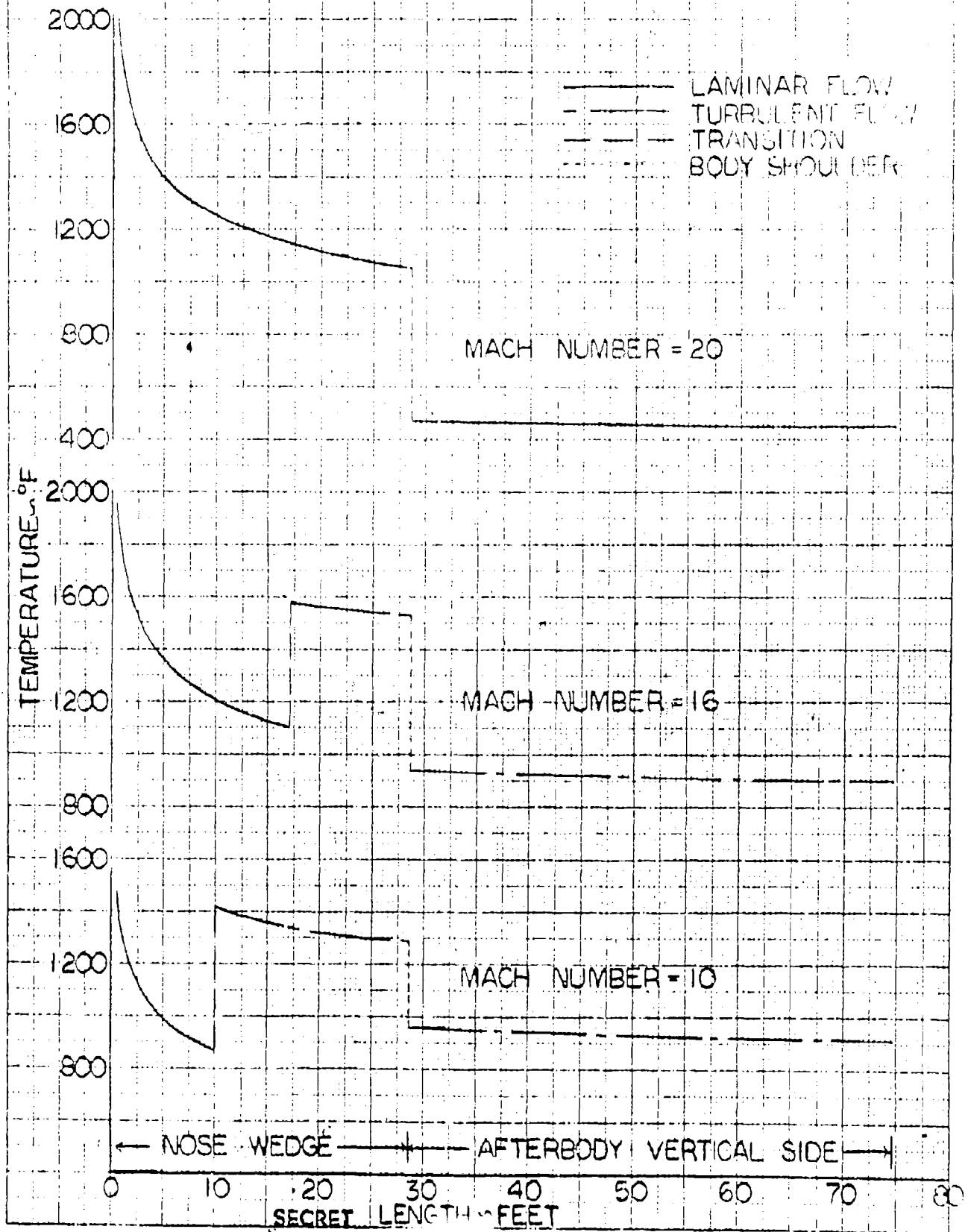


BY _____ DATE _____
 CHECKED _____ DATE _____

SECRET
BELL Aircraft CORPORATION

MODEL _____
 SHIP _____
 REPORT _____

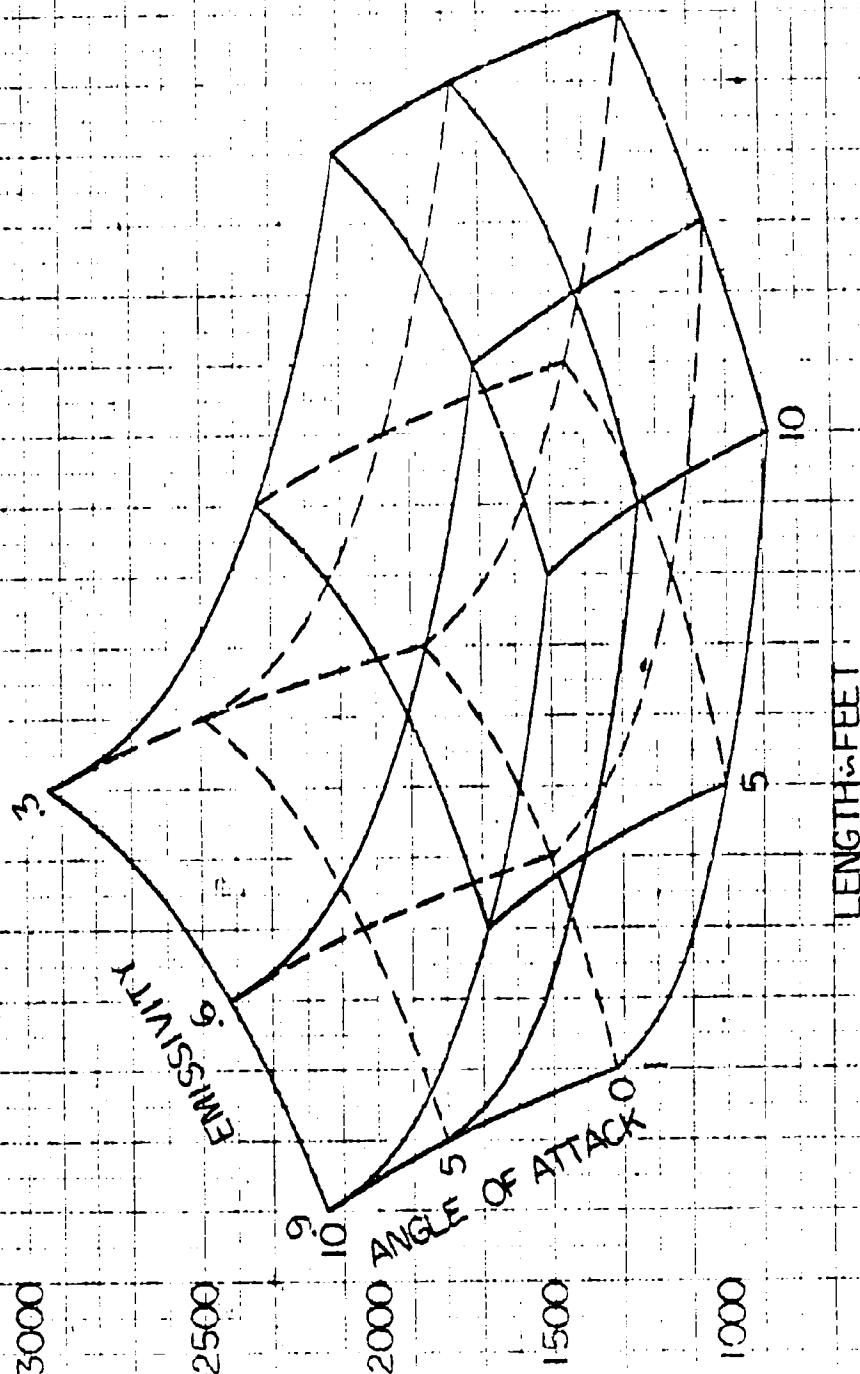
EQUILIBRIUM TEMPERATURE SIDE OF BODY



SECRET

Figure 4.6.2-6

EQUILIBRIUM TEMPERATURE
 MACH NUMBER ~20
 ALTITUDE ~198000 FT.
 LAMINAR FLOW
 BOTTOM SURFACE



BY _____ DATE _____
 CHECKED _____ DATE _____

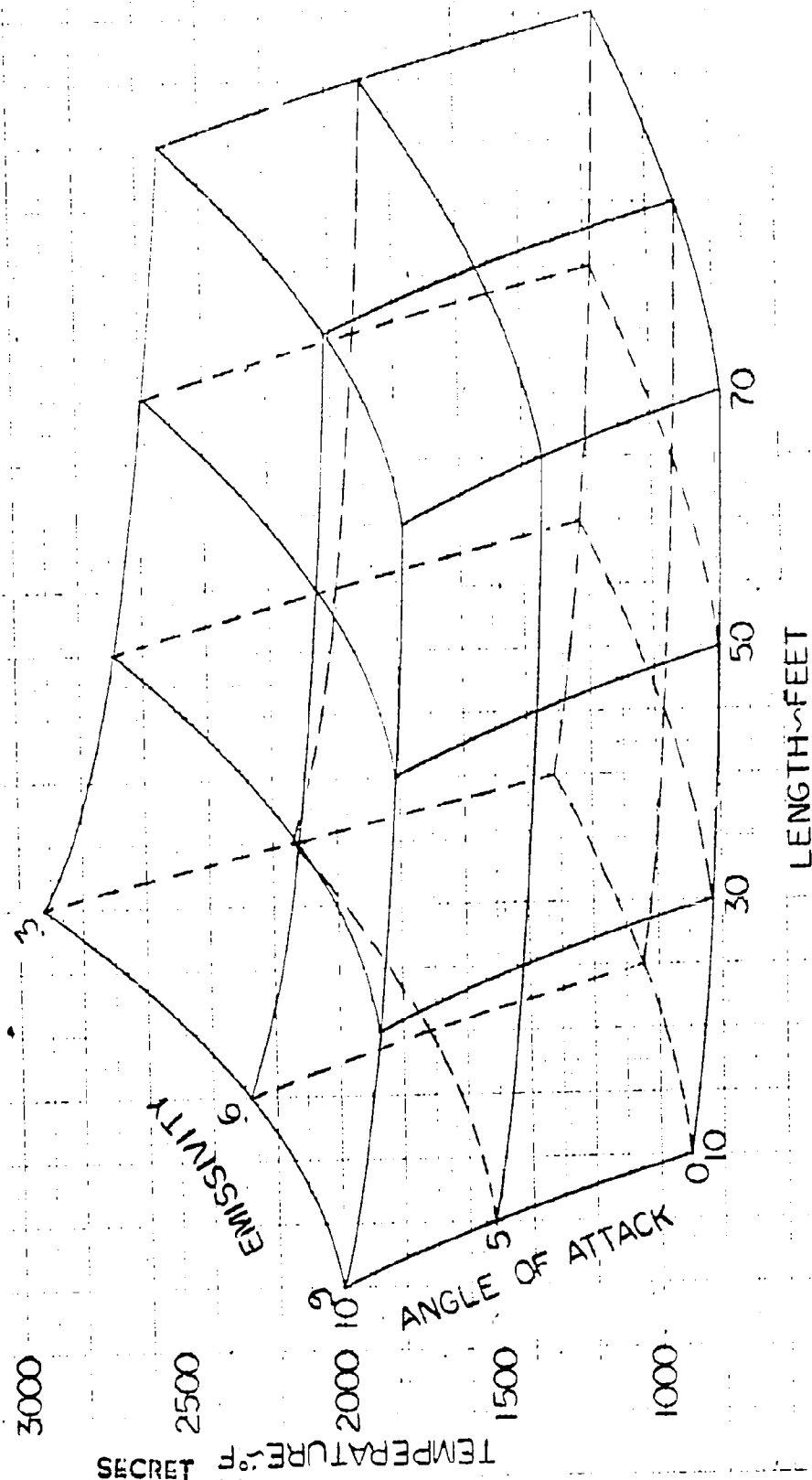
SECRET
 BELL *Aviation* CORPORATION

MODEL _____
 SHIP _____

PAGE 11137
 REPORT 113-11137

Figure 4.6.2.7

EQUILIBRIUM TEMPERATURE
 MACH NUMBER ~20
 ALTITUDE ~198000 FT.
 TURBULENT FLOW
 BOTTOM SURFACE



SECRET

BY _____ DATE _____
CHECKED _____ DATE _____

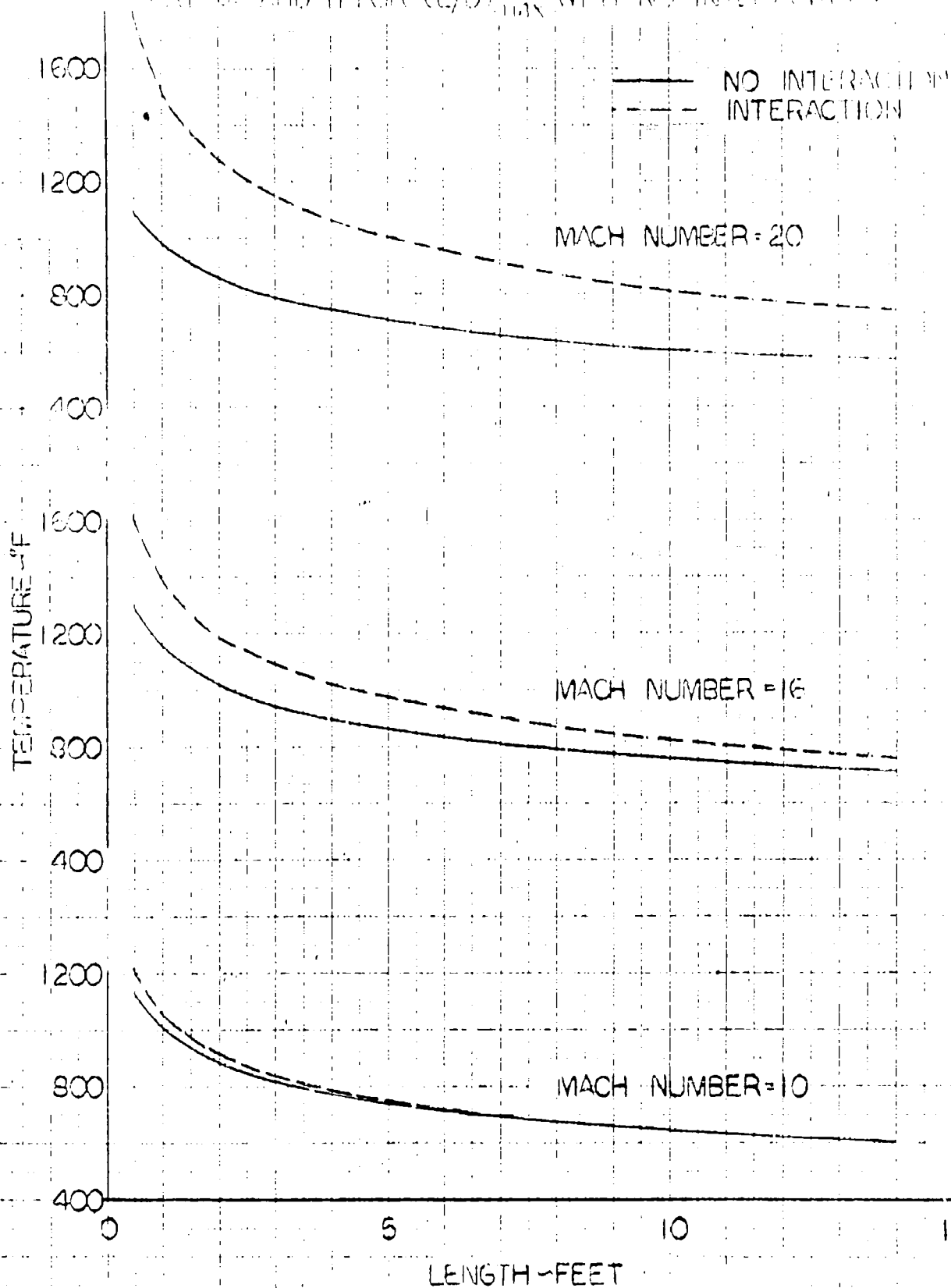
BELL *Swamp* CORPORATION

MODEL _____ PAGE 4-114
SHIP _____ REPORT 11143-215-012

EQUILIBRIUM TEMPERATURE

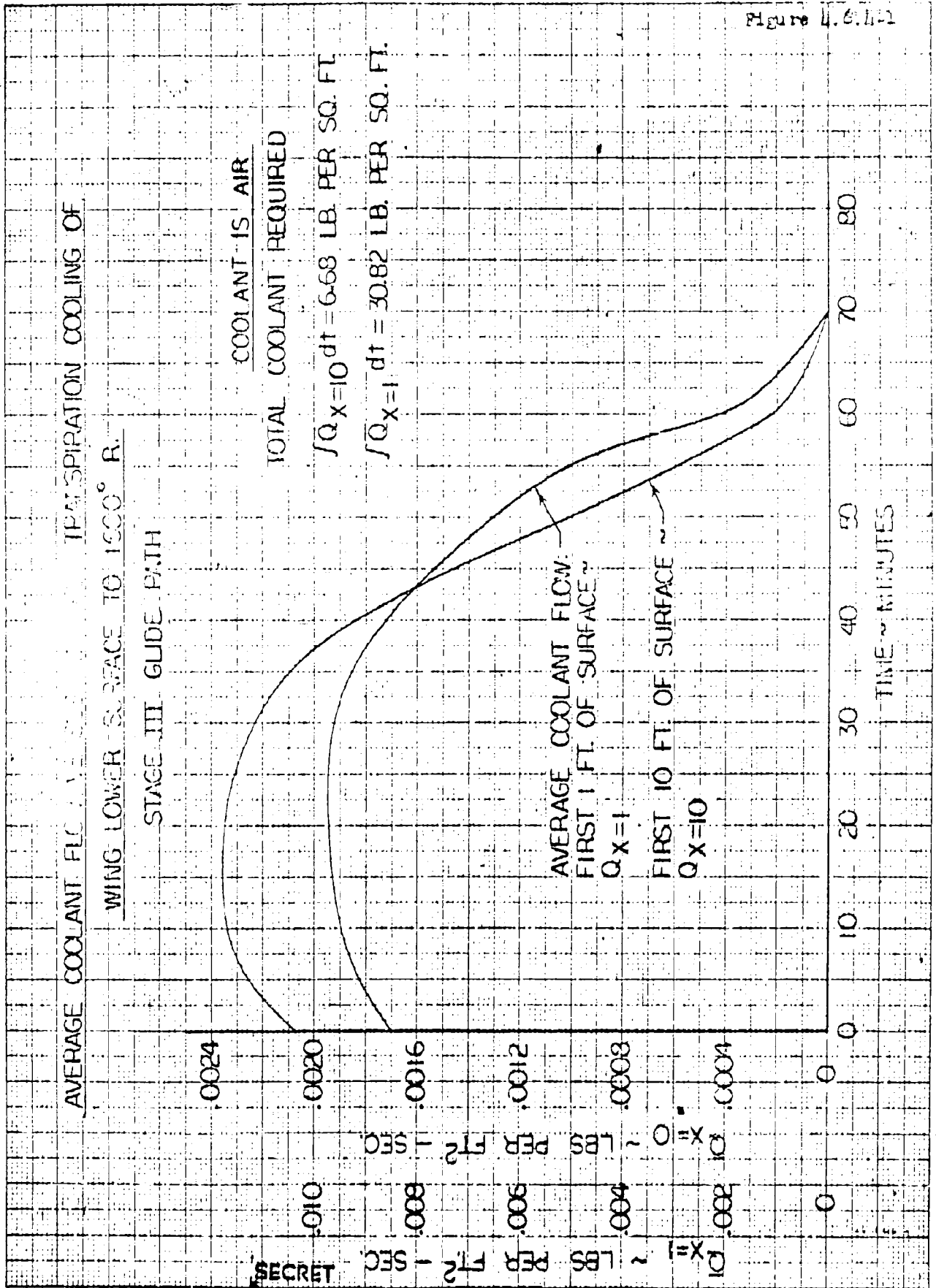
FIGURE 4-114

(CALORIC AND h FOR U_2O) WITH NO INTERACTIONS



SECRET

Figure 4.6.1-1



By _____	Date _____	BELL Aircraft CORPORATION	Model _____	Page <u>4-116</u>
Checked _____	Date _____		Missile _____	Report <u>D143-945-012</u>

4.7 Stability & Control

A hypersonic vehicle of the type of the MX-2276 will be required to be controllable and have acceptable handling characteristics throughout the regime it encounters--from the ascent, with separation of various stages, to the peak of the hypersonic glide, during the glide at hypersonic, supersonic, transonic and subsonic flight velocities and for the low-speed landing conditions. The stability and control characteristics of aircraft up to low supersonic speeds are presently understood to be a reasonable degree. The design in this regime for a vehicle such as the MX-2276 should encounter no fundamental lack in methods of analysis. In the hypersonic flight regime, however, new conditions are encountered which require a review of present methods. As shown on Appendix 4B of this report, the equations which govern the motion of the vehicle include new terms which are significant due to the high velocities which are expected -- this requires a complete reanalysis of the methods which are presently employed to investigate the dynamic stability of aircraft in order to determine the effect of the new terms on the present concepts and criterion for dynamic stability and control. The magnitude of such an analysis precluded more than an investigation of the basic equations of motion for this study -- with these equations, however, means are available by which such a study may be undertaken. In addition, considerable effort must be applied to the determination of the static and dynamic aerodynamic force and moment parameters in the hypersonic flow regime. At present, there are no known useable methods of predicting such parameters as damping in pitch, roll, etc.; however, means are available by which the problems may be attacked both on an experimental and theoretical basis -- free flight test vehicles are presently approaching the flight regimes of MX-2276 and will be able to furnish empirical data, and approximate theoretical flow models (Newtonian flow, etc.) may be employed to obtain theoretical estimates.

4.7.1 Static Stability

Some preliminary estimates of the aerodynamic static longitudinal stability of the third stage have been made. The lift and drag of the various components of the present MX-2276 configuration as given in Section 4.4 were utilized to determine the moment characteristics of the vehicle over a Mach number range from $M = 4$ to $M = 20$ and for angles of attack from $\alpha = 0^\circ$ to $\alpha = 15^\circ$. Since the methods used to determine the forces acting on the various components (Newtonian flow, shock or expansion theory, etc.) result in uniform distribution of forces on each surface area component, the moment contribution was determined by assuming that these forces acted at the center of area (or center of projected area) of the surface considered. The moment coefficient, as determined by this method is presented in figure 4.7.1-1. It is of interest to note that the principal variations in moment coefficient occur in the region $M = 4$ to $M = 8$ and that above $M = 8$ only slight variations in moment coefficient occur with Mach number at a given angle of attack.

By _____	Date _____	BELL <i>Aircraft</i> CORPORATION	Model _____	Page 4-117
Checked _____	Date _____		Missile _____	Report D143-945-012

In order to obtain an estimate of the stability margins which may exist in hypersonic flight, the center of pressure location for various angles of attack has been determined for the present configuration at $M = 20$. These results are presented in figure 4.7.1-2 and show no unusual variations. Also shown on this figure is the variation in center pressure for the configuration with a wedge-type control surface. It will be observed that adding the wedge increases the stability of the configuration.

On the basis of these preliminary investigations, it appears that no undue difficulty will be encountered in obtaining static longitudinal stability in hypersonic flight with proper location of the center of gravity of the airframe. The problem of matching the requirements for stability at hypersonic velocities with those at lower flight speeds has not been considered as yet and will require further studies. In addition, the method used to obtain the moment characteristics of the airframe have neglected the effects of shock-boundary layer interaction on the distribution of forces and moments. A preliminary evaluation of interaction (see Section 4.7.3) indicates that an appreciable effect may result and should receive further consideration.

4.7.2 Control Surfaces

The moment characteristics of several control surfaces have been studied briefly to determine the feasibility of using aerodynamic control in hypersonic flight. Several types of controls have been considered, of equal surface area, to determine the relative merits of each; (1) a trailing edge slab-sided (constant chordwise thickness) control shown on the present configuration, (2) a moveable tip control which is a portion of the outboard section of the present wing and, (3) a trailing edge wedge control formed by making a wedge of the outer wing from the 50% chord back, with upper and lower wedge angles equal to the wedge angle of the present wing.

The effectiveness of these control surfaces has been determined from inviscid two-dimensional shock or expansion theory. For the tip control surface, no data is presently available as to effects, at the Mach number considered here, of the gap between the deflected control surface and the wing, and this effect has been neglected in the present study. The effectiveness of the trailing edge controls has been determined from the stream conditions which exist immediately ahead on the wing and assuming that no shock-boundary layer interaction or separation of flow occurs. This is considered justified since for a tailless configuration the trim position of the control surface is in a trailing edge up direction for positive angles of attack. In this condition, at hypersonic velocities, the upper surface of the control is located in a region of flow which is highly expanded over the upper surface of the wing. Compression of this expanded flow does little to add to control effectiveness so that any flow effects such as shock-boundary layer interaction

SECRET

By _____	Date _____	BELL Aircraft CORPORATION	Model _____	Page 4-118
Checked _____	Date _____		Missile _____	Report D143-945-012

will have little overall result. On the bottom surface of the control, the flow is expanded from the highly compressed region which exists immediately ahead on the wing and separation in this region will have only a slight effect on the change in pressure as the flow expands from the wing to the control surface.

The variation of pitching moment coefficient with Mach number and control surface deflection is shown for the slab and tip control in figures 4.7.2-1 to 4.7.2-8 for several angles of attack. Of particular interest is the non-linearity of control effectiveness in the hypersonic range.

A comparison of this non-linearity with angle of attack and control deflection at $M = 20$ is shown in figure 4.7.2-9 for the slab, tip and wedge controls. It is notable that the slab control surface exhibits the greatest amount of non-linearity with angle of attack; however, a final selection of a control surface will depend on other factors (hinge moment, trim lift, trim lift-drag ratio, etc.) as well, and which can be evaluated only in a detail design.

The effects of control surface deflection on lift coefficient and lift-drag ratio are illustrated in figures 4.7.2-10 to 4.7.2-15. These results, which are obtained by summing the lifts and drags due to angle of attack and control deflection, show that increasing control deflection for trim results generally in a reduction in maximum lift-drag ratio and an increase in the angle of attack and lift coefficient for maximum lift-drag ratio. This will result in a reduction from the range calculated for zero control deflection and, since the angle of attack for a given lift coefficient is somewhat higher with control deflections than with no control deflection, an increase in the heat transfer.

It is apparent therefore, that selection of a control surface will result from a number of compromises which would be evaluated in a design study. The present results indicate that sufficient control effectiveness is available at hypersonic velocities to make aerodynamic control appear feasible without large aerodynamic losses.

4.7.3 Shock-Boundary Layer Interaction

The preliminary evaluation of static stability and control at hypersonic flight velocities has been made using aerodynamic parameters which were determined from inviscid fluid flow theory. As was noted in that section and also in the discussion of fluid flow regimes (see Section 5.2), the hypersonic flight path of the MX-2276 enters regions wherein the effects of fluid viscosity became of increasing importance in determining the aerodynamic pressure forces which act on a moving body. Fluid flow theories which neglect these effects may be expected to give only approximate estimates of these forces. At present, general

Form 14-1 Rev. 353

SECRET

By _____ Date _____
Checked _____ Date _____

8111

AC CORPORATION

Model _____ Page 4-119
Missile _____
Airplane _____ Report D43-945-012

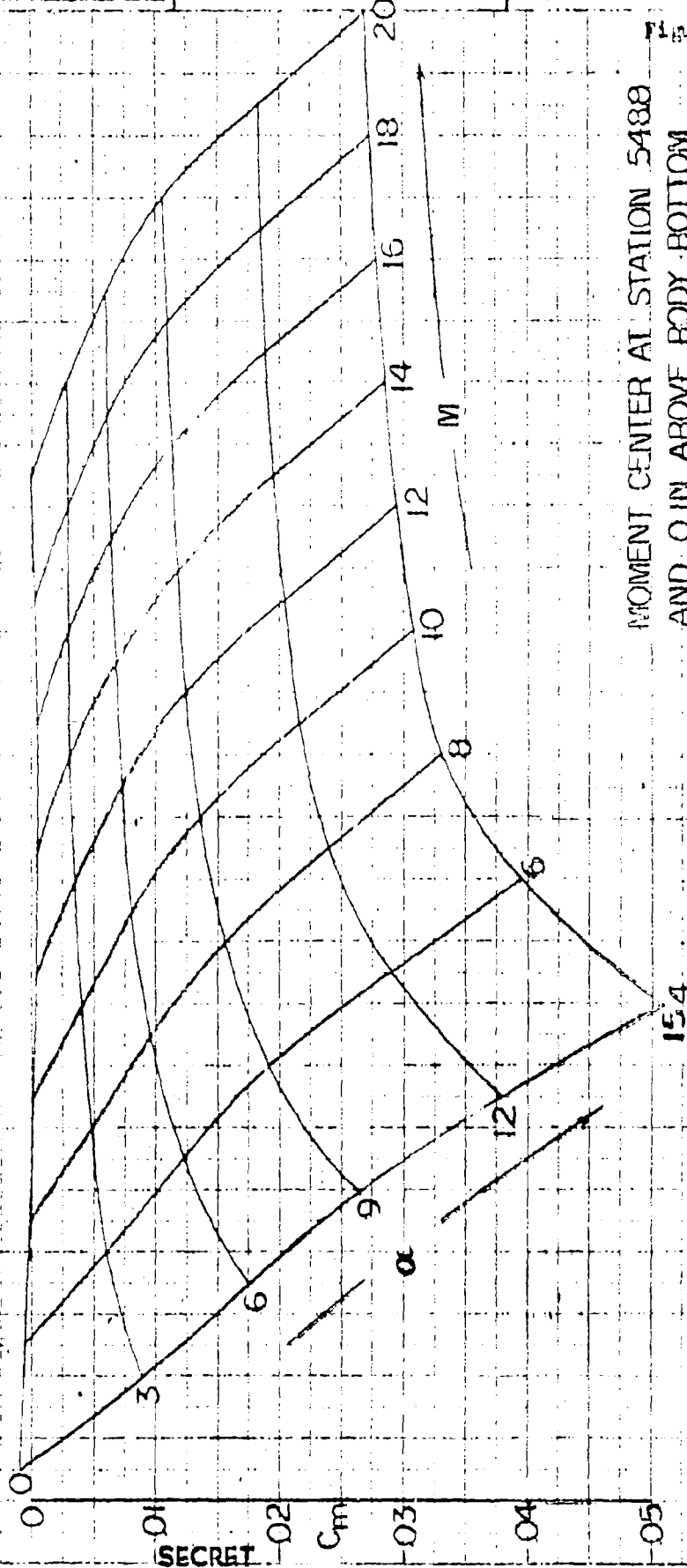
theories that will treat all of the aerodynamic shapes which it is desirable to investigate are not available. However, a preliminary theory which considers the case of the two dimensional flat plate at an angle of attack in viscous flow has been developed and is presented in Section 5.3 of this report. With this theory, it is possible to consider simple two dimensional wedge airfoil sections in order to obtain an insight to the possible effects of viscosity on forces and moments. A sample calculation has been made for a simple semi-wedge airfoil section with a chord length equal to the mean aerodynamic chord of the MX-2276 outer wing, at $M = 20$, at an angle of attack of 8° and at an altitude of 200,000 feet. Figure 4.7.3-1 presents the ratios of local pressure to free stream ambient pressure for the upper and lower surfaces of the section as determined from inviscid shock and expansion theory and from the viscous theory. For the lower surface of the section, the local pressure is considerably increased over that predicted by the inviscid theory, particularly in the region of the leading edge. For the upper surface of the wing, where inviscid expansion theory would predict pressures lower than ambient free stream, the results of the viscid theory show pressures considerably above ambient near the leading edge, decreasing as the trailing edge is approached but in this case always greater than ambient free stream. From these data, it is obvious that the forces and moments derived by integrating the pressure distribution will be appreciably influenced by the effects of fluid viscosity at the flight condition given. As an example, the section moment coefficient taken with respect to the leading edge of the simple wedge is found to be $-.0268$ from the inviscid pressure distribution and $-.0302$ from the viscid pressures while the section normal force coefficients are found to be $.0536$ and $.0623$ respectively.

The above discussion has been concerned only with the two dimensional effects of shock-boundary layer interaction. The effects on three-dimensional shapes such as bodies and wings are as yet undefined. The presently available test data for hypersonic wings have shown only negligible three-dimensional effects. However, these test data have been conducted in Mach number and Reynolds number regions wherein the present study has indicated it would not be expected that viscous effects would be large. The experimental facilities are capable of performing the necessary tests and an evaluation for the flight regimes of MX-2276 requires only that the tests be conducted at the proper conditions.

Until more data is available, approximate estimates of stability and control characteristics of hypersonic vehicles can be made using inviscid flow theory; however, the limitations of using these methods must be remembered in evaluating the results.

MX-2276 STAGE 3

PITCHING MOMENT COEFFICIENT VS.
MACH NUMBER AND ANGLE OF ATTACK



MOMENT CENTER AT STATION 5488
AND 0 IN. ABOVE BODY BOTTOM
 $x_{ref} = 896$ IN.
 $S_{ref} = 615$ FT²

Figure 4.7.1-1

BY _____ DATE _____
CHECKED _____ DATE _____

SECRET
BELL Aircraft CORPORATION

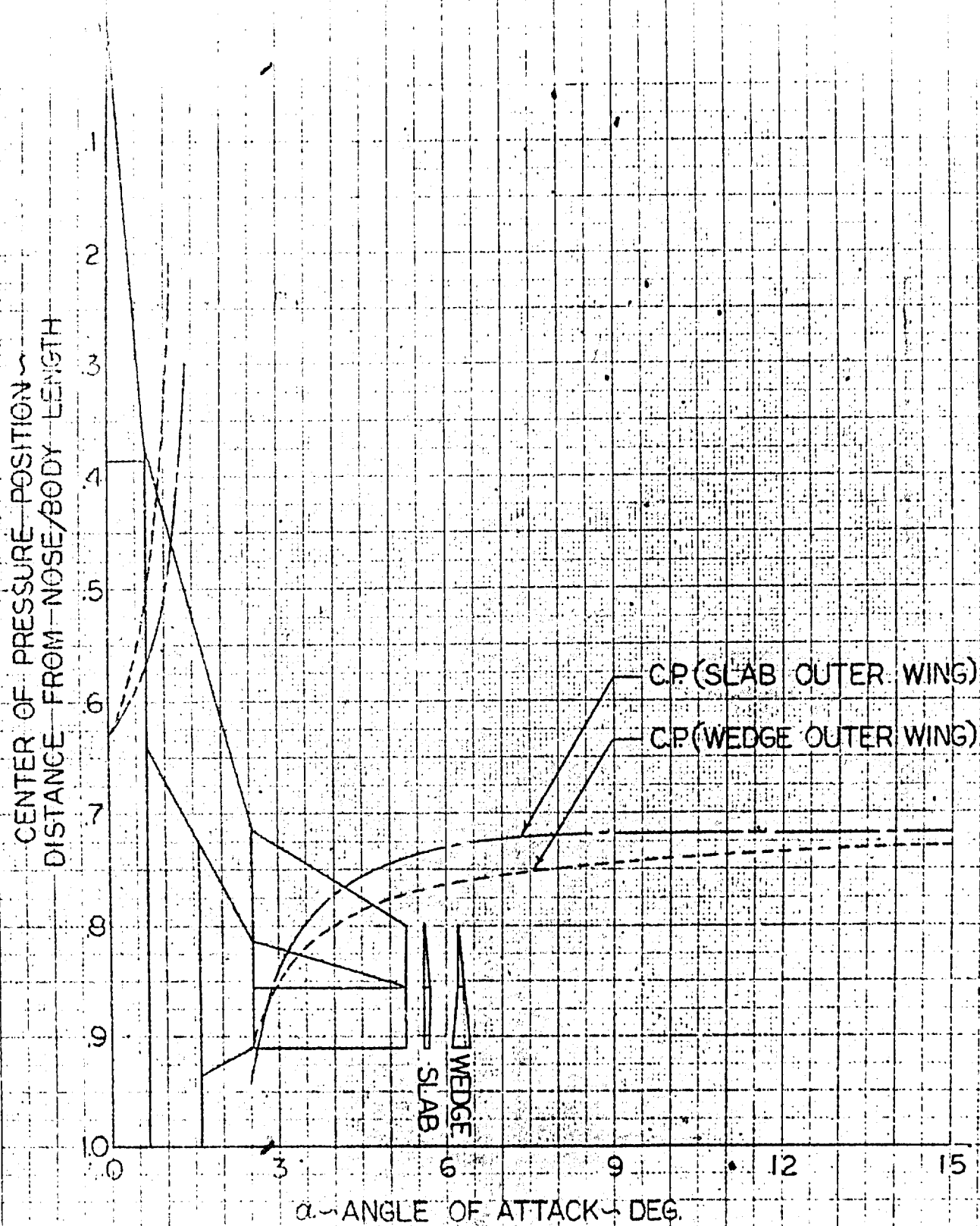
MODEL _____ PAGE 4-120
SHIP _____ REPORT D143-945-012

SECRET

STAGE 3

PRESSURE POSITION

M-20



SECRET

Best Available Copy

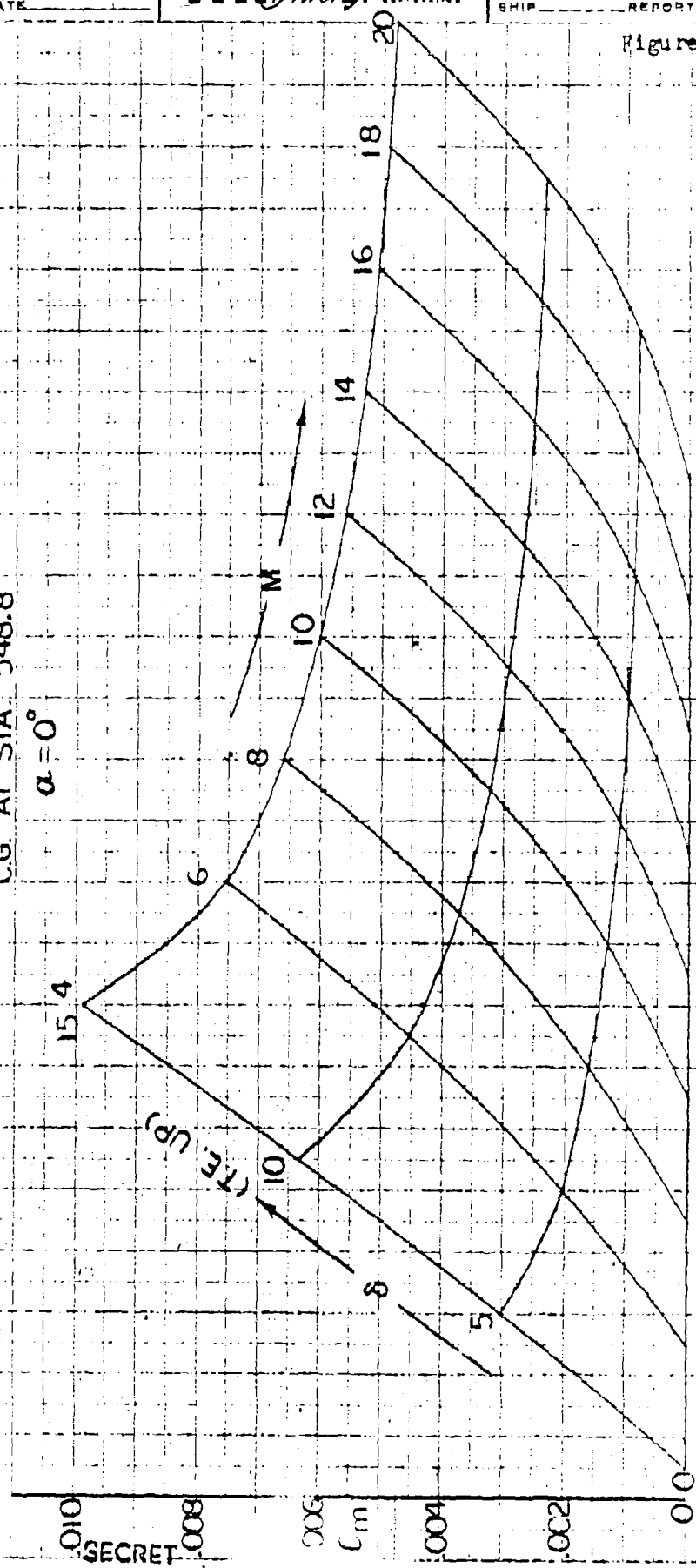
BY _____ DATE _____
 CHECKED _____ DATE _____

SECRET
BELL Aircraft CORPORATION

MODEL _____ PAGE 1-122
 SHIP _____ REPORT D143-945-012

Figure 4.7.2.1

MX-2276 STAGE 3
 SLAB CONTROL SURFACE PITCHING MOMENT COEFFICIENT
 $S_{ref} = 615 \text{ FT}^2$
 $l_{ref} = 896 \text{ IN}$
 CG. AT STA. 548.8
 $\alpha = 0^\circ$



MX-2276 STAGE 3

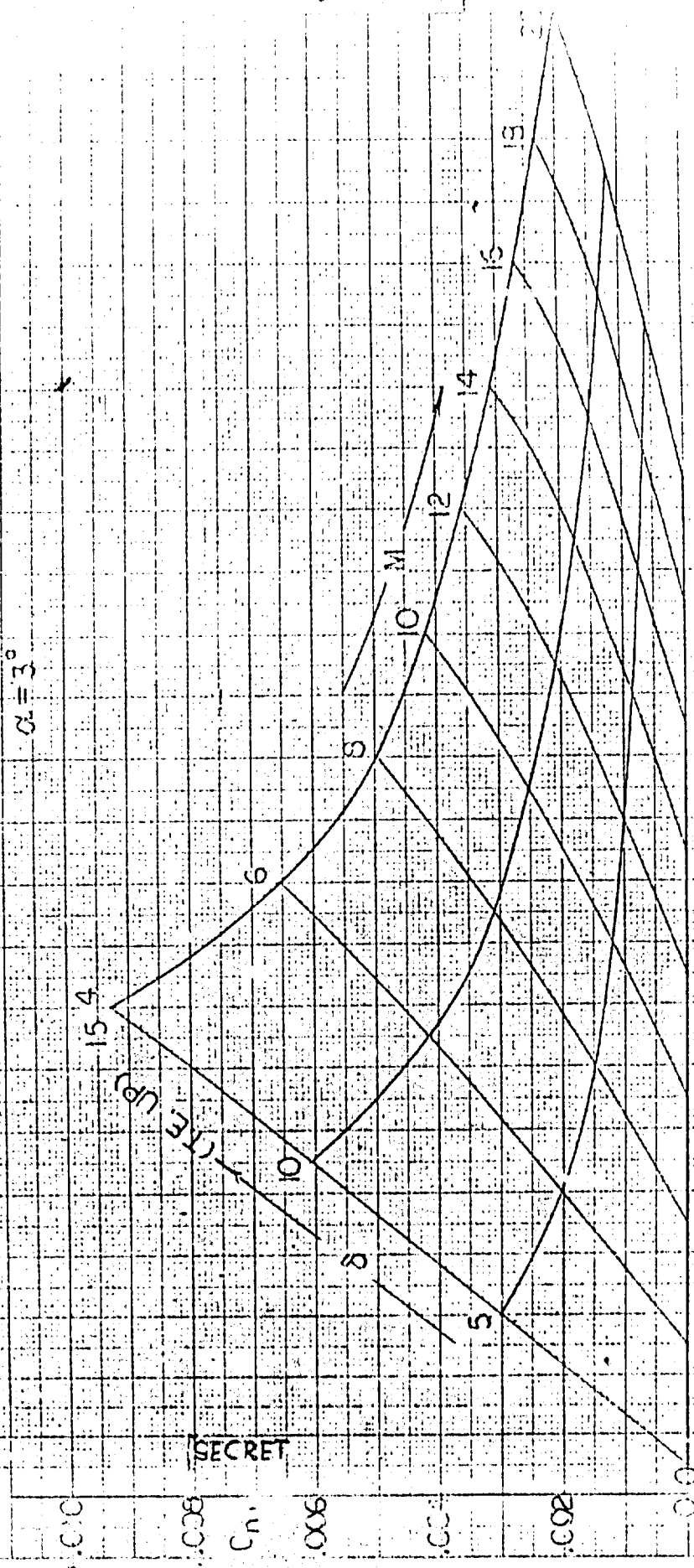
SLAB CONTROL SURFACE PITCHING MOMENT COEFFICIENT

$S_{ref} = 515 \text{ FT}^2$

$I_{ref} = 995 \text{ IN}^4$

C.G. AT STA. 543.9

$\alpha = 3^\circ$



MX-2276 STAGE 3
SLAB CONTROL SURFACE PITCHING MOMENT COEFFICIENT

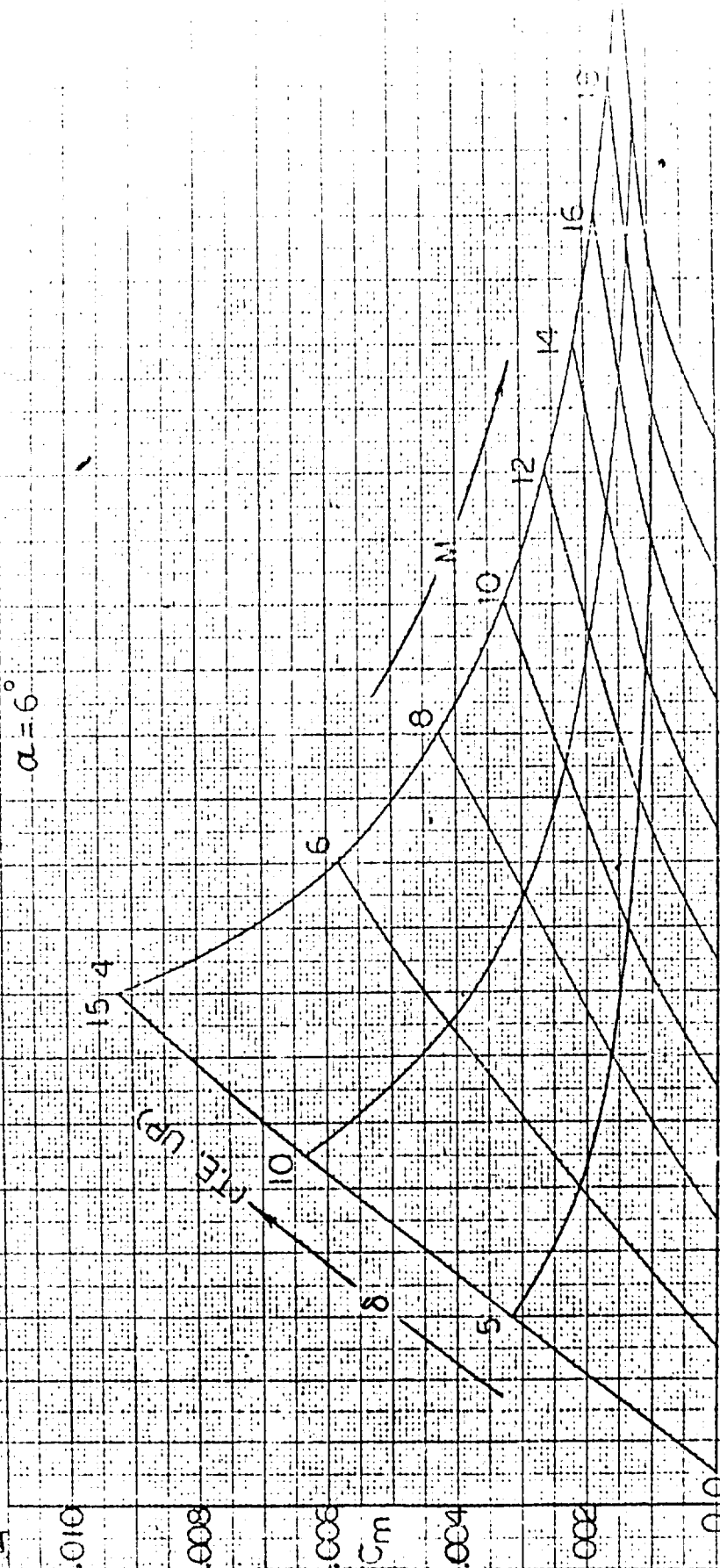
$S_{ref} = 615 \text{ FT}^2$

$l_{ref} = 606 \text{ IN}$

C.G. AT STA. 548.3

$\alpha = 6^\circ$

SECRET



MIX-2275 STAGE 3

SLAB CONTROL SURFACE PITCHING MOMENT COEFFICIENT

Set = 615-FT.2

21-5511

C.G. AT STA.	543.8
--------------	-------

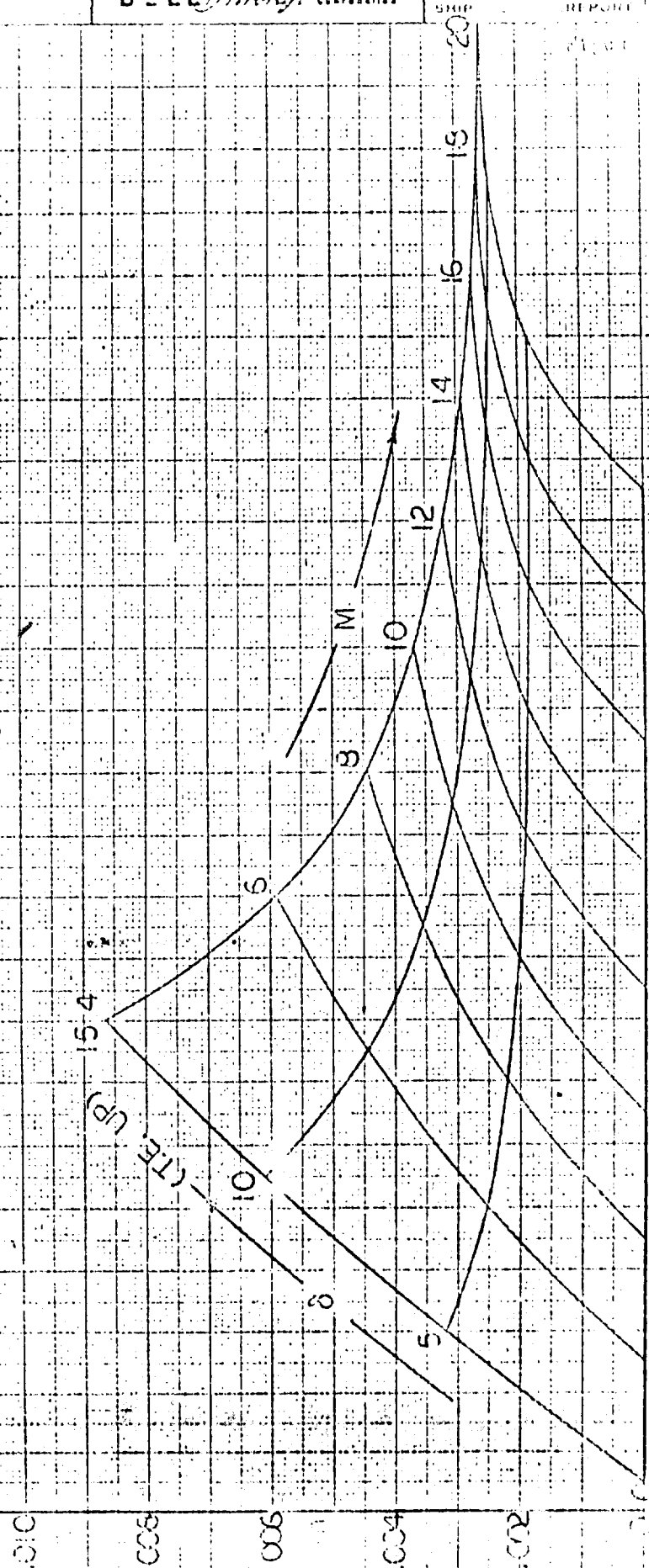
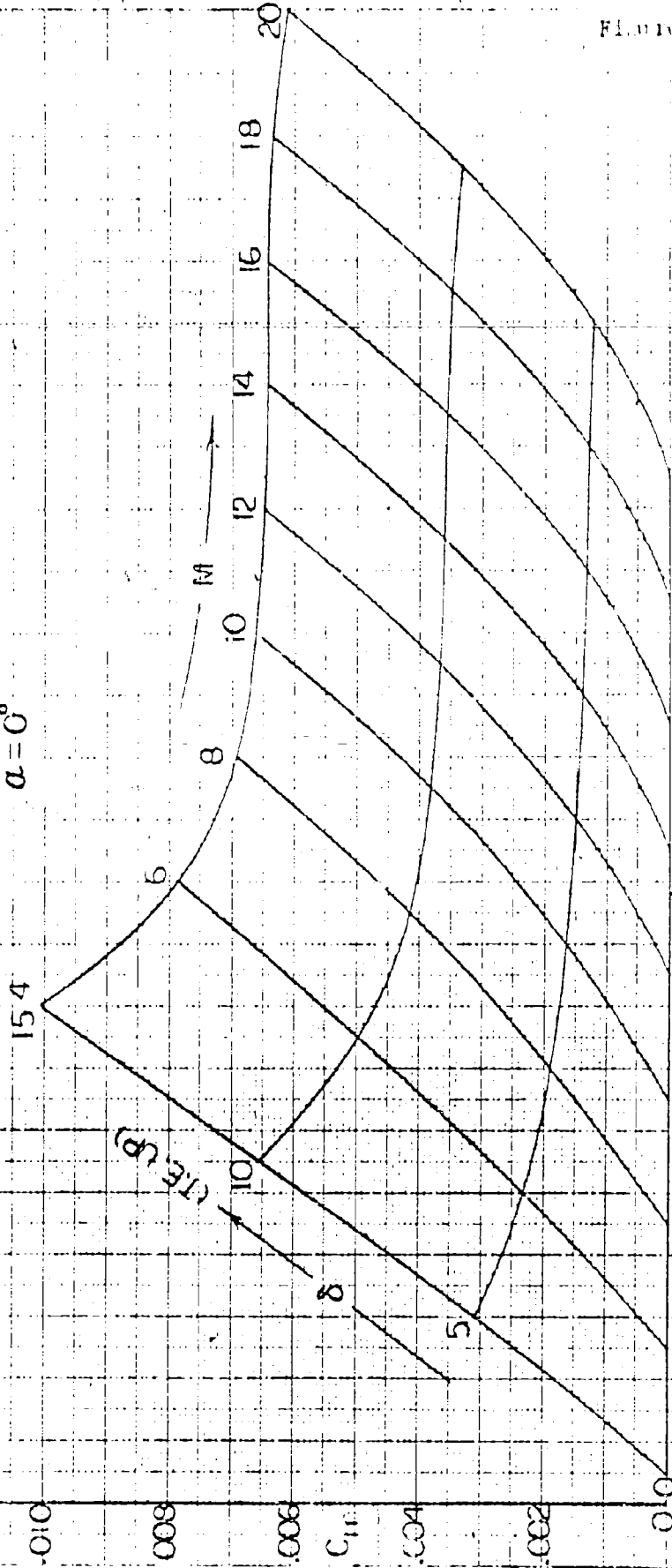
$$\frac{1}{2} \frac{d}{dt} \left(\frac{1}{2} \frac{d}{dt} \right)$$


FIGURE 4.7.2-5

10-2276 STAGE 3
 TIP CONTROL SURFACE PITCHING MOMENT COEFFICIENT
 $S_{ref} = 615 \text{ FT}^2$
 $b_{ref} = 396 \text{ IN}$
 CG AT STA 548.9
 $\alpha = 0^\circ$

SECRET



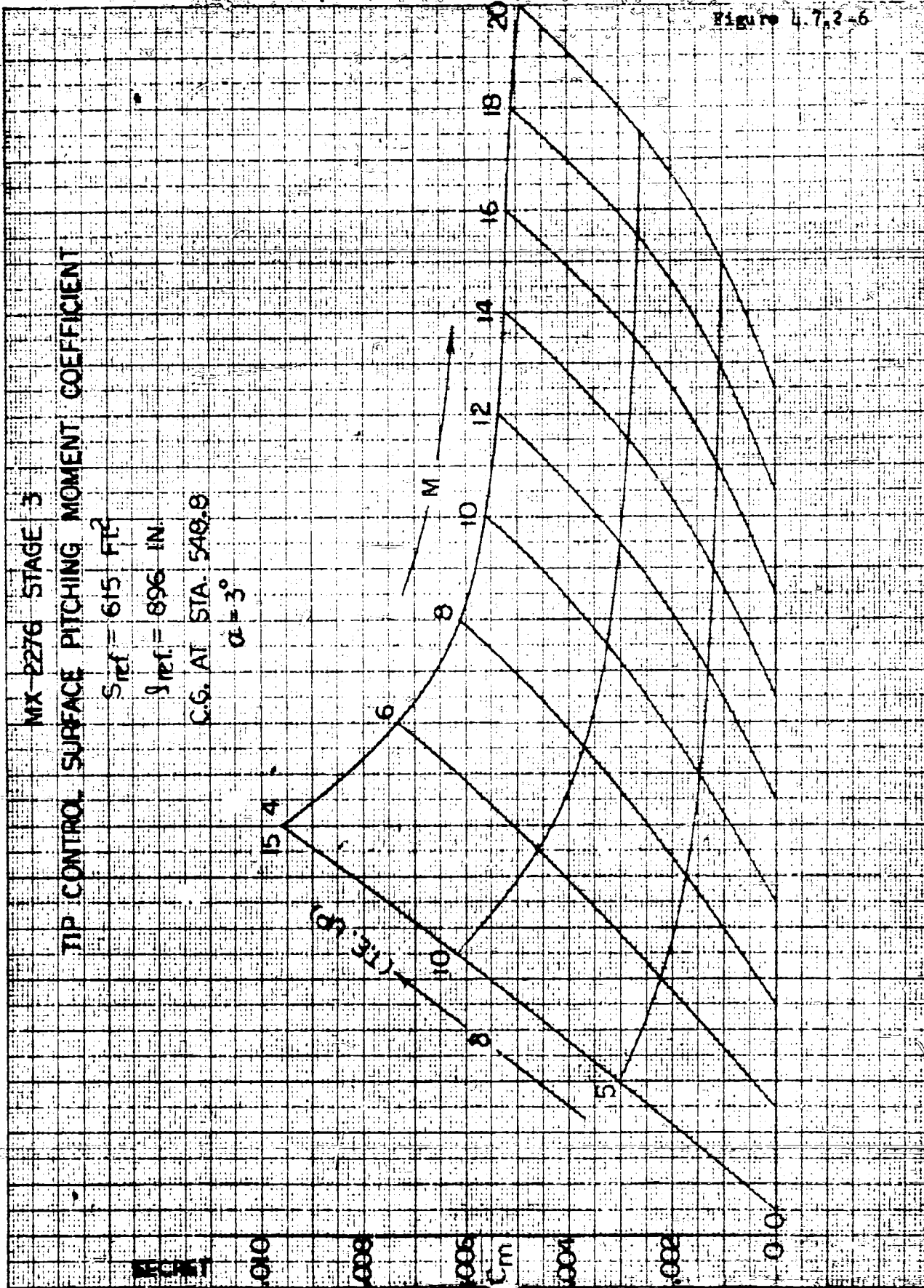


Figure 4.7.2-1

MX-2276 STAGE 3

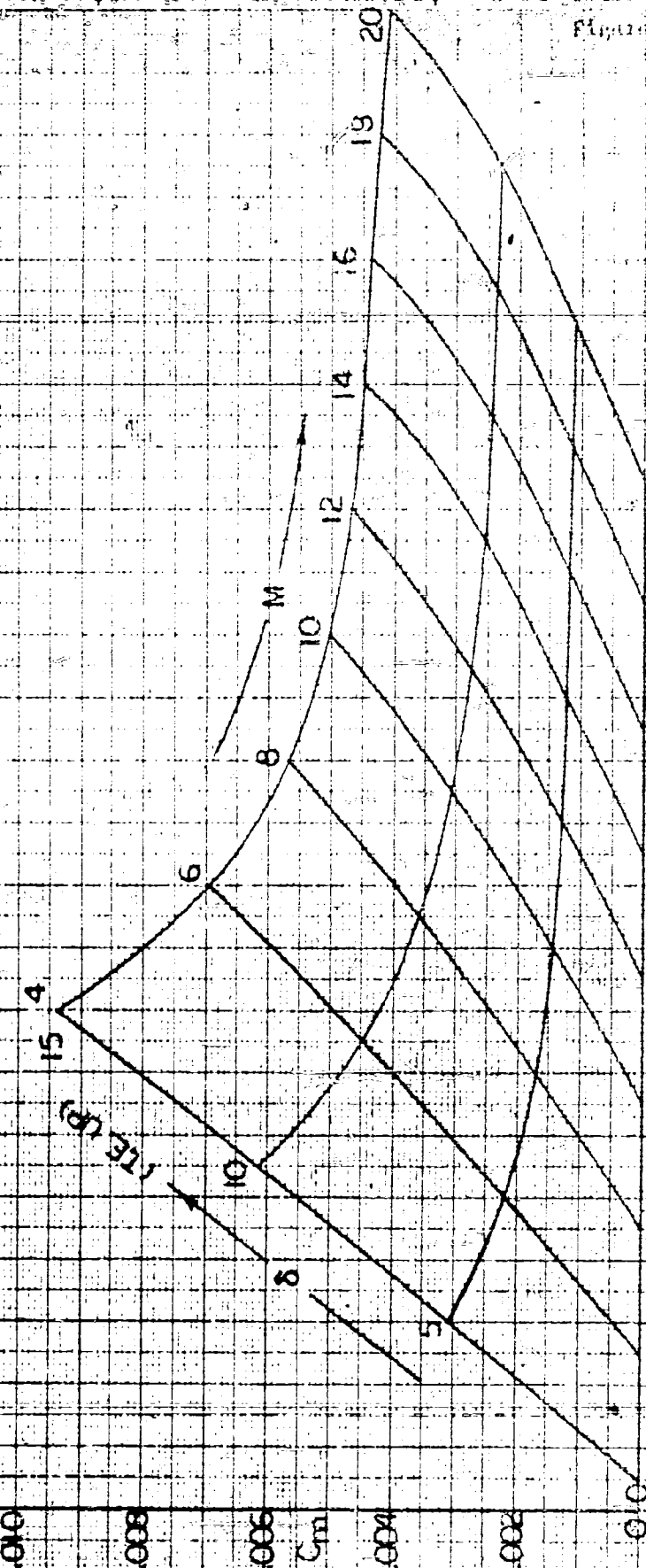
TIP CONTROL SURFACE PITCHING MOMENT COEFFICIENT

$S_{ref} = 615 \text{ FT}^2$

$l_{ref} = 896 \text{ IN.}$

C.G. AT STA. 548.8

$\alpha = 6^\circ$



BY _____ DATE _____
 CHECKED _____ DATE _____

SECRET
BELL Aircraft CORPORATION

MODEL _____ PAGE 4-129
 SHIP _____ REPORT DTIC 945-012

Figure 4.7.2-8

TIP CONTROL SURFACE PITCHING MOMENT COEFFICIENT

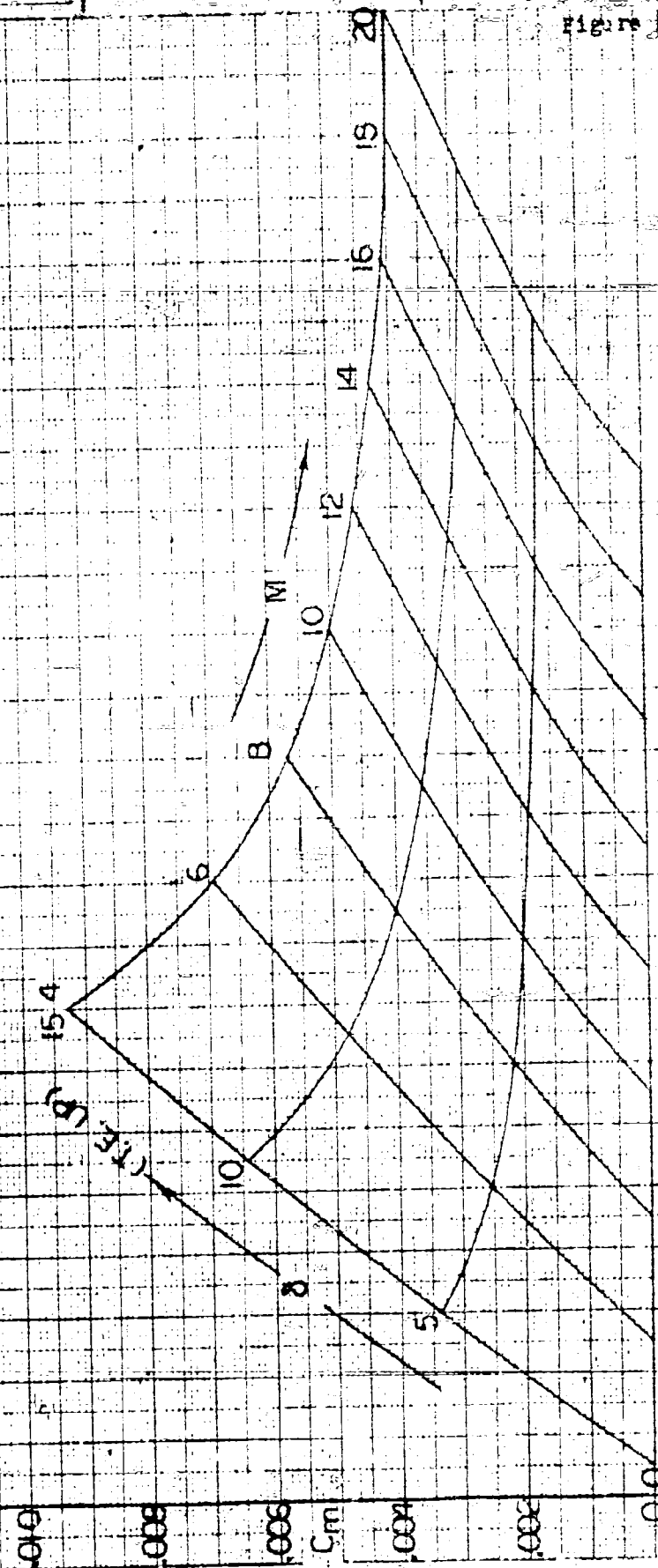
MX-2276 STAGE 3

$S_{ref} = 615 \text{ FT}^2$

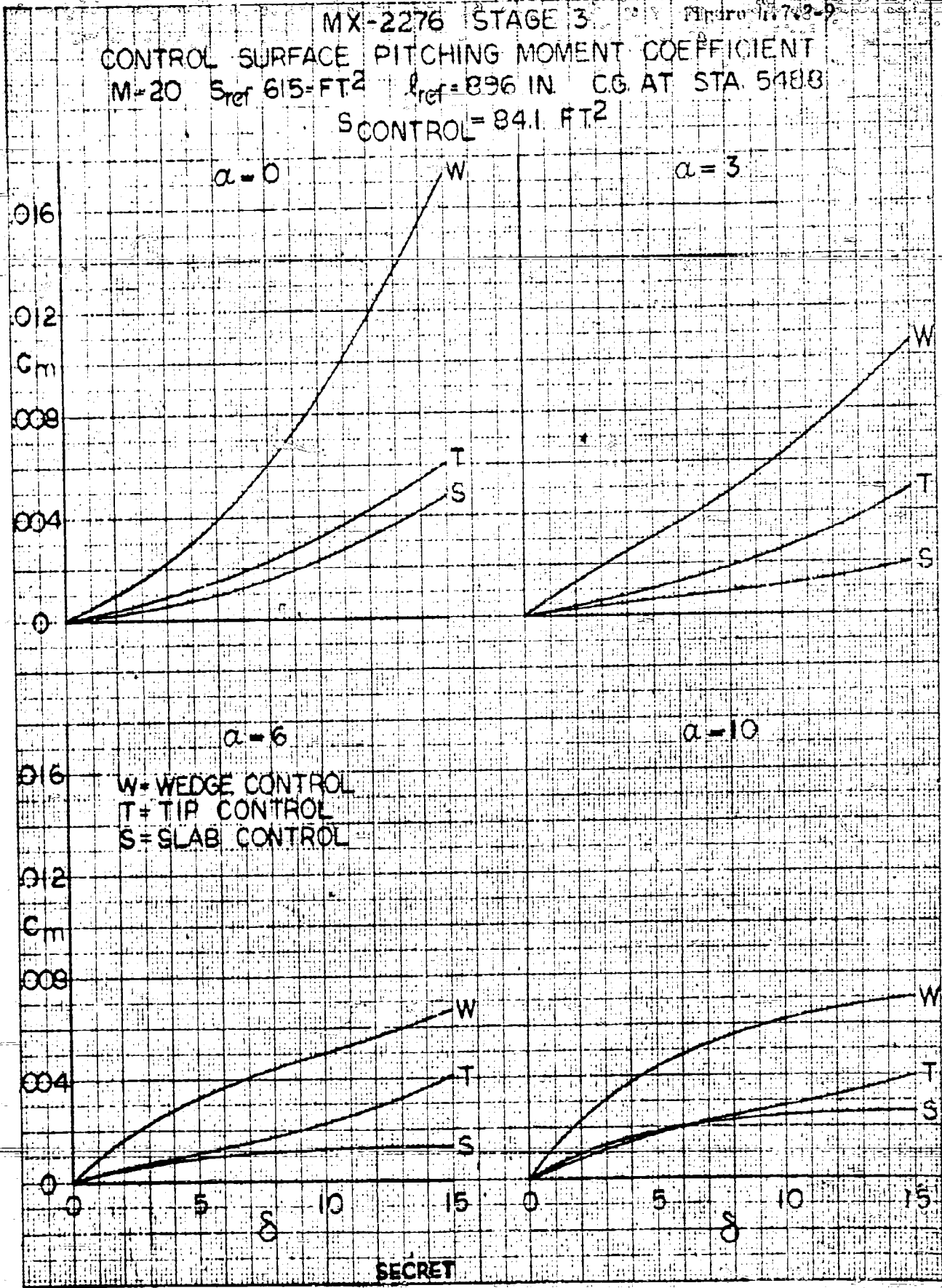
$l_{ref} = 896 \text{ IN}$

CG. AT STA. 548.8

$\alpha = 10^\circ$



SECRET

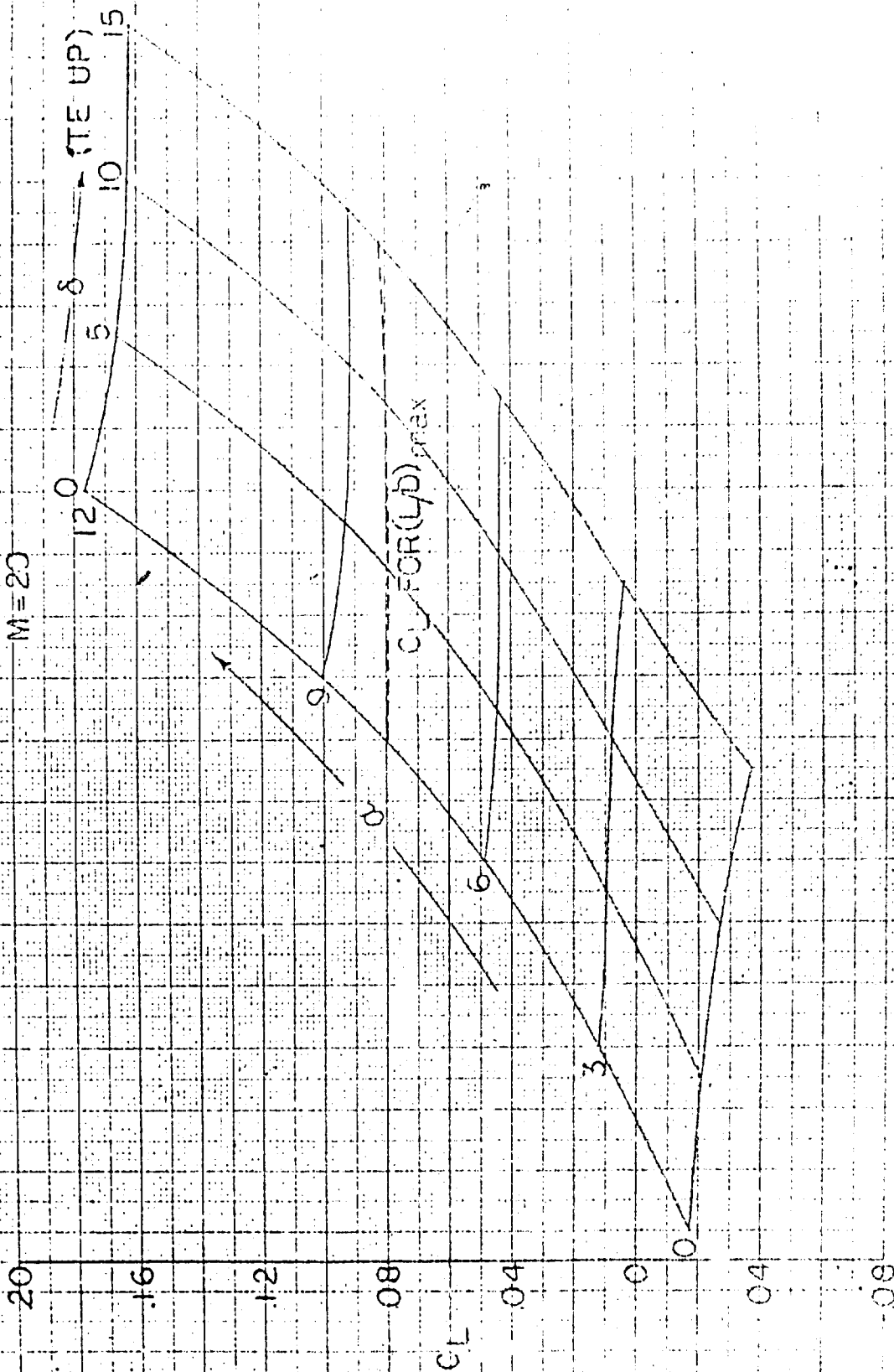


MX-2276 STAGE 3

LIFT COEFFICIENT VS ANGLE OF ATTACK
AND CONTROL SURFACE DEFLECTION

SLAB CONTROL

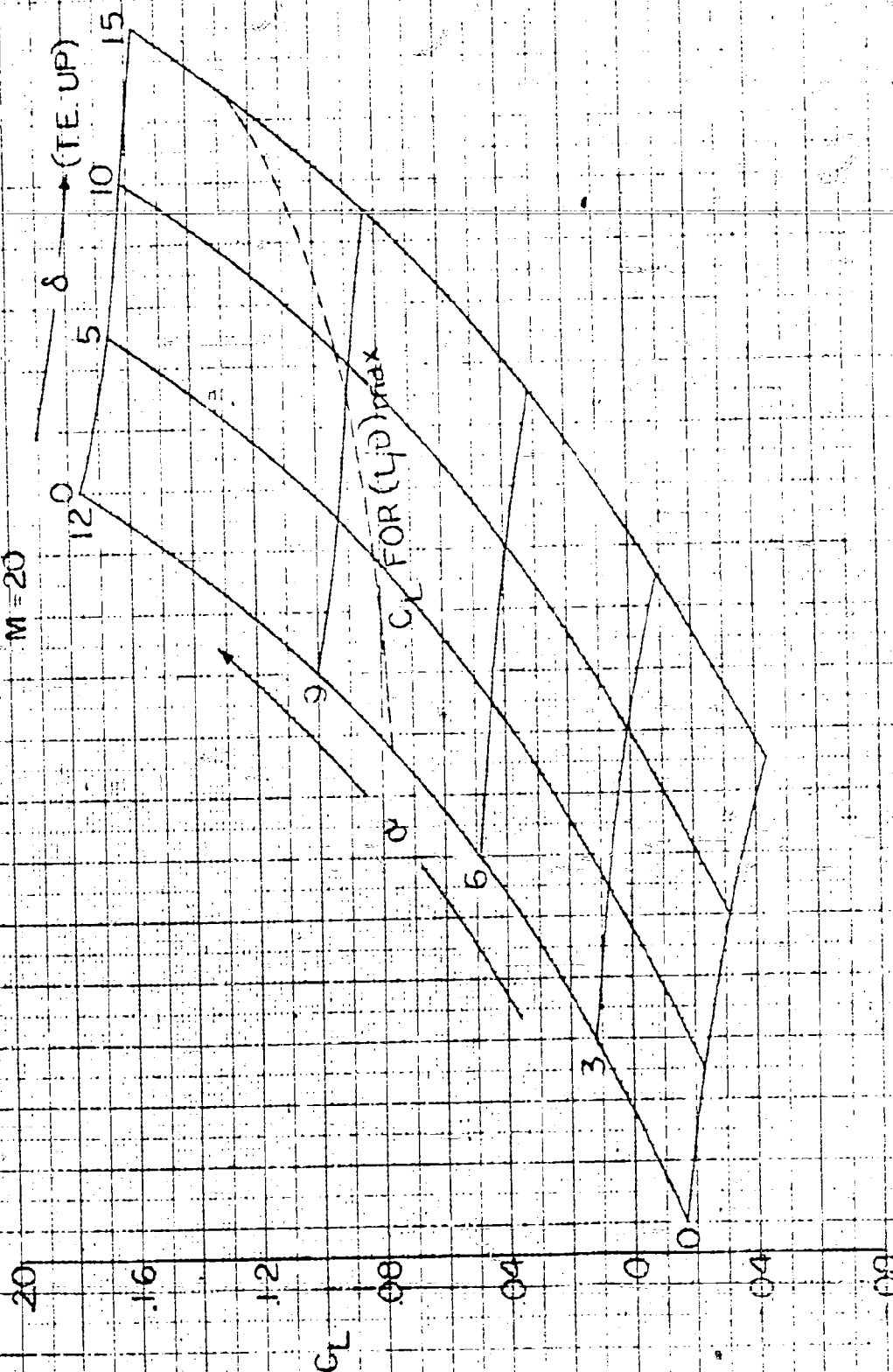
$M=20$



SECRET

MX-2276 STAGE 3
LIFT COEFFICIENT VS ANGLE OF ATTACK
AND CONTROL SURFACE DEFLECTION
TIP CONTROL

$M=20$



SECRET

EX-016 4.7.2.1

MX 2276 STAGE 3
LIFT COEFFICIENT VS ANGLE OF ATTACK
AND CONTROL SURFACE DEFLECTION
WEDGE CONTROL

M=20 120

5 10 15
(TE UP)

δ

C_L FOR $(\gamma)_{max}$

20

16

12

8

4

0

4

8

SECRET

C_L

6

3

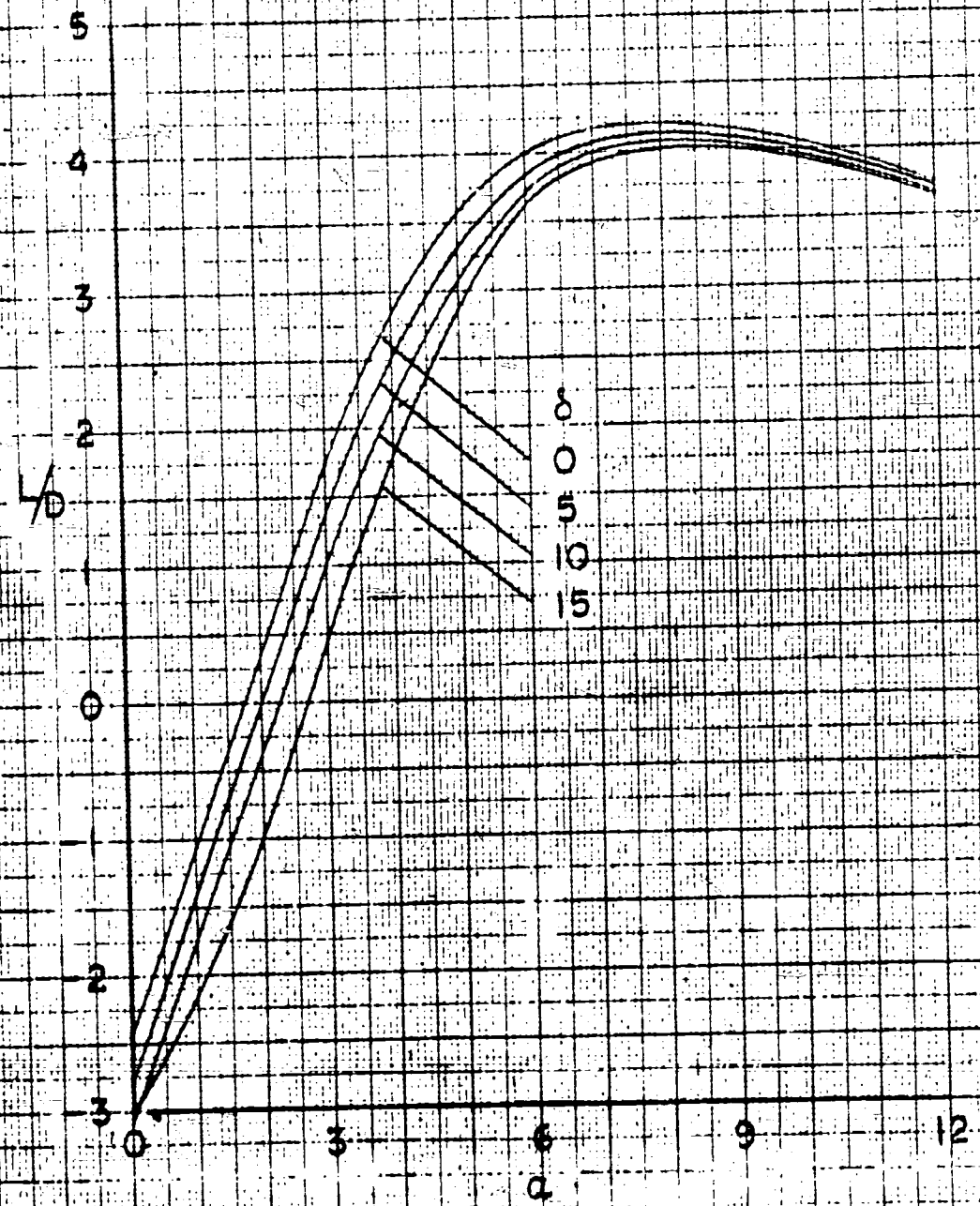
9

8

Figure 4.7.2-12

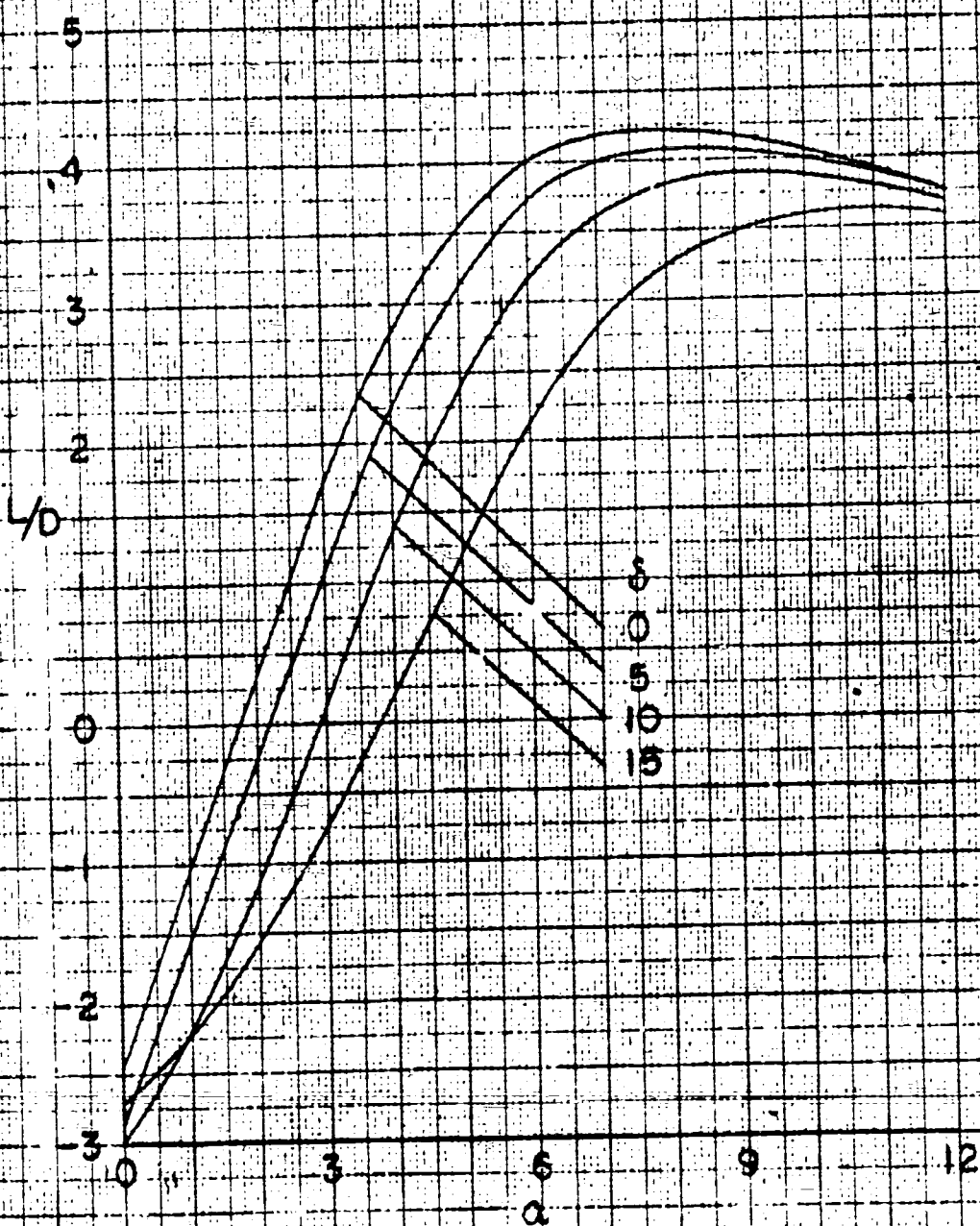
MX-2276 STAGE 3
LIFT/DRAG RATIO
M=20
h=200000 FT
SLAB CONTROL SURFACE

Figure 4.7.2-13



MX-2276 STAGE 3
LIFT/DRAG RATIO
M=20
h=200,000 FT.
TIP CONTROL SURFACE

Figure 4.7.2-11



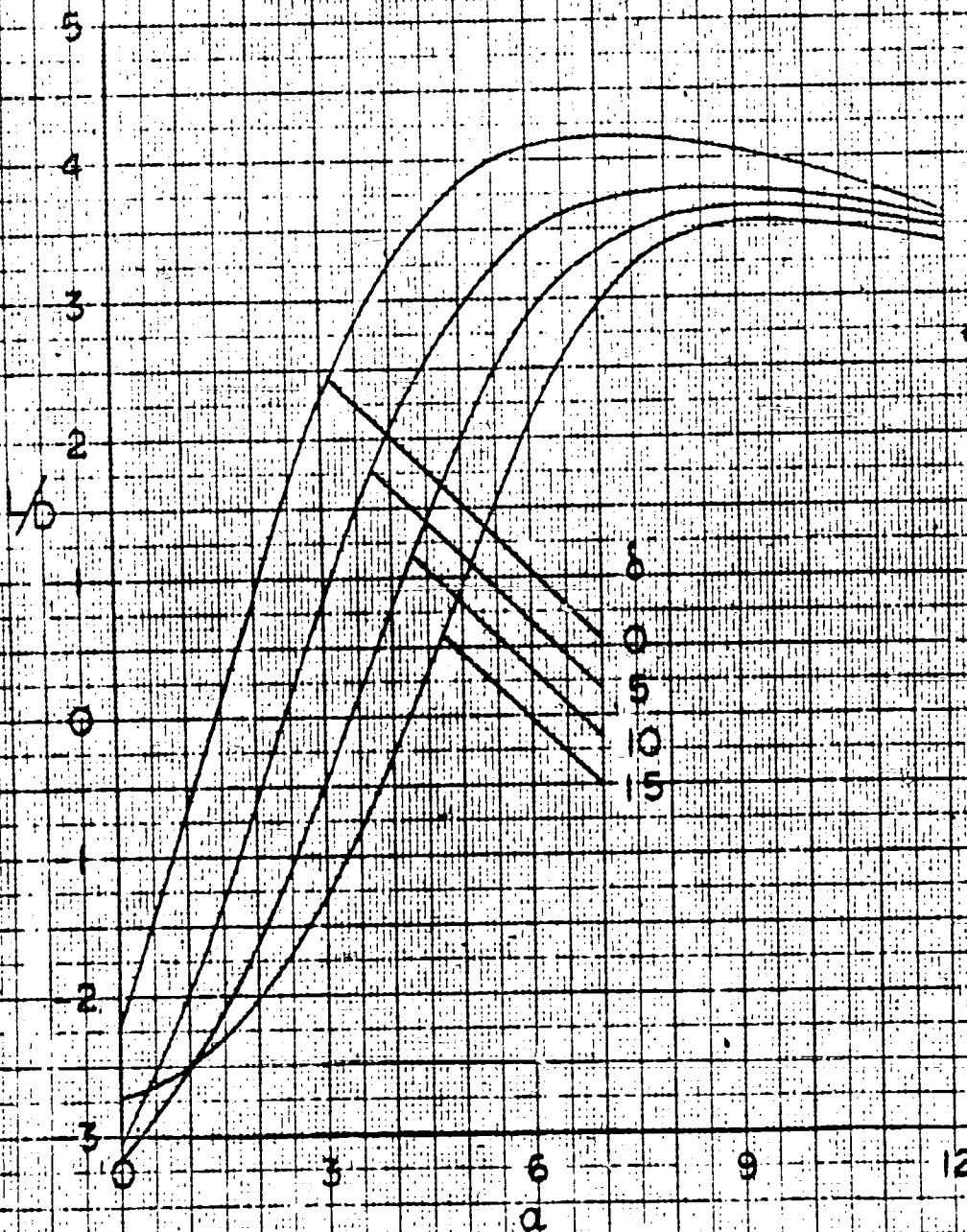
MX-2276 STAGE 3
LIFT/DRAG RATIO

Figure 4.7.2-35

$M=20$

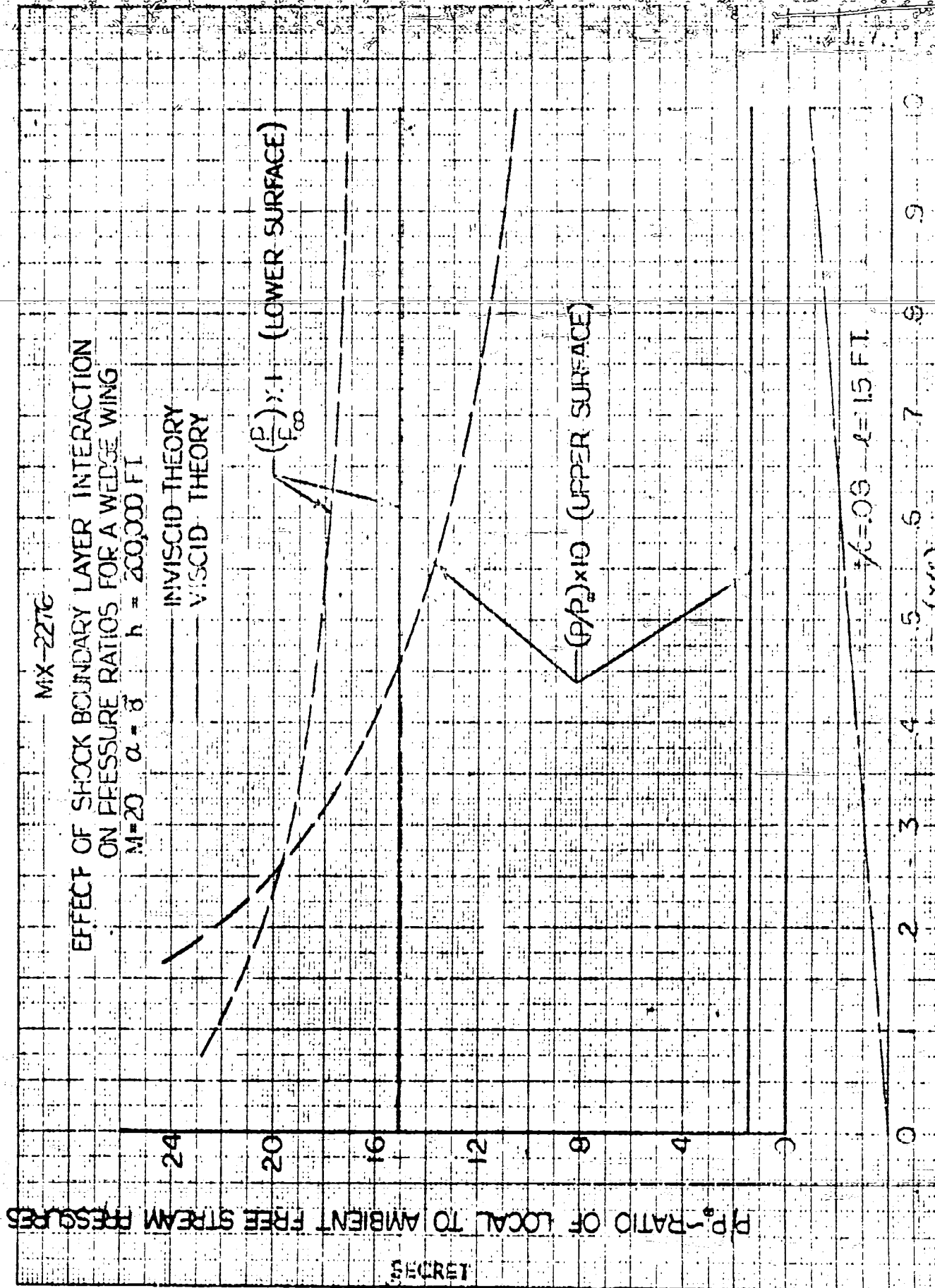
$h=200,000$ FT.

WEDGE CONTROL SURFACE



~~SECRET~~

BELL *Thompson* COMPANY



P/P_∞ - RATIO OF LOCAL TO AMBIENT FREE STREAM PRESSURES

SECRET

$\gamma/c = 0.06$ $\ell = 1.5$ FT

(x/l)

4.8 Separation

As originally described the MX-2276 system requires three stages of boost. Three separable configurations, the first and second stage boosters and the glide vehicle, are assembled adjacent to one another in a parallel arrangement. As the final stage is accelerated to the initial glide condition, the first and second stage boosters separate and drop away as their fuel loads are expended. The aerodynamics of these separations is considered in a quantitative manner hereinafter.

No definite conclusions as to the practicability of the original booster-vehicle configurations for separation are made. It is recommended that when preliminary design of the system is begun, booster-vehicle combinations be put into aerodynamic test as soon as possible as it is believed this is the only way of evaluating them in a sufficiently quantitative manner.

4.8.1 The Parallel-Booster Configurations

The parallel booster configurations considered herein are primarily the type shown for the original MX-2276 system. These are described in Reference 4.8-1; a three-view is reproduced here in Figure 4.8.1-1 for more convenient reference. This tends to tie the considerations to particular cases; however, the approach is not that specific.

The conditions for separation of the stages also are taken from Reference 4.8-1 as being typical for the system. The pertinent aerodynamic parameters for these conditions are as follows:

Separation of first from second and third stages:

Velocity	$V = 5030$ fps
Altitude	$h = 68,000$ ft.
Ambient pressure	$p_{\infty} = 104$ psf
Mach number	$M = 5.2$
Dynamic pressure	$q = 1970$ psf
Pressure after normal shock	$p_2 = 3220$ psf

Separation of second and third stage:

V	$= 13,800$ fps
h	$= 192,000$ ft.
p_{∞}	$= .902$ psf
M	$= 13.3$
q	$= 112$ psf
p_2	$= 186$ psf

It is seen from these conditions that the dynamic pressure at the separation of the first stage from the second and third is much the

greater. The shock wave cones, that contain the regions in which interference effects between surfaces are propagated, also would be larger at this lower Mach number separation. Thus, separation from the standpoint of possible difficulties, appears more critical for the first stage case. This is also heightened by the fact that the present concept calls for the first stage to be saved, i.e. glided to the ground after separation. The second stage booster, on the other hand, can be separated from the glide vehicle in a manner which destroys the booster as it is not to be salvaged. In a sense the fact that first stage separation may be more critical is fortunate because this is a much more easily realizable test condition.

4.8.1.1 Separation Times

The critical period of separation is of interest. It is defined here as the time for the base of the boosted stage to pass the nose of the booster, or the reverse; and is the time for strong aerodynamic interaction and possible collision after initiating separation. After this period down-wash effects from the stage going ahead may still be appreciable on the stage behind - say for an order of time, 10 times the above-defined critical period.

The critical periods of separation have been estimated for a number of possible rocket thrust combinations of the stages and are shown in Tables 4.8.1-1. The combinations involving steering thrust are included because it may be necessary to have these thrusts to stabilize the stages during and immediately after the separation period. The periods were estimated for the stage weights and thrusts given on Figure 4.8.1-1 and from estimates of the stage drags. Friction between the stages during separation was not considered. The period depends on the separation length over the relative acceleration of the bodies to the one half power so that the accuracy of these quantities is not critical. The expression used for the period is simply

$$t = \sqrt{\frac{2L}{32n}}$$

where L = the separation length
 n = relative acceleration in g's between the stages

It is seen that the separation periods are on the order of one to three seconds for most of the combinations and that the least time is attained by thrusting the boosters forward from the boosted stages.

4.8.1.2 Separation Events

The basic choices for separating the parallel stages appear to be: (1) by thrusting the boosted stage forward from the booster (no

By _____	Date _____	BELL Aircraft CORPORATION	Model _____	Page 4-140
Lead _____	Date _____		Missile _____	Report D113-945-012
			Airplane _____	

thrust separation would be a special case of this), or (2) by thrusting the booster forward from the boosted stage. The second case has several disadvantages, though, as indicated above, it can give the least separation period. This case puts the less valuable booster ahead of the boosted stage where its downwash affects the boosted stage and where, after its burnout, the other stage could collide with it. Also the booster motors must be burned during and for a period after separation which reduces the overall propulsive efficiency of the system. The first case appears to be the more reasonable and is considered further here.

It is felt that instantaneous aerodynamic forces during the separation of the various stages cannot be predicted with any accuracy until test data for the possible interaction configurations and conditions is available. For this reason separation is examined from the standpoint of general possibility of events.

Immediately before separation the combined configuration is assumed to be in trimmed straight line flight. If the boosted stage is thrust forward from the booster, the following appears possible. The nose of the boosted stage projects forward and a strong shock pattern with high pressures behind it will form between the bottom of this nose and the top of the booster nose. As the boosted stage continues forward (relatively) the high pressure region grows, extends back between the bodies and begins to force the bodies apart. The rocket exhaust may impinge on the booster top increasing pressure aft of the boosted stage. The relative tendencies as the boosted stage passes over the booster appear to be: (1) to force the booster down and pitch its nose down, (2) to force the boosted stage up, pitch its nose up at first and then down. Overall, there is a definite vertical separation tendency. If the aerodynamic forces and the oscillations produced by the separation can be tolerated and damped, separation in this manner appears feasible.

The large flat top and bottom surfaces of the present MX-2276 stages will tend to promote high interaction pressures and will give these extensive areas over which to act. In some areas normal shocks and the resultant high pressures undoubtedly will be produced. These may be critical to the flat surfaces which are not well suited to bear high pressure loads. The resultant total forces and moments may be more than needed or desired for the separation. The aerodynamic heating on the high pressure areas and the heating from rocket exhaust impingement also may be problems, though they are very highly transient in nature.

4.8.2 Tandem Staging

While in the original concept the stages are arranged in parallel, the feasibility of tandem staging should not be excluded from future design considerations. Some of the relative advantages of the two arrangements are as follows:

Best Available Copy

- (a) Handling - The parallel arrangement is apparently easier to erect, combine stages, and service before launch.
- (b) Stability - When the final stage is winged, it is easier to make the parallel configuration aerodynamically stable. It is more difficult to arrange the thrust axes of the rocket motors of parallel stages to pass through the overall center of gravity.
- (c) Control - Control motors would generally have longer moment arms, thus be more effective, for the tandem case.
- (d) Performance - A tandem configuration can probably be made cleaner dragwise. The parallel arrangement allows simultaneous burning of motors from several stages.
- (e) Aerodynamic Heating - The tandem stages can be arranged so that the final stage forms the nose of the complete configuration thus producing thicker boundary layers on the aft stages and less heating there. On the other hand, the final stage can be at least partially protected in the parallel arrangement, e.g., the final stage body bottom in the present MX-2276 combination.
- (f) Separation - The parallel configuration is subject to high interaction forces, large local loads, possibility of collision of stages. Tandem separation is essentially instantaneous; there is no aerodynamic interaction on the boosted stage from the booster; however, experience has shown that even the tandem separation gives large angular accelerations to the boosted stage.

4.8.3 Separation Testing

As stated before, it is believed that theoretical analyses of separation configurations will not be accurate enough to allow critical evaluations. This is based on past experience with problems of this type. Experimental evaluations will be essential and should be made as early as possible in a design program.

Static evaluation of interaction pressures and forces and overall forces and moments can be obtained in wind tunnel tests by mounting the stages on individual balances and placing them in their relative separation positions. The wind tunnel has also been used as part of the computation loop in solving dynamic separation problems. A step-by-step method is employed in which the forces and moments from the tunnel for one relative positioning of the vehicle and booster during separation are inserted in the equations of motion to determine for a selected time increment the next relative positioning in the tunnel, and so on successively.

SECRET

By _____ Date _____

BELL Aircraft CORPORATION

Model _____

Page _____

4-142

Checked _____ Date _____

Missile _____

Report _____

DL43-945-012

True dynamic evaluation, however, will have to be obtained through testing of free flight models. The flight test facilities and instrumentation techniques are available. Obviously, investigations of the MX-2276 separation at Mach number 13 may be difficult because of the high Mach number. In the interest of facility and economy, it seems most reasonable to do the majority of the preliminary and development testing at lower, more easily attained Mach numbers, find advantageous configurations there, and then check them at the higher actual separation Mach number.

Section 4.8 References

4.8-1 Anon. "Strategic Weapon System" Bell Aircraft Corporation Preliminary Design Report DL43-945-010, 15 July 1953

SECRET

SECRET

By _____ Date _____
 Checked _____ Date _____

BELL Aircraft CORPORATION

Model _____ Page 4-143
 Missile _____
 Airplane _____ Report D1143-945

TABLE 4.8.1-1

CRITICAL SEPARATION PERIODSMX-2276 PARALLEL BOOSTERS

(Separation of 1st Stage from 2nd and 3rd Stage)

	<u>Rocket Motors Burning</u> <u>1st Stage</u>	<u>2nd Stage</u>	<u>Period</u> <u>(Seconds)</u>	<u>Booster Sep.</u> <u>Direction</u>
a.	All	All	1.5	Forward
b.	All	Steering	1.3	Forward
c.	All	None	1.2	Forward
d.	Steering	All	2.3	Aft
e.	Steering	Steering	8.6	Aft
f.	None	All	1.8	Aft
g.	None	Steering	2.7	Aft
h.	None	None	3.1	Aft

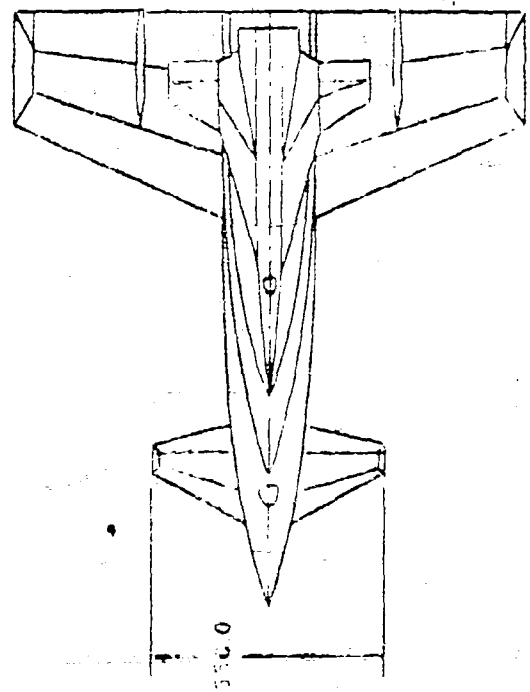
(Separation of 2nd Stage from 3rd Stage)

	<u>Rocket Motors Burning</u> <u>2nd Stage</u>	<u>3rd Stage</u>	<u>Period</u> <u>(Seconds)</u>	<u>Booster Sep.</u> <u>Direction</u>
a.	All	None	0.7	Forward
b.	Steering	None	1.7	Forward
c.	Steering	All	2.9	Forward
d.	None	All	2.0	Aft
e.	None	None	21.6	Aft

SECRET

SECRET
BELL Aircraft CORPORATION

**THREE VIEW OF MX 2276 STAGES
 (ORIGINAL CONCEPT)**



STAGE I BOOSTER	
GROSS WEIGHT	651000 POUNDS
EMPTY WEIGHT	165000 POUNDS
FULL THRUST	900000 POUNDS
STEERING THRUST	150000 POUNDS
STAGE II BOOSTER	
GROSS WEIGHT	155000 POUNDS
EMPTY WEIGHT	30000 POUNDS
FULL THRUST	300000 POUNDS
STEERING THRUST	50000 POUNDS
STAGE III GLIDE VEHICLE	
GROSS WEIGHT	45000 POUNDS
EMPTY WEIGHT	14600 POUNDS
FULL THRUST	50000 POUNDS

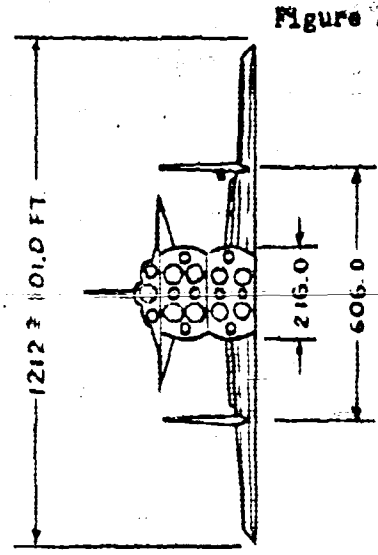
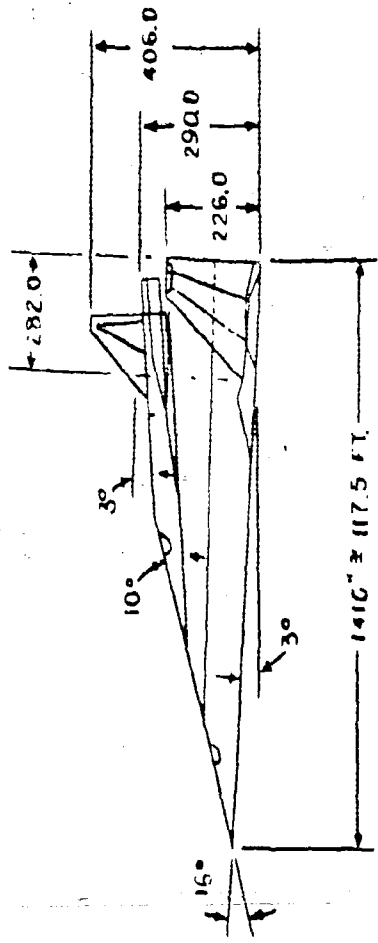


Figure 4.8.1-1



SECRET

SECRET

By _____ Date _____

Checked _____ Date _____

BELL *Corporation*

Model _____

Page _____

4-145

Missile _____

Airplane _____

Report _____

D113-945-012

4.9 Missile Trajectories.

A preliminary analysis of the zero lift trajectory of the MX-2276 missile has been made for two release conditions to illustrate the mechanics of the missile drop. Trajectories were calculated for initial velocities of 22,000 and 13,000 fps. and corresponding initial altitudes of 259,000 and 158,000 ft. respectively. The effects of earth rotation were neglected. A range of drag coefficients for the missile was used, and it was assumed that drag coefficient was constant over the range of flight velocity. Figure 4.9-1 presents the impact velocity, and the time and range interval between the time at which the carrier passes over the target and the time at which missile impact occurs. It is apparent from these results that the design of the missile will require a compromise between the desired impact velocity and the time and range interval. Figure 4.9-2 presents the line of sight angle from the carrier to the missile as a function of time from the drop point for two assumed drag coefficients.

SECRET

MX-2276

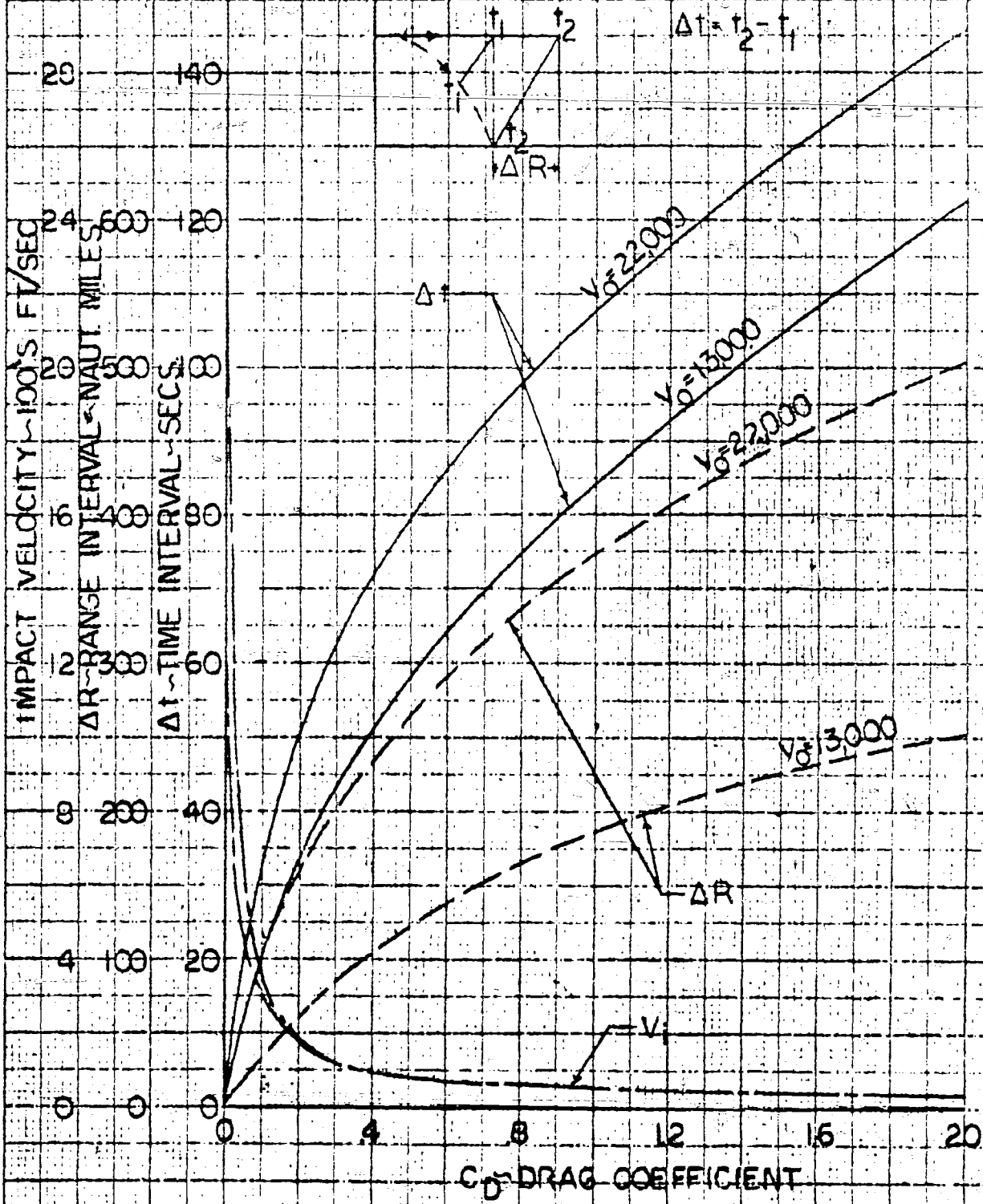
Figure 4.2-1

MISSILE ZERO LIFT TRAJECTORIES CONSTANT DRAG COEFFICIENT

$W = 4200$ lbs.

$d_{ia} = 50$ IN

$$\Delta t = t_2 - t_1$$



SECRET

RY
CHECKED

DATE
DATE

DELL *Corporation*

SHIP

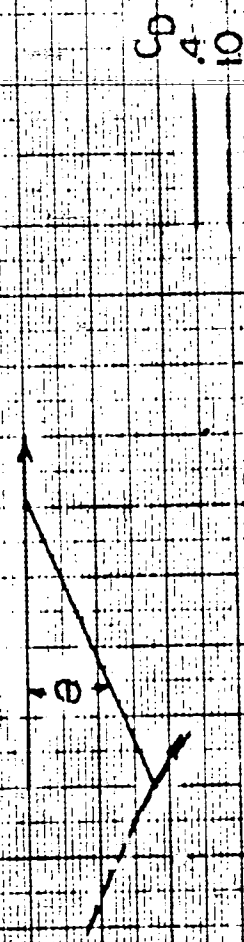
4-14?
D143-9115-012

2016 4 9-2

MX-2276
LINE OF SIGHT ANGLE FROM CARRIER TO MISSILE
CONSTANT MISSILE DRAG COEFFICIENT

W=4200 lbs.
dia=50 IN

SECRET



C_D
4.10

$V_0 = 13000$ FPS.
 $H_0 = 58000$ FT.

$V_0 = 22000$ FPS.
 $H_0 = 259000$ FT.

IMPACT

IMPACT

400

300

200

100

t - TIME OF FLIGHT - SECS

θ - LINE OF SIGHT ANGLE - DEGS

SECRET

By _____ Date _____
Checked _____ Date _____BELL *Aircraft* CORPORATIONModel _____ Page 5-1
Missile _____
Airplane _____ Report D143-915-012Section 5
Applied Research5.1 Introduction

Some of the stated objects of the present study were to take stock of the existence and accuracy of methods for analyzing the force and heat loads to which an aircraft in sustained flight will be subjected; to point out the major general and specific flow problems which need be solved in order to provide an adequate set of methods for predicting the aerodynamic performance, stability, and heating parameters in the Mach number - altitude range encompassed by MX-2276 flight, and to contribute, where possible, to the understanding of hypersonic flow problems and to the development and improvement of methods of analysis. One of the primary aims in the consideration of hypersonic flow problems was to point out the "new" or "unconventional" phenomena which are not apparent or do not occur at ordinary supersonic speeds and to attempt an assessment of the importance of such effects for MX-2276 flight.

Preliminary preparation for the study was the compilation of a complete as possible bibliography of all information pertaining to hypersonic and high altitude flight. A systematic search of the publications of government, military, and university research and development facilities, of military contractors, and of pertinent scientific periodicals was made to obtain references to all literature applicable to our work. The fields of interest in this search necessarily encompassed many areas of fundamental physics and chemistry, such as those concerned with dissociation and ionization of air at high temperatures, emissivities of gases, etc., as well as the more obvious subjects of supersonic and hypersonic flow, boundary layer theory and experiment, etc. Experience gained during our previous study of hypersonic aircraft leading to the proposal of Reference 5.4-35 and from our continued interest in the field since then served as a guide in this search. Concurrent with the setting of a literature reference file, a listing of all research facilities and of leading workers in various aspects of the field was started so that we would also have cognizance of sources of information bearing on hypersonic, high altitude flight.

During this literature survey it was recognized that a good possibility existed of there being pertinent research programs underway whose results were not yet reported in the literature or were reported by sources of which we were not yet aware. Furthermore, perusal of the available literature indicated a wide disparity of results (both theoretical and experimental) on some subjects, and in other areas of interest there apparently was no reliable information at all. Hence a series of visits to various research and industrial facilities in the country was indicated to insure overall cognizance of the field, to locate sources of information, and to discuss, on a background of knowledge of the available literature, some of the many bothersome points in the present "state of the art".

Form 14-1 Rev. 3-53

SECRET

SECRET

By _____	Date _____	BELL Aircraft Corporation	Model _____	Page <u>52</u>
Checked _____	Date _____		Missile _____	Report <u>D1143-945,012</u>

In planning the study proper it was obvious that a comprehensive and detailed monograph on aerodynamic methods and the underlying flow theory for hypersonic flight was beyond the scope of this limited study, even though the personnel performing this study had considerable background and research experience in theoretical and experimental fluid mechanics. Indeed, while the preliminary literature survey turned up over 2000 pertinent investigations on hypersonic flow and associated subjects, this branch of fluid mechanics is still relatively new and there are many gaps in theory and experiment to be filled in before the subject reaches the state where it will be amenable to a systematic, definitive treatment.

The actual plan of study adopted to carry out the objectives stated above featured several lines of approach. One approach centered about a critical investigation of the foundations and basic concepts of hypersonic flow theory to indicate the nature and types of flow patterns which could be expected to obtain; it was desired to determine both the physical problems and the basic flow equations which could adequately and consistently describe these flow problems. To this end, an analysis of the flow about a flat plate flying in the range of speeds and altitudes corresponding to the flight plan of MX-2276 was made delineating the nature and the extent of the various flow regions. In attempting to build up an overall picture of the various flow regions, however, details of the flow about a plate for various $M - Re$ combinations are required, and since there are very few experiments in the high M , low Re range of interest, these details must at present be supplied by theory. In particular, it was apparent that the bow shock-boundary layer interaction phenomena would be appreciable in parts of the $M - Re$ range of interest here.

A survey was then made of the various shock-boundary layer interaction theories to compile and correlate the information on this phenomena for use in building up a picture of the various flow regions and for predicting the pressure, shear, and heating parameters on a body in hypersonic flight. There were, however, several different theories predicting different results for some cases of shock-boundary layer interaction, while other cases of interest, e.g., the expansion side of a plate at angle of attack, had not been considered at all. It was necessary, therefore, to go into shock interaction theory in some detail in order to evaluate these theories. As a result, some improvements were made on existing theory, (flat plate, zero angle) and new theory and numerical results were obtained for the cases of interaction on a flat plate at positive and negative angles of attack. The details and results obtained are given in Section 5.3; it is shown there that the increases in pressure and skin friction coefficient due to shock interaction for all cases can be correlated in a general but simple and convenient form. The application of these results to the MX-2276 configuration is given in Sections 4.4, 4.6, and 4.7.

SECRET

SECRET

By _____ Date _____
 Checked _____ Date _____

BELL Aircraft

Model _____ Page 5-3
 Missile _____
 Airplane _____ Report D1143-945-01

The detailed investigation of shock-interaction theory led in turn to a thorough study of hypersonic inviscid flow theory, since results of the latter have an important influence on the results of interaction theory based on the two layer model. Furthermore, the so-called "Newtonian flow" approximation of inviscid hypersonic flow is an important practical method for determining pressure distributions on a body where viscous effects do not predominate, and hence the applicability and limits of this approximation merited consideration. Some contributions to an understanding of and an improvement in accuracy of the approximate hypersonic inviscid theory were made and are described in Section 5.6.

It is of interest to remark that the nature of the present type of study is illustrated by the particular problems discussed in the above paragraphs. This nature is such that in order to build up an overall perspective of hypersonic flow theory a knowledge of many details of the flow pattern is required; thus where basic flow problems have not been solved - or where existing solutions may be thought inadequate - these must be looked into in order to make progress in the overall picture. At the same time, an overall perspective of the field is required as a guide to a choice of the more significant detailed problems to investigate. Thus the nature of the study requires detailed investigations as well as overall surveys and evaluations.

In any evaluation program, furthermore, some detailed work on specific problems is necessary in order to emphasize the numerous assumptions involved, and to get a "feel" for the qualitative and quantitative effect of these assumptions on the theoretically predicted results; this is particularly true when theories are developed and partially checked experimentally in one range of M and Re and then are extrapolated to another $M - Re$ range where there are few, if any, experimental checks.

The analysis which was made to delineate the nature and the significant features of hypersonic flow is presented in Section 5.2. It serves to point out the need for fundamental investigation of slip flow and also to indicate the order of magnitude of the extent of slip flow for points on the MX-2276 flight path. Furthermore, the parameters which must be considered for similarity in experimental work in the high $M -$ low Re range are brought out by the analysis of Section 5.2.

Another line of approach followed in this study was to make probing investigations into the nature and magnitude of "new" effects arising from the high temperatures which would be realized in the boundary layer and behind strong shocks in hypersonic flight. To this end studies were made of the emissivity of air - which governs radiative heat transfer - and of the effect of dissociation of the air on

Form 20-1 Rev. 2-53

SECRET

SECRET

By _____ Date _____
Checked _____ Date _____

BELL Aircraft Corporation

Model _____ Page 5-4
Missile _____
Aircraft _____ Report DE-43-945-01

conductive heat transfer; in these cases determination of even the order of magnitude of an effect involved detailed investigations. These and other considerations of ultra high temperature effects are gathered in Section 5.4.

A third line of approach was to extend conventional supersonic flow theory to high Mach number and low densities, particularly where the results of such theories were needed for the engineering studies of the overall performance of MX-2276. The study of transpiration cooling reported in Section 5.5 falls in this category as does some work on the conditions at the nose of a blunt body; the latter is not reported separately but results are used in Section 4.6. A study of the status of theory and experiment related to determination of the transition between laminar and turbulent boundary layer flow was also made, since predictions of total skin friction for a given aircraft configuration are dependent on the assumption of a "transition point"; this is reported in Section 5.7.

As a by-product of these studies, basic physical data on the transport properties of air and on the properties of the atmosphere published in various sources were compared and compiled, and a choice was made of the tentative "standards" to be adopted for the present or future studies. These compilations are given in Reference 5.4-36 and 5.4-55. Also, a program (underway at Bell Aircraft Corporation before the start of this study) to compute basic tables of flow parameters for both shock flow and isentropic flow, incorporating the real gas effects (mainly thermal imperfections) up to dissociation temperatures was completed. The problem is discussed briefly in Section 5.4.4, and the complete tables are given in Reference 5.4-50.

This report is concerned mainly with describing the results of the more or less detailed and original investigations which were made in carrying out the objectives of the present study. It was not desirable or feasible to report on the detailed information gleaned from the literature and from discussion with many workers in the field of hypersonic aerodynamics. It is remarked, however, that the background and overall perspective of the subject thus gained is reflected in the choice and handling of the methods employed in the general aerodynamic analyses and in the recommendations for future work.

SECRET

By _____ Date _____

BELL Aircraft CORPORATION

Model _____ Page 5-5

Checked _____ Date _____

Missile _____ Report D143-945-012
Airplane _____

5.2 Fundamental Equations: Flow Regions

In 1946, Tsien (Reference 5.2-1) suggested a set of criteria which roughly divided fluid mechanics into several now familiar "realms" determined by the Mach number and Reynolds number of the flow. Essentially he defined the gasdynamic region, the slip flow region, and the molecular flow region; the nature of the flow phenomena and the form of the appropriate equations and boundary condition governing the flow is the same in each region but, of course, is considerably different amongst the regions. The aim of the present study was to delineate somewhat more precisely the various flow patterns and flow regions which would be encountered in hypersonic flight and to indicate in each region the fundamental equations and boundary conditions which must be considered in order to consistently and adequately represent the physical situation.

We start with the usual concept of a supersonic flow pattern as depicted in Figure 5.2-1a.

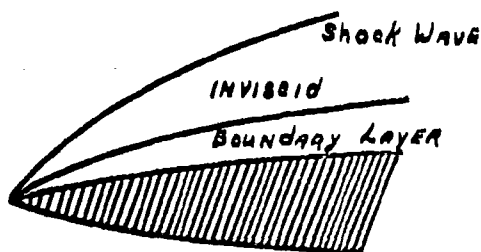


FIG. 5.2-1a

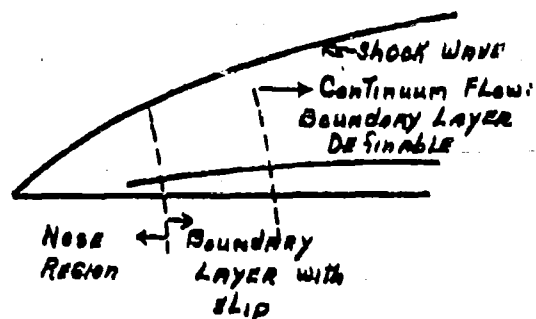


FIG. 5.2-1b

By _____ Date _____

BELL Aircraft CORPORATION

Model _____ Page 5-6

Checked _____ Date _____

Missile _____ Airplane _____ Report D-143-945-012

A shock wave - in which the flow parameters p , ρ , T , etc., change very rapidly, almost discontinuously, in essentially the stream direction - is formed in front of the body, and in the narrow boundary layer adjacent to the body the flow parameters vary rapidly (essentially) normal to the direction of flow; there are also other shock waves formed at the rear of the body and over any proturbances. The conventional approach to a theoretical analysis of this flow is in two steps. First, the equations governing the flow of a dense, inviscid, non-heat conducting gas are solved - to some degree of approximation - for the region exterior to the body (including the shock waves which are treated mathematically as discontinuities); these solutions yield velocity and pressure distributions over the body. Second, the boundary layer is treated as a separate flow region, where the equations governing this flow are those for a viscous, heat-conducting dense gas, and the boundary conditions on this flow are zero velocity on the body itself and at the outer "edge" of the boundary layer the computed velocity from the inviscid flow solution. The complete "viscous" equations - which are not in general amenable to solution - are simplified for application to boundary layer flows by an order of magnitude analysis whereby terms containing derivatives of the flow parameters along the body are neglected with respect to derivatives of these parameters normal to the body, the latter being of a higher order of magnitude in a sufficiently thin layer. The boundary layer equations are then solved - numerically or analytically - to yield friction and heat transfer coefficients on the surface, as well as an expression for the thickness of the layer.

At hypersonic speeds and low densities the boundary layer thickens appreciably, causing a change in the effective body shape which the external or inviscid flow sees and thus producing, in particular, a change in the bow shock pattern which in turn increases the pressure acting on the boundary layer and tends to thin it. When this occurs, the inviscid flow and the boundary layer can no longer be solved independently but must be considered together. This hypersonic shock-boundary layer interaction is treated in some detail in Section 5.3.

Actually, the idealized two region concept of a flow pattern is not valid at the very nose of the body, at any speed; here the velocity and temperature gradients in any direction are of the same order of magnitude and hence the flow in the whole nose region is dominated by viscous effects. At the speeds and velocities associated with ordinary supersonic flight, the nose region where a boundary layer is not definable is very small - of the order of a fraction of an inch and is ignored for all practical purposes. For an aircraft such as MX 2276, however, where hypersonic speeds are reached at high altitudes and thus low air densities, the extent of such a region can be of the order of magnitude of a foot.

By _____ Date _____

BELL *Aircraft* CORPORATION

Model _____ Page 5-7

Checked _____ Date _____

Missile _____
Airplane _____ Report D113-945-012

Furthermore even when a boundary layer is definable in low density flow, the fundamental equations governing the fluid flow and heat transfer are probably no longer the usual approximate form of the Navier-Stokes equations (which are based on the assumption of continuous flow). This assumption of a continuum cannot be justified when the mean free path in the microscopic picture of the gas is of comparable size to the smallest characteristic dimension of the flow; this dimension is the boundary layer thickness δ in the case of interest. The region in which continuum flow would be a very poor assumption could encompass several feet of the nose.

One way of looking at the flow pattern in high speed rarefied gas flow and breaking it up for analysis is shown in Figure 5.2-1b, where the surface is assumed to be a flat plate for simplicity. At some point sufficiently far downstream from the nose, a definite boundary layer region will obtain (with δ/x very small) inside of which the usual boundary layer equations will govern the flow and outside of which the flow may be considered inviscid; the two regions, however, must be solved simultaneously. Moving upstream, there are two possibilities; (a) the thickness δ of the boundary layer decreases so that the situation will obtain where the local mean free path $\lambda \approx \delta$, i.e., the continuum assumption is no longer valid, and we have a "slip flow" region; (b) even though δ decreases, δ is still small, but δ/x increases to where $\delta/x = O(1)$; in this case the continuum flow assumptions are valid, but the boundary layer simplifications where gradients normal to the flow are assumed much larger than gradients with the flow (due to the "thinness" of the layer) are no longer valid. It is not evident apriori which effect occurs closest to the nose, but the result of the analysis outlined below indicates the situation shown in Figure 5.2-1b.

The region immediately surrounding the nose is not describable in terms of a reasonably simple model; indeed, very little is known of the details of the flow in this region. Certainly any consideration of this flow must be based on the molecular picture of a fluid, and factors such as the ratio of plate thickness to mean free path and absolute value of mean free path (which determines shock thickness to some extent) will play a role in determining the flow here. Considerably more experimentation is needed to obtain an understanding of the flow in this nose region.*

*Some rarefied flow experiments have been carried and in the last few years by S.A. Shaaf and co-workers at the University of California cf. e.g., Reference 5.2-3.

By _____ Date _____

Model _____ Page 5-8

Checked _____ Date _____

BELL Aircraft CORPORATION

Missile
Airplane

Report D113-945-012

In the present analysis an attempt is made to indicate where ** the concept of a boundary layer may be expected to be valid in hypersonic flow, and where the Navier-Stokes equations may be expected to be an adequate set of equations to describe the flow; consideration is also given to when slip at the surface of the body will occur. Since the latter equations are the basis of practically all present boundary layer theories from which, in turn, methods for prediction of skin friction and heat transfer parameters are derived, these considerations can serve as a guide in evaluating the limits applicability of such methods.

The investigation was based on the assumption of the Burnett equations derived from kinetic theory (cf. e.g., References 5.2-4, 5.2-5) as the fundamental equations governing the fluid flow and heat transfer in a slightly rarefied gas. There are the most generally accepted set of equations, * although their formulation is not completely satisfactory. Assuming a thin boundary layer region with gradients normal to the surface $O(1/\delta)$ and gradients along the surface of $O(1)$, a detailed comparison was made of the order of magnitude of the Burnett terms relative to the Navier-Stokes terms. The criterion defining slip was taken to be when the ratio $\frac{\text{Burnett terms}}{\text{Navier-Stokes terms}}$ became of a significant size, thus indicating where the Navier-Stokes equations may not be adequate to describe the flow. This criterion is designated here for convenience as one for "inside slip" and indicates where the rarefaction of the gas (relative to the characteristic dimension δ of the flow) should be taken into account in obtaining a fundamental set of equations. The numerical value of the ratio which will be a significant size is, of course, an open question; in the following ratios of 1/10 and 2/10 were considered as significant.

It was found possible to equate the ratio $\frac{\text{Burnett terms}}{\text{Navier-Stokes terms}}$ to the ratio $\frac{T}{p}$ in the boundary layer, and it can be shown that the maximum of this quantity occurs at the point in the boundary layer immediately adjacent to the surface, both when the surface is considered insulated or cooled; hence $\left. \frac{T}{p} \right|_{\text{max.}} = \frac{C_f}{C_p}$. This suggested the following procedure

*The validity of these equations, however, has recently been challenged on the basis of low density shock experiments at the University of California

**i.e., distance downstream from edge of plate.

By _____ Date _____

BELL *Aircraft* CORPORATION

Model _____ Page 5-9

Checked _____ Date _____

Missile _____ Report ML 3-945-012
Airplane _____

for studying when "inside slip" - in the sense defined above - will occur: Solutions for the hypersonic flow over a flat plate were obtained, on the basis of the conventional inviscid-viscous regions picture, using the boundary layer approximation of the Navier-Stokes equations in the latter region and taking the interaction between regions into account; this is detailed in Section 5.3. From these solutions the ratio $\frac{C_f}{C_p}$ at any distance from the edge of the plate can be calculated

for any flight condition - Mach number, altitude, and angle of attack - and, in particular, the distance from the nose at which $\frac{C_f}{C_p}$ (and hence

the ratio $\frac{B.T.}{N.S.T.}$) has the value $\frac{1}{10}$ of $\frac{2}{10}$ can be determined. The

results of such a procedure are shown in Figures 5.2-4a, 4b and 4c, where the practical case of a cooled plate was considered.

The "inner slip" boundary thus calculated can be presented in another way, namely in the $M - Re$ plane. For any given flight condition, the free stream condition and the distance (from nose) where $\frac{C_f}{C_p} =$

given ratio fixed a local Reynolds number. Since the results of Section 5.3 show that C_f and C_p are each essentially functions of

$\chi = \frac{M^{5/2}}{Re^{1/2}}$ and M only (at high M); the ratio $\frac{C_f}{C_p}$ at any point on

a plate at a given angle of attack is a function of M and Re only; hence a unique* curve of $\frac{C_f}{C_p} = \text{constant}$ in the $M - Re$ plane exists

and can be readily calculated from the results displayed in Figure 5.2-4.

The "inner slip boundaries" in the $M - Re$ plane for the case of flat plate ** are shown in Figures 5.2-2 and 5.2-3 where the criteria $C_f/C_p = 0.1$ and $= .2$ were used, and the cases of the insulated and the cooled plates were considered. In Figure 5.3-2 the criteria of Tsien (Reference 5.2-1) and of Shultz, etc. (Reference 5.3-7) and Mirels (Reference 5.3-8) for the slip boundary are also shown for comparison. Of interest is the difference between the boundary for a given ratio of $\frac{B.T.}{N.S.T.}$ according as the plate is insulated or cooled.

* In the engineering sense that a single curve can be faired through calculated points.

** Here, since solutions are analytic, the boundaries can be determined analytically.

By _____	Date _____	BELL <i>Aircraft</i> CORPORATION	Model _____	Page 5-10
Checked _____	Date _____		Missile _____	Report D113-945-012
			Airplane _____	

Looking back, what was done here was to use solutions of the usual boundary layer equations (including shock-boundary layer interaction effects) to check the internal consistency of these equations by indicating where corrections to these equations are apparently necessary, and to show the results as "boundaries" in the $M - Re$ plane. These considerations only serve to point out the possible extent of rarefied gas effects on a surface in hypersonic flight. The question of the qualitative and quantitative nature of these effects remain to be determined by experimental and theoretical investigations.

The terms of "slip" is usually applied to the case where a rarefied gas does not stick to a surface but slips over it with a finite velocity. From kinetic theory, the slip velocity along the wall is given by

$$\frac{\Delta u}{U_\infty} \approx \frac{\lambda}{U_\infty} \frac{\partial u}{\partial y} + \frac{9}{4} \frac{\mu}{\rho T} \frac{\partial T}{\partial x}$$

where $\lambda \sim 1$. For constant wall temperature

$$\frac{\Delta u}{U_\infty} \approx \left(\frac{\lambda}{U_\infty} \frac{\partial u}{\partial y} \right)_w \approx \frac{a_w}{a_\infty} \frac{1}{M_\infty} \left(\frac{\mu}{\rho} \frac{\partial u}{\partial y} \right)_w \approx \frac{a_w}{a_\infty} \frac{1}{M_\infty} \frac{C_p}{C_p}$$

Since

$$\frac{\lambda}{a} = \sqrt{\frac{\pi}{2\gamma}} \frac{\mu}{\rho}$$

from simple kinetic theory. In the case of an insulated plate,

$$\frac{a_w}{a_\infty} \approx \sqrt{\frac{\gamma-1}{2}} M_\infty, \quad \text{thus} \quad \frac{\Delta u}{U_\infty} \approx K \frac{C_p}{C_p}$$

where $K < 1$. Thus it is seen that the parameters signifying slip on the boundary and "inside" slip are essentially the same at high M differing only by a numerical factor. However, the actual correction *

Note: * correction to the solution of the problem with assumed no-slip boundary condition.

By _____ Date _____

BELL *Aircraft* CORPORATION

Model _____ Page 5-11

Checked _____ Date _____

Missile _____
Airplane _____ Report D143-945-012

which say 10% slip, i.e. $\frac{\Delta u}{u_\infty} = 0.1$ will cause to some measurable

characteristic of the flow like the skin friction and the correction which would come from using a more complete set of fundamental equations to describe the flow** when $\frac{B.T.}{N.S.T.} = 0.1$ are not known;

so that the relative importance of these effects cannot be quantitatively discussed. It is of interest to note, however, that for a cooled wall $a_w \sim a_\infty$, so that $\frac{\Delta u}{u_\infty} \sim \frac{1}{M} \left(\frac{C_f}{C_p} \right)_w$; thus for high M

it appears that the effect of slip at the wall lags behind the effect of rarefaction or "inside slip" on the basic equations.

Slip boundaries for $\frac{\Delta u}{u_\infty} = 0.1$ & 0.2 and for

$T_w = 3T_\infty$ and the insulated wall are shown in Figures 5.2-2 and 5.2-3. Also, to round out Figure 5.2-3, some curves indicating where shock boundary layer interaction effects are strong ($\frac{\Delta p}{p_\infty} \geq 4$)

and weak ($\frac{\Delta p}{p_\infty} \approx 0.1$) are shown, again for the two cases of $T_w = 3T_\infty$ and the insulated wall.

* Correction to the solution of the problem with assumed no-slip boundary condition.

** Providing the proper equations were known and solutions to them could be obtained.

SECRET

By _____ Date _____

Checked _____ Date _____

BELL *Aircraft* CORPORATIONModel _____ Page 5-12Missile _____
Airplane _____ Report D143-945-012

A curve representing the values of Mach number and local free stream Reynolds number attained at the one foot point of a flat plate (zero angle) flying the MX-2276 glide path is shown to indicate what regions of the M - Re plane are of interest for this aircraft.

The details of the study outlined above, and a more complete discussion of the problem of determining the appropriate fundamental equations and boundary condition is given in Reference 5.2-8.

SECRET

By _____ Date _____

Checked _____ Date _____

BELL *Aircraft* CORPORATION

Model _____ Page 5-13

Missile _____
Airplane _____ Report D143-945-012Section 5.2 References

- 5.2-1 Tsien, H. S.: Superaerodynamics, Mechanics of Rarefied Gases. Jour. Aero. Sci., 13, 653-664 (1944)
- 5.2-2 MX-2276 Interim Technical Report: Bell Aircraft Corporation Report No. D143-945-011, Oct. 25, 1954.
- 5.2-3 Shaaf, S. A., and Maslach, G. J.: Recent Developments in Rarefied Gas Dynamics Research. Presented at U. S. Navy Symposium on Aeroballistics, Laurel, Md. October 1954.
- 5.2-4 Burnett, D.: Proc. Lond. Math. Soc. 40, 382 (1935)
- 5.2-5 Chapman, S., and Cowling, T. G.: The Mathematical Theory of Non-Uniform Gases. Cambridge University Press, (1953)
- 5.2-6 Siegel, M. K.: Boundaries of Fluid Mechanics. Jour. Aero. Sci. 17, 191, (1950)
- 5.2-7 Mirels, H.: Estimate of Slip Effect on Compressible Laminar Boundary Layer Skin Friction NACA TN 2609, January 1952.
- 5.2-8 Isenberg, J. S., Cheng, H. K, Pallone, A. J, and Roehrs, F.: Bell Aircraft Corporation, Aerodynamics Section - Theoretical Research Note No. 3, April 1955.

Figure 5.2-2

REYNOLDS NO

10² 10³ 10⁴ 10⁵

FLOW REGIONS
(FLAT PLATE)

MACH NO

SECRET

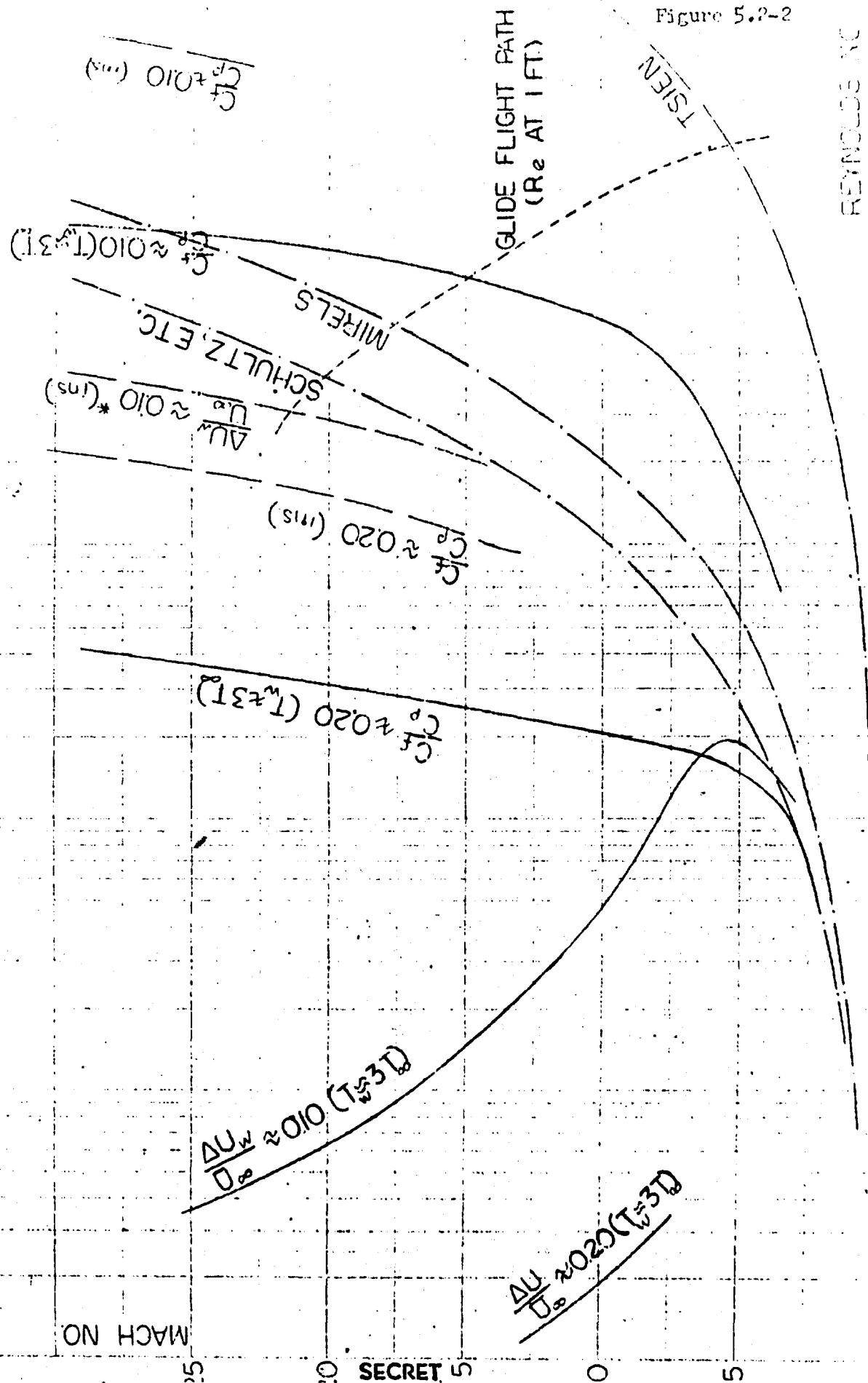
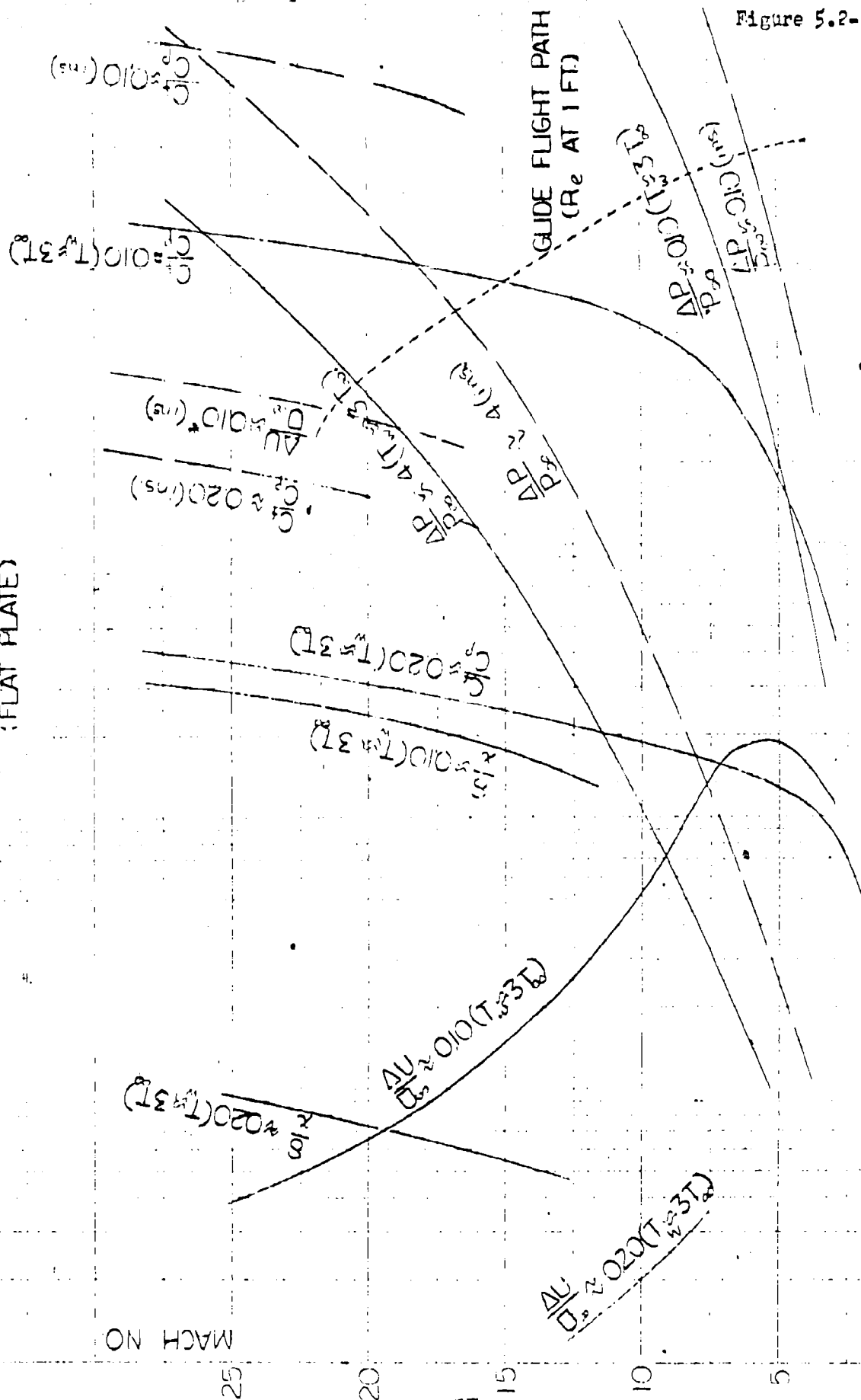
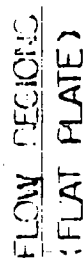


Figure 5.2-3

DESIGNING NO



DATE
DATE

REVISION
STEP

51

Figure 6

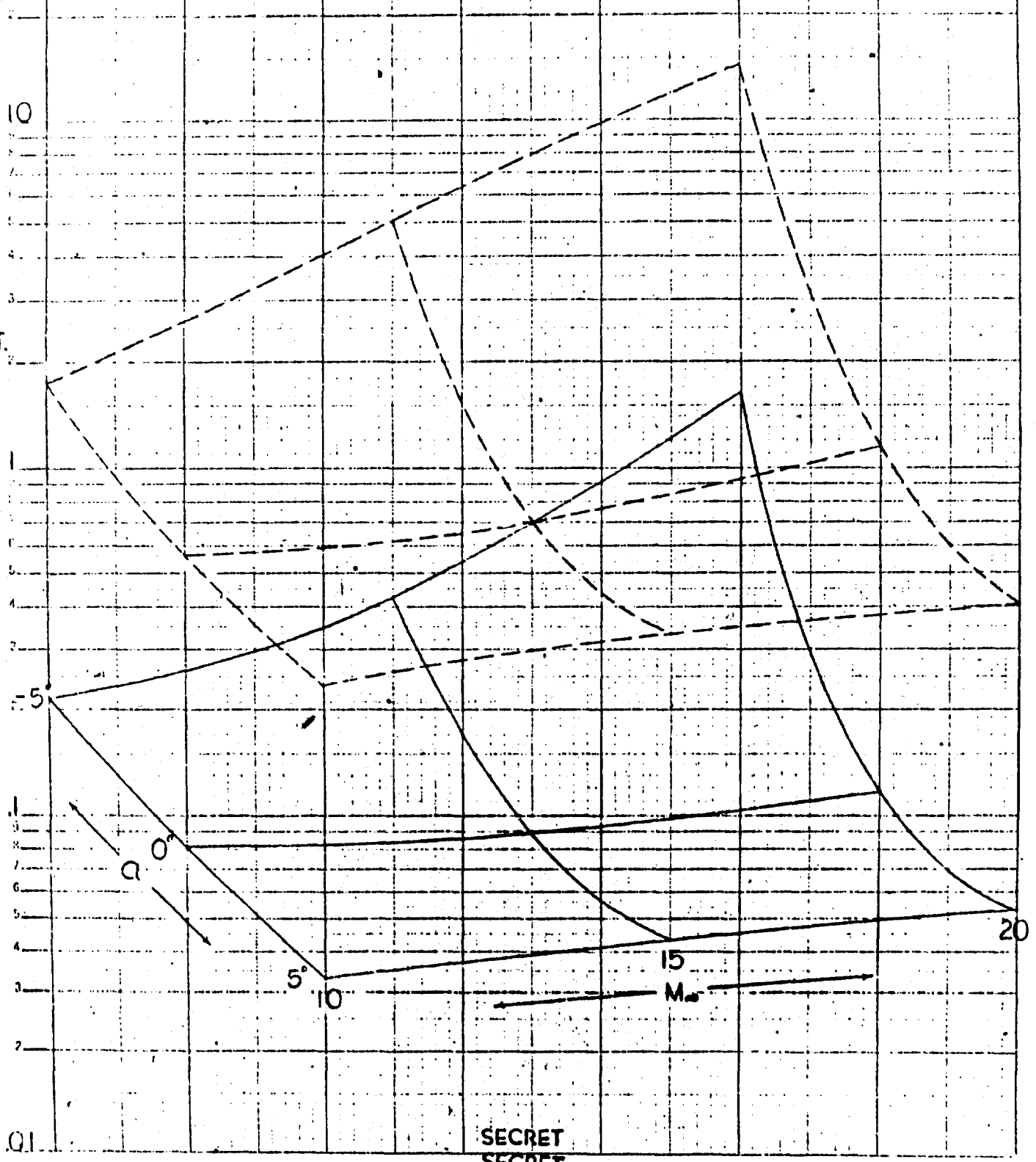
EXTENT OF SLIP REGION

DISTANCE X FROM LEADING EDGE

WHERE $\frac{\lambda}{\phi y}$ IS 1 ---
2 —

$h = 130,000$

X-FT.



EXTENT OF SLIP REGION
 DISTANCE X FROM LEADING-EDGE

WHERE $\frac{\lambda}{a} \frac{\partial u}{\partial y} = 1$ ---
 2 ---

$h = 200,000$

Figure 5.2-1b

X-FT.

10

-5°

0°

5°

10

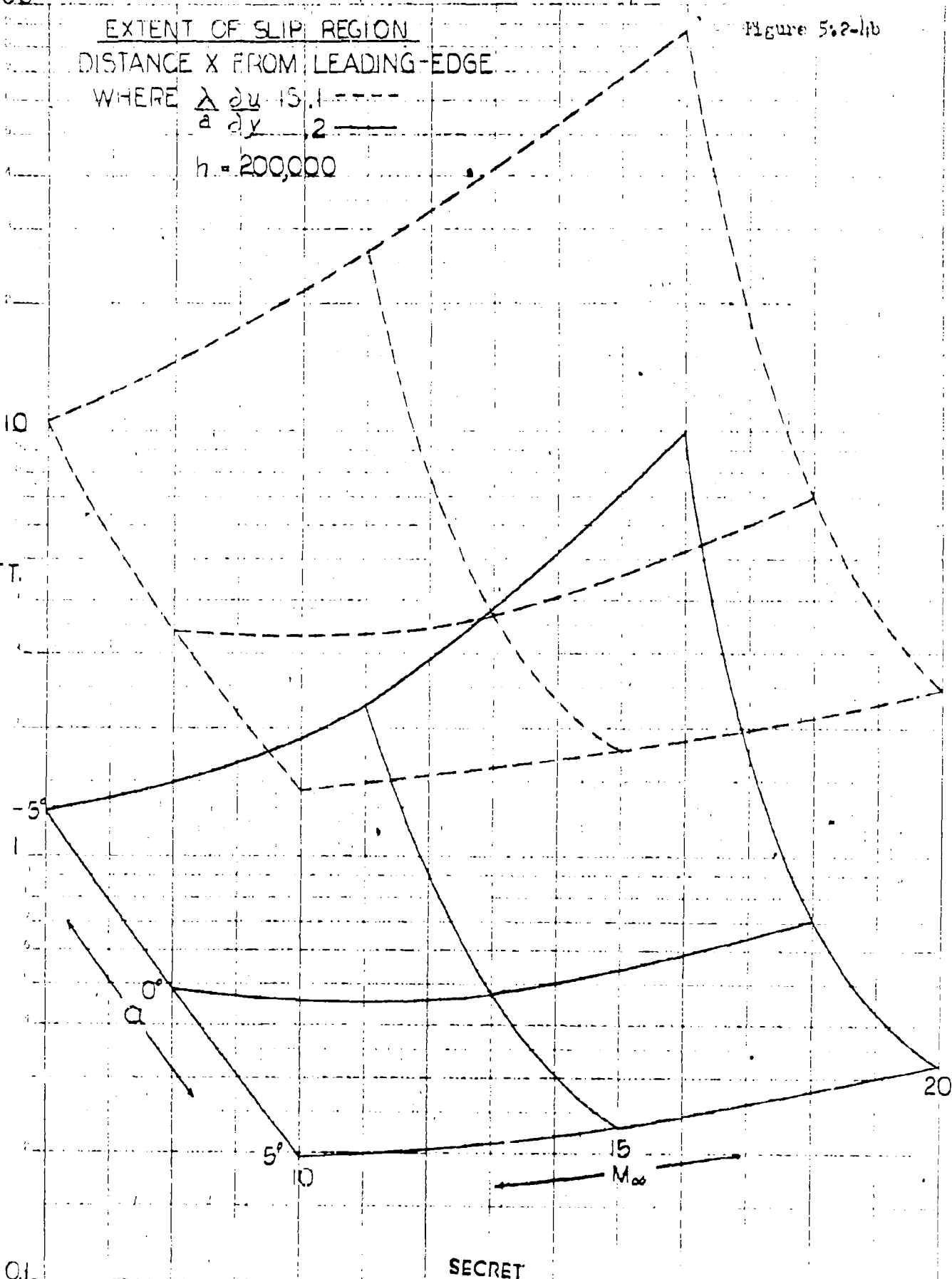
15

M_∞

20

O.I.

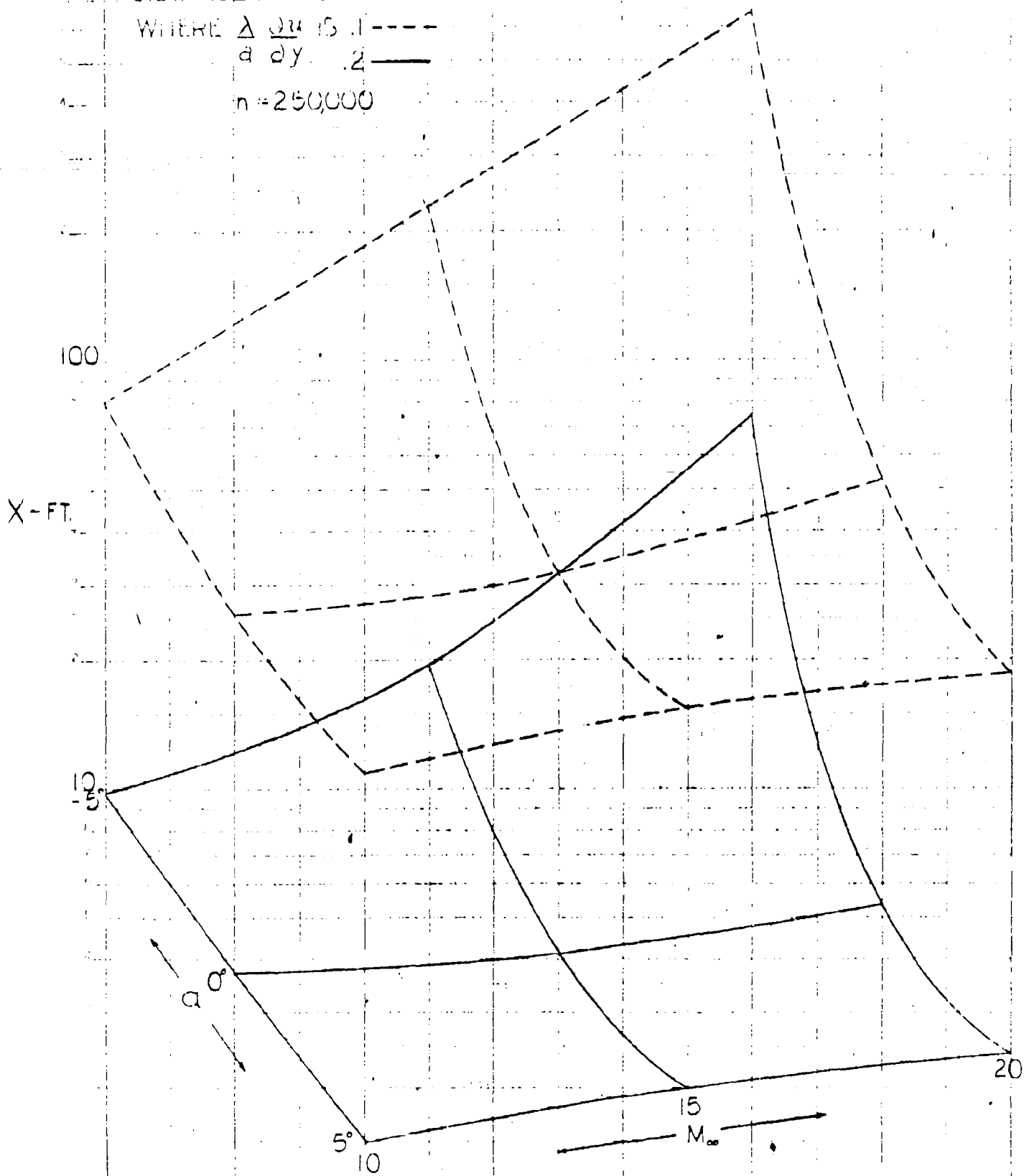
SECRET



EXTENT OF SLIP REGION
 DISTANCE X FROM LEADING-EDGE

Figure 5.2-10

WHERE $\Delta \sigma$ IS 1 ---
 2 ———
 $n = 250,000$



By _____	Date _____	BELL <i>Aircraft</i> CORPORATION	Model _____	Page <u>5-19</u>
Checked _____	Date _____		Missile _____	Report <u>D1113-915-012</u>

5.3 Bow Shock - Boundary Layer Interaction

5.3.1 Introductory Remarks

The flow over a body in supersonic flight is usually determined in two distinct steps: first the assumed inviscid flow about the body including shock waves is computed to determine, for one thing, the pressure distribution on the body; then on the assumption that viscous effects are confined to a thin boundary layer adjacent to the body, an approximate solution is found for the flow in this region - bounded by external inviscid flow and solid boundary - where the external pressure distribution is now known, thus obtaining the shear stress on and the heat loads into the body. The boundary layer solution also gives an expression for the displacement thickness of this layer which represents at any point the distance which the streamlines of the inviscid flow are deflected away from the body because of the retardation of the flow in the boundary layer (since mass flow between a streamline and the solid boundary is constant).

The deflection of the streamlines in the essentially inviscid or external flow is actually due to the physical body plus the displacement thickness. This change in the effective shape of the body changes the pressure about the body which, in turn, affects the flow in the viscous layer. At low supersonic speeds and the associated flight altitudes (relatively high density) this "interaction" effect is small, and can be neglected. In hypersonic flight, however, the high M and low Re (high altitude) both produce a rapid thickening of the boundary layer and hence a very significant interaction between inviscid - viscous flow regions; also, at high Mach numbers the bow shock wave lies close to the surface of the body (actually the edge of the boundary layer) and the region in which inviscid flow may exist behind the shock wave is very limited.

In this section the problem of the simultaneous solution of the boundary layer and the external flow equations is considered in order to obtain a theory for predicting the increases* in pressure and skin friction on the nose of a body in hypersonic flight. Some improvements are made on the existing theory (flat plate, zero angle) and new theory and numerical results are obtained for the cases of interaction on a flat plate at positive and negative angles of attack, and for the practical case of a cooled wall. It is shown how the numerical results for interaction induced pressure for all cases (zero, positive and negative angles of attack) can be correlated with respect to the parameters

$$\chi = M^{5/2}/Re^{1/2} \text{ and } M\alpha \text{ in a general but simple and convenient form;}$$

* i.e., increases over what values would be predicted by inviscid plus viscous flow solutions ignoring interaction.

By _____ Date _____

BELL Aircraft CORPORATION

Model _____ Page 5-20

Checked _____ Date _____

Missile _____
Aircraft _____ Report DL43-945-012

this is given in Figure 5.3-1. A similar correlation for $M^3 C_p$ is given in Figure 5.3-3. The general results of Figure 5.3-2 are applied to determine the pressure at the nose of a 5° wedge flying at $M = 20$ at various altitudes, as an illustration of the magnitude and the extent of the interaction effect; the results are shown in Figure 5.3-4. The specific application of these results to the MX 2276 configuration is given in Sections 4.4, 4.6 and 4.7.

The present analysis is restricted to two - dimensional flow and is based on the following assumptions:

The surface is an infinite flat plate with a mathematically sharp leading edge.*

The flow field between shock wave and surface is idealized as being divided into two regions or layers (cf. Figure 5.3-1), namely a viscous layer adjacent to the surface across which the pressure remains substantially constant, and an inviscid region between the shock and the viscous layer. In the latter region the flow is rotational due to entropy variation generated by the curved bow shock; the flow expands in this layer and the variation of centrifugal force through this expanding layer sets up a significant pressure gradient normal to the surface.

The fluid is a continuum and the flow in the boundary layer is governed by the usual Prandtl boundary layer equations approximating the full Navier-Stokes equations.** Furthermore, the fluid is assumed to be a perfect gas with constant (arbitrary) Prandtl number, constant (arbitrary) C_p , and following the Sutherland viscosity - temperature relation.

The plate is assumed to be cooled to a constant wall temperature.

The interaction problem differs from ordinary boundary layer problems in that the external flow field enters as an unknown, instead of being given. In order to obtain an analytical solution to the problem with a reasonable amount of labour, it is necessary to have an explicit expression between the induced pressure on the edge of the boundary layer and the rate of growth of this layer. It is found that when $M \frac{d\delta}{dx} \gg 1$

* Experimental evidence (cf. References 5.3-12 to 5.3-15) indicates that the result obtained for an infinite plate with a sharp leading edge cannot be indiscriminately applied to the region(s) near the leading and trailing edge(s); more theoretical and experimental work is necessary before a complete solution for the entire plate is possible.

** A discussion of the self-consistency and hence regions of validity of this assumption is given in Section 5.2.

By _____ Date _____

BELL *Aircraft* CORPORATION

Model _____ Page 5-21

Checked _____ Date _____

Missile _____ Report D143-945-012
Airplane _____

then a modified form of the tangent - wedge formula can be used - as discussed in Section 5.6 - , and when $M \frac{d\delta}{dx} < 1$, the Prandtl-Meyer relation between pressure and deflection angle can be used; when $M \frac{d\delta}{dx} \approx 1$ there is no really simple pressure - deflection relation.*

Before outlining the detailed analysis of the shock-interaction problem, it is of interest to consider this phenomena by an order of magnitude argument.

5.3.2 Order of Magnitude Considerations

The average value(s) of the temperature and velocity in the boundary layer in hypersonic flow are characterized by $\bar{T} \sim O(M_\infty)^2$ and $\bar{u} \sim O(U_\infty)$. Comparing the relative magnitude of the pressure gradient and the inertia terms in the x - momentum equations (cf. 5A-1), for instance, we obtain

$$\frac{\partial p}{\partial x} : \bar{\rho} \bar{u} \frac{\partial \bar{u}}{\partial x} \approx \frac{\Delta p}{p} : 1 \quad (1)$$

since $\frac{\partial p}{\partial x} \approx O\left(\frac{\Delta p}{L}\right)$

and $\bar{\rho} \bar{u} \frac{\partial \bar{u}}{\partial x} \approx \frac{p}{RT} \frac{\bar{u} \bar{u}}{L} \approx \frac{p \bar{M}^2}{L} \approx \frac{p}{L}$

since $RT \sim a^2$, $\bar{M} \sim 1$, and p = constant in the boundary layer. Accordingly, the pressure gradient effect is generally small when the pertur-

* In this case, however, a pressure-deflection angle relation can be obtained in series form by a perturbation from either the tangent - wedge or the Prandtl-Meyer relations.

By _____ Date _____	BELL Aircraft CORPORATION	Model _____	Page 5-22
Checked _____ Date _____		Missile _____ Airplane _____	Report D143-945-012

bation pressure is small, and becomes at most of the same order of magnitude as the inertia effect when the perturbation pressure is much larger than free stream pressure.

In the case of a flat plate at zero incidence, for example, the self-induced pressure increases with the hypersonic parameter of the external flow, i.e., $M_\infty \frac{\delta}{x}$; hence for a sufficiently small $M_\infty \frac{\delta}{x}$,

$$\frac{\partial p}{\partial x} : \bar{\rho} \bar{u} \frac{\partial \bar{u}}{\partial x} \approx 0 \left[M_\infty \frac{\delta}{x} : 1 \right], \quad (2)$$

whereas for large values of $M_\infty \frac{\delta}{x}$, say of order unity or larger, it can be seen from Equation (1) that the ratio reduces to $O(1:1)^*$.

From the above relation, it is seen that one may omit the self-induced pressure gradient effect in an order of magnitude analysis of the Navier-Stokes equations in the boundary layer, since it is at most of the same order as the inertia terms. Thus equating the rate of change of momentum to the shear stress we have

$$\bar{\rho} \bar{u} \frac{\partial \bar{u}}{\partial x} / \frac{\partial}{\partial y} \left[\mu \left(\frac{\partial \bar{u}}{\partial y} \right) \right] = 0 \quad (1) \quad (3)$$

Assuming a thin boundary layer δ and a regular velocity profile in this layer, it follows that

$$\frac{\delta}{x} \sim \frac{\mu \frac{\partial \bar{u}}{\partial y}}{\bar{\rho} \bar{u}^2} \sim \frac{\mu \frac{\partial \bar{u}}{\partial y}}{\bar{\rho} \bar{u}^2} \Big|_{\text{external flow}} \sim \frac{\tau}{\bar{p}} \sim \frac{C_f}{C_p} \quad (4)$$

where the bar denotes average values. Since $\mu \frac{\partial \bar{u}}{\partial y} \approx \frac{1}{2} \mu \frac{\partial \bar{u}}{\partial y} \Big|_{\text{max}}$

similarly $\bar{\rho} \bar{u}^2 \approx \frac{1}{2} \bar{\rho} \bar{u}^2 \Big|_{\text{max}} \approx \frac{1}{2} \bar{\rho} \bar{u}^2 \Big|_{\text{edge of layer}}$.

Now since

$$\frac{\partial \bar{u}}{\partial y} \approx \frac{\bar{u}}{\delta}, \quad \mu \frac{\partial \bar{u}}{\partial y} \approx \frac{\mu}{\bar{\rho} \bar{u} \delta} \approx \frac{\delta}{x}$$

so that

$$\frac{\delta}{x} \approx \left[\frac{\mu}{\bar{\rho} \bar{u} x} \right]^{1/2} \approx \frac{1}{R_\infty^{1/2}} \left[\frac{\mu}{\mu_\infty} \frac{T}{T_\infty} \frac{p_\infty}{p} \right]^{1/2} \quad (5)$$

By _____ Date _____

BELL Aircraft CORPORATION

Model _____ Page 5-23

Checked _____ Date _____

Missile _____ Airplane _____ Report D113-945-012

which is essentially the well known Prandtl result where now the Reynolds number based on the average properties characteristic of conditions in the boundary layer instead of on the free stream values is used. Assuming a power law viscosity - temperature relation $\mu \sim T^s$, we have, since $T \sim M_\infty^2$,

$$\frac{\delta}{L} \approx \left(\frac{p_\infty}{p} \right)^{1/2} \frac{M_\infty^{s+1}}{Re_\infty} = \frac{1}{M_\infty} \left(\frac{p_\infty}{p} \right)^{1/2} \chi \quad (6)$$

where

$$\chi = \frac{M_\infty^{s+2}}{Re_\infty^{1/2}}$$

Hence, it can be seen that, in general, compression tends to reduce the thickness of the boundary layer and expansion tends to increase it; the effect of the self-induced pressure gradient resulting from thickening of the boundary layer tends in turn to thin the boundary layer.

From Equations (4) and (6), it can be shown that

$$M_\infty^3 C_f \sim \left(\frac{p}{p_\infty} \right)^{1/2} \chi \quad (7)$$

Similarly, a consideration of energy balance in the boundary layer leads to

$$M_\infty^3 C_h \sim \left(\frac{p}{p_\infty} \right)^{1/2} \chi \quad (8)$$

where C_h is the heat transfer coefficient defined as

$$C_h = p \frac{\partial T}{\partial y} / \rho_\infty \bar{u}_\infty C_p T_0$$

Thus, the effect of compression is to increase the skin friction and the heat transfer rate, while expansion tends to reduce these parameters; the self-induced pressure gradient thus tends to increase both C_f and C_h .

For large value of the "hypersonic parameter", i.e., $M_\infty \tau' \gg 0(1)$, where τ' is an effective thickness,

$$\frac{p}{p_\infty} \sim F(M_\infty \tau'), \text{ e.g. } \frac{p}{p_\infty} \sim M_\infty^2 \left(1 + \frac{d\delta}{dx} \right)^2, \quad (9)$$

By _____ Date _____

Checked _____ Date _____

BELL Aircraft CORPORATION

Model _____ Page 5-24

Missile

Airplane

Report DL43-945-012

where α is the local inclination of the surface. For small values of M^* , i.e. $M^* \ll 1$,

$$\frac{p - p_\infty}{p_\infty} \sim M_\infty^2 \left(\alpha + \frac{d\delta}{dx} \right)^2 \quad (10)$$

In view of Equations (6), (7) and (8), it may be anticipated then that the expressions for p , C_f and C_h on the surface of a wedge in hypersonic flow will have the following functional forms for a considerable range of \mathcal{X} :

$$\begin{aligned} p/p_\infty &= F(\mathcal{X}, M_\infty) \\ M_\infty^3 C_f &= G(\mathcal{X}, M_\infty) \\ M_\infty^3 C_h &= H(\mathcal{X}, M_\infty) \end{aligned} \quad (11)$$

From the form of Equations (11) it is recognized that the important parameter in hypersonic viscous flow is \mathcal{X} .

It is emphasized that the above considerations on the relative order of magnitude of the flow parameters assumed that the velocity and temperature profiles are regular and that other effect such as the temperature distribution along the wall, etc., are not the essential features which to determine the interaction phenomena.

By _____ Date _____

BELL *Aircraft* CORPORATION

Model _____ Page 5-25

Checked _____ Date _____

Missile _____ Report D143-945-012
Airplane _____5.3.3 Outline of Analysis.

The detailed investigation was carried out along the lines of the von Karman integral method. The momentum and energy equations of the laminar boundary layer including the pressure gradient term* were formulated as two integral differential equations. Profiles for the local velocity and local stagnation enthalpy in terms of the distance from the wall were assumed, these profiles satisfying certain boundary conditions at the wall and at the outer edge of the boundary layer. With the assumption of these profiles and with the use of the Dorodnitsin transformation, discussed in Reference 5.3-11, the two integral differential equations are converted to ordinary differential equations which give essentially the variation of the boundary layer thickness and of the heat transfer parameter.

The solution of the problem for the flow over a flat surface at angle of attack α ** was obtained in two parts. In the first, a solution for the flow over the bottom of the plate was developed, using the assumption of third degree polynomials for the velocity and stagnation enthalpy profiles. The Prandtl number was left arbitrary, although it is required to be of order unity. Analytical results were obtained for the insulated and given constant wall temperature cases by expanding the solution in ascending and descending powers of the parameter X for strong and weak interaction***, respectively. For both the strong and the weak interaction cases the analytical solutions show that $p/p_\infty = f(X, M\alpha)$ and $M_{\infty}^2 C_f = g(X, M\alpha)$ for a given wall to free stream temperature ratio; results for the intermediate region can be extrapolated from the strong and weak interaction regions. All the details of the analysis are presented in Appendix 5B.

In the second part a solution for the flow over the top of the plate was developed, using a fourth degree velocity profile and a fifth degree stagnation enthalpy profile. Since in the present analysis a single boundary layer thickness is used by assumption that $Pr = 1$ instead of separate dynamical and a thermal boundary layer thicknesses, the stagnation enthalpy profiles were used here of one degree higher than the velocity profiles in order that the same number of boundary

*The pressure gradient is induced by the deflection of the inviscid flow streamlines and is a function of

$$\frac{\partial \delta}{\partial x} ; \text{ since } \left(\frac{\partial}{\partial x}\right)_1 = \frac{\partial}{\partial x} - \frac{(g - f^2)}{(e u)_1} \frac{\partial}{\partial x} (e u)_1 \quad \text{and for } X \gg 1$$

it is shown that $\delta^* \approx \delta$.

**The positive value of α corresponds to the bottom or compression side and the negative α corresponds to the top or expansion side.

***The strong interaction range was arbitrarily defined to begin at the value of X where the perturbation pressure is 800% of the asymptotic value ($X \rightarrow 0$); the weak interaction region was also defined to begin

By _____	Date _____	BELL <i>Aircraft</i> CORPORATION	Model _____	Page 5-26
Checked _____	Date _____		Missile _____	Report D143-945-012
			Airplane _____	

conditions be satisfied by the energy equation as were satisfied by the momentum equation. The practical case where the wall is assumed cooled to a uniform temperature was considered. The resulting two ordinary differential equations were solved numerically and the variation of the pressure, skin friction, and heat transfer parameters were calculated for several combinations of M , α , and altitude. It was found numerically that for $M \gg 1$ the relation $p/p_\infty = f(\chi, M\alpha)$ and $M^3 C_f = g(\chi, M\alpha)$ holds true also at the top for $\alpha \approx -10^\circ$; the results obtained for $M^3 C_f$ and p/p_∞ were correlated in χ and $M\alpha$ and plotted in Figures 5.3-3 and 5.3-2. The details of the analysis are given in Appendix 5A.

5.3.4 Discussion of Results

Numerical examples were calculated for the top and bottom of a flat surface in steady flight. For the top side the pressure and skin friction distribution were found for $M = 10, 15, 20$; $\alpha = -5^\circ, -10^\circ$, altitudes of 150,000, 200,000 and 250,000 feet and $\frac{T_w}{T_\infty} = 3$.

The results were correlated in terms of χ and $M\alpha$. The correlation was found to be very good for $M = 15$ and 20, but for $M = 10$ poorer results were obtained. The heat transfer coefficient (C_h) was found to vary between $1/2 C_f$ and $1/2.4 C_f$ for very weak and very strong interaction respectively; no curve has been plotted since in the flight regime in which we are interested $C_h \approx 1/2 C_f$.

For the bottom side of the plate numerical results for C_f and $\frac{p}{p_\infty}$ were obtained, using the method developed in Appendix 5B for the strong interaction region. The method of Lees and Probstein, Reference 5.3-1 was used for the weak interaction region since our analysis of this case was not completed at the time of computation, but it was later found that the increment in C_f and in $\frac{p}{p_\infty}$ given by Lees and Probstein are of the same order as the one given by our method. Results in the region of intermediate interaction were extrapolated from the weak and strong region.

The skin friction parameter $M^3 C_f$ and the pressure ratio $\frac{p}{p_\infty}$ are plotted as functions of χ for constant $M\alpha$ in Figures (5.3-3) and (5.3-2), respectively. It is interesting to notice that as $|\alpha|$ increases the viscous-inviscid interaction becomes weaker, and it becomes stronger as M increases. This observation is true for both top and bottom of the plate but the rates of increase or decrease are not the same.

***at χ where the perturbation pressure is 30% of the asymptotic value. Between the strong and weak interaction we have an intermediate region where no analytical solution is available.

By _____	Date _____	BELL <i>Aircraft</i> CORPORATION	Model _____	Page <u>5-27</u>
Checked _____	Date _____		Missile _____	Report <u>D143-945-012</u>

5.3.5 Remarks on Previous Work

Several attempts have been made to analyze and solve this problem of hypersonic shock-boundary layer. For the case of strong interaction there have been two distinct approaches used, insofar as the physical flow model is concerned. The first (c.f.e.g. References 5.3-3, 5.3-8) assumes that the region behind the shock wave consists of a viscous boundary layer and an inviscid region between the shock and the boundary layer, as illustrated in Figure 5.3-1. The boundary layer equations are applied to the boundary layer region and some approximation to the inviscid flow is applied to the inviscid but rotational region. The other approach (References 5.3-2, 5.3-4) assumes that the region between the shock wave and the body can be treated as a whole by the system of boundary layer equations, i.e., the edge of the boundary layer and the shock wave are made to coincide. Strictly speaking, an important assumption implied in the ordinary boundary layer equations system - namely, constant pressure across the layer - is not valid here, since near the outer edge of this layer where the viscous effect is relatively small a very strong normal pressure gradient exists due to the centrifugal force. Although the first approach - the two-layer theory - may not be appropriate at the immediate vicinity of the leading edge where the shock is close to the surface, this idealization, nevertheless, accounts for the pressure variation. In the present approach, the two-layer model has been adopted. For the weak interaction range, the distinction between a viscous and an inviscid region is more clearly the appropriate simple model.

From the mathematical viewpoint, there are also two distinct approaches. One (c.f.e.g. References 5.3-1, 5.3-3, 5.3-6, 5.3-10) assumes a linear viscosity - temperature relation which leads to relatively simple solutions of the differential equations. However, the linear viscosity-temperature relation is known to over or under estimate the fluid viscosity μ in the layer when the variation in temperature across the layer is large, such as the case of a cooled wall at high Mach number. The other approach (References 5.3-2, 5.3-4, 5.3-7, 5.3-8) employs the momentum-integral method: while the approximation to the flow details provided by this method is not precise, it nevertheless allows the use of a more accurate viscosity-temperature law. In the treatment presented in this report, the latter approach has been used. Analytic as well as numerical solutions are obtained for the case of a wedge at angle of attack, with a given wall to free stream temperature ratio - the case of practical interest. The Sutherland viscosity-temperature law has been adopted throughout, and polynomials of third and fourth degree are assumed to determine the velocity and stagnation temperature distributions. Previous works based on this approach either consider the case of an insulated wall or assume linear velocity or total temperature profiles.

SECRET

By _____ Date _____	BELL <i>Aircraft</i> CORPORATION	Model _____	Page <u>5-28</u>
Checked _____ Date _____		Missile _____ Airplane _____	Report <u>D113-945-012</u>

Figure 5.3-5 is a working chart for the correction of the $M^3 C_f$ curve in Figure 5.3-3 for the weak interaction range, based on the asymptotic conditions behind the shock wave. This correction arises essentially from the error introduced by the asymptotic formula approximating Crocco's (zero pressure gradient) result as high Mach number. This correction to Chart 5.3-3 has been utilized in the estimations of MX 2276 performance, reported in Sections 4.4, 4.6, and 4.7.

SECRET

By _____ Date _____

BELL *Aircraft* CORPORATION

Model _____ Page 5-29

Checked _____ Date _____

Missile _____
Airplane _____ Report D143-945-012Section 5.3 References

- 5.3-1 Lees, L. and Probststein, R. F.: "Hypersonic Viscous Flow Over a Flat Plate", Princeton Univ. Aero. Eng. Dept. Report 195, April 20, 1952.
- 5.3-2 Shen, S. F.: "An Estimate of Viscosity Effect in Hypersonic Flow Over an Insulated Wedge", Journal of Math & Physics, Vol. 31, N.3, October 1952, pp. 192-305.
- 5.3-3 Lees, L.: "Hypersonic Viscous Flow Over an Inclined Wedge", Readers' Forum, Journal of Aero. Sciences, Vol. 20, No. 11, Nov. 1954, pp 794-6.
- 5.3-4 Li, Ting Yi and Naganatsu, H.: "Shock Wave Effects on the Laminar Skin Friction of an Insulated Flat Plate at Hypersonic Speeds", Journal of the Aero. Sciences, Vol. 20, No. 5, May 1953, pp. 345-55.
- 5.3-5 Bertram, M. H.: "An Approximate Method for Determining the Displacement Effects and Viscous Drag of Laminar Boundary Layers in Two-Dimensional Hypersonic Flow", NACA TN 2773, September 1952.
- 5.3-6 Lees, Lester: "Hypersonic Viscous Flow Over an Inclined Wedge", Journal Aero. Sciences, Vol. 20, No. 11, Readers' Forum, November 1953.
- 5.3-7 Pai, S. I.: "A Note on Hypersonic Viscous Flow Over a Flat Plate", Journal Aero. Sciences, Vol. 20, No. 7, Readers' Forum, July 1953.
- 5.3-8 Pai, S. I.: "Hypersonic Viscous Flow Over an Insulated Wedge at an Angle of Attack", Technical Note BN-42, The Institute for Fluid Dynamics & Applied Mathematics, University of Maryland, Oct. 1954.
- 5.3-9 Shen, S. F.: "On the Boundary - Layer Equations in Hypersonic Flow", Journal Aero. Sciences, Vol. 19, No. 7, Readers' Forum, July 1952.
- 5.3-10 Probststein, R. F., and Lees, L.: "On the Recovery Factor for Hypersonic Flow with a Self-Induced Pressure Gradient", Journal Aero. Sciences, Vol. 20, No. 4, Readers' Forum, April 1953.

By _____ Date _____
 Checked _____ Date _____

BELL *Aircraft* CORPORATION

Model _____ Page 5-30
 Missile _____
 Airplane _____ Report D113-945-012

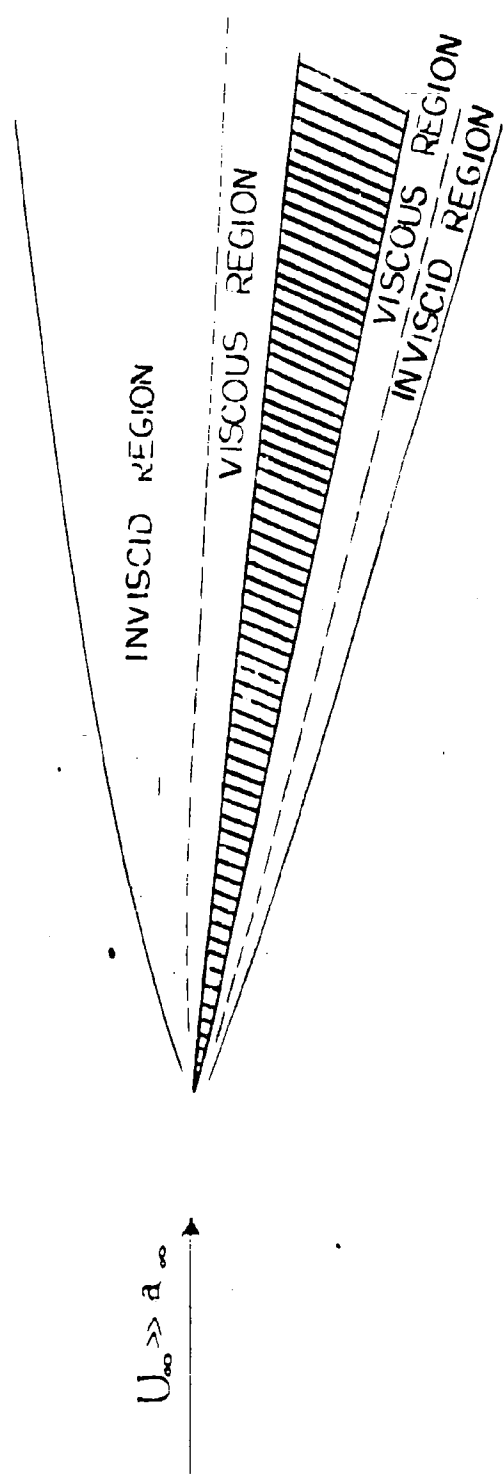
- 5.3-11 Libby, Paul A. and Morduchow, Morris: "A Method for the Calculation of the Compressible Laminar Boundary Layer with Axial Pressure Gradient and Heat Transfer, NACA TN 3157.
- 5.3-12 Ferri, A. and Libby, P.: "Note on an Interaction Between the Boundary Layer and the Inviscid Flow", Readers Forum, Journal of the Aero. Sciences, Vol. 21, February 1954, p. 130.
- 5.3-13 Schaaf, S. A.: "Recent Developments in Rarefied Gas Dynamics Research", Third Navy Symposium on Aeroballistics, Technical Session IV, October 20, 1954.
- 5.3-14 Bogdonoff, Seymour, M. and Hammitt, Andrew, G.: "Fluid Dynamic Effects at Speeds From M 11 to 15, Reprint Institute of the Aeronautical Sciences, January 1955.
- 5.3-15 Bertram, Mitchel, H.: "Viscous and Leading - Edge Thickness Effects on the Pressures on the Surface of a Flat Plate in Hypersonic Flow", Journal of the Aeronautical Sciences, Vol. 21, June 1954, p. 430.
- 5.3-16 Bogdonoff, S. and Kepler, E.: "The Separation of a Supersonic Turbulent Boundary Layer, Reprint Institute of the Aeronautical Sciences, No. 441, January 1954.
- 5.3-17 Lee, J. D.: "The Influence of High Adverse Pressure Gradient on Boundary Layers in Supersonic Flow", Institute of Aerophysics University of Toronto, Report No. 21, October 1952.
- 5.3-18 Crocco, L. and Lees, L.: "A Mixing Theory for the Interaction Between Dissipative Flows and Newly Insentropic Stream". Journal Aero. Sci., Vol. 19 No. 10, October 1952.
- 5.3-19 Ferri, A.: "Elements of Aerodynamics of Supersonic Flows", Macmillan Co., 1949.
- 5.3-20 Karman, T. and Biot, M.: "Mathematical Methods in Engineering", McGraw Hill Book Company, 1940.
- 5.3-21 Van Driest, E. R.: "Investigation of the Laminar Boundary Layer in Compressible Fluids Using the Crocco Method", North American Aviation, Inc., Report AL-1183, January 9, 1951.

BELL SECRET

TABLE PAGE 5-31
ADDITIONAL REPORT D143-945-012

Figure 5.3-1

FLOW PATTERNS

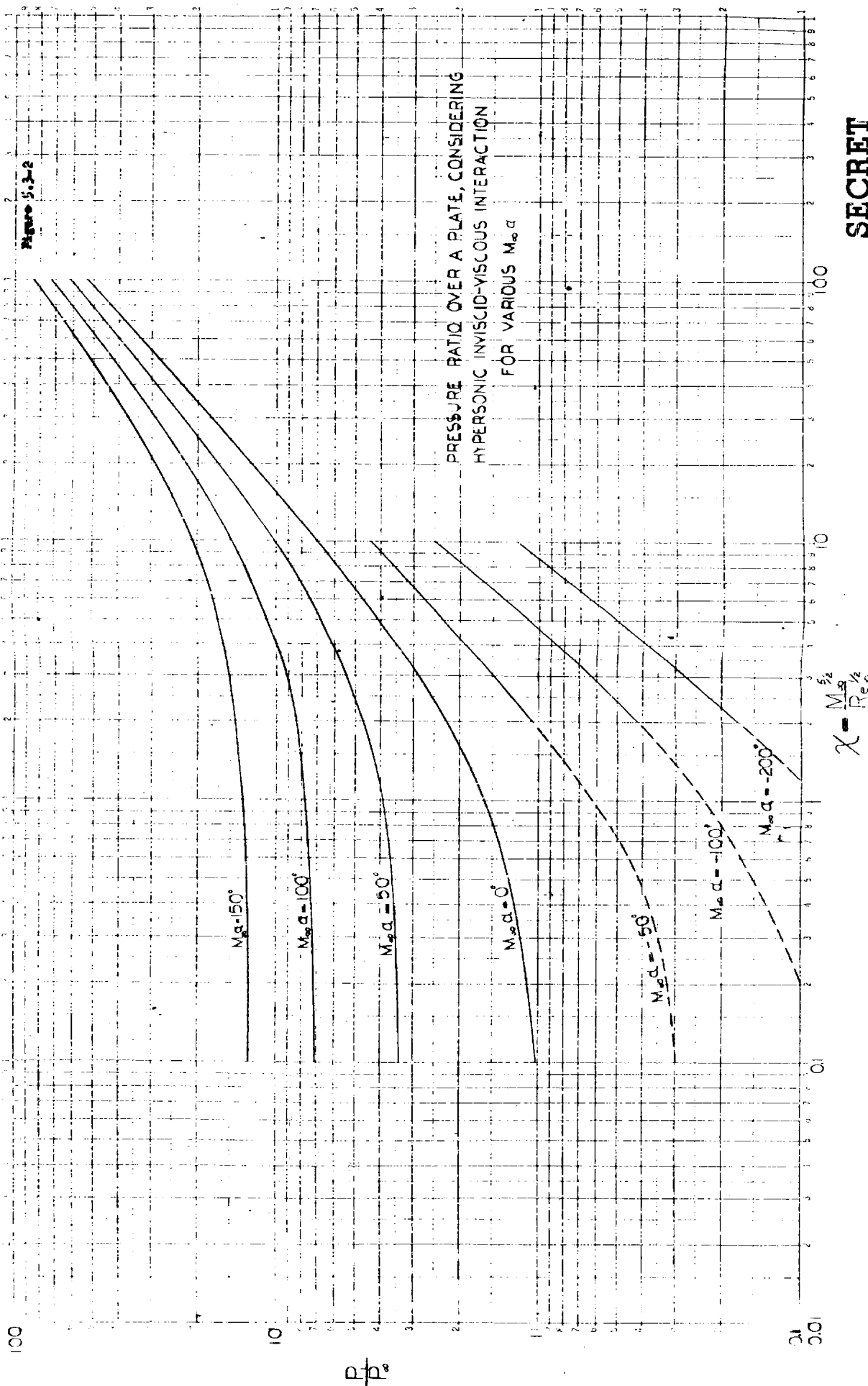


SECRET

BY _____ DATE _____
CHECKED _____ DATE _____

BELL Aircraft CORPORATION

MODEL _____ PAGE 5-32
SHIP _____ REPORT M43-945-012



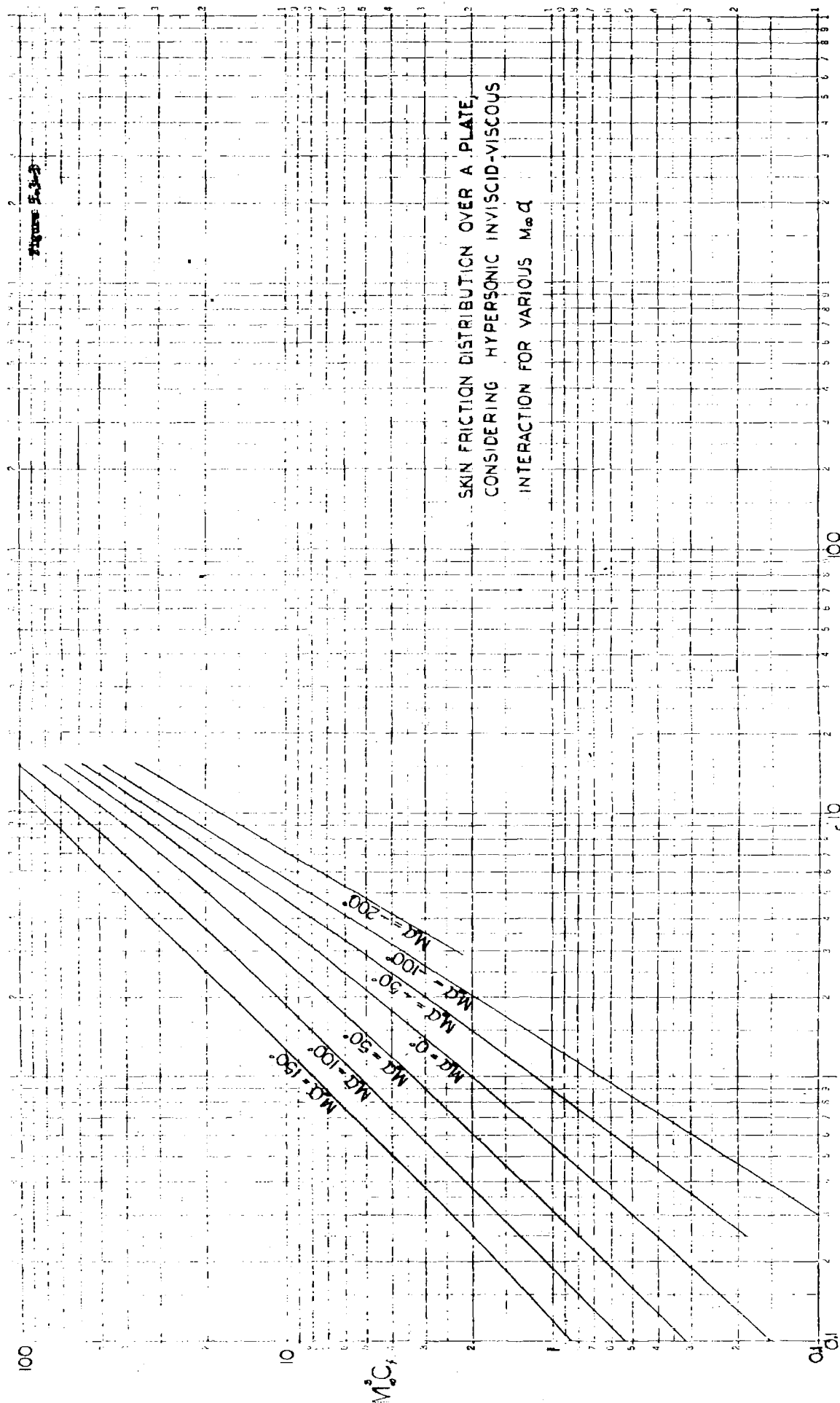
SECRET

SECRET

BY _____ DATE _____
CHECKED _____ DATE _____

BELL Aircraft CORPORATION

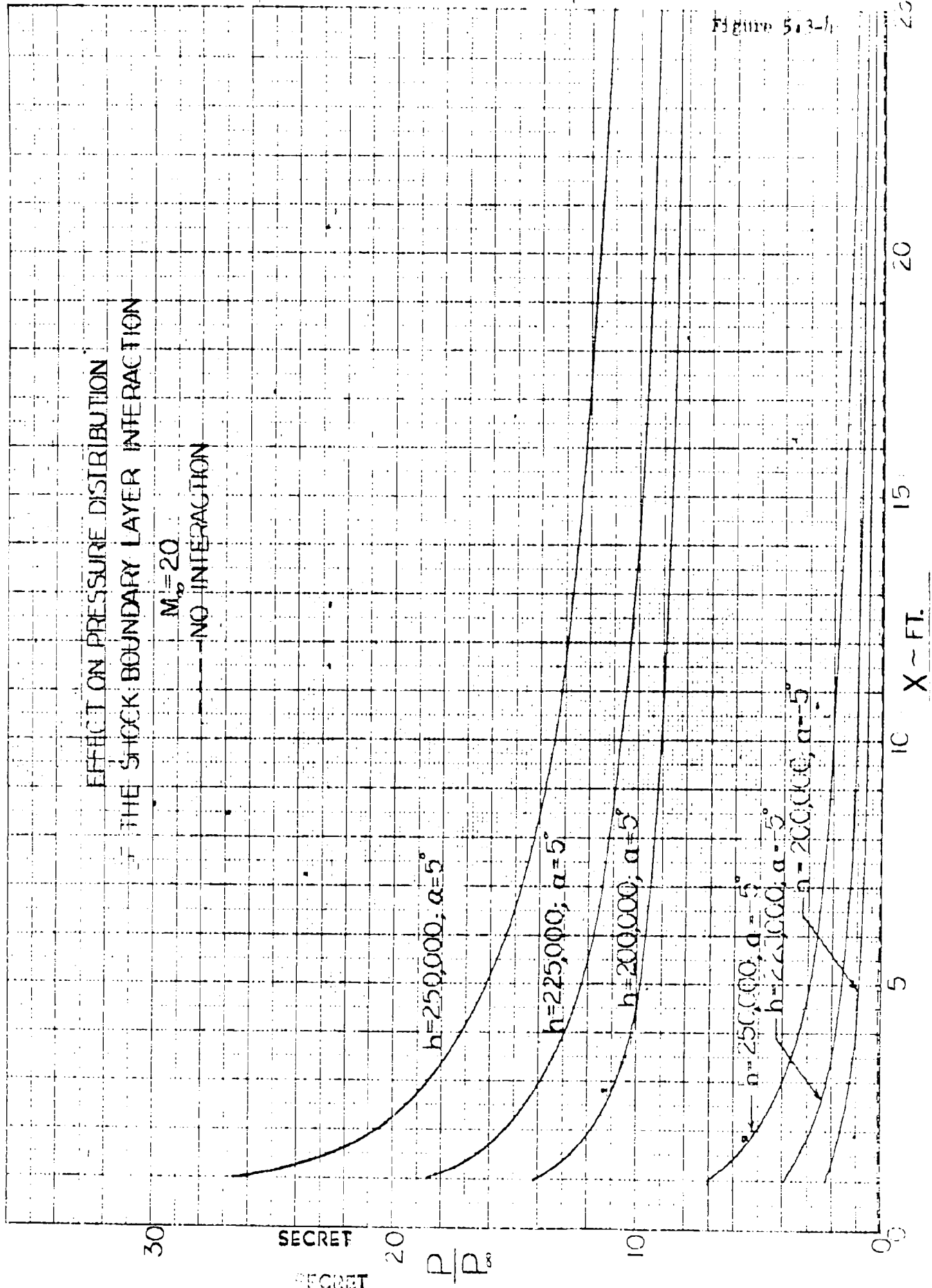
MODEL _____ PAGE 5-32
SHIP _____ REPORT DALL-945-012



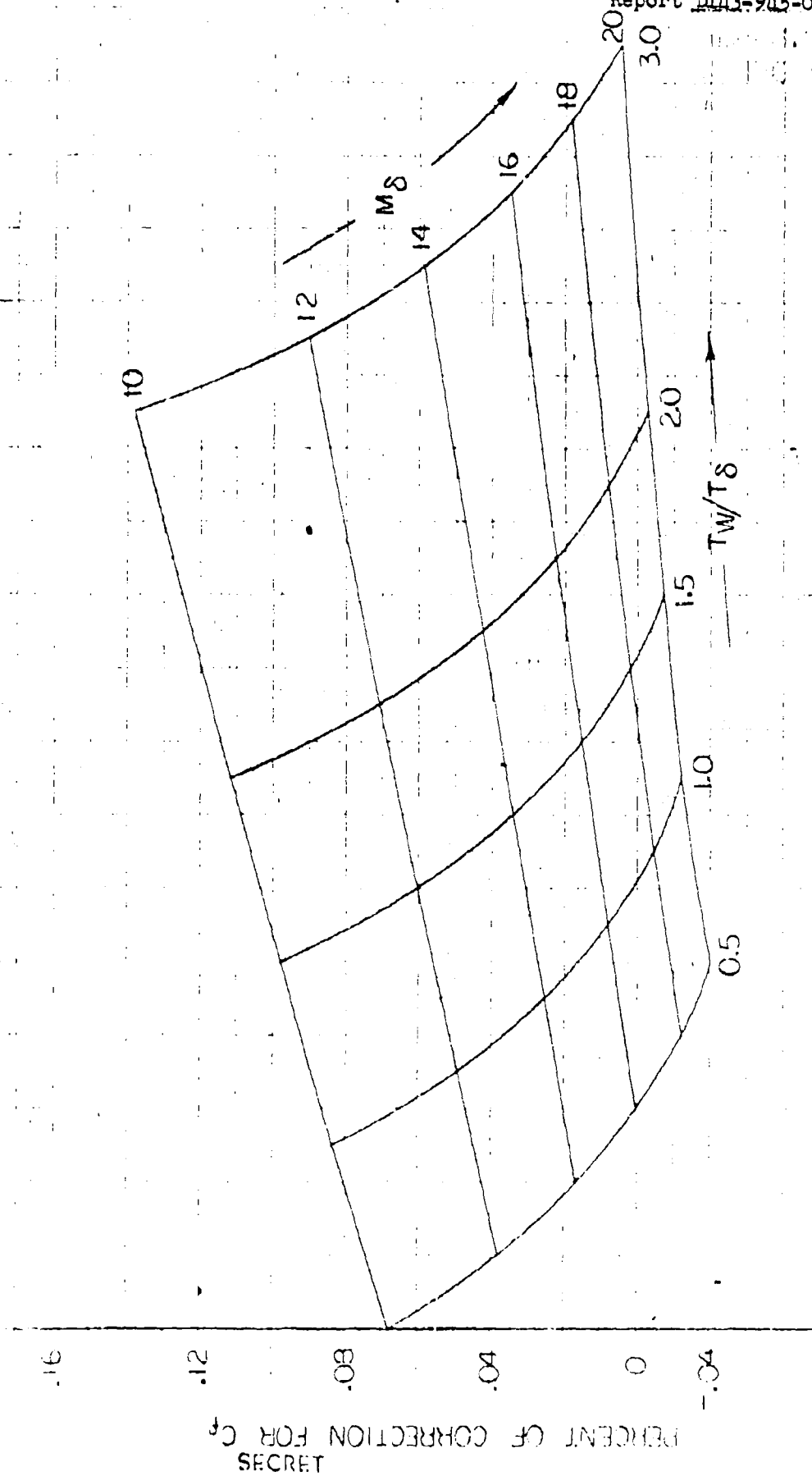
$$\chi = \frac{M_\infty^{5/2}}{Re_\infty^{1/2}}$$

SECRET

Figure 5.3-1



WORKING CHART: CORRECTION OF C_f IN THE WEAK INTERACTION RANGE



SECRET

By _____ Date _____	BELL <i>Aircraft</i> CORPORATION	Model _____	Page 5-36
Checked _____ Date _____		Missile _____ Airplane _____	Report D1143-945-012

5.4 Ultra-High Temperature Phenomena

The energy which a moving body imparts to the air in which it moves is dissipated by viscous action into heat (internal energy or molecular activity) mostly in shock waves and in the boundary layer. The amount of energy required for flight increases roughly as ρv^n , $2 < n < 3$, and at hypersonic speeds this energy is sufficient to cause appreciable changes in the structure of the air in the narrow layer right next to the body and in the neighborhood of the nose where a strong normal shock obtains. This change in structure will be reflected in changes in the measurable macroscopic properties such as μ , C_v , C_p , k , etc., but at the same time the more complicated microscopic structure and behaviour of the gas can no longer be completely and adequately described in terms of the conventional thermostatic parameters; one must resort to kinetic theory to explain and predict the behaviour of gas at high temperatures (temperature being, of course, a measure of the molecular energy or activity). Furthermore, air is a complex mixture of gases, c.f. Table 5.4-1, and its properties are determined by the properties of each of its constituents.

TABLE 5.4-1
COMPOSITION OF AIR

N ₂	78.03	Neon	0.0012
O ₂	20.99	He	0.0004
A	0.94	Krypton	0.00005
CO ₂	0.03	Xenu	0.000006
H ₂	0.01		

The principle constituents of air, N₂ and O₂ are both diatomic molecules. On the idealized kinetic theory model of a gas, the diatomic molecule has six possible degrees of freedom: 3 translational, 2 rotational, and one vibrational. For N₂ and O₂ molecules, the translational and vibrational modes are active at room temperature and higher, but the vibrational mode is frozen out.* At temperatures of 600°R and above,

* Actually what is considered is a statistical average. Even at a "low" temperature there will be some molecules possessing sufficiently high energy so that all degrees of freedom are active, but these will be so few as to have negligible effect on the average. As the temperature is raised, more and more molecules possess sufficient energy to excite all modes and hence the properties of the gas which results from an average of the properties of the molecules comprising it will be affected.

By _____ Date _____

BELL *Aircraft* CORPORATIONModel _____ Page 5-37
Missile _____
Airplane _____ Report D1143-945-012

Checked _____ Date _____

the vibrational mode (in the oxygen molecule first) becomes active, and this shows up macroscopically in increasing values for C_v and C_p with increasing temperature. At temperatures of the order of 5400°R , the O_2 molecules start to dissociate, i.e., there is sufficient energy available to some molecules to overcome the potential forces binding its atoms together, and at temperatures of about $10,000^\circ\text{R}$ ionization becomes significant.

The distribution of energy among the various possible degrees of freedom does not occur instantaneously, but requires a number of collisions before each mode is in equilibrium. While the translational mode requires so few collisions that it reaches equilibrium almost instantaneously, the rotational mode requires about 10 to 100 collisions, while the vibration mode requires about 100,000 collisions to reach equilibrium. Hence there are finite "relaxation" times before an element of gas subject to a change reacts completely to this change and reaches an equilibrium state. The actual times required are functions of density and temperature change, and at present are not too well known, although experimental investigations of relaxation times are under way. Likewise, dissociation and ionization do not occur instantaneously but rather at a finite rate which is a function of the temperature of the gas. After an element of gas has been heated to a sufficiently high temperature for a large enough time interval, then an equilibrium state will be reached where the molecules are continuously dissociating and reassociating at a constant rate but there is a certain constant percentage (characteristic of temperature and density) which are dissociated; however, a certain characteristic time is required after every change of state until equilibrium conditions at the new state are reached. Similarly for ionization.

The determination of the characteristic times is difficult and laborious theoretically, and at present the experimental approach is not clear. Furthermore, the properties of air under equilibrium dissociation and ionization conditions have yet to be calculated correctly and tabulated. Hence the probing studies of dissociation effects which have been made herein pertain to equilibrium dissociation conditions only.

An indication of the temperatures associated with hypersonic flow can be obtained from the simple ideal gas relation

$$\frac{T}{T_a} = 1 + \frac{\gamma-1}{2} M^2$$

Thus flight in air with ambient temperature $T_a \approx 500^\circ\text{R}$, the C_p , C_v variation becomes significant at around $M = 2$, dissociation becomes important at about $M = 7$ and ionization at about $M = 9$.

By _____ Date _____

BELL *Aircraft* CORPORATION

Model _____ Page 5-38

Checked _____ Date _____

Missile _____
Airplane _____ Report D143-945-012

The changes in gas properties associated with a change in microscopic structure of the air must be taken into account in predicting the force and heat loads on a hypersonic aircraft by extensions of the conventional approach, i.e., in obtaining approximate solutions to the usual boundary layer equations and shock relations at high Mach numbers. Furthermore, the possibility of relatively "new" effects in aerodynamics - like radiation from hot air in the boundary layer to the structure - need also be investigated.

Another way of looking at the thermodynamic problems associated with hypersonic flight is to consider the energy involved in body-gas interaction in the Mach number range from zero to 25, as demonstrated by a diagram of the energy spectrum of the gas on the molecular scale. The average translational kinetic energy of each molecule of air relative to the aircraft can be expressed in the form $\frac{m}{2} \frac{3a^2}{\gamma} (1 + \frac{\gamma}{3} M^2)$,

and this relationship between Mach number and kinetic energy is represented by the parabolic curve shown in Figure 5.4-1. The characteristic energy values for excitation of the vibrational energy levels, and the dissociation energies of the air molecules are indicated as well as the sublimation energies of typical solids.

From this energy diagram it can be seen that the relative kinetic energy of the typical gas molecule at high Mach numbers is sufficient to produce dissociation, and also that this relative kinetic energy is greater than the energy required to remove a single atom from a common metal, i.e., the sublimation energy. These facts suggest that thermodynamic and chemical phenomena not apparent at ordinary supersonic speeds - because there is not enough energy available to produce them - will be observed at hypersonic Mach numbers.

A number of probing studies were initiated to investigate some of the high temperature effects associated with hypersonic flow, and the results of these diverse analyses are collected in this section. Also, considerations of "new" phenomena which could possibly be of importance are gathered below in this introduction.

The question of whether or not the intensely hot air in the boundary layer radiates an appreciable amount of heat to the adjacent structure is considered in Section 5.4-1; essentially, the first step is to estimate the emissivity of air at temperatures of the order of 10,000°R and low densities. The estimates obtained from an analysis

* "new" in the sense of either not existing or not apparent at the relatively lower temperatures associated with supersonic flight.

By _____ Date _____
 Checked _____ Date _____

BELL Aircraft CORPORATION

 Model _____ Page 5-39
 Missile _____
 Airplane _____ Report D1143-945-012

based on the quantum mechanical aspects of kinetic theory show that the order of magnitude of the emissivity of air at the temperatures under consideration is sufficiently high so that radiative heat transfer appears to be an important factor at these temperatures. It remains, however, to solve the flow equations in the boundary layer including a radiative heat transfer term, in order to determine the exact way in which radiation will qualitatively and quantitatively affect the overall heat transfer picture. A prerequisite to such a detailed study is a precise knowledge of the emissivity ϵ_λ as a function of wave length λ , pressure p and temperature T . A theory has been developed to compute this quantity and is given in Appendix 5C; it was not, however, within the scope of this study to carry out the detailed numerical calculations at this stage.

Some brief thoughts and remarks on the calculation of the transport properties of dissociated gases are given in Section 5.4.2, while in Section 5.4.3, an investigation of the effects of assumed equilibrium dissociation of air on the boundary layer characteristics is reported. The results of the latter study show that skin friction and heat transfer are essentially unaffected by dissociation so long as both the stream and body temperatures are below dissociation values. It was learned during this writing that similar results (unpublished) have recently been obtained at the Rand Corporation. (Also cf. Reference 5.4-37), it appears that a similar result holds in the stagnation region of a blunt-nosed body.

In Section 5.4.4 a recently completed program (at Bell Aircraft Corporation) to compute basic tables of flow parameters for both shock flow and isentropic flow, incorporating real gas effects up to dissociation temperatures, is discussed. Since the gas flow tables are basic to any numerical analysis of the flow, it was important to determine how the actual behavior of air at high temperatures differs from that described by the standard ideal gas tables, and thus the real gas flow tables were needed as a standard of comparison. These tables are applicable to normal shocks up to a Mach number of 10 and to oblique shocks of 30° or less wave angle up to $M \approx 20$, since in these cases the temperatures behind the shock are below dissociation temperature. It should be noted also that these tables relate equilibrium states on both sides of the shock.

In the following, various thermodynamic phenomena which could possibly be of importance in hypersonic flight are pointed out, although so little is known about these phenomena at present, but that they must first be investigated experimentally to determine whether or not they will be important, and if so, to determine quantitative effects and/or a model for theoretical studies. To be sure, the methods for performing such experiments are not at all obvious, but some progress is now being made.

By _____	Date _____	BELL Aircraft CORPORATION	Model _____	Page <u>5-40</u>
Checked _____	Date _____		Missile _____	Report <u>D143-945-012</u>
			Airplane _____	

One such possibility is that of damage to the skin of a high velocity aircraft due to interaction of the air-skin molecules; Figure 5.4-1 shows that at $M = 20$ say, the energy of an air molecule is about twice the binding energy of aluminum. A few experiments by F. J. Willig, where a fast jet of about 100,000 fps impinged on an aluminum target have been conducted, where it was demonstrated that damage to the metal surface appeared as a lightly etched area. These results are very preliminary, however, and at much higher velocities than of interest to MX 2276. The problem requires further experimental study in order to understand and control any effect of this type.

The possibility of damage to a surface by a meteorite has also been noted. Here the worry is that the meteorite could either penetrate or tear a chunk out of the surface, resulting in high heating rates being induced at this "hole" because of turbulent flow or the setting up a sound wave oscillation in this hole (of e.g., Reference 5.4-52). However, the probability of contact with a meteorite larger than 1×10^{-8} grams is at most about once a day (of Reference 5.4-53) at the highest altitude reached so that this is not a problem for the glide vehicle.

Considering now the interaction of micrometeorite dust and the surface, it is estimated that particles of size 3×10^{-3} grams and larger with relative kinetic energies of 50 e.v. and greater will register about 5000 hits per hour, and will probably cause microscopic pitting. Such etching of metal by meteor dust has already been observed in high altitude rocket firings. It is not expected to be serious or to significantly affect the surface finish of a glide vehicle, however, but it would be prudent to obtain more experimental evidence of this effect.

One effect stemming from the dissociation of air at high temperatures is the possibility that ions produced by dissociation in the extremely hot layer inside the boundary layer will drift towards the surface and combine there, releasing energy and heating the surface. Again, since there are finite times in which dissociation and reassociation occur, and dissociation at the high temperatures occurs at a faster rate than dissociation at the lower temperatures, it is conceivable that some dissociated particles will be swept downstream over the body before they have time to recombine, thus alleviating the heating problem to some extent (of as yet unknown magnitude).

The ultra high temperatures reached in the boundary layer will also result in ionization of the air, and heat conduction by electron diffusion must also be considered. Some preliminary theoretical and experimental investigations in this line, particularly Reference 5.4-27 has been carried out for argon, but as yet no work on air has been reported. This problem requires considerable theoretical and experimental study,

By _____ Date _____
 Checked _____ Date _____

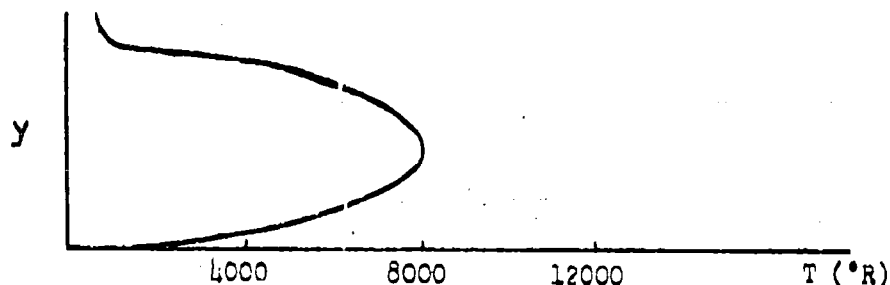
BELL & HOWELL CORPORATION

Model _____ Page 5-41
 Missile _____
 Airplane _____ Report D143-945-012

5.4.1 Radiation Transfer of Energy in Hypersonic Flow

Introduction

The conventional solution for the equilibrium temperature distribution in a boundary layer over a flat plate evaluated at a Mach number of 15 or 20, and an ambient temperature of 400°R , indicates that somewhere in the boundary layer the air reaches an ideal gas temperature of 8000 or $10,000^{\circ}\text{R}$. In obtaining equilibrium solutions it is found (cf. Section 4.6) that considerable energy is radiated out from the heated plate to drop its temperature well below the theoretical recovery temperature (almost stagnation) at given free stream conditions. However, even though the plate may thus be "radiation cooled", (to well below stagnation temperature) somewhere in the boundary layer the temperature approaches the high stagnation value. See Figure 5.4-1. The question arises as to whether the plate receives a significant amount of heat by radiation from the hot air in the boundary layer.



Several recent papers (References 5.4-27 and 5.4-33) describe experimental studies of radiation emitted by plane shock waves. These shock tube experiments demonstrate the fact that substantial amounts of energy are being transported by radiation. This result is not too surprising, since it is a well established fact that radiation is the dominate transport mechanism when the temperatures are of the order of stellar temperatures. Again, using the classical expression for heat radiated as σT^4 and, for example, taking the case where $T_w = 2000^{\circ}\text{R}$ and T_{max} in stream is $10,000^{\circ}\text{R}$ then for the stream to radiate locally as much heat as the wall does it need only have an emissivity of about $(1/5)^4 \sim .015$. However, we could find no quantitative theoretical or experimental information about the emissivity of air at the temperatures under consideration, and besides the process of radiative heat transfer at these temperatures cannot be completely represented by the engineering approach. It is known that some experiments were made at Cornell University in Summer of 1954 to try to measure the emissivity of air, using a shock tube as a source of hot air and making a spectrographic analysis of the strength of radiation emitted as a function of wave length, but this very difficult experiment did not lead to any conclusive results because of contaminating radiation given off by the shock tube itself.

SECRET

 By _____ Date _____
 Checked _____ Date _____

BELL Aircraft CORPORATION

 Model _____ Page 5-42
 Missile _____
 Airplane _____ Report D143-945-012

In order to get an estimate of even the order of magnitude of the heat radiated by the boundary layer air, it is necessary to analyse the detailed molecular state of the gas to compute its emissivity as a function of pressure, temperature, and wave length, and then to utilize this information in setting up an energy balance equation for the flow in the boundary layer. For example in regions where emission and absorption are intense the energy equation will have the additional term

$$\frac{\partial}{\partial x_j} \left(K \frac{\partial T}{\partial x_j} \right)$$

$$\text{where } K = \frac{-\sigma \lambda_R}{3} \frac{d\xi}{dT}$$

$$\xi \text{ is the energy density} = \int_0^\infty \xi_\nu d\nu$$

$$\xi_\nu = \frac{8 \pi h \nu^3}{c^3} \frac{1}{e^{h\nu/kT} - 1}$$

$$\lambda_R \text{ the radiation mean free path} = \frac{\int_0^\infty \frac{1}{K_\nu} \frac{d\xi_\nu}{dT} d\nu}{\int_0^\infty \frac{d\xi_\nu}{dT} d\nu}$$

$K_\nu = n \sigma_\nu$ where σ_ν is the absorption cross section and K_ν coefficient of spectroscopy.

The present study started off as a probing investigation to determine the order of magnitude of the emissivity of air, and when it was found that radiation would apparently be a significant factor, a more detailed theoretical study was initiated to compute essentially the emissivity of air as a function of λ , p , T , since this information is an necessary prerequisite to any serious study of radiative heat transfer.

A brief discussion of radiative energy transfer leading to an estimate of the order of magnitude of this effect is given below. The more detailed analysis leading to a method for computing ϵ_λ is given in Appendix 50 which shows that this quantity can be calculated to a reasonable approximation. It was not within the scope of the present work, however, to carry out the extensive calculations to obtain ϵ_λ . Both treatments presuppose a certain familiarity with the concepts of kinetic and quantum theories.

By _____ Date _____	BELL <i>Aircraft</i> CORPORATION	Model _____	Page 5-43
Checked _____ Date _____		Missile _____ Airplane _____	Report D143-945-012

Analysis

The model assumed for analysis is that of an ionized (or dissociated) gas in an equilibrium state, where the ionization (or dissociation) process is preceeding at a constant rate, and it is balanced by the rate of the inverse process of recombination (or reassociation). The inverse processes take place by one of two mechanisms, inelastic collision or radiative transition. The meaning of temperature used herein is that characteristic of the equilibrium thermodynamic state.

The problem of calculating equilibrium concentrations and temperatures has been discussed by Krieger and White (Reference 5.4-34). The classical engineering methods of computing radiative heat transfer are not very convenient when the medium is a gas at 5000 or 10,000 degrees Kelvin. From here on in this section temperatures are given in °K, the physicists unit, since the problem is now in the world of physics and it is convenient to use the language of physics. The average emissivity coefficient, ϵ , has a very discontinuous frequency or wave length spectral distribution and as a result its temperature variation is non-uniform. A series of papers by S.S. Penner (References 5.4-29, 5.4-30, 5.4-31 and 5.4-32) discuss some aspects of this problem, and a brief discussion of general problems is given in Reference 5.4-2.

The radiation properties of air are complicated because the two major components nitrogen and oxygen are homopolar molecules in the ground state and thus have no electric dipole moment, but the minor constituents carbon dioxide and water vapor, etc. do not have this symmetry. The non-luminous property of oxygen and nitrogen at moderate temperatures is dependent on the zero value of the dipole moment, and this property is destroyed in the case of oxygen when the temperature is raised sufficiently high to put some of the molecules in the $^3\Sigma^-$ state. The emission and absorption of radiation due to transitions between this excited state and the ground state has been studied extensively by spectroscopist, and valuable information on the subject is given in References 5.4-1, 5.4-15, 5.4-22, 5.4-25 and 5.4-26.

A general method of analyzing radiant energy transfer can be developed by extending the domain of the classical theory with the aid of some concepts from the quantum theory of radiation. One approach to this problem is to express the coefficient ϵ_λ (emissivity per wave length interval) in terms of K_λ (absorption coefficient of spectroscopy) and then relate the macroscopic K_λ to the microscopic cross section for absorption of radiation. The details of these steps are given below:

By _____ Date _____

BELL Aircraft CORPORATION

Model _____ Page 5-44

Checked _____ Date _____

Missile
Airplane Report M43-945-012

The radiant flux emitted per unit area by a hemisphere gas at temperature T , density ρ , and radius L is given by the expression $\Gamma = \pi I = \epsilon(T, \rho L) \sigma T^4$. This radiation is distributed over a spectral range and is studied by resolving it into frequency or wave length elements

$$I = \int I_\lambda d\lambda \text{ and } I_\lambda = \epsilon_\lambda E_\lambda(T) \text{ where } E_\lambda = \frac{2hc^2}{\lambda^5} \frac{1}{e^{hc/\lambda kT} - 1}$$

$$\text{Since } \int E_\lambda d\lambda = \sigma T^4 / \pi, \quad \epsilon = \frac{\int I_\lambda d\lambda}{\int E_\lambda d\lambda} = \frac{\int I_\lambda d\lambda}{\sigma T^4 / \pi}$$

The function $E_\lambda(T)$ is sketched in Figure 5.4.1-2 against the wave length to give the standard black body distribution curve for a given temperature T .

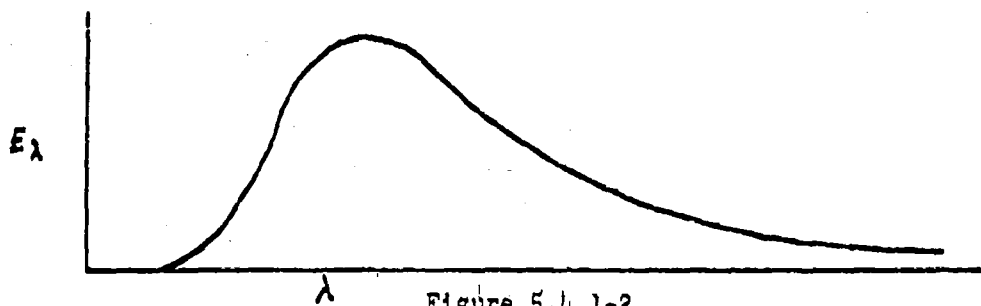


Figure 5.4.1-2

The intensity of radiation I from the gas is equal to the integral $\int I_\lambda d\lambda$

where $I_\lambda = \epsilon_\lambda E_\lambda(T)$. From Kirchhoffs relations, we know that $\epsilon_\lambda = a_\lambda$

where a_λ is the fractional absorption at the wave length λ , thus

$$I_\lambda = (1 - a_\lambda) I \quad \text{or} \quad \frac{I_\lambda}{I_\lambda} = 1 - a_\lambda$$

In absorption spectroscopy the logarithm of this intensity ratio is measured in the laboratory

$$\ln \frac{I_\lambda}{I_\lambda} = -K_\lambda L = \ln(1 - a_\lambda)$$

K_λ is called the absorption coefficient and it has the dimensions cm^{-1} . If we now obtain experimental or theoretical values of K_λ we can compute $\epsilon_\lambda = a_\lambda = 1 - e^{-K_\lambda L}$ and the ordinary emissivity

$$\epsilon = \frac{\int (1 - e^{-K_\lambda L}) E_\lambda d\lambda}{\int E_\lambda d\lambda} = \frac{\int \epsilon_\lambda E_\lambda d\lambda}{\int E_\lambda d\lambda}$$

By _____ Date _____

BELL Aircraft CORPORATION

Model _____ Page 5-45
Missile _____
Airplane _____ Report D143-945-012

Checked _____ Date _____

The above relations indicates that the emissivity ϵ is the ratio of two areas in Figure 5.4.1-3 of E_λ and $\epsilon_\lambda E_\lambda$ versus λ . As an example, consider the case where $T = 8000^\circ\text{K}$ and ϵ_λ is 0 for λ greater than .25 microns and 1 for λ less than .25 microns.

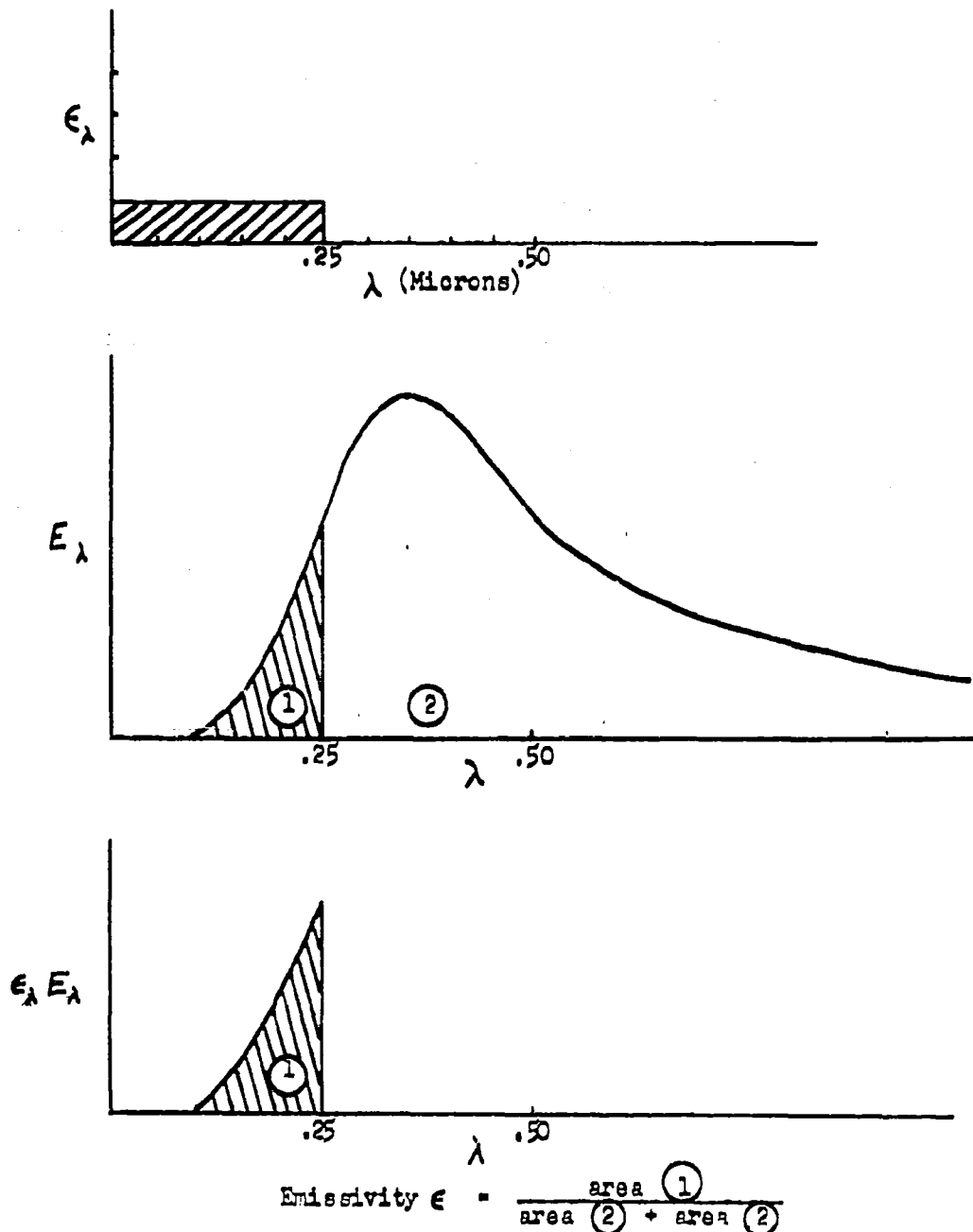


Figure 5.4.1-3

By _____ Date _____

BELL *Aircraft* CORPORATION

Model _____ Page 5-46

Checked _____ Date _____

Missile _____
Airplane _____ Report D143-945-012

The absorption coefficient K_λ is related to the microscopic absorption σ_λ by the relation $K_\lambda = N \sigma_\lambda$ where N indicates the number of molecules per unit volume. σ_λ is the absorption cross-section which can be calculated from the quantum theory of radiation for most absorption processes.

In many problems involving molecular transitions, it is difficult to calculate the cross section from theory alone, but the general theoretical relations may be used in conjunction with isolated experimental data to provide an adequate description of the absorption. In the case of diatomic molecules such as oxygen, the Frank-Condon principle may be used to obtain rapid qualitative estimates of radiative transition probabilities from the potential energy curves and energy level schemes of the molecule. This information can be used to extend low temperature absorption measurements to higher temperatures.

A quantitative description of the absorption can be established by developing a theoretical expression for the cross-section in terms of the electric dipole matrix element. The dipole matrix element can be expressed as a product of an electronic matrix element and an overlap integral of the nuclear wave functions. The electronic matrix element will remain essentially constant over large frequency intervals and can be determined from room temperature experiments. The overlap integral will be sensitive to temperature because the occupation of nuclear energy levels will change with temperature. The nuclear wave functions can be computed from the Schrödinger equation with the aid of potential energy curves available in the literature. The occupation numbers for the vibrational energy levels are determined by the basic relations of statistical mechanics.

The Schumann-Runge continuum will be responsible for a major part of the radiation emitted by air in the temperature range 3000 to 10,000 degrees Kelvin. The maximum absorption coefficients are known from spectroscopy to be of the order of 300 cm^{-1} S.T.P. and the long wave length edge of the continuum is found at wave lengths near 1600 angstroms. When the temperature of the gas is raised from a standard room temperature near 300°K to 6000 or 8000 degrees Kelvin, the continuum will move into the visible part of the spectrum and this action will contribute greatly to the average emissivity of the gas. Preliminary estimates based on the use of the Frank-Condon rule give emissivity values in excess of 10 per cent for $L = 1 \text{ cm}$, $P = 1 \text{ atm}$, $T = 8000^\circ \text{ Kelvin}$.

SECRET

By _____ Date _____

BELL *Aircraft* CORPORATIONModel _____ Page 5-47
Missile _____
Airplane _____ Report DL43-945-012

Checked _____ Date _____

As an example of the heat transfer at this condition

$$\Gamma = \pi I = \epsilon \sigma T^4 \quad T = 8000^\circ K$$

$$\epsilon = 0.1$$

$$\sigma = 5.7 \times 10^{-5} \text{ cgs}$$

$$\Gamma = (0.1)(5.7 \times 10^{-5})(4.1 \times 10^{15}) = 2.34 \times 10^{10} \frac{\text{ergs}}{\text{cm}^2 \text{ sec}}$$

$$\Gamma = 2.34 \times 10^3 \frac{\text{joules}}{\text{cm}^2 \text{ sec}} = 2.34 \times 10^3 \times \frac{926}{1054.8} \frac{\text{BTU}}{\text{ft}^2 \text{ sec}}$$

$$\Gamma = 2.05 \times 10^3 \frac{\text{BTU}}{\text{ft}^2 \text{ sec}}$$

Any realistic evaluation of the radiation problems must be made on the basis of a quantitative method. The foundation of such a method is presented in Appendix 5C.

SECRET

By _____ Date _____

BELL Aircraft CORPORATION

Model _____ Page 5-48

Checked _____ Date _____

Missile _____
Airplane _____ Report D143-945-012

5.4.2 Transport Properties of Dissociated Gases

There is currently a need for reliable information about the transport properties of dissociated air. All of the theories for combination of boundary layer characteristics involve empirical formulas for the variation of the transport coefficients as a function of temperature. The results given by these theories are sensitive to the details of the specific property or temperature law assumed.

The kinetic theory of non-uniform gases (Reference 5.4-2) gives the temperature dependence of the viscosity and heat conduction coefficient in the form $\frac{\Omega^{(2,2)*}(T)}{\sqrt{T}}$ where $\Omega^{(2,2)*}(T)$ represents the

$$\Omega^{(2,2)*}(T)$$

deviation from a rigid sphere model, and it depends on the interaction between the gas particles during the collision process. The attractive force between two normal nitrogen or oxygen molecules is a very weak one characteristic of an induced dipole - induced dipole interaction; however, in a collision between two dissociated particles the attractive force is a very strong one characteristic of the chemical bond. At dissociation temperatures, the potential energy of the weak interaction would be insignificant compared to the kinetic energy, but the interaction energy between two dissociated particles will be large compared to the kinetic energy and as a result the term $\Omega^{(2,2)*}(T)$ will be important. In other words, at dissociation temperatures the temperature dependence of μ and K could be expected to deviate appreciable from the $T^{1/2}$ variation as given by the rigid sphere model. It is noted here that this model is the basis for Hanson (Reference 5.4-39) and Moore's (Reference 5.4-38) treatments of the effect of dissociation in the boundary layer.

$Q^{(2)}$ The integral $\Omega^{(2,2)*}$ is a function of the viscous cross-section where $Q^{(2)} = 2\pi \int_0^\pi (1 - \cos^2\theta) I(\theta) \sin\theta d\theta$ and where $I(\theta)$ is the differential collision cross-section of scattering theory. The differential cross-section can be determined by standard quantum mechanical methods if the potential function $V(r)$ is known. The potential curves for the interaction of oxygen atoms are given in Reference 5.4-1 and 5.4-16 and similar information is available for other molecules in the physics journals. It appears then this would be possible to compute μ and K with reasonable accuracy at dissociation temperatures. Moreover, the calculations are closely tied in with the solutions of the radial wave equation in the radiation problem (Appendix 5C).

By _____ Date _____
 Checked _____ Date _____

BELL Aircraft CORPORATION

Model _____ Page 5-49
 Missile _____
 Airplane _____ Report D143-945-012

5.4.3 Effect of Dissociation in the Laminar Boundary Layer

A preliminary investigation was carried out in order to estimate the effects of equilibrium dissociation of air on the characteristics of the compressible laminar boundary layer over a flat plate when the temperature of the wall is assumed uniform and below the dissociation temperature for air. The results show that skin friction and heat transfer are essentially unaffected by dissociation, but that the thickness of the boundary layer is reduced and that the maximum temperature in the layer is considerably reduced.

The method applies to flow regions where the Navier-Stokes equations and the Prandtl boundary layer approximations are valid.

While the transport properties from dissociated air calculated by Krieger and White (Reference 5.4-34) are probably incorrect (because the value they assumed for the dissociation energy of nitrogen is now considered too low), their tabulated values were used because they were the only available; however, some of the conclusions which were reached in this analysis are not appreciably affected by small changes. Other results, although subject to errors, may still serve as indication of the effect of dissociation.

L. Moore has investigated the same problem in Reference 5.4-38, utilizing a differential analyzer to solve the equations; some of his results are not valid, however, since he assumed that μ/k is not affected by dissociation in calculating Prandtl number. This assumption was shown to be wrong by F. Hansen (Reference 5.4-39) and A. Kantrowitz (Reference 5.4-40); they show that the Prandtl number for dissociated air is approximately a constant of order unity by using elementary kinetic theory based on the hard sphere model, (See Figure 5.4.3-1).

In the present analysis, the method of Crocco (Reference 5.4-41) was used since it gives accurate results for variable μ , C_p , k and Pr near unity. The values of ρ , μ and i for air in dissociation equilibrium were calculated according to the method presented in part B of (Reference 5.4-38).

The laminar boundary layer equation for a compressible flow over a flat plate, including temperature variations, are

$$\text{Momentum} \quad \rho u u_x + \rho v u_y = (\mu u_y)_y \quad (1)$$

$$\text{Continuity} \quad (\rho u)_x + (\rho v)_y = 0 \quad (2)$$

$$\text{Energy} \quad \rho u i_x + \rho v i_y = \mu u^2_y + \frac{1}{Pr} (\mu i_y)_y \quad (3)$$

By _____ Date _____
 Checked _____ Date _____

BELL Aircraft CORPORATION

Model _____ Page 5-50
 Missile _____
 Airplane _____ Report D143-945-012

The enthalpy, i , includes the heat of formation of dissociated products; $C_p = di/dT$. The Prandtl number is assumed constant and its value is taken from Hansen's method (Ref. 5.4-38). Following Crocco's method, letting $i_x = 0$ we get from equation (1), (2) and (3) after some transformations.

$$K K' + 2 u_* \rho_* \mu_* = 0 \quad (4)$$

$$(i_*' + Pr \frac{u_*^2}{i_0}) K + (1 - Pr) i_*' K' = 0$$

with the following boundary conditions:

$$\text{when } u_* = 0 \quad K' = 0; \quad i_* = \frac{i_w}{i_0}$$

$$u_* = 1 \quad K = 0; \quad i_* = 1$$

where the prime denotes differentiation with respect to u_* .

Here the star subscript denotes dimensionless variable, namely

$$i_* = \frac{i}{i_0}, \quad u_* = \frac{u}{U_0}, \quad \rho_* = \frac{\rho}{\rho_0}, \quad \mu_* = \frac{\mu}{\mu_0}, \quad K(u_*) = \frac{\tau}{1/2 \rho_0 U_0} \left(\frac{U_0 \rho_0 x}{\mu_0} \right)^{1/2}$$

Examining equation (4), we observe that the transport properties of the gas appear only in the Prandtl number and in the function $\rho_* \mu_*$ of i_* . Now since Pr dissociated is approximately equal to Pr undissociated (see Figure 5.4.3-1) and since by using the method of (Ref. 5.4-38 part B) to evaluate ρ_* and μ_* we find that for $\alpha = 0$ and $M_{\infty} \leq 25$ $\rho_* \mu_*$ dissociated is within 5 percent of the undissociated value (see Figure 5.4.3-2) and for $\alpha \leq 10$ and $M_{\infty} \leq 25$ $\rho_* \mu_*$ dissociated is within 8 percent of the undissociated value we can immediately conclude that for the same initial and boundary conditions we have the same solution of equation (4) for i_* and K as a function of u_* whether the air is dissociated or not. We see, therefore, that the skin friction ($c_f = K_w / \sqrt{R_0}$)

and the heat transfer $q = 1/2 \frac{i_0}{Pr} \left(\frac{\partial i_*}{\partial u_*} \right)_w \frac{\rho_0 U_0 K_w}{\sqrt{R_0}}$ are not appreci-

ably affected by dissociation. It should be pointed out that these are tentative results and are based on the validity of the elementary kinetic theory model used in the calculation of ρ_* , μ_* and of Pr in Reference 5.4-38 and Reference 5.4-39 respectively. In order to get more accurate results the more realistic kinetic theory model of Section 5.4.2 is needed to evaluate ρ_* , μ_* and Pr.

By _____ Date _____

BELL *Aircraft* CORPORATIONModel _____ Page 5-51

Checked _____ Date _____

Missile _____
Airplane _____ Report DL43-945-012

Two numerical examples have been calculated following Crocco's method in order to estimate the effects of dissociation on the velocity and temperature profiles in the boundary layer. The first example is that of a flat plate at zero angle of attack in steady flight at a Mach number of 25 at 250,000 ft. The wall was assumed cooled to a uniform temperature equal to three times the free stream temperature. Figure 4.3-3a shows a comparison of the velocity profiles assuming undissociated air and air in equilibrium dissociation. Figure 4.3-4a shows a comparison of the temperature and enthalpy profile assuming dissociated and undissociated air.

The second example was of a flat plate at a 10° angle of attack in steady stream flight Mach number of 25 at 250,000 ft. The wall was assumed cooled to a uniform temperature equal to 3 times the free stream temperature. Figure 4.3-3b shows a comparison of velocity profile for dissociated and undissociated air and Figure 4.3-4b shows a comparison of enthalpy profiles for dissociated and undissociated air. From a comparison of these two examples it appears that the thickness of the boundary layer is reduced as dissociation occurs and the maximum temperature in the layer is greatly reduced. It is interesting to see that the slope of the velocity and temperature profiles of the wall are unchanged by dissociation. This again shows that the skin friction and heat transfer are unaffected by dissociation.

By _____ Date _____

BELL *Aircraft* CORPORATIONModel _____ Page 5-52

Checked _____ Date _____

Missile _____ Report MLL3-945-012
Airplane _____Section 5.4.3 Symbols

x, y	Geometrical coordinate parallel and perpendicular to flat plate, respectively
u, v	Velocity components of boundary layer flow in x and y direction, respectively
ρ	Mass density
μ	Coefficient of viscosity
k	Coefficient of thermal conductivity
T	Absolute temperature
i	Enthalpy, includes the heat of formation of dissociated product
c_p	$\frac{\partial i}{\partial T}$ specific heat at constant pressure
γ	Ratio of specific heat at constant pressure to specific heat at constant volume
τ	Shear stress
M	Mach number
Pr	Prandtl number ($c_p \mu / k$)
K	Shear function
S	Sutherland constant
R_o	Reynolds number ($\rho_o U_o x / \mu_o$)
c_f	Local skin-friction coefficient
q	Rate of heat transfer
i_*	i/i_o
u_*	u/U_o
e_*	e/e_o
μ_*	μ/μ_o

By _____ Date _____

BELL *Aircraft* CORPORATIONModel _____ Page 5-53

Checked _____ Date _____

Missile _____
Airplane _____ Report D113-945-012Symbols (Cont'd) M_* M/M_0 T_* T/T_0 Subscripts

- o Free stream conditions down-stream of the leading edge
- w Wall conditions
- oo Free stream conditions upstream of the leading edge

By _____ Date _____
 Checked _____ Date _____

BELL Aircraft CORPORATION

 Model _____ Page 5-51
 Missile _____
 Airplane _____ Report DL43-945-012

5.4.4 Compressible Flow Tables for a Real Gas

The shock waves occurring in hypersonic flow produce extremely high temperatures at which the air can no longer be considered as calorically perfect gas*. Also, the density increase involved can be such that the thermally perfect gas+ model can be in error. However, the standard gas dynamic tables for air, which give the relations between state parameters in isentropic flow, are based on the assumption that air is an ideal gas with constant specific heat (cf. e.g., Reference 5.4-42). Since the gas flow tables are basic to any numerical analysis of the flow, it is important to determine how the actual behavior of air differs from that described by the standard ideal gas tables; such a determination can only be made when there are real gas flow tables to serve as a standard of comparison.

A program to compute tables of flow parameters for shock flow and isentropic flow, incorporating the effects of van der Waals' forces and variable specific heat for the range of temperatures at which dissociation is considered to be negligible (up to 5400°R) was underway at Bell Aircraft before the start of the MX-2276 study contract; these calculations have been completed and the tables were issued as Reference 5.4-50.

The procedure employed for incorporating these effects in the flow equations was straightforward. However the resulting equations are extremely difficult to use directly and any general tables of the flow functions would be prohibitively voluminous. The aim in developing a method for including the real gas effects in flow problems was then to find a way of presenting the results so as to make them most generally useful without resorting to volumes and volumes of tables and graphs. Crown (Reference 5.4-43) uses correction factors which are functions of the temperature and pressure so that his method is essentially a successive approximation procedure. Tsien (Reference 5.4-44) introduces correction terms to the ideal gas relations which are products of two functions, one function depending only on Mach number, the other only on the initial conditions. This approach is more direct but still not simple. The NAVORD's report (Reference 5.4-45) includes tables of thermodynamic parameters behind normal shocks and throughout regions of constant entropy, both for a limited number of initial conditions. Several other authors (References 5.4-46 and 5.4-47) merely study representative cases in order to indicate the magnitude of error arising from neglecting the real gas effects.

* A gas with constant specific heat. C_p and C_v for air are nearly constant below 600°R but increase rapidly at higher temperatures.

+ Gas with equation of state $p = RT$

By _____ Date _____

BELL *Aircraft* CORPORATION

Model _____ Page 5-55

Checked _____ Date _____

Missile _____
Airplane _____

Report DL43-945-012

The approach followed in Reference 5.4-50 was similar to the NAVORD report, where the thermodynamic parameters are related to a single independent variable and the initial conditions. However, a significant improvement was made by choosing the initial conditions of those defined by a standard atmosphere, by extending the shock tables to the oblique case, and by including the flow parameters as functions of the thermodynamic state and an initial flow condition. Initial conditions at sea level and 36,089 feet were based on the NACA approved atmosphere (Reference 5.4-48). At the high altitudes a linear temperature profile atmosphere based on the Rocket Panel Study (Reference 5.4-49) was chosen and shock tables were calculated for the three key altitudes. Data for any intermediate altitude can be obtained by linear interpolation. In order to correlate shock and isentropic flow tables the initial flow condition is given in terms of the total or tank enthalpy rather than velocity.

The above mentioned shock flow tables were used for some sample calculations to compare shock flow in an ideal air with shock flow in a "real" air taking into account variable specific heat and real gas effects. The results are gathered in Table 5.4.4-1 and show that at Mach numbers greater than 10 and flow deviations of more than 10° the ideal gas approximation introduces noticeable error. The greatest error is in the temperature and is due to the assumption of constant specific heat. The error due to neglecting the van der Waals forces is smaller but of sufficient magnitude to merit consideration, especially since equations and tables including the effects of variable specific heat are not greatly simplified by neglecting the van der Waals forces.

When the air is heated beyond about 5400°R by shock effects, the dissociation of air at these temperatures should be taken into account in computing gas flow tables. An analysis was made of the theory underlying shock flow and isentropic flow in the dissociation range of temperature, and a procedure for calculating flow tables (using IBM equipment) was developed. Actual programming and carrying out of the extensive calculations required awaits accurate tables for the composition of air for the dissociation range of temperature. Existing tables of Hirschfelder and Curtiss, Reference 5.4-51 are based on a value of 7.54 e.v. for the dissociation energy of nitrogen, which is now generally regarded as incorrect; thus, at the present time there exist no accurate tables of the composition of air at temperatures above 5400°R. Just recently Cornell Aeronautical Laboratory and the Gas Dynamics Branch of AEDC together have started the calculation of this composition, and it was learned that the Bureau of Standards has also done work on this problem. This latter source, however, was motivated by the needs of atomic energy work and as a result the accuracies and the increments of temperature considered are not very appropriate to hypersonic flow problems. Several other leads as to

SECRET

By _____ Date _____

BELL *Aircraft* CORPORATIONModel _____ Page 5-56

Checked _____ Date _____

Missile _____
Airplane _____ Report DL43-945-012

sources which may be calculating or planning the calculation of such tables are being checked. It is hoped, however, that these tables will be made available at least in part by other sources, so that we can concentrate on our primary problems. To this end we have contacted and encouraged several possible sources regarding the possibility of their making such tables.

SECRET

SECRET

By _____ Date _____

Checked _____ Date _____

BELL *Aircraft* CORPORATIONModel _____ Page 5-57Missile _____ Report D143-945-012
Airplane _____

TABLE 5.4.4-1
Comparison of Shock Relations for Real and Ideal Gases

Altitude: 160,000 ft.

M_1	θ_2	θ_{wR}	θ_{w1}	Dev.	$(T_2/T_1)_R$	$(T_2/T_1)_1$	Dev.	$(P_2/P_1)_R$	$(P_2/P_1)_1$	Dev.
10	10°	14.35°	14.43°	.6%	2.14	2.13	0.0%	7.0	7.1	1.4%
	20°	25.25°	25.83°	2.3%	4.24	4.64	9.4%	21.3	22.0	3.3%
15	10°	13.05°	13.15°	.8%	3.12	3.19	2.2%	13.3	13.4	.7%
	20°	24.20°	24.98°	3.2%	7.45	8.72	17.0%	45.2	46.6	3.1%
20	10°	12.48°	12.72°	1.9%	4.40	4.70	6.8%	21.8	22.4	2.7%
	10°	12.16°	12.50°	2.8%	5.82	6.62	13.7%	33.0	34.0	3.0%
30	10°	11.96°	12.36°	3.3	7.54	8.88	17.8%	46.0	47.5	3.3%
5	0	Normal			5.38	5.80	7.8%	29.7	29.0	-2.4%
10	0	Normal			11.52	13.39	16.2%	77.6	74.5	-4.0%

SECRET

SECRET

By _____ Date _____

BELL *Aircraft* CORPORATION

Model _____ Page 5-58

Checked _____ Date _____

Missile _____ Report D143-945-012
Airplane _____Section 5.4 References:

- 5.4-1 G. Herzberg: Molecular Spectra and Molecular Structure, D. van Nostrand Company (1950)
- 5.4-2 J. O. Hirschfelder, C. F. Curtiss, R. Byron Bird: Molecular Theory of Gases and Liquids, John Wiley (1954)
- 5.4-3 J. E. Mayer, M. Goeppert Mayer: Statistical Mechanics, John Wiley (1940) p. 149
- 5.4-4 G. Herzberg: Atomic Spectra and Atomic Structure Dover (1944)
- 5.4-5 R. W. Ditchburn: Light, Interscience Publishers (1953) p. 576
- 5.4-6 R. W. Gurney: Introduction to Statistical Mechanics, McGraw-Hill (1949)
- 5.4-7 E. H. Kennard: The Kinetic Theory of Gases, McGraw-Hill (1938)
- 5.4-8 L. I. Schiff: Quantum Mechanics, McGraw-Hill (1949)
- 5.4-9 L. Pauling, E. B. Wilson Jr.: Introduction to Quantum Mechanics McGraw-Hill (1935)
- 5.4-10 N. F. Mott, H. S. W. Massey: Theory of Atomic Collisions, Oxford University Press (1950)
- 5.4-11 H. Heitler: The Quantum Theory of Radiation, Oxford University Press (1945)
- 5.4-12 W. Gordy, W. V. Smith, R. F. Trambarulo: Microwave Spectroscopy, John Wiley (1953), p. 207
- 5.4-13 S. Chapman, T. G. Cowling: The Mathematical Theory of Non-Uniform Gases, Cambridge University Press (1939)
- 5.4-14 G. S. Rushbrooke: Introduction to Statistical Mechanics, Oxford University Press (1949)
- 5.4-15 A. G. Gaydon: Spectroscopy and Combustion Theory, Chapman-Hall (1948)
- 5.4-16 A. G. Gaydon: Dissociation Energies and Spectra of Diatomic Molecules, Dover (1950)

SECRET

By _____	Date _____	BELL <i>Aircraft</i> CORPORATION	Model _____	Page <u>5-59</u>
Checked _____	Date _____		Missile _____	Report <u>D143-945-012</u>

- 5.4-17 R. M. Goody: The Physics of the Stratosphere, Cambridge University Press (1954)
- 5.4-18 C. N. Hinshelwood: The Kinetics of Chemical Change of Oxford University Press (1940)
- 5.4-19 H. Grad. Communications on Pure and Applied Mathematics, 2 331 (1949)
- 5.4-20 C. S. Wang-Chang, G. E. Uhlenbeck, University of Michigan, CM-681 (1951) Transport Phenomena in Polyatomic Molecules
- 5.4-21 H. M. Mott-Smith, Physics Rev. 82 885 (1951) - Solution of Boltzmann Equation for Shock Wave)
- 5.4-22 K. Watanabe, M. Zelikoff, E. C. Y. Inn - Geophysical Research Papers No. 21 - Absorption Coefficients of Several Atmospheric Gases
- 5.4-23 W. S. Benedict, E. K. Plyer, National Bureau of Standards Circular 523 (1954) - High-Resolution Spectra of Hydrocarbon Flames in the Infrared
- 5.4-24 R. Schamberg, Thesis CIT (1947) - Fundamental Differential Equations and boundary Conditions for High Speed Slip Flow, and Their Application to Several Specific Problems
- 5.4-25 R. W. Mitchburn, D. W. O. Heddle: Proc. Roy Soc. A 226, p. 509 (1954) Absorption Cross Sections in the Vacuum Ultra-Violet
- 5.4-26 E. C. G. Stueckelberg, Phys, Rev. 42 518 (1932)
- 5.4-27 H. E. Petschek, P. H. Rose, H. S. Glick, A. Kane, A. Kantrowitz, Jour. App. Phys. 26, p. 83 (1955) Spectroscopic Studies of Highly Ionized Argon Produced by Shock Waves
- 5.4-28 E. L. Resler, S. C. Lin, A. Kantrowitz, Jour. Appl. Phys. 23 (1952), p. 1390 - The Production of High Temperature Gases in Shock Tubes
- 5.4-29 S. S. Penner, Jour. Appl. Phys. 21, 685 (1950) I
- 5.4-30 S. S. Penner, D. Weber, Jour. Appl. Phys. 22 (1951) p. 1164 II

SECRET

By _____ Date _____
Checked _____ Date _____

BELL *Aircraft* CORPORATION

Model _____ Page 5-60
Missile _____
Airplane _____ Report DL43-945-012

- 5.4-31 S. S. Penner, M. H. Ostrander, H. S. Tsien, Jour. Appl. Phys. 23 (1952), p. 256
- 5.4-32 S. S. Penner, Jour. Appl. Phys. 25 660 (1954) - Approximate Emissivity Calculations for Polyatomic Molecules
- 5.4-33 R. G. Shreffler, R. H. Christian, Jour. Appl. Phys. 25 324 (1954) - Boundary Disturbance in High Explosive Shock Tubes
- 5.4-34 F. J. Krieger, W. B. White - The Rand Corporation, Project Rand Report R-1449 April 1949 - The Composition and Thermodynamic Properties of Air at Temperatures from 500 to 8000°K
- 5.4-35 Strategic Weapon System: Bell Aircraft Corporation Preliminary Design Report No. DL43-945-010, dated 15 July 1953
- 5.4-36 McKown, P. B.: Bell Aircraft Corporation Consistent Properties of Air, Aerodynamic Method Note #16, 1955
- 5.4-37 Beckwith, I. E.: The Effect of Dissociation in the Stagnation Region of a Blunt-Nosed Body, Jour. Aero. Sci. 20, 645-646 (1953)
- 5.4-38 Moore, L. L.: A Solution of the Laminar Boundary Layer Equations for a Compressible Fluid with Variable Properties, Including Dissociation, Journal of the Aeronautical Sciences, Vol. 19, August 1952
- 5.4-39 Hansen, C. Fredrick: Note on the Prandtl Number for Dissociated Air, Journal of Aeronautical Sciences, Vol. 20, Nov. 1953
- 5.4-40 Kantrowitz, A.: Preceeding of the Symposium on High Speed Aerodynamics, Polytechnic Institute of Brooklyn, Jan. 1955 (to be published)
- 5.4-41 Crocco, Luigi: Lo Strato Limite Laminare Nei Gas, Monografie Scientifiche Di Aeronautica, Numero 3, Roma, Dicembre 1946
- 5.4-42 McKown, P. B.: Tables and Graphs for Compressible Flow, Bell Aircraft Corporation, Aerodynamics Research Note 52, June 1953

Form 14-1 Rev. 3-53

SECRET

SECRET

By _____ Date _____

Checked _____ Date _____

BELL Aircraft CORPORATION

Model _____ Page 5-61
Missile _____
Airplane _____ Report D1143-945-012

- 5.4-43 Crown, J. D.: Flow of a Beattie - Bridgeman Gas With Variable Specific Heat, NAVORD Report 2148, November 1951
- 5.4-44 Tsien, H. S.: One Dimensional Flows of a Gas Characterised by van der Waals, Equation of State, J. Math. Phys. Vol. 26 No. 1, pp. 301-324, Jan. 1947
- 5.4-45 Handbook of Supersonic Aerodynamics, Vol. 5, NAVORD Report 1488 (Vol. 5) Aug. 1953
- 5.4-46 Nores, R. N.: Prandtl-Meyer Flow for a Diatomic Gas of Variable Specific Heat, NACA TN 2125, June 1950
- 5.4-47 Eggers, A. J. One Dimensional Flows of an Imperfect Diatomic Gas, NACA TN 1861, April 1949
- 5.4-48 Manual of the ICAO Standard Atmosphere, NACA TN 3182, May 1954
- 5.4-49 The Rocket Panel, Pressures, Densities and Temperatures in the Upper Atmosphere, Phys. Rev., Vol. 88, No. 5 pp. 1027-1032, Dec. 1952
- 5.4-50 McKown, P. B.: Flow Parameters for a Real Gas, Bell Aircraft Corporation Aerodynamics Research Note 56, Jan. 1955
- 5.4-51 Hirschfelder, J. O. and Curtiss, C. F.: "Thermodynamic Properties of Air, II", University of Wisconsin Report CM-518, 21 December 1948.
- 5.4-52 Ackeratt, J.: Eidgenossische Technische Hochschule, Zurich
- 5.4-53 Grimmering, G.: Probability that a Meteorite will Hit or Penetrate a Body Situated in the Vicinity of the Earth, Jour. Appl. Physics 19, 947-956, (1948)

Form 14-1 Rev. 3-51

SECRET

BY
CHECKED

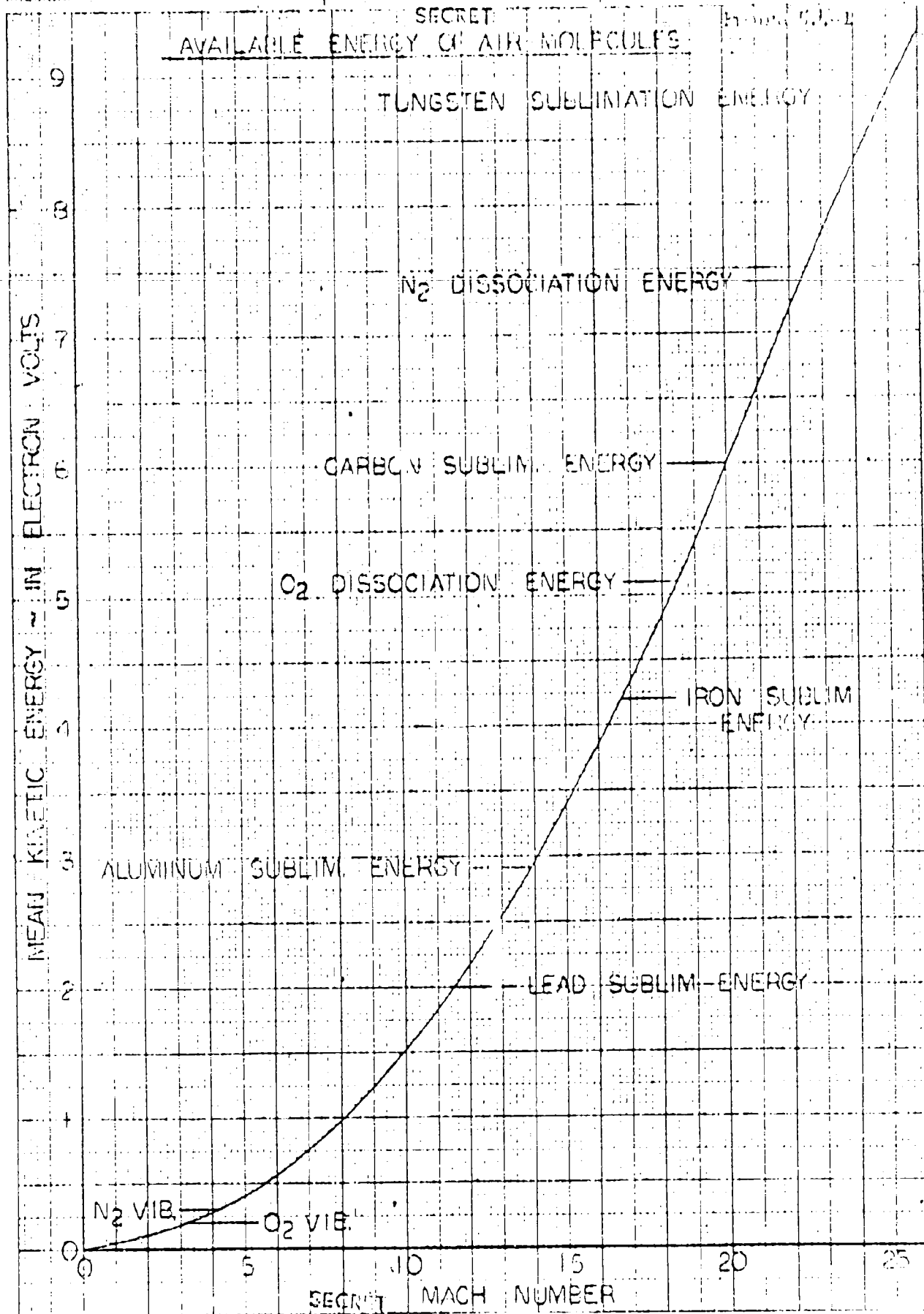
DATE
DATE

BELL

SECRET

MODEL
STOP

PAGE 5-20
REPORT DHB-517-01A



BY
CHECKED

DATE
DATE

BELL

SECRET
CORPORATION

MODEL

PAGE 5-68

BUFFALO, N. Y.

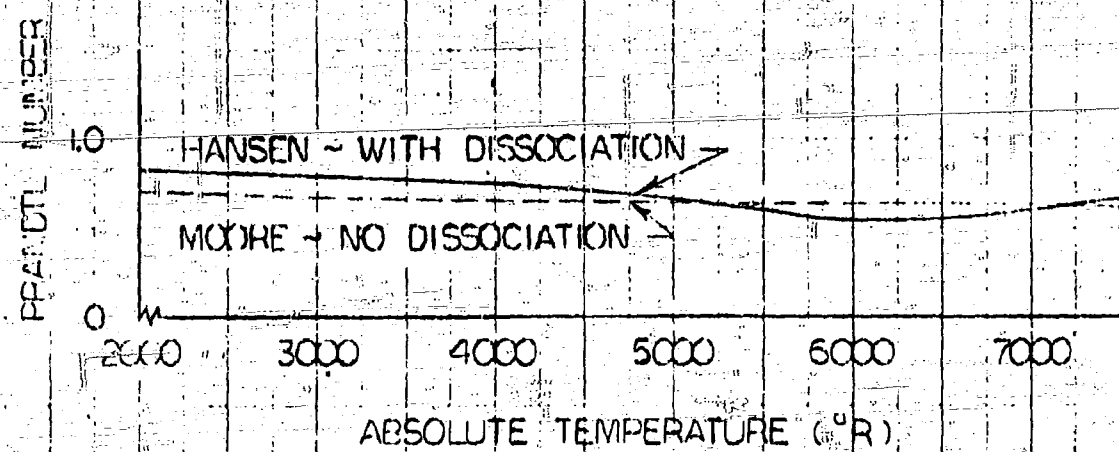
SHOWN

REPORT DHB 51-012

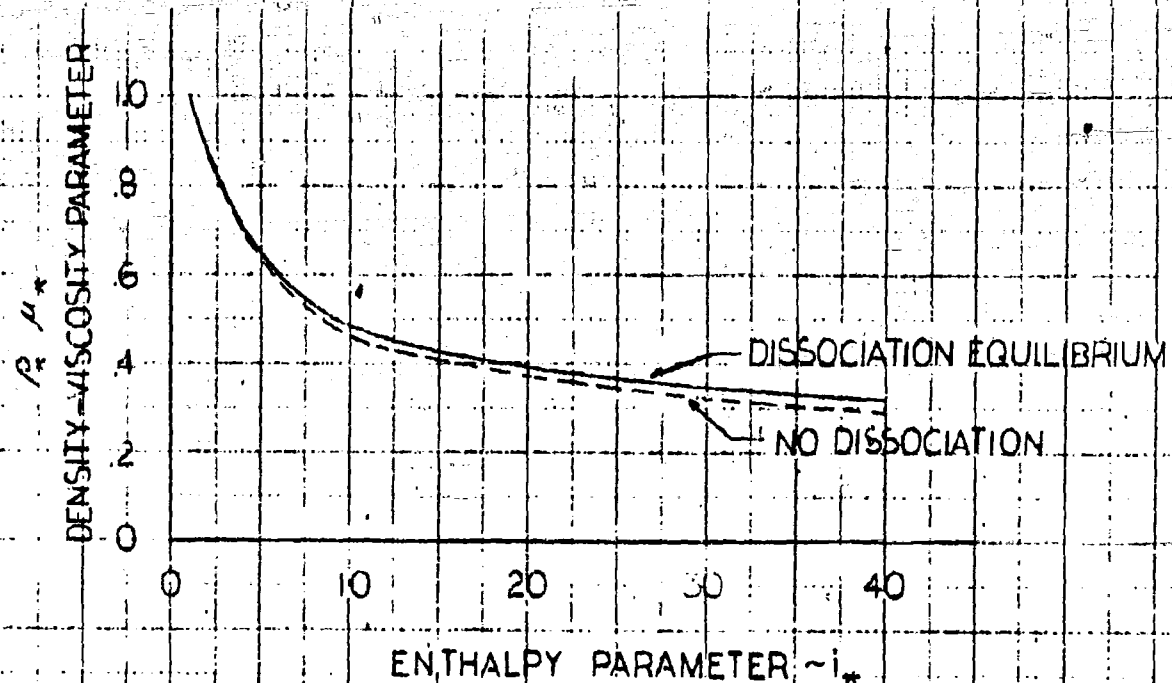
SECRET

Figure 1.4.3-2

COMPARISON OF PRANDTL NUMBER WITH AND WITHOUT DISSOCIATION



COMPARISON OF ENTHALPY PARAMETER VERSUS DENSITY - VISCOSITY PARAMETER FOR DISSOCIATED AND UNDISSOCIATED AIR



SECRET

40

SECRET

FIGURE 5.1.3-3a

VELOCITY PROFILE

OVER A PLATE IN STEADY FLIGHT

$\alpha = 0^\circ$, $M_\infty = 25$ AT 250,000 FT.

$\frac{y}{x} \sqrt{VR_x}$

30

WITHOUT DISSOCIATION →

20

10

← WITH DISSOCIATION

0

5

SECRET

y/u_∞

SECRET

10

BY _____
CHECKED _____

DATE _____
DATE _____

BELL *Shinn* CORPORATION

SECRET

MODEL _____
SHIP _____

PAGE 5-65
REPORT 113-915-012

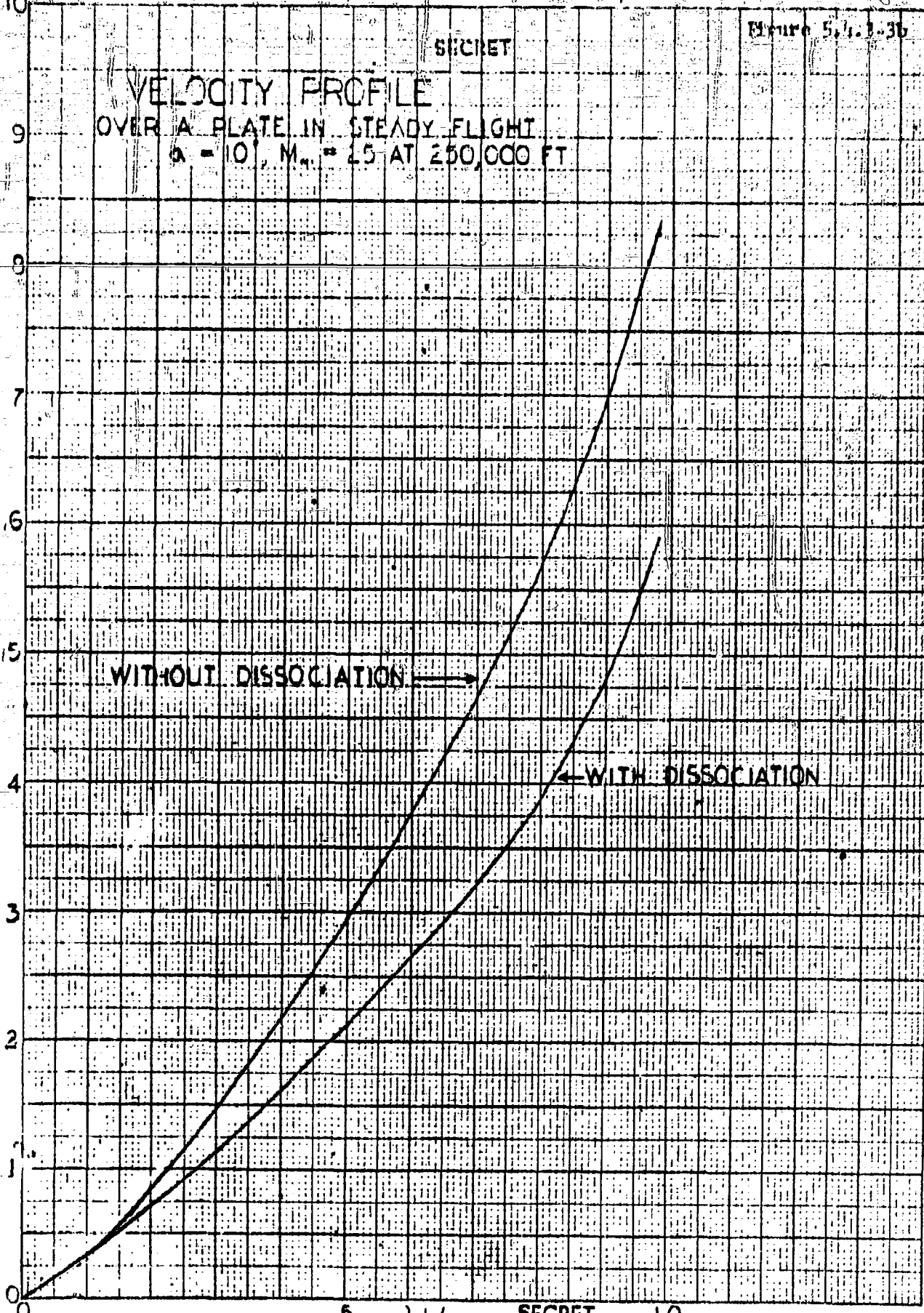
Figure 5.1.3-3b

SECRET

VELOCITY PROFILE
OVER A PLATE IN STEADY FLIGHT
 $\alpha = 10^\circ$, $M_\infty = 2.5$ AT 250,000 FT

$\frac{Y}{X}$

R



u/u_∞

SECRET

BELL

SECRET

CORPORATION

MODEL

PAGE 5-66

BY
CHECKEDDATE
DATE

BUFFALO, N. Y.

SHIP

REPORT 5113-2-50-1

March 3, 1953

SECRET

TEMPERATURE PROFILE
OVER A PLATE IN STEADY FLIGHT
 $\alpha = 10^\circ$, $M_\infty = 25$ AT 250,000

 $\frac{y}{x} \sqrt{R_x}$

4

2

0

WITHOUT DISSOCIATION

WITH DISSOCIATION

2

1

4

SECRET

BY _____ DATE _____
CHECKED _____ DATE _____

BELL Aircraft CORPORATION

SECRET

MODEL _____
SHIP _____

PAGE 5-67

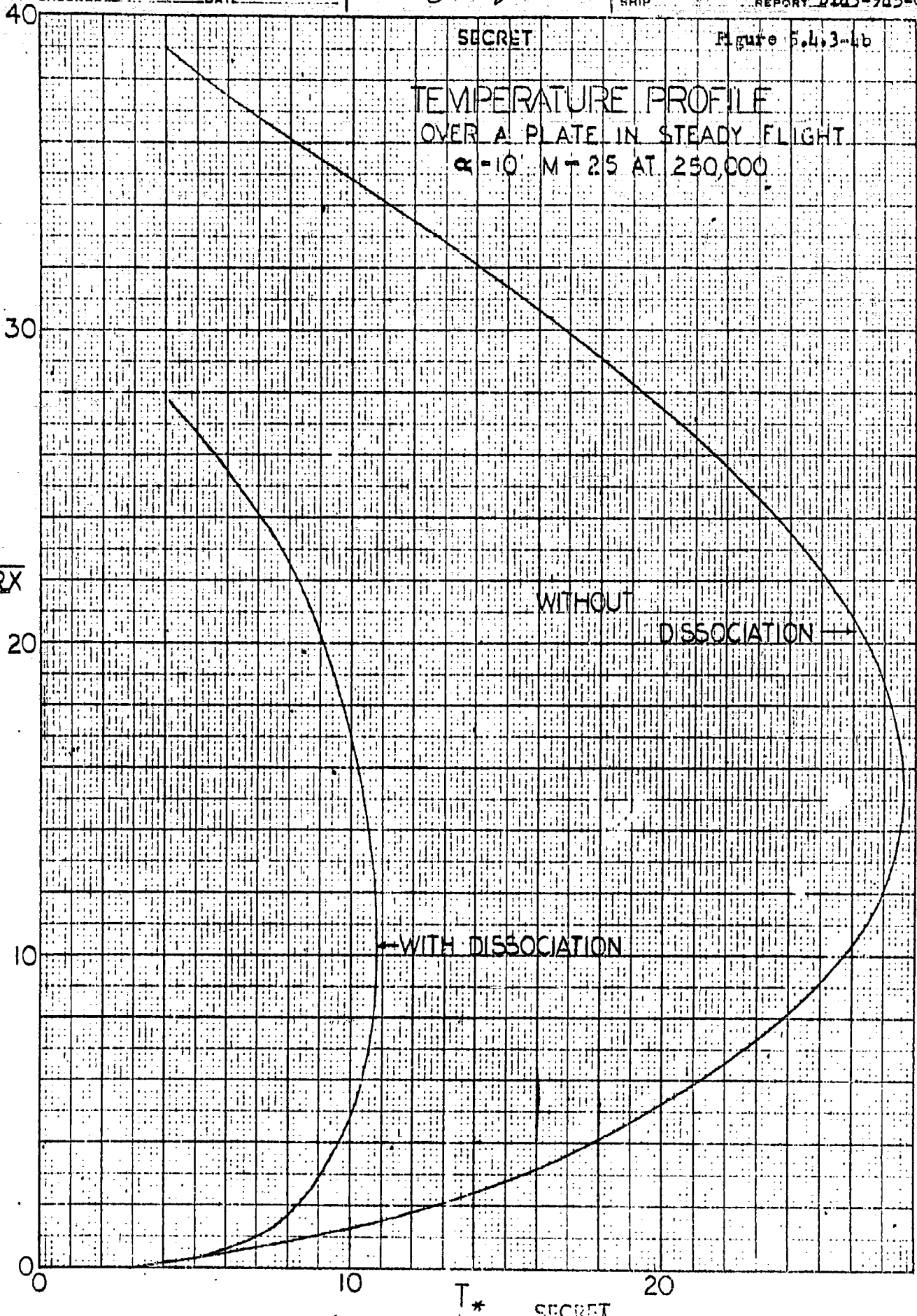
REPORT D143-945-012

SECRET

Figure 5.4.3-4b

TEMPERATURE PROFILE
OVER A PLATE IN STEADY FLIGHT
 $\alpha = 10^\circ$ $M = 25$ AT 250,000

$\frac{Y}{X} \sqrt{R_X}$



SECRET

SECRET

By _____ Date _____
 Checked _____ Date _____

BELL Aircraft CORPORATION

Model _____ Page 5-68
 Missile _____
 Airplane _____ Report D143-945-012

5.5 Transpiration Cooling

The preliminary feasibility study of the MX-2276 vehicle (Ref. 5.5-16) indicated that equilibrium skin temperature (as calculated by extrapolation of conventional supersonic laminar boundary layer methods) on the order of 2000°R could be expected on some local areas at the most critical hypersonic flight conditions. Since these temperatures are beyond the useful limits of known materials, it was evident that some method of cooling the structure locally must be considered. In order to compare the effectiveness of convection, transpiration, or film cooling* in a practical structural design, it is necessary to first obtain the aerodynamic information in transpiration cooling, and to reduce this information to a convenient form for use in structural design studies. Previous theoretical investigations (at lower Mach number to be sure) (Ref. 5.5-10 and 5.5-14) indicate that transpiration cooling would be superior in several ways to film cooling, and hence the latter was not considered in detail.

A survey and evaluation of the existing theoretical and experimental literature on the aerodynamic aspects of transpiration cooling was made (Ref's. 5.5-1 to 5.5-11) seeking a basis for the calculation of design information. Practically all of the theoretical studies examined were restricted to supersonic flow at low Mach number, generally less than 3. Hence, it was deemed necessary to develop new solutions to the equations of the compressible laminar boundary layer including the effects of transpiration cooling for Mach numbers up to 20, and to carry out the calculations for the Mach number and altitude range of interest.

The theory developed and presented (in brief) below is essentially an extension of Morduchow's approach (Ref. 5.5-1) and is based on an integral method. The essential improvements made were to assume a Sutherland relation between viscosity and temperature as used by Chapman and Rubesin (Ref. 5.5-13) instead of the linear viscosity temperature law, and to include heat radiation from the surface; the latter is an important factor at the high wall temperatures associated with the higher Mach numbers. As the end result, an approximate method was developed for computing the rate of mass flow injection of coolant required to keep a surface at a given (arbitrary) temperature under given initial free stream conditions.

* In transpiration cooling, the coolant is passed through a porous skin and enters the airstream with a finite velocity normal to the surface; in film cooling, the coolant is injected through the surface by a slot or orifice into the boundary layer at one or more points streamwise along the surface, and the coolant is spread over an area immediately downstream of the opening by viscous action of the boundary layer. With convection cooling, coolant is passed under the surface to act as a heat sink.

SECRET

By _____ Date _____

Checked _____ Date _____

BELL Aircraft CORPORATION

Model _____ Page 5-69
Missile _____
Airplane _____ Report D113-915-012

A set of exemplary design charts were calculated, typical examples of which are shown in Figs. 5.5-1 and 5.5-2. In Fig. 5.5-1 the wall temperature is constant at 1600°R and the mean coolant flow required to keep a 10 ft. plate at this temperature is shown as a function of Mach number and altitude; these charts were also made for wall temperatures ranging from 600°R to 1800°R . In Fig. 5.5-2, the altitude is fixed, and mean coolant flow is shown as a function of Mach number and surface temperature. The complete set of charts and details of the calculation are given in Ref. 5.5-12. The atmosphere used in these curves is that given in NACA TN 1200.

In evaluating the merits of transpiration cooling at the present time, many factors must be taken into account. The mechanism of transpiration cooling is to reduce the heat transfer at the surface by altering the velocity and temperature profiles in the boundary layer through mass injection into this layer. It would appear desirable, therefore, to consider a coolant other than air. This coolant - particularly a liquid like water - would absorb heat through its heat capacity and latent heat of vaporization before passing into the boundary layer at the temperature of the outside surface. However, all theories, including that given below, apply strictly only if the coolant and the flow in the boundary layer are the same gas, air in our case of interest. This stems from a basic simplification in the theory that assumes the resultant flow in the boundary layer to be homogeneous. Although it is not possible to predict the error made in assuming coolant other than air, it is expected that the results of the analysis for the modification of the velocity and temperature profiles by mass injection made for air in air would reasonably apply to other coolants, particularly when the injection rate is small (as it usually is). Since this is the most laborious part of the calculations, it is a simple matter to consider the effects of all coolants once the air-air problem is solved.

The approach adopted here is to first consider air as a coolant. If this shows merit in reducing the aerodynamic heating by modifying the flow characteristics in the boundary layer, then water or other coolant could be expected to be considerably better, even within the limits of the approximations involved and should be looked into in detail. Accordingly, a calculation of the total weight of air as a coolant required to keep the first 10' of the wing section of the proposed MX-2276 configuration at a constant temperature of 1600°R throughout its flight path was made, and the details are shown in Figure 4.6.4-1 discussed in the General Aerodynamics Section. Use of a coolant such as water could be expected to at least halve the coolant flow required in this case. The scope of the present study did not permit detailed comparison with convection cooling.

One of the considerations involved in evaluating the merit of transpiration cooling is whether or not the initial (assumed) laminar boundary layer will remain so with injection. It is known that the normal velocity associated with coolant injection has a destabilizing

By _____ Date _____

BELL Aircraft CORPORATION

Model _____ Page 5-70

Checked _____ Date _____

Missile _____
Airplane _____ Report D143-945-012

effect (cf. L. Lees - Ref. 5.5-4) but on the other hand the theory of hydrodynamic stability (Ref. 5.5-15) indicates that surface cooling tends to stabilize the boundary layer. Which trend will predominate in a given case of hypersonic flow is still an open question, and must ultimately be answered by experiment. The only known test of flow injection at supersonic speeds is that reported just recently by Nagasamatsu (Ref. 5.5-11). He injected air into the boundary layer through a spanwise series of orifices located near the leading edge of a flat plate at a Mach number 5.8. He found that transition moved upstream as the mass injected was increased to 2 percent of the boundary layer mass defect on the plate, but then any further increase in injected mass flow had very little additive effect and did not reduce transition Reynold's number to less than 2×10^6 . In comparison with this 2 percent limit, the injected mass flow percentage of the boundary layer mass flow decrement was computed for the MX-2276 glide path point with the maximum value of Q/W at the one foot station. This mass flow percentage was found to be only $1/2$ of a percent. Thus indications are that the laminar boundary layer will remain so with the low practical injection rates.

Other existing experiments with transpiration cooling were predominately concerned with the cooling of rocket combustion chambers and hot turbine blades, which is a different type of problem. Here, in low speed flow, experiments indicate good qualitative and quantitative agreement with theory (cf. Ref. 5.5-7).

Further on the question of stability of the laminar boundary layer with injection, some attempts, one just published at the time of writing, (cf. Ref. 5.5-2 and 5.5-6) have been made to investigate just how the two opposing factors of blowing and cooling combine to affect stability. The results, based on the Lin-Lees stability theory indicate that (in general) it is possible and practical to cool the surface sufficiently so that the boundary layer is stable. These conclusions must be considered with caution, since the Lin-Lees theory itself has many assumptions which restrict its applicability to low supersonic Mach number flows.

The conclusions of this study are that transpiration cooling has considerable merit as a means of cooling the critically hot parts of the MX-2276 structure, and design studies taking into account the employment of various coolants and the practical problems of porous materials, ducting and control equipment, etc. are very much in order. To this end, the method and design charts developed herein and in Ref. 5.5-12 should be of considerable use. It should be noted also that an extra dividend in the form of reduced skin friction is obtained with the use of transpiration cooling.

What is needed, however, are experiments in transpiration cooling at supersonic speeds. It is known that these are underway at several facilities (University of Michigan, NACA Langley) and are planned at

By _____	Date _____	BELL Aircraft CORPORATION	Model _____	Page 5-71
Checked _____	Date _____		Missile _____	Report D143-945-012

others when presently building test facilities are ready (e.g. Ferri's M = 6-15 tunnel at Brooklyn Polytechnic).

Analysis

The basic theory is a modification of Morduchow's work which is presented in detail in Ref. 5.5-1. Essentially, a simple expression is derived for the normal injection velocity distribution required to maintain a given, uniform temperature along a porous surface in the laminar boundary layer region of a compressible flow with a given velocity distribution outside of the boundary layer. The analysis is based on an application of the Karman - Pohlhausen method to the momentum and energy boundary layer equations and use of a heat balance equation with a Dorodnitsyn type of transformation of variables. Only the flow over a flat plate parallel to the free stream is considered here. The Sutherland relation between viscosity and temperatures as used by Chapman and Rubesin (Ref. 5.5-13) is assumed, and an additional term for the inclusion of heat radiation from the surface was included in the heat balance equation.

Initial Assumptions

(1) $Pr = 1$

(2) Velocity and enthalpy profiles are expressed by

$$u/u_1 = a_1 \eta + (6 - 3a_1) \eta^2 + (3a_1 - 8) \eta^3 + (3 - a_1) \eta^4$$

$$H/H_1 = h + b_1 \eta + (6 - 6h - 3b_1) \eta^2 + (8h - 8 + 3b_1) \eta^3 + (3 - 3h - b_1) \eta^4$$

(3) Viscosity temperature relationship is

$$\mu/\mu_1 = C_H T/T_1$$

where

$$C_H = \sqrt{\frac{T_w}{T_1}} \left(\frac{T_1 + 216}{T_w + 216} \right)$$

Introducing the Dorodnitsyn variable t defined by

$$y = \int_0^t \frac{T}{T_1} dt$$

By _____ Date _____
 Checked _____ Date _____

BELL Aircraft CORPORATION

Model _____ Page 5-72
 Missile _____
 Airplane _____ Report D143-945-012

and integrating the momentum equation from $t = 0$ to $t = \delta$ gives

$$F_1 K K' = K \Phi + F_3 \quad (1)$$

where

$$F_1 = 0.1143 + .00953 a_1 - .00397 a_1^2 \quad (2a)$$

and

$$F_3 = a_1 \quad (2b)$$

The coefficients a_1 and b_1 were found by imposing the boundary conditions at the wall,

$$u/u_1 = 0, H/H_1 = h$$

upon the momentum and energy equations, and, for zero pressure gradient are

$$a_1 = \frac{2}{1 + \frac{1}{60H} \Phi K} \quad (3a)$$

$$b_1 = \frac{2(1-h)}{1 + \frac{1}{60H} \Phi K} \quad (3b)$$

The heat balance equation is

$$\left(k \frac{\partial T}{\partial y}\right)_w = e_w v_w c_p (T_w - T_\infty) + e \sigma T_w^4 \quad (4)$$

From the expression for the enthalpy profile

$$\left(\frac{\partial T}{\partial y}\right)_w = \frac{T_1}{T_w} \frac{T_\infty}{\delta} b_1 \quad (5)$$

and substituting Eq. (5) into Eq. (4) together with the assumption that $Pr = 1.0$, we obtain, finally

$$b_1 = \frac{2(1-h)}{1 + \frac{\Phi K}{60H}} = \Phi K \left(h - \frac{T_\infty}{T_w}\right) + AK \quad (6)$$

where

$$A = \frac{e \sigma L h T_w^4}{k_w T_1 R_\infty^{1/2}} \quad (7)$$

SECRET

 By _____ Date _____
 Checked _____ Date _____
BELL *Air* CORPORATION
 Model _____ Page 5-73
 Missile _____ Report D113-915-012
 Airplane _____

Solving the above quadratic for the injection parameter, ϕ , we obtain

$$\phi = \left\{ \frac{A}{2(h - \frac{T_o}{T_e})} \left[\frac{A}{2(h - \frac{T_o}{T_e})} - \frac{6C_H}{K^2} \right] + \frac{9C_H}{K^2} \left[C_H + \frac{1}{3} \frac{1-h}{h - T_o/T_e} \right] \right\}^{1/2} - \left(\frac{3C_H}{K} + \frac{A}{2(h - T_o/T_e)} \right) \quad (8)$$

Let $B = \frac{A}{2(h - T_o/T_e)}$ and $D = C_H + \frac{1}{3} \left(\frac{1-h}{h - T_o/T_e} \right)$

Then $\phi K = \sqrt{B^2 K - 6BC_H K - 9C_H^2} = (3C_H + BK) \quad (9)$

Equation (1) can be written as

$$\frac{dK}{d\xi} = \frac{1}{F_1} \left(\frac{\phi K + F_3}{K} \right) \quad (10)$$

or $d\xi = \frac{F_1 K dK}{\phi K + F_3} \quad (11)$

or $\xi = \int_0^\xi d\xi = F_1 \int_0^K \frac{K dK}{\phi K + F_3} \quad (11b)$

However

$$F_3 = a_1 = \frac{b_1}{1-h} = \frac{1}{1-h} \left[\phi K (h - \frac{T_o}{T_e}) + AK \right]$$

thus

$$\begin{aligned} \phi K + F_3 &= \phi K \left(1 + \frac{h - T_o/T_e}{1-h} \right) + \frac{AK}{1-h} \\ &= \frac{1 - T_o/T_e}{1-h} (\phi K - BK) \end{aligned} \quad (12)$$

SECRET

By _____ Date _____

Checked _____ Date _____

BELL & HOWELL CORPORATION

Model _____ Page 5-73

Missile Airplane Report D1143-945-012

Solving the above quadratic for the injection parameter, ϕ , we obtain

$$\phi = \left\{ \frac{A}{2(h - \frac{T_0}{T_e})} \left[\frac{A}{2(h - \frac{T_0}{T_e})} - \frac{6C_H}{K^2} \right] + \frac{9C_H}{K^2} \left[C_H + \frac{1}{3} \frac{1-h}{h - T_0/T_e} \right] \right\}^{1/2} - \left(\frac{3C_H}{K} + \frac{A}{2(h - T_0/T_e)} \right) \quad (8)$$

Let $B = \frac{A}{2(h - T_0/T_e)}$ and $D = C_H + \frac{1}{3} \left(\frac{1-h}{h - T_0/T_e} \right)$

Then $\phi K = \sqrt{B^2 K - 6BC_H K - 9C_H D} - (3C_H + BK) \quad (9)$

Equation (1) can be written as

$$\frac{dK}{d\xi} = \frac{1}{F_1} \left(\frac{\phi K + F_3}{K} \right) \quad (10)$$

or $d\xi = \frac{F_1 K dK}{\phi K + F_3} \quad (11)$

or $\xi = \int_0^\xi d\xi = F_1 \int_0^K \frac{K dK}{\phi K + F_3} \quad (11b)$

However

$$F_3 = a_1 = \frac{b_1}{1-h} = \frac{1}{1-h} \left[\phi K \left(h - \frac{T_0}{T_e} \right) + AK \right]$$

thus

$$\begin{aligned} \phi K + F_3 &= \phi K \left(1 + \frac{h - T_0/T_e}{1-h} \right) + \frac{AK}{1-h} \\ &= \frac{1 - T_0/T_e}{1-h} (\phi K - EK) \end{aligned} \quad (12)$$

where

$$E = A/1 = \frac{T_c}{T_o}$$

so that

$$\xi = \int_0^K \frac{\frac{1-h}{1-T_c/T_o} F_1 K dK}{\sqrt{B^2 K^2 - 6BC_H K + 9C_H^2 D - [(B-E)K + 3C_H]}}$$

$$= \int_0^K I(K) dK \quad (13)$$

Method of Computation

1. For a selected set of free stream conditions, wall temperatures, and initial coolant temperature, C_H , k , A , B , D , and E are determined.
2. F_1 is computed from Eq. (2a) where a_1 can be found from the expression derived from the heat balance equation without radiation consideration. This expression is

$$a_1 = \frac{2}{1 + \frac{C}{6C_H}} \quad (14)$$

where

$$C = 3C_H \left\{ \left[1 + \frac{4}{3} \frac{1}{C_H} \frac{1-h}{h - \frac{T_c}{T_o}} \right]^{1/2} - 1 \right\} \quad (15)$$

The discrepancy in a_1 will have very little effect upon the numerical value for F_1 .

3. For selected values of K , the corresponding values of I are determined.
4. A plot I vs. K is made and the variation of ξ with K is determined by a graphical or numerical integration procedure. An approximate value for K at $\xi = 1.0$ can be found from

$$K (\xi = 1.0) = \sqrt{\frac{2}{F_1}} \left[C + \frac{2}{1 + \frac{C}{6C_H}} \right] \quad (16)$$

SECRET

By _____ Date _____

Checked _____ Date _____

BELL *Aircraft* CORPORATIONModel _____ Page 5-75Missile _____
Airplane _____ Report D113-915-012

5. Knowing the variation of g with K , values for g can be assumed and the corresponding K 's determined, and then the injection parameter, Φ , is computed from Eq. (9). From

$\Phi, \frac{g}{w} = \frac{q_w v_w}{c_1 u_1}$ can be determined. The curves in this report were computed for a 10 foot long flat plate with an assumed emissivity of 0.8 for a Mach number range of 5 - 20 at altitudes of 100, 200 and 300,000 feet. Since the chordwise injection parameter distribution varies approximately with the inverse square of x , this presentation was simplified by use of mean integrated values.

SECRET

SECRET

By _____ Date _____
 Checked _____ Date _____

BELL Aircraft CORPORATION

Model _____ Page 5-76
 Missile _____
 Airplane _____ Report D143-945-012

Section 5.5 - Symbols

- a_1 = Coefficient of η in velocity profile
 b_1 = Coefficient of η in enthalpy profile
 c_p = Specific heat of gas at constant pressure
 H = Stagnation Enthalpy
 h = H_w/H_1 for $Pr = 1.0$, $h = \frac{T_w}{T_e}$
 k = Coefficient of thermal conductivity
 L = Length of plate
 Pr = Prandtl number
 Q = $c_w v_w$
 Re = Reynolds number; $= c_1 u_1 L/\mu_1$
 T = Absolute temperature in $^{\circ}R$
 T_c = Initial temperature of the coolant
 T_e = Equilibrium wall temperature for zero heat transfer
 $= T_1 (1 + \frac{\gamma - 1}{2} M_1^2)$
 W = $c_1 u_1$
 t = Variable defined by $y = \int_0^t \frac{T}{T_1} dt$
 u, v = Velocities of flow parallel and perpendicular to the surface
 x, y = Distance along, and normal to the surface
 δ = Boundary layer thickness in (x, t) plane
 ϵ = Emissivity
 η = t/δ
 σ = Stephan-Boltzmann constant ($\sigma = 4.8 \times 10^{-13}$)

SECRET

SECRET

By _____	Date _____	BELL Aircraft CORPORATION	Model _____	Page 5-77
Checked _____	Date _____		Missile _____	Report D113-915-012

$$K = (\delta/L) Re^{1/2}$$

μ = Absolute viscosity

$$\xi = x/L$$

$$\phi = \frac{\rho_w v_w}{\rho_l u} Re^{1/2} \quad \text{injection parameter}$$

Subscripts

l = values at outer edge of boundary layer

w = values at wall

a prime (') denotes differentiation with respect to ξ .

SECRET

SECRET

By _____ Date _____
Checked _____ Date _____

BELL *Aircraft* CORPORATION

Model _____ Page **5-78**
Missile _____
Airplane _____ Report **D143-945-012**

Section 5.5 - References

- 5.5-1 Morduchow, M.: "On Heat Transfer Over a Sweat-Cooled Surface in Laminar Compressible Flow with a Pressure Gradient". Journal of Aeronautical Sciences, Vol. 19, No. 10, October 1952.
- 5.5-2 Klunker, E.B. & Ivey, H.R.: "An Analysis of Supersonic Aerodynamic Heating with Continuous Fluid Injection". NACA TN 1987, December 1949.
- 5.5-3 Yuan, S.W.: "Heat Transfer in a Laminar Compressible Boundary Layer on a Porous Flat Plate with Variable Fluid Injection". Polytechnic Institute of Brooklyn, TM-PIB-15, September 1950.
- 5.5-4 Lees, L.: "Stability of Laminar Boundary Layers with Injection of Cool Gas at the Wall". Princeton University, TR-11, 5 May 1948.
- 5.5-5 Dorrence & Dore: "The Effect of Mass Transfer on Compressible Turbulent Boundary Layer Skin Friction and Heat Transfer". Journal of Aeronautical Sciences, Vol. 21, No. 6, June 1954.
- 5.5-6 Low, G.M.: "The Compressible Laminar Boundary Layer with Fluid Injection". NACA TN 340A, March 1955.
- 5.5-7 Libby, Kaufman & Harrington: "An Experimental Investigation of the Isothermal Laminar Boundary Layer on a Porous Flat Plate". Polytechnic Institute of Brooklyn, TM-PIB-16, April 1952.
- 5.5-8 Eckert, E.R.G. & Livingood, J.N.B.: "Method for the Calculation of Heat Transfer in the Laminar Region of Air Flow Around Cylinders of Arbitrary Cross-section (Including Large Temperature Differences and Transpiration Cooling)". NACA TN 2744, June 1952.
- 5.5-9 Ness, N.: "On the Temperature Distribution Along a Semi-Infinite Sweat-Cooled Plate". Journal of Aeronautical Sciences, Vol. 19, No. 11, November 1952.
- 5.5-10 Eckert, E.R.G. & Livingood, J.N.B.: "Comparison of the Effectiveness of Convection, Transpiration, and Film Cooling Methods with Air as a Coolant". NACA TN 3010, October 1953.
- 5.5-11 Nagamatsu, H.T.: "Summary of Recent GARCIT Hypersonic Experimental Investigation". Journal of Aeronautical Sciences, Vol. 22, No. 3, March 1955.
- 5.5-12 Landphair, L.C.: "Transpiration Cooling of a Flat Plate in Laminar Compressible Flow". Bell Aircraft Corp. Research Note No. 76 (Unpublished).

SECRET

SECRET

By _____	Date _____	BEL CORPORATION	Model _____	Page 5-79
Checked _____	Date _____		Missile _____	Report DL43-945-012

- 5.5-13 Chapman, D.R. & Rubesin, M.W.: "Temperature and Velocity Profiles in the Compressible Laminar Boundary Layer with Arbitrary Distribution of Surface Temperature". Journal of Aeronautical Sciences, Vol. 16, No. 9, September 1949.
- 5.5-14 Knuth, E.L.: "The Mechanics of Film Cooling". California Institute of Technology, Ph. D. Thesis, 1954.
- 5.5-15 Lees, L. & Lin, C.C.: "Investigation of the Stability of the Laminar Boundary Layer in a Compressible Fluid". NACA TN 1115, September 1946.
- 5.5-16 "Strategic Weapon System". Bell Aircraft Corporation Preliminary Design Report No. DL43-945-010 dated 15 July 1953.

SECRET

BY
CHECKED

DATE

BELL

SECRET

CORPORATION

BUFFALO, N. Y.

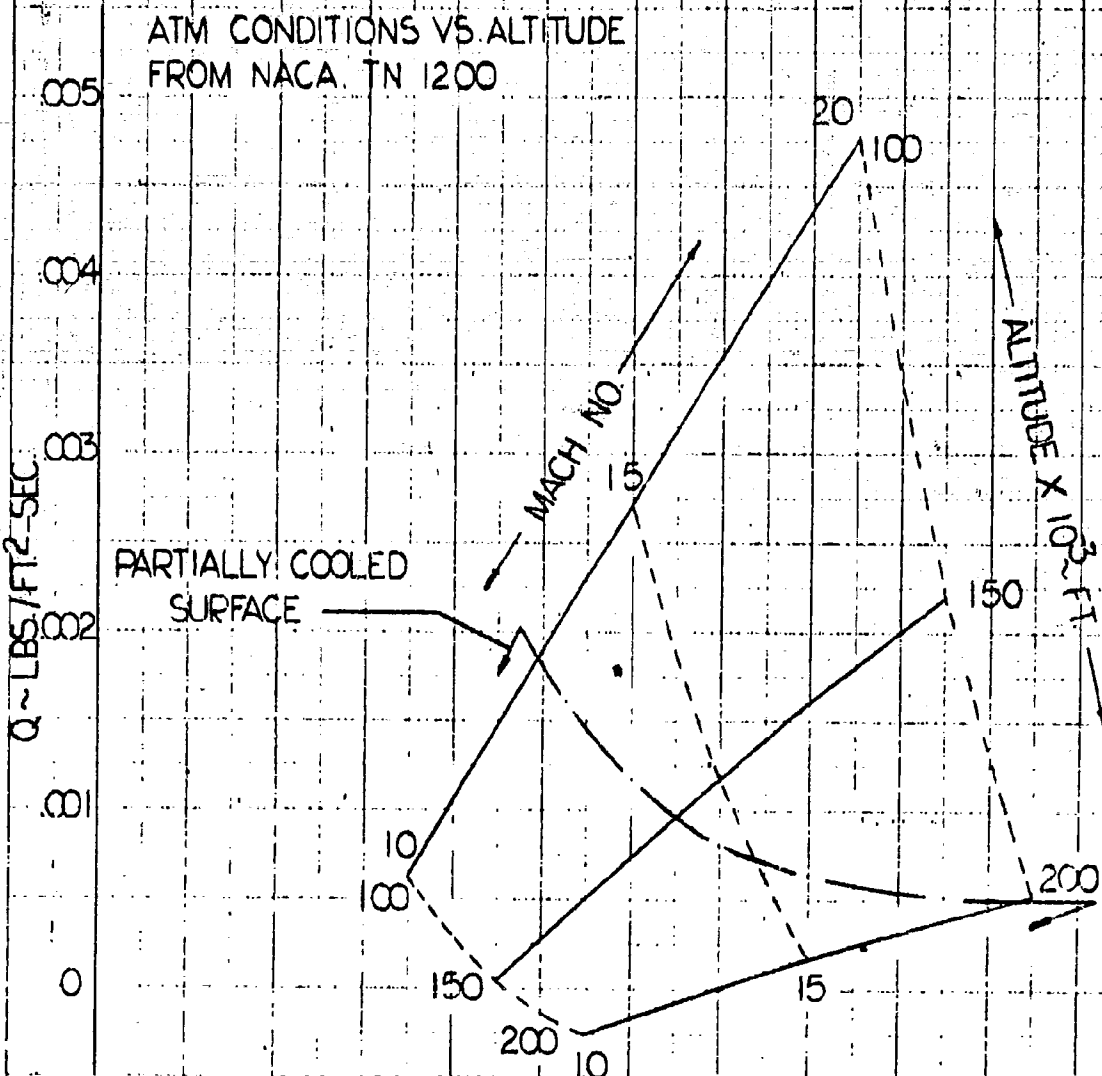
150P

PAGE 580
FROM 1213-91-112

Figure 5.5.1

MEAN COOLANT AIR FLOW FOR TRANSPIRATION
COOLING OF FLAT PLATE SURFACE TO 1600° R

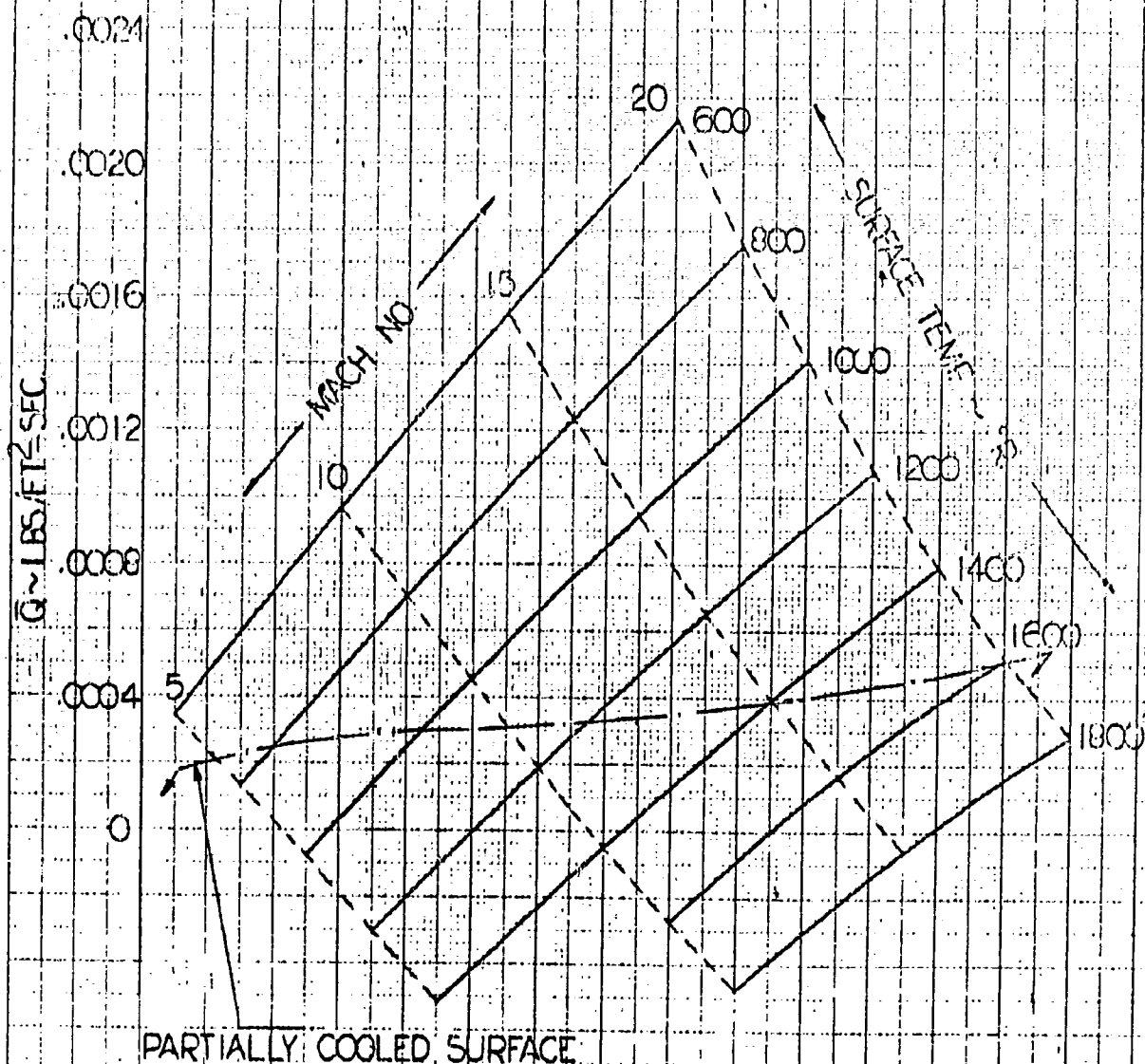
PLATE LENGTH = 10 FT.



SECRET

MEAN COOLANT AIR FLOW FOR TRANSPIRATION
 COOLING OF FLAT PLATE SURFACE

FLIGHT ALTITUDE = 20000 FT.



By _____

Checked _____

Model _____

Page 5-82

Missile
Airplane _____

Report DL43-915-012

5.6. Hypersonic Inviscid Flow

It is quite generally accepted that the trend of pressure variation predicted by the Newtonian impact theory, namely

$$p = (1/2 \rho_{\infty} U_{\infty}^2) 2 \sin^2 \alpha \quad (1)$$

agrees quite well with most of the high Mach number test results as well as with exact numerical solutions based on the method of characteristics for inviscid continuum flow. An essential assumption underlying the above formula is that the change of momentum of the flow element does not take place until its collision with the body, and this could only be true in free molecular flow under very special assumptions.

On the other hand, a simplified model which brings out the essential features of the flow of a continuous medium at high Mach number can be constructed as illustrated in Figure 5.6-1. Assuming that the Mach number is so high that the shock wave is very strong and, in addition, that the fluid is compressed to a diminishing volume by the shock, it is seen that the extent of the region between the shock and the body surface becomes necessarily small. It follows that the shock wave forms a surface envelope around the body and the fluid coasts along the body immediately behind the shock (see Figure 5.6-2). The pressure force acting on the body in such a flow model is simply the sum of the impact pressure - which is that given above by Equation (1) - and the centrifugal force arising from the infinitely dense fluid coasting along the curved body surface; the static pressure in the free stream can be ignored. If the infinitely thin layer is assumed inviscid*, the Busemann formula

$$\frac{p}{\frac{1}{2} \rho_{\infty} U_{\infty}^2} = 2 \sin^2 \alpha + 2 \cos \alpha \frac{d\alpha}{dx} \int_0^x \sin \alpha \, dx \quad (2)$$

where α is the local surface incidence, is obtained. A similar formula can be obtained for bodies of revolution.

* The assumption made in Reference 5.6-6 concerning the constancy of velocity of each individual particle while coasting along the curved body surface is actually equivalent to the assumption of an inviscid flow insofar as it affects the determination of the centrifugal force.

SECRET

By _____ Date _____

Checked _____ Date _____

BELL *Aircraft* CORPORATION

Model _____ Page 5-83

Missile _____ Report D143-945-012
Airplane _____

The Busemann formula which is deduced from a simplified continuum model reduces to the Newton impact pressure formula when applied to a wedge. The characteristics of the inviscid continuum flow under the assumption of infinite compression ratio for the shock is revealed in the additional term - the centrifugal effect (the realization of which requires an exchange of momentum amongst the fluid particles). However, comparison of results of Busemann and Newton formulas with exact numerical solutions for thin airfoils or bodies at very high Mach number in air (with ratio of specific heats $\gamma = 1.4$) seems to show that the effect predicted by the second term of Equation (2) is absent and the Newtonian impact pressure or the tangent-wedge formula gives a better numerical approximation. In particular, the prediction of the point of "zero" pressure on the surface is given to soon (i.e. too close to the nose) by Equation (2).

Now (undissociated) air with a specific heat ratio $\gamma = 1.4$ say, cannot be infinitely compressed by the strong shock; the limiting compression ratio is only

$$\frac{\rho_s}{\rho_\infty} = \frac{\gamma + 1}{\gamma - 1} \quad (3)$$

which (for no dissociation) is of the order of unity. It is seen then that fluid density is finite and variable in the layer, and the thickness of the layer grows downstream along the surface because fluid mass is being entrained in it. The concept of the flow behind the shock being confined to an infinitesimally thin layer - which forms the basis for Equation (2) - is no longer applicable, the extent of the included region (between shock and surface) being small but finite near the front and diverging from the body downstream. In the hypothetical case of a gas where $\gamma = 1$ (infinite internal degrees of freedom) the Busemann formula is satisfactory, as demonstrated by the example in Reference 5.6-6 (see also Figure 5.6-4).

In Appendix 5D a refinement of the Busemann flow model is given where the (slight) divergence of the shock wave from an (slightly) inclined surface and the thickening of the "entropy layer" (since the shock is strong and curved, the flow is rotational) is taken into account. The analogy between a steady hypersonic flow over a three (or two) dimensional thin body and unsteady cross flow (of one less dimension) is employed (cf. References 5.6-4 and 5.6-5). Thus the equivalent problem is identifiable as one involving an "entropy layer" between an advancing piston and a strong shock wave. The momentum-integral method is then applied to this entropy-layer in a similar fashion as in the ordinary viscous boundary layer problems.

SECRET

SECRET

By _____ Date _____	BELL <i>Aircraft</i> CORPORATION	Model _____	Page 5-84
Checked _____ Date _____		Missile _____ Airplane _____	Report D113-915-012

For the case of infinite Mach number, this piston theory (a similar method can be applied to the case of body of revolution) yields the Busemann formula as the zeroth order approximation when the solution is developed as an asymptotic expansion in descending powers of the limiting compression ratio, i.e. $(\frac{\gamma+1}{\gamma-1})$ this zeroth

approximation gives*

$$p^{(0)} \approx \rho_{\infty} u_{\infty}^2 \frac{d}{dx} [Y(x) Y'(x)]$$

$$\approx \rho_{\infty} u_{\infty}^2 [Y'(x)]^2 + \rho_{\infty} u_{\infty}^2 Y(x) Y''(x) \quad (4)$$

whereas the correction term accounting for the finiteness of the compression ratio, though of order of $(\frac{\gamma-1}{\gamma+1})$, is indeed not numerically

small; when applied to the wedge at incidence α , it gives the correct limiting value of the so called tangent-wedge formula

$$p \approx 1/2 \rho_{\infty} u_{\infty}^2 (\gamma + 1) \alpha^2 \quad (5)$$

and when applied to the parabolic airfoil it gives a correction so large (for $\gamma = 1.4$) that an opposite effect to that of the centrifugal is observed as shown in Figures 5.6-3 and 5.6-4. Unfortunately, such an expansion is not uniformly valid (with respect to x) and diverges at some point where the formal zeroth order (Busemann) solution yields a negative pressure.

The result in Figure 5.6-3 indicates that for flow over a slightly convex surface, the finiteness of the compression ratio causes the shock front to deviate from the surface, resulting in a stronger shock wave (than the Busemann result) and consequently a higher pressure jump which tends to balance the pressure decrease due to the centrifugal force. This fact is demonstrated clearly in the particular solution worked out for the surface (Figure 5.2-5).

* This formula shows that, to the zero order (in $\frac{\gamma-1}{\gamma+1}$), the total lift depends only on the value of $Y(x) Y'(x)$ at the trailing edge, e.g. if the local incidence at the trailing edge vanishes, the total lift vanishes (the result is also valid for a blunt i.e. provided the slope at the trailing edge is small).

SECRET

By _____ Date _____	BELL <i>Aircraft</i> CORPORATION	Model _____	Page 5-85
Checked _____ Date _____		Missile _____ Airplane _____	Report DL43-945-012

$$y \sim x^{3/4}$$

which is the type belonging to the "viscous boundary layer" thickness" near the leading edge portion of a wedge under the influence of the self-induced pressure gradient. The asymptotic solution in the development of $(\frac{\gamma-1}{\gamma+1})$ does not behave peculiarly in this case and

it agrees well numerically with the similar solution obtained directly from the momentum and energy integral relations. The results show that the pressure is higher than the tangent-wedge value by a factor of 1.14 for $\gamma = 7/5 = 1.4$ and 1.32 for $\gamma = 5/3$. This pressure increase instead of decrease from the tangent-wedge value is explainable by the fact that the location of the shock wave is found 1.36 times higher than the tangent-wedge value for $\gamma = 7/5$ and 1.4 times higher for $\gamma = 5/3$; thus in spite of the centrifugal force effect, the resultant pressure at the edge of the hypersonic boundary layer may be higher than the value provided by the tangent-wedge formula.

In the absence of solution based on the full equations, these values, namely 1.14 for $\gamma = 7/5$, 1.32 for $\gamma = 5/3$, are taken as the correction factor for the tangent-wedge formula used in the theory of shock wave - boundary layer interaction. The error in these solutions, when applied to the case of high but finite Mach number, is of the order of $1/M_\infty^2$ in comparison with unity, the first order effect of which can be determined in a similar manner as in the expansion in $(\frac{\gamma-1}{\gamma+1})$.

Date _____

BELL *Aircraft* CORPORATION

Model _____

Page _____

5-86

Date _____

Missile
Airplane _____

Report _____

D143-945-012

Section 5.6 References

- 5.6-1 Busemann, A., "Flussigkeits - und Gasbewegung, Handwörterbuch der Naturwissenschaft", 2nd Ed., Gustave Fisher, Jena, 1933 - pp. 275-277.
- 5.6-2 Grimminger, G., Williams, E.P., and Young, G.B.W., "Lift on Inclined Bodies of Revolution in Hypersonic Flow", J.A.S., Vol. 17 (1950) pp. 675-690.
- 5.6-3 Ivey, H.R., Klunker, E.B., and Bowen, E.N., "A Method for Determining the Aerodynamic Characteristics of Two- and Three-Dimensional Shapes at Hypersonic Speeds", NACA TN 1613, 1948.
- 5.6-4 Hayes, W.D., "On Hypersonic Similitude, Quant. Appl. Math.," Vol. 5 (1947), 105-106.
- 5.6-5 Van Dykes, M.D., "Application of Hypersonic Small-Disturbance Theory", J.A.S. Vol. 21, No. 3, March 1954.
- 5.6-6 Eggers, A.J., Jr., and Syverston, C.A., "Inviscid Flow about Airfoils at High Supersonic Speeds", NACA TR 1123, 1953.

BELL SECRET

WINDT

PAGE 5-87

AIRPLANE

REPORT D113-216-012

FLOW PATTERNS

Figure 5.6-1

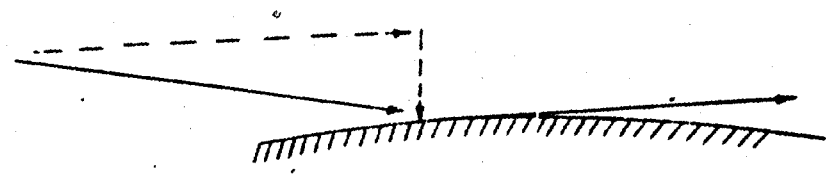


FIG. a

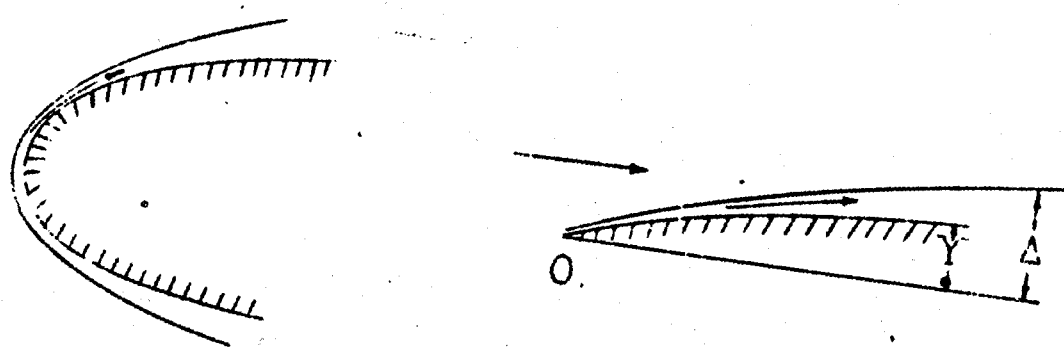


FIG. b

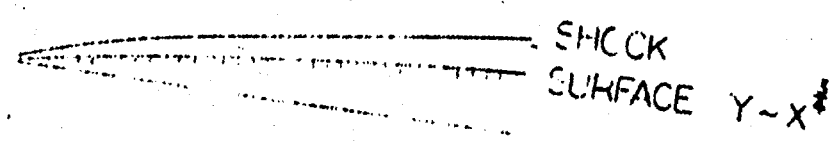


FIG. c

SECRET

BY
CHECKED

DATE
DATE

BELL

SECRET

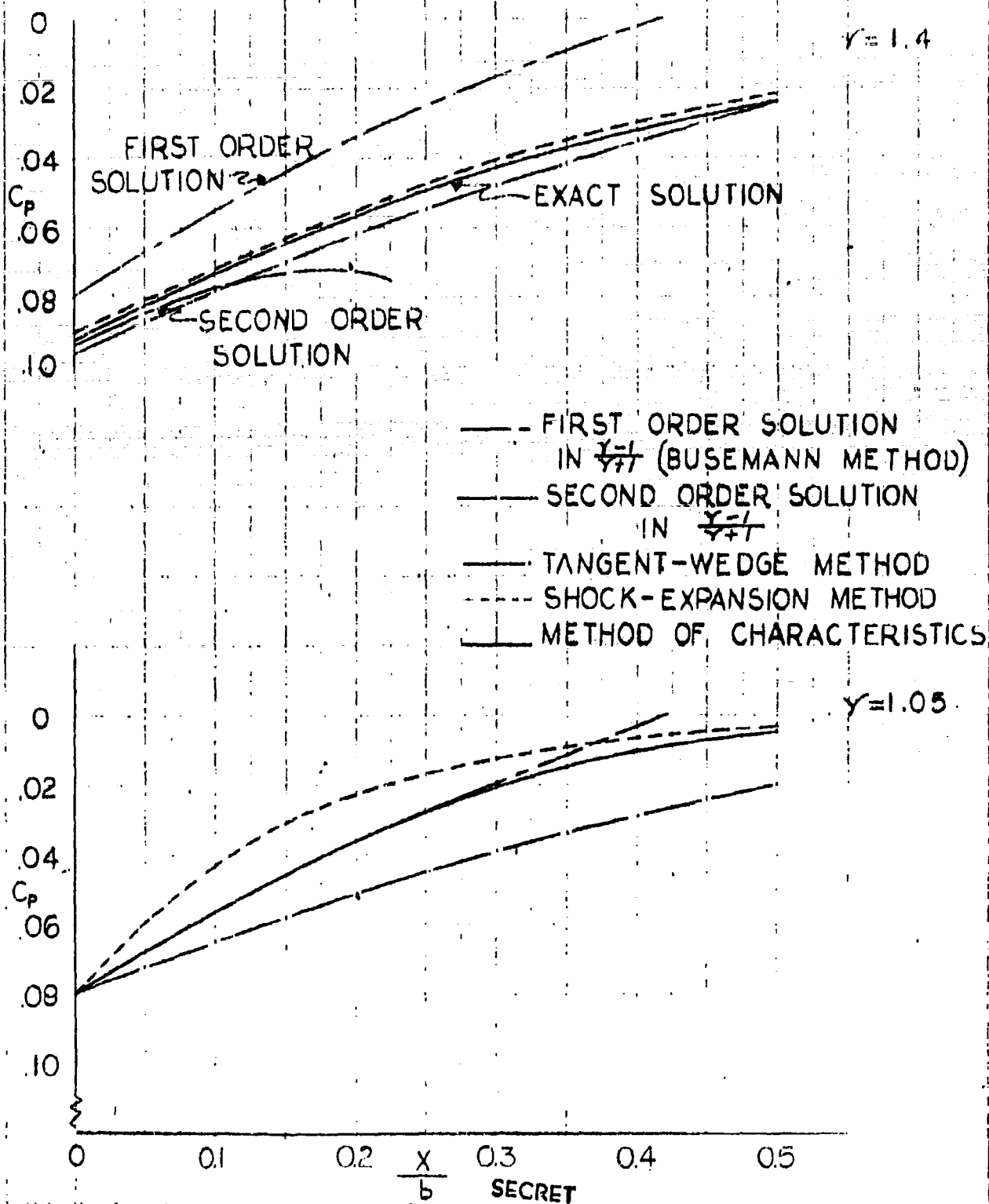
CORPORATION

DATE 5.28

REPORT 111-101

Figure 5.6.2

COMPARISON OF VARIOUS FORMULAS
AT $M_\infty = \infty$
10% - THICK BICONVEX AIRFOIL



Date _____

BELL

CORPORATION

Model _____

Page

5-69

Date _____

Missile _____
Airplane _____

Report

DL43-5

5.7 Transition

Methods have been given for the determination of the local skin friction and heat transfer parameters for the cases when the boundary layer is laminar or turbulent. In any practical computation of friction drag or aerodynamic heating, the state of the boundary layer must first be assumed, i.e., a knowledge of the transition point is required. Unfortunately, the present state of reliable knowledge on this subject leaves much to be desired. The effect and the importance of the many variables which could effect transition and the mechanism of transition itself is not yet understood; hence, the assumptions of theory are incomplete and experiments are not fully controlled. The best that can be done at the present time is to assume a transition Reynolds number based on the trends exhibited by available wind-tunnel and flight test data. In the original proposal report a transition Reynolds number $Re = 2.8 \times 10^6$ at all Mach numbers was assumed. This appears to have been conservatively low judging from the trends exhibited by the test data (Figure 5.7-1 and 5.7-2), from theoretical predictions, and by discussions with several experimenters during our visits to other research agencies. However, it is interesting to note that even on the basis of the assumed transition Reynolds number of 2.8×10^6 , the boundary layer over the wing of X-2276 (chords varying from 10 to 140 ft.) is practically all laminar for the major portion of a typical flight path where $M = 10$ and $Re/ft.$ is less than 1×10^5 .

It cannot be said that there is actually a theory for the prediction of transition Reynolds number, although the results of theoretical investigations of the stability of the laminar boundary layer in a compressible fluid (e.g., References 5.7-1 and 5.7-2) are often used as a basis for such predictions. This theory, which is also limited to the lower supersonic Mach numbers, cannot be expected to yield more than qualitative results and trends, as it is based on a linearized method of small disturbances, while transition is a non-linear problem of a different order. Besides, the model of boundary layer stability is only an approximation to the actual mechanism of transition which is still unknown.

While some sources are making extensive and laborious calculations on the stability of the laminar boundary layer, based on the Lin-Lees theory, it is felt that the usefulness of any results of this type, particularly at the high Mach numbers, are open to considerable question because of the many assumptions involved in the underlying theory and because of the sensitivity of the calculated results to actual values of the transport properties of the air used in the calculations. As has been pointed out before, the actual values of these properties are not known beyond about 20,000R, yet these values have to be assumed up to temperatures approaching 10,000R which are reached (theoretically) in the boundary layer. It is believed that the most reliable data for the near future will come from wind-

5-5-1-1-5-8-0-2-7-5

BY _____ Date _____	BELL <i>Aircraft</i> CORPORATION	Model _____	Page <u>5-90</u>
Checked _____ Date _____		Missile _____ Airplane _____	Report <u>D143-945-012</u>

tunnel and, particularly, free flight tests. It is known that pertinent tests of this nature are now underway or planned. It seems apparent, therefore, that any reliable information on transition point must come from carefully instrumented and analyzed flight tests, where all possible controlling factors are considered. These are needed, particularly at Mach numbers greater than three. There seems to be some hope that with research missiles now reaching towards Mach ten, that flight test transition data in this neighborhood will be available in the next year or so.

A survey of experimental data on determination of the transition point has been made and the results are summarized in Figures 5.7-1 and 5.7-2. As can be seen from Figure 5.7-1 no sharply definitive results can be found because of the varied tunnel characteristics, although, apparently, trends can be established. In the wind tunnel, the transition point is located through examination of the plots of recovery factor or skin friction coefficient versus Reynolds number, or through Schlieren photographs or other visual methods such as china clay, etc. For firing range flight tests such as those in Reference 5.7-3, shadowgraph methods can be used to find the transition point or, if telemetered data is available, graphical analyses as mentioned above are used.

The effects of various parameters on the location of the transition point has been investigated experimentally. These parameters include: addition and removal of heat, surface roughness, angle of attack, wind tunnel turbulence, free-stream stagnation pressures, and leading edge thickness. References 5.7-4 to 5.7-11 found that heating of the surface results in earlier transition while cooling has the reverse effect, as predicted by the small disturbance theory of boundary layer stability (cf. Reference 5.7-1). However, the stabilizing effect of heat removal is greatly reduced if flow disturbances are present such as those caused by roughness, tunnel turbulence, or transition inducing devices (see References 5.7-4 and 5.7-5). Reference 5.7-4 shows that if the insulated plate friction coefficient is large, the transition Reynold's number is greatly influenced by heat flow; if small, heat flow effects are greatly reduced. Increased surface roughness results in earlier transition; as does an increased angle of attack upon the transition on the upper surface of the model (as illustrated in References 5.7-3, 5.7-12, 5.7-13). Transition Reynold's number increases with the free-stream stagnation pressure and also with the leading edge thickness of the model, according to Reference 5.7-14. Wind tunnel turbulence may have great effect upon the location of transition area, tending to decrease the transition Reynold's number as the degree of turbulence increases. Therefore, wind tunnel results are often characteristic of the tunnel used, since stream-turbulence is a function of the tunnel design. In Reference 5.7-15, a conical model was tested in various NACA supersonic wind tunnels. Tunnel flow characteristics were so varied, that no conclusive results could be found. However, in most cases at least, trends can be established through wind tunnel experimentation even though specific data may be questionable.

SECRET

By _____	Date _____	BELL Aircraft CORPORATION	Model _____	Page 5-91
Checked _____	Date _____		Missile _____	Report DL43-945-012

Section 5.7 - References

- 5.7-1 Lees, L.: "The Stability of the Laminar Boundary Layer in a Compressible Fluid". NACA TN 1360, July 1947.
- 5.7-2 Lees, L. & Lin, C.C.: "Investigation of the Stability of the Laminar Boundary Layer in a Compressible Fluid". NACA TN 1115, September 1946.
- 5.7-3 Jedlicka, V.R.; Welins, H.E.; and Seiff, A.: "Experimental Determination of Boundary Layer Transition on a Body of Revolution at $M = 3.5$ ". NACA RM A53L18, March 15, 1954.
- 5.7-4 Czarnecki, K.R. and Sinclair, A.R.: "Preliminary Investigation of the Effects of Heat Transfer on Boundary Layer Transition on a Parabolic Body of Revolution (NACA RM-10) at a Mach number of 1.61". NACA TN 3165, April 1954.
- 5.7-5 Kline, S.V. and Shapiro, A.H.: "Experimental Investigation of the Effects of Cooling on Friction and on Boundary Layer Transition for Low Speed Gas Flow at the Entry of a Tube". NACA TN 3048, November 1953.
- 5.7-6 Frick, C.W., Jr. and McCullough, G.P.: "Tests of a Heated Low-Drag Airfoil". NACA 12-3-42, December 3, 1952.
- 5.7-7 Scherrer, R.: "Comparison of Theoretical and Experimental Heat Transfer Characteristics of Bodies of Revolution at Supersonic Speeds". NACA Report 1055, 1951.
- 5.7-8 Scherrer, R.; Winbrow, W.R.; and Gown, F.E.: "Heat Transfer and Boundary Layer Transition on a Heated Cone at a Mach Number of 1.53". NACA RM A8L28, January 10, 1949.
- 5.7-9 Scherrer, R.: "Boundary Layer Transition on a Cooled 20° Cone at Mach Numbers of 1.5 and 2.0". NACA TN 2131, July 1950.
- 5.7-10 Liepmann, H.W. and Fila, G.H.: "Investigation of Effects of Surface Temperature and Simple Roughness Elements on Boundary Layer Transition". NACA Report 890, 1947.
- 5.7-11 Higgins, R.W. and Pappas, C.C.: "An Experimental Investigation of the Effect of Surface Heating on Boundary Layer Transition on a Flat Plate in Supersonic Flow". NACA TN 2351, April 1951.
- 5.7-12 Dryden, H.L.: "Review of Published Data on the Effect of Roughness on Transition from Laminar to Turbulent Flow". Journal of Aeronautical Sciences, Vol. 20, No. 7, July 1953.

SECRET

SECRET

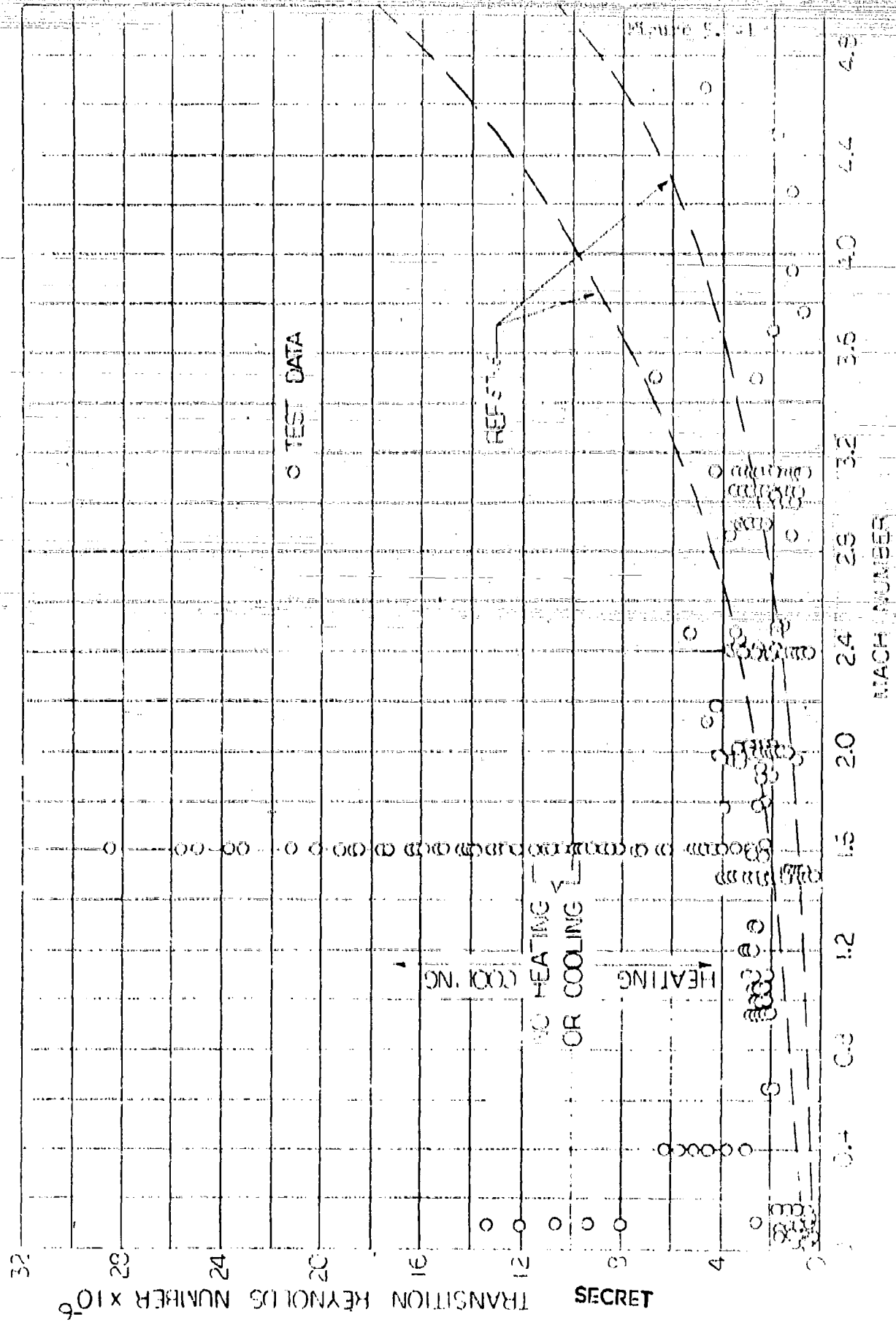
Date _____	BELL <i>Aircraft</i> CORPORATION	Model _____	Page <u>5-92</u>
Checked _____ Date _____		Missile _____	Report <u>DL43-945-012</u>
		Airplane _____	

- 5.7-13 Czarnecki, K.R.; Robinson, R.B.; and Hilton, J.R., Jr.; "Investigation of Distributed Surface Roughness on a Body of Revolution at a Mach Number of 1.61". NACA TN 3230, June 1954.
- 5.7-14 Brinick, P.F. and Diaconis, N.S.; "Boundary Layer Development and Skin Friction at Mach Number 3.05", NACA TN 2742, July 1952.
- 5.7-15 Ross, A.O.; "Determination of Boundary Layer Transition Reynold's Numbers by Surface Temperature Measurement of a 10° Cone in Various NACA Supersonic Wind Tunnels". NACA TN 3020, October 1953.
- 5.7-16 Gazley, C.; "Boundary Layer Stability and Transition in Supersonic Flow." General Electric Report R52-A0506, May 1952.

SECRET

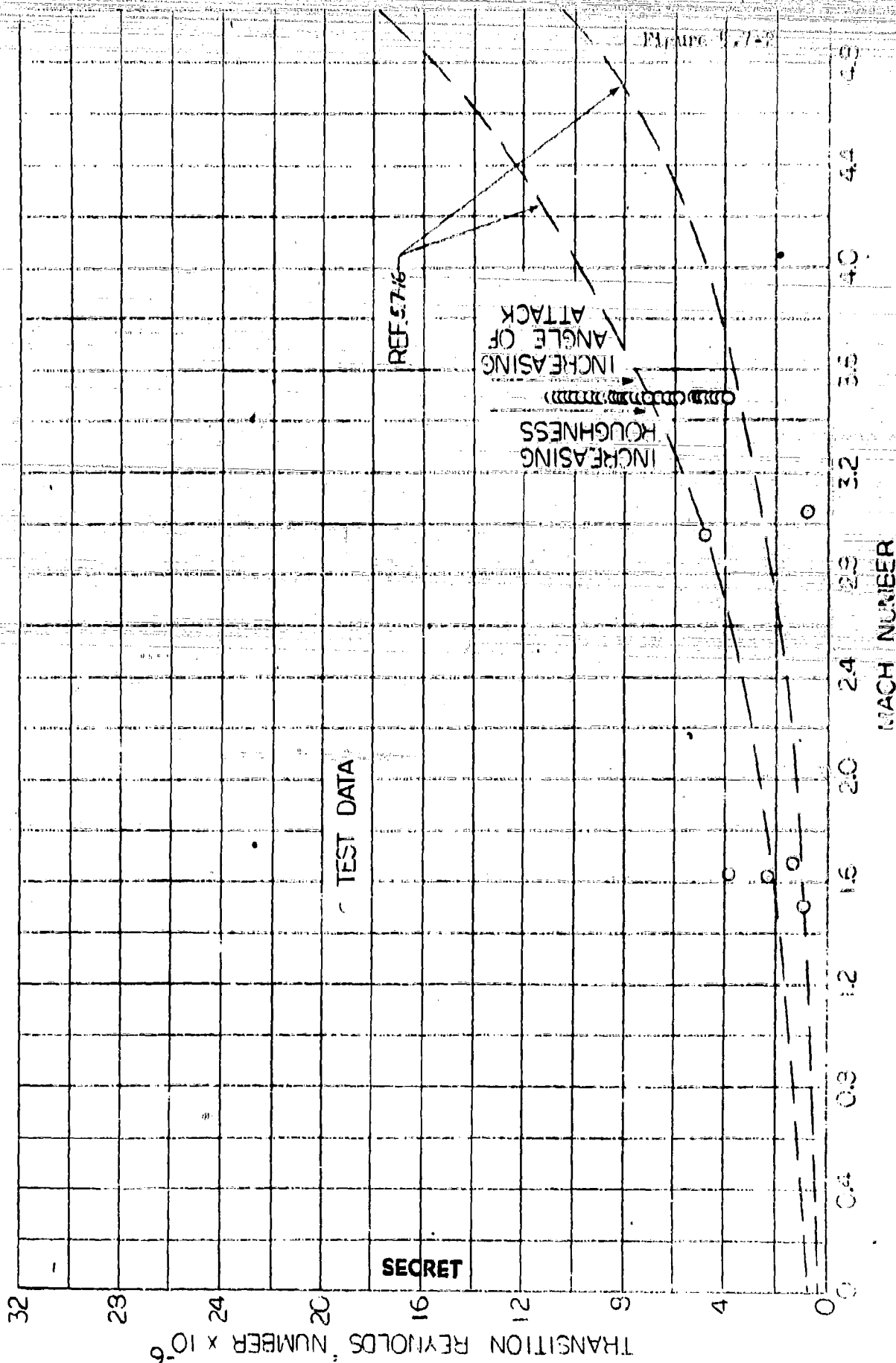
EXPERIMENTAL BOUNDARY LAYER TRANSITION DATA

WIND TUNNEL TESTS



EXPERIMENTAL BOUNDARY LAYER TRANSITION DATA

FLIGHT TESTS



By _____	Date _____	BELL Aircraft CORPORATION	Model _____	Page <u>6-1</u>
Checked _____	Date _____		Missile _____	Report <u>D113-945-012</u>

Section 6

Test Facilities

It would be short-sighted to consider the problems of a system or contemplate their solution without some knowledge of the test facilities in which the problems could be investigated. In this section some of the available facilities and those planned or under development - which are noteworthy with respect to MX-2276 - are briefly discussed and some basic information on the facilities presented. More complete information than presented here will be necessary for detailed test planning. This should be obtained during the next MX-2276 phase for the facilities of particular interest.

A bar graph showing the coverage of the Mach number range by the various facility types is shown in Figure 6.-1. Tables 6.-1 to 6.-3 present information on the different facilities and possible MX-2276 uses. As a general conclusion it can be said that there are now a limited number of facilities with which most MX-2276 hypersonic aerodynamic problems can be attacked and that in the near future (say within 2 to 3 years) a considerable number of new facilities of larger size and/or increased test ranges will be available.

6.1 Wind Tunnels

The wind tunnel is usually the preferred aerodynamic test tool if the data desired is within its limitations. Wind tunnel testing is the least expensive and time consuming (e.g. as compared to flight test), test conditions can be carefully controlled, and instrumentation is relatively less complicated and more accurate. Unfortunately, it is generally difficult to simulate all the important hypersonic flight parameters simultaneously in the wind tunnel. But this is not to say the wind tunnel will not be invaluable to the MX-2276; past experience has shown it definitely worthwhile to compromise certain parameters in order to investigate the effects of others; e.g. in the past few years supersonic wind tunnel testing has generally been at flight Mach number but at less than flight Reynolds numbers. The several types of wind tunnels, their abilities and limitation, are discussed hereafter under their respective headings.

6.1.1 Supersonic Wind Tunnels

There are a number of supersonic wind tunnels (M 5) in this country today in which MX-2276 testing could be carried out. These are generally well known so that a listing is not included here. Many of the tunnels do not provide either sufficient stream Reynolds numbers or temperature for true flight simulation; but for general configuration development and evaluation in this Mach number range these quantities usually are not considered of first importance.

Best Available Copy

6.1.2 Heat Transfer Tunnels

The inability of the supersonic wind tunnel, designed for general test work, to produce flight temperatures has led to a class of tunnels planned for use in high temperature flow and heat transfer studies. A number of these are described in Table 6.-1. It will be noted that none of these are ready for testing though they are definitely in work. Further it will be seen that these tunnels are limited in Mach number range and that several use the products of H_2 and O_2 combustion as test media instead of air.

6.1.3 Low Density Wind Tunnels

The purpose of this type of tunnel is to investigate the special fluid flow phenomena which occur in high altitude, low density flight, such as slip flow effects which may be significant to MX-2276. The only facility cited here is that at the University of California at Berkeley (Table 6.-1) which has produced much of the empirical slip flow regime information available today.

6.1.4 Hypersonic Wind Tunnels

The hypersonic wind tunnels which may be useful to MX-2276 are described in Table 6.-1. For the hypersonic tunnels using air as test media the supply air is generally heated to temperatures on the order of $1000^\circ F$ to prevent condensation of the air components; however, this does not even approach the stagnation temperatures needed for flight temperature simulation. On the other hand, the hypersonic tunnels can produce Reynolds numbers comparable to those of MX-2276 flight. This type of tunnel thus can be used to investigate general hypersonic flow phenomena excepting those which are the products of the extreme flight stagnation and recovery temperatures - such as real gas and dissociation effects.

6.1.5 Shock Tubes and Impulse Wind Tunnels

The shock tube has become well known as a tool for basic flow investigations. Because of its unique abilities and low cost a number have been built and are operated by universities and research organizations. Of particular interest to MX-2276 is that shocks waves strong enough to cause measurable relaxation intervals, dissociation, and ionization can be produced in the shock tube. The shock tube is limited by the very short time in which steady test flow exists at the test section and in maximum Mach number, which is between $M = 2$ and 3 for real air.

An outgrowth of added interest to MX-2276 is the shock tube driven impulse wind tunnel in which shock tube technique is used to produce an initial high energy column of air at low supersonic Mach number that is

Best Available Copy

By _____	Date _____	BELL <i>Aircraft</i> CORPORATION	Model _____	Page <u>6-3</u>
Checked _____	Date _____		Missile _____	Report <u>D143-945-012</u>

then expanded through a nozzle to hypersonic Mach numbers. The resultant flow temperatures are of the same order as those of flight. This then gives a tool for the study of high temperature hypersonic phenomena. Its severest limit is the very short steady flow times - less than .001 seconds - which make instrumentation very difficult. Other possible limitations are that the period of steady flow may be so short that the boundary layer is not fully established on the test models and that high temperature phenomena such as dissociation may first occur (prematurely) in the shock tube instead of at the model. In general this technique is still in the development stage and its full potentialities and/or limitations remain to be fixed. People working in this field feel they will be able to measure model pressures, heat transfer rates, and even drags with usable accuracies.

Another type of impulse wind tunnel uses supply air almost instantaneously compressed to very high pressures and temperatures by a piston driven either by explosion or by rapidly released, compressed, bottled gas. The test conditions again are high temperature - hypersonic. The test time is improved to the order of 1 second; otherwise, the above limitations generally apply to this type also. Several of both types of impulse wind tunnel are given in Table 6.-1.

6.2 Ballistic Ranges

The capabilities of several ballistic facilities are shown in Table 6.-2. Advantages of ballistic range testing are in the real flight conditions that can be produced and the elimination of the air flow non-uniformities and turbulence which inherently exist in wind tunnels. In addition, variable density ranges allow very wide Reynolds number latitude so that they are natural tools for boundary layer studies. Spark pictures of excellent quality which allow examination of the boundary layer structure are common. Disadvantages are the small models and the complicated instrumentation techniques necessary. However, the methods of obtaining such characteristic ballistic quantities as drag and stability have been well developed.

New techniques are being developed to study aero-thermodynamic phenomena. For example in the NOL Bromine range the dissociation in the wakes of projectiles is determined by observing absorption of light waves. The dissociated bromine does not stop 2 angstrom waves while molecular bromine does. Relaxation phenomena are being studied by measuring the distance of bow waves from the noses of spherical models. A sharp focusing schlieren technique is used to eliminate the distortion of the light rays through the shock.

The NACA-Ames Free Flight Wind Tunnel in which models are fired from a gun upstream through the supersonic flow is herein classed as more of a ballistic facility than a wind tunnel, as data from it is basically obtained by ballistic techniques. Advantages of this combination of wind tunnel and ballistic facilities are increased Mach number, Reynolds number, and temperature ranges.

SECRET

Page 6-4

Model _____
Missile _____
Airplane _____

Report D113-945-012

BELL Aircraft CORPORATION

By _____ Date _____

Checked _____ Date _____

6.3 Flight Test Vehicles

The difficulty of achieving simultaneous simulation of all flight parameters in earth bound test facilities and the limitations of the facilities which do have this ability have been touched upon briefly in the preceding discussions. It is evident that there is a need for flight test data to confirm and augment the information from these facilities. Further it is evident that to develop (even of small scale) flight test vehicles to reach the MX-2276 operational conditions is a large task in itself. It is encouraging, therefore, to find several efforts of this magnitude already underway. These are the hypersonic flight test efforts of the NACA PARD division and the development of a hypersonic test vehicle (HTV) by the Aerophysics Development Company. Some information on the NACA vehicles and the HTV are given in Table 6.-3. It will be noted that the vehicles enter the Mach number regimes where aero-thermodynamic effects are expected to become significant, though they do not as yet reach the ultimate MX-2276 conditions. Thus far the primary goal of these vehicles is to obtain aerodynamic heating information. It is reasonable to expect other types having the same performances to obtain drag, stability and control and separation information.

The problems and difficulties of pilotless flight test are many, e.g. instrumentation capacities of vehicles (as above) are limited and instrumentation is generally less accurate (than wind tunnel instrumentation). Overall, the operation of a flight test program is most expensive per data point obtained.

Best Available Copy

SECRET

SECRET

Table 6-1
 Test Facility Information
 Wind Tunnels

Facility	Type	Test Section Size	Mach No. Reynolds No.	Max. Supply Press. & Temp.	Status	Suitability and Comment W.R.T. to W-2276
1. NACA Ames	Heat Transfer Flight T_{01} to $M = 4$	10 x 10 in.	$M_{max} = 6$		Development	General heating studies - effects on configuration development
2. Naval Ordnance Lab. Heat Transfer W.T.	Heat Transfer	15 x 15 cm (tentative)	$M = 2 - 5$	$P_0 = 10$ atmos. $T_0 = 250^\circ C$	Under Construction	Basic heat transfer work - surfaces, leading edges, cooling
3. University of Texas	Heat Transfer Flight T_{01} to $M = 5$		$M_{max} = 5$		Development	Basic boundary layer and heating studies
4. Convair - Atlas Hydrogen-Oxygen W.T.	Heat Transfer 5×10^6 ftu/ft ² /hr with Turb. B.L.	5.6 x 5.6 in.	$V = 10,000$ fps $M = 2.76$	$P_0 = 515$ psia $T_0 = 6300^\circ R$	Development	Transpiration cooling, materials evaluations, thermal shock studies
5. Polytechnic Inst. of Brooklyn Hydrogen-Oxygen W.T.	Heat Transfer	$\sim 9 - 12$ in. dia.	Subsonic	$T_0 = 1600^\circ F$	Development	Heat Transfer, transpiration cooling of leading edge, noses
6. University of California at Berkeley	Low Density Supersonic W.T.	~ 5 in. dia.	$M_{max} = 6$ $Re \approx 10 - 10,000$		Operational	Boundary layer studies, slip plane effects, instrumentation calib.
7. NACA - Langley 11 inch Hypersonic W.T.	Hypersonic Intermittent	10 x 10.5 in.	$M = 6.94 - 10$ at $M = 6.9$ $Re = 1.5 \times 10^6/ft$ $-3.0 \times 10^6/ft$	$P_0 = 2-28$ atmos. $T_0 = 1300^\circ R$	Operational (M-10 development)	Configuration development general aerodynamic studies
8. MACA - Ames 10 x 14 in. Supersonic W.T.	Supersonic Continuous	10 x 14 in. (nominal)	$M = 2.7 - 6.3$ at $M = 6.3$ $Re \approx 1.7 \times 10^6/ft$	$P_0 = 6$ atmos. $T_0 = 400^\circ F$	Operational	Configuration development general aerodynamic studies
9. Cal. Tech. Hypersonic W.T. Leg No. 1	Hypersonic Continuous	5 x 5 in.	$M = 2 - 7$ $Re \approx 2 \times 10^4$ 5×10^5	$P_0 = 1000$ psi $T_0 = 860^\circ R$	Operational Present Nozzle $M = 5.8$	Boundary layer studies Transition Shock - B.L. interaction
Leg No. 2	Hypersonic Continuous	5 x 5 in.	$M = 4 - 11$	$P_0 = 150$ atmos. $T_0 = 1500^\circ R$	Operational Present Nozzle $M = 8.0$	Transpiration cooling
10. Naval Ordnance Lab. Hypersonic W.T.	Hypersonic Continuous	12 x 12 cm	$M = 5 - 9$	$P_0 = 15 - 675$ psi $T_0 \rightarrow 800^\circ R$	Operational	Basic hypersonic flow and B.L. studies
11. Applied Physics Lab. JHU Hypersonic W.T.	Hypersonic	2 in. dia.	$M = 9.07$ with Nitrogen gas $M = 15.2$ with Helium gas		Operational Plan Impulse drive for this W.T.	Basic hypersonic flow and B.L. studies. Slip flow and vibrational relaxation noted in this W.T.

SECRET

SECRET

Table 6-1 (Cont'd.)
 Test Facility Information
 Wind Tunnels

Facility	Type	Test Section Size	Mach No. Reynolds No.	Max. Supply Press. & Temp.	Status	Reliability and Comment w.r.t. to MX-2276
12. Princeton Univ. Helium Hypersonic W.T.	Hypersonic Intermittent	3 1/4 in. dia. Nominal max	M = 10 - 15 Re = 6×10^6 - 1.8×10^6 /in.	Po = 1500 psi To = unheated	Operational	Basic hypersonic flow and B.L. studies - Shock - B.L. interaction
13. Univ. of Minnesota Channel 1	Supersonic Intermittent	6 x 8 in.	M = 1.5 - 8.2	Po = 40 atmos To (planned) = 900 °F	Operational & Dev. - Present Max = 5.6	Configuration development General aerodynamic evaluation
Channel 2	Hypersonic Intermittent	12 x 12 in.	M = 3 - 10	Po = 70 atmos To (planned) = 3000 °F	Operational & Dev. - Present Max = 5.5	
14. ARDC Tunnel E-1	Supersonic Intermittent	12 x 12 in.	M = 1.2 - 5.5 Re = 22×10^6 /ft	Po = 60 psi To = 100 °F	Operational	Configuration development - L/D, stability, control effectiveness
Tunnel E-2	Hypersonic Intermittent	12 x 12 in.	M = 4.5 - 10 Re = 46×10^6 /ft	Po = 2500 psi To = 1500 °F	Ready early 1956	
Tunnel A	Supersonic Continuous	40 x 40 in.	M = 1.2 - 5.5 Re = 16×10^6 /ft	Po = 200 psi To = 100 °F	Ready late 1955	Above in more detail complete configuration B.L. studies - transition, heat transfer
Tunnel B	Hypersonic Continuous	40 x 40 in.	M = 4.5 - 10 Re = $7 \frac{1}{2} \times 10^6$ /in.	Po = 2500 psi To = 1500 °F	Ready early 1959	
15. Jet Propulsion Lab. - CIT Hypersonic W.T.	Hypersonic Continuous	16 x 16 in.	M = 9 - 10 Re = $.4 \times 10^6$ /in.	Po = 50 atmos To = 1000 °F	Ready Aug. 1957	Configuration development general hypersonic aerodynamics studies
16. Aberdeen - NRL Hypersonic W.T.	Hypersonic Continuous	13 x 15 in.	M = 10	Po = 100 atmos To = 1500 °F	Hardware in 2 - 3 years	Configuration development general hypersonic studies
17. United Aircraft Corp. Hypersonic W.T.	Hypersonic Intermittent	6 x 6 in.	M = 5 - 8		Under Construction	Flow + B.L. studies
18. NACA - Langley Gasdynamics Lab.	Supersonic Hypersonic Blowdown Impulse		M = 7 nozzle operating	Storage Bottles 5000 psi To = 1500 °F	Hypersonic Research Starting	General hypersonic flow research Aero-thermodynamic

SECRET

SECRET

Table 6.-1 (Cont'd.)
Test Facility Information
Wind Tunnels

Facility	Type	Test Section Size	Mach No. Reynolds No.	Max. Supply Press. & Temp.	Status	Suitability and Comment w.r.t. to XE-2276
19. Cornell Aeronautical Lab. Shock - Tube W.T.	Impulse $t \approx 1/1000$ sec.		$M \approx 13$	$T_0 = 7000^\circ R$	Development	Aero-thermodynamic research Dissociation, ionisation, relaxation as above
20. Cal. Tech. Shock - Tube W.T.	Impulse $t \approx 1/1000$ sec.	3 x 10 in. (7 in. dia. window)	$M \approx 6$	$T_0 = 7000^\circ R$	Development	
21. NACA - Ames Open Tunnel	Impulse $t \approx .6$ sec.		$M \approx 7$ Potential - $V_{max} = 8000$ fps	$T_0 = 3000^\circ R$ Potential - $T_0 = 6000^\circ R$	Development	Fundamental studies Heat transfer, dissociation
22. Polytechnic Inst. Brooklyn Hypersonic Facility	Impulse	12 in. dia.	$M = 6 \text{ \& } 15$	3000 psi 4000 R Heater	Development	Fundamental studies Heat transfer, cooling on leading edges, surfaces

SECRET

SECRET

Table 6.-2
Test Facility Information
Ballistic Facilities

Facility	Type	Max. Projectile Size	Velocity or Mach No.	Status	Suitability or Comment
1. Naval Ordnance Lab. a) Unpressurized Range b) Pressurized Range	Atmospheric Pressure Variable Density from .01 - 6 atmos.	~40 mm dia. 40 mm dia.	V → 5000 fps V → 5000 fps V = 7000 fps gun in development	Operational Operational	Boundary layer transition study - Project Atlas has initiated same; to include effects of wall to stream temperature variation on B.L. stability
c) Bromine Range	Pressurized - Variable gas test media	~20 mm dia.	V → 6000 fps M = 13 in Bromine	Operational	Fundamental aero-thermodynamic research - relaxation, dissociation phenomena
2. Aberdeen - BRL a) Two atmospheric Ranges b) Variable Density Range	Atmospheric Pressure Variable Density Variable gas test media	75 mm dia. ~20 mm dia.	V → 4000 fps V → 4000 fps	Operational Shut-down	As (a), (b) above but more limited. Might try stage separations study with big gun. Equipped with Interferometer Fundamental aero-thermodynamic research
3. NORTS a) Ballistic Range b) Light Gas Gun	Explosively Compressed Helium Accelerates Model	50 cal.	M = 4 - 5 (normal gun) V → 10,000 fps	Operational Ready for firing in 1954 Results unknown as yet	As (a) above. B.L. transition studies being made for OGE Drag, stability of bodies B.L. transition research Aero-thermodynamic research
4. MACA - Ames a) Free-Flight Wind Tunnel b) Hypersonic Gun	Model fired up supersonic stream Explosively Compressed Helium Accelerates Model	3 in. dia. For ~1/2 in. length Rg = 5 x 10 ⁶ - 17 x 10 ⁶ at M = 4 (M = 2 nozzle) Rg = 24 x 10 ⁶ - 15 x 10 ⁶ at M = 10 (M = 2 nozzle.) 22 cal. - 22 cal. sabot 1/8 in. Al. sphere model (typical)	Gun V → 6600 fps M = 2 W.T. nozzle Total M → 10 M = 3 W.T. nozzle Total M → 13 Potential V → 20,000 fps V = 15,000 fps attained	Operational Development Useful data in ~ 2 years	Configuration drag, stability, Boundary layer transition; skin friction research Fundamental aero-thermodynamic research - dissociation, ionization, relaxation.

SECRET

BY _____ DATE _____
CHECKED _____ DATE _____

SECRET

Table 6-3
Test Facility Information
Flight Test Vehicles

Vehicle	Stages	Final Stage Size	Mach No.	Instrumentation	Status	Suitability or Comment v.r.t. to MX-2276
1. MACA - PARAD Div. a) 2 Stage Vehicle	2 Solid Rockets	Dia. = 7 in. Length = 12 ft.	M ~ 5.6	4 Channel telemeter Doppler Radar Tracking Radar	Firings made	Models fired to date to check rocket test techniques and obtain heat transfer data.
b) 3 Stage Vehicle	3 Solid Rockets	Dia. = 6 in. Length = 6 ft.	M ~ 7		Firings made	B.L. transition, drag, stability, separation tests also seem feasible.
c) 4 Stage Vehicle	4 Solid Rockets	Dia. = 6 in. Length = 6 ft.	M ~ 10	7 quantities telemetered Doppler Radar Tracking Radar	1 Firing Reported	
2. Aerophysics Development Co. - Hypersonic Test Vehicle	2 Stages Vehicle - 4 Loki rkts. Booster - a) 7 Loki rkts. or b) 13 Loki rkts.	Dia. = 6 in. Length = 7.5 ft.	Booster (a) M → 12 at h = 50,000 ft. Booster (b) M → 14 h → 100 mi with 40 lb. payload h → 100 mi with 10 lb. payload and 40,000 ft. air launch	Magnetic tape recorder - recovered after descent - 5 channels	Development Test 4 Boosters Fired.	Primarily designed for heat transfer and materials investigations and as sounding rocket. Could be instrumented for B.L. transition, possibly for transportation cooling at nose. ADC also proposes to fire pellets from nose of HTU with shaped charge - to give velocity of 26,000 fps.

SECRET

By _____ Date _____
 Checked _____ Date _____
BELL *aircraft* CORPORATION
 Model _____ Page 4A-1
 Missile _____
 Airplane _____ Report D143-945-012

APPENDIX 4A

COMPRESSIBLE SKIN FRICTION AND HEAT TRANSFER METHOD

A basic step to be considered in the calculation of viscous heating is the estimation of the heat transfer coefficient. Implicit in this estimation is the consideration of the closely related skin friction coefficient. The method proposed for the estimation of these coefficients is the use of the well-known constant property incompressible relations extended to supersonic and hypersonic conditions by evaluating the air properties in these relations at a reference temperature, a weighted mean temperature which occurs within the boundary layer. The reference temperature is expressed as a function of the wall, stream, and recovery temperatures (and thus Mach number). This semi-empirical theory was derived for laminar flow but from its agreement with test results also appears to be applicable to turbulent flow. It is well-adapted to engineering calculations and has been used in other hypersonic studies (References 4.6-6 and 4.6-7).

Eckert (Reference 4.6-4) in a recent survey of heat transfer also recommends this approach and shows that excellent agreement can be obtained with the more exact theories in the laminar flow case and with the available experimental data in the turbulent flow case. Eckert presents and discusses the method in considerable detail. Therefore, it is presented only in brief form here for the sake of completeness and for interpretation regarding this current study.

The following relations are those used herein for incompressible flow. In their use and extension, two dimensional flat plate flow with no pressure or temperature gradient is implied. The symbols used are given in the table following this section. The wall shearing stress is expressed as:

$$\tau_w = c_f \frac{\rho}{2} v^2 \quad (1)$$

For laminar flow the skin friction coefficient and Stanton numbers are:

$$\frac{c_f}{2} = \frac{0.332}{\sqrt{Re}} = \frac{0.332}{\sqrt{\frac{\rho v x}{\mu}}} \quad (2)$$

$$St = \frac{h}{c_p \rho v} = \frac{c_f}{2} (Pr)^{-2/3} \quad (3)$$

By _____ Date _____
 Checked _____ Date _____
BELL *Aircraft* CORPORATION
 Model _____ Page 4A-8
 Missile _____
 Airplane _____ Report D243-945-012

For turbulent flow the skin friction coefficient and Stanton numbers are:

$$\frac{c_f}{2} = 0.0296 Re^{-0.2} = 0.0296 \left(\frac{V_\infty x}{\mu} \right)^{-0.2} \quad (4)$$

$$St = \frac{h}{c_p \rho V} = \frac{c_f}{2} S \quad (5)$$

where in the turbulent case the $Pr^{-2/3}$ is replaced by a constant S . A reasonable choice for this constant appears to be $S = 1.2$ (Reference 4.6-4). If the pressure across the boundary layer is assumed constant, the following expressions for heat transfer coefficients can be obtained for laminar flow from Equations (2) and (3):

$$h = 928.0 \left(\frac{P_b V_b}{x} \right)^{0.5} \left(\frac{\mu}{T} \right)^{0.5} \frac{c_p}{Pr^{2/3}} \quad (6)$$

For turbulent flow from Equations (4) and (5):

$$h = 10.66 \frac{(P_b V_b)^{0.8}}{x^{0.2}} \frac{\mu^{0.2}}{T^{0.8}} c_p \quad (7)$$

The question then arises, at what temperature should the temperature variant properties, μ , c_p , and Pr be evaluated. The boundary layer profile varies considerably as a function of velocity and wall temperature. Rutesin and Johnson (reference 4.6-5) have advanced a constant property solution for laminar flow based upon the reference temperature:

$$\frac{T'}{T_b} = 1 + 0.45 \left(\frac{T_w}{T_b} - 1 \right) + 0.032 M_\infty^2 \quad (8)$$

This relation also has been used in turbulent analyses, e.g. References 4.6-6 and 4.6-7.

Reference 4.6-9 presents the following relationship for T'/T_b :

$$\frac{T'}{T_b} = 1 + 0.45 \left(\frac{T_w}{T_b} - 1 \right) + 0.035 M_\infty^2 \quad (9)$$

Use of these reference temperatures have given good correlation with the turbulent skin friction data obtained from wind tunnel tests by Chapman and Kester (Reference 4.6-3) and with turbulent data from the NACA Ames free flight wind tunnel. The T' method has also been compared with the friction coefficients from tests of low speed flow in heated pipes with good correlation.

By _____ Date _____

BELL Aircraft CORPORATION

Model _____ Page 4A-3
Missile _____
Airplane _____ Report D143-945-012

Checked _____ Date _____

Eckert has modified the coefficients in the T' relation to read:

$$\frac{T'}{T_g} = 1 + 0.50 \left(\frac{T_w}{T_g} - 1 \right) + 0.22 \left(\frac{T_r}{T_g} - 1 \right) \quad (10)$$

or for comparison with the previous relations this can be written as:

Laminar Flow

$$\frac{T'}{T_g} = 1 + 0.50 \left(\frac{T_w}{T_g} - 1 \right) + 0.0374 M_g^2 \quad (10a)$$

Turbulent Flow

$$\frac{T'}{T_g} = 1 + 0.50 \left(\frac{T_w}{T_g} - 1 \right) + 0.0396 M_g^2 \quad (10b)$$

using perfect gas relations and appropriate recovery factors. This latter relation appears to have been derived from the more exact laminar theory for a greater range of temperatures than the above equation of Johnson and Rubesin.

The relation for T'/T_g given in Equation (10) has been used with the incompressible relations for the laminar flow skin friction to obtain a comparative check with the theory of Crocco, Reference 4.6-10. For this example $T_g = 400^\circ\text{R}$. and the air properties as a function of the temperature given in Reference 4.6-11 were used. This comparison is given for T_w/T_g of 2 and 4 in Figure 4A-1. The comparison is only carried to $M = 1$ because the properties of μ are not tabulated beyond 3400°R . which is the T' for this condition. The figure shows that this T' relation gives excellent agreement with the Crocco theory.

The preceding T' relations have been used with the incompressible relations stated to give the curves shown in Figure 4A-2 which are compared with available turbulent data. It was assumed that $r = 0.9$, $\gamma = 1.4$ and that

$$\frac{\mu'}{\mu_g} = \left(\frac{T'}{T_g} \right)^{0.72}$$

The representation advanced by Eckert, Equation (10) appears to give the best overall correlation. In view of this correlation, the Eckert T' relation was adopted.

The following equations give the relationship of compressible skin friction coefficient to incompressible coefficient for both laminar and turbulent flow:

By _____ Date _____

BELL Aircraft CORPORATION

Model _____ Page 4A-4

Checked _____ Date _____

Missile _____ Airplane _____ Report D143-945-012

Laminar flow

$$\frac{c_{f_c}}{c_{f_1}} = \left(\frac{\mu'}{\mu_s} \right)^{0.5} \left(\frac{\rho'}{\rho_s} \right)^{0.5} \quad (11a)$$

Turbulent flow

$$\frac{c_{f_c}}{c_{f_1}} = \left(\frac{\mu'}{\mu_s} \right)^{0.2} \left(\frac{\rho'}{\rho_s} \right)^{0.8} \quad (11b)$$

where the c_f 's are both defined by the relation $c_f = \frac{\tau_w}{0.5 \rho V^2}$ and

and the primed quantities are evaluated at the reference temperature. The above equations have been evaluated and are plotted versus T'/T_s in Figure 4A-3 using 400°R as a base. The solid lines represent the functions that are obtained by using the NBS-NACA tables (Reference 4.6-11) for the air properties.

The effective temperatures encountered in the proposed MX-2276 flight plan will be greater than 3400°R. One then wonders how to extend the curves reasonably. Power law variations of the air properties with temperature suggest themselves because of their convenience and because they have been commonly used as approximations in this situation in skin friction work. The power laws which were chosen to match these curves are:

Laminar flow

$$\frac{c_{f_c}}{c_{f_1}} = \left(\frac{T'}{T_s} \right)^{-0.17} \quad (12a)$$

Turbulent flow

$$\frac{c_{f_c}}{c_{f_1}} = \left(\frac{T'}{T_s} \right)^{-0.668} \quad (12b)$$

These power laws were chosen in order to match the curves given by the air properties particularly in the temperature region of 3000°R. It is seen that the power law representations are very good for turbulent flow but less accurate for the laminar skin friction coefficient. However, the total c_{f_c}/c_{f_1} variation is small and of less importance.

Similarly, from the heat transfer coefficient equations, the following equations give the relation of compressible heat transfer coefficients to the incompressible coefficients for both laminar and turbulent flow:

By _____ Date _____
 Checked _____ Date _____

BELL Aircraft CORPORATION

 Model _____ Page 4A-5
 Missile _____
 Airplane _____ Report D143-945-012

Laminar flow

$$\frac{h_0}{h_1} = \left(\frac{\mu'}{\mu_s} \frac{\rho'}{\rho_s} \right)^{0.5} \left(\frac{c_{p1}}{c_{ps}} \right) \left(\frac{Pr_s}{Pr_1} \right)^{2/3} \quad (13a)$$

Turbulent flow

$$\frac{h_0}{h_1} = \left(\frac{\mu'}{\mu_s} \right)^{0.2} \left(\frac{\rho'}{\rho_s} \right)^{0.8} \left(\frac{c_{p1}}{c_{ps}} \right) \quad (13b)$$

These equations are evaluated and plotted as a function of T'/T_s in Figure 4A-4. The solid lines represent the functions that are obtained by using the NBS-NACA tables (Reference 4.6-11). However, the Prandtl number is given only to 1800°R in these tables; after this point it was assumed the Prandtl number has a constant value of 0.715, after Chapman and Cowling. The other property values at the higher temperatures also are felt to be less certain and it must be stated that at the higher values of T' , particularly above 1800°R, the validity of the curves becomes less certain.

As was done for the skin friction coefficients, power law variations of the air properties with temperature were assumed in order to extend this available information:

Laminar flow

$$\frac{h_0}{h_1} = \left(\frac{T_1}{T_s} \right)^{-0.040} \quad (14a)$$

Turbulent flow

$$\frac{h_0}{h_1} = \left(\frac{T_1}{T_s} \right)^{-0.576} \quad (14b)$$

These power laws match the curves given by the air properties particularly in the temperature range below 1800°R. It is seen that the power law representation is reasonably good for the turbulent case, although it appears to be less accurate for the laminar heat transfer. The total h_0/h_1 correction is small and of less importance.

It will be noted that the effects of wall-to-stream temperature ratios T_w/T_s on the skin friction coefficient in turbulent flow are quite large. Other boundary layer theories advanced (e.g. Van Driest Reference 4.6-12) also show this. Data from NACA Ames free flight wind tunnel (Reference 4.6-13), presented in Figure 4A-2, also indicate the increase in skin friction and heat transfer with decreasing T_w/T_s for turbulent flow. This has also been confirmed in discussions with the NACA Langley Field Division concerning their free flight tests at $R = 5$. However, recent turbulent flow tests at the

By _____ Date _____

Checked _____ Date _____

BELL Aircraft CORPORATION

Model _____ Page 4A-6

Missile _____ Report D143-945-012
Airplane _____

1. Ordnance Laboratory hypersonic wind tunnel reported by Lobb (Reference 4.6-14) at $M = 5, 6.8, \text{ and } 7.7$, and unpublished data from both NOL and Johns Hopkins University Applied Physics Laboratory hypersonic tunnels at $M = 9$ do not show this trend. They show no appreciable effect of T_w/T_s or if anything a slight decrease in skin friction coefficient as the wall temperature decreases from the recovery temperature. There is some question as to the validity of these latter tests because they were made on the tunnel walls where the boundary layer development has not been exactly typical of flat plate flow; but in the area of measurement the streamwise pressure gradients were small and the boundary layer measurement techniques appear to have been excellent. More experimental information is needed to resolve these differences. If the effects of T_w/T_s are as indicated by NOL and APL, the present method is conservative in this respect, as their points agree well with the curve of cf_c/cf_1 for the condition $T_w = T_r$ predicted by the present method.

Finally using the power law representation the heat transfer coefficients for laminar and turbulent flow are given by the following:

Laminar flow

$$h_c = \frac{0.00963}{T_s^{0.04}} \left(\frac{V_\infty P_\infty}{x} \right)^{0.5} \left(\frac{h_c}{h_1} \right)_L \quad (15a)$$

Turbulent flow

$$h_c = \frac{0.0334}{T_s^{0.576}} \left(\frac{V_\infty P_\infty}{x} \right)^{0.8} \left(\frac{h_c}{h_1} \right)_T \quad (15b)$$

where the values of h_c/h_1 correspond to the proper values T'/T_s .

Heat Transfer Equations

The convective heat transfer per unit area is:

$$Q_v = h_c (T_r - T_w) \quad (16)$$

where the recovery temperature, T_r , is given by the relation:

$$r = \frac{T_r - T_s}{T_t - T_s} \quad (17)$$

$$\text{or } T_r = T_s + r (T_t - T_s)$$

$$\text{where } T_t - T_s = \frac{V_\infty^2}{2 J c_p}$$

The recovery factor, r , for laminar flow is closely approximated by $r = \sqrt{Pr}$ and for turbulent flow by $r = \sqrt{Pr}$, and is evaluated at the

By _____ Date _____

Checked _____ Date _____

BELL Aircraft CORPORATION

Model _____

Page 4A-7

Missile _____

Airplane _____

Report D143-945-012

reference temperature, T' . However, since the Prandtl number is almost invariant with temperature the recovery factor was assumed to be constant, i.e. $r_L = .85$, $r_T = .9$. The adiabatic temperature rise $T_t - T_g$, at hypersonic speeds is very large; thus \bar{c}_p can be expected to vary significantly. The variation of c_p with temperature is approximated from Reference 4.6-15 by:

$$c_p = c_{p1} \left\{ 1 + \frac{\gamma-1}{\gamma} \left(\frac{5500}{T} \right)^2 \frac{\exp\left(\frac{5500}{T}\right)}{\left[1 - \exp\left(\frac{5500}{T}\right) \right]^2} \right\} \quad (18)$$

Equating the change in kinetic energy to the change in the total heat or enthalpy when the air is brought to rest and integrating from T_g to T_t gives:

$$v_g^2 = 12,003 \left\{ T_t - T_g + \frac{1572}{\exp\left(\frac{5500}{T_t}\right) - 1} - \frac{1572}{\exp\left(\frac{5500}{T_g}\right) - 1} \right\} \quad (19)$$

The values of $T_t - T_g$ obtained from this function are plotted in Figure 4A-5. The right side of the plot gives the relationship between $T_t - T_g$ and velocity for a $T_g = 400^\circ R$. The left side of the plot gives a correction term dependent upon the actual T_g . Figure 4A-6 gives a comparison of the adiabatic temperature rise for a constant specific heat, $0.24 \frac{\text{Btu}}{\text{lb.}^\circ \text{F.}}$, to the variable specific heat

outlined above using $T_g = 400^\circ R$. The reduction in stagnation temperature rise for variable specific heat is significant. Also shown on this plot are .85 and .9 (approximately the laminar and turbulent recovery factors respectively) times $T_t - T_g$ to indicate the recovery temperature rise.

By _____ Date _____

BELL *Aircraft* CORPORATIONModel _____ Page 4A-8

Checked _____ Date _____

Missile _____ Airplane _____ Report D143-945-012APPENDIX 4A AERODYNAMIC HEATING SYMBOLS

c_f	Skin friction coefficient	dimensionless
c_p	Specific heat, constant pressure	Btu/lb °F
\bar{c}_p	Mean specific heat, constant pressure	Btu/lb °F
c_v	Specific heat, constant volume	Btu/lb °F
g	Gravitational constant	ft/sec ²
h	Convective heat transfer coefficient	Btu/ft ² °F hr
J	Mechanical equivalent of heat	ft lb/Btu
M	Mach number	dimensionless
P	Pressure	lb/ft ²
Pr	Prandtl number	dimensionless
Q	Rate of heat flow	Btu/ft ² hr
r	Recovery factor	dimensionless
R_0	Gas constant	ft-lb/°F lb.
Re	Reynolds number	dimensionless
St	Stanton number	dimensionless
T	Temperature	°R
V	Velocity	ft/sec
w	Specific weight	lb/ft ³
x	Distance from leading edge	ft
y	Thickness of skin	ft
α	Absorptivity	dimensionless
γ	Ratio c_p/c_v	dimensionless
ϵ	Emissivity	dimensionless
θ	Time	sec
μ	Viscosity	lb sec/ft ²

SECRET

By _____ Date _____
 Checked _____ Date _____

BELL *Aircraft* CORPORATION

Model _____ Page 4A-9
 Missile _____
 Airplane _____ Report D143-245-012

ρ Density slug/ft³
 σ Stefan Boltzmann constant $\frac{\text{Btu}}{\text{ft}^2 \cdot ^\circ\text{R} \cdot \text{hr.}}$
 ω Power law exponent dimensionless

Subscripts

c Compressible flow
 i Incompressible flow
 L Laminar flow
 r Recovery
 t Stagnation
 T Turbulent flow
 v Convention
 w Wall condition
 δ Local stream

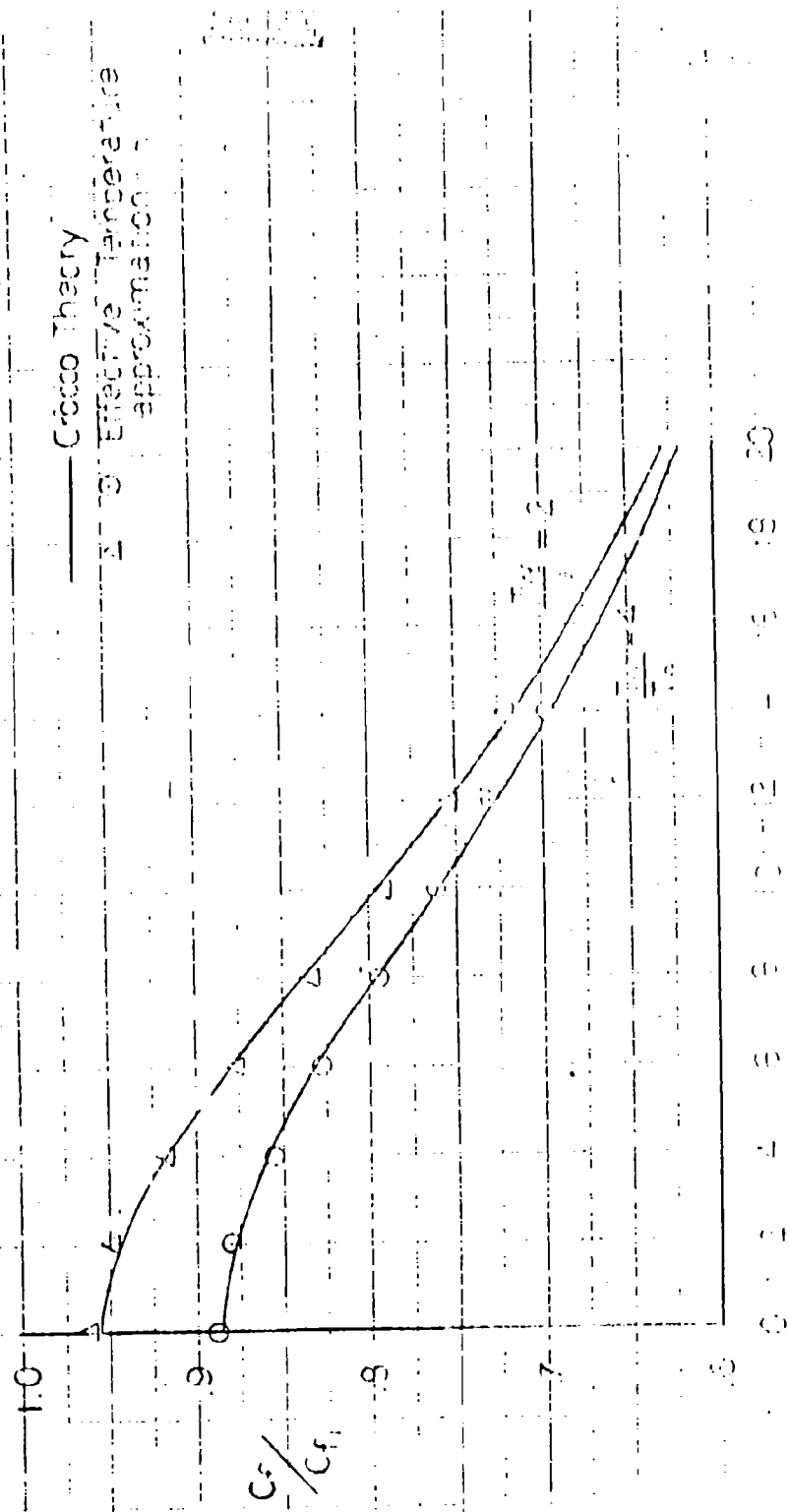
Superscript

' Reference temperature condition

SKIN FRICTION COEFFICIENT

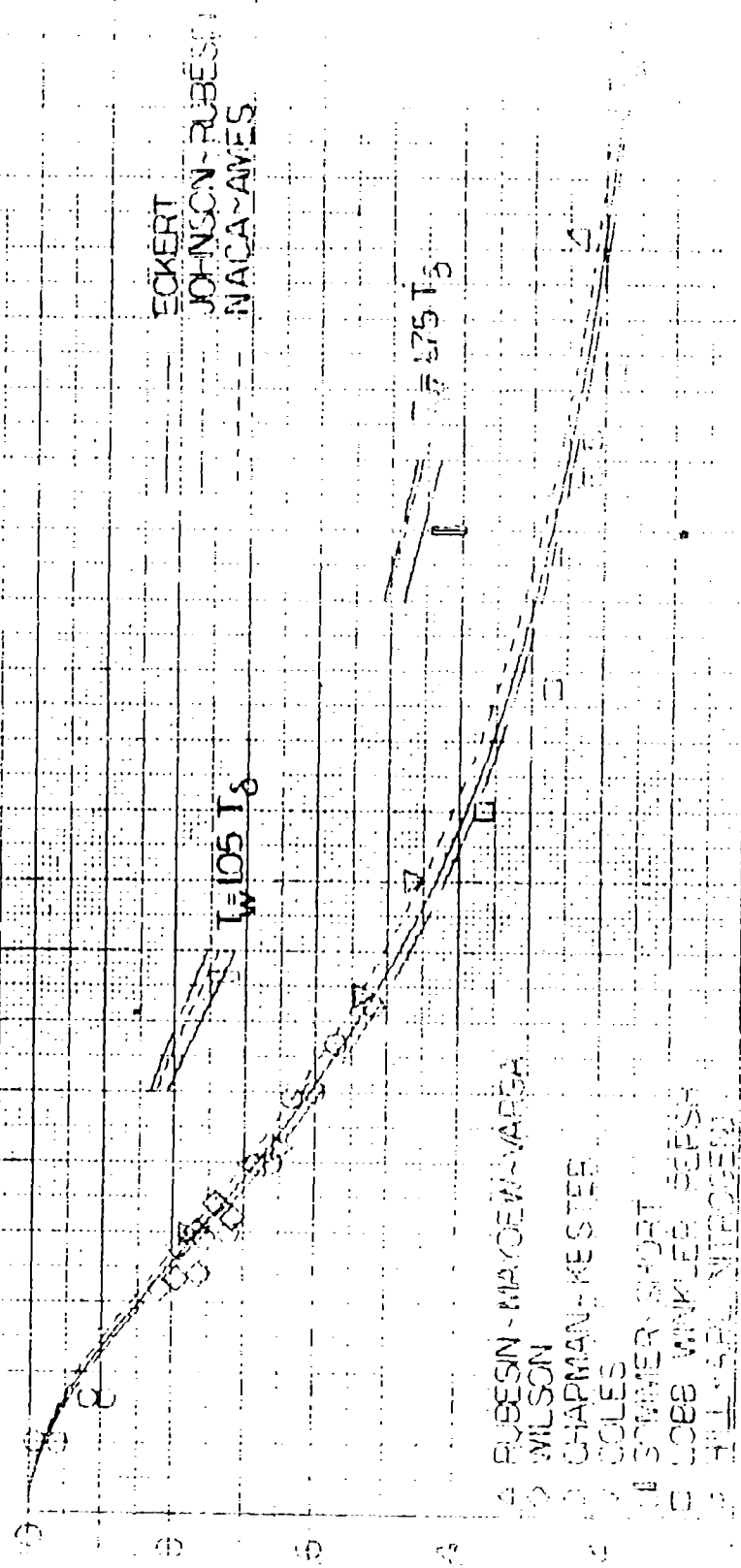
CORRECTION FACTOR

LAMINAR FLOW

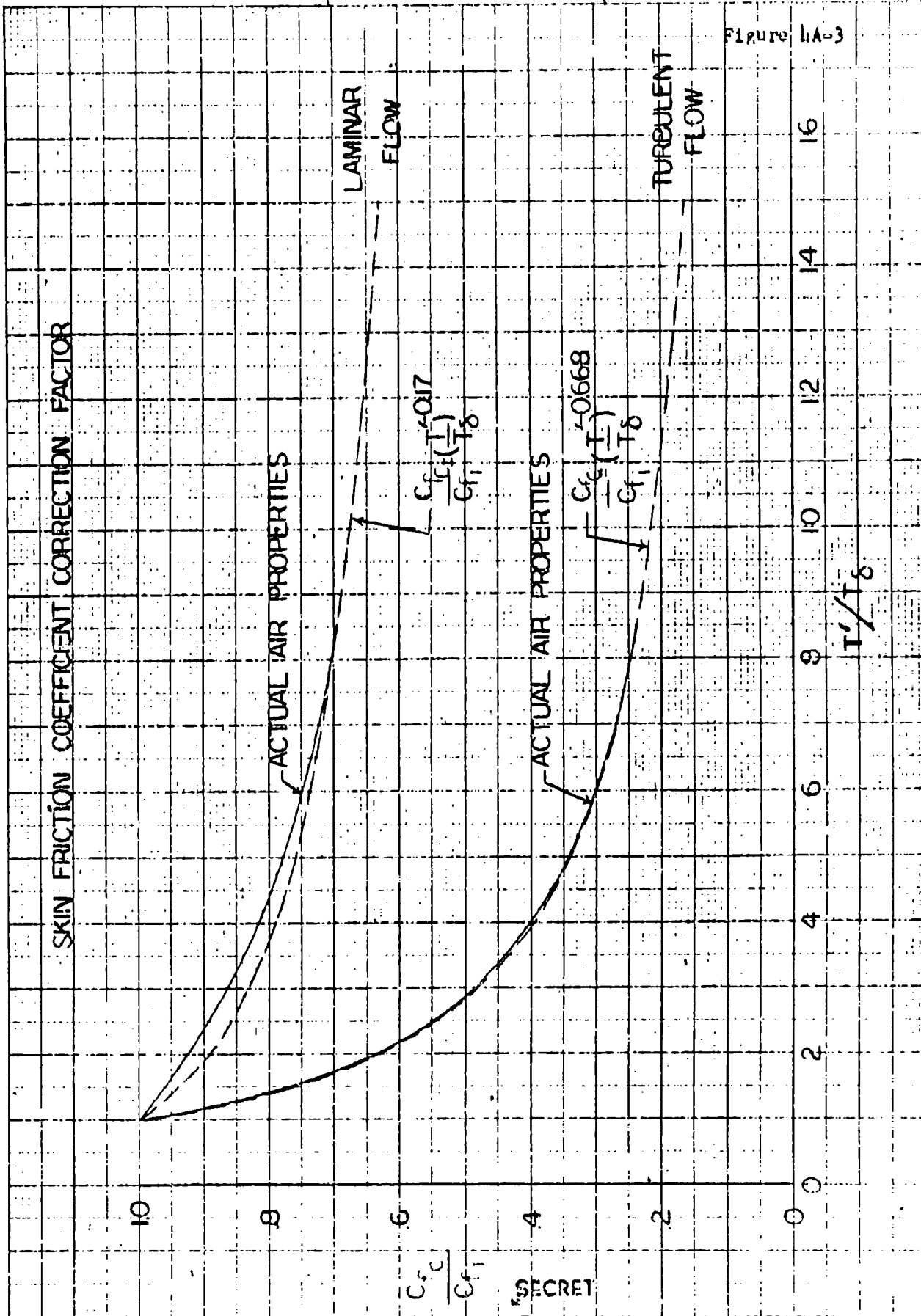


VARIATION OF COMPRESSIBLE SKIN FRICTION COEFFICIENT

TURBULENT FLOW



MACH NUMBER



SECRET

BY _____
CHECKED _____

DATE _____
DATE _____

BELL *Aircraft* CORPORATION

SECRET

MODEL _____
SHIP _____

REPORT _____

PAGE 11A-13
D113-945-072

HEAT TRANSFER COEFFICIENT CORRECTION FACTOR

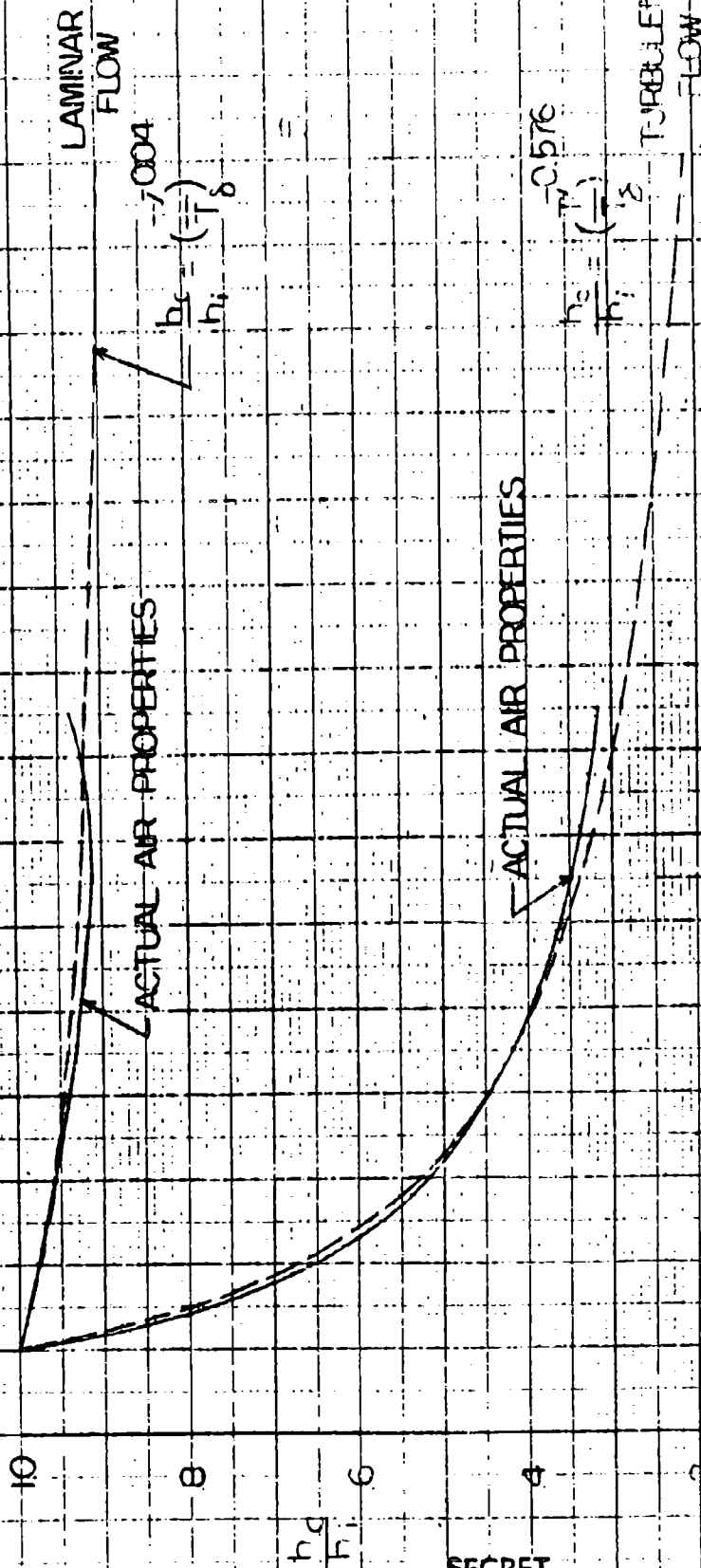


FIGURE 11A-13

SECRET

BY _____
CHECKED _____

DATE _____
DATE _____

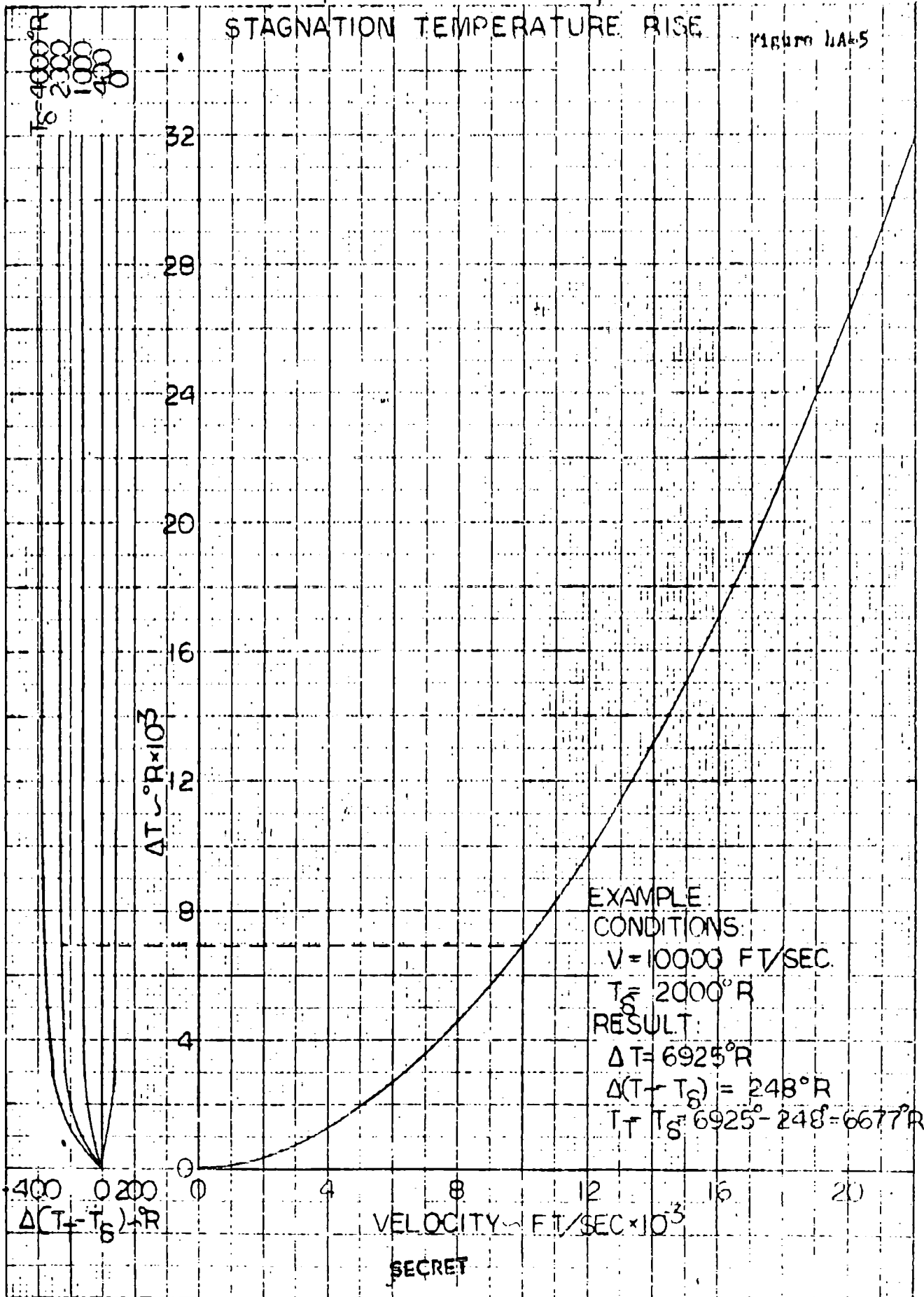
SECRET
BELL *Aircraft* CORPORATION

MODEL _____
SHIP _____

PAGE **1A-11**
REPORT **DL13-915-012**

STAGNATION TEMPERATURE RISE

Figure 1A-5



SECRET

APPENDIX 11B

EQUATIONS OF MOTION OF AN AIRCRAFT

In order to conduct a detailed study of the problems involved in hypersonic flight, it is essential to both performance and stability analyses that the equations which are employed accurately describe the motion of the vehicle.

Previously, the equations of linear motion for an aircraft had been simplified to a great extent by neglecting terms which were small in magnitude mostly due to relatively small flight velocities. The effects of centrifugal and Coriolis accelerations, gravity variations with altitude and earth orientation, and the earth's rotation were neglected compared with those of lift, drag, thrust, and weight of the aircraft. Therefore, the apparent, i.e. relative, motions of the aircraft seen by an earth fixed observer could be calculated using the following familiar equations.

$$T \cos \gamma - D - W \sin \gamma = m \frac{d^2 x}{dt^2} \quad (1a)$$

$$T \sin \gamma + L - W \cos \gamma = m \left(\frac{dx}{dt} \right) \left(\frac{d\gamma}{dt} \right) \quad (1b)$$

where: m is the mass of the aircraft

W is the weight of the aircraft

T is the thrust

L is the aerodynamic lift

D is the aerodynamic drag

x is the linear displacement of the aircraft in the flight direction

SECRET

BY _____ DATE _____
CHECKED _____ DATE _____

BELL Aircraft CORPORATION

MODEL _____ PAGE 4B-2
AIRPLANE _____ REPORT D143-945-012

~~SECRET~~

δ is the angle between the flight direction and the horizontal.

γ is the angle between the thrust line and the flight direction.

Herein, the complete equations of linear motion are derived so as to include most all the effects not found in Equation 1. Since the inclusion of all the forces acting on a body moving in space obviously results in highly complex expressions, the effects of making certain simplifying assumptions has been investigated.

As the equations of motion can be derived so that the motions are relative to any arbitrary axis system, special consideration must be given to the choice of an axis system which proves most convenient and useful. Since, in this case, it is of primary interest to determine aircraft range relative to the earth, the equations of motion are derived to yield displacements relative to an observer fixed on the earth's surface as caused by forces acting along well known aircraft axes.

The motion of the earth in space is to be considered, therefore the first step in the evaluation consists of determining which of the various motions and the factors which cause them are important to the analysis. This is accomplished by evaluating the maximum possible magnitude of the various terms.

If we consider a coordinate system fixed at the center of the sun, the position vector of a point in space may be expressed as the sum of the vectors relating the origins of all intermediate coordinate systems and the position of the point with respect to the final system as follows. If z is the position vector of a point with respect to the sun, ℓ is the position vector of the origin of an axis system located at the center of the earth taken with respect to the sun, R is the position vector of the

Form 84-1 Rev. 1046

~~SECRET~~

SECRET

origin of an axis system located on the surface of the earth and taken with respect to the earth's center, and x is the position vector of the point with respect to the axis system located on the earth's surface, then

$$z = \ell + R + x$$

If we consider the center of the sun to be motionless in space then by Newton's Law for constant mass

$$\frac{\sum F}{m} = \frac{d^2 z}{dt^2}$$

where $\sum F$ represents the vector sum of all the external forces acting on the mass m . Differentiating the vector z can be shown to result in the vector equation.

$$\begin{aligned} \frac{d^2 z}{dt^2} = & \omega \times (\omega \times [\ell + R + x]) + 2(\omega \times \Omega \times R) + \Omega \times (\Omega \times [R + x]) \\ & + 2([\Omega + \omega] \times v) + a \end{aligned}$$

where ω is the angular velocity of the earth about the sun, Ω is the angular velocity of the earth about its axis and v and a are the respective velocity and acceleration vectors of the point with respect to the axis system fixed on the earth's surface. It is assumed that the distance of the earth from the sun (ℓ) and the radius of the earth (R) are constant. The maximum magnitude of the vector terms can be evaluated by assigning the following approximately values to the parameters

$$\begin{aligned} |\ell| &= 93.0 \times 10^6 \text{ statute miles} & |\omega| &= 2.0 \times 10^{-7} \frac{\text{rad}}{\text{sec}} \\ |R| &= 4.0 \times 10^3 \text{ statute miles} & |\Omega| &= 7.3 \times 10^{-5} \frac{\text{rad}}{\text{sec}} \\ |x| &= 50 \text{ statute miles} & |v| &= 20,000 \text{ ft/sec} \end{aligned}$$

which result in

$$\begin{aligned} |\omega \times (\omega \times [\ell + R + x])| &= 0.019 \text{ ft/sec}^2 \\ |2(\omega \times \Omega \times R)| &= 0.0006 \text{ ft/sec}^2 \\ |(\Omega \times (\Omega \times [R + x]))| &= 0.11 \text{ ft/sec}^2 \\ |2([\Omega + \omega] \times v)| &= 3.1 \text{ ft/sec}^2 \end{aligned}$$

SECRET

SECRET

With these results, and considering that $\omega \ll \Omega$ and $x \ll R$, it is seen that sufficient accuracy is obtained with the expression.

$$\frac{\Sigma F}{M} = \frac{d^2 x}{dt^2} = (\Omega \times \Omega \times R) + 2(\Omega \times v) + a$$

which contains only the angular velocity of the earth and the relative velocity and acceleration of the point with respect to the earth.

The accelerations of a mass at a point in space due to the gravitational attractions of the sun and moon can be evaluated from Newton's gravitational law which states that the attractive force (F_g) between two masses (M_1 and M_2) is given by

$$F_g = G \frac{M_1 M_2}{r^2}$$

where G is a constant = $3.44 \text{ ft}^4/\text{lb. sec}^4$ and r is the intervening distance. The acceleration of the mass M_1 due to this attractive force is then expressed by

$$\frac{F_g}{M_1} = \frac{GM_2}{r^2}$$

If we assign the following values

	SUN	MOON
M_2	0.137×10^{30} slugs	0.504×10^{22} slugs
r	0.491×10^{12} ft	0.124×10^{10} ft

Then the accelerations are found to be

$$\frac{F_g}{M_1} \text{ SUN} = 0.019 \text{ ft/sec}^2$$

$$\frac{F_g}{M_1} \text{ MOON} = 0.0001 \text{ ft/sec}^2$$

SECRET

SECRET

which are negligible when compared to the acceleration of the mass M_1 due to earth's attraction (32.2 ft/sec^2 at the earth's surface).

It is therefore established that for the present study only the rotation and gravitational attraction of the earth need be considered in expressing the equations of motion.

The forces acting on the aircraft cause "absolute"* accelerations relative to the assumed inertial axis system located at the center of the earth. Thus, the aircraft at an instant of time may be located in space relative to this fixed axis system $X_1 Y_1 Z_1$ as shown in Figure 4B-1.

where: point A is the aircraft's center of gravity

r is the radial distance from the origin (O) to the point A

μ is the angle measured in the $X_1 Y_1$ plane

λ is the angle measured in the AOZ_1 plane

At any instant of time an observer, who is also located in space coincident with point A but stationary with respect to the earth's surface, will see the aircraft moving with a relative velocity, V , in some direction. Hence, a second axis system is established with the observer at the origin. This axis system, herein called $X_2 Y_2 Z_2$ is illustrated by Figures 4B-2 and 4B-3.

where: The $X_2 Y_2$ plane is parallel to a plane tangent to the earth's surface at point A'.

Z_2 is in the direction of r , the instantaneous vertical, and perpendicular to the $X_2 Y_2$ plane.

* The term "absolute" will be used to indicate the acceleration, velocity, etc. referred to an inertial system.

SECRET

SECRET

X_2 is in the direction of instantaneous east.

Y_2 is in the direction of instantaneous south.

ξ , the azimuth angle, is measured from east in the $X_2 Y_2$ plane.

γ , the flight path angle, is measured in a vertical plane containing the velocity vector and perpendicular to the $X_2 Y_2$ plane. It is that angle between the velocity vector and its projection onto the $X_2 Y_2$ plane.

Likewise, there is a third axis system which is located in the aircraft and rotates with it. This axis system is a right hand system orientated in the well known standard manner of aircraft axes (i.e. either body or stability axes) in which the X axis is arbitrarily placed along the thrust line, chord line, flight direction, etc. Herein, this axis system is denoted as the $X_3 Y_3 Z_3$ system. It is along these axes that the aerodynamic, thrust, and gravity forces are most recognisable. Thus the linear motions of the aircraft along these axes are derived using the quantities apparent to the observer rotating with the earth; namely: relative velocity, flight path and azimuth angles.

Now that the axis systems to be used in the derivation of the equations of motion have been illustrated, all that remains is the choice of the physical principle upon which the equations of motion are based. The familiar $F = ma$ cannot be used because it refers to a system of constant mass and an aircraft, especially, a rocket propelled aircraft, with an operating propulsion system is obviously not such a system. Therefore, the following principle is used in the derivation.

SECRET

SECRET

"If one has a system S of particles, then the vector sum of all the exterior forces acting on S is equal to the time rate of change of the total momentum of S plus the rate at which momentum is being transferred out of S by particles that are leaving S." This principle can be expressed by the following equations.

$$\begin{vmatrix} F_{X_1} \\ F_{Y_1} \\ F_{Z_1} \end{vmatrix} = \frac{d}{dt} \begin{vmatrix} M\bar{V}_{X_1} \\ M\bar{V}_{Y_1} \\ M\bar{V}_{Z_1} \end{vmatrix} + \dot{m} \begin{vmatrix} \bar{V}_{X_1} - v_{X_{1e}} \\ \bar{V}_{Y_1} - v_{Y_{1e}} \\ \bar{V}_{Z_1} - v_{Z_{1e}} \end{vmatrix} \quad (2)$$

where: F_{X_1} , F_{Y_1} and F_{Z_1} are the sum of the exterior forces acting on the aircraft in the X_1 , Y_1 and Z_1 directions respectively.

M is the mass of the aircraft at any time.

\dot{m} is the rate at which propellants are being consumed.

\bar{V}_{X_1} , \bar{V}_{Y_1} , \bar{V}_{Z_1} are the absolute velocities of the body in the X_1 , Y_1 , Z_1 directions respectively.

$v_{X_{1e}}$, $v_{Y_{1e}}$, and $v_{Z_{1e}}$ are the velocities relative to the

aircraft at which mass is leaving the system in the X_1 , Y_1 and Z_1 directions respectively.

By re-arranging equation (2) and taking note of the fact that

$\frac{dM}{dt} = -\dot{m}$, the following equation results.

SECRET

SECRET

$$\frac{1}{M} \begin{pmatrix} F_{X_1} + \dot{m}V_{X_{1e}} \\ F_{Y_1} + \dot{m}V_{Y_{1e}} \\ F_{Z_1} + \dot{m}V_{Z_{1e}} \end{pmatrix} = \frac{d}{dt} \begin{pmatrix} \bar{V}_{X_1} \\ \bar{V}_{Y_1} \\ \bar{V}_{Z_1} \end{pmatrix} \quad (3)$$

or

$$\frac{1}{M} (F_1 + \dot{m}V_{1e}) = \frac{d}{dt} (\bar{V}_1) \quad (3a)$$

where:*

$$(F_1 + \dot{m}V_{1e}) = \begin{pmatrix} F_{X_1} + \dot{m}V_{X_{1e}} \\ F_{Y_1} + \dot{m}V_{Y_{1e}} \\ F_{Z_1} + \dot{m}V_{Z_{1e}} \end{pmatrix}$$

$$(\bar{V}_1) = \begin{pmatrix} \bar{V}_{X_1} \\ \bar{V}_{Y_1} \\ \bar{V}_{Z_1} \end{pmatrix}$$

Since the forces along the aircraft's axes are ordinarily used in predicting performance it is convenient to derive the "apparent" accelerations along these axes. These accelerations are then integrated to give velocity and displacement increments relative to the earth

- * Such similar notation for matrixes will be used throughout the remainder of the derivation. The subscript denotes the axis system to which the quantity is referred.
- * The term "apparent" indicates the accelerations, velocities, etc. as seen by the observer on the earth's surface.

SECRET

SECRET

fixed observer. So that the equations are in terms of quantities recognizable to the observer, the transformation from the axis system $X_1 Y_1 Z_1$ to the $X_3 Y_3 Z_3$ system is necessary; this is accomplished in two steps. The first is a transformation from the $X_1 Y_1 Z_1$ system to the $X_2 Y_2 Z_2$ system. This is accomplished in the following manner.

$$(\bar{v}_2) = (\bar{l})(\bar{v}_1) \quad (4)$$

where (\bar{l}) is a transformation matrix as given by:

$$(\bar{l}) = \begin{vmatrix} \cos \mu & , & -\sin \mu & , & 0 \\ \cos \lambda \sin \mu & , & \cos \lambda \cos \mu & , & \sin \lambda \\ -\sin \lambda \sin \mu & , & -\sin \lambda \cos \mu & , & \cos \lambda \end{vmatrix} \quad (5)$$

in which the angles μ and λ are those previously illustrated in Figure 1. Likewise, the absolute velocities along the $X_3 Y_3 Z_3$ axes can be obtained by a second transformation

$$(\bar{v}_3) = (l)(\bar{v}_2) \quad (6)$$

where (l) is the transformation matrix given by:

$$(l) = \begin{vmatrix} \cos \theta \cos \psi & , & \cos \theta \sin \psi & , & -\sin \theta \\ -\cos \phi \sin \psi + \sin \phi \sin \theta \cos \psi & , & \cos \phi \cos \psi + \sin \phi \sin \theta \sin \psi & , & \sin \phi \cos \theta \\ \sin \phi \sin \psi + \cos \phi \sin \theta \cos \psi & , & -\sin \phi \cos \psi + \cos \phi \sin \theta \sin \psi & , & \cos \phi \cos \theta \end{vmatrix} \quad (7)$$

In which the angles, ψ , θ , and ϕ are angular rotations from the $X_2 Y_2 Z_2$ axis system to the $X_3 Y_3 Z_3$ axis system in the yaw, pitch and roll planes respectively. The order of rotation is in the yaw, pitch and roll directions. It should be noted that the angle θ is perfectly arbitrary and need not be the "pitch angle".

SECRET

SECRET

Combining equations (4) and (6)

$$(\bar{v}_3) = (\ell)(\bar{\ell})(\bar{v}_1) \quad (8)$$

Differentiating equation (8) with respect to time

$$\frac{d}{dt}(\bar{v}_3) = \left[\frac{d}{dt}(\ell) \right] (\bar{\ell})(\bar{v}_1) + (\ell) \left[\frac{d}{dt}(\bar{\ell}) \right] (\bar{v}_1) + (\ell)(\bar{\ell}) \left[\frac{d}{dt}(\bar{v}_1) \right] \quad (9)$$

Differentiating equation (6); substituting the results in equation (9), and making use of equation (4) to substitute for (\bar{v}_1) and $(\bar{\ell})(\bar{v}_1)$

$$(\ell)(\bar{\ell}) \left[\frac{d}{dt}(\bar{v}_1) \right] = (\ell) \left[\frac{d}{dt}(\bar{v}_2) \right] - (\ell) \left[\frac{d}{dt}(\bar{\ell}) \right] (\bar{\ell})^{-1}(\bar{v}_2) \quad (10)$$

By multiplying both sides of equation (3a) by the quantity $(\ell)(\bar{\ell})$ and substituting into equation (10) the following matrix equation is derived

$$(\bar{a}_3) = \frac{1}{M} (\ell)(\bar{\ell})(F_1 + \dot{m}v_{10}) = (\ell) \left\{ \frac{d}{dt}(\bar{v}_2) - \left[\frac{d}{dt}(\bar{\ell}) \right] (\bar{\ell})^{-1}(\bar{v}_2) \right\} \quad (11)$$

where: (\bar{a}_3) are the absolute accelerations along the X_3 , Y_3 and Z_3 axes respectively.

The right side of equation (11) is expanded to give

$$(\ell) \begin{pmatrix} \frac{d}{dt} \bar{v}_{X_2} + \bar{v}_{Y_2} \cos \lambda \dot{\mu} - \bar{v}_{Z_2} \sin \lambda \dot{\mu} \\ \frac{d}{dt} \bar{v}_{Y_2} - \bar{v}_{Z_2} \dot{\lambda} - \bar{v}_{X_2} \cos \lambda \dot{\mu} \\ \frac{d}{dt} \bar{v}_{Z_2} + \bar{v}_{X_2} \sin \lambda \dot{\mu} + \bar{v}_{Y_2} \dot{\lambda} \end{pmatrix} \quad (12)$$

As \bar{v}_{X_2} , \bar{v}_{Y_2} and \bar{v}_{Z_2} are the absolute velocities of the aircraft's c.g. in the direction X_2 , Y_2 and Z_2 it can easily be seen from figures 1 and 2 that;

SECRET

$$\bar{v}_{x_2} = V \cos \delta \cos \xi + r \omega \sin \lambda \quad (13a)$$

$$\bar{v}_{y_2} = V \cos \delta \sin \xi \quad (13b)$$

$$\bar{v}_{z_2} = -V \sin \delta \quad (13c)$$

where ω is the rotational velocity of the earth.

It is also apparent that

$$\dot{\mu} = \omega + \frac{V \cos \delta \cos \xi}{r \sin \lambda} \quad (14a)$$

$$\dot{\lambda} = \frac{V \cos \delta \sin \xi}{r} \quad (14b)$$

$$\frac{dr}{dt} = V \sin \delta \quad (14c)$$

Using equations (13) and (14) to substitute for the values of $\frac{d\bar{v}_2}{dt}$, \bar{v}_2 , $\dot{\mu}$ and $\dot{\lambda}$ the following expressions for a_{x_3} , a_{y_3} and a_{z_3} are derived.

$$\begin{aligned} \bar{a}_{x_3} = & \dot{V} \left[\cos \delta \cos \xi (\cos \theta \cos \psi) + \cos \delta \sin \xi (\cos \theta \sin \psi) + \sin \delta (\sin \theta) \right] \\ & - V \dot{\delta} \left[\sin \delta \cos \xi (\cos \theta \cos \psi) + \sin \delta \sin \xi (\cos \theta \sin \psi) - \cos \delta (\sin \theta) \right] \\ & - V \dot{\xi} \left[\cos \delta \sin \xi (\cos \theta \cos \psi) - \cos \delta \cos \xi (\cos \theta \sin \psi) \right] \\ & + V \omega \left[(\sin \delta \sin \lambda + \cos \delta \sin \xi \cos \lambda) (\cos \theta \cos \psi) \right] \\ & - \sin \lambda \left(\omega + \frac{V \cos \delta \cos \xi}{r \sin \lambda} \right) \left[(V \cos \delta \cos \xi + r \omega \sin \lambda) (\sin \theta) - (V \sin \delta) (\cos \theta \cos \psi) \right] \\ & - \cos \lambda \left(\omega + \frac{V \cos \delta \cos \xi}{r \sin \lambda} \right) \left[(V \cos \delta \cos \xi + r \omega \sin \lambda) (\cos \theta \sin \psi) - (V \cos \delta \sin \xi) (\cos \theta \cos \psi) \right] \\ & + \frac{V \cos \delta \sin \xi}{r} \left[(V \sin \delta) (\cos \theta \sin \psi) - (V \cos \delta \sin \xi) (\sin \theta) \right] \end{aligned} \quad (15a)$$

By _____ Date _____
 Checked _____ Date _____

BELL Aircraft CORPORATION

Model _____ Page 4B-12
 Missile _____
 Airplane _____ Report D143-945-012

$$\begin{aligned}
 \bar{a}_{Y_3} = \dot{V} & \left[\cos \gamma \cos \xi (-\cos \phi \sin \psi + \sin \phi \sin \theta \cos \psi) + \cos \delta \sin \xi (\cos \phi \cos \psi \right. \\
 & + \sin \phi \sin \theta \sin \psi) - \sin \delta (\sin \phi \cos \theta) \Big] \\
 & - V \dot{\delta} \left[\sin \gamma \cos \xi (-\cos \phi \sin \psi + \sin \phi \sin \theta \cos \psi) \right. \\
 & + \sin \gamma \sin \xi (\cos \phi \cos \psi + \sin \phi \sin \theta \sin \psi) + \cos \delta (\sin \phi \cos \theta) \Big] \\
 & - V \dot{\xi} \left[\cos \gamma \sin \xi (-\cos \phi \sin \psi + \sin \phi \sin \theta \cos \psi) - \cos \delta \cos \xi (\cos \phi \cos \psi \right. \\
 & + \sin \phi \sin \theta \sin \psi) \Big] + V \Omega \left[(\sin \gamma \sin \lambda + \cos \delta \sin \xi \cos \lambda) (-\cos \phi \sin \psi \right. \\
 & + \sin \phi \sin \theta \cos \psi) \Big] + \sin \lambda \left(\Omega + \frac{V \cos \delta \cos \xi}{r \sin \lambda} \right) \left[(V \cos \delta \cos \xi \right. \\
 & + r \Omega \sin \lambda) (\sin \phi \cos \theta) + V \sin \delta (-\cos \phi \sin \psi + \sin \phi \sin \theta \cos \psi) \Big] \\
 & - \cos \lambda \left(\Omega + \frac{V \cos \gamma \cos \xi}{r \sin \lambda} \right) \left[(V \cos \delta \cos \xi + r \Omega \sin \lambda) (\cos \phi \cos \psi \right. \\
 & + \sin \phi \sin \theta \sin \psi) - V \cos \delta \sin \xi (-\cos \phi \sin \psi + \sin \phi \sin \theta \cos \psi) \Big] \\
 & + \frac{V \cos \delta \sin \xi}{r} \left[V \sin \delta (\cos \phi \cos \psi + \sin \phi \sin \theta \sin \psi) \right. \\
 & \left. + V \cos \delta \sin \xi (\sin \phi \cos \theta) \right] \quad (15b)
 \end{aligned}$$

$$\begin{aligned}
 \bar{a}_{Z_3} = \dot{V} & \left[\cos \delta \cos \xi (\sin \phi \sin \psi + \cos \phi \sin \theta \cos \psi) + \cos \delta \sin \xi (-\sin \phi \cos \psi \right. \\
 & + \cos \phi \sin \theta \sin \psi) - \sin \delta (\cos \phi \cos \theta) \Big] - V \dot{\delta} \left[\sin \gamma \cos \xi (\sin \phi \sin \psi \right. \\
 & + \cos \phi \sin \theta \cos \psi) + \sin \gamma \sin \xi (-\sin \phi \cos \psi + \cos \phi \sin \theta \sin \psi) \\
 & + \cos \delta (\cos \phi \cos \theta) \Big] - V \dot{\xi} \left[\cos \delta \sin \xi (\sin \phi \sin \psi + \cos \phi \sin \theta \cos \psi) \right. \\
 & - \cos \delta \cos \xi (-\sin \phi \cos \psi + \cos \phi \sin \theta \sin \psi) \Big] + V \Omega \left[(\sin \gamma \sin \lambda \right. \\
 & + \cos \delta \sin \xi \cos \lambda) (\sin \phi \sin \psi + \cos \phi \sin \theta \cos \psi) \Big] \\
 & + \sin \lambda \left(\Omega + \frac{V \cos \delta \cos \xi}{r \sin \lambda} \right) \left[V \sin \delta (\sin \phi \sin \psi + \cos \phi \sin \theta \cos \psi) \right. \\
 & + (V \cos \gamma \cos \xi + r \Omega \sin \lambda) (\cos \phi \cos \theta) - \cos \lambda \left(\Omega + \frac{V \cos \gamma \cos \xi}{r \sin \lambda} \right) \left[(V \cos \delta \cos \xi \right. \\
 & + r \Omega \sin \lambda) (-\sin \phi \cos \psi + \cos \phi \sin \theta \sin \psi) - V \cos \delta \sin \xi (\sin \phi \sin \psi \\
 & + \cos \phi \sin \theta \cos \psi) \Big] + \frac{V \cos \delta \sin \xi}{r} \left[V \sin \delta (-\sin \phi \cos \psi \right. \\
 & + \cos \phi \sin \theta \sin \psi) + V \cos \delta \sin \xi (\cos \phi \cos \theta) \Big] \quad (15c)
 \end{aligned}$$

SECRET

By _____ Date _____	BELL Aircraft CORPORATION	Model _____ Page <u>4B-19</u> Missile _____ Airplane _____ Report <u>M43-945-012</u>
Checked _____ Date _____		

The matrix quantity $(\bar{L})(\bar{J})(F_1 + \dot{m}V_1)$ is the sum of aerodynamic, gravity, and thrust forces acting along the three axes of the aircraft. For rocket propelled aircraft these are as follows:

$$(\bar{L})(\bar{J})(F_1 + \dot{m}V_1) = \begin{pmatrix} F'_{X_3} - gM \sin \theta + \dot{m}V_{X_3} + [(P_e - P_A)A_e]_{X_3} \\ F'_{Y_3} + gM \sin \phi \cos \theta + \dot{m}V_{Y_3} + [(P_e - P_A)A_e]_{Y_3} \\ F'_{Z_3} + gM \cos \phi \cos \theta + \dot{m}V_{Z_3} + [(P_e - P_A)A_e]_{Z_3} \end{pmatrix} \quad \begin{matrix} (16a) \\ (16b) \\ (16c) \end{matrix}$$

where: A_e is the area of the rocket exit
 P_e is the pressure of the exhaust at the exit
 P_A is the ambient pressure of the atmosphere at the altitude under consideration
 F'_{X_3} , F'_{Y_3} , and F'_{Z_3} are the aerodynamic forces acting along the X_3 , Y_3 and Z_3 axes
 g is the gravitational acceleration constant at both the altitude under consideration and orientation with respect to the earth.

In the normal rocket aircraft the quantity $\dot{m}V_{Y_3} + [(P_e - P_A)A_e]_{Y_3}$, which is a sideward rocket thrust, is zero. Furthermore, if one makes the simplification of measuring θ to the thrust line so that the thrust is acting along the X_3 axis (for such a choice of θ the $X_3 Y_3 Z_3$ system is a body axis system) it is obvious that the rocket thrust in the Z_3 direction given by $\dot{m}V_{Z_3} + [(P_e - P_A)A_e]_{Z_3}$ is zero.

When equations (15) and (16) are combined a very complex expression for the aircraft motion results. However, if the simplifying

SECRET

By _____ Date _____
 Checked _____ Date _____

BELL Aircraft CORPORATION

Model _____ Page 4B-14
 Missile _____ Report M43-945-012
 Airplane _____

assumptions are made that $\psi = \xi$ (case of no sideslip) and that $\Theta = \delta$ (the angular rotation in the pitch plane of the $X_3 Y_3 Z_3$ axis system is through the angle δ from the horizontal to the flight direction making the $X_3 Y_3 Z_3$ a stability axis system) the following simplified general equations result.

$$\ddot{v} = \frac{T}{M} \cos \psi - \frac{D}{M} - (g - r\Omega^2 \sin^2 \lambda) \sin \delta + r\Omega^2 \sin \lambda \cos \lambda \cos \delta \sin \xi \quad (17a)$$

$$\begin{aligned} v \dot{\xi} \cos \phi \cos \delta - v \dot{\gamma} \sin \phi &= \frac{Y}{m} + (g - r\Omega^2 \sin^2 \lambda) \sin \phi \cos \delta \\ &+ r\Omega^2 \sin \lambda \cos \lambda (\cos \phi \cos \xi + \sin \phi \sin \delta \sin \xi) \\ &+ 2v\Omega \left[\cos \lambda (\cos \phi \cos \delta) - \sin \lambda (\sin \phi \cos \xi \right. \\ &\left. - \cos \phi \sin \delta \sin \xi) \right] - \frac{v^2}{r} (\sin \phi \cos \delta - \cos \phi \cos^2 \delta \cos \xi \cot \lambda) \quad (17b) \end{aligned}$$

$$\begin{aligned} v \dot{\delta} \cos \phi + v \dot{\xi} \sin \phi \cos \delta &= \frac{L}{M} + \frac{T}{M} \sin \psi - (g - r\Omega^2 \sin^2 \lambda) \cos \phi \cos \delta \\ &+ r\Omega^2 \sin \lambda \cos \lambda (\sin \phi \cos \xi - \cos \phi \sin \delta \sin \xi) \\ &+ 2v\Omega \left[\cos \lambda (\sin \phi \cos \delta) + \sin \lambda (\cos \phi \cos \xi \right. \\ &\left. + \sin \phi \sin \delta \sin \xi) \right] + \frac{v^2}{r} (\cos \phi \cos \delta + \sin \phi \cos^2 \delta \cos \xi \cot \lambda) \quad (17c) \end{aligned}$$

In arriving at equations (17) from equations (15) and (16) it should be remembered that the aerodynamic lift force, L , and drag forces, D , are in the negative Z_3 and X_3 directions respectively, and that the aerodynamic side force (represented by Y) is in the positive Y_3 direction. It is assumed that the thrust line is displaced from the flight path direction by the angle ψ , i.e. the inclination at the thrust line from the horizontal is given by the angle $\psi + \delta$.

SECRET

By _____ Date _____	BELL Aircraft CORPORATION	Model _____	Page 4B-15
Checked _____ Date _____		Missile _____ Airplane _____	Report D143-945-012

If additional restrictions are placed upon equation (17), as done in Reference 3; namely: 1) the aircraft is flying in the equatorial plane, 2) the aircraft is flying towards the east, and 3) the angle of bank is maintained zero, then equation (17) is reduced to the form as given in Reference 3. These equations are repeated below.

$$\dot{V} = \frac{T}{M} \cos \nu - \frac{D}{M} - (g - r\Omega^2) \sin \delta \quad (18a)$$

$$V \dot{\delta} \cos \delta = \frac{Y}{M} \quad (18b)$$

$$V \dot{\delta}^2 = \frac{L}{M} + \frac{T}{M} \sin \nu - (g - r\Omega^2) \cos \delta + 2V\Omega \sin \delta + \frac{V^2}{r} \cos \delta \quad (18c)$$

It is seen by comparison of equation (18) with the equations resulting from the combination of equations (15) and (16) that the equations given in Reference 3 are a special case of the general equations of motion. Hence, in using equation (18) to calculate the performance of an aircraft, the limitations placed upon the flight conditions should be realized.

As equations of linear motion (see equations (15) and (16)) are now available in their most complete form, it is possible, by using one of several methods, to calculate the flight path relative to the earth of an aircraft flying in any direction at any latitude. However, as shown the equations of linear motion are extremely complex for the general case. The possibility of neglecting terms and making simplifying assumptions will have to be investigated in hopes that the amount of labor and time to calculate fairly accurate flight paths may be reduced.

SECRET

SECRET

BY _____ DATE _____
CHECKED _____ DATE _____

BELL Aircraft CORPORATION

MODEL _____ PAGE 4B-16
AIRPLANE _____ REPORT DL43-945-012

The equations of linear motion have derived for flight about a rotating earth. Similar expressions will now be derived for angular motion about the aircraft axis. For this derivation, the assumptions of an inertial axis at the center of the earth will be continued and only earth curvature and rotation will be considered, in addition to the angular motions of the vehicle with respect to the earth.

The law of conservation of angular momentum may be expressed as the vector equation

$$N_1 = \frac{d(L_1)}{dt} \quad (19)$$

where N_1 is the vector sum of all torques (moments) acting on the system and L_1 is the total angular momentum of the system being considered, measured with respect to the inertial $X_1 Y_1 Z_1$ axis system illustrated in Figure 4B-1. As with the equations of linear motion, it is more convenient to express the equations of angular motion with respect to the $X_3 Y_3 Z_3$ (aircraft axis) system, for which the moments of inertia and aerodynamic moments are most recognizable.

The total angular momentum may be expressed in vector form as

$$\left(\frac{dL_1}{dt}\right) = \left(\frac{dL_3}{dt}\right) + \omega_3 \times L_3 \quad (20)$$

where L_3 is the angular momentum measured with respect to the $X_3 Y_3 Z_3$ axis system and ω_3 is the angular velocity of the $X_3 Y_3 Z_3$ axis system with respect to the inertial $X_1 Y_1 Z_1$ axis system. Substituting equation (20) into equation (19) and expressing the vector equation in its components, results in the following:

Para B'-1 Rev. 1046

SECRET

$$N_{X_3} = \left(\frac{dL_{X_3}}{dt} \right) + \omega_{Y_3} L_{Z_3} - \omega_{Z_3} L_{Y_3} \quad (21a)$$

$$N_{Y_3} = \left(\frac{dL_{Y_3}}{dt} \right) + \omega_{Z_3} L_{X_3} - \omega_{X_3} L_{Z_3} \quad (21b)$$

$$N_{Z_3} = \left(\frac{dL_{Z_3}}{dt} \right) + \omega_{X_3} L_{Y_3} - \omega_{Y_3} L_{X_3} \quad (21c)$$

where the components of angular momentum are given by equation (22)

$$L_{X_3} = I_{X_3X_3} \omega_{X_3} + I_{X_3Y_3} \omega_{Y_3} + I_{X_3Z_3} \omega_{Z_3} \quad (22a)$$

$$L_{Y_3} = I_{Y_3X_3} \omega_{X_3} + I_{Y_3Y_3} \omega_{Y_3} + I_{Y_3Z_3} \omega_{Z_3} \quad (22b)$$

$$L_{Z_3} = I_{Z_3X_3} \omega_{X_3} + I_{Z_3Y_3} \omega_{Y_3} + I_{Z_3Z_3} \omega_{Z_3} \quad (22c)$$

wherein $I_{X_3X_3}$, $I_{X_3Y_3}$, etc. are the components of moments and products of inertia taken with respect to the $X_3 Y_3 Z_3$ axis system and are given by

$$I_{X_3X_3} = \sum_1 m_1 (y_{13}^2 + z_{13}^2)$$

$$I_{X_3Y_3} = - \sum_1 m_1 x_{13} y_{13}$$

$$I_{X_3Z_3} = - \sum_1 m_1 x_{13} z_{13}$$

etc.

Differentiating equations (22) and substituting these results in equations (21) gives

$$\begin{aligned} N_{X_3} = & \omega_{X_3} \frac{d}{dt} (I_{X_3X_3}) + I_{X_3X_3} \dot{\omega}_{X_3} + \omega_{Y_3} \frac{d}{dt} (I_{X_3Y_3}) \\ & + I_{X_3Y_3} \dot{\omega}_{Y_3} + \omega_{Z_3} \frac{d}{dt} (I_{X_3Z_3}) + I_{X_3Z_3} \dot{\omega}_{Z_3} \\ & + \omega_{Y_3} (I_{Z_3X_3} \omega_{X_3} + I_{Z_3Y_3} \omega_{Y_3} + I_{Z_3Z_3} \omega_{Z_3}) \\ & - \omega_{Z_3} (I_{Y_3X_3} \omega_{X_3} + I_{Y_3Y_3} \omega_{Y_3} + I_{Y_3Z_3} \omega_{Z_3}) \quad (23a) \end{aligned}$$

Form 34-1 Rev. 10-66

SECRET

$$\begin{aligned}
 N_{Y_3} &= \omega_{X_3} \frac{d}{dt} (I_{Y_3 X_3}) + I_{Y_3 X_3} \dot{\omega}_{X_3} + \omega_{Y_3} \frac{d}{dt} (I_{Y_3 Y_3}) \\
 &+ I_{Y_3 Y_3} \dot{\omega}_{Y_3} + \omega_{Z_3} \frac{d}{dt} (I_{Y_3 Z_3}) + I_{Y_3 Z_3} \dot{\omega}_{Z_3} \\
 &+ \omega_{Z_3} (I_{X_3 X_3} \omega_{X_3} + I_{X_3 Y_3} \omega_{Y_3} + I_{X_3 Z_3} \omega_{Z_3}) \\
 &- \omega_{X_3} (I_{Z_3 X_3} \omega_{X_3} + I_{Z_3 Y_3} \omega_{Y_3} + I_{Z_3 Z_3} \omega_{Z_3}) \quad (23b) \\
 N_{Z_3} &= \omega_{X_3} \frac{d}{dt} (I_{Z_3 X_3}) + I_{Z_3 X_3} \dot{\omega}_{X_3} + \omega_{Y_3} \frac{d}{dt} (I_{Z_3 Y_3}) \\
 &+ I_{Z_3 Y_3} \dot{\omega}_{Y_3} + \omega_{Z_3} \frac{d}{dt} (I_{Z_3 Z_3}) + I_{Z_3 Z_3} \dot{\omega}_{Z_3} \\
 &+ \omega_{X_3} (I_{Y_3 X_3} \omega_{X_3} + I_{Y_3 Y_3} \omega_{Y_3} + I_{Y_3 Z_3} \omega_{Z_3}) \\
 &- \omega_{Y_3} (I_{X_3 X_3} \omega_{X_3} + I_{X_3 Y_3} \omega_{Y_3} + I_{X_3 Z_3} \omega_{Z_3}) \quad (23c)
 \end{aligned}$$

The angular velocity ω_3 is found by taking the sum of angular velocity of the $X_3 Y_3 Z_3$ axis system with respect to the $X_2 Y_2 Z_2$ axis system and the angular velocity of the $X_2 Y_2 Z_2$ axis system with respect to the inertial $X_1 Y_1 Z_1$ axis system so that

$$\begin{vmatrix} \omega_{X_3} \\ \omega_{Y_3} \\ \omega_{Z_3} \end{vmatrix} = k \begin{vmatrix} \dot{\phi} \\ \dot{\theta} \\ \dot{\psi} \end{vmatrix} + l \begin{vmatrix} \frac{V}{r} \cos \gamma \sin \xi \\ \frac{V}{r} \cos \gamma \cos \xi - \Omega \sin \lambda \\ -\Omega \cos \lambda \end{vmatrix} \quad (24)$$

where l is a transformation matrix given by equation (7) and k is a transformation matrix which may be expressed as

SECRET

$$k = \begin{vmatrix} 1 & 0 & -\sin \theta \\ 0 & \cos \phi & \sin \phi \cos \theta \\ 0 & -\sin \phi & \cos \phi \cos \theta \end{vmatrix} \quad (25)$$

Substituting for ϕ and k and expanding the right hand side of equation (24) then gives

$$\begin{aligned} \omega_{x_3} = \dot{\phi} - \dot{\psi} \sin \theta + \frac{V}{r} \cos \theta \cos \theta \sin (\xi - \psi) \\ + \Omega (\cos \lambda \sin \theta - \sin \lambda \cos \theta \sin \psi) \end{aligned} \quad (26a)$$

$$\begin{aligned} \omega_{y_3} = \dot{\phi} \cos \phi + \dot{\psi} \sin \phi \cos \theta - \frac{V}{r} \cos \theta [\cos \phi \cos (\xi - \psi) \\ + \sin \phi \sin \theta \sin (\xi - \psi)] - \Omega \sin \lambda (\cos \phi \cos \psi \\ - \sin \phi \sin \theta \sin \psi - \sin \phi \cos \theta \cot \lambda) \end{aligned} \quad (26b)$$

$$\begin{aligned} \omega_{z_3} = \dot{\psi} \cos \phi \cos \theta - \dot{\phi} \sin \phi + \frac{V}{r} \cos \theta [\sin \phi \cos (\xi - \psi) \\ + \cos \phi \sin \theta \sin (\xi - \psi)] + \Omega \sin \lambda (\sin \phi \cos \psi \\ - \cos \phi \sin \theta \sin \psi - \cos \phi \cos \theta \cot \lambda) \end{aligned} \quad (26c)$$

When equations (26) and their derivatives are substituted into equations (23) the complete equations of angular motion in terms of the applied moments N_3 result. Since these equations are greatly detailed and hence space consuming, they will not be presented here. Some simplifications to these equations are possible however. If we assume that the hypersonic glide vehicle will possess at least a vertical plane of symmetry so that

$$I_{x_3 y_3} = I_{y_3 x_3} = I_{y_3 z_3} = I_{z_3 y_3} = 0$$

BY _____ DATE _____

CHECKED _____ DATE _____

BELL Aircraft CORPORATION

MODEL _____ PAGE LB-20

AIRPLANE _____ REPORT DL43-945-012

and

$$I_{X_3 Z_3} = I_{Z_3 X_3} \quad (27)$$

then equations (23) reduce the following form

$$\begin{aligned} N_{X_3} = & \omega_{X_3} \frac{d}{dt}(I_{X_3 X_3}) + I_{X_3 X_3} \dot{\omega}_{X_3} + \omega_{Z_3} \frac{d}{dt}(I_{X_3 Z_3}) \\ & + I_{X_3 Z_3} \dot{\omega}_{Z_3} + \omega_{Y_3} \omega_{Z_3} (I_{Z_3 Z_3} - I_{Y_3 Y_3}) + \omega_{X_3} \omega_{Z_3} I_{X_3 Z_3} \end{aligned} \quad (28a)$$

$$\begin{aligned} N_{Y_3} = & \omega_{Y_3} \frac{d}{dt}(I_{Y_3 Y_3}) + I_{Y_3 Y_3} \dot{\omega}_{Y_3} + \omega_{X_3} \omega_{Z_3} (I_{X_3 X_3} - I_{Z_3 Z_3}) \\ & + I_{X_3 Z_3} (\omega_{Z_3}^2 - \omega_{X_3}^2) \end{aligned} \quad (28b)$$

$$\begin{aligned} N_{Z_3} = & \omega_{X_3} \frac{d}{dt}(I_{X_3 Z_3}) + I_{X_3 Z_3} \dot{\omega}_{X_3} + \omega_{Z_3} \frac{d}{dt}(I_{Z_3 Z_3}) \\ & + I_{Z_3 Z_3} \dot{\omega}_{Z_3} + \omega_{X_3} \omega_{Y_3} (I_{Y_3 Y_3} - I_{X_3 X_3}) - \omega_{Y_3} \omega_{Z_3} I_{X_3 Z_3} \end{aligned} \quad (28c)$$

and if in addition the time rates of change of moments and products of inertia may be neglected then

$$\begin{aligned} N_{X_3} = & I_{X_3 X_3} \dot{\omega}_{X_3} + I_{X_3 Z_3} \dot{\omega}_{Z_3} + \omega_{Y_3} \omega_{Z_3} (I_{Z_3 Z_3} - I_{Y_3 Y_3}) \\ & + \omega_{X_3} \omega_{Z_3} I_{X_3 Z_3} \end{aligned} \quad (29a)$$

$$\begin{aligned} N_{Y_3} = & I_{Y_3 Y_3} \dot{\omega}_{Y_3} + \omega_{X_3} \omega_{Z_3} (I_{X_3 X_3} - I_{Z_3 Z_3}) \\ & + I_{X_3 Z_3} (\omega_{Z_3}^2 - \omega_{X_3}^2) \end{aligned} \quad (29b)$$

$$\begin{aligned} N_{Z_3} = & I_{Z_3 Z_3} \dot{\omega}_{Z_3} + I_{X_3 Z_3} \dot{\omega}_{X_3} + \omega_{X_3} \omega_{Y_3} (I_{Y_3 Y_3} - I_{X_3 X_3}) \\ & - \omega_{Y_3} \omega_{Z_3} I_{X_3 Z_3} \end{aligned} \quad (29c)$$

7
SECRET

BY _____ DATE _____
CHECKED _____ DATE _____

BELL *Aircraft* CORPORATION

MODEL _____ PAGE 40-21
AIRPLANE _____ REPORT D143-945-012

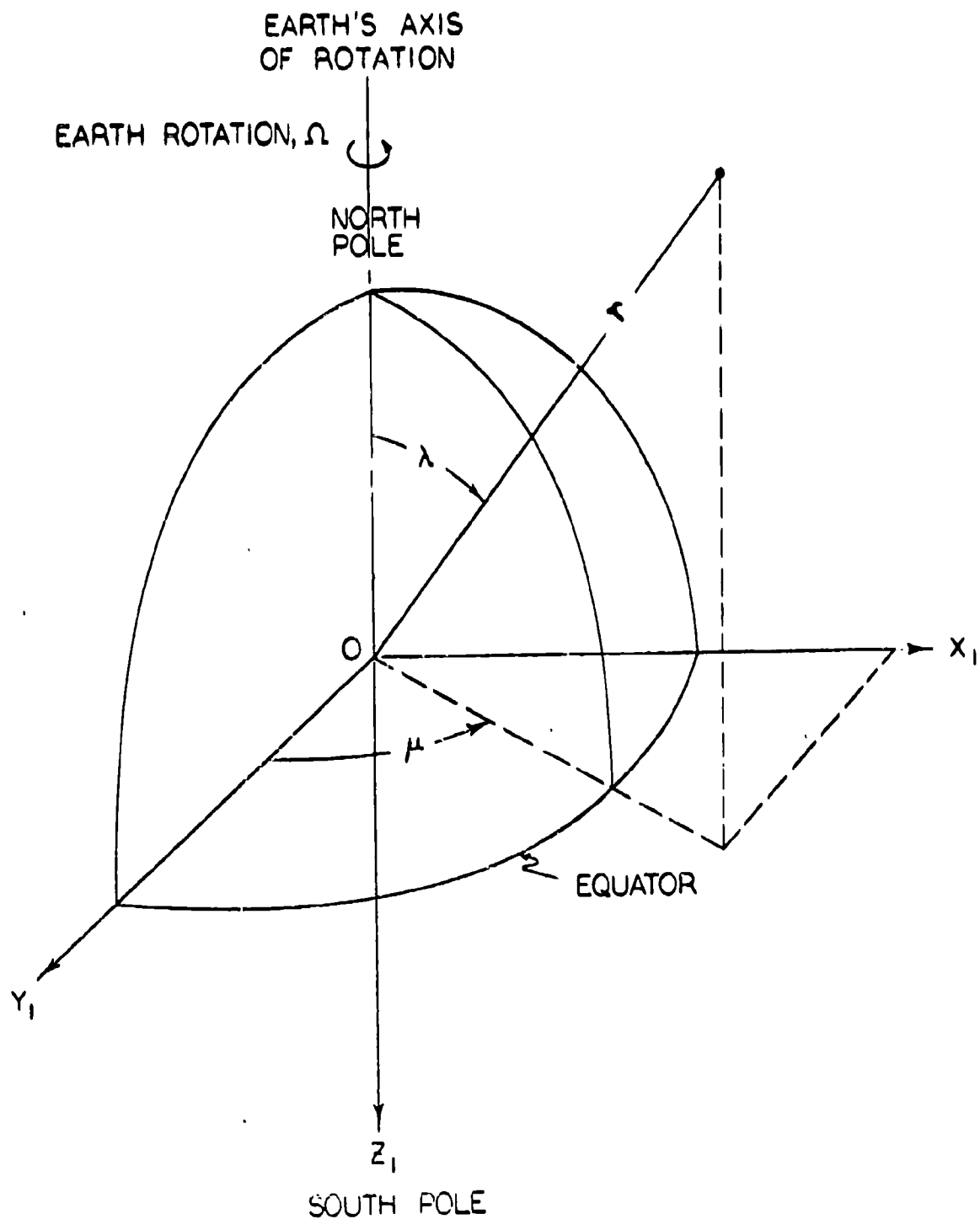
At this phase of the study, it is not possible to determine what further simplifications can be made. The equations of linear and angular motion as presented here, form the basis by which the motion of the vehicle in six degrees of freedom, including the effects of earth rotation and curvature, may be analyzed-in particular the dynamic behavior of such a vehicle may be studied once the necessary aerodynamic and kinematic parameters have been determined. Further analysis will be required to determine whether or not the dynamic motions can be derived in an analytical fashion. Certainly at least, with the present equations means are available by which the dynamic stability and control characteristics may be studied by the use of analogue computing equipment, provide sufficient equipment is available to handle the complexity of the equations.

SECRET

BY _____ DATE _____
 CHECKED _____ DATE _____

BELL Aircraft CORPORATION

MODEL _____ PAGE 4B-22
 AIRPLANE _____ REPORT D143-245-012



Form 34-1 Rev. 10-56

FIGURE 4B-1

SECRET

J

DATE _____

DATE

MODEL

PAGE

LB-23

AIRPLANE

REPORT D143-945-012

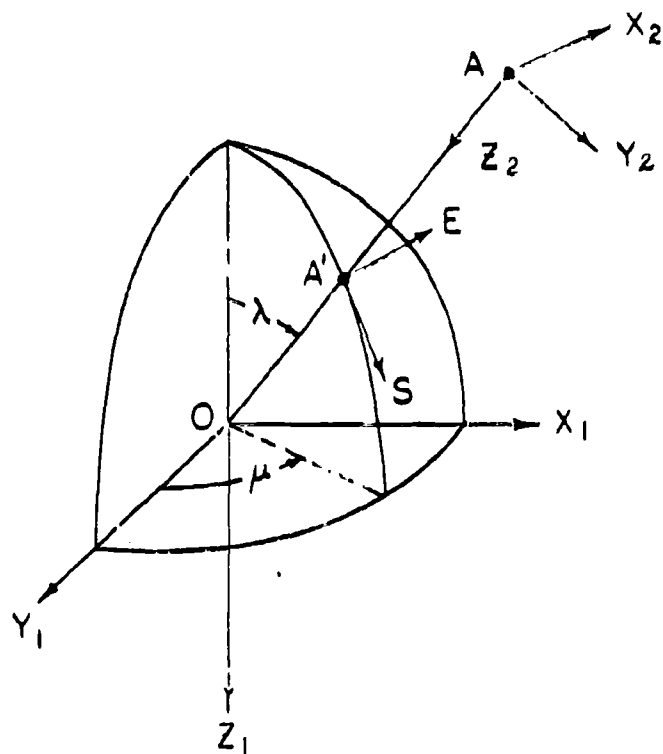


FIGURE 4B-2

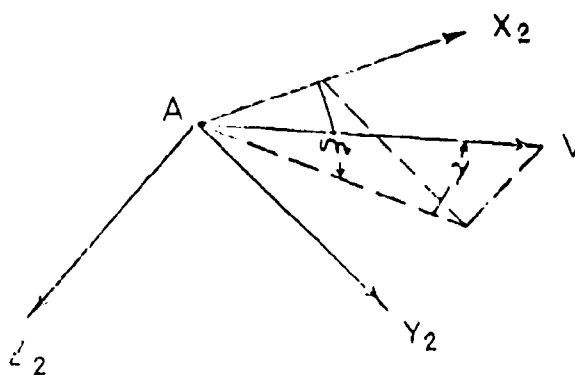


FIGURE 4B-3

6671 - 7103

By _____ Date _____

BELL Aircraft CORPORATION

Model _____ Page 5A-1

Checked _____ Date _____

Missile _____
Airplane _____ Report D143-945-012APPENDIX 5A

Steady, two-dimensional flow in the laminar compressible boundary layer over a flat surface or one whose radius of curvature is large compared with the boundary layer thickness is governed by the following equations:

Momentum

$$\rho u u_x + \rho v u_y = -p_x + (\mu u_y)_y \quad (1)$$

$$p_y = 0 \quad (2)$$

Continuity

$$(\rho u)_x + (\rho v)_y = 0 \quad (3)$$

Energy

$$\rho u H_x + \rho v H_y = (\mu H_y)_y \quad (4)$$

where $H = c_p T + 1/2 u^2$

State

$$p = \rho R T \quad (5)$$

Further, it is assumed that the viscosity is related to the temperature by the Sutherland law

$$\mu/\mu_0 = (T/T_0)^{3/2} (T_0 + S)/(T + S), \quad (6)$$

where S is a constant which for air is $216^\circ R$ and where the subscript 0 denotes reference condition.

From the momentum equation, the external pressure p can be expressed in term of the external velocity distribution as

$$\frac{\partial p}{\partial x} = \frac{dp}{dx} = -\rho_1 u_1 u_{1x}$$

The boundary conditions on the flow are

$$\text{at } y = 0: u = v = 0 \quad H = H_w \quad (7)$$

$$\text{at } y = \delta: u = u_1, u_y = 0 \quad H = H_1 = H_s, H_y = 0 \quad (8)$$

By _____ Date _____

BELL Aircraft CORPORATION

Model _____ Page 5A-2

Checked _____ Date _____

Missile _____
Airplane _____ Report D143-945-012

To start the analysis, Equation (1) is converted into the following integral differential equation:

$$\frac{d}{dx} \left\{ \rho_1 u_1^2 \int_0^{\delta} \frac{\rho}{\rho_1} \frac{u}{u_1} \left(1 - \frac{u}{u_1}\right) dy \right\} + \rho_1 u_1 u_{1x} \int_0^{\delta} \frac{\rho}{\rho_1} \left(\frac{\rho}{\rho_1} - \frac{u}{u_1}\right) dy = (\mu u_y)_w \quad (9)$$

With the use of Equation (3), Equation (9) is more conveniently handled by introducing Dorodnitsin transformation. Accordingly the new variable is defined such that for a given value of x .

$$dt = \frac{\rho}{\rho_1} dy \quad (10)$$

This implies the introduction of a new boundary layer thickness in the $x - t$ plane defined must conveniently by the inverse transformation.

$$\delta = \int_0^{\delta_t} \frac{\rho_1}{\rho} dt \quad (11)$$

Now using Equations (10) and (11), Equation (9) becomes

$$\frac{d}{dx} \left\{ \rho_1 u_1^2 \delta_t \int_0^1 \frac{u}{u_1} \left(1 - \frac{u}{u_1}\right) d\tau \right\} + \rho_1 u_1 u_{1x} \delta_t \int_0^1 \left\{ \frac{H}{H_1} \left(1 + \frac{\gamma-1}{2} M_1^2\right) - \frac{\gamma-1}{2} M_1^2 \left(\frac{u}{u_1}\right)^2 - \frac{u}{u_1} \right\} d\tau = \mu_w \frac{T_1}{T_w} \frac{u_1}{\delta_t} \left[\left(\frac{u}{u_1}\right)_\tau \right]_w \quad (12)$$

This can be written as

$$\frac{F_1}{2} \Lambda' + F_1 \Lambda (\ln(F_1 O))' + F_2 \Lambda (\ln \frac{u_1}{u_0})' = \left[\left(\frac{u}{u_1}\right)_\tau \right]_w \quad (13)$$

$$\text{where } \Lambda = \frac{\rho_0 u_0 \rho_1 u_1}{\mu_0 \mu_w} \frac{T_w}{T_1} \delta_t^2, \quad \xi = \frac{\rho_0 u_0 x}{\mu_0} \quad (14)$$

and the prime denotes differentiation with respect to ξ

By _____ Date _____
 Checked _____ Date _____

BELL Aircraft CORPORATION

Model _____ Page 5A-3
 Missile _____
 Airplane _____ Report D143-945-012

$$F_1 = \int_0^1 \frac{u}{U_1} \left(1 - \frac{u}{U_1}\right) d\tau$$

$$F_2 = \left(1 + \frac{\gamma-1}{2} M_1^2\right) \int_0^1 \left(\frac{H}{H_1} - \left(\frac{u}{U_1}\right)^2\right) d\tau \quad (15)$$

$$0^2 = \frac{\rho_1}{\rho_0} \frac{U_1}{U_0} \frac{T_1}{T_w} \frac{\mu_w}{\mu_0} = \frac{\rho_1}{\rho_0} \frac{U_1}{U_0} \frac{H_1}{H_w} \frac{1}{\left(1 + \frac{\gamma-1}{2} M_1^2\right)} \frac{\mu_w}{\mu_0}$$

$$\tau = \frac{t}{\delta_t} \quad (16)$$

Now equation (13) is in a form amenable to approximate solution following the integral method of von Karman.

Similarly the energy equation becomes:

$$\int_0^\delta \rho u H_x dy + \int_0^\delta \rho v H_y dy = -(\mu H_y)_w \quad (17)$$

or

$$\frac{d}{dx} \left\{ \rho_1 U_1 \int_0^\delta \frac{\rho}{\rho_1} \frac{u}{U_1} \left(H_1 - H\right) dy \right\} = (\mu H_y)_w \quad (18)$$

Applying Dorodnitsin transformation to Equation (18) we get:

$$\frac{d}{dx} \left\{ \rho_1 U_1 \delta_t \int_0^1 \frac{u}{U_1} \left(1 - \frac{H}{H_1}\right) d\tau \right\} = \frac{\mu_w}{\delta_t} \frac{T_1}{T_w} \left[\left(\frac{H}{H_1}\right)_\tau \right]_w \quad (19)$$

and introducing the variable Λ and ξ the above equation becomes:

$$\frac{F_3}{2} \Lambda' + F_3 \Lambda \left(\ln(F_3 Q) \right)' = \left[\left(\frac{H}{H_1}\right)_\tau \right]_w \quad (20)$$

where

$$F_3 = \int_0^1 \frac{u}{U_1} \left(1 - \frac{H}{H_1}\right) d\tau \quad (21)$$

Equation (20) is now also in a form amenable to solution by an integral procedure. To get an integral solution, we assume velocity and enthalpy distributions in the form:

By _____ Date _____
 Checked _____ Date _____

BELL *Aircraft* CORPORATION

Model _____ Page 5A-4
 Missile _____
 Airplane _____ Report D143-945-012

$$\frac{u}{u_1} = \sum_{i=0}^4 a_i \tau^i \quad (22)$$

$$\frac{H}{H_1} = \sum_{i=0}^5 b_i \tau^i \quad (23)$$

The boundary conditions are, at $\tau = 0$

$$\rho_1 u_1 u_{1x} = (\mu u_y)_y, (\mu H_y)_y = 0, \frac{H}{H_1} = W$$

and at $\tau = 1$:

$$\left(\frac{u}{u_1}\right)_\tau = \left(\frac{u}{u_1}\right)_{\tau\tau} = \left(\frac{H}{H_1}\right)_{\tau\tau} = \left(\frac{H}{H_1}\right)_\tau = 0, \left(\frac{u}{u_1}\right) = 1, \left(\frac{H}{H_1}\right) = 1$$

Substituting the above boundary conditions in equation (22) and (23), we get

$$b_0 = W \quad a_1 = (2 + 2/3)$$

$$b_1 = \left[\left(\frac{H}{H_1}\right)_\tau\right]_W = b \quad a_2 = -2$$

$$b_2 = \frac{1}{2} \left[\left(\frac{H}{H_1}\right)_{\tau\tau}\right]_W$$

The velocity and enthalpy profiles can be evaluated in terms of W , b and b_2 . They are

$$\frac{u}{u_1} = (2\tau - 2\tau^3 + \tau^4) - W\left(\frac{\tau}{3} + \tau^2 - \tau^3 + \frac{\tau^4}{3}\right)$$

and

$$\begin{aligned} \frac{H}{H_1} = & 1 - (1 - W)(1 - 10\tau^3 + 15\tau^4 - 6\tau^5) + b(\tau - 6\tau^3 + 8\tau^4 - 3\tau^5) \\ & + b_2(\tau^2 - 3\tau^3 + 3\tau^4 - \tau^5) \end{aligned}$$

SECRET

By _____ Date _____	BELL Aircraft CORPORATION	Model _____ Page <u>5A-5</u> Missile _____ Airplane _____ Report <u>D143-945-012</u>
Checked _____ Date _____		

Using the above equations, the F integrals can be evaluated in terms of W, b and b₂. We obtain

$$F_1 = 37/315 - 22/945 - z^2/2268 \quad (24)$$

$$F_2 = (1 + \frac{\gamma-1}{2} M_1^2) (\frac{263}{630} + \frac{1}{2} (1-w) - \frac{712}{3780} - \frac{z^2}{2268} + \frac{b}{10} + \frac{b_2}{60})$$

$$F_3 = (1-w) (\frac{17}{70} + \frac{312}{2520}) - b (\frac{79}{1260} + \frac{192}{7560}) - b_2 (\frac{319}{27720} + \frac{112}{27720})$$

where b₂ and z are given by:

$$b_2 = b^2 \left(\frac{1}{2W} \left(\frac{T_w}{T_w + s} \right) - \frac{1}{4W} - b^2 f(W) \right), \quad (24a)$$

$$z = \left\{ \frac{\Lambda W}{2M_1} \frac{\partial M_1}{\partial \xi} + 2b(f(W)) \right\} \left\{ 1 - \frac{b}{3} (f(W)) \right\}^{-1}$$

Now equations (14) and (20) are transformed to a form where (Λ) is the dependant variable and (M₁) is the independent variable.

Using the isentropic equations and γ = 1.4, we have:

$$Q = \left(\frac{M_1}{M_0} \right)^{1/2} \left\{ \frac{(1 + \frac{\gamma-1}{2} M_0^2)^3}{(1 + \frac{\gamma-1}{2} M_1^2)^4} \right\}^{1/2} \frac{\mu_w}{\mu_0}^{1/2}$$

and for hypersonic flow, M₁ >> 1, Q reduces to

$$Q = \frac{2}{(\gamma-1)} \frac{M_0^{2.5}}{M_1^{3.5}} \left(\frac{\mu_w}{\mu_0} \right)^{1/2}$$

Since the variable term in F₁ and F₃ are relatively small (cf. equation 24); following Reference (5.3-6) we let F₁' = F₃' = 0.

Thus equation (14) becomes

$$\begin{aligned} \frac{F_1}{2} \frac{d\Lambda}{dM_1} - \frac{3.5 F_1 \Lambda}{M_1} + F_2 \Lambda \left(\frac{1}{M_1} - \frac{\gamma-1}{2} \right) \frac{M_1}{(1 + \frac{\gamma-1}{2} M_1^2)} \\ = (2 + \frac{z}{3}) \left(\frac{dM_1}{d\xi} \right)^{-1} \end{aligned} \quad (25)$$

By _____ Date _____

BELL Aircraft CORPORATION

Model _____ Page 5A-6

Checked _____ Date _____

Missile _____ Report D143-945-012
Airplane _____

Denoting $\frac{d}{dM_1}$ by (\cdot) $\frac{\lambda}{\lambda_0} = \lambda$ and regrouping terms, Equation (25) becomes:

$$\lambda' - \frac{7\lambda}{M_1} - \frac{\lambda}{3F_1 M_1 (1 - 1/3 b f(W))} + 2 \frac{F_2}{F_1} \lambda \left(\frac{1}{M_1} - \frac{(\frac{\gamma-1}{2}) M_1}{1 + \frac{\gamma-1}{2} M_1^2} \right) \\ = \left\{ 1 + \frac{b f(W)}{3 - b f(W)} \right\} \frac{4}{F_1 \lambda_0} \left(\frac{dM_1}{d\xi} \right)^{-1} \quad (26)$$

In order to evaluate $dM_1/d\xi$ we must choose a region in which we want our equation to describe the flow. In this method, since very little is known about the region close to the leading edge, and since we would like to have a method which will be valid, independent of the leading edge effect, we shall start our solution downstream of the leading edge using the two-region theory. Thus we use the results available to start the problem and join our solution downstream of the leading edge. Therefore, using isentropic expansion (Reference 5.3-19).

$$\frac{dM_1}{d\xi} = - \frac{\gamma-1}{2} M_1^2 \frac{\mu_0}{\rho_0 u_0} \frac{\partial^2 \delta}{\partial x^2} \quad (27)$$

Since for $M \gg 1$ it will be shown later that $\left(\frac{v}{u}\right)_1 = \frac{\partial \delta^*}{\partial x} \approx \frac{\partial \delta}{\partial x}$

If we apply the same transformation to equation (20) we get

$$F_3 \lambda' - \frac{F_3 \lambda}{M_1} = \frac{4b}{\lambda_0} \frac{dM_1}{d\xi} \quad (28)$$

Using the initial condition we can now solve numerically equations (26) and (28) and find the parameters b and λ as a function of ξ . Now b can be found at once as a function of λ if we eliminate λ' between equation (26) and (28) by multiplying equation (26) by F_3 , multiply equation (28) by F_1 and subtracting the resulting equations. Equation (26) can then be solved numerically using ADAMS method (Reference 5.3-20).

By _____ Date _____
 Checked _____ Date _____

BELL Aircraft CORPORATION

Model _____ Page 5A-7
 Missile _____
 Airplane _____ Report D143-945-012

In our case the problem was started by means of the method described in Appendix 5B using the solution determined for several values of M , α , and R_∞ for a flat plate in steady flight.

In terms of the parameter Q , Λ , Z and b the coefficients C_f and C_h are:

$$C_f = \frac{2\tau}{\rho_\infty U_\infty^2} = \frac{2\rho_0 U_1 U_0}{\rho_\infty U_\infty^2} \frac{Q}{\Lambda^{1/2}} \left(2 + \frac{2}{3}\right) \quad (29)$$

$$C_h = \frac{q_w}{\rho_\infty U_\infty^2} = \left\{ \frac{2(2 + \frac{2}{3})}{b} \frac{U_1}{U_\infty} \right\}^{-1} C_f \quad (30)$$

The C_f and $\frac{p_\infty}{p_0}$ for the various M , α , and R_∞ were correlated and plotted in Figure 5.3-2 and 5.3-3. C_h was found to be approximately $1/2 C_f$ for all the cases computed.

This method can be improved by using $P_r = \text{constant}$ (not necessarily 1) and by using the exact expression for $(\frac{v}{U})_1$ which is found as follows

$$\begin{aligned} \rho_1 v_1 &= \frac{\partial}{\partial x} \int_0^\delta \rho u \, dy - \int_0^\delta \rho u \frac{\partial}{\partial x} (dy) \\ &= \frac{\partial}{\partial x} \int_0^\delta \rho u \, dy - \left(\rho_1 u_1 \frac{\partial \delta}{\partial x} \right) \\ (\rho u)_1 &= \frac{\partial}{\partial x} \rho_1 u_1 \int_0^\delta \left(1 - \frac{\rho u}{\rho_1 u_1} \right) dy - \int_0^\delta \frac{\partial}{\partial x} (\rho_1 u_1) dy \\ \left(\frac{\rho v}{\rho U} \right)_1 &= \frac{\partial \delta^*}{\partial x} - \left(\frac{\delta - \delta^*}{\rho_1 u_1} \right) \frac{\partial}{\partial x} (\rho_1 u_1) \end{aligned}$$

In the case considered in this paper we assume $\delta^* \approx \delta$ and therefore

$$\left(\frac{v}{U} \right)_1 = \frac{\partial \delta}{\partial x}$$

SECRET

By _____ Date _____

Checked _____ Date _____

BELL *Handwritten* CORPORATIONModel _____ Page 5A-8Missile _____
Airplane _____ Report D143-945-012

Since in terms of our variable

$$\delta^* = \delta_1(P_2 = P_1)$$

$$\delta = \delta_1(P_2 = P_1 + \frac{7}{10} + \frac{2}{60})$$

and P_2 being the dominating term for $M \gg 1$ then $\delta \approx \delta^*$. This assumption gets better as the wall temperature increases.

SECRET

SECRET

By _____	Date _____	BELL Aircraft CORPORATION	Model _____	Page 5A-9
Checked _____	Date _____		Missile _____	Report D143-945-012

APPENDIX 5A LIST OF SYMBOLS

$F_{1, 2, 3}$	Integrals defined after equations (15) and (21)
O	Function of M_0 and M_1 (cf. equation 24b)
H	Stagnation enthalpy = $\frac{u^2}{2} + c_p T$
M	Mach number
p	Static pressure
R	Gas constant
R_∞	Reynolds number ($\rho_\infty U_\infty x / \mu_\infty$)
S	Sutherland constant, 216°R for air
T	Absolute temperature
t	Transformed variable (cf. equation 16)
u	Velocity component in x direction
U	Potential flow velocity in x direction
v	Velocity component in the y direction
W	Ratio of stagnation enthalpy at the wall in potential flow
x	Coordinate along the surface
y	Coordinate normal to the surface
Z	Pressure gradient parameter; (cf. equations 24a)
γ	Ratio of specific heats
δ	Boundary layer thickness
δ^*	Boundary layer displacement thickness
λ	Non-dimensional boundary layer thickness ratio ($\lambda = \delta / \delta_0$)
μ	Coefficient of viscosity

By _____ Date _____
 Checked _____ Date _____

BELL Aircraft CORPORATION

Model _____ Page 5A-10
 Missile _____
 Airplane _____ Report D143-945-012

ξ Non-dimensional space coordinate ($\xi = \frac{\rho_o U_o x}{\mu_o}$), or

$$\frac{T_w}{T_o} \frac{\mu_o}{\mu_w} \frac{R_o}{M_o^2}$$

ρ Mass density

Λ Non-dimensional boundary layer thickness parameter

$$(\Lambda = \rho_1 U_1 \rho_o U_o \delta_t^2 T_w / \mu_w \mu_o T_1)$$

τ t / δ_t

Subscripts

- ()_w Value at the surface, $y = 0$ for any value of x
- ()₁ Value at the outer edge of the boundary layer
- ()_o Value at $x = 0$
- ()_t Value in the $x - t$ or $\xi - \tau$ plane
- ()_s Stagnation values
- ()_∞ Value at infinity upstream
- ()_∞ Value at infinity downstream

By _____ Date _____

BELL *Aircraft* CORPORATION

Model _____ Page 5B-1

Checked _____ Date _____

Missile _____
Airplane _____ Report D143-945-012

APPENDIX 5B *

The Momentum Integral Method for Hypersonic Viscous Flow

It can be shown that the Prandtl boundary theory remains valid in the hypersonic flow range ($M_\infty \gg 1$) under the following assumptions:

(I) The fluid can be considered as a continuum and the flow field is describable by the Navier-Stokes equations; (II) A sufficiently thin laminar boundary layer with continuous slope exists; (III) The curvature of the body surface is sufficiently small.

The second condition may be written, if the thickness of the layer δ is introduced, as

$$\frac{\delta}{x} \ll 1 \quad (\text{II})'$$

and the first condition, together with the second condition above, may be taken arbitrarily as the criterion[†]

$$\left(\frac{\text{shearing stress}}{\text{pressure}} \right)_{\text{max.}} = \left(\frac{C_f}{C_p} \right)_{\text{wall}} \ll 1 \quad (\text{I})'$$

With the aid of the continuity equation, the momentum and energy integral relations can be written in the usual form

$$\delta^* M^2 \frac{d}{dx} \frac{\rho_1}{\rho_\infty} \psi = \frac{k_{11}}{\rho_\infty U_\infty} \left(\frac{\partial u}{\partial y} \right)_w + \delta^{**} \frac{d}{dx} \left(\frac{p_2}{p_\infty} \right) \quad (1)$$

and

$$\frac{\delta^*}{2} M^2 \frac{d}{dx} \frac{\rho_1}{\rho_\infty} \psi = \frac{k_{11}}{\rho_\infty U_\infty} \left(\frac{\partial T}{\partial y} \right)_w \quad (2)$$

* The criteria (I) and (II) can be shown to be equivalent in order of magnitude, i.e.,

$$\left(\frac{C_f}{C_p} \right)_{\text{wall}} \sim \frac{\delta}{x} \ll 1$$

although not equal numerically.

† The nomenclature used here is that defined in Appendix 5A.

By _____ Date _____
 Checked _____ Date _____

BELL Aircraft CORPORATION

 Model _____ Page 5B-2
 Missile _____
 Airplane _____ Report D143-945-012

where

$$\left. \begin{aligned}
 \mathcal{Q} &\equiv \int_0^\delta \frac{\rho}{\rho_1} \frac{u}{u_1} \left(1 - \frac{u}{u_1}\right) dy \\
 \mathcal{Q} &\equiv \int_0^\delta \frac{\rho}{\rho_1} \frac{u}{u_1} (1 - R) dy \\
 \delta^* &\equiv \int_0^\delta \left(1 - \frac{\rho u}{\rho_1 u_1}\right) dy \\
 R &\equiv \frac{c_p T + \frac{1}{2}(u^2 + v^2)}{c_p T_\infty + \frac{1}{2}u_\infty^2} = \frac{(c_p T_\theta)}{(c_p T_\theta)_\infty} = \frac{(c_p T_\theta)_1}{(c_p T_\theta)_1}
 \end{aligned} \right\} \quad (3)$$

$$\left. \begin{aligned}
 \delta^* &\equiv \int_0^\delta \left(1 - \frac{\rho u}{\rho_1 u_1}\right) dy \\
 R &\equiv \frac{c_p T + \frac{1}{2}(u^2 + v^2)}{c_p T_\infty + \frac{1}{2}u_\infty^2} = \frac{(c_p T_\theta)}{(c_p T_\theta)_\infty} = \frac{(c_p T_\theta)_1}{(c_p T_\theta)_1}
 \end{aligned} \right\} \quad (4)$$

and

$$\frac{v}{u_1} = \frac{d\delta^*}{dx} - [\delta_1^* - \delta] \frac{d}{dx} \ln(\rho u_1) \quad (5)$$

Assuming the body to be very thin, (and $\frac{\delta}{x} \ll 1$), it is consistent to assume also that $u_1 \approx U_\infty$. Since $M_\infty \gg 1$, then $M_1 \gg 1$, while $M_\infty > M_1$; then⁺

$$\frac{\rho}{\rho_1} = O\left\{\frac{1}{\frac{\delta}{x} - 1} M_1^2\right\} \ll 1$$

thus

$$\begin{aligned}
 \delta^* &\approx \delta \\
 \left(\frac{v}{u_1}\right) &\approx \frac{d\delta}{dx}
 \end{aligned} \quad (6)$$

⁺Here the conventional notation is used, namely $x = O(y)$ means

$$\lim_{y \rightarrow 0} \frac{x}{y} = \text{constant} \neq 0, \text{ and } x = o(y) \text{ means } \lim_{y \rightarrow 0} \frac{x}{y} = 0$$

By _____ Date _____

BELL Aircraft CORPORATION

Model _____ Page 5B-3

Checked _____ Date _____

Missile
Airplane

Report D143-245-012

On the wall the x-momentum equation reduces to

$$\left. \frac{\partial p}{\partial x} \right|_w \approx \left. \frac{\partial}{\partial y} \left(\mu \frac{\partial u}{\partial y} \right) \right|_w \quad (7)$$

While the energy equation becomes

$$\frac{\partial}{\partial y} k \frac{\partial}{\partial y} \left[R - \frac{1}{Pr} (1 - Pr) \left(\frac{u}{u_1} \right)^2 \right] = 0 \quad (8)$$

Introducing the Dorednitzin-Stewartson transformation

$$t = \int_0^y \frac{\rho}{\rho_1} dy' = \int_0^y \frac{T_1}{T} dy' \quad (9)$$

$$\tau = (t / \delta_t)$$

where

$$\delta_t = \int_0^\delta \frac{\rho}{\rho_1} dy' \quad (10)$$

one has

$$2\eta \frac{d}{d\zeta} \left[\eta \int_0^1 \bar{u} (1 - \bar{u}) d\tau \right] = 2 \left(\frac{\partial \bar{u}}{\partial \tau} \right)_{\tau=0} p^* \\ + \frac{\gamma - 1}{\gamma} \int_0^1 (R - \bar{u}^2) d\tau \cdot \eta^2 \cdot \frac{d}{d\zeta} \ln p^* \quad (11)$$

By _____ Date _____

BELL Aircraft CORPORATION

Model _____ Page 5B-4

Checked _____ Date _____

Missile _____ Report D143-945-012
Airplane _____

$$(Pr) \eta \frac{d}{d\delta} \left[\eta \int_0^1 \bar{u} (1 - R) d\tau \right] = \left(\frac{\partial R}{\partial \tau} \right)_{\tau=0} p^*, \quad (12)$$

$$- \frac{\gamma-1}{\gamma} \left(\frac{T_w}{T_s} \right) \eta^2 \frac{d}{d\delta} \frac{1}{p^*} = 2 \left(\frac{\partial^2 \bar{u}}{\partial \tau^2} \right)_{\tau=0} - \frac{T_w - S}{T_w + S} \left(\frac{T_s}{T_w} \right) \left(\frac{\partial \bar{u}}{\partial \tau} \right)_{\tau=0} \left(\frac{\partial R}{\partial \tau} \right)_{\tau=0} \quad (13)$$

where

$$\bar{u} = u/u_1, \quad p^* = p/M_\infty^2 p_\infty, \quad (Pr) = \frac{\mu C_p}{k}$$

and C_p is assumed to be a constant, $T_s = \frac{\gamma-1}{2} M_\infty^2$, S is the Sutherland constant, and

$$\delta \equiv \frac{T_w}{T} \frac{\mu_\infty}{\mu_w} \frac{Re_\infty}{M_\infty^2} \quad (14)$$

$$\eta \equiv \frac{\gamma-1}{\gamma} \frac{T_w}{T_s} \frac{\mu_\infty}{\mu_w} \frac{Re_\infty}{M_\infty^2} \left(\frac{\delta}{x} \right) p^* / \int_0^1 (R - \bar{u}^2) d\tau$$

The subscripts ∞ , w , and s refer to the free stream, wall and stagnation quantities, respectively. In deriving Equation (13) the Sutherland viscosity-temperature relation has been used.

In determining the above system of equations, the energy equation on the wall has not been used. It can be shown that the error introduced by ignoring this condition is of the order of $(1 - Pr)$. The above three differential equations of the first order, together with an appropriate formula relating pressure to the normal velocity at the edge of the layer, or

$$\frac{p}{p_\infty} = F \left(M_\infty \frac{d\delta}{dx} \right),$$

are sufficient to determine (with proper initial conditions), η , p^* and two other unknown functions which characterize the distribution of velocity and of the total enthalpy across the layer. Since the external "entropy-layer" is at least as thick as δ , and the change in velocity

By _____ Date _____
 Checked _____ Date _____

BELL Aircraft CORPORATION

Model _____ Page 5B-5
 Missile _____
 Airplane _____ Report D143-245-012

is of the order of the larger of $U_{\infty} \left(\frac{\delta}{x}\right)^2$ and $U_{\infty} \alpha^2$, the vorticity there is at most of the order of $\frac{U_{\infty}}{x} \left(\frac{\delta}{x}\right)$, which is smaller by one order of magnitude than the vorticity in the boundary layer; one may, therefore, assume $u = u_1$, and $\left(\frac{\partial u}{\partial y}\right) = 0$ at the edge (but $\frac{\partial^2 u}{\partial y^2} \neq 0$), and write

$$\bar{u} = 1 - (1 - \tau)^2 (1 - a\tau) \quad (15)$$

One can also write for R

$$R = 1 - (1 - \tau)^2 \left[1 - \frac{T_w}{T_s} - b\tau \right] \quad (16)$$

where a and b are unknown functions of ξ or x . Note that the temperature on the wall has also been accounted for in Equation (16). Substituting Equations (15) and (16), into Equations (11), (12) and (13), we have

$$2p^* \eta \frac{d}{d\xi} \left[\eta \left(\frac{2}{15} - \frac{1}{60} a - \frac{1}{105} a^2 \right) \right] = 2(2 + a) p^{*2} \quad (17)$$

$$+ \frac{\gamma - 1}{2} \eta^2 \frac{dp^*}{d\xi} \left(\frac{2}{15} + 1/3 \frac{T_w}{T_s} + \frac{1}{12} b - \frac{a}{10} - \frac{a^2}{105} \right)$$

$$(Pr) \eta \frac{d}{d\xi} \left\{ \eta \left[\frac{2}{15} \left(1 - \frac{T_w}{T_s} \right) - 1/20 b + 1/30 \left(1 - \frac{T_w}{T_s} \right) a - \frac{1}{105} a b \right] \right\} \quad (18)$$

$$= (2 - 2 \frac{T_w}{T_s} + b) p^*$$

and

$$- \frac{\gamma - 1}{\gamma} \eta^2 \frac{d}{d\xi} p^* = p^{*2} \frac{T_s}{T_w} \left[4(1 + 2a) + \frac{T_w - T_s}{T_w + T_s} (2 + a) \frac{T_s}{T_w} (2 - 2 \frac{T_w}{T_s} + b) \right] \quad (19)$$

SECRET

By _____ Date _____

Checked _____ Date _____

BELL *Aircraft* CORPORATION

Model _____ Page 5B-6

Missile _____ Report D113-945-012
Airplane _____

The skin friction coefficient can then be expressed as

$$C_f \equiv \frac{\mu_w \left(\frac{\partial u}{\partial y} \right)_w}{\frac{1}{2} \rho_\infty U_\infty^2} = 2 \frac{(2+a) p^*}{\eta} \quad (20)$$

and the heat transfer coefficient ** as

$$C_h \equiv \frac{k_w \left(\frac{\partial T}{\partial y} \right)_w}{\rho_\infty U_\infty C_p (T_\infty - T_w)} = \frac{T_\infty}{Pr (T_\infty - T_w)} \cdot \frac{[2 (1 - \frac{T_w}{T_\infty}) + b] p^*}{\eta} \quad (21)$$

and thus

$$\frac{C_f}{C_h} = 2 Pr \left(1 - \frac{T_w}{T_\infty} \right) \frac{2+a}{2 (1 - \frac{T_w}{T_\infty}) + b} \quad (22)$$

With an additional relation - the pressure formula - one can proceed to obtain a solution either numerically - using step-wise integration or iteration - or analytically by expanding the solution in powers of the variable ξ . For points near the leading edge, where the interaction is strong, one expands the solutions in ascending powers of ξ ; for points far downstream, where the interaction is weak, one expands the solutions in descending powers of ξ .

The formula deduced from Prandtl-Meyer flow may be used when the shock, if it exists, is very weak. This is

$$\frac{p}{p_1} = \left[1 + \frac{\gamma-1}{2} M_1^2 \left(\frac{d\delta}{dx} + \alpha \right) \right]^{\frac{2\gamma}{\gamma-1}} \quad (23)$$

where p_1 and M_1 are the arbitrary reference pressure and Mach number belonging to the same state.

In the absence of a better formula, the so-called "tangent-wedge formula" may be used whenever the shock involved is strong enough. This can be expressed as (continued next page)

**Note that this definition differs from that employed by Crocco (reference 5.3-21).

By _____ Date _____
 Checked _____ Date _____

BELL Aircraft CORPORATION

Model _____ Page 5B-7
 Missile _____
 Airplane _____ Report D143-945-012

$$\frac{p}{p_{\infty}} = 1 + \frac{\gamma}{2} (\gamma + 1) M_{\infty}^2 \left[\frac{d\delta}{dx} + \alpha \right]^2 \left\{ \frac{1}{2} + \frac{1}{4} + \frac{1/(\gamma + 1)^2}{(M_{\infty}^2 - 1) \left[\frac{d\delta}{dx} + \alpha \right]^2} \right\}$$

$$= \frac{\gamma}{2} (\gamma + 1) M_{\infty}^2 \left[\frac{d\delta}{dx} + \alpha \right]^2 + \frac{3\gamma + 1}{\gamma + 1} + O \left(\frac{1}{M^2 \left[\frac{d\delta}{dx} + \alpha \right]^2} \right), \quad (21)$$

and strictly speaking, should be considered as an empirical formula in application.

It has been estimated by the calculations in Appendix 5D that for $M_{\infty} \gg 1$ and near the leading edge the error involved in using equation (21) may be not too large for ideal air ($\gamma = 1.4$), the correction factor being $(1.14)^{1/2}$ in the resulting pressure, and $(1.14)^{3/8}$ in the skin friction. For the strong interaction solution obtained here, this factor has been taken into account.

Since the solutions are singular near the leading edge, a suitable transformation of the variable in each of the expansions is introduced.

Strong Shock - Boundary Layer Interaction

The governing of equations consist of Equations (17), (18), (19) and

$$p^{**} = k \frac{\gamma}{2} (\gamma + 1) \left(\frac{\gamma - 1}{2} \right)^2 \frac{d}{d\xi} \left[\frac{\eta}{p^{**}} \int_0^1 (R - \bar{u}^2) d\tau + \alpha^2 \right] \quad (25)$$

$$+ \left(\frac{3\gamma + 1}{\gamma + 1} \right) \frac{1}{M_{\infty}^2}$$

only the highest order terms are retained in Equation (25), and the factor k is intended as a correction to the tangent-wedge formula. We thus have four equations for the four unknowns are η , p^{**} , a and b .

In view of the singular behavior of the solution to this system as $\xi \rightarrow 0$, the variable

$$\zeta = \xi^{1/4} \quad (26)$$

is introduced, and it is assumed that (for $\zeta \ll 1$)

By _____ Date _____

Checked _____ Date _____

BELL Aircraft CORPORATION

Model _____ Page 58-8

Missile _____
Airplane _____ Report D113-945-012

$$\left. \begin{aligned} \eta &= H_0 \xi + H_1 \xi^2 + \dots \\ p^* &= P_0 \xi^{-2} + P_1 \xi^{-1} + \dots \\ a &= a_0 + a_1 \xi + \dots \\ b &= b_0 + b_1 \xi + \dots \end{aligned} \right\} \quad (27)$$

The expressions of Equation (27) are substituted into Equations (17), (18), (19), and (25), and the leading terms of each of the resultant equations are, respectively,

$$\left. \begin{aligned} \left[\textcircled{1} + \frac{\gamma-1}{2} \textcircled{2} \right] H_0^2 &= 4(2+a_0) P_0 \\ \frac{P_r}{4} \textcircled{3} H_0^2 &= \left[2 \left(1 - \frac{T_w}{T_s} \right) + b_0 \right] P_0 \\ \frac{\gamma-1}{2\gamma} H_0^2 &= \textcircled{4} P_0 \\ k \frac{\gamma}{2} (\gamma+1) \left(\frac{\gamma-1}{2} \right)^2 \frac{9}{16} \textcircled{2}^2 H_0^2 &= P_0^3 \end{aligned} \right\} \quad (28)$$

$$\textcircled{1} = \int_0^1 \bar{u}(1-\bar{u}) d\tau = \frac{2}{15} - \frac{a_0}{20} - \frac{a_0^2}{105}$$

$$\textcircled{2} = \int_0^1 (R - \bar{u}^2) d\tau = \frac{7}{15} - \frac{1}{3} \left(1 - \frac{T_w}{T_s} \right) + \frac{b_0}{12} - \frac{a_0}{10} - \frac{a_0^2}{105} \quad (29)$$

$$\textcircled{3} = \int_0^1 \bar{u}(1-R) d\tau = \frac{2}{15} \left(1 - \frac{T_w}{T_s} \right) - \frac{b_0}{20} + \frac{a_0}{30} \left(1 - \frac{T_w}{T_s} \right) - \frac{a_0 b_0}{105}$$

$$\textcircled{4} = \frac{T_s}{T_w} \left\{ 4(1+2a_0) + \frac{T_w - S}{T_w + S} \frac{T_s}{T_w} (2+a_0) \left[2 \left(1 - \frac{T_w}{T_s} \right) + b_0 \right] \right\}$$

By _____ Date _____
 Checked _____ Date _____

BELL *Aircraft* CORPORATION

Model _____ Page 5B-9
 Missile _____
 Airplane _____ Report D143-945-012

Simultaneous solution on the Equations (28) then yields the parameters H_0 , P_0 , a_0 and b_0 . The coefficients of the second order terms involve H_1 , P_1 , a_1 and b_1 and are:

$$H_0 \left[3/2 \textcircled{1} + \frac{\gamma-1}{2} \textcircled{2} \right] H_1 + \left\{ -4(2+a_0) + \frac{1}{2} \frac{H_0^2}{P_0} \textcircled{1} + \frac{\gamma-1}{8} \frac{H_0^2}{P_0} \textcircled{2} \right\} P_1 \\ - H_0^2 \left[2 \frac{P_0}{H_0^2} + \left(\frac{1}{60} + \frac{2a_0}{105} \right) + \frac{\gamma-1}{4} \left(\frac{1}{10} + \frac{2a_0}{105} \right) \right] a_1 \\ + \frac{\gamma-1}{48} H_0^2 b_1 = 0, \quad (30.a)$$

$$3 \textcircled{3} H_0 H_1 + 2a_1 H_0^2 \left\{ \frac{1}{30} \left(1 - \frac{T_w}{T_0} \right) - \frac{b_0}{105} \right\} - H_0^2 \left\{ \frac{1}{10} + \frac{2a_0}{105} + \frac{4}{\gamma} \frac{P_0}{H_0^2} \right\} b_1 \\ + \left\{ -\frac{4}{Pr} \left[2 \left(1 - \frac{T_w}{T_0} \right) + b_0 \right] \right\} P_1 = 0, \quad (30.b)$$

$$\left\{ \frac{\gamma-1}{\gamma} \frac{H_0}{P_0} \right\} H_1 + \left\{ \frac{\gamma-1}{\gamma} \frac{1}{4} \frac{H_0^2}{P_0^2} - 2 \textcircled{4} \frac{1}{P_0} \right\} P_1 \\ - \left[\frac{T_w - S}{T_w + S} \left(\frac{T_0}{T_w} \right)^2 (2 + a_0) \right] b_1 \\ - \left[8 \frac{T}{T_w} + \frac{T_w - S}{T_w + S} \left(\frac{T_0}{T_w} \right)^2 (2 - 2 \frac{T_w}{T_0} + b_0) \right] a_1 = 0, \quad (30.c)$$

$$- \left\{ \frac{\gamma-1}{2} \frac{\textcircled{2}}{P_0} \right\} H_1 + \left\{ \frac{1}{k} \frac{1}{\gamma} (\gamma+1) - \frac{4}{3} (\gamma-1) \frac{P_0}{H_0} \frac{1}{\textcircled{2}} + \frac{\textcircled{2}(\gamma-1)}{2} \frac{H_0}{P_0^2} \right\} P_1 \\ - \left\{ \frac{\gamma-1}{24} \frac{H_0}{P_0} \right\} b_1 + \frac{\gamma-1}{2} \frac{H_0}{P_0} \left\{ \frac{1}{10} + \frac{2a_0}{105} \right\} a_1 = \alpha \quad (30.d)$$

This is a linear algebraic system which can be solved for H_1 , P_1 , a_1 and b_1 .

By _____ Date _____

BELL Aircraft CORPORATION

Model _____ Page 5B-10

Checked _____ Date _____

Missile _____ Airplane _____ Report D113-945-012

It is clear that the second order terms give the angle of attack effect, since all the unknowns appearing in them are linear in α . The leading terms which do not contain α , give the solution at zero angle of attack (when $M \frac{d\delta}{dx} \gg 1$).

In the first order system, one finds for the insulated case, $a_0 = 2.333$, $b_0 = 0$, (for $\delta = 7/5 = 1.4$); $a_0 = 0.399$, $b_0 = 0$, (for $\delta = 5/3$);

$$\frac{P^{(0)}}{P_\infty} = \frac{3}{4} \delta^k \sqrt{k (\delta^2 - 1)(1 + 2a_0)} \left[\frac{7}{15} - \frac{a_0}{10} - \frac{a_0^2}{105} \right] \bar{X}, \quad (31)$$

$$\text{and } M_\infty^3 C_f^{(0)} = \frac{\sqrt{3}}{2} \left[k \frac{2(\delta + 1)}{1 + 2a_0} \right]^{1/4} (2 + a_0) \left[\frac{7}{15} - \frac{a_0}{10} - \frac{a_0^2}{105} \right] \bar{X}^{3/2}, \quad (32)$$

where the value of k is to be taken from Appendix 5D as 1.14 for $\delta = 7/5$ and 1.36 for $\delta = 5/3$.

and where

$$\bar{X} = \frac{M_{co}^3}{R_{co}^{1/2}} \sqrt{\frac{\mu_w}{\mu_\infty} \frac{T_\infty}{T_w}} \approx \left(\frac{2}{\delta - 1} \right)^{1/4} \sqrt{1 + \frac{9}{T_\infty}} \left(\frac{M_{co}^2 + 1/2}{R_{co}^{1/2}} \right), \quad (33)$$

the superscript (o) referring to the asymptotic values near the leading edge.

If the power law $\mu \sim T^\omega$ is used instead of the Sutherland law ^{*}, then

$$\bar{X} \approx \left(\frac{\delta - 1}{2} \right)^{\omega - \frac{1}{2}} \frac{M^2 + \omega}{R_{co}^{1/2}} \quad (34)$$

For the "cooled" wall of constant temperature with $\frac{T_w}{T_{co}} = 3$, $M_\infty = 20$, and $\delta = 1.4$, we obtain $a_0 = -1.2805$, $b_0 = -1.462$,

$$P_0 = k^{1/2} \left(\frac{\delta}{2} \right)^{1/2} (\delta + 1)^{1/2} \left(\frac{\delta - 1}{2} \right)^{3/4} \frac{3}{4} \textcircled{2} \sqrt{\frac{2(2 + a)}{\frac{1}{2} \textcircled{1} + \delta - 1} \textcircled{2}},$$

^{*} It is of interest to note that the results of different authors vary (within the same order of magnitude) divergently (5.3). The present result provides the highest value for the self-induced pressure.

By _____ Date _____
 Checked _____ Date _____

BELL Aircraft CORPORATION

Model _____ Page 5B-11
 Missile _____
 Airplane _____ Report D143-945-012

$$\frac{p^{(o)}}{p} = p_o \left(\frac{T_w}{T_\infty} \right)^{1/4} \left(\frac{T_\infty + S}{T_w + S} \right)^{1/2} \frac{(20)^3}{Re_\infty^{1/2}}$$

$$C_f^{(o)} = \sqrt{2(2+a)} \sqrt{\frac{1}{2} \textcircled{1} + \frac{\gamma-1}{11} \textcircled{2}} \sqrt{P} \left(\frac{\gamma-1}{11} \right)^{-3/4} \quad (35)$$

$$\times \left(\frac{T_w}{T_\infty} \right)^{-3/4} \left(\frac{M_\infty}{M_w} \right)^{-3/4} \left(Re_\infty \right)^{-3/4},$$

where $\textcircled{1}$ and $\textcircled{2}$ refer to the expressions given by (29).

An analytic expression for the asymptotic value of p/p_∞ and c_f can be obtained for sufficiently small value of T_w/T_∞ , i.e., for

$$\frac{2}{(\gamma-1)} \frac{T_w}{M_\infty^2} \ll 1 \quad (36)$$

$$\text{as}$$

$$\frac{p^{(o)}}{p} = \frac{9}{11} \left[\frac{2}{35} k \gamma (\gamma+1) \right]^{1/2} \left[\frac{3 (\frac{\gamma-1}{2})^3}{(1 + \frac{\gamma-1}{2}) Pr} \right]^{1/4}$$

$$\times \left[\frac{T_w}{T_\infty} \frac{T_w + S}{T_\infty + S} \right]^{1/2} \left[\frac{T_w + S}{T_\infty - S} \right]^{1/4} \chi \quad (37)$$

and

$$M_\infty^3 C_f^{(o)} = \frac{9(3)^{3/8}}{(70)^{3/4}} k^{3/8} \left(1 + \frac{\gamma-1}{2} \right)^{5/8} \left(\frac{\gamma-1}{2} \right)^{1/8}$$

$$\times \gamma^{1/4} (\gamma+1)^{1/4} \left(\frac{T_w}{T_\infty} \frac{T_\infty + S}{T_w + S} \right)^{3/4} \left(\frac{T_\infty + S}{T_\infty - S} \right)^{3/8} \chi$$

where *

$$\chi = \frac{M_\infty^2 + 1/2}{Re^{1/2}} \quad (38)$$

* It should be noted that for a given (low) wall temperature, as Mach number M increases, the slope in the velocity and temperature profiles increases.

By _____ Date _____

BELL Aircraft CORPORATION

Model _____ Page 5B-12

Checked _____ Date _____

Missile _____ Report D143-945-012
Airplane _____

It can be also be shown that

$$C_f^{(0)} / C_h^{(0)} = 1 + \delta$$

Inspection of Equations (38) and (33) shows that with the assumption of the Sutherland viscosity-temperature relation, the essential parameter in the problem of hypersonic viscous flow is

$M_{\infty}^{5/2} / R_{e_{\infty}}^{1/2}$ for both insulated ($T_w \approx T_B$) cases and the cooled wall ($T_w / T_B \ll 1$), (instead of $M_{\infty}^3 / R_{e_{\infty}}^{1/2}$) obtained in References 5.3-1 and 5.3-3 which was based on the linear viscosity law.

Figures 5.3-2 and 5.3-3 appearing in the text were computed, at the time the angle of attack effect which is the solution of the linear algebraic system Equation (30) had not been carried out explicitly. From results obtained from a flow model similar to that used by Shen and Pai, References 5.3-2 and 5.3-8, we obtained

$$\frac{p}{p_{\infty}} \approx \left(\frac{p}{p_{\infty}} \right)_{\alpha=0} \left[1 + \frac{8}{7} \frac{\alpha}{\left(\frac{\delta}{x} \right)_{\alpha=0}} \right]$$

$$C_f \approx (C_f)_{\alpha=0} \left[1 + \frac{4}{7} \frac{\alpha}{\left(\frac{\delta}{x} \right)_{\alpha=0}} \right]$$

under the assumption of an insulated wall, a linear velocity profile, and $\delta = 7/5 = 1.4$. This expression served as a basis for the estimation of the angle of attack effect on C_f and (p/p_{∞}) shown in Figures 5.3-2 and 5.3-3. A check at $M_{\infty} = 20$, $T_w/T_{\infty} = 3$, with the calculation obtained later reveals that the error involved in the coefficients $\frac{8}{7}$ and $\frac{4}{7}$ appeared above about 20% or less which is of the

same order of magnitude as terms neglected in the computation of the angle of attack effect.

By _____ Date _____

Checked _____ Date _____

BELL Aircraft CORPORATION

Model _____ Page 5B-13

Missile _____ Report D143-945-012
Airplane _____Effect of a Small Induced Pressure Gradient on
Laminar Skin Friction and Heat Transfer

For the area of weak interaction, which is necessarily at some distance downstream of the leading edge, one can develop the solution into descending powers of ξ , and the appropriate transformation is

$$\zeta = \xi^{1/2} \quad (39)$$

The first order equation system obviously reduces to the ordinary case of a flat plate (at zero incidence and zero pressure gradient). The first order correction accounting for the change in pressure (Δp) may then be obtained. In fact, if only the first order effect is of primary interest, the percentage changes in skin friction and in the rate of heat transfer depends only on the ratio ($\Delta p/p_{\infty}$).

The first order solution (zero pressure gradient) satisfies the following algebraic equations

$$H_0^2 \left(\frac{2}{15} - \frac{a_0}{60} - \frac{a_0^2}{105} \right) - 2(2 + a_0) p_0'' = 0$$

$$\frac{(Pr) H_0^2}{2} \left[\frac{2}{15} \left(1 - \frac{T_W}{T_g} \right) - \frac{b_0}{20} + \frac{a_0}{30} \left(1 - \frac{T_W}{T_g} \right) - \frac{a_0 b_0}{105} \right] - \left[2 \left(1 - \frac{T_W}{T_g} \right) + b_0 \right] p_0'' = 0 \quad (40)$$

$$4(1 + 2a_0) + \frac{T_W - S}{T_W + S} \frac{T_g}{T_W} (2 + a_0) \left[2 \left(1 - \frac{T_W}{T_g} \right) + b_0 \right] = 0$$

$$p_0'' = p_{\infty}'' = \frac{1}{N_{\infty}^2} \left(\frac{p_{\infty}}{p_0} \right)$$

where $H_0 = \eta / \sqrt{\xi}$, which yields the zero angle asymptotic solutions for high Mach number. It is of interest to note that, even with zero pressure gradient, the skin friction coefficients for insulated and cooled wall ($\frac{T_W}{T_g} \leq 1$) can both be expressed in the asymptotic form

$$M_{\infty}^3 C_f = \text{const. } X \quad (41)$$

provided the Sutherland viscosity-temperature law is used.

SECRET

By _____ Date _____

BELL Aircraft CORPORATION

Model _____ Page 5B-14

Checked _____ Date _____

Missile

Airplane

Report DL13-945-012

The first order correction for the pressure gradient effect can then be obtained from the following linear algebraic system for a and b in terms of the solution of Equation (40) and p :

$$2(2 + a_0) \frac{\Delta \eta}{\eta_0} - 2 \Delta a$$

$$+ \left[\frac{\gamma - 1}{\gamma} \left(\frac{2}{15} + \frac{1}{3} \frac{T_W}{T_B} + \frac{b_0}{12} - \frac{a_0}{10} - \frac{a_0^2}{105} \right) \frac{H_0^2}{P_0^*} - 2(2 + a_0) \right] \frac{\Delta p}{P_{-\infty}} = 0$$

$$\left(\frac{\Delta \eta}{\eta_0} \right) - \left(\frac{\Delta p}{P_{-\infty}} \right) - \frac{\Delta b}{2(1 - \frac{T_W}{T_B}) + b_0} = 0$$

$$\frac{\gamma - 1}{2\gamma} \frac{H_0^2}{P_0^*} \left(\frac{\Delta p}{P_{-\infty}} \right) - \left(\frac{T_B}{T_W} \right)^2 \frac{T_W - S}{T_W + S} (2 + a_0) \Delta b \quad (12)$$

$$- \left\{ \gamma \frac{T_B}{T_W} + \left(\frac{T_B}{T_W} \right)^2 \frac{T_W - S}{T_W + S} \left[2(1 - \frac{T_W}{T_B}) + b_0 \right] \right\} \Delta a = 0$$

It follows from Equations (20) and (21) that

$$\left. \begin{aligned} \frac{\Delta C_f}{C_{f_0}} &= \left(\frac{\Delta a}{2 + a_0} \right) + \left(\frac{\Delta p}{P_{-\infty}} \right) - \left(\frac{\Delta \eta}{\eta_0} \right) \\ \frac{\Delta C_h}{C_{h_0}} &= \left(\frac{\Delta b}{2(1 - \frac{T_W}{T_B}) + b_0} \right) + \left(\frac{\Delta p}{P_{-\infty}} \right) - \left(\frac{\Delta \eta}{\eta_0} \right) \end{aligned} \right\} \quad (13)$$

where the subscript (0) refers to the case of zero pressure gradient.

By _____ Date _____
 Checked _____ Date _____

BELL Aircraft CORPORATION

Model _____ Page 58-15
 Missile _____ Report: D143-245-012
 Airplane _____

Since from Equation (42),

$$\frac{\Delta a}{2 + a_0} = \frac{\gamma - 1}{8\gamma} \frac{4 \left(\frac{T_W}{T_B} \right)^2 \left(\frac{T_W + S}{T_W - S} \right) + \gamma \left[2 \left(1 - \frac{T_W}{T_B} \right) + b_0 \right]}{(2 + a_0) \left\{ 2 \left[2 \left(1 - \frac{T_W}{T_B} \right) + b_0 \right] + 8 \frac{T_W}{T_B} \frac{T_W + S}{T_W - S} \right\}} \\ \times \left(\frac{2}{15} + \frac{1}{3} \frac{T_W}{T_B} + \frac{b_0}{12} - \frac{a_0}{10} - \frac{a_0^2}{105} \right) \frac{H_0^2}{P_\infty^*} \left(\frac{\Delta p}{P_\infty} \right)$$

and

$$\frac{\Delta b}{2 \left(1 - \frac{T_W}{T_B} \right) + b_0} = \frac{1}{2 + a_0} \left\{ - \frac{\gamma - 1}{8} \left(\frac{2}{15} + \frac{1}{3} \frac{T_W}{T_B} + \frac{b_0}{12} - \frac{a_0}{10} - \frac{a_0^2}{105} \right) \frac{H_0^2}{P_\infty^*} \frac{\Delta p}{P_\infty} + \Delta a_1 \right\} \quad (44)$$

and in view of the second of Equation (42), one arrives at

$$\left(\frac{\Delta c_h}{c_{h_0}} \right) = 0 \left(\frac{\Delta p}{P_\infty} \right) \quad (45)$$

and

$$\left(\frac{\Delta c_f}{c_{f_0}} \right) = \left\{ \frac{\gamma - 1}{8} \left(\frac{2}{15} + \frac{1}{3} \frac{T_W}{T_B} + \frac{b_0}{12} - \frac{a_0}{10} - \frac{a_0^2}{105} \right) \frac{H_0^2}{P_\infty^*} \right\} \left(\frac{\Delta p}{P_\infty} \right) \quad (46)$$

Thus to the first order of approximation, the rate of heat transfer at the wall is practically unaffected by the change in pressure, and the local skin friction increases proportionally to the local increase in pressure.

The coefficient of $\left(\frac{\Delta p}{P_\infty} \right)$ in Equation (46) reduces simply to

$3.69 \left(\frac{\gamma - 1}{\gamma} \right)$ for an insulated wall and to $\frac{\gamma - 1}{\gamma}$ for a cooled wall

$\left(\frac{T_W}{T_B} \ll 1 \right).$

By _____ Date _____

BELL Aircraft CORPORATION

Model _____ Page 5B-16

Checked _____ Date _____

Missile _____ Report D143-945-012
Airplane _____

For $(M_\infty \alpha)^2 \gg 1$, and on the "compression side", one can deduce from the tangent-wedge formula that

$$\frac{\Delta p}{p_\infty} = \frac{36}{35} \left(\frac{\gamma - 1}{2} \right)^{3/4} \left\{ \frac{\frac{3}{2} \left(1 + \frac{S}{T_\infty} \right)}{\gamma (\gamma + 1) \frac{117}{840}} \right\}^{1/2} \chi \frac{1}{(M_\infty \alpha)^2} \quad (47)$$

(for insulated wall)

and

$$\frac{\Delta p}{p_\infty} = 2 \left(\frac{\gamma - 1}{2} \right)^{3/4} \left\{ \frac{\left(\frac{2}{70} \right) T_\infty + S}{\gamma (\gamma + 1) T_W + S} \right\}^{1/2} \frac{12}{(Pr)} \frac{T_W}{T_\infty} \frac{T_W + S}{T_W - S} \left\{ \right\}^{1/4} \chi \frac{1}{(M_\infty \alpha)^2}$$

(for $T_W \quad T_S$)

where

$$\chi = M_\infty^{5/2} / Re_\infty^{1/2}$$

Thus it can be seen that the interaction effect decreases with increasing angle of attack.

While $M_\infty \alpha \ll 1$ on the compression side, and also on the "expansion" side, it can be seen from the Prandtl-Meyer solution that

$$\left(\frac{\Delta p}{p_\infty} \right) = \frac{\gamma}{2} \left(\frac{\gamma - 1}{2} \right)^{3/4} \left[\frac{7}{15} + \frac{1}{20} - \frac{1}{420} \right] \left\{ 3 \frac{\left(1 + \frac{S}{T_\infty} \right)}{\frac{2}{15} + \frac{1}{120} - \frac{1}{420}} \right\}^{1/2} \frac{M_\infty^{5/2}}{Re_\infty^{1/2}}$$

(for insulated wall)

and

$$\left(\frac{\Delta p}{p_\infty} \right) = \frac{\gamma}{2} \left(\frac{\gamma - 1}{2} \right)^{3/4} \left\{ 2 \frac{T_\infty + S}{T_W + S} \left(\frac{2}{15} + \frac{1}{30} - \frac{1}{105} \right) \right\}^{1/2} \frac{M_\infty^{5/2}}{Re_\infty^{1/2}}$$

$$\times \left\{ \frac{12}{(Pr)} \frac{T_W}{T_\infty} \frac{T_W + S}{T_W - S} \right\}^{1/4} \frac{M_\infty^{5/2}}{Re_\infty^{1/2}}$$

(for cooled wall)

(48)

By _____ Date _____
 Checked _____ Date _____
BELL *Aircraft* CORPORATION
 Model _____ Page 50-1
 Missile _____
 Airplane _____ Report D143-945-01

APPENDIX 50

The absorption cross-sections $\sigma(\nu)$ are fundamental quantities in a quantitative theory of radiation. The theoretical expressions for the absorption cross sections are derived on the basis of a quantum mechanical theory of radiation. The details of the derivation are determined by the specific nature of the spectra. Since we are primarily concerned with the absorption continuum of oxygen, the major part of this appendix is devoted to a derivation of the cross sections describing this type of absorption. The cross-sections for line spectra are included for completeness, but no derivation is given. The radiation problems involving line spectra are discussed in many books and papers (References 5.4-1, 5.4-11, 5.4-29 and 5.4-30).

The expression for the cross section for absorption due to transitions between bound states may be written:

$$\sigma(\nu) = \frac{8\pi^3 \nu}{3hc} (1 |\mu| f)^2 S(\nu, \nu_0)$$

$$\text{or } \sigma(\lambda) = \frac{8\pi^3}{3hc\lambda_0} (1 |\mu| f)^2 S(\lambda, \lambda_0)$$

where $(1 |\mu| f)$ is the matrix element for an electric dipole transition and $S(\nu, \nu_0)$ is the shape function for the line. The exact expression for the shape function depends on the state of the gas; the natural line shape is expressed as $S = \frac{\Gamma}{2\pi} \frac{1}{(\nu - \nu_0)^2 + \frac{1}{4}\Gamma^2}$ where Γ = the transition

probability; the doppler broadening gives a shape function

$$S = \sqrt{\frac{m}{2\pi kT}} \frac{e^{-\frac{m}{2kT}(\nu - \nu_0)^2}}{\nu_0^2} \quad \text{and collision broadening; usually}$$

has an expression similar to the natural line shape with $\Gamma = \frac{1}{\tau_0}$ where τ_0 is the mean time between collisions.

Transitions which go from bound states to continuum states are responsible for continuous type absorption spectra, and the corresponding cross section is:

$$\sigma(\nu) = \frac{32\pi^4 \nu m^2}{3h^3 c} (1 |\mu| f)^2$$

where m is the reduced mass of the two body system, ν is the velocity of the reduced particle in the final state.

By _____ Date _____

BELL *Aircraft* CORPORATION

Model _____ Page 50-2

Checked _____ Date _____

Missile _____ Report D143-945-012
Airplane _____

The above equation can be derived in a straight forward manner from the principles of the quantum theory of radiation (Reference 5.4-11). The derivation is sketched below.

$$d\sigma = \frac{2\pi}{hc} |H'|^2 \rho_E d\Omega$$

$$\text{where } |H'|^2 = \frac{e^2}{m^2 c^2} \left(\frac{2\pi \hbar c^2}{\omega} \right) \left| \int \psi_1^* p_0 e^{-i \underline{k} \cdot \underline{r}} \psi_f d\tau \right|^2$$

and

m Reduced mass

\underline{k} Propagation vector

ρ_E Density of final states

p_0 Component of momentum in the direction of the polarization vector $\underline{\epsilon}$

In the visible and near ultra violet region of the spectrum

$$|\underline{k}| = \frac{2\pi}{\lambda} \approx \frac{2\pi}{10^{-5}}$$

\underline{r} is the order of molecular dimensions $\sim 10^{-7} - 10^{-8}$

$$\therefore \underline{k} \cdot \underline{r} \sim 2\pi (10^{-2}) \text{ or less and } e^{i \underline{k} \cdot \underline{r}} \sim 1$$

If we define $\theta = \angle (\underline{k}, \underline{k})$

$\phi = \angle$ between $\underline{k}, \underline{k}$, plane and $\underline{\epsilon}, \underline{k}$ plane

then $p_0 = P \sin \theta \cos \phi$

since $P = m \underline{v}$

and $\underline{v} = i \omega \underline{r}$ where $\omega = \frac{E_f - E_i}{\hbar}$

because we are using eigen functions of the time independent Schrodinger equation

Using the above relations we write

$$|H'|^2 = \frac{1}{m_0^2} \left(\frac{2\pi\hbar c^2}{\omega} \right) \sin^2 \theta \cos^2 \phi \omega^2 m^2 (1|\mu|f)^2$$

where $(1|\mu|f)$ is the dipole matrix element $\int \psi_1^* e \underline{r} \psi_f d\tau$

The final states in the transition will be closely approximated by the eigen functions for free particles over most of physical space; therefore, we can set the density of final states ρ_E equal to

$$\frac{k m d\Omega}{(2\pi)^3 \hbar^2} \quad \text{or} \quad \frac{m^2 v d\Omega}{(2\pi)^3 \hbar^3}$$

If we substitute the above relations into the original expression for the differential cross section, we find:

$$d\sigma = \frac{m^2 v \omega}{2\pi_0 \hbar^3} (1|\mu|f)^2 \sin^2 \theta \cos^2 \phi d\Omega$$

The total cross section is found by integrating the above expression over the solid angle $d\Omega$.

$$\sigma = \int d\sigma = \frac{2}{3} \frac{m^2 v \omega}{\hbar^3 c} (1|\mu|f)^2$$

or

$$\sigma = \frac{32\pi}{3} \frac{\hbar m^2 v v}{\hbar^3 c} (1|\mu|f)^2$$

The matrix element $(1|\mu|f)$ can be split into two parts in the case of electronic transitions in molecular radiation problems (see Reference 5.4-1, 5.4-2 and 5.4-26).

$$(1|\mu|f) = (1^0|\mu^0|f^0)(1^n|f^n)$$

where $(1^0|\mu^0|f^0)$ is the electronic dipole matrix element and

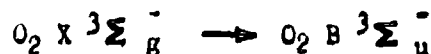
$$(1^n|f^n) = \int \psi_1^{*n} \psi_f^n d\tau$$

is the overlap integral of the initial and final nuclear wave functions.

The electronic dipole matrix element $\langle i^0 | \mu^0 | f^0 \rangle$ is difficult to compute, but it can be determined by spectroscopic measurements at room temperature. The matrix element is determined from the "f" number of spectroscopy by the equation

$$f = \frac{8\pi^2 \nu m}{3he^2} \langle i | \mu | f \rangle^2$$

where m and e are the mass and charge of the electron respectively. The f number for the



transition has the value .259 (see Reference 5.4-25), and this gives the matrix element the value 2.84×10^{-18} esu or 2.84 debye units.

The final step in the cross section calculation is the determination of the overlap integral for the nuclear wave functions. These wave functions are solutions of the time independent Schrodinger equation for the reduced system of the nuclei.

$$\frac{1}{r^2} \frac{\partial}{\partial r} r^2 \frac{\partial \psi}{\partial r} + \frac{1}{r^2 \sin \theta} \frac{\partial}{\partial \theta} \left(\sin \theta \frac{\partial \psi}{\partial \theta} \right) + \frac{1}{r^2 \sin^2 \theta} \frac{\partial^2 \psi}{\partial \phi^2} + \frac{8\pi^2 m}{h^2} [E - V(r)] \psi = 0$$

where E is the characteristic energy value and $V(r)$ is the potential energy function for a given electronic configuration. Approximate solutions for the initial bound states are given in the literature (Reference 5.4-9).

$$\psi_1 = \frac{1}{\sqrt{\pi} r} e^{-\alpha r} \left\{ \frac{(2l+1)(l-l_0)}{2(l+l_0)!} \right\} P_l^{l_0}(\cos \theta) \times \left\{ \frac{\alpha}{\pi} \sqrt{\frac{1}{V}} \right\}^{\frac{1}{2}} e^{-\frac{\alpha}{2} S^2} H_V(\sqrt{\alpha} S)$$

where $\alpha = \frac{8\pi^2 m V_0}{h^2}$

$$S = r - r_0 - a$$

$$V_0 = \frac{1}{2\pi} \sqrt{\frac{E}{h}}$$

$$a = \frac{l(l+1)\sigma r_0}{3l(l+1)\sigma + 2(l+1)}$$

$$V_0 = (V + \frac{1}{2}) h V_0 + l(l+1) \frac{h^2}{8\pi^2 \mu r_0^2} \sigma^2 + \text{etc.}$$

By _____ Date _____

BELL Aircraft CORPORATION

Model _____ Page 50-5

Checked _____ Date _____

Missile _____
Airplane _____ Report D113-945-012

The values of V_e and σ are given in the literature for nitrogen, oxygen and many other diatomic molecules (Reference 5.4-14). For oxygen

$$\frac{h V_e}{k_B} = 2.23 \times 10^3 \text{ egs} \quad \text{and} \quad \frac{\sigma}{k_B} = 2.07 \text{ egs}$$

The final states in the continuum are known to have the asymptotic solutions

$$\psi_{k\ell} = (2\ell + 1) i^{\ell} e^{i\eta_{\ell}} P_{\ell}(\cos \theta) \sin \left(kr - \frac{\ell\pi}{2} + \eta_{\ell} \right)$$

where $k = \frac{p}{h}$ and η_{ℓ} is a phase angle.

The general solution is of the form $A_{\ell} P_{\ell}(\cos \theta) F_{\ell}(r)$ where $F_{\ell}(r)$ satisfies the radial equation

$$\frac{d^2}{dr^2} (r F) + \left\{ k^2 - u(r) - \frac{\ell(\ell+1)}{r^2} \right\} (r F)$$

$$u(r) = \frac{2m}{\hbar^2} V(r)$$

The potential function $V(r)$ is available in the literature for many molecules; in particular the potentials which are significant for the Schumann-Runge transitions are presented on page 64 of Reference 5.4-16. The solution to the radial equation can be obtained by joining the asymptotic expression to a numerical solution in the region of the turning point with the aid of the W.K.B. approximation. If we indicate this solution by $S_{k\ell}(r) = r F_{k\ell}(r)$ our final wave function

$$\psi_{k\ell} = (2\ell + 1) i^{\ell} e^{i\eta_{\ell}} P_{\ell} \frac{S_{k\ell}}{r}(r)$$

When the above initial and final wave functions are substituted into the overlap integral and integrated over the angles θ and ϕ , the integral is reduced in the following manner:

$$\int \psi_i^{*} \psi_f d\tau = \int \psi_{\nu\ell M}^{*} \psi_{k\ell} r^2 dr d\Omega =$$

$$\delta_{\ell\ell'} \sqrt{2} (2\ell + 1)^{\frac{1}{2}} \sqrt{2\pi} \left(\left[\frac{\alpha}{\pi} \right]^{\frac{1}{2}} \frac{1}{2\sqrt{V}} \right)^{\frac{1}{2}} \frac{1}{r_{\infty}}$$

$$\int_0^{\infty} \alpha S^2 \Pi_V(\sqrt{\alpha} S) \times [k_{\infty} S_{k\ell}(r)] dr$$

SECRET

By _____ Date _____

Checked _____ Date _____

BELL *Aircraft* CORPORATION

Model _____ Page 50-6

Missile _____
Airplane _____ Report 0143-945-012

When $v = 0$ the integrand above is simply the product of a gaussian curve times a distorted sine wave. A modest computational program is needed to complete the preceding development and provide a good quantitative description of the continuum radiation of oxygen.

SECRET

By _____ Date _____
 Checked _____ Date _____

BELL Aircraft CORPORATION

Model _____ Page 5D-1
 Missile _____
 Airplane _____ Report D143-945-012

APPENDIX 5D

The Piston Analogy and the Limiting Solutions in Hypersonic Flow

The analogy between the problem of a steady two or three dimensional hypersonic inviscid flow over a thin body and the unsteady cross-flow problem has been pointed out by Hayes and Van Dyke, References 5.6-4 and 5.6-5. In this treatment we shall consider only the two dimensional case, where the equivalent cross-flow problem is that of a piston advancing at a speed comparable to the speed of the shock wave starting instantaneously from rest at time $t = 0$. Let the distance of the piston surface and the shock from their identical starting position at $t = 0$ be Y and Δ , respectively. Referring to Figure 5D-1, the conservation laws of mass, momentum and energy give the integral relations

$$\rho_0 \Delta = \int_Y^\Delta \rho dy \quad (1)$$

$$\int_0^t (p_w - p_\infty) dt = \int_Y^\Delta \rho v dy \quad (2)$$

$$\int_0^t p_w \dot{Y}(t) dt = \int_Y^\Delta \left[\frac{\partial v}{\partial t} p' + \frac{1}{2} \rho v^2 \right] dy \quad (3)$$

where ρ , v , p are the density, normal velocity and pressure, respectively, and the subscripts ∞ and w refer to the values in the free stream and at the piston wall, respectively.

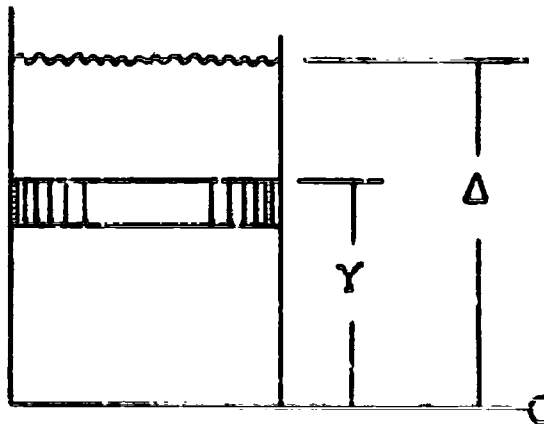


FIGURE 5D-1

By _____ Date _____

BELL Aircraft CORPORATION

Model _____ Page 5D-2

Checked _____ Date _____

Missile _____
Aircraft _____ Report D143-945-012

The above relations can be rearranged as

$$\rho_{\infty} \Delta = \int_Y^{\Delta} \rho \, dy \quad (1)$$

$$\int_0^t (p_w - p_{\infty}) \, dt = \rho_{\infty} \dot{Y} \Delta + \int_Y^{\Delta} \rho (v - \dot{Y}) \, dy \quad (2)$$

$$\begin{aligned} \int_0^t p_w \dot{Y} \, dt - \dot{Y} \int_0^t (p_w - p_{\infty}) \, dt &= \frac{1}{\gamma-1} \int_Y^{\Delta} p \, dy \\ &= -\frac{1}{\gamma} \rho_{\infty} \dot{Y}^2 \Delta + \frac{1}{\gamma} \int_Y^{\Delta} \rho (v - \dot{Y})^2 \, dy \quad (3) \end{aligned}$$

The conditions across the shock are

$$p_0 / p_{\infty} = (1 + \mu^2) \frac{\dot{\Delta}^2}{a_{\infty}^2} + \mu^2 \quad (4)$$

$$\rho_0 / \rho_{\infty} = \frac{\dot{\Delta}^2 / a_{\infty}^2}{1 + \mu^2 + \mu^2 \dot{\Delta}^2 / a_{\infty}^2} \quad (5)$$

$$v_0 / \dot{\Delta} = (1 + \mu^2) \left[1 + a_{\infty}^2 / \dot{\Delta}^2 \right] \quad (6)$$

where $\mu^2 = \frac{\gamma-1}{\gamma+1}$

The boundary condition at the piston wall is

$$v_w = \dot{Y} \quad (7)$$

All the integrals of the form $\int_Y^{\Delta} dy$ (integrating across the "entropy-layer") may be approximated by the use of a linear variation law for ρ , p and v under the integral signs namely

By _____ Date _____

BELL Aircraft CORPORATION

Model _____ Page 5D-3

Checked _____ Date _____

Missile _____ Airplane _____ Report D143-945-012

$$\rho = \rho_w + (\rho_a - \rho_w) \frac{v - Y}{\Delta - Y}$$

$$p = p_w + (p_a - p_w) \frac{v - Y}{\Delta - Y} \quad (8)$$

$$v = Y + (v_a - Y) \frac{Y - Y}{\Delta - Y}$$

In this manner the system (1), (2), (3) is reduced to the following:

$$\int_0^t (\rho_w - \rho_a) dt = \rho_w \dot{Y} \Delta + \frac{v_a - Y}{\delta} \left[\rho_w \Delta + \rho_a (\Delta - Y) \right] \quad (9)$$

$$\begin{aligned} \int_0^t \rho_w \dot{Y} dt &= \dot{Y} \int_0^t (\rho_w - \rho_a) dt = \frac{\Delta - Y}{2(v_a - 1)} (\rho_w + \rho_a) \\ &= -\frac{1}{2} \rho_w \Delta \dot{Y}^2 + \frac{(v_a - Y)^2}{2\delta} \left[\rho_w \Delta + \rho_a (\Delta - Y) \right] \quad (10) \end{aligned}$$

Where the unknowns involve ρ_w , ρ_a , v_a , δ and Δ . Equations (9) and (10), together with equations (4), (5) and (6) are sufficient to determine the solution.

Consider the limiting solution corresponding to the case of

$$\delta \rightarrow \frac{v_a}{\Delta} \gg 1, \quad (11)$$

$$\text{i.e., } \Delta^2 / v_a^2 \gg 1$$

$$\text{Then } \rho_a / \rho_w (1 + \mu^2) \rightarrow \frac{\Delta^2}{v_a^2}$$

$$\rho_a / \rho_w \rightarrow 1 / \mu^2 \quad (12)$$

$$v_a / \Delta \rightarrow 1 - \mu^2$$

By _____ Date _____

Checked _____ Date _____

BELL *Aircraft* CORPORATION

Model _____ Page 5D-4

Missile _____ Report D143-945-012
Airplane _____

So that the system of Equations (9) and (10) reduces finally to

$$\int_0^t P_W dt = \rho_\infty \Delta \dot{Y} + \frac{\rho_\infty}{6} \left[(1 - \mu^2) \dot{\Delta} - \dot{Y} \right] \left[2\Delta + \frac{\Delta - Y}{\mu^2} \right] \quad (13)$$

$$\text{and } \int_0^t P_W \dot{Y} dt = \dot{Y} \int_0^t P_W dt = \frac{1 - \mu^2}{4\mu^2} (\Delta - Y) P_W = \quad (14)$$

$$\rho_\infty \frac{(1 - \mu^2)^2}{4\mu^2} (\Delta - Y) \dot{\Delta}^2 - \frac{\rho_\infty}{2} \dot{Y}^2 + \frac{\rho_\infty}{12} \left[\Delta + \frac{1}{\mu^2} (\Delta - Y) \right] \left[(1 - \mu^2) \dot{\Delta} - \dot{Y} \right]^2$$

where Δ and P_W are the two unknowns

Expanding the solution in the asymptotic series

$$\begin{aligned} P_W &= p^{(0)} + \mu^2 p^{(1)} + \mu^4 p^{(2)} + \dots \\ \Delta &= \Delta^{(0)} + \mu^2 \Delta^{(1)} + \mu^4 \Delta^{(2)} + \dots \end{aligned} \quad (15)$$

yields, from Equations (13) and (14), the explicit solutions

$$\Delta^{(0)} = Y(t) \quad (16)$$

$$\int_0^t p^{(0)} dt = \rho_\infty \dot{Y} \Delta^{(0)} = \rho_\infty \dot{Y} Y, \quad (17)$$

$$\int_0^t p^{(1)} dt = \rho_\infty \left[\dot{Y} \Delta^{(1)} + \frac{1}{6} (\dot{\Delta}^{(1)} - \dot{Y}) (\Delta^{(1)} + 2Y) \right], \quad (18)$$

and

$$\left[\frac{d}{dt} Y \dot{Y} + \dot{Y}^2 \right] \Delta^{(1)} = 2Y \dot{Y}^2 - 4 \int_0^t Y \ddot{Y} dt. \quad (19)$$

By _____ Date _____
 Checked _____ Date _____

BELL *Aircraft* CORPORATION

Model _____ Page 5D-5
 Missile _____ Report D143-945-012
 Airplane _____

Equations (16) and (17) which are identifiable as the Newton impact formula when the effect of surface curvature is ignored gives the Busemann result after substituting $x = U_{\infty} t$, (Reference 5.6-1 and 5.6-3).

For the family of surfaces

$$Y = K x^{\sigma} \quad (20)$$

where σ is an arbitrary parameter, the "similar solution"

$$\begin{aligned} \Delta &= A x^{\sigma} \\ p &= B x^{2\sigma-2} \end{aligned} \quad (21)$$

can be obtained without resorting to the asymptotic development of Equation (15) and Equations (13) and (14) are reduced to a system of algebraic equations for the determination of the coefficients A and B which are functions of the specific heat ratio γ . The case $\sigma = 1$ is trivial, as it leads simply to the well-known limiting values for a wedge:

$$\begin{aligned} \Delta &= \frac{\gamma+1}{2} K x \\ p &= \frac{1}{2} \rho_{\infty} U_{\infty}^2 (\gamma+1) K^2 \end{aligned} \quad (22)$$

For $\sigma = 3/4$, i.e., $Y = K x^{3/4}$, which expresses the growth of a hypersonic viscous boundary layer near the leading edge, it gives, for $\gamma = 1.4$,

$$\begin{aligned} \Delta &= 1.63 K x^{3/4} \\ p &= (1/2) \rho_{\infty} U_{\infty}^2 (1.53) K^2 x^{-1/2} \end{aligned} \quad (23)$$

For $\gamma = 1.67$, we have

$$\begin{aligned} \Delta &= 1.99 K x^{3/4} \\ p &= (1/2) \rho_{\infty} U_{\infty}^2 (1.78) K^2 x^{-1/2} \end{aligned} \quad (24)$$

By _____ Date _____

BELL *Aircraft* CORPORATIONModel _____ Page 21-6

Checked _____ Date _____

Missile _____ Airplane _____ Report DX 3-9-5-012

Using the so-called tangent-wedge method,

i.e.,

$$p = \frac{1}{2} \rho_{\infty} u_{\infty}^2 (\gamma + 1) \left(\frac{dy^2}{dx^2} \right), \quad (H_{\infty} \gg 1), \quad (25)$$

the similarity of the solution to the case, but the value of p given by Equation (25) is found to differ by the ratios 1 : 1.1, for $\gamma = 1.4$, and 1 : 1.13 for $\gamma = 1.67$.



DEPARTMENT OF THE AIR FORCE
HEADQUARTERS 88TH AIR BASE WING (AFMC)
WRIGHT-PATTERSON AIR FORCE BASE OHIO

17 March 2006

88 CG/SCCMF
3810 Communications Blvd
Wright-Patterson AFB OH 45433-7802

Defense Technical Information Center
Attn: Ms. Kelly Akers (DTIC-R)
8725 John J. Kingman Rd, Suite 0944
Ft Belvoir VA 22060-6218

Dear Ms. Akers,

This concerns Technical Report AD073754, MX-2276 Advanced Strategic Weapon System. Aerodynamics, 23 April 1955. This technical report, previously Unclassified/Limited Distribution, is now releasable to the public. The attached AFMC Form 559 verifies that it was reviewed by release authorities at Air Force Research Lab Air Vehicles Directorate (AFRL/VA) and determined to be fully releasable to the public.

Please call me at (937) 522-3091 if you have any questions.

Sincerely

A handwritten signature in cursive script, reading "Lynn Kane", is written above the typed name.

Lynn Kane
Freedom of Information Act Analyst
Management Services Branch
Base Information Management Division

Attachment
AFMC Form 559, RUSH - Freedom of Information Act